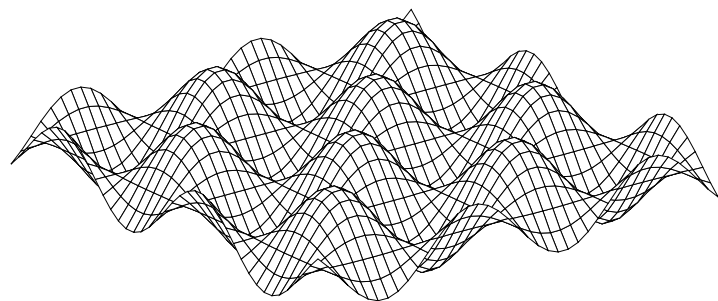


Aircraft Responses to Atmospheric Turbulence

Lecture Notes AE4304

J.A. Mulder, J.C. van der Vaart, W.H.J.J. van Staveren,
Q.P. Chu & M. Mulder

November 2020



Copyright © 2020, by Delft University of Technology, Faculty of Aerospace Engineering (section Control and Simulation), Delft, The Netherlands.

All rights reserved. No part of this publication may be reproduced, stored in a retrieval system or transmitted in any form or by any means, electronic mechanical, photocopying, recording or otherwise, without the prior written consent of the Delft University of Technology, Faculty of Aerospace Engineering, Delft, The Netherlands.

Publisher:

Delft University of Technology
Faculty of Aerospace Engineering
P.O. Box 5058
2600 GB Delft
The Netherlands
Tel.: 31-15-2 78 2094
Fax : 31-15-2 78 6480

Acknowledgements

The Lecture Notes in the present form have a long history and are the result of a continuing effort by quite a number of members and former members of the section Control and Simulation of the Faculty for Aerospace Engineering of Delft University of Technology.

Professor O.H. Gerlach's lecture notes on "Stochastische Processen" to which in particular K. Moelker contributed, may be considered as the prototype of the present lecture notes. Under the name "Vliegeigenschappen III" the lecture course was, during a number of years, given by G.A.J. van de Moesdijk, who extended the subject matter with a number of valuable additions.

A first draft of the present notes was conceived about thirty years ago by professor Bob Mulder, dr Hans van der Vaart and dr Qi Ping Chu, together with dr Martin Laban (at that time a PhD student). This first draft was adapted, including its lay-out, adding many Matlab examples and plots, by ir Arun Karwal, at that time a master student. The second draft was formed by dr Qi Ping Chu and dr Jan-Willem van Staveren (PhD student). The third draft has been modified by professor Max Mulder and dr Mung Lam (PhD student), who made considerable changes to Chapters 2, 3, and 5 in 2006. The fourth draft was concluded in 2015, after prof. Max Mulder finished rewriting Chapter 4. The current draft, again revising Chapters 2 to 5, was completed by him in November 2020.

In some form or other, parts of the original work by present or former staff members have been included in these notes. Apart from the contributions of those already mentioned, the work of M. Baarspul, H.L. Jonkers and F.K. Kappetijn is mentioned here. These contributions are gratefully acknowledged. Of course the full responsibility for any errors or omissions remains entirely with the present author.

prof.dr.ir. M. Mulder

Section Control and Simulation
Department Conrol and Operations
Faculty of Aerospace Engineering
Delft University of Technology
Delft, The Netherlands

Contents

Acknowledgements	i
List of Tables	ix
List of Figures	xi
List of Symbols	xix
Frames of Reference	xxxv
1 Introduction	1
1.1 Contents	1
1.2 Structure	1
2 Scalar Stochastic Processes	3
2.1 An introduction to stochastic processes	3
2.2 The probability distribution function	4
2.3 The probability density function	5
2.4 Moments of the probability density function	5
2.5 The uniform and normal distributions	7
2.5.1 The uniform distribution	7
2.5.2 The normal (or Gaussian) distribution	7
2.6 The joint probability distribution- and density functions	8
2.7 The conditional probability density function	9
2.8 Moments of the joint probability density function	9
2.9 Uncorrelated, orthogonal and independent stochastic variables	11
2.10 The product-, covariance- and correlation functions	12
2.11 Ergodic processes	14
2.12 White noise	15
2.12.1 Definition used in the lecture notes	15
2.12.2 Other definitions	16
2.13 Central limit theorem	16

2.14 Examples	17
2.14.1 Example 2.1	17
2.14.2 Example 2.2	17
2.14.3 Example 2.3	20
2.14.4 Example 2.4	22
2.14.5 Example 2.5	23
2.15 Problems	25
2.16 Summary	27
3 Spectral Analysis of Continuous Time Stochastic Processes	47
3.1 Introduction	47
3.2 Fourier analysis	49
3.3 The continuous-time Fourier Series	49
3.3.1 Derivation	49
3.3.2 Complex form of the Fourier series expansion	52
3.3.3 Properties of the Fourier series	53
3.4 The continuous-time Fourier transform	54
3.4.1 Derivation and definitions	54
3.4.2 Properties of the Fourier transform and some basic Fourier transform pairs	56
3.5 The power spectral density function	61
3.5.1 Derivation	61
3.5.2 Auto- and cross-power spectral density functions	62
3.5.3 Integrating the power spectral density function	63
3.6 Dynamic system analysis in the frequency-domain	63
3.7 White noise, colored noise and shaping filters	67
3.7.1 White noise	67
3.7.2 Colored noise and shaping filters	68
3.8 Frequency-domain analysis using PSDs	68
3.8.1 Estimation of the FRF using PSDs	68
3.8.2 Estimation of the noise spectrum PSDs	70
3.8.3 Definition of the Coherence	70
3.9 Examples and problems	71
3.9.1 Example 3.1	71
3.9.2 Example 3.2	72
3.9.3 Example 3.3	73
3.9.4 Problem 3.1	76
3.9.5 Problem 3.2	77
3.10 Summary	77

4 Spectral Analysis of Discrete Time Stochastic Processes	91
4.1 Introduction	91
4.2 Sampling and signal reconstruction	92
4.2.1 Sampling: from C to D	93
4.2.2 Signal reconstruction: from D to C	96
4.3 The Discrete-time Fourier Transform	98
4.4 The Discrete Fourier Transform	101
4.4.1 Definition of the DFT	101
4.4.2 Properties of the DFT	102
4.4.3 Leakage	103
4.5 The Fast Fourier Transform	105
4.6 The calculation of spectral estimates	108
4.6.1 The periodogram as an estimate for the discrete-time power spectral density	108
4.6.2 Properties of the periodogram	109
4.6.3 The periodogram as an estimate for the continuous-time power spectral density	112
4.6.4 Conclusions	112
4.7 Smoothed estimators for power spectral densities	112
4.7.1 Bartlett's procedure	113
4.7.2 Window functions: the 'indirect' and 'direct' method	113
4.8 Examples and problems	116
4.8.1 Example 4.1: the DFT	116
4.8.2 Example 4.2: the FFT	117
4.8.3 Example 4.3	118
4.8.4 Example 4.4	122
4.8.5 Example 4.5	127
4.8.6 Problem 4.1	133
4.8.7 Problem 4.2	133
4.9 Summary	134
5 Multivariable Stochastic Processes	151
5.1 Introduction	151
5.2 Probability distribution, probability density, mean value and covariance . .	152
5.3 Linear transformations	154
5.4 The covariance function matrix and the spectral density matrix	155
5.5 Dynamic multivariable system analysis in the frequency domain	156
5.6 Dynamic multivariable system analysis in the time domain	159
5.6.1 Continuous time	160
5.6.2 Discrete time	164
5.7 The impulse response method	167
5.8 Examples and problems	171

5.8.1 Example 5.1	171
5.8.2 Example 5.2	176
5.8.3 Example 5.3	180
5.8.4 Example 5.4	181
5.8.5 Problem 5.1	185
5.8.6 Problem 5.2	185
5.9 Summary	185
6 Description of Atmospheric Turbulence	197
6.1 Introduction	197
6.2 Meteorological aspects of atmospheric turbulence	198
6.2.1 Vertical stability	198
6.2.2 Windshear	199
6.3 Different kinds of turbulence	199
6.3.1 Turbulence near the ground	200
6.3.2 Turbulence in clouds	200
6.3.3 Clear-air turbulence	200
6.3.4 Mountain wave turbulence	201
6.4 Statistical aspects of atmospheric turbulence	201
6.4.1 Introduction	201
6.4.2 The Navier-Stokes equations	201
6.4.3 A general statistical description	204
6.4.4 Two fundamental correlation functions	206
6.4.5 The integral scale of turbulence	207
6.5 The von Kármán spectra	207
6.6 The Dryden spectra	209
6.7 Quantitative description of turbulence parameters at low altitude	212
6.7.1 The intensity of turbulence	213
6.7.2 The scale of turbulence	213
6.8 Examples	214
6.8.1 Example 6.1	214
6.8.2 Example 6.2	216
6.8.3 Example 6.3	218
6.9 Summary	220
7 Symmetric Aircraft Response to Atmospheric Turbulence	233
7.1 Introduction	233
7.2 The symmetric aerodynamic forces and moments due to atmospheric turbulence	233
7.3 Derivation of the gust derivatives for longitudinal aircraft motion	236
7.3.1 Introduction	236
7.3.2 Derivation of gust derivatives with respect to \hat{u}_g	237

7.3.3	Derivation of gust derivatives with respect to α_g	244
7.4	Equations for the symmetric motions of aircraft in atmospheric turbulence	246
7.4.1	Introduction	246
7.4.2	The symmetric equations of motion for aircraft in atmospheric turbulence	247
7.5	Modeling the gust penetration effect	248
7.6	Examples and problems	254
7.6.1	Example 7.1	254
7.6.2	Example 7.2	258
7.6.3	Example 7.3	267
7.6.4	Example 7.4	271
7.6.5	Problem 7.1	277
7.7	Summary	277
8	Asymmetric Aircraft Response to Atmospheric Turbulence	295
8.1	Introduction	295
8.2	The two-dimensional autocovariance functions of stationary homogeneous isentropic turbulence	296
8.3	The two-dimensional power spectral density functions of stationary homogeneous turbulence	298
8.4	Elementary two-dimensional fields of flow	300
8.5	The force and moments due to gust velocities parallel to the longitudinal axis	302
8.6	The force and moments due to gust velocities parallel to the lateral axis	304
8.7	The force and moments due to gust velocities parallel to the vertical axis	305
8.8	The power spectra of the rolling and yawing moments due to gust velocities parallel to the longitudinal and the vertical axes	307
8.9	Approximation of the effective one-dimensional power spectral densities	309
8.10	Summary of the expressions for the aerodynamic force and moments	310
8.11	Equations for the asymmetric motions of an aircraft in atmospheric turbulence	311
8.12	Equations of motion in state-space form for asymmetric aircraft motions in atmospheric turbulence	312
8.13	Modeling the gust penetration-effect for asymmetric aircraft motions	316
8.13.1	Introduction	316
8.13.2	Derivation of the aerodynamic frequency response function of the aerodynamic force coefficient C_Y with respect to β_g	316
8.13.3	Derivation of the aerodynamic frequency response function of the aerodynamic moment coefficient C_l with respect to β_g	317
8.13.4	Derivation of the aerodynamic frequency response function of the aerodynamic moment coefficient C_n with respect to β_g	318
8.13.5	Derivation of asymmetric steady and unsteady gust derivatives	318
8.14	Examples and problems	319
8.14.1	Example 8.1	319

8.14.2 Example 8.2	326
8.14.3 Example 8.3	329
8.14.4 Problem 8.1	332
8.15 Summary	332
9 Aircraft Responses According to Etkin's 4 Point Model	355
9.1 Introduction	355
9.2 A general statistical description	355
9.3 Correlation functions and the integral scale of turbulence	357
9.4 The turbulence inputs for the linear field approximation	359
9.5 Etkin's four point model	364
9.5.1 Introduction	364
9.5.2 Correlations and spectra	365
9.5.3 Equations of motion	368
9.5.4 Frequency domain simulations	369
9.5.5 Time domain simulations	370
9.6 Examples	373
9.6.1 Example 9.1	373
9.6.2 Example 9.2	376
9.6.3 Example 9.3	381
9.7 Summary	388
References	415

List of Tables

2.1	Definition of the moments and central moments of the probability density function.	28
2.2	Moments and central moments of the joint probability density function.	29
2.3	Some characteristics of product-, covariance-, and correlation functions.	30
2.4	“Theoretical” versus “practical” calculation of the 6 most important statistical properties.	31
3.1	Properties of the Fourier transform.	78
3.2	Some basic Fourier transforms.	79
3.3	Properties of the power spectral density function (note that we assume zero-mean signals in this table).	80
3.4	Average value, correlations and spectral densities of linear dynamic system outputs.	81
3.5	Standard integrals for the calculation of the variance.	82
3.6	Standard integrals for the calculation of the variance.	83
4.1	Relations between continuous-time and discrete-time transforms.	135
4.2	Examples of time- and frequency-domain windows	135
7.1	Symbols appearing in the general state-space representation (Equations (7.104) and (7.109)).	278
7.2	Calculation of the symmetric gust derivatives.	279
8.1	$\frac{I_{\hat{u}_g}(0,B)}{\sigma_{\hat{u}_g}^2}$ and $\frac{I_{\alpha_g}(0,B)}{\sigma_{\alpha_g}^2}$ as a function of B	334
8.2	τ_1 , τ_2 and τ_3 in the approximated power spectral density function of the horizontal gust velocity, as a function of B	335
8.3	τ_4 , τ_5 and τ_6 in the approximated power spectral density function of the horizontal gust velocity, as a function of B	336
8.4	Symbols appearing in the general state-space representation (Equations (8.87) and (8.99)).	337

8.5	Calculation of the asymmetric gust derivatives. The gust derivatives marked with an asterisk (*) should be used in conjunction with the effective one-dimensional input periodograms $I_{\hat{u}_g \hat{u}_g}(\omega)$ and $I_{\alpha_g \alpha_g}(\omega)$	338
9.1	Additional symbols appearing in the general state-space representation for Etkin's Four Point Aircraft model. Symmetric aircraft models.	389
9.2	Additional symbols appearing in the general state-space representation for Etkin's Four Point Aircraft model. Asymmetric aircraft models.	389

List of Figures

2.1	Some common deterministic input signals used for system analysis. Note that the horizontal axes show time in seconds.	32
2.2	An example of a stochastic input signal.	32
2.3	The concept of the ensemble of a stochastic process.	32
2.4	Realizations of stochastic processes with different average value (a), different amplitude (b) or different speed of fluctuations (c).	33
2.5	Part of the ensemble of a stochastic process.	34
2.6	Expected value as an ensemble averaging.	34
2.7	Uniform probability density function, $\bar{x} \sim \mathcal{U}(a, b)$	34
2.8	The Gaussian probability density- and distribution functions, $\bar{x} \sim \mathcal{N}(\mu, \sigma)$ (plotted here with $\mu_{\bar{x}} = 0$, $\sigma_{\bar{x}} = 1$).	35
2.9	Graphical representation of the joint probability density function $f_{\bar{x}\bar{y}}(x, y)$. .	35
2.10	Graphical representation of the conditional probability density function. .	36
2.11	Auto covariance functions of stochastic processes $\bar{x}(t)$ and $\bar{y}(t)$ (one realization).	36
2.12	Cross covariance functions two stochastic processes $\bar{x}(t)$ and $\bar{y}(t)$ (one realization).	37
2.13	Averaged auto and cross covariance functions, for two stochastic processes $\bar{x}(t)$ and $\bar{y}(t)$, over 500 realizations.	37
2.14	Difference between ensemble average and time average.	38
2.15	'Ideal' versus 'practical' white noise.	39
2.16	The sum of two random variables with equal, uniform, probability density functions (top) yields a random variable with a triangular probability density function (bottom).	40
2.17	Time history, auto product / covariance / correlation functions.	41
2.18	Graphical impression of a joint Gaussian probability density function, here with $\mu_{\bar{x}} = \mu_{\bar{y}} = 0$, $\sigma_{\bar{x}} = \sigma_{\bar{y}} = 1$, $K_{\bar{x}\bar{y}} = 0$	42
2.19	Equi-probability ellipses of the joint Gaussian distribution.	43
2.20	Equi-probability ellipses of the <i>normalized</i> joint Gaussian distribution. .	43
2.21	Randomness in Matlab (Example 2.4).	44

2.22	Signal $x(t)$ and the probability density function of the stochastic variable \bar{x} , used in Example 2.5.	44
2.23	Signals $x(t)$ of Problem 2.7.	45
3.1	Two different stochastic signals with equal average and variance but with totally different frequency contents.	84
3.2	Graphical representation of a Fourier series expansion. The signal $x(t)$ consists of 3 cosine functions and 1 sine function.	84
3.3	Graphical representation of a complex Fourier series expansion of $x(t)$ in Figure 3.2.	84
3.4	The block function $b(t)$ and its Fourier transform $B(\omega)$, the sinc-function. .	85
3.5	The effect of changing T in $b(t)$ on the Fourier transform $B(\omega)$	86
3.6	The periodic block function $b(t)$, and the scaled Fourier series coefficients $\{c'_k\} = T_0 \{c_k\}$. These coefficients are equal to the Fourier transform of an aperiodic block function (the dotted sinc-function, see also Figure 3.4) at the integer multiples of the fundamental frequency $k \frac{2\pi}{T_0}$	87
3.7	Power spectral density of ideal white noise with intensity $W = 1$	87
3.8	A linear time-invariant system with input $\bar{u}(t)$ and output $\bar{y}(t)$	88
3.9	An LTI system with stochastic input $\bar{u}(t)$ and response $\bar{x}(t)$ perturbed by random noise.	88
3.10	Power spectral density function of $\bar{x}(t) = \sin(2\pi t) + 1$	88
3.11	Typical runway profile.	88
3.12	Power spectral density $S_{\bar{u}\bar{u}}(\gamma)$ of runway roughness from experimental data. Taken from (AGARD, 1975).	89
3.13	Landing gear suspension as a 1 DOF mass-spring-damper system.	89
3.14	Cross power - and auto power spectral densities of aircraft displacements and auto power spectral density of normal acceleration.	90
4.1	Duality of the block transformation.	136
4.2	The sampling process.	136
4.3	Example of impulse-train sampled spectrum	137
4.4	Illustration of the aliasing effect.	138
4.5	Impulse-train sampling overview 1.	138
4.6	Ideal signal reconstruction scheme.	139
4.7	Conversion of the CT pulse train model $z(n\Delta t)$ to a discrete time series $x[n]$	139
4.8	Impulse-train sampling overview 2: sampling complete.	140
4.9	Frequency in discrete time.	141
4.10	The Discrete Fourier Transform; positive and negative frequencies.	142
4.11	The ‘view’ of the DFT on the discrete-time spectrum.	142
4.12	Illustration of the ‘leakage’ phenomenon (right).	142
4.13	Second illustration of the ‘leakage’ phenomenon.	143

4.14	A discrete sample of $\bar{x}(t)$ and the resulting auto-covariance function, drawn in MATLAB as a continuous line.	143
4.15	Auto spectral density function of $\bar{x}(t)$, drawn in MATLAB as a continuous line.	144
4.16	A discrete sample of $\bar{x}(t)$ and the resulting auto-covariance function, drawn in MATLAB as discrete samples.	144
4.17	Auto spectral density function of $\bar{x}(t)$, drawn in MATLAB as discrete samples.	145
4.18	A discrete-time sample of $\bar{w}(t)$ and the resulting auto-covariance function.	145
4.19	Auto spectral density function of $\bar{w}(t)$	146
4.20	Filter input ‘white’ noise signal $\bar{w}(t)$ (a), resulting input signal of surface irregularities $\bar{u}(t)$ (b) and suspension system output signal $\bar{y}(t)$ (c).	147
4.21	Digitally calculated power spectral density functions, compared to analytically derived power spectral density functions (dashed lines).	148
4.22	Digitally calculated auto power spectral density functions (using <code>pwelch.m</code> : blue, using <code>smooth.m</code> : red), compared to the analytically derived power spectral density functions (dashed green lines).	149
4.23	Digitally calculated results (using <code>pwelch.m</code> : blue, using <code>smooth.m</code> : red), compared to the analytically derived reference (dashed green lines).	150
5.1	A first order continuous LTI system driven by a white noise input signal.	186
5.2	Covariance of discrete white noise input signals and output signals of a continuous system simulated with MATLAB’s <code>lsim</code> function, driven by the discrete input signals.	186
5.3	1 DOF mass-spring-damper system.	187
5.4	Responses of the elements of the covariance matrix to a white noise input signal. Second order system, initial conditions zero.	188
5.5	Responses of the elements of the covariance matrix to initial conditions. Second order system, no noise input signal.	189
5.6	Responses of the elements of the covariance matrix to white noise input and initial conditions. Second order system.	190
5.7	Response to a white noise input signal of limited duration.	191
5.8	The effect of a stepwise change in white noise input intensity.	192
5.9	The response of the variance of the displacement to a white noise input signal calculated using the impulse response method. Second order system.	193
5.10	The response of the ensemble variable $x(t)$ and variances of the second order system to a white noise input signal calculated using time responses. The number of replications is 15.	194
5.11	The response of the ensemble variable $x(t)$ and variances of the second order system to a white noise input signal calculated using time responses. The number of replications is 150.	195

5.12	The response of the ensemble variable $x(t)$ and variances of the second order system to a white noise input signal calculated using time responses. The number of replications is 1500.	196
6.1	Breakdown of the ‘flight in atmospheric turbulence’ problem.	221
6.2	Vertical instability. If the geometric lapse rate $ \lambda $ at height h is larger than $ \beta $, a parcel rising Δh from P will have at Q a temperature $T' > T$ where T is the temperature of the surrounding air (Q). It will tend to continue to rise.	221
6.3	Conditions for vertical stability. The diagram summarizes the stability conditions for both unsaturated and saturated air.	222
6.4	Definition of vertical (a) and horizontal (b) windshear.	222
6.5	Percent of time clear-air turbulence reported by pilots with respect to jet-stream core (Endlich & McLean, 1957).	223
6.6	Cross-section of conditions associated with a typical mountain wave (Kuettnér & Jenkins, 1953).	224
6.7	Correlations in isotropic turbulence a) Longitudinal correlation, $f(\xi)$ and b) Lateral correlation, $g(\xi)$	225
6.8	General shape of the correlation curves $f(\xi)$ and $g(\xi)$	225
6.9	a) The longitudinal von Kármán spectrum, b) the lateral von Kármán spectrum.	226
6.10	Reference frame and separation distance vector definition.	226
6.11	a) The longitudinal Dryden spectrum, b) the lateral Dryden spectrum.	226
6.12	a) The longitudinal Dryden spectrum, b) the lateral Dryden spectrum.	227
6.13	Modelling of atmospheric turbulence.	227
6.14	Standard deviation of vertical gust velocity as a function of altitude.	228
6.15	Scale of (longitudinal) turbulence as a function of altitude.	229
6.16	Schematic view of aircraft.	230
6.17	Correlation coefficient of turbulence velocity at two points as a function of scale length. Dryden turbulence model.	230
6.18	Dryden spectra for vertical turbulence for two values of L_g : Solid line: $L_g = 150$ m; dashed line $L_g = 1500$ m.	231
6.19	Approximated white noise \bar{w} (a), and resulting vertical turbulence signal \bar{w}_g for $L_g = 150$ m (continuous line) and $L_g = 1500$ m (dashed line) (b).	232
7.1	The velocities in the horizontal OXY -plane.	280
7.2	Positive directions of the gust velocities u_g , v_g and w_g	280
7.3	A sinusoidal elementary field of flow.	281
7.4	Positioning of the centre of gravity and arbitrary point P in a measurement frame of reference $OX_mY_mZ_m$	281
7.5	The influence of the finite dimensions of an aircraft.	281

7.6	Aircraft responses to vertical turbulence for the Ce-500 ‘Citation’ for $V = 59.9 \text{ m/s}$ ($L_g=150 \text{ m}$, $\sigma=1 \text{ m/s}$).	282
7.7	Auto power spectral densities of symmetric aircraft motion variables due to vertical turbulence for the Ce-500 ‘Citation’.	283
7.8	Impulse responses of symmetric aircraft motion variables (vertical turbulence) for the Ce-500 ‘Citation’.	284
7.9	(Cross) products of impulse responses for the Ce-500 ‘Citation’.	285
7.10	Growth in time of the covariance matrix calculated by integrating the (cross) products of the impulse responses (vertical turbulence) for the Ce-500 ‘Citation’.	286
7.11	Growth in time of the covariance matrix of symmetric aircraft motion variables (response to vertical turbulence) for the Ce-500 ‘Citation’.	287
7.12	Power spectral density of the normal acceleration due to vertical turbulence for controlled (dashed line) and uncontrolled aircraft (continuous line) for the Ce-500 ‘Citation’.	288
7.13	Power spectral density of the normal acceleration due to vertical (continuous line) and horizontal turbulence (dashed line) for the Ce-500 ‘Citation’.	289
7.14	Aircraft responses due to horizontal turbulence for the Ce-500 ‘Citation’.	290
7.15	Analytically derived power spectral densities and periodograms of the motion variables for the Ce-500 ‘Citation’. The periodograms have been calculated from time-domain data (previous figure).	291
7.16	Aircraft responses due to vertical turbulence for the Ce-500 ‘Citation’.	292
7.17	Analytically derived power spectral densities and periodograms of the motion variables for the Ce-500 ‘Citation’. The periodograms have been calculated from time-domain data (previous figure).	293
8.1	‘Symmetric’ and ‘asymmetric’ gust.	339
8.2	The components of the velocity in two points of the $O_eX_eY_e$ plane.	339
8.3	The one-dimensional covariance functions $f(r)$ and $g(r)$	340
8.4	The velocities u_g and v_g in the $O_eX_eY_e$ -plane, resolved in components along- and perpendicular to O_eP	340
8.5	Graphical impression of the (2D) auto power spectral density $S_{u_g u_g}(\Omega_x L_g, \Omega_y L_g)$	341
8.6	Two-dimensional elementary flowfield, symmetric with respect to the $O_eX_eZ_e$ -plane, in which the components of the gust velocity u_g , v_g or w_g change sinusoidally in the X_e - as well as in the Y_e -direction.	341
8.7	Two-dimensional elementary flowfield, antisymmetric with respect to the $O_eX_eZ_e$ -plane.	342
8.8	The two-dimensional flowfield, represented by a one-dimensional field rotated about the Z_e -axis over the angle $\arctan \frac{\Omega_y}{\Omega_x}$	342
8.9	Two-dimensional symmetric (a) and antisymmetric flowfields (b).	343
8.10	Two-dimensional elementary flowfield, resulting from the numerical superposition of Figures 8.9(a) and 8.9(b).	343

8.11	The contribution to the rolling moment by a chordwise strip of the wing of width dy at a distance y from the plane of symmetry (a), and description of the gust penetration effect for asymmetric aircraft motions (b).	344
8.12	The non-dimensional function $h(\Omega_y \frac{b}{2})$ for three different spanwise lift distributions.	345
8.13	The effective one-dimensional power spectral density function of the horizontal gust velocity for different values of $B = \frac{b}{2L_g}$	346
8.14	The effective one-dimensional power spectral density function of the vertical gust velocity for different values of $B = \frac{b}{2L_g}$	347
8.15	The effective one-dimensional power spectral density function of the horizontal gust velocity for three different spanwise lift distributions at two different values for B	348
8.16	Gust responses of the asymmetric motion variables for the Ce-500 ‘Citation’.	349
8.17	Gust responses of the asymmetric motion variables for the Ce-500 ‘Citation’ (continued).	350
8.18	Power spectral density of the roll angle for the Ce-500 ‘Citation’ for two feedback gains. The dashed line represents the aircraft’s response with a wing-leveler active.	351
8.19	Growth in time of the covariance of the roll angle for $K_\varphi = 0$ (a) and $K_\varphi = -0.1$ (b).	352
8.20	Aircraft responses due to lateral horizontal turbulence β_g for the Ce-500 ‘Citation’.	353
8.21	Analytically derived power spectral densities and periodograms of the motion variables. The periodograms have been calculated from time-domain data (previous figure).	354
9.1	The downwash at point (x,y) of a planar aircraft.	390
9.2	The downwash at point (x,y) of a planar aircraft due to rolling and yawing.	390
9.3	The turbulence inputs r_{1g} and r_{2g}	390
9.4	Linearization of the gust fields.	391
9.5	The influence of the dimensions of aircraft on the gust field linearization (747 and Cessna ‘Citation II’).	391
9.6	The “four point” aircraft model.	391
9.7	The “four point” model and separation vectors ξ	392
9.8	Dimensional autocorrelation function $R_{u_g u_g}$ for Etkin’s “four point” model.	392
9.9	Dimensional autocorrelation function $R_{v_g v_g}$ for Etkin’s “four point” model.	393
9.10	Dimensional autocorrelation function $R_{w_g w_g}$ for Etkin’s “four point” model.	393
9.11	Dimensional autocorrelation function $R_{p_g p_g}$ for Etkin’s “four point” model.	394
9.12	Dimensional autocorrelation function $R_{q_g q_g}$ for Etkin’s “four point” model.	394
9.13	Dimensional autocorrelation function $R_{r_{1g} r_{1g}}$ for Etkin’s “four point” model.	395
9.14	Dimensional autocorrelation function $R_{r_{2g} r_{2g}}$ for Etkin’s “four point” model.	395
9.15	Dimensional crosscorrelation function $R_{w_g q_g}$ for Etkin’s “four point” model.	396

9.16	Dimensional crosscorrelation function $R_{v_g r_1 g}$ for Etkin's "four point" model.	396
9.17	Dimensional crosscorrelation function $R_{v_g r_2 g}$ for Etkin's "four point" model.	397
9.18	Dimensional crosscorrelation function $R_{r_1 g r_2 g}$ for Etkin's "four point" model.	397
9.19	Auto power spectral density function $S_{\hat{u}_g \hat{u}_g}$ for Etkin's "four point" model ($L_g = 150$ m).	398
9.20	Auto power spectral density function $S_{\beta_g \beta_g}$ for Etkin's "four point" model ($L_g = 150$ m).	398
9.21	Auto power spectral density function $S_{\alpha_g \alpha_g}$ for Etkin's "four point" model ($L_g = 150$ m).	399
9.22	Auto power spectral density function $S_{\frac{p_{g,b}}{2V} \frac{p_{g,b}}{2V}}$ for Etkin's "four point" model ($L_g = 150$ m).	399
9.23	Auto power spectral density function $S_{\frac{q_g \bar{c}}{V} \frac{q_g \bar{c}}{V}}$ for Etkin's "four point" model ($L_g = 150$ m).	400
9.24	Auto power spectral density function $S_{\frac{r_{1,g,b}}{2V} \frac{r_{1,g,b}}{2V}}$ for Etkin's "four point" model ($L_g = 150$ m).	400
9.25	Auto power spectral density function $S_{\frac{r_{2,g,b}}{2V} \frac{r_{2,g,b}}{2V}}$ for Etkin's "four point" model ($L_g = 150$ m).	401
9.26	Cross power spectral density function $S_{\alpha_g \frac{q_g \bar{c}}{V}}$ for Etkin's "four point" model ($L_g = 150$ m).	401
9.27	Cross power spectral density function $S_{\beta_g \frac{r_{1,g,b}}{2V}}$ for Etkin's "four point" model ($L_g = 150$ m).	402
9.28	Cross power spectral density function $S_{\beta_g \frac{r_{2,g,b}}{2V}}$ for Etkin's "four point" model ($L_g = 150$ m).	402
9.29	Cross power spectral density function $S_{\frac{r_{1,g,b}}{2V} \frac{r_{2,g,b}}{2V}}$ for Etkin's "four point" model ($L_g = 150$ m).	403
9.30	Power spectral density of \hat{u} for the Ce-500 'Citation' due to symmetrical gust u_g ($L_g = 150$ m).	403
9.31	Power spectral density of α for the Ce-500 'Citation' due to symmetrical gust u_g ($L_g = 150$ m).	404
9.32	Power spectral density of θ for the Ce-500 'Citation' due to symmetrical gust u_g ($L_g = 150$ m).	404
9.33	Power spectral density of $\frac{q_g \bar{c}}{V}$ for the Ce-500 'Citation' due to symmetrical gust u_g ($L_g = 150$ m).	405
9.34	Power spectral density of \hat{u} for the Ce-500 'Citation' due to symmetrical gust w_g ($L_g = 150$ m).	405
9.35	Power spectral density of α for the Ce-500 'Citation' due to symmetrical gust w_g ($L_g = 150$ m).	406
9.36	Power spectral density of θ for the Ce-500 'Citation' due to symmetrical gust w_g ($L_g = 150$ m).	406

9.37	Power spectral density of $\frac{q\bar{c}}{V}$ for the Ce-500 'Citation' due to symmetrical gust w_g ($L_g = 150$ m).	407
9.38	Power spectral density of β for the Ce-500 'Citation' due to asymmetrical gust u_g ($L_g = 150$ m).	407
9.39	Power spectral density of ϕ for the Ce-500 'Citation' due to asymmetrical gust u_g ($L_g = 150$ m).	408
9.40	Power spectral density of $\frac{pb}{2V}$ for the Ce-500 'Citation' due to asymmetrical gust u_g ($L_g = 150$ m).	408
9.41	Power spectral density of $\frac{rb}{2V}$ for the Ce-500 'Citation' due to asymmetrical gust u_g ($L_g = 150$ m).	409
9.42	Power spectral density of β for the Ce-500 'Citation' due to asymmetrical gust v_g ($L_g = 150$ m).	409
9.43	Power spectral density of ϕ for the Ce-500 'Citation' due to asymmetrical gust v_g ($L_g = 150$ m).	410
9.44	Power spectral density of $\frac{pb}{2V}$ for the Ce-500 'Citation' due to asymmetrical gust v_g ($L_g = 150$ m).	410
9.45	Power spectral density of $\frac{rb}{2V}$ for the Ce-500 'Citation' due to asymmetrical gust v_g ($L_g = 150$ m).	411
9.46	Power spectral density of β for the Ce-500 'Citation' due to asymmetrical gust w_g . ($L_g = 150$ m)	411
9.47	Power spectral density of ϕ for the Ce-500 'Citation' due to asymmetrical gust w_g ($L_g = 150$ m).	412
9.48	Power spectral density of $\frac{pb}{2V}$ for the Ce-500 'Citation' due to asymmetrical gust w_g ($L_g = 150$ m).	412
9.49	Power spectral density of $\frac{rb}{2V}$ for the Ce-500 'Citation' due to asymmetrical gust w_g ($L_g = 150$ m).	413

List of Symbols

A	system matrix
a_z	acceleration along the aircraft's Z -axis
B, C	input matrix
B	$\frac{b}{2L_g}$
C	output matrix
\bar{c}	mean aerodynamic wing chord
$c.g.$	aircraft's centre of gravity
$C(i, j)$	element (i, j) of covariance matrix
C_L	lift coefficient
C_l	$\frac{L}{\frac{1}{2}\rho V^2 S b}$ rolling moment coefficient
C_{l_g}	C_l due to turbulence
C_{l_p}	$\frac{\partial C_l}{\partial \frac{pb}{2V}}$
$C_{l_{pw}}$	contribution of the wing to C_{l_p}
C_{l_r}	$\frac{\partial C_l}{\partial \frac{rb}{2V}}$
$C_{l_{rw}}$	contribution of the wing to C_{l_r}
C_{l_w}	contribution of the wing to C_l
$C_{l_{ug}}$	$\frac{\partial C_{l_g}}{\partial \hat{u}_g}$
$C_{l_{\alpha_g}}$	$\frac{\partial C_{l_g}}{\partial \alpha_g}$
C_{l_β}	$\frac{\partial C_l}{\partial \beta}$
$C_{l_{\beta_g}}$	$\frac{\partial C_{l_g}}{\partial \beta_g}$

$C_{l_{\dot{\beta}}}$	$\frac{\partial C_l}{\partial \frac{\dot{\beta}b}{V}}$
$C_{l_{\dot{\beta}_g}}$	$\frac{\partial C_{l_g}}{\partial \frac{\dot{\beta}_g b}{V}}$
$C_{l_{\delta_a}}$	$\frac{\partial C_l}{\partial \delta_a}$
$C_{l_{\delta_r}}$	$\frac{\partial C_l}{\partial \delta_r}$
C_m	$\frac{M}{\frac{1}{2}\rho V^2 S \bar{c}}$ pitching moment coefficient
$C_{m_{a.c.}}$	C_m about the aerodynamic centre of the wing plus fuselage for $C_{L_w} = 0$
C_{m_g}	C_m due to turbulence
C_{m_h}	contribution of the horizontal tailplane to C_m
C_{m_q}	$\frac{\partial C_m}{\partial \frac{q c}{V}}$
C_{m_u}	$\frac{1}{\frac{1}{2}\rho V S \bar{c}} \frac{\partial M}{\partial u}$
$C_{m_{u_g}}$	$\frac{\partial C_m}{\partial \dot{u}_g}$
$C_{m_{\dot{u}_g}}$	$\frac{\partial C_m}{\partial \frac{\dot{u}_g \bar{c}}{V}}$
C_{m_w}	contribution of the wing plus fuselage to C_m
C_{m_α}	$\frac{\partial C_m}{\partial \alpha}$
$C_{m_{\alpha_g}}$	$\frac{\partial C_{m_g}}{\partial \alpha_g}$
$C_{m_{\dot{\alpha}}}$	$\frac{\partial C_m}{\partial \frac{\dot{\alpha} \bar{c}}{V}}$
$C_{m_{\dot{\alpha}_g}}$	$\frac{\partial C_{m_g}}{\partial \frac{\dot{\alpha}_g \bar{c}}{V}}$
C_{m_δ}	$\frac{\partial C_m}{\partial \delta}$
C_n	$\frac{N}{\frac{1}{2}\rho V^2 S b}$ yawing moment coefficient
C_{n_g}	C_n due to turbulence

C_{n_p}	$\frac{\partial C_n}{\partial \frac{pb}{2V}}$
$C_{n_{pw}}$	contribution of the wing plus fuselage to C_{n_p}
C_{n_r}	$\frac{\partial C_n}{\partial \frac{rb}{2V}}$
$C_{n_{rw}}$	contribution of the wing plus fuselage to C_{n_r}
$C_{n_{ug}}$	$\frac{\partial C_{n_g}}{\partial \hat{u}_g}$
$C_{n_{\alpha_g}}$	$\frac{\partial C_{n_g}}{\partial \alpha_g}$
C_{n_β}	$\frac{\partial C_n}{\partial \beta}$
$C_{n_{\beta_g}}$	$\frac{\partial C_{n_g}}{\partial \beta_g}$
$C_{n_{\dot{\beta}}}$	$\frac{\partial C_n}{\partial \frac{\dot{\beta}b}{V}}$
$C_{n_{\dot{\beta}_g}}$	$\frac{\partial C_{n_g}}{\partial \frac{\dot{\beta}_gb}{V}}$
$C_{n_{\delta_a}}$	$\frac{\partial C_n}{\partial \delta_a}$
$C_{n_{\delta_r}}$	$\frac{\partial C_n}{\partial \delta_r}$
C_X	$\frac{X}{\frac{1}{2}\rho V^2 S}$ aerodynamic force coefficient along the aircraft's X -axis
C_{X_g}	C_X due to turbulence
C_{X_q}	$\frac{\partial C_X}{\partial \frac{qc}{V}}$
C_{X_u}	$\frac{1}{\frac{1}{2}\rho VS} \frac{\partial X}{\partial u}$
$C_{X_{ug}}$	$\frac{\partial C_X}{\partial \hat{u}_g}$
$C_{X_{\dot{u}_g}}$	$\frac{\partial C_X}{\partial \frac{\dot{\hat{u}}_g c}{V}}$
C_{X_0}	C_X in the steady flight condition
$C_{\bar{x}\bar{x}}(i)$	covariance matrix of the state vector \underline{x} at time i

$C_{xy}(\tau)$	covariance function of x and y
C_{X_α}	$\frac{\partial C_X}{\partial \alpha}$
$C_{X_{\alpha_g}}$	$\frac{\partial C_{X_g}}{\partial \alpha_g}$
$C_{X_{\dot{\alpha}}}$	$\frac{\partial C_X}{\partial \dot{\alpha}^c \underline{V}}$
$C_{X_{\dot{\alpha}_g}}$	$\frac{\partial C_{X_g}}{\partial \dot{\alpha}_g^c \underline{V}}$
C_{X_δ}	$\frac{\partial C_X}{\partial \delta}$
C_Y	$\frac{Y}{\frac{1}{2}\rho V^2 S}$ aerodynamic force coefficient along the aircraft's Y -axis
C_{Y_g}	C_Y due to turbulence
C_{Y_p}	$\frac{\partial C_Y}{\partial \frac{pb}{2V}}$
C_{Y_r}	$\frac{\partial C_Y}{\partial \frac{rb}{2V}}$
$C_{n_{rw}}$	contribution of the wing plus fuselage to C_{n_r}
$C_{Y_{u_g}}$	$\frac{\partial C_{Y_g}}{\partial \hat{u}_g}$
$C_{Y_{\alpha_g}}$	$\frac{\partial C_{Y_g}}{\partial \alpha_g}$
C_{Y_β}	$\frac{\partial C_Y}{\partial \beta}$
$C_{Y_{\beta_g}}$	$\frac{\partial C_{Y_g}}{\partial \beta_g}$
$C_{Y_{\dot{\beta}}}$	$\frac{\partial C_Y}{\partial \dot{\beta}^b \underline{V}}$
$C_{Y_{\dot{\beta}_g}}$	$\frac{\partial C_{Y_g}}{\partial \dot{\beta}_g^b \underline{V}}$
$C_{Y_{\delta_a}}$	$\frac{\partial C_Y}{\partial \delta_a}$
$C_{Y_{\delta_r}}$	$\frac{\partial C_Y}{\partial \delta_r}$
C_Z	$\frac{Z}{\frac{1}{2}\rho V^2 S}$ aerodynamic force coefficient along the aircraft's Z -axis

C_{Z_g}	C_Z due to turbulence
C_{Z_h}	contribution of the horizontal tailplane to C_Z
C_{Z_q}	$\frac{\partial C_Z}{\partial \frac{q^c}{V}}$
C_{Z_u}	$\frac{1}{\frac{1}{2}\rho VS} \frac{\partial Z}{\partial u}$
$C_{Z_{u_g}}$	$\frac{\partial C_Z}{\partial \hat{u}_g}$
$C_{Z_{\dot{u}_g}}$	$\frac{\partial C_Z}{\partial \frac{\dot{u}_g^c}{V}}$
C_{Z_w}	contribution of the wing plus fuselage to C_Z
C_{Z_0}	C_Z in the steady flight condition
C_{Z_α}	$\frac{\partial C_Z}{\partial \alpha}$
$C_{Z_{\alpha_g}}$	$\frac{\partial C_{Z_g}}{\partial \alpha_g}$
$C_{Z_{\dot{\alpha}}}$	$\frac{\partial C_Z}{\partial \frac{\dot{\alpha}^c}{V}}$
$C_{Z_{\dot{\alpha}_g}}$	$\frac{\partial C_{Z_g}}{\partial \frac{\dot{\alpha}_g^c}{V}}$
C_{Z_δ}	$\frac{\partial C_Z}{\partial \delta}$
D	$\frac{d}{dt}$ differential operator
D_b	$\frac{b}{V} \frac{d}{dt}$ non-dimensional differential operator, asymmetric motions
D_c	$\frac{\bar{c}}{V} \frac{d}{dt}$ non-dimensional differential operator, symmetric motions
$E\{ \}$	expectation operator
$F\{ \}$	Fourier operator
$F_{\bar{x}}(x)$	probability distribution function
$F_{\bar{x}\bar{y}}(x, y)$	two-dimensional probability distribution function

$f_{\bar{x}}(x)$	probability density function
$f_{\bar{x}\bar{y}}(x, y)$	two-dimensional probability density function
g	acceleration due to gravity
$H(\omega)$	transfer function
$h(t)$	impulse response function
Im	imaginary part of a complex variable or function
$I_{\hat{u}_g}(\Omega L_g, B)$	power spectral density function of \hat{u}_g (asymmetric aircraft motions)
$I_{\alpha_g}(\Omega L_g, B)$	power spectral density function of α_g (asymmetric aircraft motions)
I_X	moment of inertia about the aircraft's X -axis
I_Y	moment of inertia about the aircraft's Y -axis
I_Z	moment of inertia about the aircraft's Z -axis
I_{XZ}	product of inertia
j	$\sqrt{-1}$
K_X	non-dimensional radius of gyration, $\mu_b K_X^2 = \frac{I_X}{\rho S b^3}$
K_Y	non-dimensional radius of gyration, $\mu_c K_Y^2 = \frac{I_Y}{\rho S c^3}$
K_Z	non-dimensional radius of gyration, $\mu_b K_Z^2 = \frac{I_Z}{\rho S b^3}$
K_{XZ}	non-dimensional radius of gyration, $\mu_b K_{XZ} = \frac{I_{XZ}}{\rho S b^3}$
$K_{xy}(\tau)$	normalized covariance function of x and y
K_θ	gain factor of automatic pilot
K_q	gain factor of automatic pilot

k_b	reduced frequency $\frac{\omega b}{V}$
k_c	reduced frequency $\frac{\omega c}{V}$
L	aerodynamic moment about the aircraft's X -axis
L_g	scale of turbulence
l	wavelength of elementary flowfield
l_h	horizontal taillength
l_v	vertical taillength
l_{α_g}	
l_β	
l_{β_g}	
l_p	stability-, gust- and input derivatives in abbreviated notation, see Chapter 8
l_r	
l_{u_g}	
l_{δ_a}	
l_{δ_r}	
M	aerodynamic moment about the aircraft's Y -axis
m	moment
m	$\frac{W}{g}$ aircraft mass
m_q	
m_u	
m_{u_g}	

$m_{\dot{u}_g}$

m_α stability-, gust- and input derivatives in abbreviated notation, see Chapter 7

 m_{α_g} $m_{\dot{\alpha}_g}$ m_δ m_θ

N aerodynamic moment about the aircraft's Z -axis

n number/order of equations

n $\frac{a_z}{g}$ normal acceleration factor at the aircraft's centre of gravity

 n_{α_g} n_β n_{β_g}

n_p stability-, gust- and input derivatives in abbreviated notation, see Chapter 8

 n_r n_{u_g} n_{δ_a} n_{δ_r}

p rolling velocity about the aircraft's X -axis

$Prob$ Probability

q pitching velocity about the aircraft's Y -axis

r	yawing velocity about the aircraft's Z -axis
Re	real part of a complex variable or function
$R_{xy}(\tau)$	correlation function of x and y
S	wing area
$S_{xy}(\omega)$	power spectral density function of x and y
s_b	$\frac{Vt}{b}$ non-dimensional parameter indicating time (asymmetric aircraft motions)
$s_{\bar{c}}$	$\frac{Vt}{\bar{c}}$ non-dimensional parameter indicating time (symmetric aircraft motions)
t	time
T	sampling time interval, period
Δt	$t_k - t_{k-1}$ discretization time interval
u	component of \underline{V} along the aircraft's X -axis
u_g	component of \underline{V}_g along the aircraft's X_e -axis
\hat{u}_g	$\frac{u_g}{V}$
\hat{u}_{g_h}	value of \hat{u}_g at the aerodynamic centre of the horizontal tailplane
\hat{u}_{g_w}	value of \hat{u}_g at the aerodynamic centre of the wing plus fuselage
\hat{u}_{g_x}	value of \hat{u}_g at a point with abscissa x
$\underline{u}(t)$	input vector
V	velocity of the aircraft's centre of gravity relative to the earth
V_a	velocity of the aircraft's centre of gravity relative to the surrounding air
V_{a_h}	value of V_a at the aerodynamic centre of the horizontal tailplane

V_{a_w}	value of V_a at the aerodynamic centre of the wing plus fuselage
V_g	gust velocity: difference between $V_{w_{tot}}$ and V_w
V_w	mean velocity of the air relative to the earth
$V_{w_{tot}}$	total velocity of the air relative to the earth
v	component of \underline{V} along the Y -axis
v_g	component of \underline{V}_g along the Y_e -axis
W	aircraft weight
W	white noise intensity matrix
W_k	$\frac{W}{\Delta t}$ discretized white noise covariance matrix
$\bar{w}(t)$	white noise input vector
w	component of \underline{V} along the Z -axis
w_g	component of \underline{V}_g along the Z_e -axis
X	aerodynamic force along the aircraft's X -axis
x	abscissa of the aircraft's centre of gravity in an earth-fixed frame of reference
x	abscissa of a point of the aircraft in an aircraft-fixed frame of reference
Δx	distance between two points in the turbulent atmosphere, along the aircraft's flight path
x_h	abscissa of the aerodynamic centre of the horizontal tail in an aircraft-fixed frame of reference
$\underline{x}(t)$	state vector
x_q	
x_u	

x_{u_g} $x_{\dot{u}_g}$

x_α stability-, gust- and input derivatives in abbreviated notation, see Chapter 7

 x_{α_g} $x_{\dot{\alpha}_g}$ x_δ x_θ

Y aerodynamic force along the aircraft's Y -axis

y y -coordinate of a point of the aircraft in an aircraft-fixed frame of reference

 y_{α_g} y_β y_{β_g}

y_p stability-, gust- and input derivatives in abbreviated notation, see Chapter 8

 y_r y_{u_g} y_{δ_a} y_{δ_r} y_φ

$\underline{y}(t)$ output vector

Z aerodynamic force along the aircraft's Z -axis

z	z coordinate of a point of the aircraft in an aircraft-fixed frame of reference
Z_h	contribution of the horizontal tail to the aerodynamic force Z
Z_w	contribution of the wing plus fuselage to the aerodynamic force Z
z_q	
z_u	
z_{u_g}	
$z_{\dot{u}_g}$	
z_α	stability-, gust- and input derivatives in abbreviated notation, see Chapter 7
z_{α_g}	
$z_{\dot{\alpha}_g}$	
z_δ	
z_θ	

Greek Symbols

α	$\frac{w}{V}$ angle of attack
α_g	$\frac{w_g}{V}$ gust angle of attack
α_g^*	auxiliary variable in turbulence shaping filter state equation
β	$\frac{v}{V}$ gust sideslip angle
γ	flight path angle
$\delta(t)$	Dirac function
δ_a	aileron deflection
δ_e	elevator deflection
δ_r	rudder deflection
ϵ	downwash angle
θ	angle of pitch
μ	central moment
μ_b	$\frac{m}{\rho S b}$ relative aircraft mass (asymmetric aircraft motions)
μ_c	$\frac{m}{\rho S c}$ relative aircraft mass (symmetric aircraft motions)
μ_x	mean value of x
ψ	angle of yaw
ρ	air density
ξ	damping ratio
σ	sidewash angle
σ_x^2	variance of x

$\Phi(t, t_0)$	transition matrix
φ	aircraft roll angle
Ψ	discretized input distribution matrix
τ	time constant
τ	time variable in covariance function
Ω	spatial circular frequency
ω	circular frequency
ζ	damping ratio

Superscripts

T	transpose of matrix
-1	inverse of matrix
$-$	stochastic variable (scalar, vector or function)

Subscripts

a	quantities relative to surrounding airmass
$c.g.$	centre of gravity
g	gust, turbulence
h	parameters for the horizontal tailplane
k	discrete (time)
v	vertical tailplane
w	wing plus fuselage

Vectors are underlined, stochastic variables are overlined.

Frames of Reference

Two frames of reference are used,

1. The **stability frame of reference**: an aircraft-fixed right-handed frame of reference $OXYZ$. The origin O lies in the aircraft's centre of gravity, the positive X -axis lies in the plane of symmetry OXZ and points forward in the direction of the undisturbed velocity V : in the undisturbed symmetric flight condition, about which the turbulence or other 'inputs' causes small deviations, the X -axis coincides with the vector of the velocity of the centre of gravity relative to the undisturbed atmosphere. The positive Y -axis points to the right, the positive Z -axis points downwards. For disturbed aircraft motions, the stability frame of reference remains fixed to the aircraft.
2. An **earth-fixed**, right handed frame of reference $O_eX_eY_eZ_e$. The origin O_e has a fixed position relative to the earth. In the undisturbed flight condition mentioned above, the X_e -, Y_e - and Z_e -axes coincide with the corresponding axes of the stability frame of reference $OXYZ$.

Chapter 1

Introduction

1.1 Contents

The main subject of these lecture notes is the mathematical description of atmospheric turbulence and the way in which atmospheric turbulence affects the aircraft's motions. Only cases of rigid aircraft with or without active stabilization, perturbed by normally distributed atmospheric turbulence are considered.

The influence of turbulence on the aircraft motions and trajectory is of great importance for several reasons. The aspect of safety for the strength and fatigue of the structure is evident. Also of great interest is the way in which turbulence causes the aircraft to deviate from its desired flight path, especially during take-off, approach and landing. Other important aspects of the aircraft turbulence response concern the aircraft ride qualities and passenger comfort. For developments like gust response alleviation, a proper modelling of turbulence and its effects on the aircraft responses is mandatory.

Prerequisites for the present course are a basic knowledge of statistics, ordinary differential equations, rigid aircraft flight dynamics, complex analysis including Fourier- and Laplace transforms, mathematical systems theory and principles of classic and modern multivariable control theory.

1.2 Structure

These lecture notes consist of two parts. The first part, Chapters 2 through 5, can be considered an introduction to stochastic processes. The second part, Chapters 6 through 9, describe the way in which atmospheric turbulence and its effects on the aircraft motion can be modelled.

Scalar processes are considered in Chapters 2 through 4. Chapter 2 recapitulates basic statistical notions like probability and probability density, covariance and correlation. Chapter 3 is on spectral analysis in continuous time and derives some important results which may be used in practical calculations. As most stochastic processes are sampled in discrete time, a separate chapter is devoted to discrete-time stochastic processes, including a concise treatment of the Fast Fourier Transform (FFT), Chapter 4. Continuous-time and discrete-time multivariable stochastic processes are the subject of Chapter 5.

Many of the techniques discussed in these first chapters prove to be very useful in describing the aircraft atmospheric flight dynamics. Note that whereas the third-year course “Flight Dynamics” discussed the aircraft dynamic response to deterministic input signals like the aileron, elevator and rudder (Mulder et al., 2013), in this course the aircraft dynamic response to stochastic input signals is studied. Together, these courses yield a complete description of the aircraft flight dynamics, essential for both the design of automated flight control systems and flight guidance systems for pilot manual control.

Atmospheric turbulence as a physical process of the Earth atmosphere is introduced in Chapter 6, which also gives the Dryden- and von Kármán turbulence spectra and their filter equations needed for simulation in time and space. Chapters 7 and 8 introduce the mathematical models of the mechanics of turbulence effects on the aerodynamic forces and moments. The so-called gust derivatives enable the calculation of the statistical properties of the trajectory, the linear- and angular accelerations, the loads etc., once the turbulence spectra and the aircraft dynamics are known. Chapter 9 describes the aircraft response to turbulence in a fundamentally different manner, using Etkin’s four-point model (Etkin, 1972). It will be shown that both methods, however, yield approximately the same results.

Most chapters end with a number of examples, many of which have been calculated using Matlab. Complete listings of the `m` sources are included and are also made available via Brightspace. Students are invited to check the examples, to work out similar cases or to adapt the scripts according to their own needs and include them in their own files.

Chapter 2

Scalar Stochastic Processes

2.1 An introduction to stochastic processes

The dynamics of a system can be studied by examining the system output when a certain input signal is applied. Input signals often used for this purpose, are the impulse function, the step function or sine functions, see Figure 2.1. These functions have as a common feature that their value at any given instant in time is known and can be predicted exactly. We will classify these functions as deterministic.

Another class of input signals can be considered whose values cannot be predicted exactly and show some uncertainty. The irregular movements of turbulent air in the atmosphere are an example of such an input signal for an aircraft. Such a non-deterministic function is called a stochastic function of time, see for example Figure 2.2.

The function given in Figure 2.2 is, however, just one of the many possible that can originate from the same physical process, for example atmospheric turbulence. The set of all possible functions is called a stochastic process. The function plotted in Figure 2.2 is a possible realization of the stochastic process. All realizations together are referred to as the ensemble, see Figure 2.3. Although stochastic functions are more or less unpredictable in their nature, there appear to be differences between stochastic processes, for example in average value, average amplitude or average fluctuation speed of the functions. Figure 2.4 shows some examples.

Another important property in which stochastic processes can differ is the stationarity of the process. A stochastic process is called “strict sense stationary” (in this reader, stationary, for short) if the statistical functions describing the process (like its probability density) do not vary in time. A process is called “wide sense stationary” when its mean and auto covariance are time-invariant and its second moment (all discussed below) is finite for all times. A strict sense stationary process is also wide-sense stationary, but not

the other way around. In the following, the stochastic processes considered are all assumed stationary, although it is not easy in practice to state whether a stochastic process is really stationary, or not.

The phenomena that form the basis for a stochastic process are often not known in sufficient detail to allow an exact prediction of the stochastic functions. Therefore, stochastic processes are described in terms as used in the theory of statistics and probability. What follows is a brief review of some fundamental elements of probability theory.

2.2 The probability distribution function

As a starting point in the study of stochastic processes the stochastic variable is introduced. This is a variable whose value depends on random circumstances. Some values of such a variable are more likely than others. This fact is expressed quantitatively by the probability distribution function $F_{\bar{x}}$ of the stochastic variable \bar{x} :

$$F_{\bar{x}}(x) = \Pr\{\bar{x} \leq x\} \quad (2.1)$$

or in words: the distribution function for the stochastic variable \bar{x} , as a function of a deterministic quantity x , describes the probability that the stochastic variable \bar{x} takes on values smaller than or equal to a certain value x .

The notion of ‘probability’ can be illustrated as follows: in Figure 2.5 a part of the ensemble of the stochastic variable $\bar{x}(t)$ is shown. Let n be the number of realizations of the process under consideration and i the number of realizations where at $t = t_1$ holds $\bar{x} \leq x$, then:

$$F_{\bar{x}}(x) = \lim_{n \rightarrow \infty} \frac{i}{n}$$

Because the stochastic process is assumed to be stationary, $F_{\bar{x}}(x)$ does not depend on the choice of t_1 .

The probability of an event occurring must lie between 0 (impossibility) and 1 (certainty), it can never become negative. Hence, the probability distribution function $F_{\bar{x}}$ must be a monotonously increasing function of x :

$$F_{\bar{x}}(a) \leq F_{\bar{x}}(b) \quad \text{if} \quad a \leq b$$

It then follows that:

$$F_{\bar{x}}(-\infty) = 0$$

$$F_{\bar{x}}(+\infty) = 1$$

2.3 The probability density function

The derivative with regard to x of the distribution function is called the probability density function and is defined as:

$$\begin{aligned} f_{\bar{x}}(x) = \frac{dF_{\bar{x}}(x)}{dx} &= \lim_{\Delta x \rightarrow 0} \frac{\Pr\{\bar{x} \leq x + \Delta x\} - \Pr\{\bar{x} \leq x\}}{\Delta x} \\ &= \lim_{\Delta x \rightarrow 0} \frac{\Pr\{x < \bar{x} \leq x + \Delta x\}}{\Delta x} \end{aligned} \quad (2.2)$$

Because the probability distribution function monotonously increases, its derivative, the probability density function (p.d.f. for short) is always larger than or equal to zero:

$$f_{\bar{x}}(x) \geq 0$$

We obtain:

$$\begin{aligned} \int_{-\infty}^{+\infty} f_{\bar{x}}(x) dx &= F_{\bar{x}}(+\infty) - F_{\bar{x}}(-\infty) = 1 - 0 = 1 \\ \int_{-\infty}^a f_{\bar{x}}(x) dx &= F_{\bar{x}}(a) - F_{\bar{x}}(-\infty) = F_{\bar{x}}(a) \\ \int_a^b f_{\bar{x}}(x) dx &= F_{\bar{x}}(b) - F_{\bar{x}}(a) = \Pr\{a < \bar{x} \leq b\} \end{aligned} \quad (2.3)$$

2.4 Moments of the probability density function

Often it will be difficult to determine the functions $f_{\bar{x}}(x)$ and $F_{\bar{x}}(x)$ of a stochastic process explicitly. Instead we may concentrate on alternative quantities which are somehow related to the probability functions $f_{\bar{x}}(x)$ and $F_{\bar{x}}(x)$. Such alternative quantities are for instance the most likely or expected values of \bar{x} , of \bar{x}^2 , of \bar{x}^3 etc. The expected value is denoted in the following by the expectation operator $E\{\cdot\}$. The expected value of \bar{x} , $E\{\bar{x}\}$, is defined as the average of the values of \bar{x} over the whole ensemble of the stochastic process, see Figure 2.6.

We now introduce the i -th moment m_i of the probability density function as:

$$m_i = E\{\bar{x}^i\} = \int_{-\infty}^{+\infty} x^i f_{\bar{x}}(x) dx \quad (2.4)$$

where i is the order of the moment. The first order moment:

$$m_1 = E\{\bar{x}\} = \int_{-\infty}^{+\infty} x f_{\bar{x}}(x) dx$$

is known as the mean or average $\mu_{\bar{x}}$ of the random variable \bar{x} . Intuitively, a comparison with the center of gravity location of a mechanical system can be made.

The second order moment:

$$m_2 = E\{\bar{x}^2\} = \int_{-\infty}^{+\infty} x^2 f_{\bar{x}}(x) dx$$

can then be compared with the moment of inertia of a mechanical system about a certain axis of a frame of reference.

Closely related to the moments of the probability density function are the central moments of $f_{\bar{x}}(x)$. These are the moments of $f_{\bar{x}}(x)$ relative to the average $\mu_{\bar{x}}$.

The i -th order central moment is defined as:

$$m'_i = E\{(\bar{x} - \mu_{\bar{x}})^i\} = \int_{-\infty}^{+\infty} (x - \mu_{\bar{x}})^i f_{\bar{x}}(x) dx \quad (2.5)$$

For the first order central moment m'_1 holds:

$$\begin{aligned} m'_1 &= E\{(\bar{x} - \mu_{\bar{x}})\} = \int_{-\infty}^{+\infty} (x - \mu_{\bar{x}}) f_{\bar{x}}(x) dx \\ &= \int_{-\infty}^{+\infty} x f_{\bar{x}}(x) dx - \mu_{\bar{x}} \cdot \int_{-\infty}^{+\infty} f_{\bar{x}}(x) dx \\ &= \mu_{\bar{x}} - \mu_{\bar{x}} = 0 \end{aligned}$$

The second order central moment:

$$m'_2 = E\{(\bar{x} - \mu_{\bar{x}})^2\} = \int_{-\infty}^{+\infty} (x - \mu_{\bar{x}})^2 f_{\bar{x}}(x) dx$$

will now be called the variance $\sigma_{\bar{x}}^2$ of the stochastic process. Its square root is known as the standard deviation $\sigma_{\bar{x}}$ (Korn & Korn, 1968; Burington & May Jr., 1970). Table 2.1 summarizes the first three moments and central moments.

2.5 The uniform and normal distributions

2.5.1 The uniform distribution

A simple and often very useful probability density function is the uniform distribution, where all possible outcomes of the stochastic variable \bar{x} have the same probability:

$$f_{\bar{x}}(x) = \begin{cases} \frac{1}{b-a} & : a \leq x \leq b \\ 0 & : \text{elsewhere} \end{cases} \quad (2.6)$$

with $[a, b]$ the range of possible outcomes, so $\bar{x} \sim \mathcal{U}(a, b)$. see Figure 2.7. An example of a (discrete) uniform distribution is ‘throwing a dice’ (possible outcomes 1, 2, 3, 4, 5 and 6) where with a “pure dice” all outcomes have probability 1/6.

The first moment of this uniformly distributed random variable is found to be:

$$m_1 = E\{\bar{x}\} = \frac{1}{2}(a+b)$$

And for the second order central moment:

$$m'_2 = E\{(\bar{x} - \mu_{\bar{x}})^2\} = \sigma_{\bar{x}}^2 = \frac{1}{12}(b-a)^2$$

2.5.2 The normal (or Gaussian) distribution

The most common probability density function of stochastic variables is the Gaussian or ‘normal’ probability density function:

$$f_{\bar{x}}(x) = \frac{1}{\sigma\sqrt{2\pi}} e^{-\frac{(x-\mu)^2}{2\sigma^2}} \quad (2.7)$$

Figure 2.8 shows the Gaussian probability density- and distribution functions. For a Gaussian probability density function the first moment is found to be (see (Billingsley, 1986; Mathai & Pederzoli, 1977)):

$$m_1 = E\{\bar{x}\} = \mu_{\bar{x}} = \mu$$

and for the second order central moment:

$$m'_2 = E\{(\bar{x} - \mu_{\bar{x}})^2\} = \sigma_{\bar{x}}^2 = \sigma^2$$

So the parameters μ and σ , that together fully characterize the probability density function, correspond with the average and standard deviation of the stochastic process.

If $m_1 = 0$ the higher order moments are given by:

$$\begin{aligned} m_{2k+1} &= 0 \\ m_{2k} &= 1 \cdot 3 \cdot 5 \cdots (2k-1)\sigma^{2k} \end{aligned}$$

(for $k = 1, 2, 3, \dots$) which means that if the first and second moment of a normal distribution are known, all higher moments can be calculated, or, the first and second moment completely characterize the normal p.d.f. It is often important to realize that for a zero-average stochastic process with a normal distribution, the following values hold:

$$\begin{aligned} F_{\bar{x}}(+\sigma) - F_{\bar{x}}(-\sigma) &= 0.6827 \\ F_{\bar{x}}(+2\sigma) - F_{\bar{x}}(-2\sigma) &= 0.9545 \\ F_{\bar{x}}(+3\sigma) - F_{\bar{x}}(-3\sigma) &= 0.9973 \end{aligned}$$

According to the Central Limit Theorem (CLT, see Section 2.13, and (Billingsley, 1986; Fabian & Hannan, 1985; Papoulis, 1991; Patel & Read, 1982)) the probability density function of a stochastic process the outcome of which originates from a large number of random circumstances tends towards the Gaussian distribution. This is why this density function is labelled ‘normal’ and this also explains why it is so important in the study of physical ‘real-life’ stochastic phenomena.

In the following it is assumed that, unless stated otherwise, all stochastic variables have a normal distribution. In the special case of atmospheric turbulence this is a reasonable assumption when the normal distribution is only used for values of the stochastic variable not much larger than 2σ or 3σ . For the calculation of the required strength of the aircraft structure, however, the extreme values of vertical gusts are of importance. The probability of these extremes occurring, cannot simply be determined using a normal distribution because it is questionable whether the ‘tails’ of the normal distribution give an accurate description of atmospheric turbulence. It should therefore be used with caution.

2.6 The joint probability distribution- and density functions

The concepts of probability distribution functions and probability density functions will now be extended to two (or more) stochastic variables.

The two-dimensional joint probability distribution function $F_{\bar{x}\bar{y}}(x, y)$ of the stochastic variables \bar{x} and \bar{y} is defined as the probability of $\bar{x} \leq x$ while simultaneously $\bar{y} \leq y$. Formally this can be written as:

$$F_{\bar{x}\bar{y}}(x, y) = \Pr\{\bar{x} \leq x \wedge \bar{y} \leq y\} \quad (2.8)$$

From this definition the following characteristics of the joint probability distribution function can easily be derived:

$$\begin{aligned} F_{\bar{x}\bar{y}}(-\infty, -\infty) &= 0 \\ F_{\bar{x}\bar{y}}(+\infty, +\infty) &= 1 \\ F_{\bar{x}\bar{y}}(x, +\infty) &= F_{\bar{x}}(x) \\ F_{\bar{x}\bar{y}}(+\infty, y) &= F_{\bar{y}}(y) \end{aligned} \quad (2.9)$$

The first of the above equation is called the *impossibility* characteristic of $F_{\bar{x}\bar{y}}(x, y)$, while the second equation is called the *certainty* characteristic of $F_{\bar{x}\bar{y}}(x, y)$. Assuming that $F_{\bar{x}\bar{y}}(x, y)$ is twice differentiable (which is the case for a normal distribution), the joint probability density function $f_{\bar{x}\bar{y}}(x, y)$ is defined as:

$$\begin{aligned} f_{\bar{x}\bar{y}}(x, y) &= \frac{\partial^2 F_{\bar{x}\bar{y}}(x, y)}{\partial x \partial y} \\ &= \lim_{\Delta x \rightarrow 0} \lim_{\Delta y \rightarrow 0} \frac{\Pr\{x < \bar{x} \leq x + \Delta x \wedge y < \bar{y} \leq y + \Delta y\}}{\Delta x \Delta y} \end{aligned} \quad (2.10)$$

The joint probability density function $f_{\bar{x}\bar{y}}(x, y)$ may be represented as a three-dimensional surface, see Figure 2.9, for which the volume contained underneath the surface equals 1. The elementary volume shown represents the probability that $x \leq \bar{x} \leq x + \Delta x$ and $y \leq \bar{y} \leq y + \Delta y$.

From the definition of the joint probability density function the following characteristics can be deduced:

$$\begin{aligned} f_{\bar{x}\bar{y}}(x, y) &\geq 0 \\ \int_{-\infty}^{y_1} \int_{-\infty}^{x_1} f_{\bar{x}\bar{y}}(x, y) dx dy &= F_{\bar{x}\bar{y}}(x_1, y_1) \\ \int_{-\infty}^{+\infty} f_{\bar{x}\bar{y}}(x, y) dy &= f_{\bar{x}}(x) \\ \int_{-\infty}^{+\infty} f_{\bar{x}\bar{y}}(x, y) dx &= f_{\bar{y}}(y) \end{aligned} \quad (2.11)$$

2.7 The conditional probability density function

In Section 2.6 we showed how the one-dimensional probability density function $f_{\bar{x}}(x)$ can be obtained from the corresponding two-dimensional probability density function $f_{\bar{x}\bar{y}}(x, y)$. Suppose now, that instead of allowing the stochastic variable \bar{y} to have any value, we restrict our attention only to those cases for which \bar{y} equals some value y_1 . The conditional probability density function $f_{\bar{x}}(x | y_1)$ is then defined as, see Figure 2.10:

$$f_{\bar{x}}(x | y_1) = \frac{f_{\bar{x}\bar{y}}(x, y_1)}{f_{\bar{y}}(y_1)} \quad (2.12)$$

2.8 Moments of the joint probability density function

Also for two-dimensional probability density functions the moments and central moments of the probability density function are defined. The joint moment m_{ij} is defined as:

$$m_{ij} = E\{\bar{x}^i \bar{y}^j\} = \int_{y=-\infty}^{+\infty} \int_{x=-\infty}^{+\infty} x^i y^j f_{\bar{x}\bar{y}}(x, y) dx dy \quad (2.13)$$

The sum $n = i + j$ will be denoted as the order of the joint moment.

The first order joint moments m_{10} and m_{01} are the averages $\mu_{\bar{x}}$ and $\mu_{\bar{y}}$:

$$\begin{aligned} m_{10} &= \int_{y=-\infty}^{+\infty} \int_{x=-\infty}^{+\infty} x f_{\bar{x}\bar{y}}(x, y) dx dy = \int_{x=-\infty}^{+\infty} x \left[\int_{y=-\infty}^{+\infty} f_{\bar{x}\bar{y}}(x, y) dy \right] dx \\ &= \int_{x=-\infty}^{+\infty} x f_{\bar{x}}(x) dx = \mu_{\bar{x}} \\ m_{01} &= \mu_{\bar{y}} \end{aligned}$$

The second order joint moment m_{11} is known as the average product $R_{\bar{x}\bar{y}}$:

$$R_{\bar{x}\bar{y}} = E\{\bar{x}\bar{y}\} = \int_{-\infty}^{+\infty} \int_{-\infty}^{+\infty} xy f_{\bar{x}\bar{y}}(x, y) dx dy$$

Once again we may ‘correct’ for the average values $\mu_{\bar{x}}$ and $\mu_{\bar{y}}$ and introduce the joint central moment m'_{ij} :

$$m'_{ij} = E\{(\bar{x} - \mu_{\bar{x}})^i (\bar{y} - \mu_{\bar{y}})^j\} = \int_{-\infty}^{+\infty} \int_{-\infty}^{+\infty} (x - \mu_{\bar{x}})^i (y - \mu_{\bar{y}})^j f_{\bar{x}\bar{y}}(x, y) dx dy \quad (2.14)$$

The second order joint central moment m'_{11} is referred to as the covariance $C_{\bar{x}\bar{y}}$:

$$C_{\bar{x}\bar{y}} = E\{(\bar{x} - \mu_{\bar{x}})(\bar{y} - \mu_{\bar{y}})\} = \int_{-\infty}^{+\infty} \int_{-\infty}^{+\infty} (x - \mu_{\bar{x}})(y - \mu_{\bar{y}}) f_{\bar{x}\bar{y}}(x, y) dx dy \quad (2.15)$$

The notion of covariance can be interpreted as a joint variance. When $\bar{y} = \bar{x}$, it is a proper variance:

$$C_{\bar{x}\bar{y}}|_{\bar{y}=\bar{x}} = C_{\bar{x}\bar{x}} = E\{(\bar{x} - \mu_{\bar{x}})^2\} = \sigma_{\bar{x}}^2$$

The other two second order joint central moments m'_{20} and m'_{02} turn out to equal the variances $\sigma_{\bar{x}}^2$ and $\sigma_{\bar{y}}^2$:

$$m'_{20} = \int_{y=-\infty}^{+\infty} \int_{x=-\infty}^{+\infty} (\bar{x} - \mu_{\bar{x}})^2 f_{\bar{x}\bar{y}}(x, y) dx dy$$

$$\begin{aligned}
&= \int_{x=-\infty}^{+\infty} (x - \mu_{\bar{x}})^2 \left[\int_{y=-\infty}^{+\infty} f_{\bar{x}\bar{y}}(x, y) dy \right] dx \\
&= \int_{x=-\infty}^{+\infty} (x - \mu_{\bar{x}})^2 f_{\bar{x}}(x) dx = \sigma_{\bar{x}}^2 \\
m'_{02} &= \sigma_{\bar{y}}^2
\end{aligned}$$

The relation between the average product $R_{\bar{x}\bar{y}}$ and the covariance $C_{\bar{x}\bar{y}}$ is found to be:

$$\begin{aligned}
C_{\bar{x}\bar{y}} &= m'_{11} = E\{(\bar{x} - \mu_{\bar{x}})(\bar{y} - \mu_{\bar{y}})\} \\
&= E\{\bar{x}\bar{y}\} - \mu_{\bar{y}}E\{\bar{x}\} - \mu_{\bar{x}}E\{\bar{y}\} + \mu_{\bar{x}}\mu_{\bar{y}} \\
&= R_{\bar{x}\bar{y}} - \mu_{\bar{x}}\mu_{\bar{y}}
\end{aligned} \tag{2.16}$$

We can normalize the covariance by dividing by the product of the standard deviations of the stochastic variables involved. This is how the correlation $K_{\bar{x}\bar{y}}$ is defined:

$$K_{\bar{x}\bar{y}} = \frac{C_{\bar{x}\bar{y}}}{\sigma_{\bar{x}}\sigma_{\bar{y}}} = E\left\{\frac{\bar{x} - \mu_{\bar{x}}}{\sigma_{\bar{x}}} \cdot \frac{\bar{y} - \mu_{\bar{y}}}{\sigma_{\bar{y}}}\right\} \tag{2.17}$$

The stochastic variables \bar{x} and \bar{y} are said to be uncorrelated if $K_{\bar{x}\bar{y}} = 0$ and fully correlated if $|K_{\bar{x}\bar{y}}| = 1$.

In Table 2.2 the first two joint moments, joint central moments and their physical meaning are summarized.

2.9 Uncorrelated, orthogonal and independent stochastic variables

In the previous sections some important variables describing the statistics of stochastic processes were introduced. In this section we will take a more detailed look into characteristics describing the coherence relationship between stochastic variables.

Two stochastic variables are called uncorrelated if:

$$E\{\bar{x}\bar{y}\} = E\{\bar{x}\} \cdot E\{\bar{y}\} \tag{2.18}$$

Two stochastic variables are called orthogonal if:

$$E\{\bar{x}\bar{y}\} = 0 \tag{2.19}$$

Two stochastic variables are called independent if:

$$f_{\bar{x}\bar{y}}(x, y) = f_{\bar{x}}(x) \cdot f_{\bar{y}}(y) \quad (2.20)$$

Based on these formal definitions the following facts are stated:

$$\begin{aligned} \text{Uncorrelated: } & \left\{ \begin{array}{lcl} E\{\bar{x}\bar{y}\} & = & E\{\bar{x}\} E\{\bar{y}\} \\ C_{\bar{x}\bar{y}} & = & 0 \\ \sigma_{\bar{x}+\bar{y}}^2 & = & \sigma_{\bar{x}}^2 + \sigma_{\bar{y}}^2 \\ \bar{x} - \mu_{\bar{x}} & \text{and} & \bar{y} - \mu_{\bar{y}} \text{ are orthogonal} \end{array} \right. \\ \text{Independent: } & \left\{ \begin{array}{lcl} \bar{x} & \text{and} & \bar{y} \text{ are uncorrelated} \\ f_{\bar{x}\bar{y}}(x, y) & = & f_{\bar{x}}(x) \cdot f_{\bar{y}}(y) \end{array} \right. \end{aligned}$$

Based on these characteristics it becomes clear that independence implies uncorrelation but uncorrelation does not imply independence. Uncorrelation forms a weaker condition than independence.

2.10 The product-, covariance- and correlation functions

In Section 2.1 it was mentioned that a stochastic process is the set of all stochastic functions that can originate from some physical process. A realization $\bar{x}(t)$ is a function of time, sometimes called a signal, see for example Figure 2.2. It is possible to assign a distribution function and a density function to a stochastic process. These functions are in general also a function of time:

$$F_{\bar{x}}(x; t) = \Pr\{\bar{x}(t) \leq x\} \quad (2.21)$$

$$f_{\bar{x}}(x; t) = \frac{\partial F_{\bar{x}}(x; t)}{\partial x} = \lim_{\Delta x \rightarrow 0} \frac{\Pr\{x < \bar{x}(t) \leq x + \Delta x\}}{\Delta x} \quad (2.22)$$

We are now interested in the joint distribution of two stochastic processes $\bar{x}(t)$ and $\bar{y}(t)$. In general this is a function of four variables, namely x, y, t_1 and t_2 :

$$F_{\bar{x}\bar{y}}(x, y; t_1, t_2) = \Pr\{\bar{x}(t_1) \leq x \wedge \bar{y}(t_2) \leq y\}$$

It is assumed that the processes under consideration are stationary. This means that not the absolute values of t_1 and t_2 are important, but only the difference $t_2 - t_1$. Writing $\tau = t_2 - t_1$ we can reformulate the joint distribution- and density functions as:

$$F_{\bar{x}\bar{y}}(x, y; \tau) = \Pr\{\bar{x}(t) \leq x \wedge \bar{y}(t + \tau) \leq y\} \quad (2.23)$$

$$f_{\bar{x}\bar{y}}(x, y; \tau) = \frac{\partial^2 F_{\bar{x}\bar{y}}(x, y; \tau)}{\partial x \partial y} \quad (2.24)$$

So the joint distribution of two stationary stochastic processes that are shifted an interval τ in time depends only on the magnitude of τ and not of the instant in time t at which the joint distribution is considered.

Now the probability distribution- and -density functions of stochastic processes are defined, we can use the notation of moments of the joint probability density function of two stochastic processes. These moments (and central moments) are in general a function of τ , and are therefore called moment functions. The moment function $m_{ij}(\tau)$ is defined as:

$$m_{ij}(\tau) = E\{\bar{x}(t)^i \bar{y}(t + \tau)^j\} = \int_{-\infty}^{+\infty} \int_{-\infty}^{+\infty} x^i y^j f_{\bar{x}\bar{y}}(x, y; \tau) dx dy \quad (2.25)$$

and the central moment function $m'_{ij}(\tau)$ as:

$$\begin{aligned} m'_{ij}(\tau) &= E\{(\bar{x}(t) - \mu_{\bar{x}})^i (\bar{y}(t + \tau) - \mu_{\bar{y}})^j\} \\ &= \int_{-\infty}^{+\infty} \int_{-\infty}^{+\infty} (x - \mu_{\bar{x}})^i (y - \mu_{\bar{y}})^j f_{\bar{x}\bar{y}}(x, y; \tau) dx dy \end{aligned} \quad (2.26)$$

The timeshift τ is important in expressions with $\bar{x}(t)$ and $\bar{y}(t + \tau)$, but also in expressions with $\bar{x}(t)$ and $\bar{x}(t + \tau)$. Similar to the definitions stated in Section 2.8 we can define the average product function, the covariance function and the correlation function. If these functions relate to two stochastic processes they are called cross product function $R_{\bar{x}\bar{y}}(\tau)$, cross covariance function $C_{\bar{x}\bar{y}}(\tau)$ and cross correlation function $K_{\bar{x}\bar{y}}(\tau)$, if they relate to one stochastic process with a timeshift, they are called auto product function $R_{\bar{x}\bar{x}}(\tau)$, auto covariance function $C_{\bar{x}\bar{x}}(\tau)$ and auto correlation function $K_{\bar{x}\bar{x}}(\tau)$:

$$\begin{aligned} R_{\bar{x}\bar{y}}(\tau) &= E\{\bar{x}(t)\bar{y}(t + \tau)\} \\ &= \int_{-\infty}^{+\infty} \int_{-\infty}^{+\infty} xy f_{\bar{x}\bar{y}}(x, y; \tau) dx dy \end{aligned} \quad (2.27)$$

$$\begin{aligned} C_{\bar{x}\bar{y}}(\tau) &= E\{(\bar{x}(t) - \mu_{\bar{x}})(\bar{y}(t + \tau) - \mu_{\bar{y}})\} \\ &= \int_{-\infty}^{+\infty} \int_{-\infty}^{+\infty} (x - \mu_{\bar{x}})(y - \mu_{\bar{y}}) f_{\bar{x}\bar{y}}(x, y; \tau) dx dy \end{aligned} \quad (2.28)$$

$$\begin{aligned} K_{\bar{x}\bar{y}}(\tau) &= \frac{C_{\bar{x}\bar{y}}(\tau)}{\sigma_{\bar{x}} \sigma_{\bar{y}}} = E\left\{\frac{\bar{x}(t) - \mu_{\bar{x}}}{\sigma_{\bar{x}}} \cdot \frac{\bar{y}(t + \tau) - \mu_{\bar{y}}}{\sigma_{\bar{y}}}\right\} \\ &= \int_{-\infty}^{+\infty} \int_{-\infty}^{+\infty} \frac{x - \mu_{\bar{x}}}{\sigma_{\bar{x}}} \frac{y - \mu_{\bar{y}}}{\sigma_{\bar{y}}} f_{\bar{x}\bar{y}}(x, y; \tau) dx dy \end{aligned} \quad (2.29)$$

Similar definitions hold for the auto functions $R_{\bar{x}\bar{x}}(\tau)$, $C_{\bar{x}\bar{x}}(\tau)$ and $K_{\bar{x}\bar{x}}(\tau)$ by substituting $\bar{y}(t + \tau) = \bar{x}(t + \tau)$.

The auto product- and auto covariance functions are a measure of the coherence between the values of the stochastic process $\bar{x}(t)$ at time t and at time $t + \tau$. From $R_{\bar{x}\bar{x}}(\tau)$ and $C_{\bar{x}\bar{x}}(\tau)$ we may learn whether that stochastic process exhibits ‘fast’ or ‘slow’ fluctuations in time. Figure 2.11 shows an example, computed using just one realisation of the processes, which means that this computation is a realisation itself, i.e., it is an *estimate*.

The cross covariance function $C_{\bar{x}\bar{y}}(\tau)$ gives us some idea of the coherence between the values of a stochastic process \bar{x} at time t and another stochastic process \bar{y} at time $t + \tau$. Figure 2.12 shows an example of the cross covariance function, again computed using just one realisation of the processes.

The importance of either increasing the observation time in estimating the product, covariance, and correlation functions from data, or averaging over many (hundreds, thousands, ...) of realizations is illustrated in Figure 2.13. Here, the estimates of the auto covariance and cross covariance functions of the same processes \bar{x} and \bar{y} as above are shown, but now based on averaging the obtained functions over 500 realizations. Clearly, we approximate the ‘true’ functions when we average or, equivalently, have a longer observation time. The symmetry properties are much more clear now. Note that when a longer observation time is not possible, for instance because the process we are studying ‘dies out’ in time, only averaging over many responses is possible. This is known as ‘Monte Carlo simulation’.

Some important characteristics of these functions are summarized in Table 2.3. Note that in this table we assume that the stochastic variables have no periodical components. Clearly, all auto-functions are **even** functions.¹ The cross-functions are neither even, nor odd, but have a symmetry relative to which signal is moved in what direction relative to the other, e.g., $R_{\bar{x}\bar{y}}(\tau) = R_{\bar{y}\bar{x}}(-\tau)$.

2.11 Ergodic processes

All expressions derived so far, are of theoretical value only since they require either ensemble averages (that is, infinite observation times...) or the probability density or distribution functions. In any practical situation we often have just one realization available for analysis; the probability density function is seldom known. To make the step to more practical applications we introduce the concept of an ergodic process.

A stochastic process is called ergodic if its ensemble average can be replaced by its time

¹An **even** function is symmetric with respect to the zero value of its ‘running variable’, here τ , so w.r.t. $\tau=0$, i.e., $x(-\tau) = x(\tau)$. An **odd** function is anti-symmetric with respect to $\tau=0$, i.e. $x(-\tau) = -x(\tau)$. It can be shown that all functions $x(\tau)$ can be described as the sum of an even and odd function, using: $x_e(\tau) = \frac{1}{2}(\tau(t) + \tau(-t))$ and $x_o(\tau) = \frac{1}{2}(\tau(t) - \tau(-t))$, where $x_e(\tau)$ is even, $x_o(\tau)$ is odd, and $x_e(\tau) + x_o(\tau) = x(\tau)$.

average. Moulded in a more formal mathematical definition we have:

$$\mathbb{E}\{g[\bar{x}(t)]\} = \lim_{T \rightarrow \infty} \frac{1}{2T} \int_{-T}^{+T} g[\bar{x}(t)] dt \quad (2.30)$$

The expression can also be interpreted as: when the observation time increases, the time average will approximate the ensemble average. In Eq. (2.30), $g[\cdot]$ denotes any function of the stochastic variable \bar{x} . Figure 2.14 illustrates the difference between ensemble averaging and time averaging (Newland, 1984).

Notice that if a process is ergodic it must also be stationary, because an average along a single realization will (in theory) extend from $t = -\infty$ to $t = +\infty$ and will therefore be independent of time. If the time and ensemble averages are the same, the ensemble averages must therefore be independent of absolute time, and so the process must be stationary.

Once we assume the stochastic process to be ergodic we may use the practical fact that a single realization is completely representative for the ensemble. Example 2.4 illustrates the effects of observation time, and the difference between e.g. a theoretical average (the ensemble), and the average you obtain with one or more realisations. In addition, Table 2.4 illustrates how statistical properties can be calculated in a more practical way.

Remember that in a true practical application the time interval is usually limited and in case of digital data recording, the integral will be replaced by a summation. We will return to the effects of sampling and finite time intervals in Chapter 4.

2.12 White noise

2.12.1 Definition used in the lecture notes

The most chaotic stochastic process that exists is called ‘white noise’. For the sake of simplicity, the process is assumed to have zero mean. A sample function of *approximated* white noise is generated using the MATLAB random-generator, see Figure 2.15(a). The white noise which we define and use in the lecture notes physically cannot exist, as its values range between $-\infty$ and $+\infty$, its energy is infinite, hence it is a theoretical concept.

When regarding this process $\bar{w}(t)$ at time t and time $t+\tau$, as the function values are totally random, the only value for τ where there exists any coherence between the function values is $\tau = 0$. As a result, the covariance function of white noise has the form of a Dirac pulse:²

$$C_{\bar{w}\bar{w}}(\tau) = W \delta(\tau) \quad (2.31)$$

²The Dirac delta function (aka the unit impulse function) is a *generalized function*. It is not defined in

The parameter W is called the intensity of the white noise. The Dirac pulse $\delta(\tau)$ is defined zero for all values of τ except for $\tau = 0$ where $\delta(\tau)$ is infinite. It has the integral property:

$$\int_{-\infty}^{+\infty} \delta(t) dt = 1$$

The Dirac pulse is graphically represented by an arrow, see Figure 2.15(b). The value the Dirac pulse ‘carries’ is either represented through the size of the arrow, or by a number located next to the arrow and all arrows have the same size; this latter form is recommended.

Substitution of $\tau = 0$ in $C_{\bar{w}\bar{w}}(\tau)$ yields:

$$C_{\bar{w}\bar{w}}(0) = \sigma_{\bar{w}}^2 = \infty,$$

implying an infinite variance. Also, the correlation function $K_{\bar{w}\bar{w}}(\tau)$ is not defined for this type of white noise. It is clear that this stochastic process can not exist physically, like the Dirac pulse, but we will see that this abstraction is extremely useful in the mathematical treatment of systems and signals. In practice, a stochastic variable \bar{x} is called ‘white’ if:

$$C_{\bar{x}\bar{x}}(\tau) \approx 0 \quad \text{for } |\tau| > \epsilon \tag{2.32}$$

The auto covariance function of ‘practical’ white noise looks like Figure 2.15(c) where the auto covariance function of the approximated white noise of Figure 2.15(a) is plotted. The auto correlation function is illustrated in Figure 2.15(d).

2.12.2 Other definitions

Note that many other forms of white noise exist. For instance, consider the string of zeros and ones (the 0/1 bits) used in digital telecommunication. At the receiver’s end, except for trivial cases, these 0/1 bits will be completely independent of each other: knowing the bit value at this moment (and the past bits) gives us no opportunity at all to predict what the next bit will be. Hence, this binary sequence is perfectly ‘white’ as well, but has a limited power and, with that, variance.

2.13 Central limit theorem

The central limit theorem (CLT) states that the probability density function of a stochastic process, the outcome of which originates from a large number of random circumstances

terms of its values, but rather how it acts inside an integral when multiplied by a smooth function $f(t)$:

$$\int_{-\infty}^{+\infty} f(t)\delta(t - \tau) dt = f(\tau)$$

This is known as the ‘sifting property’.

tends towards the Gaussian distribution (Billingsley, 1986; Fabian & Hannan, 1985; Papoulis, 1991; Patel & Read, 1982)).

Why is this? The origin of the CLT can be explained as follows. Assume a stationary stochastic process which generates random variable \bar{x} , with a uniform probability density function $f_{\bar{x}}(x)$, illustrated in Figure 2.16(a). Suppose that we would take one sample of this process, and call it x_1 , and then take another sample of this process x_2 . Define $\bar{y} = x_1 + x_2$. What would be the probability density function of \bar{y} ?

The answer comes from probability theory, and states that $f_{\bar{y}}(y)$ can be computed by taking the *convolution* of $f_{\bar{x}}(x)$ and $f_{\bar{x}}(x)$ (Papoulis, 1991):

$$f_{\bar{y}}(y) = f_{\bar{x}}(x) \star f_{\bar{x}}(x) = \int_{-\infty}^{+\infty} f_{\bar{x}}(y-x) f_{\bar{x}}(x) dx$$

The convolution of a uniform distribution with another uniform distribution yields the triangular distribution drawn in Figure 2.16(b). This distribution does not ‘look like’ a normal distribution quite yet, but this changes when we would add a third sample of the process \bar{x} to \bar{y} : $\bar{y} = x_1 + x_2 + x_3$. Using the same steps as above, we get that $f_{\bar{y}}(y)$ becomes the convolution of the triangular probability density function with the uniform probability density function, and the resulting p.d.f would already resemble that of a normal distribution much closer.

Concluding, when summing-up the outcomes of a large number of (independent) stochastic processes, each with their own individual probability density functions, the probability distribution of the random variable that results from this summation equals the convolution of the individual p.d.f.’s, which in real life ‘converges’ to a normal distribution.

2.14 Examples

2.14.1 Example 2.1

Show that for the cross correlation function holds: $|K_{\bar{x}\bar{y}}(\tau)| \leq 1$ and give a physical interpretation.

The cross correlation is a measure of the coherence of two stochastic variables \bar{x} and \bar{y} . To see that $-1 \leq K_{\bar{x}\bar{y}} \leq 1$, observe the two extreme cases of maximum coherence: $\bar{y}_1 = \bar{x}$ and $\bar{y}_2 = -\bar{x}$:

$$\begin{aligned} K_{\bar{x}\bar{y}_1} &= E\left\{\frac{(\bar{x} - \mu_{\bar{x}})^2}{\sigma_{\bar{x}}^2}\right\} = \frac{\sigma_{\bar{x}}^2}{\sigma_{\bar{x}}^2} = 1 \\ K_{\bar{x}\bar{y}_2} &= E\left\{\frac{-(\bar{x} - \mu_{\bar{x}})^2}{\sigma_{\bar{x}}^2}\right\} = \frac{-\sigma_{\bar{x}}^2}{\sigma_{\bar{x}}^2} = -1 \end{aligned}$$

Taking $\bar{x} = \bar{x}(t)$ and $\bar{y} = \bar{y}(t + \tau)$ we can see that also for the correlation function holds: $-1 \leq K_{\bar{x}\bar{y}}(\tau) \leq 1$.

2.14.2 Example 2.2

Given a stationary ergodic stochastic process \bar{x} , each of whose sample functions is a sine wave of amplitude, period and mean value 1, or, a realization $\bar{x}(t)$ is given by:

$$\bar{x}(t) = \sin(2\pi t + \phi) + 1 \quad (2.33)$$

Calculate the auto product-, auto covariance- and auto correlation function.

The time history of a realization (here $\phi = 0$) is given in Figure 2.17(a). Since \bar{x} is an ergodic process, we may calculate $R_{\bar{x}\bar{x}}(\tau)$, $C_{\bar{x}\bar{x}}(\tau)$ and $K_{\bar{x}\bar{x}}(\tau)$ by computing the time average of a realization $\bar{x}(t)$ instead of taking the ensemble average of \bar{x} . As we have an analytical description of a realization (which in practice is seldom the case!) we can write, using Equation (2.33) and the results in Table 2.4:

$$\begin{aligned} R_{\bar{x}\bar{x}}(\tau) &= E\{\bar{x}(t)\bar{x}(t + \tau)\} \\ &= \lim_{T \rightarrow \infty} \frac{1}{2T} \int_{-T}^{+T} (\sin(2\pi t) + 1) \cdot (\sin(2\pi(t + \tau)) + 1) dt \end{aligned}$$

Using goniometric transformation formulae and integral tables (Dwight, 1957) we find:

$$\begin{aligned} R_{\bar{x}\bar{x}}(\tau) &= 1 + \cos(2\pi\tau) \cdot \lim_{T \rightarrow \infty} \frac{1}{T} \int_0^{+T} \sin^2(2\pi t) dt \\ &= 1 + \frac{1}{2} \cos(2\pi\tau) \end{aligned}$$

Using the relation between the auto product- and auto covariance function:

$$C_{\bar{x}\bar{x}}(\tau) = R_{\bar{x}\bar{x}}(\tau) - \mu_{\bar{x}}^2 \leftrightarrow R_{\bar{x}\bar{x}}(\tau) = \mu_{\bar{x}}^2 + C_{\bar{x}\bar{x}}(\tau)$$

we find:

$$C_{\bar{x}\bar{x}}(\tau) = \frac{1}{2} \cos(2\pi\tau)$$

The variance $\sigma_{\bar{x}}^2 = E\{(\bar{x}(t) - \mu_{\bar{x}})^2\} = C_{\bar{x}\bar{x}}(0) = \frac{1}{2}$, and the auto correlation function is given by:

$$K_{\bar{x}\bar{x}}(\tau) = \frac{C_{\bar{x}\bar{x}}(\tau)}{\sigma_{\bar{x}}^2} = \cos(2\pi\tau)$$

The three functions are plotted in Figure 2.17(b)-2.17(d).

We see that the correlation function has its maximum value for $\tau = 0, \pm 1, \pm 2, \dots$. This is because the functions:

$$\begin{aligned}\bar{x}_1(t) &= \sin(2\pi t) + 1 \quad \text{and} \\ \bar{x}_2(t) &= \sin(2\pi(t + \tau)) + 1\end{aligned}$$

are fully in phase and thus have maximum correlation for these values of τ . For $\tau = \pm\frac{1}{2}, \pm 1\frac{1}{2}, \pm 2\frac{1}{2}, \dots$, however, these two functions have an opposite phase and the auto correlation function $K_{\bar{x}\bar{x}}(\tau) = -1$. The following MATLAB .m-file plots the time history, auto product-, auto covariance- and auto correlation function of a stochastic process of which a description of a time history is available.

Inputting $\bar{x}(t) = \sin(2\pi t) + 1$ for a total time interval of 10 seconds, a sample time of 0.01 seconds and no noise, produces Figure 2.17. Inputting $\bar{x}(t) = 0$, a time interval of 10 seconds, sample time of 0.01 seconds and noise, yields Figure 2.15(a), Figure 2.15(c) and Figure 2.15(d).

Listing 2.1: Example 2.2

```
% Exempl22    Calculates the signal, the auto product function, the
%               auto-covariance function and the auto correlation function
%               of an arbitrary signal.
%
% Chapter 2 of the lecture notes ae4-304.
%
% Program revised August 1992, February 2004 [MM], October 2014 [M
% Rodriguez]

clc; close all; clear all;

disp(' Example 2.2 ');
disp(' ');
disp(' Calculates signal, auto product-, -covariance- and ');
disp(' -correlation function of a stochastic signal x(t). ');
disp(' ');
disp(' This program can produce Figures 2.14 and 2.16 of the ');
disp(' lecture notes ae4-304. ');

%
% create time axis
T      = input(' Enter total time interval T : ');
dt     = input(' Enter sampling time interval dt : ');

t = [-T/2:dt:T/2];
N = length(t);

%
% create signal
x      = input(' Enter function definition x(t) = : ');
int   = input(' Enter noise intensity : ');

x = x + sqrt(int)*randn(1,N);
```

```

fprintf('\n\n');
fprintf('    Signal mean      = %f\n',mean(x));
fprintf('    Signal variance = %f\n',cov(x));
fprintf('    Signal std.dev. = %f\n',sqrt(cov(x)) );

% compute variables of interest
r=xcorr(x,'unbiased');          % auto product function
c=xcov (x,'unbiased');         % auto covariance function
k=c/(std(x)^2);                % auto correlation function

% plot results
figure
subplot(2,1,1);
plot(t+T/2,x);
xlabel('time'); ylabel('x (t)'); title('signal');

subplot(2,1,2);
plot(t,r((T/2)/dt:3*(T/2)/dt));
xlabel('tau'); ylabel('Rxx (tau)'); title('auto product function');

figure
subplot(2,1,1)
plot(t,c((T/2)/dt:3*(T/2)/dt));
xlabel('tau'); ylabel('Cxx (tau)'); title('auto covariance function');

subplot(2,1,2)
plot(t,k((T/2)/dt:3*(T/2)/dt));
xlabel('tau'); ylabel('Kxx (tau)'); title('auto correlation function');

% EOF

```

2.14.3 Example 2.3

Section 2.5 introduced the Gaussian or ‘normal’ probability density function of a stochastic variable. Using the concept of the joint probability density function $f_{\bar{x}\bar{y}}(x, y)$ of two random variables, we introduce the two-dimensional normal probability density function:

$$f_{\bar{x}\bar{y}}(x, y) = \frac{1}{2\pi\sigma_{\bar{x}}\sigma_{\bar{y}}\sqrt{1 - K_{\bar{x}\bar{y}}^2}} e^{-\frac{G}{2}} \quad (2.34)$$

with:

$$G = \frac{1}{1 - K_{\bar{x}\bar{y}}^2} \left(\frac{(x - \mu_{\bar{x}})^2}{\sigma_{\bar{x}}^2} - \frac{2K_{\bar{x}\bar{y}}(x - \mu_{\bar{x}})(y - \mu_{\bar{y}})}{\sigma_{\bar{x}}\sigma_{\bar{y}}} + \frac{(y - \mu_{\bar{y}})^2}{\sigma_{\bar{y}}^2} \right) \quad (2.35)$$

where $K_{\bar{x}\bar{y}}$ is the correlation coefficient between \bar{x} and \bar{y} as given by Equation (2.17).

If \bar{x} and \bar{y} are uncorrelated, their correlation coefficient is zero. Substituting $K_{\bar{x}\bar{y}} = 0$ in Equation (2.35) yields:

$$f_{\bar{x}\bar{y}}(x, y)|_{K_{\bar{x}\bar{y}}=0} = \frac{1}{2\pi\sigma_{\bar{x}}\sigma_{\bar{y}}} e^{-\frac{1}{2} \left(\frac{(x - \mu_{\bar{x}})^2}{\sigma_{\bar{x}}^2} + \frac{(y - \mu_{\bar{y}})^2}{\sigma_{\bar{y}}^2} \right)} = f_{\bar{x}}(x) \cdot f_{\bar{y}}(y)$$

Or: when two stochastic variables have a joint Gaussian distribution and if they are uncorrelated, they are also independent.

To get a graphical impression of the influence of $K_{\bar{x}\bar{y}}$ in the joint normal density function, see Figure 2.18, produced with MATLAB for $\mu_{\bar{x}} = \mu_{\bar{y}} = K_{\bar{x}\bar{y}} = 0$ and $\sigma_{\bar{x}} = \sigma_{\bar{y}} = 1$:

Listing 2.2: Example 2.3

```
% Exampl23      Calculate and plot the 2-dimensional Normal (Gaussian)
%
% Chapter 2 of the lecture notes ae4-304.
%
% Program revised August 1992, February 2004 [MM], October 2014 [M
% Rodriguez]

clc; close all; clear all;

disp(' Example 2.3');
disp(' ')
disp(' Calculate and plot the 2-dimensional Normal (Gaussian)');
disp(' probability density function.');
disp(' ');
disp(' This program can produce Figures 2-17, 2-18 and 2-19 of');
disp(' the lecture notes ae4-304.');

x = -3:0.1:3; y = x;

% Definition of distribution parameters
mx = input(' Average value of stochastic variable x : ');
sx = input(' Standard deviation of x : ');
my = input(' Average value of stochastic variable y : ');
sy = input(' Standard deviation of y : ');
Kxy = input(' Correlation coefficient between x and y, 0<Kxy<1 : ');

if abs(Kxy) > 0.99 | abs(Kxy) < 0
    return
    disp(' Correlation coefficient should be between 0 and 1')
end

fmax=1/(2*pi*sx*sy*sqrt(1-Kxy ^ 2));
for i=1:length(x)
    for j=1:length(y)
        G=((x(i)-mx)^2/sx^2-2*Kxy*(x(i)-mx)*(y(j)-my)/...
            (sx*sy)+(y(j)-my)^2/sy^2);
    end
end
```

```

G=G/(1-Kxy^2);
fxy(j,i)=fmax*exp(-G/2);
end
end

figure(1)
mesh(x,y,fxy);
title('The 2-dimensional Normal p.d.f.')
figure(2)
contour(x,y,fxy);
title('The 2-dimensional Normal p.d.f. viewed from above')

% EOF

```

Cutting the surface in Figure 2.18 with the plane $f_{\bar{x}\bar{y}}(x, y) = c$ with:

$$0 < c < f_{max} = \frac{1}{2\pi\sigma_{\bar{x}}\sigma_{\bar{y}}\sqrt{1 - K_{\bar{x}\bar{y}}^2}} \quad (2.36)$$

yields (substitute in Eq. (2.34)):

$$\begin{aligned} c &= f_{max} e^{-\frac{G}{2}} \\ q &= \frac{G}{2} \quad \text{with } q = -\ln\left(\frac{c}{f_{max}}\right) \quad (0 < c < f_{max} \rightarrow q > 0) \\ \frac{(x - \mu_{\bar{x}})^2}{\sigma_{\bar{x}}^2} - \frac{2K_{\bar{x}\bar{y}}(x - \mu_{\bar{x}})(y - \mu_{\bar{y}})}{\sigma_{\bar{x}}\sigma_{\bar{y}}} + \frac{(y - \mu_{\bar{y}})^2}{\sigma_{\bar{y}}^2} &= 2q(1 - K_{\bar{x}\bar{y}}^2) \end{aligned}$$

This is the equation of an equi-probability ellipse ($f_{\bar{x}\bar{y}}(x, y)$ is constant on this ellipse) with origin $(\mu_{\bar{x}}, \mu_{\bar{y}})$ and (because here $\sigma_{\bar{x}} = \sigma_{\bar{y}} = 1$) the central axes under an angle of 45° with the X - and Y -axes. To examine the influence of the correlation coefficient $K_{\bar{x}\bar{y}}$, several cross-sections of the density function taken at a height of $c = 0.1f_{max}$ (see Equation (2.36)) have been plotted in Figure 2.19.

From Figure 2.19 it can be concluded that when $K_{\bar{x}\bar{y}} = 0$ it is always possible to transform the ellipse to a circle by regarding the normalized distribution $\left(\frac{(x - \mu_{\bar{x}})}{\sigma_{\bar{x}}}, \frac{(y - \mu_{\bar{y}})}{\sigma_{\bar{y}}}\right)$ instead of (x, y) (effectively, this is a scaling of the axes), while for $K_{\bar{x}\bar{y}} \neq 0$ this transformation still yields an ellipse. Figure 2.19 shows that the value for $K_{\bar{x}\bar{y}}$ is a measure of the skewedness of the ellipse. For $K_{\bar{x}\bar{y}} = 1$ the ellipse becomes a straight line: the stochastic variables \bar{x} and \bar{y} are fully correlated and an increase in x determines the increase in y .

2.14.4 Example 2.4

When using programs like Matlab to simulate a stochastic process, it is important to realize that in almost all cases one works in discrete time (i.e., with samples) and that, since the number of samples is limited, you are by definition working with a limited observation time.

This example shows some results of running a script that computes the average and standard deviation of an array of normally-distributed random numbers which represent samples from a random process \bar{x} (average $\mu_{\bar{x}} = 0$; standard deviation $\sigma_{\bar{x}} = 1$).

Figure 2.21 shows the results of 30 repetitions of obtaining these random numbers, for three observation times per repetition: 1, 10 and 100 seconds. The sampling frequency is 100 Hz, so a 1 second observation time means we have generated 100 random numbers. For each trial i , we compute the average of this array of random numbers. After running the 30 trials we can then compute the average of the averages, and the standard deviation of that average. Mathematically speaking, for each trial i we obtain an *estimate* $\hat{\mu}_{\bar{x}_i}$ of the average, which is typically non-zero even when simulating a zero-mean process. See for instance the first estimate in the top plot, which equals ≈ -0.14 . When repeating this process 30 times we can estimate the average of the 30 averages obtained, $\hat{\mu}_{\hat{\mu}_{\bar{x}}}$ and the standard deviation of the 30 averages obtained, $\hat{\sigma}_{\hat{\mu}_{\bar{x}}}$. All are estimates!

Consider the top plot in Figure 2.21. The dots show the 30 estimated averages, for each trial i , the horizontal line shows the estimated average of these 30 averages, the dotted lines show the \pm one standard-deviation lines ($\mu + \sigma, \mu - \sigma$). Every time one runs Matlab, one obtains different numbers, different estimates for the averages, etc. Our simulation *is* a random process.³

The top plot in Figure 2.21 shows that none of the estimated averages (over 100 numbers each) is exactly zero, and also the estimated average of the average (which would equal the average of one observation that is 30 seconds..., so $30 \times 100 = 3000$ numbers) is close to, but also not exactly equal to zero. Also, the standard deviation is not zero.

The center and bottom plots show the results of the same script but now with an observation time of, respectively, 10 and 100 seconds. Clearly, when the length of the observation increases, the estimates of the averages, and also the estimated average (and standard deviation) of these averages, become smaller and smaller, and converge to the ‘true’ value of 0: $|\hat{\mu}_{100}| < |\hat{\mu}_{10}| < |\hat{\mu}_1|$. The same holds when one would look at the standard deviation – the *estimated* standard deviation to be more exact – which would approximate the true value of 1 better and better for longer observation times.

To make a long story short, in our simulations we are always using *estimates* of the true stochastic properties (here, average and standard deviation, but the same holds for covariance functions, like in Figure 2.11 and Figure 2.12) of the random process we are simulating. Only when the observation time becomes very long, and providing that the

³When you run a script like this in Matlab, close Matlab, open Matlab, and run the script again you would obtain the same numbers. This is because the Matlab random number generator uses the same ‘seed’. To prevent this to happen, initialize the random number generator in the script with a different seed every time you run it, e.g., make the seed equal to the time in milliseconds of your computer clock.

estimator applied is unbiased, i.e., it does not have a systematic deviation even when observation time (or, equivalently, the number of samples) goes to infinity, these estimates will converge to the true variables of that process: $\hat{\mu}_{\bar{x}} \rightarrow \mu_{\bar{x}}$, $\hat{\sigma}_{\bar{x}} \rightarrow \sigma_{\bar{x}}$

2.14.5 Example 2.5

One of the main applications of probability theory in these lecture notes lies in the characterisation of signals and systems. Consider the signal $x(t)$ illustrated in Figure 2.22(a), a periodical signal (period 4 seconds) which is fully deterministic. What if we would be able to take just one sample of this signal, at an arbitrary time t' , then clearly that sample is a random variable (let's call it \bar{x}). Using the description of the signal $x(t)$ we can derive the probability distribution function, density function, and all other statistical properties of that random variable \bar{x} .

What is crucial to understand is that when we would look at the signal from a probabilistic perspective, we have to consider the range of possible values that \bar{x} may have (so perspective 'AA' in Figure 2.22(a)) and then see 'how often' these values occur.

In this simple example it is clear that \bar{x} is never smaller than 1 and never larger than 6. In fact, for 25% of the time (1 second of the period of 4) the signal equals exactly 1 and for 25% of the time (again, 1 second of the 4) the signal equals 6. For all other times (so the remaining 2 seconds of the period) the signal value changes linearly, from 1 to 6, so the remaining 50% of the time the signal is *equally* distributed between 1 and 6. Hence, between 1 and 6 $f_{\bar{x}}(x)$ has a constant value; integrating $f_{\bar{x}}(x)$ from 1 to 6 (range is 5) would account for a probability of 0.5 (50% of the time, remember?), hence the constant value equals $0.5/5=0.1$.

The probability density function $f_{\bar{x}}(x)$ can be derived just from these simple observations, resulting in Figure 2.22(b). Similarly, $F_{\bar{x}}(x)$ can be obtained just by reasoning (or through integrating $f_{\bar{x}}(x)$), and with $f_{\bar{x}}(x)$ known all other variables like the average $\mu_{\bar{x}}$ and variance $\sigma_{\bar{x}}^2$ can be computed:

$$\begin{aligned}\mu_{\bar{x}} &= \int_{-\infty}^{\infty} x f_{\bar{x}}(x) dx = 0.25 \cdot 1 + 0.1 \cdot \frac{1}{2}(6^2 - 1^2) + 0.25 \cdot 6 = 7/2 \\ \sigma_{\bar{x}}^2 &= \int_{-\infty}^{\infty} (x - \mu_{\bar{x}})^2 f_{\bar{x}}(x) dx \\ &= \int_{-\infty}^{\infty} x^2 f_{\bar{x}}(x) dx - \mu_{\bar{x}} \mu_{\bar{x}} \\ &= (0.25 \cdot 1^2 + 0.1 \cdot \frac{1}{3}(6^3 - 1^3) + 0.25 \cdot 6^2) - (7/2)^2\end{aligned}$$

$$= 25/6$$

The standard deviation $\sigma_{\bar{x}}$ is $\frac{5}{6}\sqrt{6}$ which is ≈ 2 , reasonable when considering Figure 2.22(a). The reader should check how to compute these integrals with Dirac functions inside.

Now, what is the chance that \bar{x} equals 1? What is the chance that \bar{x} equals 3?

2.15 Problems

Problem 2.1

Compute the average and variance of a random variable with probability density function:

$$f_{\bar{x}}(x) = \begin{cases} 4x(9 - x^2)/81 & : 0 \leq x \leq 3 \\ 0 & : \text{else} \end{cases}$$

Problem 2.2

Show that the expectation operator $E\{\cdot\}$ is a linear operator, or, implying $E\{a\bar{x} + b\bar{y}\} = aE\{\bar{x}\} + bE\{\bar{y}\}$.

Problem 2.3

What does the auto covariance function of an ergodic process with a realization $\bar{x}(t) = \sin(2\pi t) + 1$, corrupted with white noise look like?

Problem 2.4

A stochastic process is composed of an ensemble of sample functions, each of which is a sine wave with amplitude a and frequency ω . The frequency is the same for all samples, but the amplitude varies randomly from sample to sample. Each sample also has a different phase angle ψ .

The process can be described as:

$$\bar{x}(t) = \bar{a} \sin(\omega t - \bar{\psi})$$

A typical realization $x_i(t)$ therefore looks like:

$$x_i(t) = a_i \sin(\omega t - \psi_i)$$

where a_i and ψ_i are constant for the sample.

If the joint probability density function for a and ψ is given by:

$$f_{\bar{a}\bar{\psi}}(a, \psi) = \begin{cases} \frac{1}{2\pi a_0} \left(1 + \left(2\frac{a}{a_0} - 1 \right) \cos \psi \right) & : 0 \leq \psi \leq 2\pi, 0 \leq a \leq a_0 \\ 0 & : \text{else} \end{cases}$$

determine the ensemble averages $E\{\bar{x}^2\}$ and $E\{\bar{x}^2 | \psi_0\}$ where the latter denotes $E\{\bar{x}^2\}$ for those samples where $\psi = \psi_0$ (or: $\psi_0 < \psi < \psi_0 + d\psi_0$). Is $\bar{x}(t)$ a stationary stochastic process? Is it ergodic?

Problem 2.5

Using the transform:

$$\begin{aligned} x &= u \cos(45^\circ) - v \sin(45^\circ), \\ y &= u \sin(45^\circ) + v \cos(45^\circ), \end{aligned}$$

find the equation of the equi-probability circle of the cross-section of a joint normalized Gaussian density function ($\mu_{\bar{x}} = \mu_{\bar{y}} = 0$, $\sigma_{\bar{x}} = \sigma_{\bar{y}} = 1$) with $K_{\bar{x}\bar{y}} = 0$.

Problem 2.6

Prove the entries in Table 2.1, Table 2.2 and Table 2.3.

Problem 2.7

Derive the probability distribution function and the probability density function of the random variable \bar{x} which results from taking one random sample of the following four deterministic and periodical (period T_0) signals, illustrated in Figure 2.23:

Signal 1: square block wave

$$x(t) = \begin{cases} A & : 0 < t < \frac{T_0}{2} \\ -A & : \text{else} \end{cases}$$

with amplitude A .

Signal 2: piecewise linear wave

$$x(t) = \begin{cases} \frac{8A}{9} \frac{5}{T_0} t & : 0 < t < \frac{T_0}{5} \\ \frac{8A}{9} + \frac{A}{9} \frac{5}{4T_0} (t - \frac{T_0}{5}) & : \text{else} \end{cases}$$

with amplitude A .

Signal 3: exponential decay

$$x(t) = Ae^{-t/\tau}$$

with amplitude A and time constant τ in seconds; we define constant $a = Ae^{-T_0/\tau}$.

Signal 4: rectified sine wave

$$x(t) = |A \sin(\omega_1 t)|,$$

with amplitude A and frequency ω_1 in rad/s. Note that $T_0 \neq \frac{2\pi}{\omega_1}$!

Problem 2.8

In the board game ‘‘Settlers of Catan’’ participants must throw two dices, yielding two random variables \bar{x}_1 (dice 1) and \bar{x}_2 (dice 2) which have the same probability density function $f_{\bar{x}}(x)$. Draw the probability density function $f_{\bar{x}}(x)$.

In the game, one adds the numbers of the two dices together, yielding a random variable $\bar{y} = \bar{x}_1 + \bar{x}_2$. You can safely assume independence. Use the material discussed in the section dealing with the central limit theorem to derive the probability density function $f_{\bar{y}}(y)$ of \bar{y} . Draw $f_{\bar{y}}(y)$.

Problem 2.9

Consider a random variable \bar{x} with mean $\mu_{\bar{x}}$, standard deviation $\sigma_{\bar{x}}$, etc. We now define another random variable \bar{y} , as:

$$\bar{y} = a\bar{x} + b$$

with real-valued constants a, b . Compute the average and standard deviation of \bar{y} . Compute the auto- and cross-product, -covariance and -correlation functions of \bar{x} and \bar{y} . Repeat your calculations for the case $a = 0$.

Problem 2.10

Compute the average and standard deviation of the random variable \bar{y} the p.d.f. of which is drawn in Figure 2.16(b).

Problem 2.11

Consider the ‘binary’ 0/1 white noise introduced in Section 2.12.2. What is its probability density function? Compute the average and standard deviation of this process.

2.16 Summary

In this chapter we presented the basic theory for scalar stochastic processes. We have introduced the probability distribution function, the probability density function and the moments and central moments. Furthermore, we defined the same probability properties for joint stochastic processes. Finally, we discussed the auto- and cross-product, -covariance and -correlation functions, and defined uncorrelated, orthogonal, independent and ergodic processes.

$m_0 = \int_{-\infty}^{+\infty} f_{\bar{x}}(x) dx$	$= 1$
$m_1 = \int_{-\infty}^{+\infty} x f_{\bar{x}}(x) dx$	$= \mu_{\bar{x}}$ (average)
$m_2 = \int_{-\infty}^{+\infty} x^2 f_{\bar{x}}(x) dx$	$= \sigma_{\bar{x}}^2 + \mu_{\bar{x}}^2$
<hr/>	
$m'_0 = \int_{-\infty}^{+\infty} f_{\bar{x}}(x) dx$	$= 1$
$m'_1 = \int_{-\infty}^{+\infty} (x - \mu_{\bar{x}}) f_{\bar{x}}(x) dx$	$= 0$
$m'_2 = \int_{-\infty}^{+\infty} (x - \mu_{\bar{x}})^2 f_{\bar{x}}(x) dx$	$= \sigma_{\bar{x}}^2$ (variance)

Table 2.1: Definition of the moments and central moments of the probability density function.

m_{00}	$= \int_{-\infty}^{+\infty} \int_{-\infty}^{+\infty} f_{\bar{x}\bar{y}}(x, y) dx dy$	$= 1$
m_{10}	$= \int_{-\infty}^{+\infty} \int_{-\infty}^{+\infty} x f_{\bar{x}\bar{y}}(x, y) dx dy$	$= \mu_{\bar{x}}$
m_{01}	$= \int_{-\infty}^{+\infty} \int_{-\infty}^{+\infty} y f_{\bar{x}\bar{y}}(x, y) dx dy$	$= \mu_{\bar{y}}$
m_{11}	$= \int_{-\infty}^{+\infty} \int_{-\infty}^{+\infty} xy f_{\bar{x}\bar{y}}(x, y) dx dy$	$= R_{\bar{x}\bar{y}} = C_{\bar{x}\bar{y}} + \mu_{\bar{x}}\mu_{\bar{y}}$
m_{20}	$= \int_{-\infty}^{+\infty} \int_{-\infty}^{+\infty} x^2 f_{\bar{x}\bar{y}}(x, y) dx dy$	$= \sigma_{\bar{x}}^2 + \mu_{\bar{x}}^2$
m_{02}	$= \int_{-\infty}^{+\infty} \int_{-\infty}^{+\infty} y^2 f_{\bar{x}\bar{y}}(x, y) dx dy$	$= \sigma_{\bar{y}}^2 + \mu_{\bar{y}}^2$
m'_{00}	$= \int_{-\infty}^{+\infty} \int_{-\infty}^{+\infty} f_{\bar{x}\bar{y}}(x, y) dx dy$	$= 1$
m'_{10}	$= \int_{-\infty}^{+\infty} \int_{-\infty}^{+\infty} (x - \mu_{\bar{x}}) f_{\bar{x}\bar{y}}(x, y) dx dy$	$= 0$
m'_{01}	$= \int_{-\infty}^{+\infty} \int_{-\infty}^{+\infty} (y - \mu_{\bar{y}}) f_{\bar{x}\bar{y}}(x, y) dx dy$	$= 0$
m'_{11}	$= \int_{-\infty}^{+\infty} \int_{-\infty}^{+\infty} (x - \mu_{\bar{x}})(y - \mu_{\bar{y}}) f_{\bar{x}\bar{y}}(x, y) dx dy$	$= C_{\bar{x}\bar{y}}$
m'_{20}	$= \int_{-\infty}^{+\infty} \int_{-\infty}^{+\infty} (x - \mu_{\bar{x}})^2 f_{\bar{x}\bar{y}}(x, y) dx dy$	$= \sigma_{\bar{x}}^2$
m'_{02}	$= \int_{-\infty}^{+\infty} \int_{-\infty}^{+\infty} (y - \mu_{\bar{y}})^2 f_{\bar{x}\bar{y}}(x, y) dx dy$	$= \sigma_{\bar{y}}^2$

Table 2.2: Moments and central moments of the joint probability density function.

Auto functions	Cross functions
$R_{\bar{x}\bar{x}}(\tau) = R_{\bar{x}\bar{x}}(-\tau)$ $C_{\bar{x}\bar{x}}(\tau) = C_{\bar{x}\bar{x}}(-\tau)$ $K_{\bar{x}\bar{x}}(\tau) = K_{\bar{x}\bar{x}}(-\tau)$	$R_{\bar{x}\bar{y}}(\tau) = R_{\bar{y}\bar{x}}(-\tau) \neq R_{\bar{x}\bar{y}}(-\tau)$ $C_{\bar{x}\bar{y}}(\tau) = C_{\bar{y}\bar{x}}(-\tau) \neq C_{\bar{x}\bar{y}}(-\tau)$ $K_{\bar{x}\bar{y}}(\tau) = K_{\bar{y}\bar{x}}(-\tau) \neq K_{\bar{x}\bar{y}}(-\tau)$
$\tau = 0$	
$R_{\bar{x}\bar{x}}(0) = \sigma_{\bar{x}}^2 + \mu_{\bar{x}}^2$ $C_{\bar{x}\bar{x}}(0) = \sigma_{\bar{x}}^2$ $K_{\bar{x}\bar{x}}(0) = 1$	$R_{\bar{x}\bar{y}}(0) = R_{\bar{x}\bar{y}}$ $C_{\bar{x}\bar{y}}(0) = C_{\bar{x}\bar{y}}$ $K_{\bar{x}\bar{y}}(0) = K_{\bar{x}\bar{y}}$
$\tau \rightarrow \infty$	<p>here we assume that the signals have no periodic components!</p>
$\lim_{\tau \rightarrow \infty} R_{\bar{x}\bar{x}}(\tau) = \mu_{\bar{x}}^2$ $\lim_{\tau \rightarrow \infty} C_{\bar{x}\bar{x}}(\tau) = 0$ $\lim_{\tau \rightarrow \infty} K_{\bar{x}\bar{x}}(\tau) = 0$	$\lim_{\tau \rightarrow \infty} R_{\bar{x}\bar{y}}(\tau) = \mu_{\bar{x}}\mu_{\bar{y}}$ $\lim_{\tau \rightarrow \infty} C_{\bar{x}\bar{y}}(\tau) = 0$ $\lim_{\tau \rightarrow \infty} K_{\bar{x}\bar{y}}(\tau) = 0$

Table 2.3: Some characteristics of product-, covariance-, and correlation functions.

STATISTICAL PROPERTY		“THEORETICAL”		“PRACTICAL”	
Name	Symbol	Ensemble Average	Probability Density	Time Average	
Average	$\mu_{\bar{x}}$	$E\{\bar{x}\}$	$\int_{-\infty}^{+\infty} x f_{\bar{x}}(x) \, dx$	$\lim_{T \rightarrow \infty} \frac{1}{2T} \int_{-T}^{+T} x(t) \, dt$	
Variance	$\sigma_{\bar{x}}^2$	$E\{(\bar{x} - \mu_{\bar{x}})^2\}$	$\int_{-\infty}^{+\infty} (x - \mu_{\bar{x}})^2 f_{\bar{x}}(x) \, dx$	$\lim_{T \rightarrow \infty} \frac{1}{2T} \int_{-T}^{+T} x(t)^2 \, dt - \mu_{\bar{x}}^2$	
Auto Product	$R_{\bar{x}\bar{x}}(\tau)$	$E\{\bar{x}(t)\bar{x}(t + \tau)\}$		$\lim_{T \rightarrow \infty} \frac{1}{2T} \int_{-T}^{+T} x(t) x(t + \tau) \, dt$	
Auto Covariance	$C_{\bar{x}\bar{x}}(\tau)$	$E\{(\bar{x}(t) - \mu_{\bar{x}})(\bar{x}(t + \tau) - \mu_{\bar{x}})\}$		$\lim_{T \rightarrow \infty} \frac{1}{2T} \int_{-T}^{+T} x(t) x(t + \tau)' \, dt - \mu_{\bar{x}}^2$	
Cross Product	$R_{\bar{x}\bar{y}}(\tau)$	$E\{\bar{x}(t)\bar{y}(t + \tau)\}$		$\lim_{T \rightarrow \infty} \frac{1}{2T} \int_{-T}^{+T} x(t) y(t + \tau) \, dt$	
Cross Covariance	$C_{\bar{x}\bar{y}}(\tau)$	$E\{(\bar{x}(t) - \mu_{\bar{x}})(\bar{y}(t + \tau) - \mu_{\bar{y}})\}$		$\lim_{T \rightarrow \infty} \frac{1}{2T} \int_{-T}^{+T} x(t) y(t + \tau) \, dt - \mu_{\bar{x}} \mu_{\bar{y}}$	

Table 2.4: “Theoretical” versus “practical” calculation of the 6 most important statistical properties.

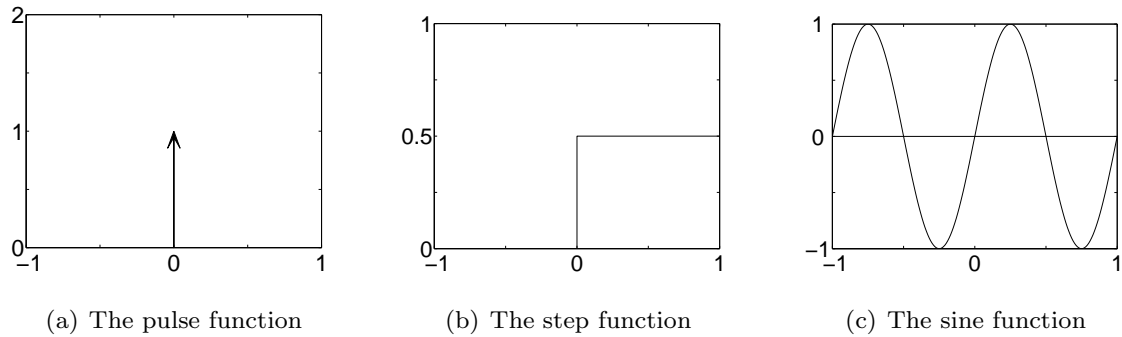


Figure 2.1: Some common deterministic input signals used for system analysis. Note that the horizontal axes show time in seconds.



Figure 2.2: An example of a stochastic input signal.

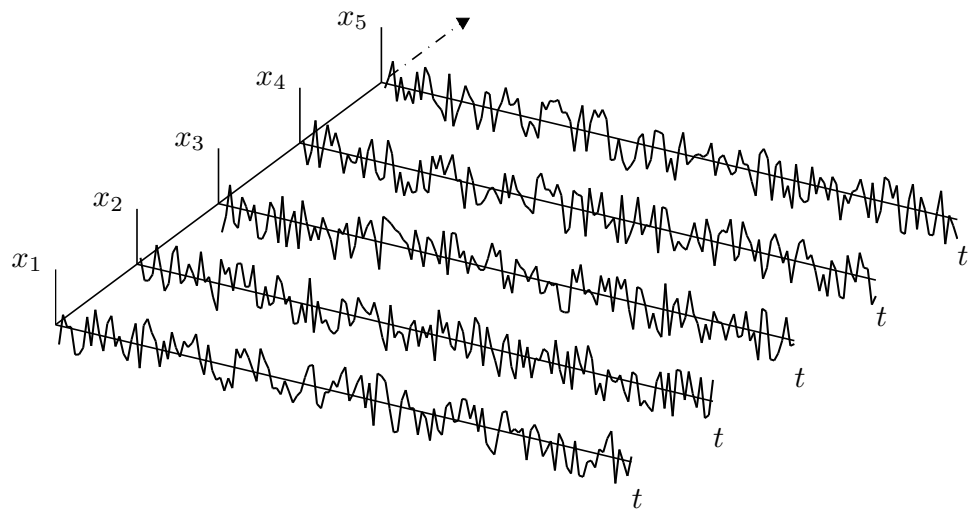


Figure 2.3: The concept of the ensemble of a stochastic process.

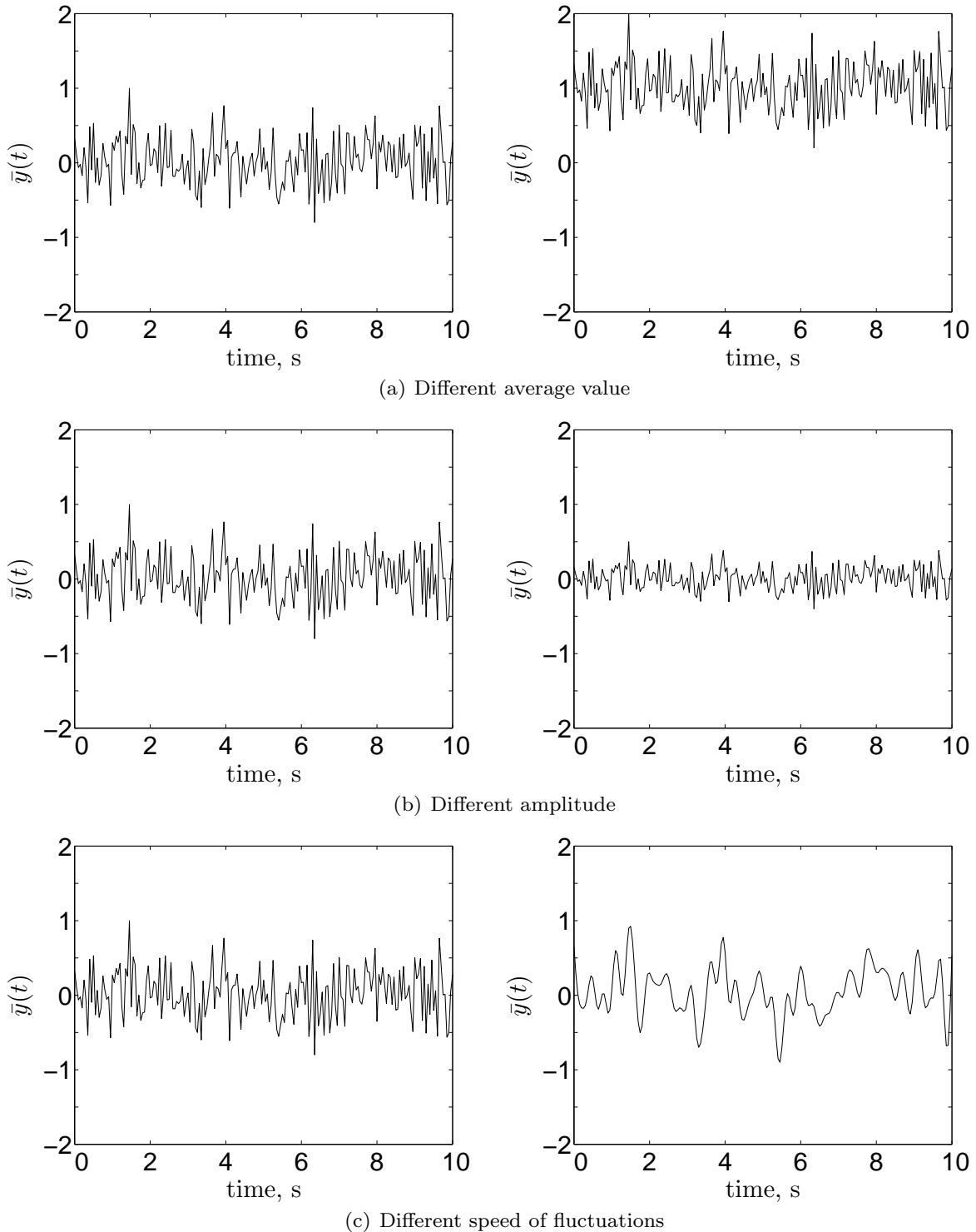


Figure 2.4: Realizations of stochastic processes with different average value (a), different amplitude (b) or different speed of fluctuations (c).

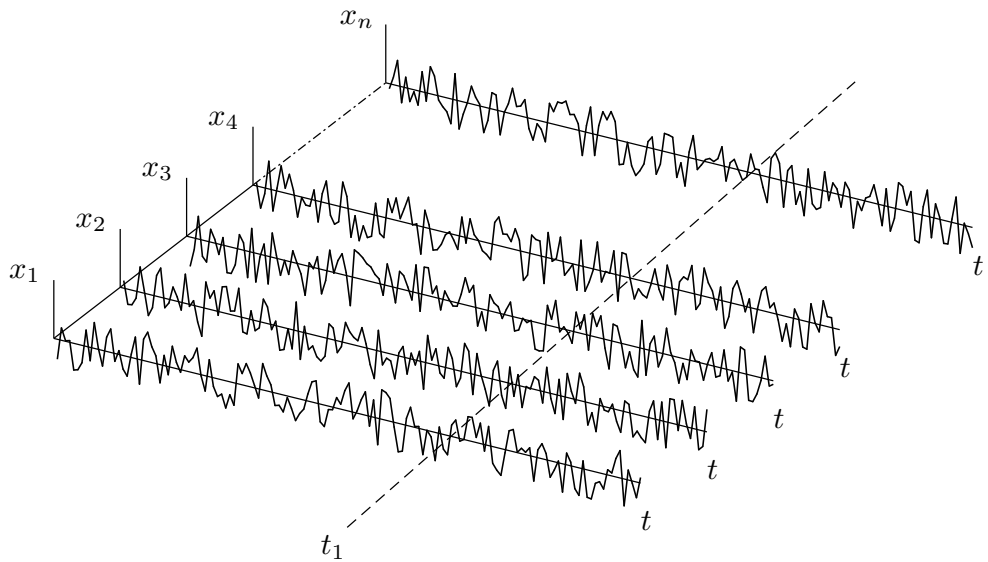


Figure 2.5: Part of the ensemble of a stochastic process.

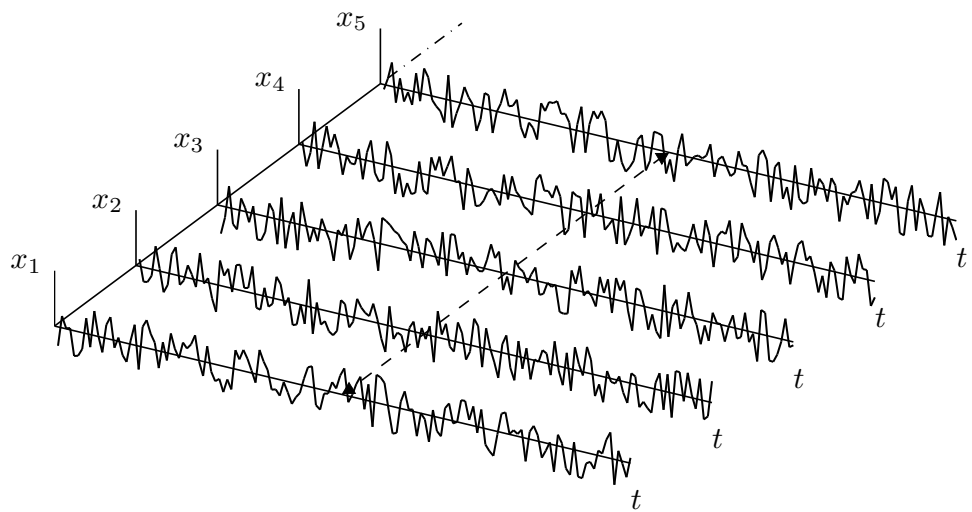


Figure 2.6: Expected value as an ensemble averaging.

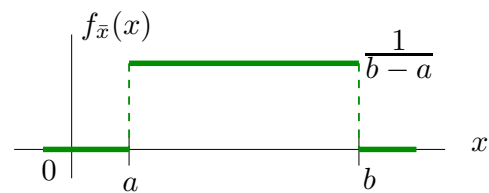


Figure 2.7: Uniform probability density function, $\bar{x} \sim \mathcal{U}(a, b)$.

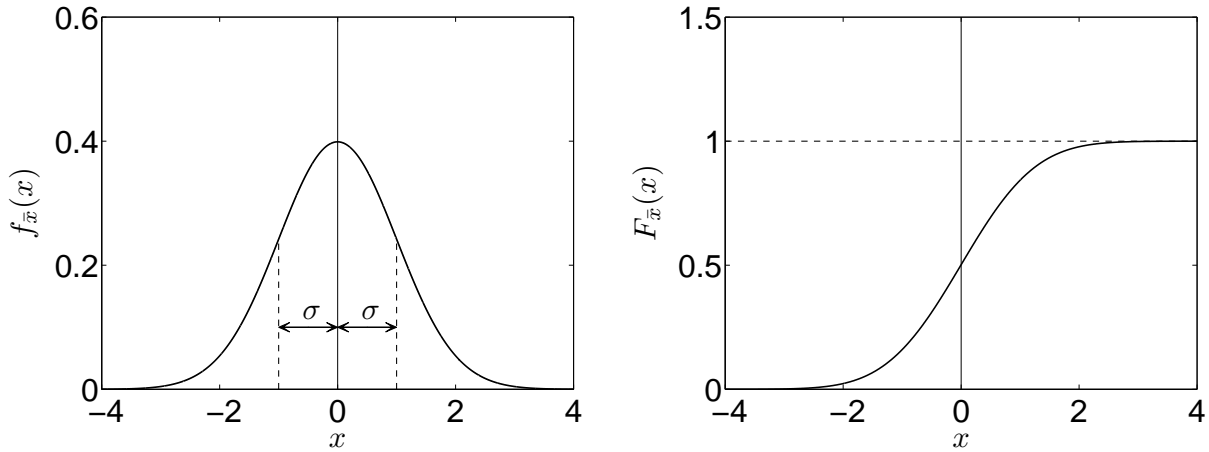


Figure 2.8: The Gaussian probability density- and distribution functions, $\bar{x} \sim \mathcal{N}(\mu, \sigma)$ (plotted here with $\mu_{\bar{x}} = 0$, $\sigma_{\bar{x}} = 1$).

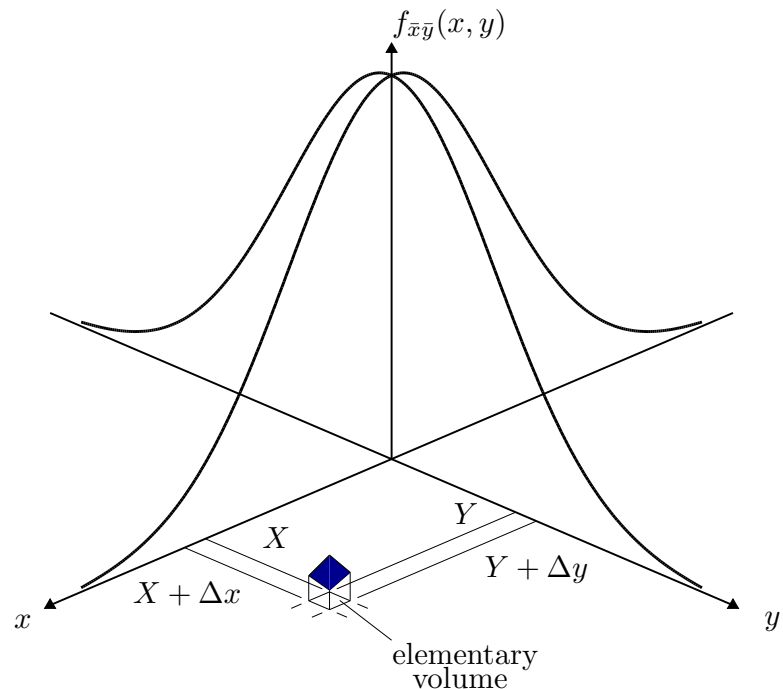


Figure 2.9: Graphical representation of the joint probability density function $f_{\bar{x}\bar{y}}(x, y)$.

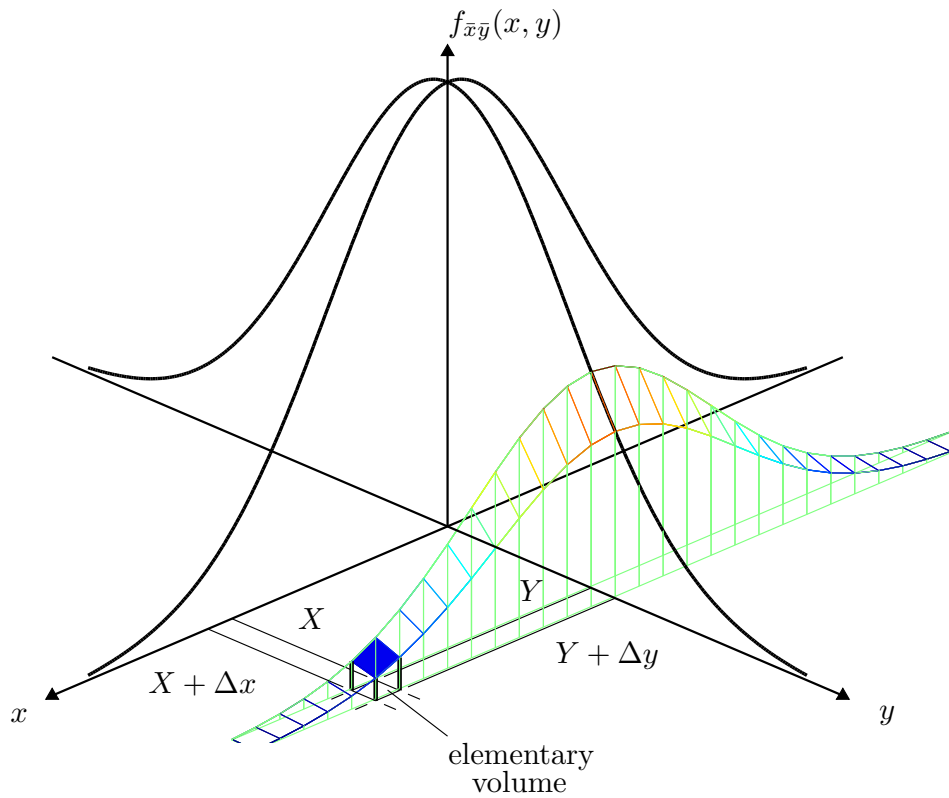


Figure 2.10: Graphical representation of the conditional probability density function.

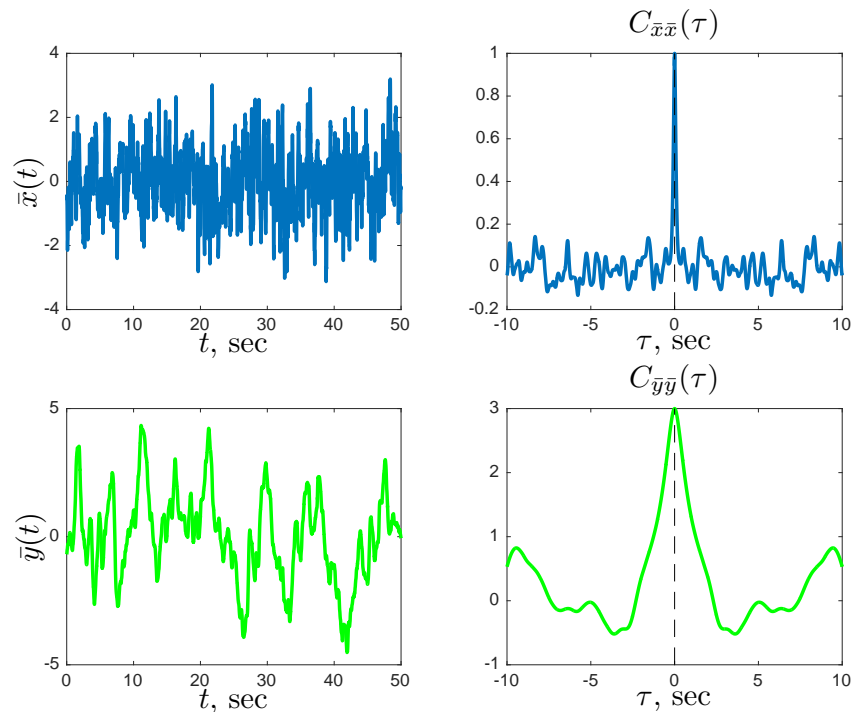


Figure 2.11: Auto covariance functions of stochastic processes $\bar{x}(t)$ and $\bar{y}(t)$ (one realization).

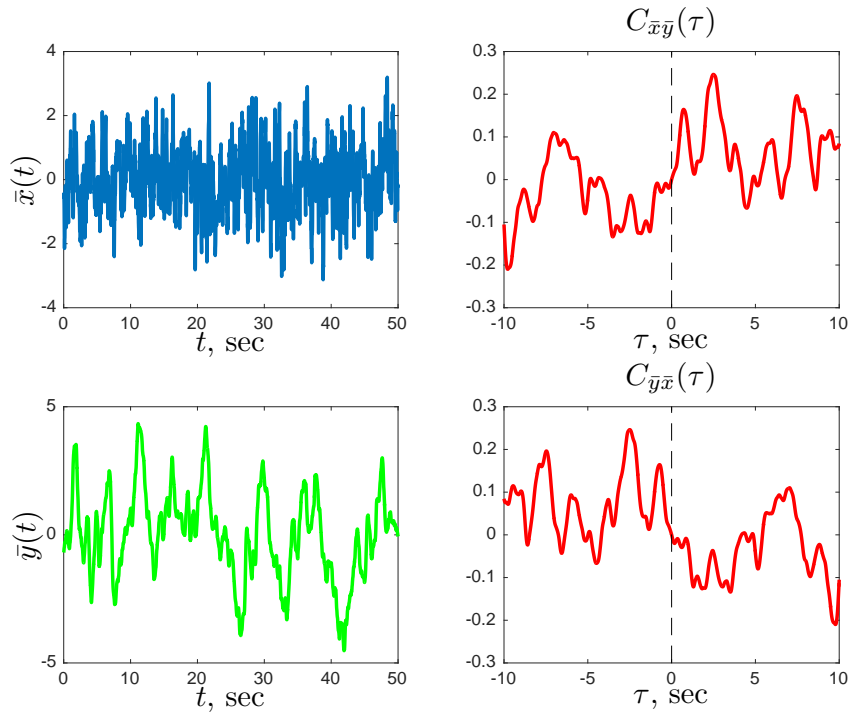


Figure 2.12: Cross covariance functions two stochastic processes $\bar{x}(t)$ and $\bar{y}(t)$ (one realization).

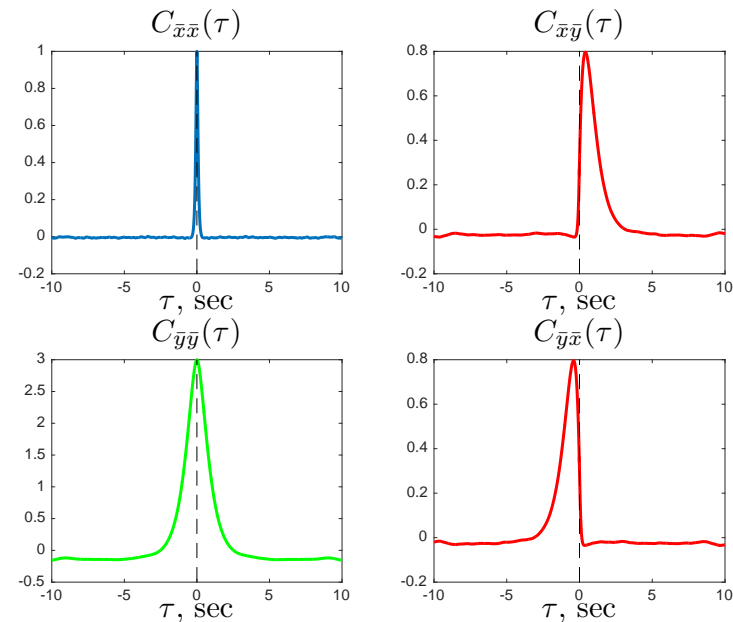


Figure 2.13: Averaged auto and cross covariance functions, for two stochastic processes $\bar{x}(t)$ and $\bar{y}(t)$, over 500 realizations.

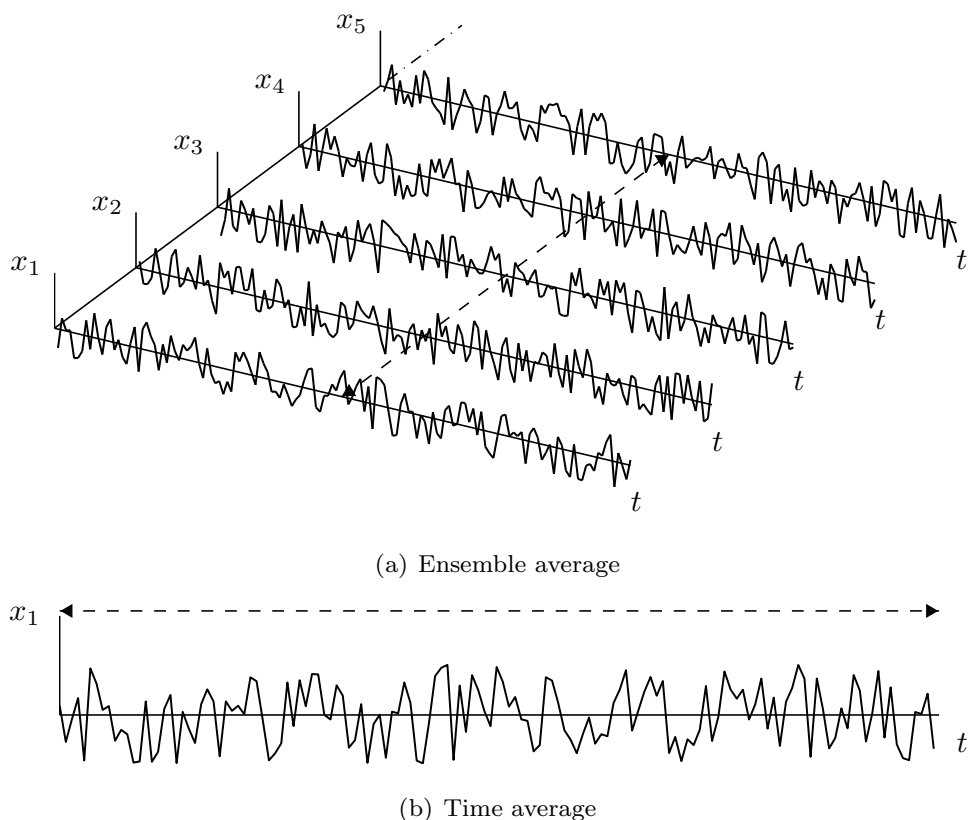


Figure 2.14: Difference between ensemble average and time average.

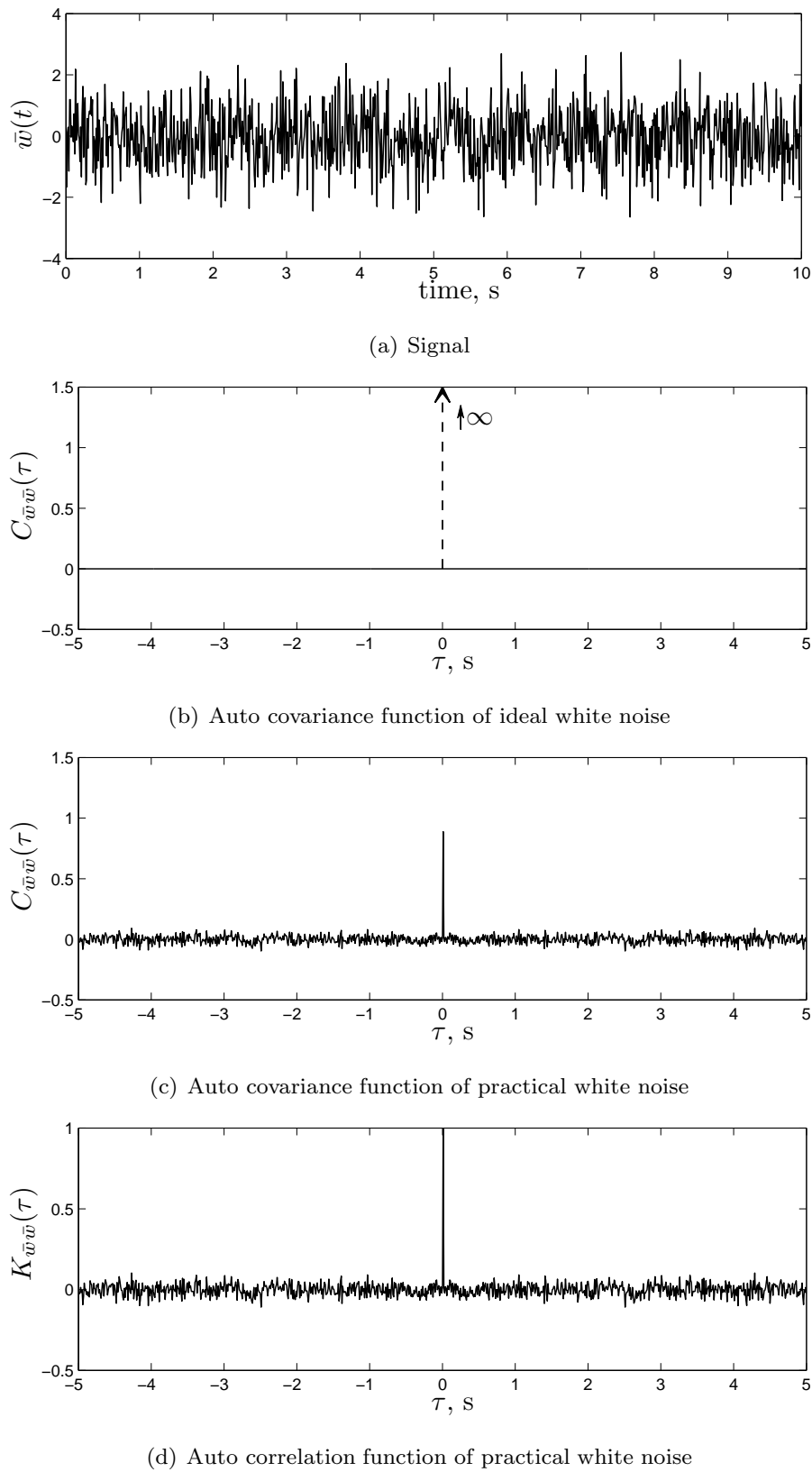


Figure 2.15: ‘Ideal’ versus ‘practical’ white noise.

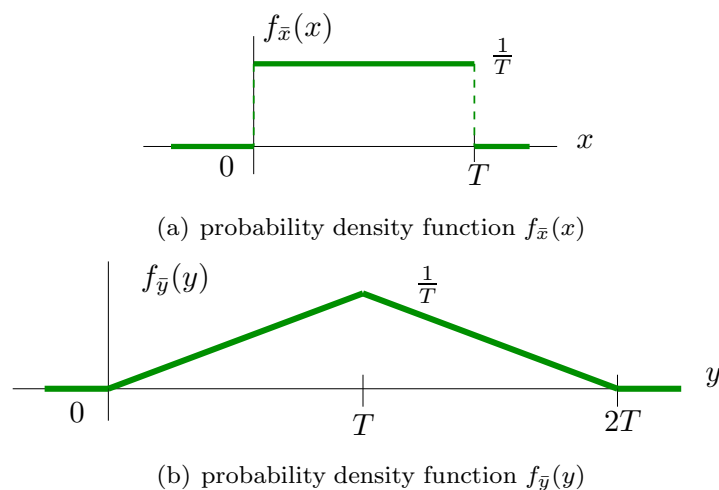


Figure 2.16: The sum of two random variables with equal, uniform, probability density functions (top) yields a random variable with a triangular probability density function (bottom).

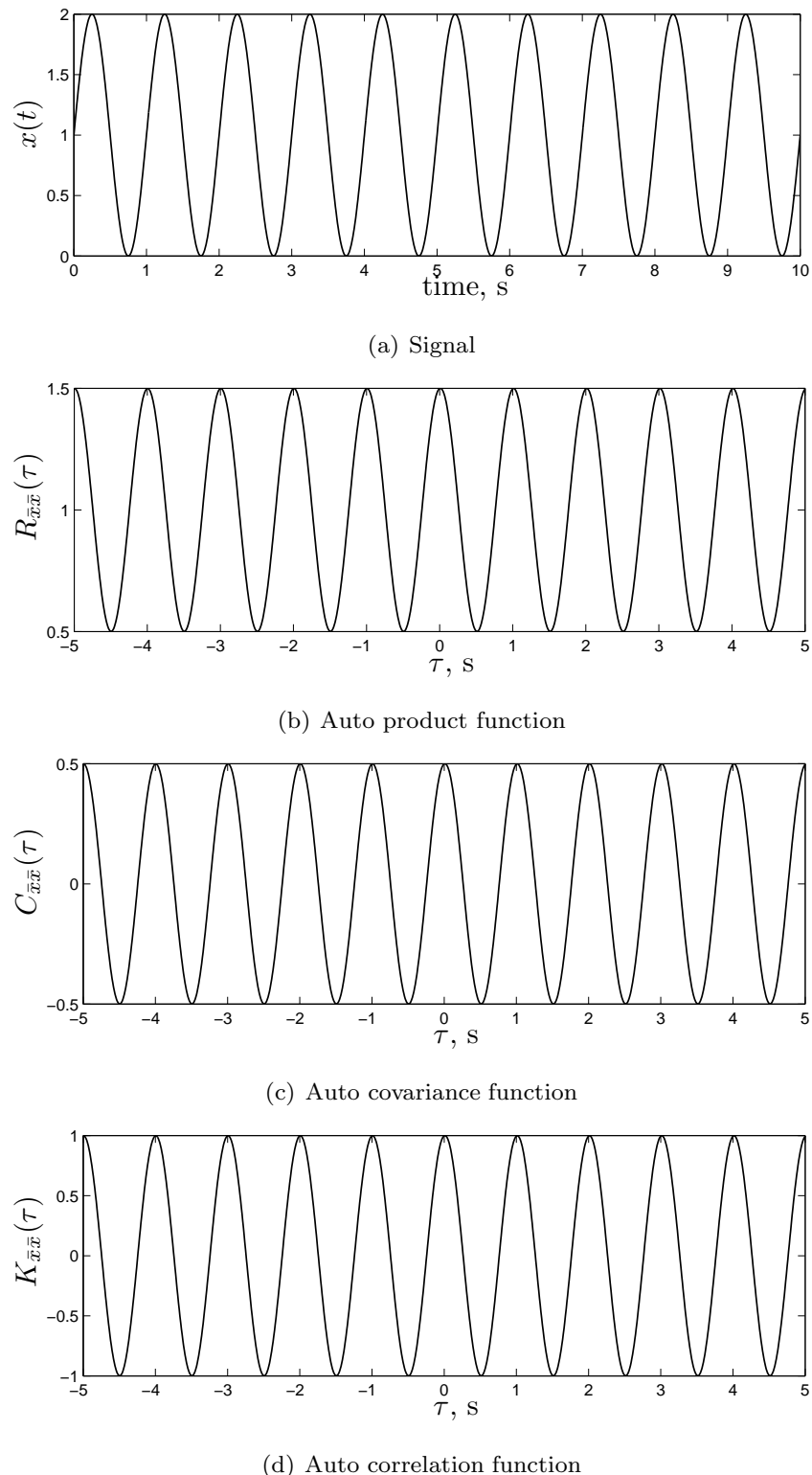


Figure 2.17: Time history, auto product / covariance / correlation functions.

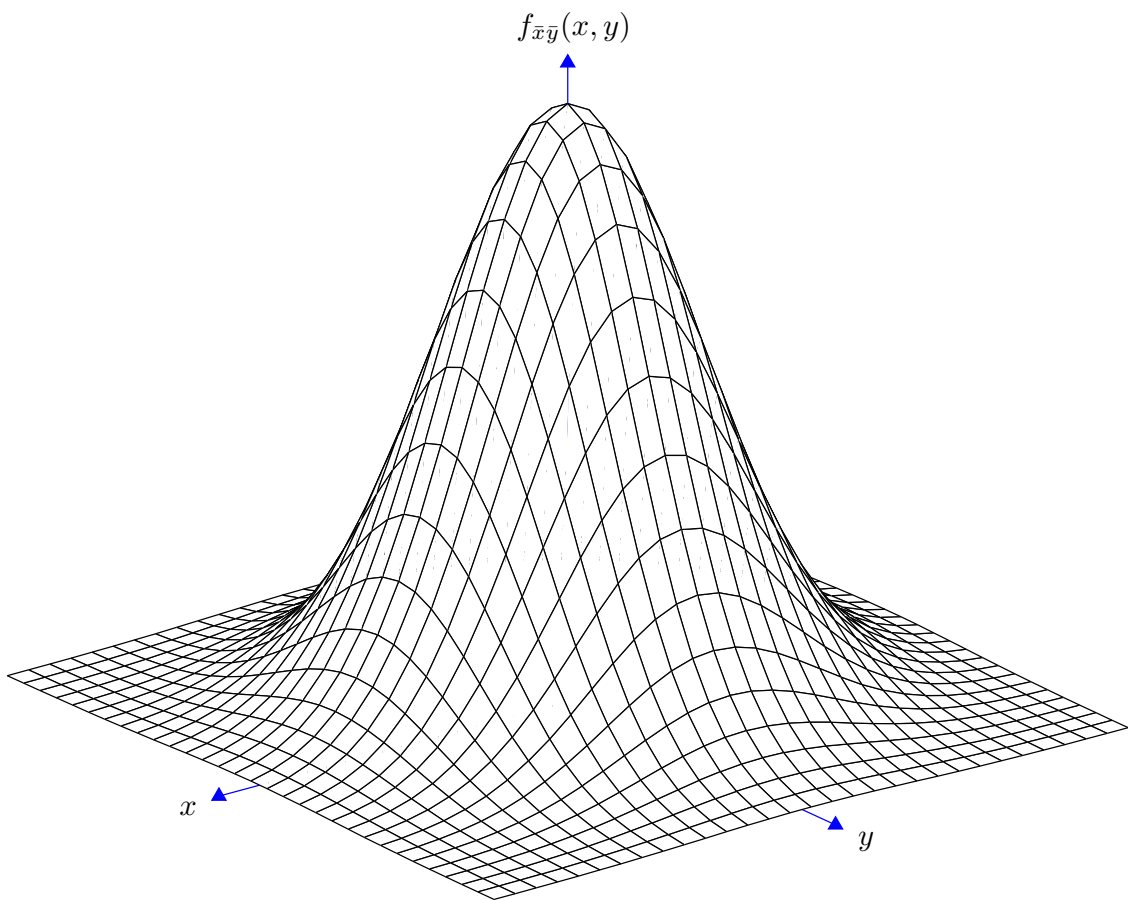


Figure 2.18: Graphical impression of a joint Gaussian probability density function, here with $\mu_{\bar{x}} = \mu_{\bar{y}} = 0, \sigma_{\bar{x}} = \sigma_{\bar{y}} = 1, K_{\bar{x}\bar{y}} = 0$.

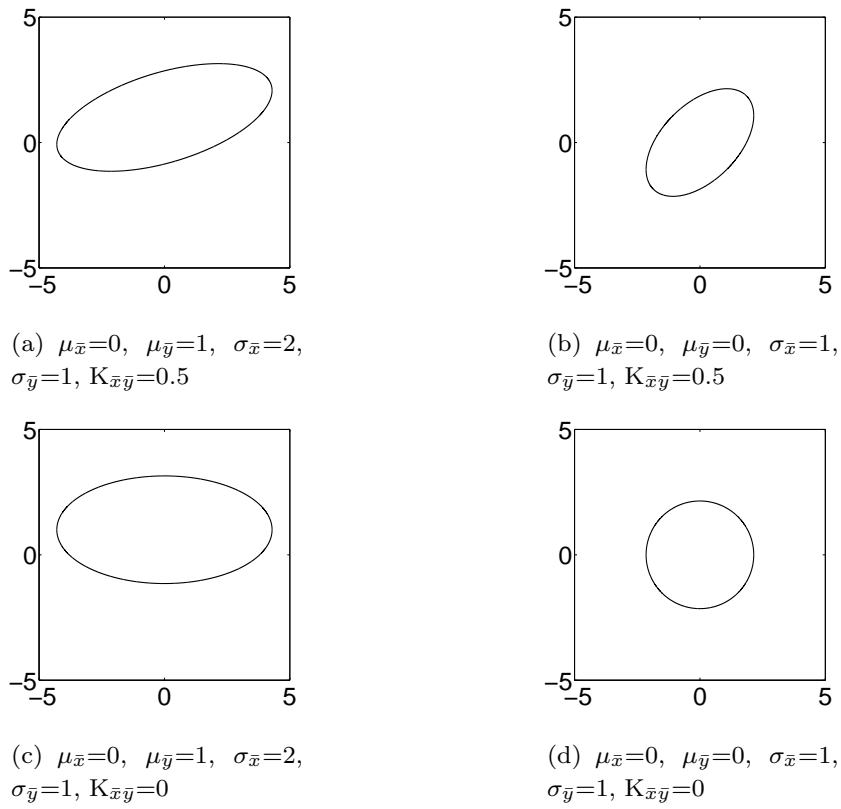


Figure 2.19: Equi-probability ellipses of the joint Gaussian distribution.

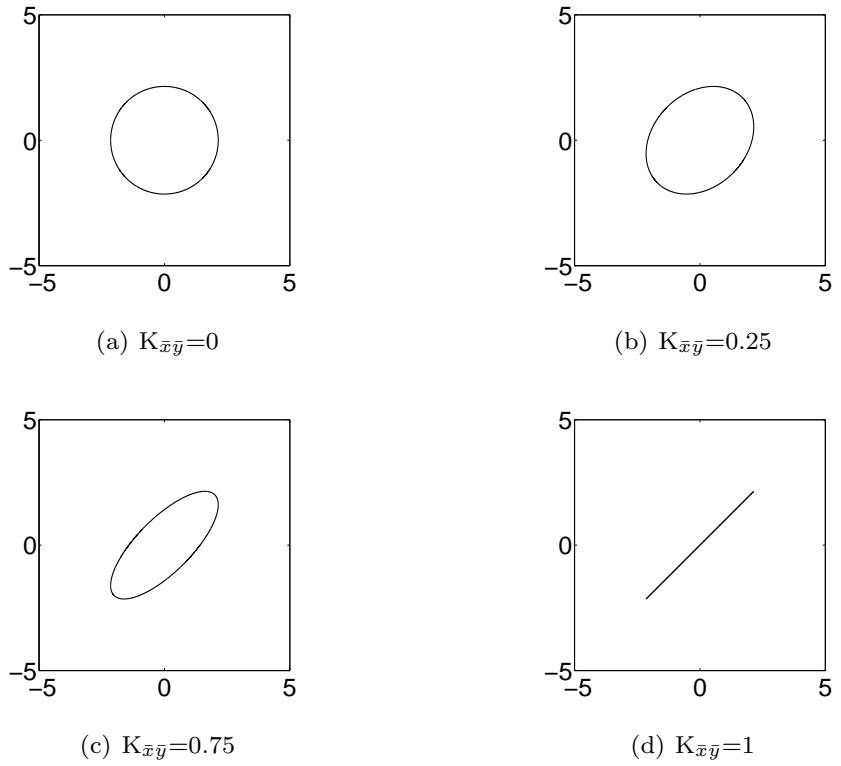


Figure 2.20: Equi-probability ellipses of the *normalized* joint Gaussian distribution.

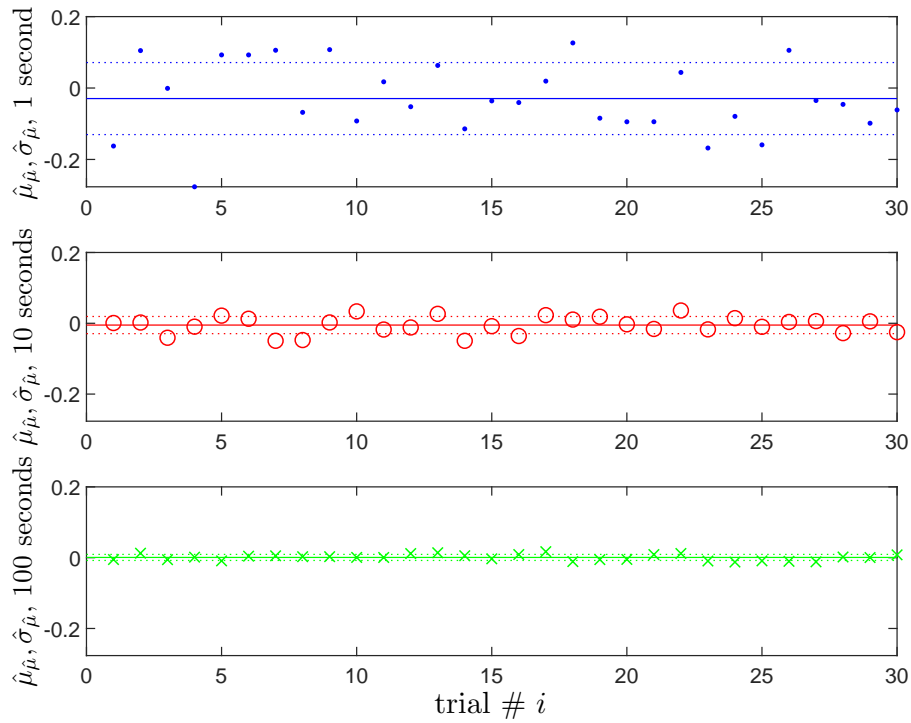


Figure 2.21: Randomness in Matlab (Example 2.4).

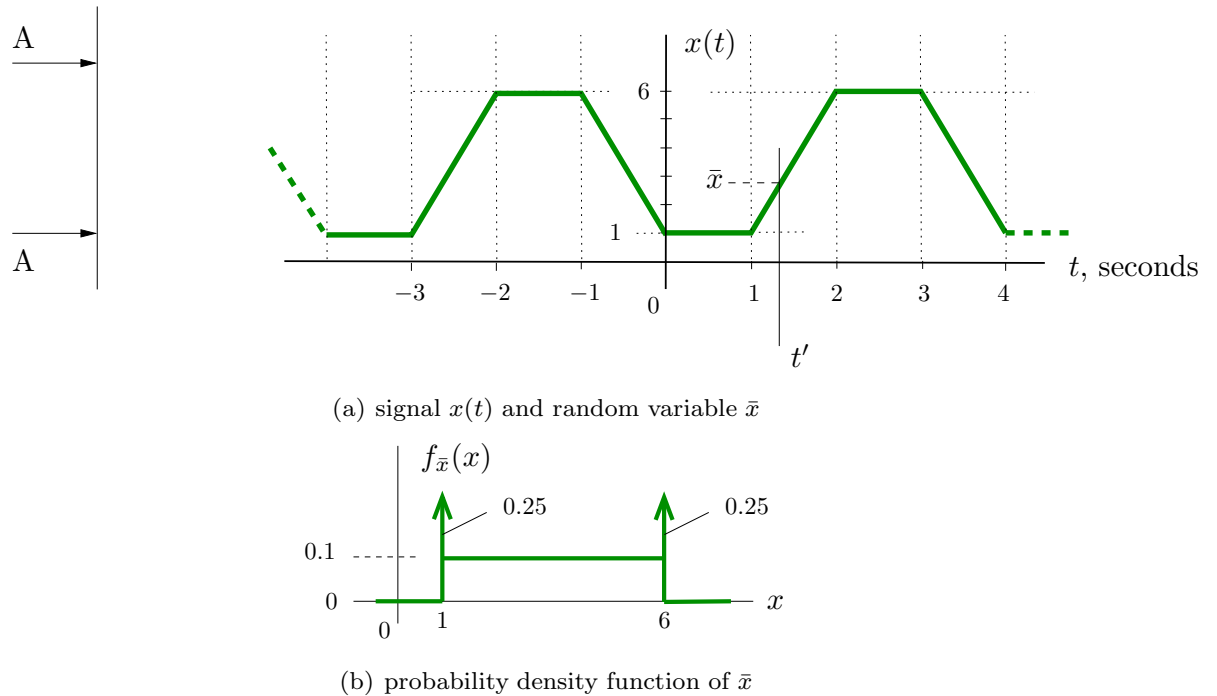


Figure 2.22: Signal $x(t)$ and the probability density function of the stochastic variable \bar{x} , used in Example 2.5.

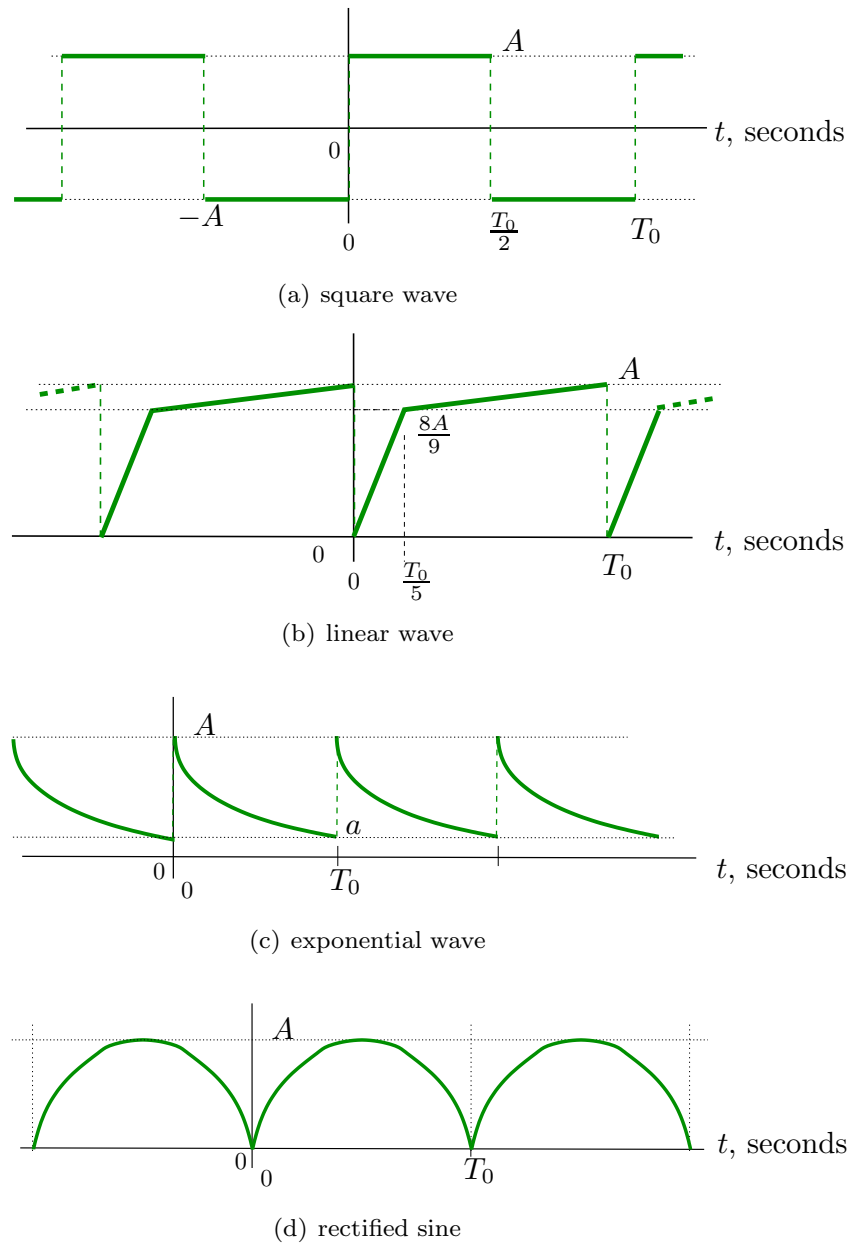


Figure 2.23: Signals $x(t)$ of Problem 2.7.

Chapter 3

Spectral Analysis of Continuous Time Stochastic Processes

3.1 Introduction

So far we have been dealing with stochastic processes in the time-domain only. The average value $\mu_{\bar{x}}$, the variance $\sigma_{\bar{x}}^2$, the covariance function $C_{\bar{x}\bar{y}}(\tau)$, etc., proved to be useful parameters for characterizing the time-domain properties of a stochastic process. In order to find some useful parameters to describe the frequency-domain characteristics of stochastic processes, consider Figure 3.1, in which two stochastic variables are shown with equal average values and equal variances. Yet it is clear that these signals exhibit different characteristics in the frequency-domain.

An intuitively attractive approach in the search for useful stochastic characteristics would be to apply a direct frequency-domain decomposition of the stochastic signal $\bar{x}(t)$,

time-domain	frequency-domain
$\bar{x}(t)$	Gain : $ X(\omega) $ Argument : $\arg(X(\omega))$

The result would be a plot of the amplitude and phase of the signal as a function of frequency ω .

However, in practice it turns out that such an approach would lead to two problems.

First there is the problem that for a signal of infinite duration the integral,

$$\int_{-\infty}^{+\infty} |\bar{x}(t)| dt$$

is infinite and cannot be transformed into the frequency-domain. By limiting the time interval from $-\infty < t < +\infty$ to $-T < t < T$, $T < \infty$, this problem can in principle be solved. Yet, as it will turn out to be in the next Chapter, other difficulties will result when considering only a limited part of the signal.

A second problem arises when spectra of different realizations of the same physical process are compared. It turns out that the complete frequency-domain representation in gain and argument is not unique but is different for each realization. This result is not surprising since the gain $|X(\omega)|$ and argument $\arg(X(\omega))$ as a function of ω completely specify the time history of the stochastic variable. Since time histories of different realizations are different, it is obvious that the frequency-domain representation will also differ between realizations.

It will be shown that, in the limit case, the variable $|X(\omega)|^2$ as a function of ω is characteristic for all realizations. This function represents the distribution of energy of a signal over different frequencies ω and is defined as the spectral density function $S_{\bar{x}\bar{x}}(\omega)$, which will be introduced in Section 3.5. The signal spectrum fully characterizes the stochastic process *only* for an infinitely long observation interval, the limit case mentioned above. In practice, with limited observation lengths, it will be shown that the power spectral density of a signal for a certain observation time $(-T, T)$ only *approximates* the ‘real’ power spectral density. Again, the power spectral density for a particular realization of a stochastic process, is essentially a realization in itself. Repeating the observations N times, computing the power spectral density N times and then averaging it, would result in an *estimate* of the ‘real’ power spectral density. Yet, clearly this would be equivalent to considering the stochastic process for an observation time N times as long, i.e., $(-T \cdot N, T \cdot N)$.

This chapter will treat the general frequency-domain techniques in detail, such as for example Fourier analysis and the power spectral density function, and their relation with time-domain characteristics for the description of stochastic processes will be shown. The response of dynamic systems on stochastic input signals in the frequency-domain will be another important topic. Note that it is assumed that all signals are real-valued. Complex-valued functions are not considered.

We will focus on the continuous-time case, and the discussion is merely of theoretical interest. The discrete-time case will be described separately in Chapter 4. Because most of the time series treated in real-life are essentially discrete-time ‘samples’ of a continuous-

time process, the discrete counterpart of the techniques discussed in this chapter is of great practical interest indeed. Yet, it would be difficult to understand the intricacies of discrete-time signal processing without knowing the continuous-time theory on which it is based.

3.2 Fourier analysis

In the general theory of signals there is a powerful technique known as **signal decomposition**. In decomposing a signal, the signal concerned is viewed as a linear combination of so-called ‘basis functions’. The value of this method strongly depends on the selection of specific basis functions that have some special properties. The Fourier series expansion relies on sinusoids as its basic components. This has proven to be a successful choice, for two reasons.

First, the response of a linear dynamic system to a sinusoidal input signal is well-known. It yields a sinusoidal output signal that has exactly the same frequency, but may have different phase and amplitude relative to the input signal. The degree to which the phase and amplitude differ, only depends on the dynamics of the system in-between. This observation forms the basis of dynamic system description in the frequency-domain. Frequency response functions (FRFs) are used to relate the input signal to the output signal as a function of frequency. and describe the frequency response of the system acting in-between.

Second, recall the superposition property of linear systems. It states that the response of a linear system to a sum of input signals equals the sum of the responses of that system to each individual input signal. That is, when y_1 is the response of the system to input signal u_1 and y_2 the response to u_2 , then the response to $u = u_1 + u_2$ equals $y = y_1 + y_2$. So, when we can describe the input signal using a sum of ‘basis functions’, like sinusoids, then the response of the system to that input signal will be equal to the sum of the system response to each individual basis function.

In the following sections, the continuous-time Fourier series expansion (CTFS) and the continuous-time Fourier transform (CTFT) will be briefly recapitulated. Many good textbooks exist on this topic, and can be recommended for further reading (e.g., (Bracewell, 1986; Oppenheim, Willsky, & Hamid, 1997)).

3.3 The continuous-time Fourier Series

3.3.1 Derivation

The continuous-time Fourier Series (CTFS) is valid for signals that are periodic with a finite period T . Any periodic signal $\bar{x}(t)$ can be approximated over the time interval $[t_0, t_0 + T]$

by a Fourier series expansion, $\tilde{x}(t)$, consisting of N sine and cosine functions,

$$\begin{aligned}\tilde{x}(t) &= \sum_{k=0}^{N-1} [a_k \cos k\omega_0 t + b_k \sin k\omega_0 t] \\ &= a_0 + \sum_{k=1}^{N-1} [a_k \cos k\omega_0 t + b_k \sin k\omega_0 t].\end{aligned}\quad (3.1)$$

Note that in the CTFS b_0 always equals 0.

The fundamental frequency ω_0 appearing in Equation (3.1) should be chosen such that all basis functions ‘fit’ an integer number of times in the interval $[t_0, t_0 + T]$. If the following choice for the fundamental frequency ω_0 is made:

$$\omega_0 = 2\pi \frac{1}{T}, \quad (3.2)$$

then this constraint is met perfectly (Bracewell, 1986). In this case, one can prove that all basic signals are orthogonal functions and will form a frame. This property will play an important role in the selection of coefficients a_k and b_k . Note that the frequency $k\omega_0$ is called the k^{th} harmonic.

A quadratic loss function J for judging the quality of the signal approximation of $\bar{x}(t)$ by $\tilde{x}(t)$, can be defined as:

$$\begin{aligned}J(a_0, a_1, a_2, \dots, a_{N-1}, b_1, b_2, \dots, b_{N-1}) &= \int_{t_0}^{t_0+T} [\bar{x}(t) - \tilde{x}(t)]^2 dt = \\ &= \int_{t_0}^{t_0+T} \left[\bar{x}(t) - \left(a_0 + \sum_{k=1}^{N-1} [a_k \cos k\omega_0 t + b_k \sin k\omega_0 t] \right) \right]^2 dt.\end{aligned}\quad (3.3)$$

Necessary conditions for J to be minimum with respect to the parameters a_0 , a_k and b_k are:

$$\frac{\partial J}{\partial a_0} = \frac{\partial J}{\partial a_\ell} = \frac{\partial J}{\partial b_\ell} = 0,$$

for $\ell = 1, 2, \dots, N-1$. Let us first consider parameter a_0 . If $\frac{\partial J}{\partial a_0} = 0$ then:

$$\int_{t_0}^{t_0+T} 2 \left[\bar{x}(t) - \left(a_0 + \sum_{k=1}^{N-1} [a_k \cos k\omega_0 t + b_k \sin k\omega_0 t] \right) \right] \cdot (-1) dt = 0,$$

so:

$$\begin{aligned}\int_{t_0}^{t_0+T} \bar{x}(t) dt &= \int_{t_0}^{t_0+T} a_0 dt + \int_{t_0}^{t_0+T} \sum_{k=1}^{N-1} [a_k \cos k\omega_0 t + b_k \sin k\omega_0 t] dt \\ &= Ta_0 + \sum_{k=1}^{N-1} \left(a_k \int_{t_0}^{t_0+T} \cos k\omega_0 t dt + b_k \int_{t_0}^{t_0+T} \sin k\omega_0 t dt \right).\end{aligned}$$

Note that the two integral terms on the right-hand side are zero for all k , and we obtain:

$$\boxed{a_0 = \frac{1}{T} \int_{t_0}^{t_0+T} \bar{x}(t) dt}. \quad (3.4)$$

Hence, a_0 can be considered the *average* of $\bar{x}(t)$ over the interval $[t_0, t_0 + T]$. We will come back to this property later.

We continue with deriving an expression for variables a_k . If $\frac{\partial J}{\partial a_\ell} = 0$ (for $\ell = 1, 2, \dots, N-1$) then:

$$\int_{t_0}^{t_0+T} 2 \left[\bar{x}(t) - \left(a_0 + \sum_{k=1}^{N-1} [a_k \cos k\omega_0 t + b_k \sin k\omega_0 t] \right) \right] \cdot (-\cos \ell\omega_0 t) dt = 0,$$

so:

$$\begin{aligned} \int_{t_0}^{t_0+T} \bar{x}(t) \cos \ell\omega_0 t dt &= \int_{t_0}^{t_0+T} a_0 \cos \ell\omega_0 t dt \\ &+ \int_{t_0}^{t_0+T} \sum_{k=1}^{N-1} [a_k \cos k\omega_0 t \cos \ell\omega_0 t + b_k \sin k\omega_0 t \cos \ell\omega_0 t] dt \\ &= a_0 \int_{t_0}^{t_0+T} \cos \ell\omega_0 t dt \\ &+ \sum_{k=1}^{N-1} \left(a_k \int_{t_0}^{t_0+T} \cos k\omega_0 t \cos \ell\omega_0 t dt + b_k \int_{t_0}^{t_0+T} \sin k\omega_0 t \cos \ell\omega_0 t dt \right). \end{aligned}$$

Note that the first integral term on the right-hand side is zero for all ℓ . Moreover, all basic cosine and sine functions are orthogonal at the interval $[t_0, t_0 + T]$, that is:

$$\begin{aligned} \int_{t_0}^{t_0+T} \sin k\omega_0 t \cos \ell\omega_0 t dt &= 0, \\ \int_{t_0}^{t_0+T} \sin k\omega_0 t \sin \ell\omega_0 t dt &= \begin{cases} 0 & \text{if } k \neq \ell \\ \frac{T}{2} & \text{if } k = \ell, \end{cases} \\ \int_{t_0}^{t_0+T} \cos k\omega_0 t \cos \ell\omega_0 t dt &= \begin{cases} 0 & \text{if } k \neq \ell \\ \frac{T}{2} & \text{if } k = \ell. \end{cases} \end{aligned} \quad (3.5)$$

Hence, we obtain:

$$\int_{t_0}^{t_0+T} \bar{x}(t) \cos \ell\omega_0 t dt = a_\ell \frac{T}{2},$$

or, substituting k for ℓ :

$$\boxed{a_k = \frac{2}{T} \int_{t_0}^{t_0+T} \bar{x}(t) \cos k\omega_0 t \, dt}, \quad (3.6)$$

for $k = 1, 2, \dots, N-1$. Similarly, we can derive for b_k :

$$\boxed{b_k = \frac{2}{T} \int_{t_0}^{t_0+T} \bar{x}(t) \sin k\omega_0 t \, dt}, \quad (3.7)$$

for $k = 1, 2, \dots, N-1$.

Interestingly, we see that Equations 3.6 and 3.7 can be interpreted as the *average product function* (see Chapter 2) of the original signal $\bar{x}(t)$ and the cosine and sine basis functions, respectively, for frequencies that are an integer multiple of the fundamental frequency ω_0 . For each frequency $k\omega_0$ the Fourier series coefficients can therefore be considered as the ‘average’ of what the signal has ‘in common’ with the orthogonal basis functions with that frequency $k\omega_0$. The Fourier series coefficient a_0 , the signal’s average, can also be considered this way, namely as the average product of the original signal with a cosine signal that has ‘zero frequency’. A cosine signal with zero frequency is the limit case of a signal that fluctuates extremely slow, i.e., it equals one in the time interval $[t_0, t_0 + T]$.¹

3.3.2 Complex form of the Fourier series expansion

The complex form is another useful way to define the Fourier series expansion. Here, the complex exponential $e^{j\omega t}$ is the basis function that will be used to approximate the signal. The complex exponential is a complex vector with constant length 1 that rotates counterclockwise (for positive ω) or clockwise (for negative ω) in the complex plane.

Recall Euler’s formulae:

$$\begin{aligned} \cos \omega t &= \frac{1}{2} [e^{j\omega t} + e^{-j\omega t}], \\ \sin \omega t &= \frac{1}{2j} [e^{j\omega t} - e^{-j\omega t}], \end{aligned} \quad (3.8)$$

and apply them to the original Fourier series, Equation (3.1). This results in the following alternative representation:

$$\boxed{\tilde{x}(t) = \sum_{k=-N+1}^{N-1} c_k e^{jk\omega_0 t}}, \quad (3.9)$$

where the original real-valued coefficients a_k and b_k are substituted by the complex-valued coefficients c_k defined as:

$$c_0 = a_0 \text{ and } c_k = \frac{1}{2}(a_k - jb_k), \quad c_{-k} = \frac{1}{2}(a_k + jb_k), \quad \text{for } k = 1, 2, \dots, N-1. \quad (3.10)$$

¹Note that a sine signal with ‘zero frequency’ is zero in the time interval $[t_0, t_0 + T]$, and therefore b_0 equals zero in the CTFS.

In other words:

$$a_0 = c_0 \text{ and } a_k = 2 \operatorname{Re}\{c_k\}, \quad b_k = -2 \operatorname{Im}\{c_k\}, \quad \text{for } k = 1, 2, \dots, N-1.$$

or, as we are dealing with complex numbers c_k and c_{-k} :

$$|c_k| = |c_{-k}| = \frac{1}{2} \sqrt{a_k^2 + b_k^2} \quad \text{and} \quad \angle c_k = \arctan \frac{-b_k}{a_k}, \quad \angle c_{-k} = \arctan \frac{b_k}{a_k} \quad (3.11)$$

Substituting (3.6), (3.7) and (3.8) in the expression for c_k , (3.10), one obtains:

$$\begin{aligned} c_k &= \frac{1}{2}(a_k - jb_k) = \frac{1}{2} \cdot \frac{2}{T} \left(\int_{t_0}^{t_0+T} \bar{x}(t) \cos k\omega_0 t \, dt - j \int_{t_0}^{t_0+T} \bar{x}(t) \sin k\omega_0 t \, dt \right) \\ &= \frac{1}{T} \int_{t_0}^{t_0+T} \bar{x}(t) \frac{1}{2} [e^{jk\omega_0 t} + e^{-jk\omega_0 t}] \, dt - j \int_{t_0}^{t_0+T} \bar{x}(t) \frac{1}{2j} [e^{jk\omega_0 t} - e^{-jk\omega_0 t}] \, dt \\ &= \frac{1}{T} \int_{t_0}^{t_0+T} \bar{x}(t) e^{-jk\omega_0 t} \, dt \end{aligned}$$

A similar argument holds for negative k , yielding:

$c_k = \frac{1}{T} \int_{t_0}^{t_0+T} \bar{x}(t) e^{-jk\omega_0 t} \, dt,$

(3.12)

which holds for all (positive and negative) integer k . Hence, we get a *two-sided* Fourier series expansion.

Equations (3.9) and (3.12), which are each others inverse, are known as the complex form of the Fourier series expansion. Equation 3.9 is known as the synthesis-equation, because it constructs, or ‘synthesizes’, a signal using complex exponential basis functions. Equation 3.12 is known as the analysis-equation, because it allows us to analyze how the signal can be constructed using basis functions.

Figure 3.2 shows an example of a Fourier series expansion for a zero-mean signal $\bar{x}(t)$ (hence, $a_0=0$) that consists of three cosine functions (a_k -terms) and one sine function (b_k -terms). Figure 3.3 shows the complex Fourier series description of this signal.

3.3.3 Properties of the Fourier series

In this subsection some properties of the CTFS will be briefly discussed.

First, it can be shown that when the number of Fourier series coefficients, N , increases, that the approximation improves:

$$\lim_{N \rightarrow \infty} \tilde{\bar{x}}(t) = \bar{x}(t),$$

for all signals within in the finite interval $[t_0, t_0 + T]$. Note that when considering an arbitrary (and therefore possibly non-periodic...) signal in this interval, applying the Fourier series yields an approximated signal $\tilde{x}(t)$ that is *always* periodic with period T . That is, the signal $\tilde{x}(t)$ will be exactly the same in an arbitrary time interval $[t_0 + nT; t_0 + (1 + n)T]$. For a signal with period T the Fourier series will be an exact description. But for an aperiodic signal the Fourier series description will only approximate the original signal in the interval $[t_0, t_0 + T]$. We will discuss this further below, when we derive the Fourier transform.

Second, it can be shown that for even functions the Fourier series expansion will only have cosine terms, i.e., $b_k = 0 \forall k$. Similarly, for odd functions the Fourier series expansion only has sine terms, i.e., $a_k = 0 \forall k$.

Third, it can be shown that the average of the squared signal equals the sum of the Fourier series coefficients. For the infinite CTFS expansion one obtains:

$$\frac{1}{T} \int_{t_0}^{t_0+T} \bar{x}^2(t) dt = a_o^2 + \sum_{k=1}^{\infty} \frac{1}{2} (a_k^2 + b_k^2) = \sum_{k=-\infty}^{\infty} |c_k|^2.$$

This is known as *Parseval's theorem for the Fourier series expansion*.

Fourth, it can be shown that the Fourier series expansion of the n^{th} derivative of a function $\bar{x}(t)$ equals:

$$\frac{d^n \bar{x}(t)}{dt^n} = \sum_{k=-\infty}^{\infty} (jk\omega_0)^n c_k e^{jk\omega_0 t}.$$

Fifth, it can be shown that for signals that are anti-symmetric *within* the interval T , i.e., $\bar{x}(\omega_0 t + \pi) = -x(\omega_0 t)$, the CTFS coefficients are zero for even k ($\pm 2, \pm 4, \dots$). This is known as the ‘half-wave odd’-property of a signal.

Finally, consider the Fourier series expansion of signals $\bar{x}_1(t) = \sin \omega_0 t$ and $\bar{x}_2(t) = \cos \omega_0 t$. Using Equation 3.12 it can be shown that the Fourier series coefficients of $\bar{x}_1(t)$ are all zero, except c_1 and c_{-1} which equal $\frac{1}{2j}$ and $\frac{-1}{2j}$, respectively. Similarly, the Fourier series coefficients of $\bar{x}_2(t)$ are all zero as well, except c_1 and c_{-1} which equal $\frac{1}{2}$ and $\frac{1}{2}$, respectively. We see that the Fourier series expansion of the odd sine function is odd, and the Fourier series expansion of the even cosine function is even.

3.4 The continuous-time Fourier transform

3.4.1 Derivation and definitions

The Fourier series expansion is able to perfectly describe any periodic (period T) signal. One may ask oneself whether such a description also exists for an aperiodic signal. It can be shown that this is indeed possible, namely by assuming that an aperiodic signal is periodic *with an infinite period T*.

Apply the Fourier series expansion to the stochastic function $\bar{x}(t)$ valid at an infinite time interval $-\infty < t < +\infty$. Starting from the complex form of the Fourier series expansion, Equations (3.9) and (3.12):

$$\begin{aligned}\tilde{x}(t) &= \sum_{k=-\infty}^{+\infty} c_k e^{jk\omega_0 t}, \\ c_k &= \frac{1}{T} \int_{t_0}^{t_0+T} \bar{x}(t) e^{-jk\omega_0 t} dt.\end{aligned}$$

The initial time instant t_0 can be defined as $t_0 = -\frac{1}{2}T$, and the integration interval becomes $[-\frac{T}{2}, \frac{T}{2}]$. The resulting expression for $\tilde{x}(t)$ is then, substituting $\frac{1}{T} = \frac{\omega_0}{2\pi}$:

$$\tilde{x}(t) = \lim_{T \rightarrow \infty} \left(\sum_{k=-\infty}^{+\infty} \frac{\omega_0}{2\pi} \left[\int_{-\frac{1}{2}T}^{+\frac{1}{2}T} \bar{x}(t) e^{-jk\omega_0 t} dt \right] e^{jk\omega_0 t} \right). \quad (3.13)$$

When the fundamental period T is extended to infinity, the fundamental frequency becomes infinitesimal ($\omega_0 \rightarrow d\omega$), the discrete frequency becomes continuous ($k\omega_0 \rightarrow \omega$), and the sum becomes an integral with limits $\omega = -\infty$ and $\omega = +\infty$:

$$\tilde{x}(t) = \frac{1}{2\pi} \int_{-\infty}^{+\infty} \underbrace{\left[\int_{-\infty}^{+\infty} \bar{x}(t) e^{-j\omega t} dt \right]}_{\Delta} e^{j\omega t} d\omega. \quad (3.14)$$

The integral Δ in Equation (3.14) is known as the Fourier integral:

$$\int_{-\infty}^{+\infty} \bar{x}(t) e^{-j\omega t} dt. \quad (3.15)$$

This equation represents a continuous ‘Fourier spectrum’ or ‘frequency spectrum’ of the signal $\bar{x}(t)$.

Equation (3.15) is defined as the Fourier transform $\bar{X}(\omega)$ of signal $\bar{x}(t)$, while Equation (3.14) is defined as the inverse Fourier transform. That is, we obtain the transformation pair:

$$\bar{X}(\omega) = \mathcal{F}\{\bar{x}(t)\} = \int_{-\infty}^{+\infty} \bar{x}(t) e^{-j\omega t} dt \quad (3.16)$$

$$\bar{x}(t) = \mathcal{F}^{-1}\{\bar{X}(\omega)\} = \frac{1}{2\pi} \int_{-\infty}^{+\infty} \bar{X}(\omega) e^{j\omega t} d\omega \quad (3.17)$$

Note that there is no universal convention as to where the factor of $\frac{1}{2\pi}$ should be located, in the inverse Fourier transform, Equation (3.17) or in the Fourier transform itself, Equation

(3.16).² Further note that when not the radial frequency ω (in rad/s) but the ‘real’ frequency $f = \frac{1}{T}$ (in Herz) is used, the whole $\frac{1}{2\pi}$ -term disappears. In fact, many of the Fourier transform characteristics are much easier to derive and understand when working with frequency in Herz.

Similar to the Fourier Series expansion, Equations (3.16) and (3.17) are known as the analysis and synthesis equations, respectively. Note that whereas the Fourier series describes a signal in the frequency domain using Fourier series coefficients $\{c_k\}$ at discrete frequencies $k\omega_0$, the Fourier transform describes the signal using a continuous frequency-domain function $\bar{X}(\omega)$, valid for all frequencies ω .

3.4.2 Properties of the Fourier transform and some basic Fourier transform pairs

Some of the most important properties of the Fourier transform are shown in Table 3.1, while Table 3.2 lists some important Fourier transform function pairs. Below some of these pairs will be elaborated in more detail, as they will prove to be important and useful in the next chapters.

Fourier transform of function $x(t) = 1 \forall t$

Rule (Table 3.2):

$$\mathcal{F}\{1\} = 2\pi\delta(\omega)$$

In Chapter 2 it was stated that the Dirac function (or delta function) $\delta(t)$ is a *generalized function*. This means that it is not defined in terms of its values, but rather how it acts inside an integral when multiplied by a smooth function $f(t)$:

$$\int_{-\infty}^{\infty} f(t)\delta(t) dt = f(0).$$

This is called the sifting property of the Dirac function. As will be shown in the next chapter, Dirac functions do not physically exist. Rather, they are mathematical constructs that help us to more easily prove certain system and signal characteristics.

Proof: use the “inverse proof”:

$$Z(\omega) = 2\pi \delta(\omega)$$

²This often causes confusion. Some adopt a factor of $\frac{1}{2}$ in front of the Fourier transform and a factor $\frac{1}{\pi}$ in the inverse Fourier transform (or vice versa). A common factor, $\frac{1}{\sqrt{2\pi}}$, in both the Fourier transform and the inverse Fourier transform is sometimes seen as well. Probably the most widely used option is no scale factor in front of the Fourier transform, leaving the full $\frac{1}{2\pi}$ factor in the inverse transformation such as in Equation (3.17).

$$\begin{aligned}
z(t) &= \mathcal{F}^{-1}\{Z(\omega)\} \\
&= \frac{1}{2\pi} \int_{-\infty}^{\infty} 2\pi \delta(\omega) e^{j\omega t} d\omega \\
&= \frac{2\pi}{2\pi} \int_{-\infty}^{\infty} \delta(\omega) e^{j\omega t} d\omega \\
&= 1 e^0
\end{aligned}$$

q.e.d.

The interesting thing is that a function that is constant, i.e., very ‘broad’ in the time domain, becomes a very ‘narrow’ function in the frequency domain. Also, the ‘constant’ value becomes a Dirac pulse at ‘zero frequency’. Recall the discussion of a signal’s average and the zero-frequency component c_0 in the CTFS.

Fourier transform of a cosine function

Rule (Table 3.2): $\boxed{\mathcal{F}\{\cos \omega_0 t\} = \pi [\delta(\omega - \omega_0) + \delta(\omega + \omega_0)]}$

Remember, $\mathcal{F}\{1\} = \int_{-\infty}^{\infty} 1 \cdot e^{-j\omega t} dt = 2\pi\delta(\omega)$.

Proof:

$$\begin{aligned}
\mathcal{F}\{\cos \omega_0 t\} &= \int_{-\infty}^{\infty} \cos \omega_0 t \cdot e^{-j\omega t} dt \\
&= \int_{-\infty}^{\infty} \frac{1}{2} (e^{j\omega_0 t} + e^{-j\omega_0 t}) e^{-j\omega t} dt \\
&= \frac{1}{2} \int_{-\infty}^{\infty} (e^{j(\omega_0 - \omega)t} + e^{-j(\omega_0 + \omega)t}) dt \\
&= \frac{1}{2} \int_{-\infty}^{\infty} e^{j(\omega_0 - \omega)t} dt + \frac{1}{2} \int_{-\infty}^{\infty} e^{j(\omega_0 + \omega)t} dt \\
&= \frac{1}{2} 2\pi \delta(\omega - \omega_0) + \frac{1}{2} 2\pi \delta(\omega + \omega_0) \\
&= \pi (\delta(\omega - \omega_0) + \delta(\omega + \omega_0))
\end{aligned}$$

q.e.d.

Similar to the previous example, recall the discussion of the Fourier series expansion of the cosine function. All Fourier series coefficients were zero, except c_1 and c_{-1} which were equal to $\frac{1}{2}$. Now, one may ask oneself, what is the relation between these Fourier series coefficients and the Fourier transform? It appears that when using the CTFT to transform a periodic signal (with fundamental frequency ω_0), the Fourier series coefficients become equal to Dirac pulses at integer multiples of the fundamental frequency, weighted with 2π . Indeed, as is shown in (Oppenheim et al., 1997), the Fourier transform of a periodic signal with Fourier series coefficients $\{c_k\}$ can be interpreted as a train of impulses occurring at the harmonically related frequencies (i.e., integer multiples of the fundamental frequency ω_0), and for which the *area of the impulse* at the k^{th} harmonic $k\omega_0$ is 2π the k^{th} Fourier series coefficient c_k . That is:

$$\bar{X}(\omega) = \sum_{k=-\infty}^{\infty} 2\pi c_k \delta(\omega - k\omega_0).$$

Note that the ‘weighting’ of the impulses is only necessary because the radial frequency ω is used. When the frequency f (in Herz) was used we would obtain:

$$\bar{X}(f) = \sum_{k=-\infty}^{\infty} c_k \delta(f - kf_0),$$

with $f_0 = 1/T = \omega_0/2\pi$ the fundamental frequency.

Fourier transform of a block function

A block function $b(t)$ can be defined as:

$$b(t) = \begin{cases} 1 & , |t| < T/2 \\ 0.5 & , |t| = T/2 \\ 0 & , |t| > T/2 \end{cases}$$

Rule (Table 3.2): $B(\omega) = \mathcal{F}\{b(t)\} = T \cdot \text{sinc}(\frac{\omega}{2\pi}T) = T \cdot \frac{\sin \omega T/2}{\omega T/2}$

Here, the ‘sinc’ function appears which is very important function in signal analysis. It is defined as:

$$\text{sinc}(\Delta) = \frac{\sin(\pi\Delta)}{\pi\Delta}.$$

The block and sinc functions are illustrated in Figure 3.4, for $T=1$ sec. Note that the sinc function has one big peak at $\omega = 0$, with amplitude T (the width of the block in the time domain), and is zero for all frequencies ω equal to $k\frac{2\pi}{T}$, with k an integer.

Proof:

$$\begin{aligned} B(\omega) &= \int_{-\infty}^{\infty} x(t) e^{-j\omega t} dt = \int_{-T/2}^{+T/2} e^{-j\omega t} dt \\ &= \int_{-T/2}^{+T/2} (\cos \omega t - j \sin \omega t) dt = \int_{-T/2}^{+T/2} \cos \omega t dt - j \int_{-T/2}^{+T/2} \sin \omega t dt \end{aligned}$$

Note that a cosine is an even function and that a sine is an odd function.

Hence, the second integral on the right-hand side is zero $\forall T$.

$$\begin{aligned} &= 2 \int_0^{+T/2} \cos \omega t dt = 2 \int_0^{+T/2} d \frac{1}{\omega} \sin \omega t \\ &= 2 \left(\frac{1}{\omega} \sin \omega t \right) \Big|_{t=0}^{T/2} = 2 \frac{\sin \omega T/2}{\omega} = T \cdot \frac{\sin \omega T/2}{\omega T/2} \end{aligned} \quad \text{q.e.d.}$$

Figure 3.5 shows the block function and its Fourier transform for several values of T . It is clear from this figure that when T increases, the sinc function looks more and more like a Dirac delta-function. In fact, the sinc function mimics the Dirac function in many other ways as well, and can therefore be seen as a good ‘approximation’ of the purely theoretical concept of impulses. The peak gets higher (because it equals T , remember)

and the number of zero-crossings increases as well (because the sinc function crosses zero for frequencies ω equal to $k\frac{2\pi}{T}$, for integer k). Again, the ‘broader’ the block, the ‘narrower’ the frequency domain description. When $T \rightarrow \infty$ (i.e., $b(t) = 1 \forall t$), $B(\omega)$ becomes a Dirac delta-function $\delta(\omega)$. The area of $B(\omega)$ integrated in the frequency domain, equals the area below the block in the time domain, T , scaled with 2π . Again, this scale factor is only because we use the radial frequency ω .

Inverse Fourier transform of a block function: duality

Now consider a block function $B(\omega)$ in the frequency domain, which can be defined as:

$$B(\omega) = \begin{cases} 1 & , |\omega| < W/2 \\ 0.5 & , |\omega| = W/2 \\ 0 & , |\omega| > W/2 \end{cases}$$

It can be shown (see (Oppenheim et al., 1997)) that the inverse Fourier transform of this block function yields a sinc function in the time-domain. That is:

$$\mathcal{F}^{-1}\{B(\omega)\} = \frac{W}{2\pi} \cdot \text{sinc}\left(\frac{W}{2\pi} t\right) = \frac{\sin W/2 t}{\pi t}.$$

Note that $B(\omega)$ represents the frequency response function of an ‘ideal’ low-pass filter, as it passes the signal perfectly for all frequencies until $\omega = \frac{W}{2}$, beyond which it does not pass the signal at all. We see that the impulse response function of the ideal low-pass filter is *non-causal*: the sinc function is non-zero for negative time t . The ideal low-pass filter is therefore not feasible.

Even more important to note is that Fourier transforming a time-domain block yields a sinc function in the frequency domain, and Fourier transforming a time-domain sinc function yields a block in the frequency domain. This is a typical example of the duality property of the Fourier transform. It can be generalized as (Oppenheim et al., 1997):

$$\text{If } x(t) \xleftrightarrow{\mathcal{F}} X(\omega) \text{ then } X(t) \xleftrightarrow{\mathcal{F}} 2\pi x(-\omega).$$

Therefore, when we have one Fourier transform pair $\{x(t), X(\omega)\}$ (e.g., block in time domain, sinc in frequency domain) we can easily find the other pair $\{X(t), x(\omega)\}$ (e.g., block in frequency domain, sinc in time domain).

Fourier transform of a *periodic* block function

As a final example of the Fourier transform, let us consider the block function introduced above, but now *periodic* with fundamental period T_0 and fundamental frequency $\omega_0 = 2\pi/T_0$:

$$b_p(t) = \begin{cases} 1 & , |t| < T/2 + nT_0 \\ 0.5 & , |t| = T/2 + nT_0 \quad \text{for integer } n \\ 0 & , |t| > T/2 + nT_0 \end{cases}$$

This function is illustrated in Figure 3.6. Since $b_p(t)$ is a periodic function, the Fourier series expansion can be calculated. It can be shown that (Oppenheim et al., 1997):

$$c_0 = \frac{T}{T_0}, \text{ and } c_k = 2 \frac{\sin k\omega_0 T/2}{k\omega_0 T_0} = \frac{\sin k\omega_0 T/2}{k\pi} \text{ for } k \neq 0.$$

Figure 3.6 shows the Fourier series coefficients c_k for the integer multiples of the fundamental frequency ω_0 , scaled with T_0 . The figure also shows the Fourier transform of the a-periodic block function $b(t)$, the sinc function $B(\omega)$ derived above. It can be seen that the scaled Fourier series components of the periodic block function correspond exactly with the Fourier-transformed aperiodical block. How can this be explained?

Starting with the aperiodic block $b(t)$, one could consider the periodic block $b_p(t)$ as an ‘approximation’ of $b(t)$, when the period T_0 becomes very large. In fact, when T_0 becomes ∞ , both signals are exactly the same. Let’s consider the Fourier series expansion of the periodic block once more. The synthesis equation is:

$$\tilde{b}_p(t) = \sum_{k=-\infty}^{\infty} c_k e^{j k \omega_0 t}.$$

The analysis equation is, with, just for convenience, the integration time interval between $-T_0/2$ and $T_0/2$:

$$c_k = \frac{1}{T_0} \int_{-T_0/2}^{T_0/2} b_p(t) e^{-j k \omega_0 t} dt.$$

Now since $b_p(t) = b(t)$ in $[-T_0/2, T_0/2]$ and because $b(t)=0$ outside this interval, we get:

$$\begin{aligned} c_k &= \frac{1}{T_0} \int_{-T_0/2}^{T_0/2} b(t) e^{-j k \omega_0 t} dt = \frac{1}{T_0} \int_{-\infty}^{\infty} b(t) e^{-j k \omega_0 t} dt. \\ \iff T_0 c_k &= \int_{-\infty}^{\infty} b(t) e^{-j k \omega_0 t} dt. \end{aligned}$$

Therefore, defining the ‘envelope’ $B(\omega)$ of $T_0 c_k$ as:

$$B(\omega) = \int_{-\infty}^{\infty} b(t) e^{-j \omega t} dt,$$

the Fourier series coefficients c_k can be expressed as:

$$c_k = \frac{1}{T_0} B(k\omega_0).$$

When substituting these coefficients in the synthesis equation we obtain:

$$\tilde{b}_p(t) = \sum_{k=-\infty}^{\infty} \frac{1}{T_0} B(k\omega_0) e^{j k \omega_0 t},$$

or, with $\omega_0 = 2\pi/T_0$:

$$\tilde{b}_p(t) = \frac{1}{2\pi} \sum_{k=-\infty}^{\infty} B(k\omega_0) e^{j k \omega_0 t} \omega_0.$$

When $T_0 \rightarrow \infty$, $b_p(t)$ approaches $b(t)$. This is the same procedure as followed in our derivation of the Fourier transform. Apparently, for periodic signals the complex exponentials have amplitudes $\{c_k\}$ and occur at a discrete set of harmonically related frequencies $k\omega_0$. For aperiodic signals these complex exponentials occur at a continuum of frequencies and have ‘amplitude’ equal to $B(\omega) \cdot (\mathrm{d}\omega/2\pi)$.

In Figure 3.6, increasing T_0 would cause a more ‘dense’ concentration of Fourier series coefficients, scaled with T_0 . But the ‘envelope’ of the scaled coefficients, i.e., the Fourier transform of $b(t)$ shown with the dotted line in Figure 3.6, would remain the same. This envelope is not a function of T_0 , but depends only on the block width T . In the limit case, i.e., when $T_0 \rightarrow \infty$, an infinite number of Fourier series coefficients would exactly describe the ‘envelope’. The Fourier series becomes the Fourier transform.

3.5 The power spectral density function

3.5.1 Derivation

Our main interest in the frequency-domain is in the average amount of power per unit of frequency generated by the product of two stochastic variables $\bar{x}(t)$ and $\bar{y}(t)$. In this section it will be shown, for zero-mean signals, how the power spectral density function $S_{\bar{x}\bar{y}}(\omega)$ is found as a Fourier transform of the covariance function $C_{\bar{x}\bar{y}}(\tau)$. Note that for non zero-mean signals, i.e., the ‘general case’, the power spectral density function is in fact the Fourier transform of the cross-product function $R_{\bar{x}\bar{y}}(\tau)$. Of course, the difference between these definitions only occurs at the zero frequency $\omega = 0$.

Consider two stochastic processes $\bar{x}(t)$ and $\bar{y}(t)$ which are approximated by two signals $\bar{a}(t)$ and $\bar{b}(t)$,

$$\begin{aligned} \text{if } -T \leq t \leq +T, \quad \bar{a}(t) &= \bar{x}(t) & \text{else} \quad \bar{a}(t) &= 0, \\ \bar{b}(t) &= \bar{y}(t) & \bar{b}(t) &= 0. \end{aligned} \quad (3.18)$$

On the time interval $-T \leq t \leq T - \tau$ it follows that,

$$\bar{a}(t) \bar{b}(t + \tau) = \bar{x}(t) \bar{y}(t + \tau). \quad (3.19)$$

The covariance function $C_{\bar{a}\bar{b}}(\tau)$ can then be written as,

$$C_{\bar{a}\bar{b}}(\tau) = \frac{1}{2T - \tau} \int_{-T}^{T-\tau} (\bar{a}(t) - \mu_{\bar{a}})(\bar{b}(t + \tau) - \mu_{\bar{b}}) \, dt.$$

assuming the signals are zero-mean (if this is not the case, it is easy to correct for an offset), the covariance function $C_{\bar{a}\bar{b}}(\tau)$ equals the cross-product function $R_{\bar{a}\bar{b}}(\tau)$ and is written as:

$$C_{\bar{a}\bar{b}}(\tau) = \frac{1}{2T - \tau} \int_{-T}^{T-\tau} \bar{a}(t)\bar{b}(t + \tau) \, dt \quad (= R_{\bar{a}\bar{b}}(\tau)). \quad (3.20)$$

Apply the inverse Fourier transform on $\bar{B}(\omega)$, Equation (3.17),

$$\bar{b}(t + \tau) = \frac{1}{2\pi} \int_{-\infty}^{+\infty} \bar{B}(\omega) e^{j\omega(t+\tau)} d\omega. \quad (3.21)$$

Substitute this result in Equation (3.20):

$$C_{\bar{a}\bar{b}}(\tau) = \frac{1}{2T - \tau} \int_{-T}^{T-\tau} \bar{a}(t) \left(\frac{1}{2\pi} \int_{-\infty}^{+\infty} \bar{B}(\omega) e^{j\omega\tau} d\omega \right) e^{j\omega t} dt, \quad (3.22)$$

Changing the order of integration yields:

$$C_{\bar{a}\bar{b}}(\tau) = \frac{1}{2\pi} \frac{1}{2T - \tau} \int_{-\infty}^{+\infty} \bar{B}(\omega) e^{j\omega\tau} \left(\int_{-T}^{T-\tau} \bar{a}(t) e^{j\omega t} dt \right) d\omega. \quad (3.23)$$

The second integral is recognized as the following Fourier transform (c.f. Equation (3.16)):

$$\int_{-T}^{T-\tau} \bar{a}(t) e^{j\omega t} dt = \bar{A}(-\omega), \quad \text{for } T \rightarrow \infty. \quad (3.24)$$

For the limit $T \rightarrow \infty$ the covariance function $C_{\bar{a}\bar{b}}(\tau)$ equals $C_{\bar{x}\bar{y}}(\tau)$:

$$C_{\bar{x}\bar{y}}(\tau) = \lim_{T \rightarrow \infty} C_{\bar{a}\bar{b}}(\tau) = \lim_{T \rightarrow \infty} \frac{1}{2T} \frac{1}{2\pi} \int_{-\infty}^{+\infty} \bar{B}(\omega) \bar{A}(-\omega) e^{j\omega\tau} d\omega. \quad (3.25)$$

At this moment we introduce the power spectral density function $S_{\bar{x}\bar{y}}(\omega)$ as:

$$S_{\bar{x}\bar{y}}(\omega) = \lim_{T \rightarrow \infty} \frac{1}{2T} \bar{B}(\omega) \bar{A}(-\omega). \quad (3.26)$$

Substitution of definition (3.26) in equation (3.25) yields the relation between the covariance function $C_{\bar{x}\bar{y}}(\tau)$ and the power spectral density function $S_{\bar{x}\bar{y}}(\omega)$,

$$S_{\bar{x}\bar{y}}(\omega) = \mathcal{F}\{C_{\bar{x}\bar{y}}(\tau)\} = \int_{-\infty}^{+\infty} C_{\bar{x}\bar{y}}(\tau) e^{-j\omega\tau} d\tau \quad (3.27)$$

$$C_{\bar{x}\bar{y}}(\tau) = \mathcal{F}^{-1}\{S_{\bar{x}\bar{y}}(\omega)\} = \frac{1}{2\pi} \int_{-\infty}^{+\infty} S_{\bar{x}\bar{y}}(\omega) e^{j\omega\tau} d\omega \quad (3.28)$$

3.5.2 Auto- and cross-power spectral density functions

Similar to the treatment of correlation functions in Section 2.10 we may distinguish two different situations. First:

$$\begin{cases} \bar{x}(t) &= \bar{x}(t) \\ \bar{y}(t) &= \bar{x}(t + \tau), \end{cases} \quad (3.29)$$

where only one signal is considered, resulting in the auto-covariance function $C_{\bar{x}\bar{x}}(\tau)$ and the auto-power spectral density function $S_{\bar{x}\bar{x}}(\omega)$.

Second:

$$\begin{cases} \bar{x}(t) &= \bar{x}(t) \\ \bar{y}(t) &= \bar{y}(t + \tau), \end{cases} \quad (3.30)$$

in which two different signals are considered giving rise to the cross-covariance function $C_{\bar{x}\bar{y}}(\tau)$ and the cross-power spectral density function $S_{\bar{x}\bar{y}}(\omega)$.

Some of the most important properties of the power spectral density function are summarized in Table 3.3.

3.5.3 Integrating the power spectral density function

From the formula for the auto-power spectral density function (Table 3.3):

$$S_{\bar{x}\bar{x}}(\omega) = \lim_{T \rightarrow \infty} \frac{1}{2T} \bar{A}(\omega) \bar{A}(-\omega) = \lim_{T \rightarrow \infty} \frac{1}{2T} |\bar{A}(\omega)|^2, \quad (3.31)$$

its interpretation as the ‘time-average amount of power as function of frequency ω ’, becomes clear.

Furthermore, in Section 2.12 the variance was expressed as:

$$\sigma_x^2 = C_{\bar{x}\bar{x}}(\tau = 0).$$

Substituting this result in Equation 3.28 yields:

$$\sigma_x^2 = \frac{1}{2\pi} \int_{-\infty}^{+\infty} S_{\bar{x}\bar{x}}(\omega) d\omega = \frac{1}{\pi} \int_0^{+\infty} S_{\bar{x}\bar{x}}(\omega) d\omega, \quad (3.32)$$

an important result, as we now have obtained a method for determining the variance of a signal *in the frequency-domain* by integrating the auto power spectral density function.

3.6 Dynamic system analysis in the frequency-domain

The dynamics of a system can be studied in the frequency-domain by examining the power spectral density of the system output signal resulting from an input signal with a given, or known, power spectral density.

Suppose that the relation between the input signal $\bar{u}(t)$ and the output signal $\bar{y}(t)$ is given by the system’s impulse response function $h(t)$. The corresponding description in

the frequency-domain of linear dynamic systems can be based on either the Laplace- or the Fourier transform,

$$\text{Laplace} : Y(s) = H(s) U(s) \quad (3.33)$$

$$\text{Fourier} : Y(\omega) = H(\omega) U(\omega) \quad (3.34)$$

The Laplace transform $H(s)$ is called the ‘transfer function’, while the Fourier transform $H(\omega)$ is referred to as the ‘frequency response function’ (FRF). A system description based on the Laplace transform is more or less equivalent to a description based on the Fourier transform. However, the more general Laplace transform is particularly well-suited to study transient phenomena while the Fourier transform is more conveniently used for frequency responses. In this section we will constrain our problem to time-invariant responses only and make use of the Fourier transform.

Let us first concentrate on calculating the expected value $\mu_{\bar{y}}$ of the system output signal $\bar{y}(t)$,

$$\begin{aligned} \mu_{\bar{y}} &= E\{\bar{y}(t)\} \\ &= E\{\bar{u}(t) * h(t)\} \\ &= E\left\{\int_{-\infty}^{+\infty} \bar{u}(t - \tau) h(\tau) d\tau\right\} \\ &= \int_{-\infty}^{+\infty} E\{\bar{u}(t - \tau)\} h(\tau) d\tau \\ &= \mu_{\bar{u}} \int_{-\infty}^{+\infty} h(\tau) d\tau \end{aligned} \quad (3.35)$$

This result will form the basis for an equivalent expression in the frequency-domain. For that purpose the Fourier transform of the impulse response is used:

$$H(\omega) = \int_{-\infty}^{+\infty} h(\tau) e^{-j\omega\tau} d\tau \quad (3.36)$$

Substitution of $\omega = 0$ yields:

$$H(0) = \int_{-\infty}^{+\infty} h(\tau) d\tau. \quad (3.37)$$

The relation between the expected values $\mu_{\bar{u}}$ and $\mu_{\bar{y}}$ in the frequency-domain is then:

$$\mu_{\bar{y}} = H(0) \mu_{\bar{u}}. \quad (3.38)$$

Next, we will search for a similar relation between the input power spectral density function $S_{\bar{u}\bar{u}}(\omega)$ and the output power spectral density function $S_{\bar{y}\bar{y}}(\omega)$, for zero-mean random processes $\bar{u}(t)$ and $\bar{y}(t)$, so that the product functions $R_{\bar{u}\bar{y}}(\tau)$, $R_{\bar{y}\bar{u}}(\tau)$ and $R_{\bar{y}\bar{y}}(\tau)$ equal the covariance functions $C_{\bar{u}\bar{y}}(\tau)$, $C_{\bar{y}\bar{u}}(\tau)$ and $C_{\bar{y}\bar{y}}(\tau)$ (in practice, if stochastic processes are not zero-mean, the average may be subtracted from all measured values to ‘normalize’ the signal). For that purpose, the covariance functions $C_{\bar{u}\bar{y}}(\tau)$, $C_{\bar{y}\bar{u}}(\tau)$ and $C_{\bar{y}\bar{y}}(\tau)$ will first be considered in the time domain.

$$\begin{aligned} C_{\bar{u}\bar{y}}(\tau) &= E\{\bar{u}(t) \bar{y}(t + \tau)\} \\ &= E\{\bar{u}(t) \int_{-\infty}^{+\infty} \bar{u}(t + \tau - \theta) h(\theta) d\theta\} \\ &= \int_{-\infty}^{+\infty} E\{\bar{u}(t) \bar{u}(t + \tau - \theta)\} h(\theta) d\theta \\ &= \int_{-\infty}^{+\infty} C_{\bar{u}\bar{u}}(\tau - \theta) h(\theta) d\theta \\ &= C_{\bar{u}\bar{u}}(\tau) * h(\tau). \end{aligned} \quad (3.39)$$

$$\begin{aligned} C_{\bar{y}\bar{u}}(\tau) &= C_{\bar{u}\bar{y}}(-\tau) \\ &= C_{\bar{u}\bar{u}}(-\tau) * h(-\tau) \\ &= C_{\bar{u}\bar{u}}(\tau) * h(-\tau). \end{aligned} \quad (3.40)$$

$$\begin{aligned} C_{\bar{y}\bar{y}}(\tau) &= E\{\bar{y}(t) \bar{y}(t + \tau)\} \\ &= E\{\bar{y}(t) \int_{-\infty}^{+\infty} \bar{u}(t + \tau - \theta) h(\theta) d\theta\} \end{aligned}$$

$$\begin{aligned}
&= \int_{-\infty}^{+\infty} \mathbb{E}\{\bar{y}(t) \bar{u}(t + \tau - \theta)\} h(\theta) d\theta \\
&= \int_{-\infty}^{+\infty} C_{\bar{y}\bar{u}}(\tau - \theta) h(\theta) d\theta \\
&= C_{\bar{y}\bar{u}}(\tau) * h(\tau) \\
&= C_{\bar{u}\bar{u}}(\tau) * h(-\tau) * h(\tau). \tag{3.41}
\end{aligned}$$

From the previous section, we have seen how the power spectral density function arises as a Fourier transform of the covariance function. Keeping in mind that the Fourier transform of a convolution product yields a product of Fourier transforms (Table 3.1), the power spectral density functions $S_{\bar{u}\bar{y}}(\omega)$, $S_{\bar{y}\bar{u}}(\omega)$ and $S_{\bar{y}\bar{y}}(\omega)$ become:

$$\begin{aligned}
S_{\bar{u}\bar{y}}(\omega) &= \mathcal{F}\{C_{\bar{u}\bar{y}}(\tau)\} \\
&= \mathcal{F}\{C_{\bar{u}\bar{u}}(\tau) * h(\tau)\} \\
&= H(\omega) S_{\bar{u}\bar{u}}(\omega). \tag{3.42}
\end{aligned}$$

$$\begin{aligned}
S_{\bar{y}\bar{u}}(\omega) &= \mathcal{F}\{C_{\bar{y}\bar{u}}(\tau)\} \\
&= \mathcal{F}\{C_{\bar{u}\bar{u}}(\tau) * h(-\tau)\} \\
&= H(-\omega) S_{\bar{u}\bar{u}}(\omega). \tag{3.43}
\end{aligned}$$

$$\begin{aligned}
S_{\bar{y}\bar{y}}(\omega) &= \mathcal{F}\{C_{\bar{y}\bar{y}}(\tau)\} \\
&= \mathcal{F}\{C_{\bar{u}\bar{u}}(\tau) * h(-\tau) * h(\tau)\} \\
&= H(-\omega) H(\omega) S_{\bar{u}\bar{u}}(\omega) \\
&= |H(\omega)|^2 S_{\bar{u}\bar{u}}(\omega). \tag{3.44}
\end{aligned}$$

To find the variance of an output signal $\sigma_{\bar{y}}^2$ we can substitute (3.44) in (3.32):

$$\sigma_{\bar{y}}^2 = \frac{1}{\pi} \int_0^{+\infty} S_{\bar{y}\bar{y}}(\omega) d\omega = \frac{1}{\pi} \int_0^{+\infty} |H(\omega)|^2 S_{\bar{u}\bar{u}}(\omega) d\omega \tag{3.45}$$

Some remarks concerning the Fourier transform $H(\omega)$ appearing in Equations (3.42), (3.43) and (3.44) should be made here.

A practical calculation of the frequency response function $H(\omega)$ would require a rather cumbersome calculation of the system's impulse response function followed by a difficult application of the general Fourier transform, Equation (3.16). There exists, however, a much more convenient procedure based on the more general Laplace transform defined as:

$$H(s) = \mathcal{L}\{h(t)\} = \int_{-\infty}^{+\infty} h(t) e^{-st} dt. \quad (3.46)$$

The Laplace transform is particularly well-suited to find the transfer function $H(s)$ of a differential equation directly, see (Boyce & DiPrima, 1977).

The Laplace transform bears a straightforward relationship with the Fourier transform when the complex variable s is restricted to be purely imaginary. To see this relationship, consider $X(s)$ as specified in Equation (3.46) with s expressed as $s = j\omega$ so that:

$$H(\omega) = \int_{-\infty}^{+\infty} h(t) e^{-j\omega t} dt. \quad (3.47)$$

We recognize the right hand side of Equation (3.47) as the Fourier transform, Equation (3.16). Table 3.4 summarizes the results found in this section.

3.7 White noise, colored noise and shaping filters

3.7.1 White noise

In Section 2.12 the (theoretical) concept of white noise was introduced. The auto covariance function of white noise had the form of a Dirac pulse and was given by Equation (2.31):

$$C_{\bar{w}\bar{w}}(\tau) = W \delta(\tau).$$

Again, using Table 3.2, the power spectral density of white noise is now given by:

$$S_{\bar{w}\bar{w}}(\omega) = \int_{-\infty}^{+\infty} C_{\bar{w}\bar{w}}(\tau) e^{-j\omega\tau} d\tau = W. \quad (3.48)$$

The spectral density of white noise is constant over the total frequency range $-\infty < \omega < +\infty$, see Figure 3.7. So, a signal that is very 'narrow' in the time domain, like the auto-covariance function of white noise, becomes very 'broad' in the frequency domain. This is one of the many symmetries in the Fourier transform pairs.

Using (3.32):

$$\sigma_{\bar{w}}^2 = \frac{1}{\pi} \int_0^{+\infty} S_{\bar{w}\bar{w}}(\omega) d\omega = \infty,$$

confirming in the frequency-domain the result of Section 2.12 that white noise has infinite variance and cannot physically exist.

A signal is often called ‘white’ if it has a spectral density:

$$S_{\bar{w}\bar{w}}(\omega) = W,$$

over a frequency range $-\omega_1 < \omega < \omega_1$, where ω_1 extends well past all the frequencies of interest (Kwakernaak & Sivan, 1972).

3.7.2 Colored noise and shaping filters

Consider a linear time-invariant (LTI) system with input $\bar{u}(t)$ and output $\bar{y}(t)$, Figure 3.8. Assume that the input $\bar{u}(t)$ is a white noise process $\bar{w}(t)$ with the power spectral density:

$$S_{\bar{u}\bar{u}}(\omega) = W \quad \forall \omega.$$

Then according to Equation (3.44) the power spectral density of the output $\bar{y}(t)$ can be described as:

$$S_{\bar{y}\bar{y}}(\omega) = |H(\omega)|^2 \cdot W.$$

The variance of $\bar{y}(t)$ can then be calculated using Equation (3.32):

$$\sigma_{\bar{y}}^2 = W \cdot \left\{ \frac{1}{2\pi} \int_{-\infty}^{+\infty} |H(\omega)|^2 d\omega \right\},$$

where the integral between brackets corresponds to the integral I in Table 3.6. Hence, the output of the LTI system is ‘filtered’ white noise, also known as colored noise. The frequency response function $H(\omega)$ is known as the shaping filter.

3.8 Frequency-domain analysis using PSDs

3.8.1 Estimation of the FRF using PSDs

Consider an LTI system, characterized by its impulse response function $h(t)$, or, equivalently, its frequency response function $H(\omega)$. The system has a stochastic input signal $\bar{u}(t)$, and therefore a stochastic response $\bar{x}(t)$. Now, assume we can not measure $\bar{x}(t)$. Rather, the measurement $\bar{y}(t)$ is corrupted with measurement errors $\bar{n}(t)$. I.e., the measured signal $\bar{y}(t)$ equals $\bar{x}(t) + \bar{n}(t)$, Figure 3.9. From the measured “input” and “output”

signals, $\bar{u}(t)$ and $\bar{y}(t)$, respectively, can we obtain an estimate of the system frequency response function?

First, the measured output signal with random noise can be described as:

$$\bar{y}(t) = \bar{x}(t) + \bar{n}(t) = \bar{u}(t) \star h(t) + \bar{n}(t). \quad (3.49)$$

$$\bar{y}(t) = \int_{-\infty}^{+\infty} h(\sigma) \bar{u}(t - \sigma) d\sigma + \bar{n}(t). \quad (3.50)$$

Shifting Equation (3.50) with time τ yields:

$$\bar{y}(t + \tau) = \int_{-\infty}^{+\infty} h(\sigma) \bar{u}(t + \tau - \sigma) d\sigma + \bar{n}(t + \tau). \quad (3.51)$$

Then multiply Equation (3.51) with a ‘help signal’, $\bar{z}(t)$, of which the properties will be selected later:

$$\bar{z}(t) \bar{y}(t + \tau) = \int_{-\infty}^{+\infty} h(\sigma) \bar{z}(t) \bar{u}(t + \tau - \sigma) d\sigma + \bar{z}(t) \bar{n}(t + \tau).$$

Taking the expectation of this equation yields (for zero-mean signals):

$$C_{\bar{z}\bar{y}}(\tau) = \int_{-\infty}^{+\infty} h(\sigma) C_{\bar{z}\bar{u}}(\tau - \sigma) d\sigma + C_{\bar{z}\bar{n}}(\tau). \quad (3.52)$$

We can now eliminate the noise effect by choosing a signal $\bar{z}(t)$ that is uncorrelated with $\bar{n}(t)$. Assume that $\bar{u}(t)$ is uncorrelated with $\bar{n}(t)$ (which is often the case when considering the situation of corrupted measurements), we then obtain (with $C_{\bar{u}\bar{n}}(\tau)=0$):

$$C_{\bar{u}\bar{y}}(\tau) = \int_{-\infty}^{+\infty} h(\sigma) C_{\bar{u}\bar{u}}(\tau - \sigma) d\sigma.$$

In the frequency domain this becomes Equation (3.42):

$$S_{\bar{u}\bar{y}}(\omega) = H(\omega) \cdot S_{\bar{u}\bar{u}}(\omega).$$

Hence, we can obtain the frequency response function using the quotient of two PSDs:

$$H(\omega) = \frac{S_{\bar{u}\bar{y}}(\omega)}{S_{\bar{u}\bar{u}}(\omega)}.$$

(3.53)

3.8.2 Estimation of the noise spectrum PSDs

Consider the same LTI system from the previous section above. Now, the question is: How can we obtain an estimate of the PSD of the noise signal $\bar{n}(t)$?

To solve this, Equation (3.49) will be shifted with time τ :

$$\begin{aligned}\bar{y}(t) &= \bar{x}(t) + \bar{n}(t) \\ \bar{y}(t + \tau) &= \bar{x}(t + \tau) + \bar{n}(t + \tau),\end{aligned}\tag{3.54}$$

so that the following holds:

$$\bar{y}(t)\bar{y}(t + \tau) = \bar{x}(t)\bar{x}(t + \tau) + \bar{n}(t)\bar{n}(t + \tau) + \bar{x}(t)\bar{n}(t + \tau) + \bar{n}(t)\bar{x}(t + \tau).\tag{3.55}$$

Then taking the expectation of Equation (3.55) and assuming that all means are zero, the auto covariance of the output signal is:

$$C_{\bar{y}\bar{y}}(\tau) = C_{\bar{x}\bar{x}}(\tau) + C_{\bar{n}\bar{n}}(\tau) + C_{\bar{x}\bar{n}}(\tau) + C_{\bar{n}\bar{x}}(\tau).\tag{3.56}$$

When $\bar{u}(t)$ and $\bar{n}(t)$ are uncorrelated, so are $\bar{x}(t)$ and $\bar{n}(t)$, i.e., $C_{\bar{x}\bar{n}}(\tau) = C_{\bar{n}\bar{x}}(\tau) = 0$:

$$C_{\bar{y}\bar{y}}(\tau) = C_{\bar{x}\bar{x}}(\tau) + C_{\bar{n}\bar{n}}(\tau)\tag{3.57}$$

In the frequency domain this becomes:

$$S_{\bar{y}\bar{y}}(\omega) = S_{\bar{x}\bar{x}}(\omega) + S_{\bar{n}\bar{n}}(\omega),\tag{3.58}$$

where (Equation (3.44)):

$$S_{\bar{x}\bar{x}}(\omega) = |H(\omega)|^2 S_{\bar{u}\bar{u}}(\omega).$$

Hence, we can obtain the PSD of the unknown noise using:

$S_{\bar{n}\bar{n}}(\omega) = S_{\bar{y}\bar{y}}(\omega) - |H(\omega)|^2 S_{\bar{u}\bar{u}}(\omega)$

$$\tag{3.59}$$

3.8.3 Definition of the Coherence

Again, consider the LTI system from Section 3.8.1. Now, the question is: what is the contribution of the systems's response to the measured output signal as compared to the contribution of the noise signal?

The answer is expressed in the quotient of $S_{\bar{x}\bar{x}}(\omega)$ and $S_{\bar{y}\bar{y}}(\omega)$:

$$\begin{aligned}\frac{S_{\bar{x}\bar{x}}(\omega)}{S_{\bar{y}\bar{y}}(\omega)} &= \frac{|H(\omega)|^2 S_{\bar{u}\bar{u}}(\omega)}{S_{\bar{y}\bar{y}}(\omega)} \\ &= \frac{\frac{|S_{\bar{u}\bar{y}}(\omega)|^2}{S_{\bar{u}\bar{u}}^2(\omega)} S_{\bar{u}\bar{u}}(\omega)}{S_{\bar{y}\bar{y}}(\omega)} \\ &= \frac{|S_{\bar{u}\bar{y}}(\omega)|^2}{S_{\bar{u}\bar{u}}(\omega) S_{\bar{y}\bar{y}}(\omega)}.\end{aligned}\tag{3.60}$$

The square root of this quotient is referred to as the coherence $\Gamma_{\bar{u}\bar{y}}(\omega)$ between the system input $\bar{u}(t)$ and its measured output $\bar{y}(t)$:

$$\boxed{\Gamma_{\bar{u}\bar{y}}(\omega) = \sqrt{\frac{|S_{\bar{u}\bar{y}}(\omega)|^2}{S_{\bar{u}\bar{u}}(\omega)S_{\bar{y}\bar{y}}(\omega)}}} \quad (3.61)$$

The coherence is a measure of the linear relationship between the input signal and the output signal of a system. It always has a value between 0 (no coherence) and 1 (full coherence).

3.9 Examples and problems

3.9.1 Example 3.1

In Example 2.2 a ‘stochastic’ ergodic process was examined with the time function,

$$\bar{x}(t) = \sin(2\pi t) + 1,$$

as a “realization” of a non-zero-mean process ($\mu_{\bar{x}} = 1$).

The power spectral density of a zero-mean stochastic signal can be determined with the auto covariance using Equation (3.27):

$$S_{\bar{x}\bar{x}}(\omega) = \int_{-\infty}^{+\infty} C_{\bar{x}\bar{x}}(\tau) e^{-j\omega\tau} d\tau.$$

However, for a non-zero-mean signal the power spectral density needs to be corrected for the mean. This can be done by using the relation between the auto product- and the auto covariance function:

$$R_{\bar{x}\bar{x}}(\tau) = C_{\bar{x}\bar{x}}(\tau) + \mu_{\bar{x}}^2.$$

The auto covariance function of the stochastic process was found to be Equation (2.14.2):

$$C_{\bar{x}\bar{x}}(\tau) = \frac{1}{2} \cos(2\pi\tau),$$

and the spectral density is then:

$$\begin{aligned} S_{\bar{x}\bar{x}}(\omega) &= \int_{-\infty}^{+\infty} R_{\bar{x}\bar{x}}(\tau) e^{-j\omega\tau} d\tau \\ &= \int_{-\infty}^{+\infty} \left(\frac{1}{2} \cos(2\pi\tau) + 1 \right) e^{-j\omega\tau} d\tau \\ &= \int_{-\infty}^{+\infty} \frac{1}{2} \cos(2\pi\tau) e^{-j\omega\tau} d\tau + \int_{-\infty}^{+\infty} 1 e^{-j\omega\tau} d\tau. \end{aligned} \quad (3.62)$$

Using the standard Fourier-transforms in Table 3.2, this power spectral density can be expressed using the Dirac-function:

$$S_{\bar{x}\bar{x}}(\omega) = \frac{\pi}{2} (\delta(\omega - 2\pi) + \delta(\omega + 2\pi)) + 2\pi\delta(\omega), \quad (3.63)$$

where the second term of Equation (3.63) represents a weighted impulse at $\omega = 0$ rad/s due to the mean, see Figure 3.10. Again, a ‘constant’ in the time domain becomes a weighted dirac-pulse at ‘zero frequency’ in the frequency domain.

3.9.2 Example 3.2

If we know the auto spectral density $S_{\bar{x}\bar{x}}(\omega)$ of a stationary random process we can use this to calculate the variance of the process according to Equation (3.32). Also, the spectral density of the derived process can be determined by differentiating \bar{x} . Starting with the covariance function:

$$C_{\bar{x}\bar{x}}(\tau) = E\{\bar{x}(t) \bar{x}(t + \tau)\},$$

differentiate with respect to τ yields:

$$\frac{d}{d\tau} C_{\bar{x}\bar{x}}(\tau) = E\{\bar{x}(t) \dot{\bar{x}}(t + \tau)\}.$$

For a stationary process holds: $E\{\bar{x}(t) \dot{\bar{x}}(t + \tau)\} = E\{\bar{x}(t - \tau) \dot{\bar{x}}(t)\}$. Differentiating again with respect to τ gives:

$$\frac{d^2}{d\tau^2} C_{\bar{x}\bar{x}}(\tau) = -E\{\dot{\bar{x}}(t - \tau) \dot{\bar{x}}(t)\} = -C_{\dot{\bar{x}}\dot{\bar{x}}}(\tau), \quad (3.64)$$

where $C_{\dot{\bar{x}}\dot{\bar{x}}}(\tau)$ is the covariance function of the derived process. The next step is to consider Equation (3.28):

$$C_{\bar{x}\bar{x}}(\tau) = \frac{1}{2\pi} \int_{-\infty}^{+\infty} S_{\bar{x}\bar{x}}(\omega) e^{j\omega\tau} d\omega.$$

Differentiating twice with respect to τ yields:

$$\frac{d^2}{d\tau^2} C_{\bar{x}\bar{x}}(\tau) = -\frac{1}{2\pi} \int_{-\infty}^{+\infty} \omega^2 S_{\bar{x}\bar{x}}(\omega) e^{j\omega\tau} d\omega = -C_{\dot{\bar{x}}\dot{\bar{x}}}(\tau). \quad (3.65)$$

Writing: $C_{\dot{\bar{x}}\dot{\bar{x}}}(\tau) = \mathcal{F}^{-1}\{S_{\dot{\bar{x}}\dot{\bar{x}}}(\omega)\}$ (recall Equation (3.28)) we see that:

$$S_{\dot{\bar{x}}\dot{\bar{x}}}(\omega) = \omega^2 S_{\bar{x}\bar{x}}(\omega), \quad (3.66)$$

or in words: the auto power spectral density of a differentiated process is ω^2 times the auto power spectral density of the original process. This result may also be verified by noticing that the Fourier transform of the time derivative of a signal is: $\mathcal{F}\{\frac{dx}{dt}\} = j\omega X(\omega)$, where $X(\omega)$ is $\mathcal{F}\{x(t)\}$, Table 3.1.

3.9.3 Example 3.3

When the auto power spectral density of an input signal \bar{u} acting on a system is known, the cross power spectral density $S_{\bar{u}\bar{y}}$ of input signal \bar{u} and output signal \bar{y} and the auto spectral density $S_{\bar{y}\bar{y}}$ of the output signal can be calculated with Equations (3.42) and (3.44):

$$\begin{aligned} S_{\bar{u}\bar{y}}(\omega) &= H(\omega) S_{\bar{u}\bar{u}}(\omega), \\ S_{\bar{y}\bar{y}}(\omega) &= |H(\omega)|^2 S_{\bar{u}\bar{u}}(\omega), \end{aligned}$$

where $H(\omega)$ is the frequency response function of the system.

Consider the case that we want to know the spectral density of the normal acceleration of an aircraft taxiing at a constant speed V over a runway with surface irregularities. A typical profile of these irregularities is shown in Figure 3.11 where the height \bar{u} of the surface above a horizontal datum is plotted as a function of the distance x along the runway. Instead of varying with time, the input is a function of distance. Long wavelength irregularities correspond to low-frequency components in the time domain and short wavelength irregularities correspond to high-frequency components. The angular frequency ω is replaced by the wavenumber γ (rad/m), expressing the rate of change varying with distance. Spectral densities can now be expressed using γ instead of ω :

$$S_{\bar{u}\bar{u}}(\gamma) = \int_{-\infty}^{+\infty} C_{\bar{u}\bar{u}}(\xi) e^{-j\gamma\xi} d\xi, \quad (3.67)$$

with:

$$C_{\bar{u}\bar{u}}(\xi) = E\{\bar{u}(x) \bar{u}(x + \xi)\}, \quad (3.68)$$

where ξ is the ‘spatial lag’, analogous to the time lag τ . A spectral density for a particular runway was found to be (see (AGARD, 1975) and Figure 3.12):

$$S_{\bar{u}\bar{u}}(\gamma) = \frac{6.3 \cdot 10^{-4}}{(1 + 0.16\gamma^2)(1 + 49\gamma^2)} \left[\frac{\text{m}^2}{\text{rad}/\text{m}} \right]. \quad (3.69)$$

We can relate the time with the distance using the constant speed V :

$$\omega = V\gamma \quad \text{and} \quad \tau = \frac{\xi}{V}, \quad (3.70)$$

or:

$$S_{\bar{u}\bar{u}}(\omega) = \int_{-\infty}^{+\infty} C_{\bar{u}\bar{u}}(\tau) e^{-j(V\gamma)\frac{\xi}{V}} \cdot \frac{1}{V} d\xi = \frac{1}{V} S_{\bar{u}\bar{u}}(\gamma = \frac{\omega}{V}). \quad (3.71)$$

Substitution of Equation (3.69) in Equation (3.71) yields:

$$S_{\bar{u}\bar{u}}(\omega) = \frac{1}{V} \cdot \frac{6.3 \cdot 10^{-4}}{[1 + (\tau_1\omega)^2][1 + (\tau_2\omega)^2]} \left[\frac{\text{m}^2}{\text{rad}/\text{s}} \right], \quad (3.72)$$

with $\tau_1 = 0.4/V$ and $\tau_2 = 7/V$.

The main landing gear suspension system can be modelled as a one-degree-of-freedom mass-damper-spring system (Baarspul, 1990), see Figure 3.13:

$$m\ddot{y} + c\dot{y} + ky = c\dot{u} + ku, \quad (3.73)$$

where the input signal to the suspension system is the time varying function $\bar{u}(Vt) = \bar{u}(x)$ of surface irregularities and the output signal $\bar{y}(t)$ the displacement above a horizontal datum. The transfer function of this system is given by:

$$H_{\bar{y}\bar{u}}(s) = \frac{cs + k}{ms^2 + cs + k}. \quad (3.74)$$

The cross power spectral density of the surface irregularities and the vertical displacement of the aircraft and the auto spectral density of this displacement is found combining Equations (3.42), (3.44), (3.72) and (3.74) and substituting $s = j\omega$:

$$S_{\bar{u}\bar{y}}(\omega) = \frac{cj\omega + k}{-m\omega^2 + cj\omega + k} \cdot \frac{1}{V} \cdot \frac{6.3 \cdot 10^{-4}}{[1 + (\tau_1\omega)^2][1 + (\tau_2\omega)^2]} \quad (3.75)$$

$$\begin{aligned} S_{\bar{y}\bar{y}}(\omega) &= |H_{\bar{y}\bar{u}}(\omega)|^2 S_{\bar{u}\bar{u}}(\omega) = H_{\bar{y}\bar{u}}(\omega) H_{\bar{y}\bar{u}}(-\omega) S_{\bar{u}\bar{u}}(\omega) = \\ &= \frac{cj\omega + k}{-m\omega^2 + cj\omega + k} \cdot \frac{-cj\omega + k}{-m\omega^2 - cj\omega + k} \cdot \frac{1}{V} \cdot \frac{6.3 \cdot 10^{-4}}{[1 + (\tau_1\omega)^2][1 + (\tau_2\omega)^2]} \\ &= \frac{c^2\omega^2 + k^2}{m^2\omega^4 + (c^2 - 2mk)\omega^2 + k^2} \cdot \frac{1}{V} \cdot \frac{6.3 \cdot 10^{-4}}{[1 + (\tau_1\omega)^2][1 + (\tau_2\omega)^2]}. \end{aligned} \quad (3.76)$$

Keeping in mind that for the normal acceleration a_z we can write:

$$a_z(t) = \ddot{y}(t),$$

we can use (3.66) to find the auto power spectral density of the normal acceleration:

$$S_{\bar{a}_z\bar{a}_z}(\omega) = \omega^4 S_{\bar{y}\bar{y}}(\omega). \quad (3.77)$$

In Figure 3.14 the calculated power spectral densities of Equations (3.75)-(3.77) are plotted with MATLAB for a landing gear suspension system where $m=2290$ kg, $c=20000$ Ns/m and $k=183000$ N/m, approximately according to the landing gear dynamics of the DHC-2 ‘Beaver’ at a taxiing speed of 10 m/s (Baarspul, 1990).

Listing 3.1: Example 3.3

```
% Exempl33.m
%
% Chapter 3
%
% Calculates power spectral densities of displacement and
% acceleration as a result of runway surface irregularities.
```

```
% The landing gear is modelled as a second order 1-DOF
% mass-spring-damper system, the input power spectral
% density is taken from AGARD-R-632.
% The output power spectral density is calculated with
%
%           Syy(w) = |H(w)|^2 * Suu(w)
%
% while the power spectral density of the acceleration is found with
%
%           Saa(w) = w^4 Syy(w)
%
% Revised August 1992, February 2004 [MM], October 2014 [M Rodriguez]

clc; close all; clear all;

disp(' Example 3.3');
disp(' Calculates power spectral densities of displacement and');
disp(' acceleration as a result of runway surface irregularities.');
disp(' The landing gear is modelled as a second order 1-DOF');
disp(' mass-spring-damper system, the input power spectral');
disp(' density is taken from AGARD-R-632.');
disp(' The output power spectral density is calculated with');
disp('');
disp('           Syy(w) = |H(w)|^2 * Suu(w)');
disp('');
disp(' while the power spectral density of the acceleration is');
disp(' found with:');
disp('');
disp('           Saa(w) = w^4 Syy(w)');
disp('');
disp(' This program produces Figure 3.14 of the lecture notes:');
disp(' Aircraft Responses to Atmospheric Turbulence.')

omega=logspace(-2,2,100); % frequency axis

% INPUT POWER SPECTRAL DENSITY OF 'RUNWAY RUMBLE'

% Ground speed. Can be changed.
V = input(' Enter ground speed V [m/s] : ');

tau1=0.4/V; tau2=7/V;
for i=1:100
    Suu(i)=((6.3e-4)/V)/((1+(tau1*omega(i))^2)*(1+(tau2*omega(i))^2));
end

% LANDING GEAR DATA. TAKEN FROM DHC-2 'Beaver'
%
% aircraft mass. Can be changed.
m = input(' Enter aircraft mass m [kg] : ');

c=20000; % damping constant. Can be changed.
k=183000; % spring constant. Can be changed.
```

```
% CALCULATION OF FREQUENCY RESPONSE USING TRANSFER FUNCTION H(s)
num=[c k]; den=[m c k];
h=freqs(num,den,omega);

% CALCULATION OF CROSS- AND AUTO POWER SPECTRAL DENSITIES
Suy = h.*Suu;
Syy = (abs(h).^2).*Suu;
Saa = (omega.^4).*Syy;

% PLOTTING RESULTS
clf
subplot(2,2,1);
loglog(omega,real(Suy));
xlabel('frequency, rad/s');
ylabel('Re (Suy)');
axis(10.^[-2 2 -12 0]); axis(axis);
grid
title('Cross P.S.D.')

subplot(2,2,2);
semilogx(omega,imag(Suy));
xlabel('frequency, rad/s');
ylabel('Im (Suy)');
grid
axis([10^{(-2)} 10^2 -2e-6 0]); axis(axis);

subplot(2,2,3);
loglog(omega,Syy);
xlabel('frequency, rad/s');
ylabel('Syy, m^2/Hz');
grid
axis(10.^[-2,2,-12,0]); axis(axis);
title('Auto P.S.D. input')

subplot(2,2,4);
loglog(omega,Saa);
xlabel('frequency, rad/s');
ylabel('Saa, (m^2/s^4)/Hz');
grid
axis(10.^[-2 2 -13 2]); axis(axis);
title('Auto P.S.D. output');

% EOF
```

3.9.4 Problem 3.1

Using MATLAB, investigate the influence of the take-off weight on the variance of the normal acceleration during take-off by integrating the power spectral density found in

Example 3.3:

$$\sigma_{\bar{a}_z}^2 = \frac{1}{\pi} \int_0^{+\infty} S_{\bar{a}_z \bar{a}_z}(\omega) d\omega.$$

Make a plot of the variance as a function of the aircraft's total mass.

3.9.5 Problem 3.2

Approximate the ‘runway rumble’ of Example 3.3 with ‘practical’ white noise of a suitable intensity for its power spectral density,

$$S_{\bar{w}\bar{w}}(\omega) = W \quad \text{for} \quad -\omega_0 < \omega < \omega_0,$$

and calculate the variance of the normal acceleration using Tables 3.5 and 3.6.

3.10 Summary

In this chapter the theory of spectral analysis for continuous-time stochastic processes was introduced. After the theory of Fourier analysis and the power spectral density function were introduced, the relationship between covariance functions and power spectral density functions was discussed. Finally, the relationship between input- and output power spectral density functions, which appear to be related by the system impulse response functions, was established.

Property	Signal	Fourier Transform
Linearity	$a x(t) + b y(t)$	$a X(\omega) + b Y(\omega)$
Time delay	$x(t - t_0)$	$\{e^{-j\omega t_0}\} X(\omega)$
Multiplication	$x(t) y(t)$	$\frac{1}{2\pi} X(\omega) * Y(\omega)$
Convolution	$x(t) * y(t)$	$X(\omega) Y(\omega)$
Time derivative	$\dot{x}(t)$	$j\omega X(\omega)$
Integral of Parseval	$\int_{-\infty}^{+\infty} x^2(t) dt$	$\frac{1}{2\pi} \int_{-\infty}^{+\infty} X(\omega) ^2 d\omega$

Table 3.1: Properties of the Fourier transform.

Signal $\bar{x}(t)$	Fourier transform $X(\omega)$	Fourier transform $X(f)$
1	$2\pi \delta(\omega)^3$	$\delta(f)$
$\delta(t)$	1	1
$\sum_{n=-\infty}^{+\infty} \delta(t - nT)$	$\frac{2\pi}{T} \sum_{k=-\infty}^{+\infty} \delta(\omega - k\frac{2\pi}{T})$	$\frac{1}{T} \sum_{k=-\infty}^{+\infty} \delta(f - k\frac{1}{T})$
$\cos k\omega_0 t$	$\pi[\delta(\omega - k\omega_0) + \delta(\omega + k\omega_0)]$	$\frac{1}{2}[\delta(f - kf_0) + \delta(f + kf_0)]$
$\sin k\omega_0 t$	$\frac{\pi}{j}[\delta(\omega - k\omega_0) - \delta(\omega + k\omega_0)]$	$\frac{1}{2j}[\delta(f - kf_0) + \delta(f + kf_0)]$
$\bar{x}(t) = \begin{cases} 1, & t < \frac{1}{2}T \\ 0, & t > \frac{1}{2}T \end{cases}$ $\frac{W}{2\pi} \text{sinc}\left(\frac{Wt}{2\pi}\right) = \frac{\sin(tW/2)}{\pi t}$	$T \text{sinc}\left(\frac{\omega T}{2\pi}\right) = T \frac{\sin(\omega T/2)}{\omega T/2}$ $\bar{B}(\omega) = \begin{cases} 1, & \omega < \frac{1}{2}W \\ 0, & \omega > \frac{1}{2}W \end{cases}$ with $W=2\pi F$	$T \text{sinc}(fT) = T \frac{\sin(\pi fT)}{\pi fT}$ $\bar{B}(f) = \begin{cases} 1, & f < \frac{1}{2}F \\ 0, & f > \frac{1}{2}F \end{cases}$

Table 3.2: Some basic Fourier transforms.

³The relation between the frequency Dirac-functions $\delta(f)$ and $\delta(\omega)$, with $f = \frac{\omega}{2\pi}$ in Hz is:

$$2\pi\delta(\omega) = \delta\left(\frac{\omega}{2\pi}\right) = \delta(f).$$

This can be derived from integral property of the Dirac-function:

$$\int_{-\infty}^{+\infty} \delta(\omega) d\omega = \int_{-\infty}^{+\infty} \delta(f) df = 1.$$

Auto spectral density function $S_{\bar{x}\bar{x}}(\omega)$	Cross spectral density function $S_{\bar{x}\bar{y}}(\omega)$
$S_{\bar{x}\bar{x}}(\omega) = \int_{-\infty}^{+\infty} C_{\bar{x}\bar{x}}(\tau) e^{-j\omega\tau} d\tau$ $C_{\bar{x}\bar{x}}(\tau) = \frac{1}{2\pi} \int_{-\infty}^{+\infty} S_{\bar{x}\bar{x}}(\omega) e^{j\omega\tau} d\omega$	$S_{\bar{x}\bar{y}}(\omega) = \int_{-\infty}^{+\infty} C_{\bar{x}\bar{y}}(\tau) e^{-j\omega\tau} d\tau$ $C_{\bar{x}\bar{y}}(\tau) = \frac{1}{2\pi} \int_{-\infty}^{+\infty} S_{\bar{x}\bar{y}}(\omega) e^{j\omega\tau} d\omega$
$S_{\bar{x}\bar{x}}(\omega) = \lim_{T \rightarrow \infty} \frac{1}{2T} \bar{A}(\omega) ^2$	$S_{\bar{x}\bar{y}}(\omega) = \lim_{T \rightarrow \infty} \frac{1}{2T} \bar{B}(\omega) \bar{A}(-\omega)$
$S_{\bar{x}\bar{x}}(\omega)$ is a real function $S_{\bar{x}\bar{x}}(\omega) = S_{\bar{x}\bar{x}}(-\omega)$	$S_{\bar{x}\bar{y}}(\omega)$ is a complex function $\begin{aligned} \text{Re } \{S_{\bar{x}\bar{y}}(\omega)\} &= \text{Re } \{S_{\bar{x}\bar{y}}(-\omega)\} \\ \text{Im } \{S_{\bar{x}\bar{y}}(\omega)\} &= -\text{Im } \{S_{\bar{x}\bar{y}}(-\omega)\} \\ S_{\bar{x}\bar{y}}(\omega) &= S_{\bar{y}\bar{x}}(-\omega) = S_{\bar{y}\bar{x}}^*(\omega) \end{aligned}$
$\begin{aligned} \frac{1}{2\pi} \int_{-\infty}^{+\infty} S_{\bar{x}\bar{x}}(\omega) d\omega &= C_{\bar{x}\bar{x}}(0) \\ &= E\{\bar{x}^2\} \\ &= \sigma_x^2 \end{aligned}$	$\begin{aligned} \frac{1}{2\pi} \int_{-\infty}^{+\infty} S_{\bar{x}\bar{y}}(\omega) d\omega &= C_{\bar{x}\bar{y}}(0) \\ &= E\{\bar{x}\bar{y}\} \end{aligned}$

Table 3.3: Properties of the power spectral density function (note that we assume zero-mean signals in this table).

$\mu_{\bar{y}}$	$=$	$H(0) \mu_{\bar{u}}$
$C_{\bar{u}\bar{y}}(\tau)$	$=$	$h(\tau) * C_{\bar{u}\bar{u}}(\tau)$
$C_{\bar{y}\bar{u}}(\tau)$	$=$	$h(-\tau) * C_{\bar{u}\bar{u}}(\tau)$
$C_{\bar{y}\bar{y}}(\tau)$	$=$	$h(-\tau) * h(\tau) * C_{\bar{u}\bar{u}}(\tau)$
$S_{\bar{u}\bar{y}}(\omega)$	$=$	$H(\omega) S_{\bar{u}\bar{u}}(\omega)$
$S_{\bar{y}\bar{u}}(\omega)$	$=$	$H(-\omega) S_{\bar{u}\bar{u}}(\omega)$
$S_{\bar{y}\bar{y}}(\omega)$	$=$	$ H(\omega) ^2 S_{\bar{u}\bar{u}}(\omega)$

Table 3.4: Average value, correlations and spectral densities of linear dynamic system outputs.

$I_1 = \frac{b_0^2}{2a_0a_1}$	
$I_2 = \frac{a_0b_1^2 + a_2b_0^2}{2a_0a_1a_2}$	
$I_3 = \frac{a_0a_3(2b_0b_2 - b_1^2) - a_0a_1b_2^2 - a_2a_3b_0^2}{2a_0a_3(a_0a_3 - a_1a_2)}$	
$I_4 = \frac{a_0b_3^2(a_0a_3 - a_1a_2) + a_0a_1a_4(2b_1b_3 - b_2^2) - a_0a_3a_4(b_1^2 - 2b_0b_2) + a_4b_0^2(a_1a_4 - a_2a_3)}{2a_0a_4(a_0a_3^2 + a_1^2a_4 - a_1a_2a_3)}$	

Table 3.5: Standard integrals for the calculation of the variance.

The list of integrals in Table 3.5 has been derived in (Newland, 1984) for the evaluation of the integral:

$$I_n = \frac{1}{2\pi} \int_{-\infty}^{+\infty} |H(\omega)|^2 d\omega,$$

where $H(s)$ is given rather than $H(\omega)$:

$$H(s) = \frac{b_0 + b_1s + b_2s^2 + b_3s^3 + b_4s^4 + \dots + b_{n-1}s^{n-1}}{a_0 + a_1s + a_2s^2 + a_3s^3 + a_4s^4 + \dots + a_ns^n}.$$

Provided that the transfer function describes a stable system, the integrals have the values stated in Table 3.5.

$H(\omega)$	I
$\frac{1}{1+j\omega\tau}$	$\frac{1}{2\tau}$
$\frac{1}{1+2\zeta\frac{j\omega}{\omega_0}+\left(\frac{j\omega}{\omega_0}\right)^2}$	$\frac{\omega_0}{4\zeta}$
$\frac{1}{(1+j\omega\tau_1)(1+j\omega\tau_2)}$	$\frac{1}{2(\tau_1+\tau_2)}$
$\frac{1+j\omega\tau}{1+2\zeta\frac{j\omega}{\omega_0}+\left(\frac{j\omega}{\omega_0}\right)^2}$	$\frac{\omega_0}{4\zeta}(1 + \omega_0^2\tau^2)$
$\frac{1+j\omega\tau_1}{(1+j\omega\tau_2)(1+j\omega\tau_3)}$	$\frac{1}{2(\tau_2+\tau_3)} \left(1 + \frac{\tau_1^2}{\tau_2\tau_3}\right)$
$\frac{1}{(1+j\omega\tau)\left\{1+2\zeta\frac{j\omega}{\omega_0}+\left(\frac{j\omega}{\omega_0}\right)^2\right\}}$	$\frac{1}{2} \frac{\frac{\omega_0}{2\zeta}+\omega_0^2\tau}{1+2\zeta\omega_0\tau+\omega_0^2\tau^2}$

Table 3.6: Standard integrals for the calculation of the variance.

An alternative for Table 3.5 is given in Table 3.6, using the frequency response function $H(\omega)$ rather than the transfer function $H(s)$.

$$I = \frac{1}{2\pi} \int_{-\infty}^{+\infty} |H(\omega)|^2 d\omega.$$

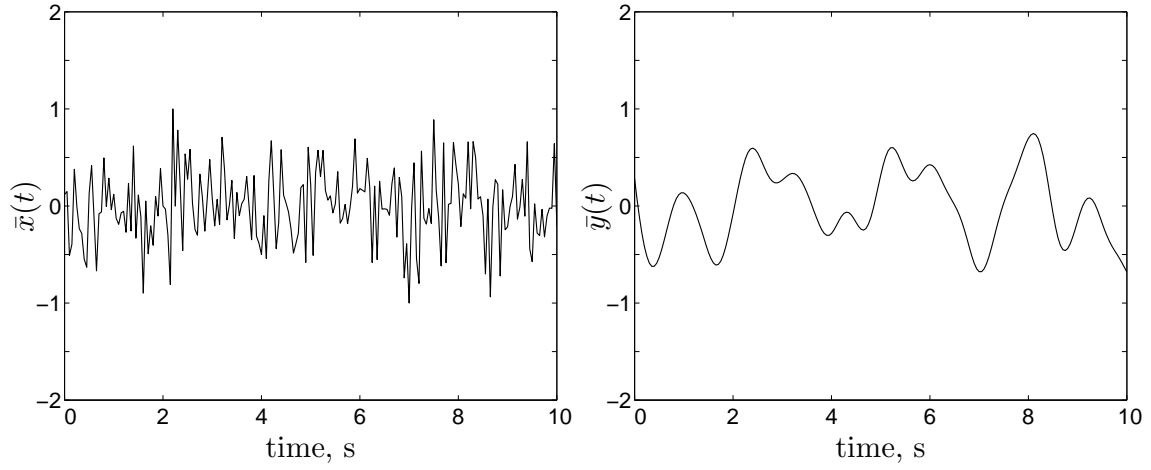


Figure 3.1: Two different stochastic signals with equal average and variance but with totally different frequency contents.

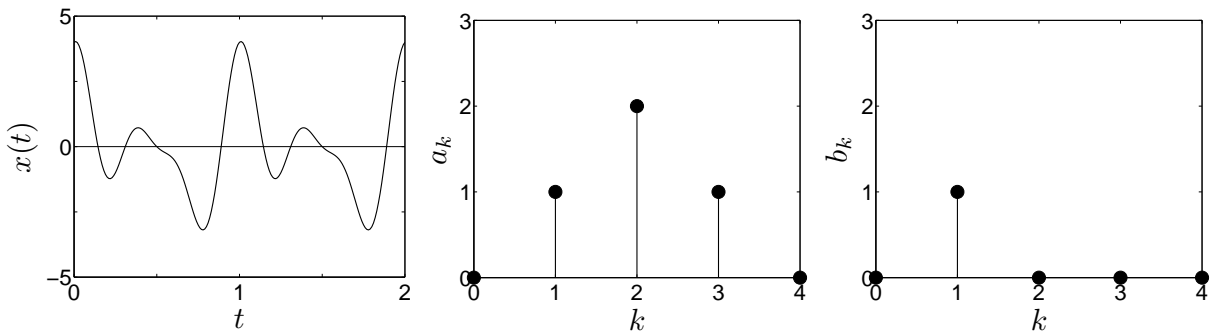


Figure 3.2: Graphical representation of a Fourier series expansion. The signal $x(t)$ consists of 3 cosine functions and 1 sine function.

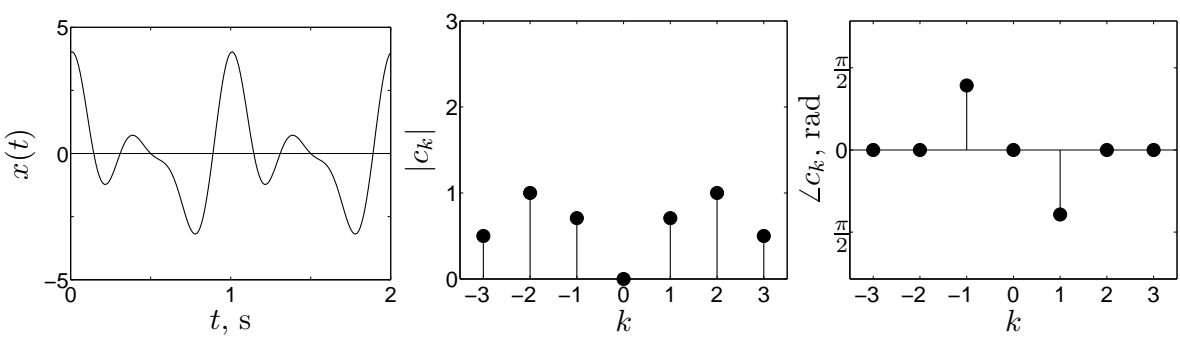


Figure 3.3: Graphical representation of a complex Fourier series expansion of $x(t)$ in Figure 3.2.

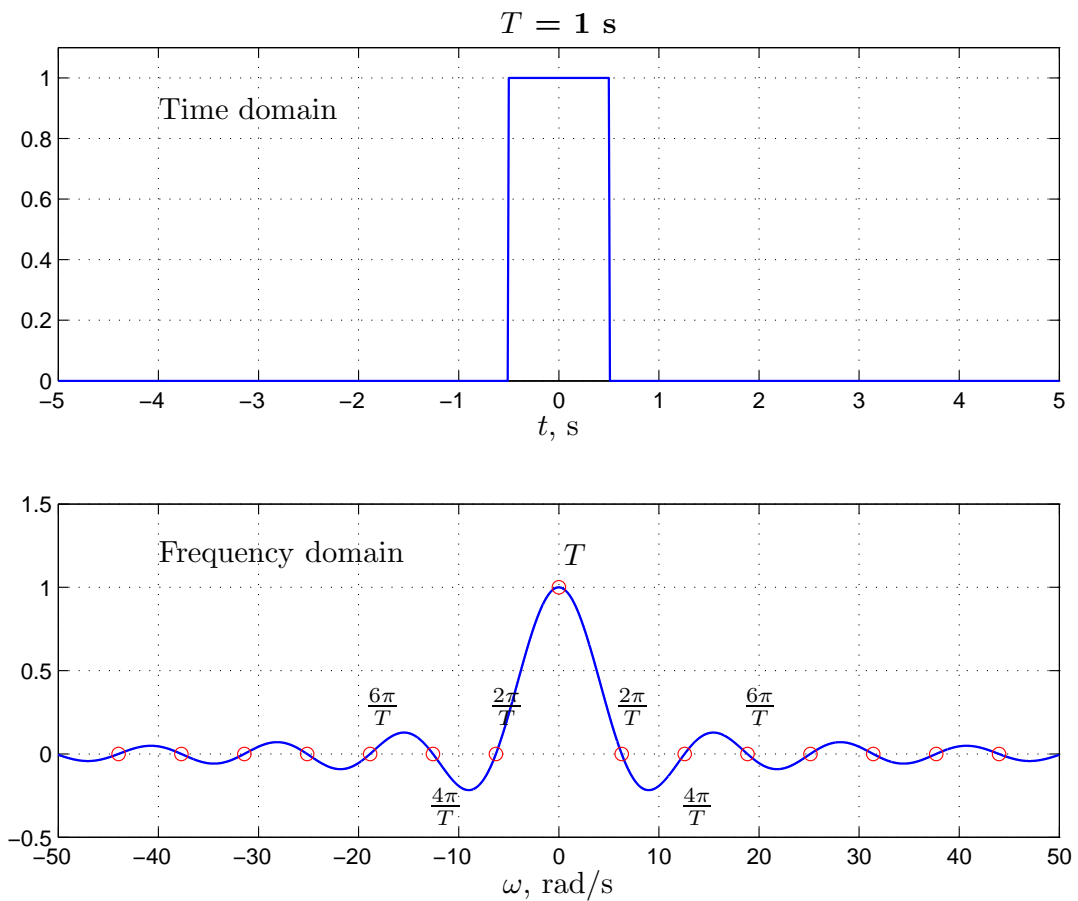


Figure 3.4: The block function $b(t)$ and its Fourier transform $B(\omega)$, the sinc-function.

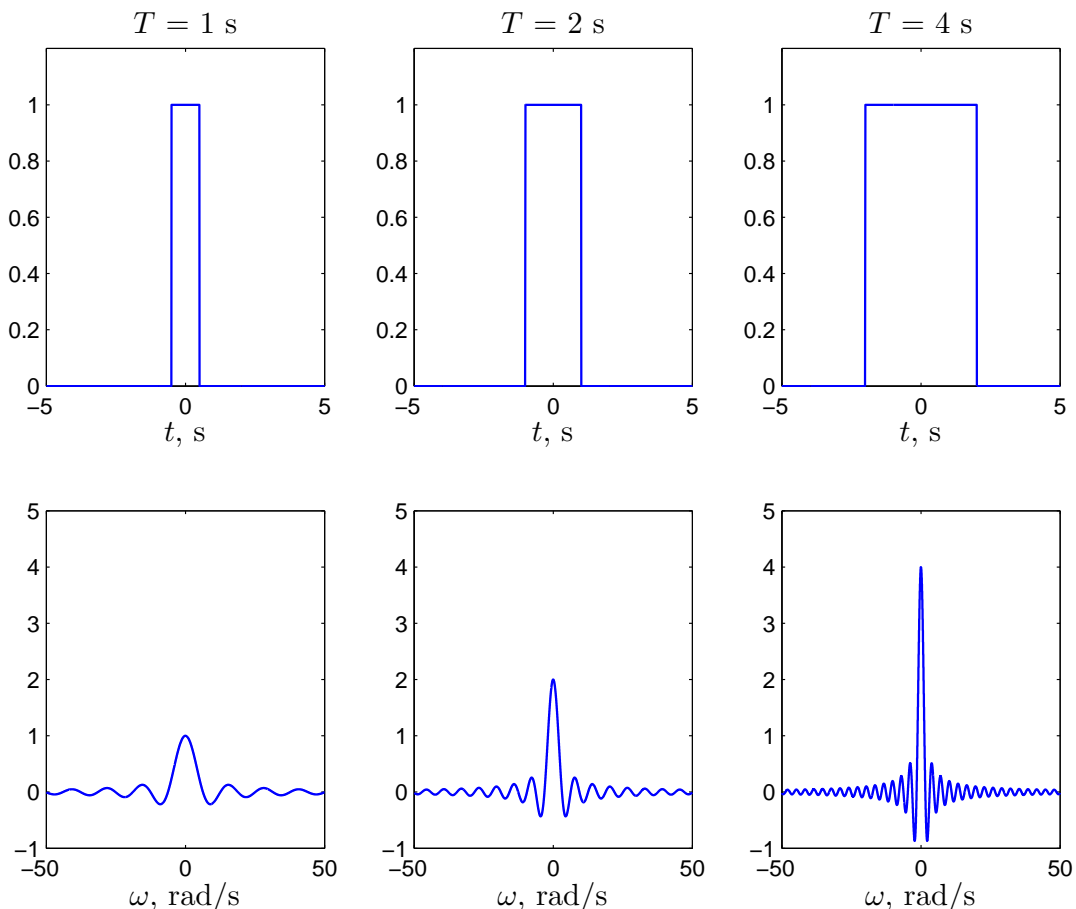


Figure 3.5: The effect of changing T in $b(t)$ on the Fourier transform $B(\omega)$.

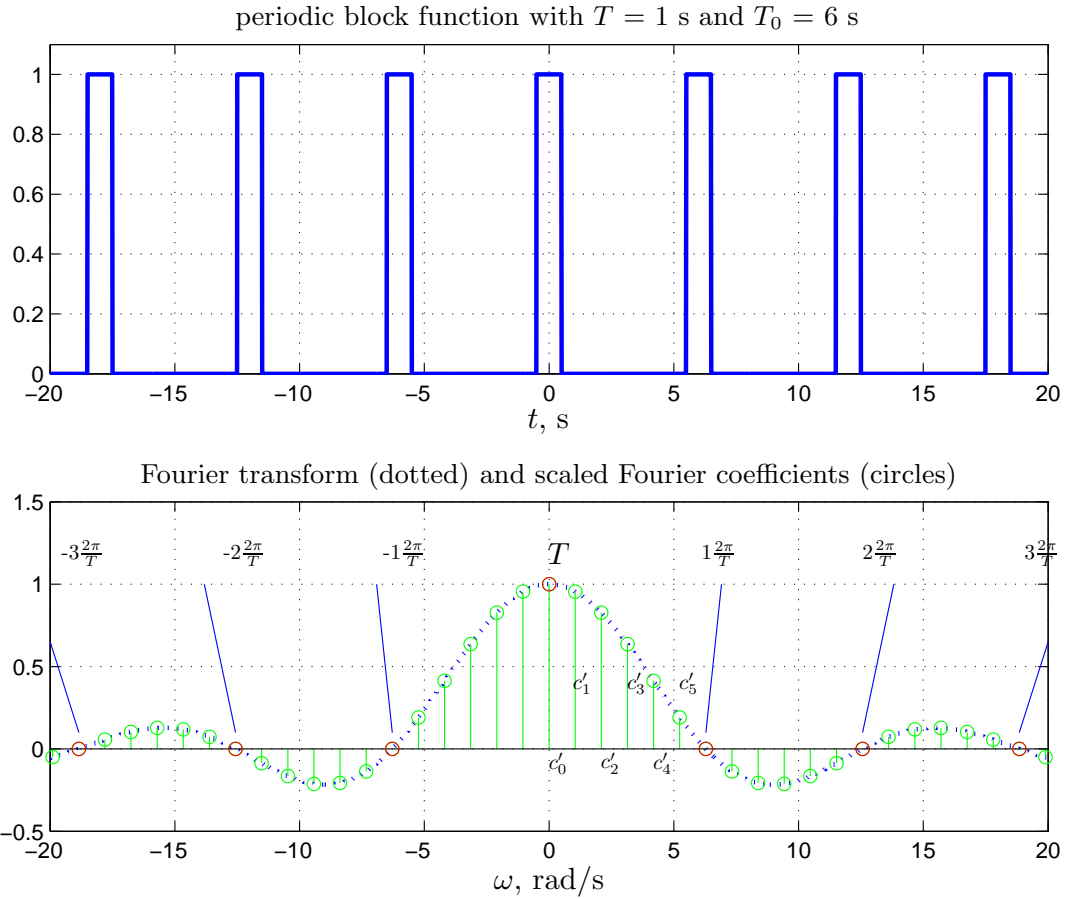


Figure 3.6: The periodic block function $b(t)$, and the scaled Fourier series coefficients $\{c'_k\} = T_0 \{c_k\}$. These coefficients are equal to the Fourier transform of an aperiodic block function (the dotted sinc-function, see also Figure 3.4) at the integer multiples of the fundamental frequency $k\frac{2\pi}{T_0}$.

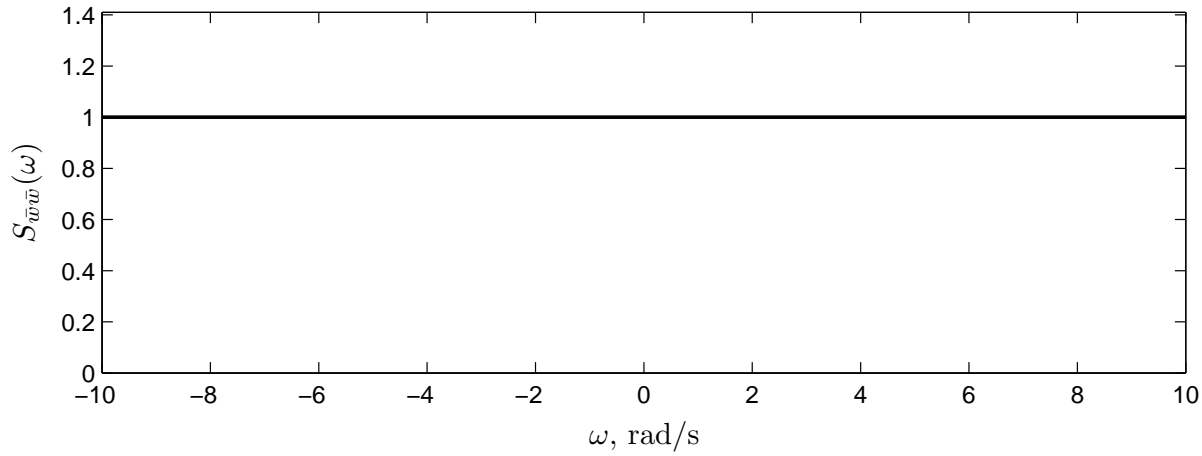


Figure 3.7: Power spectral density of ideal white noise with intensity $W = 1$.

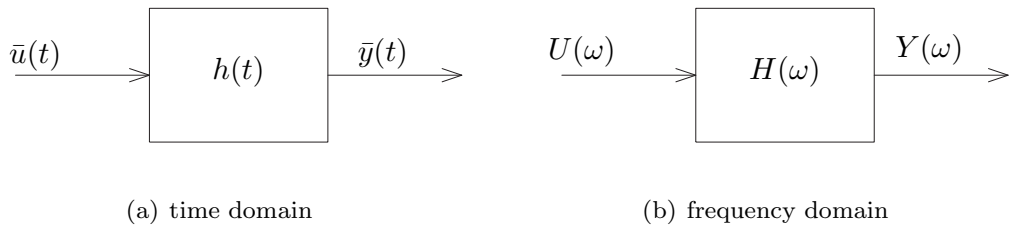


Figure 3.8: A linear time-invariant system with input $\bar{u}(t)$ and output $\bar{y}(t)$.

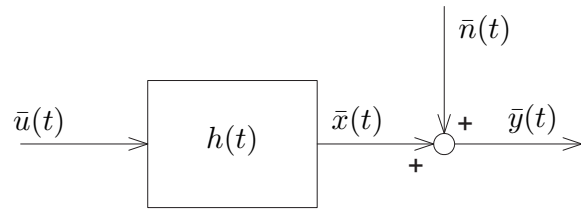


Figure 3.9: An LTI system with stochastic input $\bar{u}(t)$ and response $\bar{x}(t)$ perturbed by random noise.

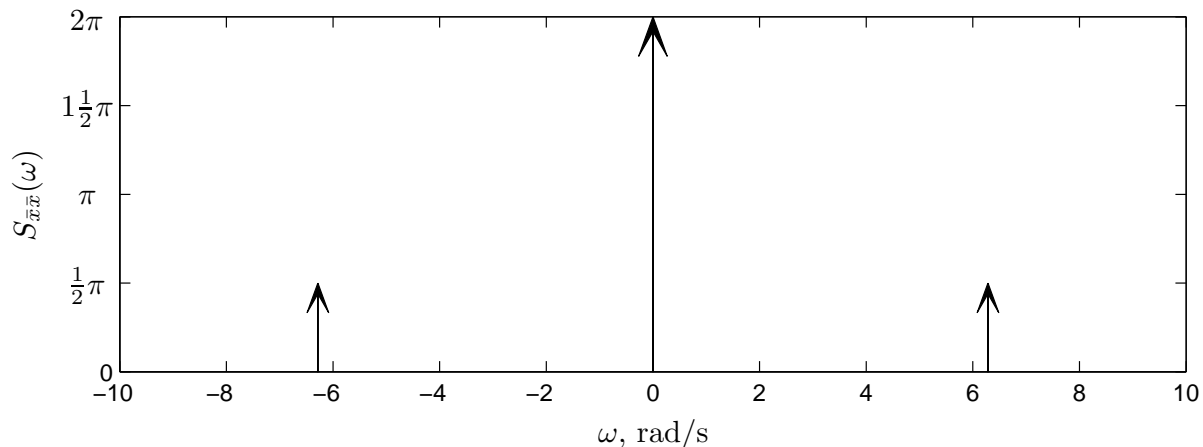


Figure 3.10: Power spectral density function of $\bar{x}(t) = \sin(2\pi t) + 1$.

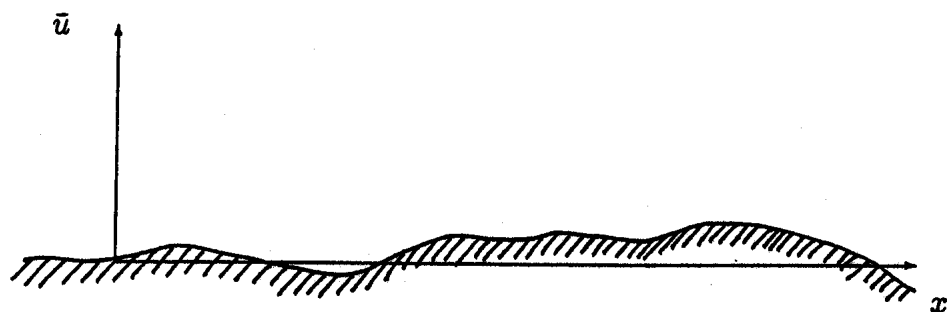


Figure 3.11: Typical runway profile.

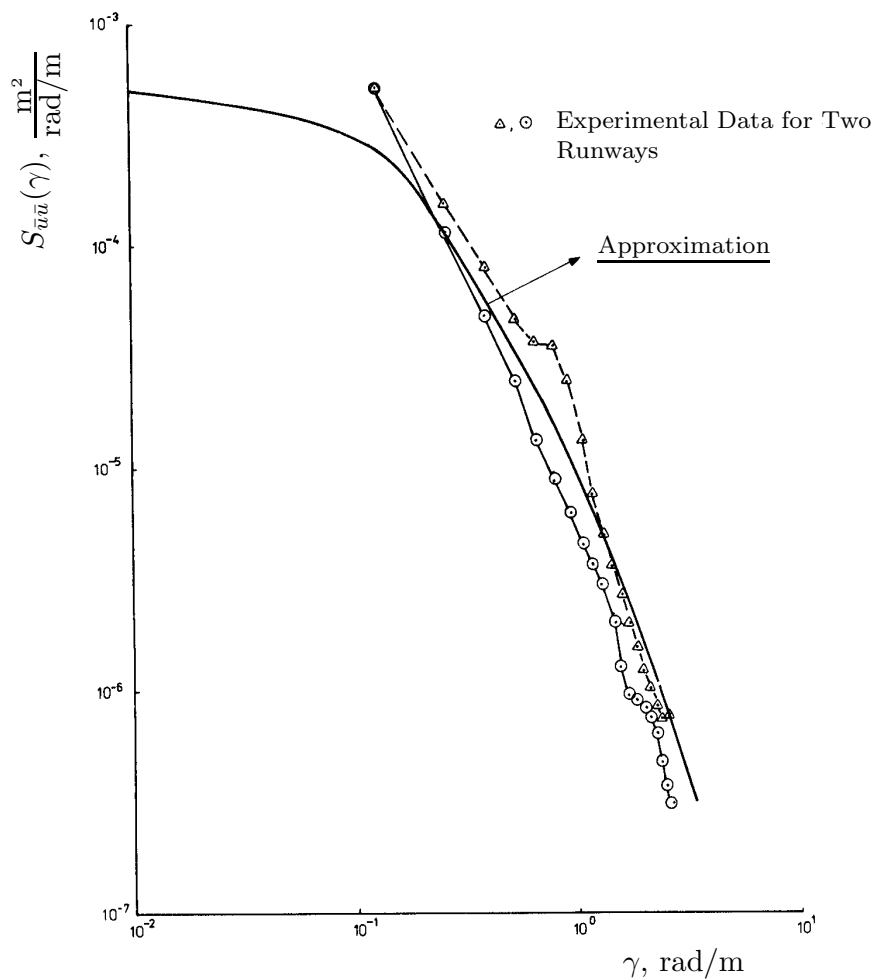


Figure 3.12: Power spectral density $S_{\bar{u}\bar{u}}(\gamma)$ of runway roughness from experimental data. Taken from (AGARD, 1975).

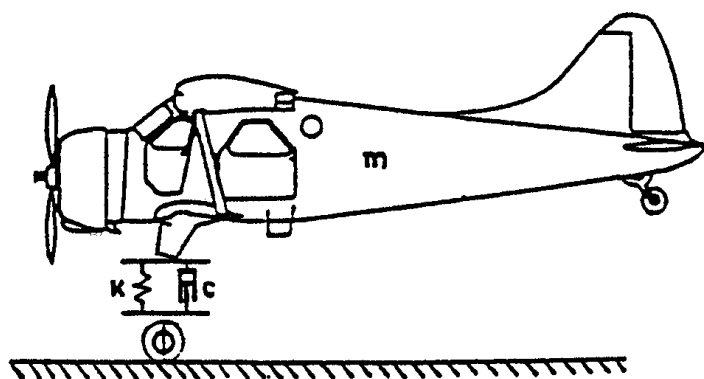


Figure 3.13: Landing gear suspension as a 1 DOF mass-spring-damper system.

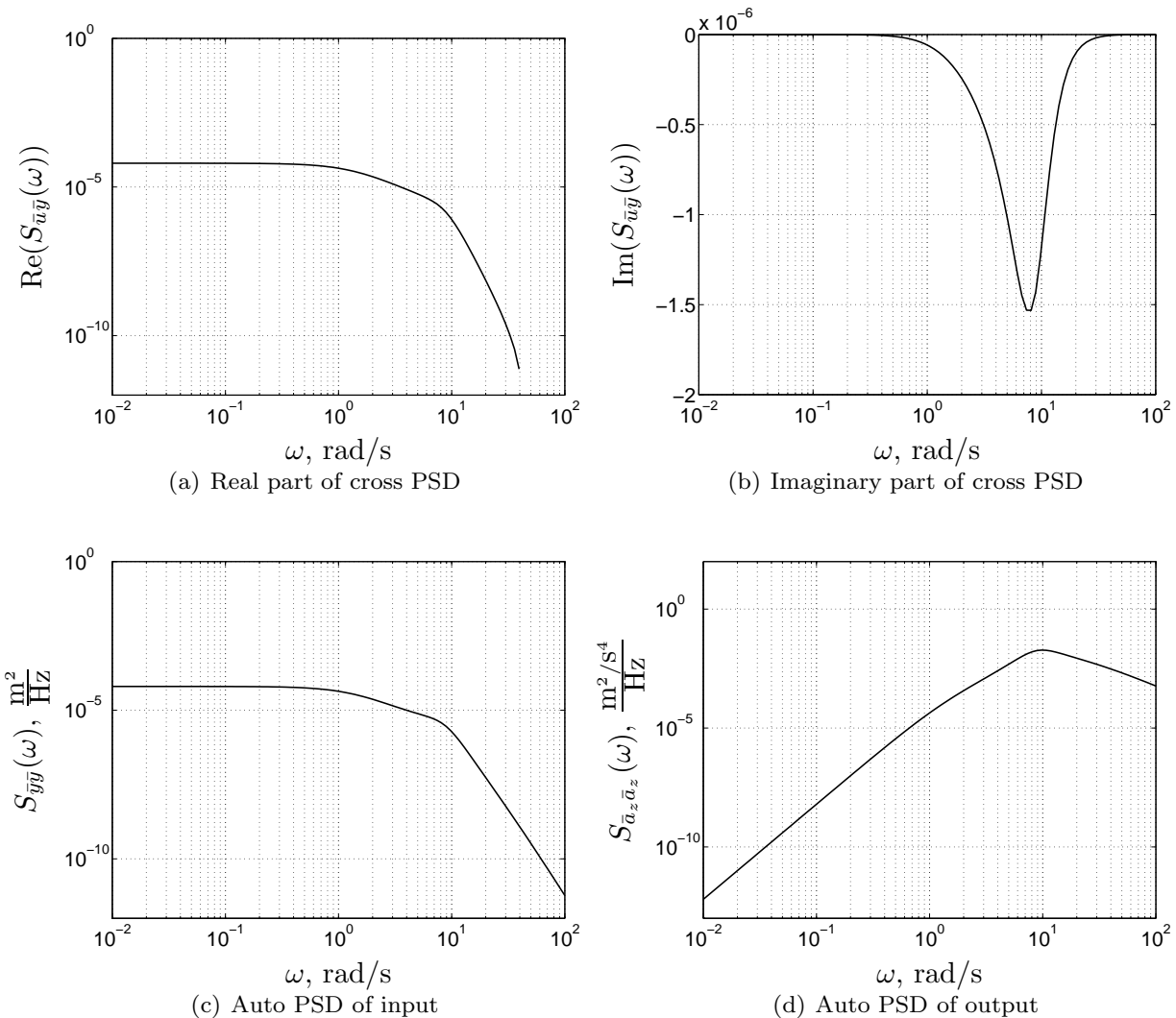


Figure 3.14: Cross power - and auto power spectral densities of aircraft displacements and auto power spectral density of normal acceleration.

Chapter 4

Spectral Analysis of Discrete Time Stochastic Processes

4.1 Introduction

The techniques for continuous-time signal Fourier analysis, as developed in Chapter 3, are of great theoretical value for analysis and insight into the properties of continuous-time stochastic signals and processes. Yet, a practical computer-based application will usually require the use of *discrete* time series. The present chapter addresses the subject of spectral analysis of discrete-time stochastic processes.

To highlight the differences between continuous-time and discrete-time signals in the frequency domain is important because these differences are more pronounced in the frequency domain as compared with the time domain (c.f. Chapter 2: no distinction was made between the continuous time and discrete time cases). Moreover, the approach of using discrete time systems sometimes leads to different techniques for the calculation of important frequency domain characteristics such as the power spectral density function.

In order to estimate power spectral density functions from measured data, the obvious method would be to estimate the covariance function first and then to apply a Fourier transform. This approach has long been the basis of practical calculation procedures which follow the ‘classical’ mathematical route by which spectral densities are defined as Fourier transforms of covariance functions (c.f. Section 3.5). However, this procedure has changed with the availability of the Fast Fourier Transform (or FFT for short) since the 1960’s.

The Fast Fourier Transform is a remarkably efficient way for calculating the Fourier transform of a finite length discrete time series. Basically, the FFT works by partitioning the original sequence into a number of shorter sequences. It then calculates the Fourier

transforms of each subsequence and combines the results together to yield the Fourier transform of the full sequence. An enormous reduction in computer time can be achieved since Fourier transformation of the short subsequences is relatively fast.

As for the calculation of the power spectral densities, it has become a common procedure to calculate these *directly* from the original time series by application of the FFT. The method of this procedure has had a great impact on the way discrete time signals and systems are being analysed in the frequency domain.

Section 4.2 introduces the effects of sampling, i.e., transforming a continuous-time signal to a discrete time series. We will briefly discuss the Shannon sampling theorem, aliasing effects and the process of ideal signal reconstruction. The Continuous-Time Fourier Transform (CTFT) of Chapter 3 will be used to understand what happens when impulse-train sampling a continuous-time signal.

Section 4.3 will then take the theory one step further, and introduce what happens when really dealing with *numbers* in a computer, where all references to time (and frequency, for that matter) disappear. We will briefly discuss the discrete-time frequency, and the Discrete-Time Fourier Transform (DTFT) that comes with it.

In Section 4.4 we will then finally introduce our main engineering tool, the **Discrete Fourier Transform (DFT)**, its properties and main assumptions, and relate it to the DTFT. Phenomena like leakage will be briefly discussed. Section 4.5 explains the mechanism behind the Fast Fourier Transform which is a practical tool for rapidly calculating the discrete Fourier Transform.

Section 4.6 shows the impact the FFT has had on calculating power spectral density functions. It will be shown how a direct calculation of spectral estimates is now feasible without the need for calculating covariance functions first. Section 4.7 discusses some methods to improve spectral estimates through applying window functions in time and frequency domain.

The chapter concludes with examples and problems in Section 4.8.

4.2 Sampling and signal reconstruction

In Section 4.2.1 several methods to *sample* continuous-time signals will be presented. The *reconstruction* of continuous-time signals from sampled data is explained in Section 4.2.2.

4.2.1 Sampling: from C to D

An often used CTFT pair

Before we discuss the process of sampling, a frequently used Fourier transform pair will be defined, as this pair will show to be useful (and often used) in understanding the sampling process and the discrete-time Fourier analysis.

Figure 4.1 illustrates that the CTFT of a unit pulse (or block) signal $b(t)$ (width T , so $b(t) = \Pi(\frac{t}{T})$), defined in the time domain, becomes a sinc-function in the frequency domain:

$$b(t) = \Pi\left(\frac{t}{T}\right) \xleftrightarrow{\mathcal{F}} B(\omega) = T \text{sinc}\left(\frac{\omega T}{2\pi}\right) \quad (4.1)$$

It can be shown that the sinc-function $B(\omega)$ has zeros at frequencies $\omega = m\frac{2\pi}{T}$ (for $m \in \mathbb{Z} \setminus \{0\}$); the area in time equals the height of the sinc-function $B(\omega)$ at zero frequency, T .

Similarly, because of duality (discussed in Section 3.4.2), the inverse CTFT of a unit pulse (or block) $b(\omega)$ (width W , so $b(\omega) = \Pi(\frac{\omega}{W})$), defined in the frequency domain, becomes a sinc-function in the time domain:

$$B(t) = \frac{W}{2\pi} \text{sinc}\left(\frac{tW}{2\pi}\right) \xleftrightarrow{\mathcal{F}} b(\omega) = \Pi\left(\frac{\omega}{W}\right) \quad (4.2)$$

The sinc-function $B(t)$ has zeros at times $t = m\frac{2\pi}{W}$ (for $m \in \mathbb{Z} \setminus \{0\}$); the area in frequency equals the height of the sinc-function $B(t)$ at zero time, scaled with $\frac{1}{2\pi}$, namely $\frac{W}{2\pi}$.

Impulse-train sampling

Figure 4.2 illustrates our ‘model’ of the sampling process. The analog for sampling is that the continuous-time signal $x(t)$ is multiplied with a continuous-time *sampling function* $y(t)$, resulting in a new *continuous-time* signal $z(t)$. The sampling function can be thought of to be a ‘valve’, or ‘switch’, which is either open (signal passed) or closed (signal blocked). The ‘switch’ is opened every Δt seconds, called the *sampling time*, and remains open for τ seconds. To conserve the original signal’s energy, we multiply the signal with the inverse of the time that the switch is open, $1/\tau$.

In the limit-case, τ is infinitesimally small, the switch is opened for only a tiny fraction of a second, yielding a ‘sample’ of $x(t)$ every Δt seconds: $z(t) = x(n\Delta t)$. Because $z(t)$ and $x(t)$ have the same energy, this process can be considered a multiplication of $x(t)$ with an infinite set of Dirac-functions $\delta(t)$ that occur every Δt seconds.¹ In other words, the sampled signal $z(t)$ can be considered an infinite set of Dirac-pulses, one every Δt seconds,

¹These infinite sets of Dirac-functions are also known as ‘Dirac-combs’.

where the *area* of each Dirac pulse at time $t = n\Delta t$ equals the *value* of the continuous-time signal $x(t)$ at that time t . This is the mathematical model of the sampling process that we will use to understand what happens when moving a continuous-time signal to discrete time. It is known as the **impulse-train sampling** model.

From Chapter 3 we know that a multiplication of two signals in the time domain:

$$z(t) = x(t) \cdot y(t), \quad (4.3)$$

corresponds to a convolution operation in the frequency domain (Table 3.2):

$$Z(\omega) = \frac{1}{2\pi} X(\omega) \star Y(\omega) = \frac{1}{2\pi} \int_{-\infty}^{+\infty} X(\xi) Y(\omega - \xi) d\xi \quad (4.4)$$

Let $x(t)$ be the continuous time (possibly aperiodic) signal which is to be sampled, and let $X(\omega)$ denote its continuous time Fourier transform. For the signal $y(t)$ we choose the following ‘pulse train’ in the time domain:

$$y(t) = \sum_{n=-\infty}^{+\infty} \delta(t - n\Delta t), \quad (4.5)$$

which is referred to as the sampling function, with Δt as the sampling period (or sampling time) and the fundamental frequency $\omega_s = \frac{2\pi}{\Delta t}$ as the sampling frequency.

According to Table 3.2 the CTFT of $y(t)$ equals:

$$Y(\omega) = \frac{2\pi}{\Delta t} \sum_{k=-\infty}^{+\infty} \delta(\omega - k\frac{2\pi}{\Delta t}), \quad (4.6)$$

or, equivalently:

$$Y(\omega) = \omega_s \sum_{k=-\infty}^{+\infty} \delta(\omega - k\omega_s), \quad (4.7)$$

which both represent a ‘pulse train’ (or Dirac comb) in the frequency domain.

Let’s continue to investigate the sampled signal $z(t)$, Eq. (4.4):

$$\begin{aligned} Z(\omega) &= \frac{1}{2\pi} X(\omega) \star Y(\omega) \\ &= \frac{1}{2\pi} \int_{-\infty}^{\infty} X(\xi) Y(\omega - \xi) d\xi && \text{definition of convolution} \\ &= \frac{1}{2\pi} \int_{-\infty}^{\infty} X(\xi) \left(\frac{2\pi}{\Delta t} \sum_{k=-\infty}^{\infty} \delta(\omega - \xi - k\omega_s) \right) d\xi && \text{substitute Eq. (4.6)} \\ &= \frac{1}{\Delta t} \sum_{k=-\infty}^{\infty} \int_{-\infty}^{\infty} X(\xi) \delta(\omega - \xi - k\omega_s) d\xi && \text{reverse } \sum \text{ and } \int \\ &= \frac{1}{\Delta t} \sum_{k=-\infty}^{\infty} X(\omega - k\omega_s) && \text{use sifting property} \end{aligned}$$

We see that the CTFT of $Z(\omega)$ is a **periodic** function of frequency, consisting of an infinite sum of replications of $X(\omega)$, scaled by $\frac{1}{\Delta t}$ and shifted by $k\omega_s$, for integer k :

$$Z(\omega) = \frac{1}{\Delta t} \sum_{k=-\infty}^{\infty} X(\omega - k\omega_s) \quad (4.8)$$

with sampling frequency $\omega_s = \frac{2\pi}{\Delta t}$. This is our main result so far.

Example

Figure 4.3 illustrates an example of the effects of impulse-train sampling a continuous-time signal $x(t)$ with CTFT transform $X(\omega)$. We assume that $x(t)$ is a real and even signal, hence its CTFT is also a real and even function of frequency ω . $X(\omega)$ is zero for all frequencies, except between $\pm\omega_M$ which here equals $\pm 2\pi$ rad/s (± 1 Hz), where it has a triangular shape, see Figure 4.3(a).

Now, suppose that $x(t)$ is sampled with 4 Hz and the CTFT (!) of the impulse-train sampled signal $z(t)$, $Z(\omega)$, is illustrated in Figure 4.3(b). What is obtained, is a **scaled** series of copies, also known as **aliases**, occurring at all integer multiples of the sampling frequency ω_s which equals 8π rad/s. That is, the magnitude of $Z(\omega)$ equals the magnitude of $X(\omega)$ multiplied with $1/\Delta t$ (or, the sampling frequency f_s in Hz), and $Z(\omega)$ ‘repeats itself’ at each integer multiple $k \in \mathbb{Z}$ of the sampling frequency ω_s .

Aliasing

From the above, one may ask oneself, what would be a proper choice of the sampling frequency ω_s ? The answer to this question can be easily found when considering the example discussed above. We see that $Z(\omega)$ consists of scaled copies of the original spectrum $X(\omega)$ placed at integer multiples of the sample frequency ω_s . But what if the sampling frequency would be chosen too small, so small that, e.g., the first alias occurring at $1 \cdot \omega_s$ (or at $-1 \cdot \omega_s$ for that matter) will start to *interfere* with the original placed $0 \cdot \omega_s$ rad/s? In that case, the frequency-content of the copies will be *added together* at the frequencies where they overlap, and the lumped spectrum will have a different shape at these frequencies.

This is illustrated in Figure 4.4 where the sampling frequency ω_s is chosen too small, and the first alias (in green) comes too close to the original -1- (in red), leading in spectrum overlap. The resulting sampled spectrum -2- is ‘aliased’ and looks different from the original at the frequencies of overlap. When transforming the discrete time samples back to continuous time, as will be discussed in the following paragraph, the reconstructed signal will not be equal to the original signal!

At what frequency does the overlap first occur? Well, that can be easily seen from Figure 4.3 as well. When we define the maximum frequency at which the original spectrum

$X(\omega)$ has a non-zero value to be ω_M ; then the first copy at positive frequencies will have a non-zero value from $\omega_s - \omega_M$ to $\omega_s + \omega_M$. The difference in frequency between the original and the first copy (at positive frequencies) equals $\omega_s - \omega_M - \omega_M$ and *only* when this difference is larger than zero no overlap will occur, i.e.: $\omega_s > 2\omega_M$.

Hence, from the above we can conclude that, in order to avoid any aliasing effects the sampling frequency should be large enough. Generally speaking, many stochastic processes that are studied are somehow band-limited, that is, the process is bounded in energy typically at higher frequencies. When sampling a signal $x(t)$ which is band-limited, i.e., its spectrum $X(\omega)$ has power or energy up to and including ω_M , it should be sampled with a sampling frequency that is larger (not equal!) than $2\omega_M$. This is known as **Shannon's Sampling Theorem**.

The maximum frequency where the original spectrum has a non-zero value, multiplied with 2, is called the Nyquist rate: $2\omega_M$. The minimum frequency at which the sampler should sample the continuous-time process to avoid aliasing to occur is called the Nyquist frequency: $\omega_s/2 > \omega_M$. Hence, whereas the former depends on the *signal* to be sampled, the latter is a requirement for the sampling function.

Sampling overview #1

Figure 4.5 illustrates our progress in understanding the sampling of continuous-time signals so far. The top row shows what ‘happens’ in the time domain, the bottom row shows what happens in the frequency domain. Let’s briefly recapitulate before we carry on.

In the time domain, the original signal $x(t)$ (left) is multiplied with the impulse-train sampling function $y(t)$ (middle), resulting in the continuous-time (!, it is a model of discrete time, so we refer to it as “discrete time” in Figure 4.5) sample sequence $z(n\Delta t)$ (right). Note that although Figure 4.5 suggests that the amplitude of the Dirac pulses changes, it is in fact the *weight* of the Dirac pulse that changes: each Dirac pulse at $n\Delta t$ seconds ‘carries’ the original signal *value* $x(n\Delta t)$ through its weight.

In the frequency domain, the spectrum of the original signal $X(\omega)$ (left) is convolved with an infinite set of Dirac functions occurring at $k\omega_s$, each with weight $2\pi/\Delta t$ (middle), yielding a scaled and periodic spectrum $Z(\omega)$ of the sample sequence $z(n\Delta t)$ (right).

4.2.2 Signal reconstruction: from D to C

The transformation of the signal $z(n\Delta t)$ back to continuous time is called **signal reconstruction**. *Ideally*, we would be able to define an ideal reconstruction filter $R(\omega)$ that perfectly passes through all signal strength within $[-\omega_s/2, \omega_s/2]$, beyond which all signal strength is blocked, and would have a gain of Δt . This filter would simply get rid of all

the aliases, except for the one centered around zero, as illustrated in Figure 4.6.

The ideal reconstruction filter thus equals the ideal low-pass filter $R(\omega)$:

$$R(\omega) = \Delta t \Pi\left(\frac{\omega}{\omega_s}\right), \quad (4.9)$$

with $\omega_s = \frac{2\pi}{\Delta t}$ the sampling frequency.

The time-domain equivalent of this ideal filter is a sinc-function, see Eq. (4.2):

$$r(t) = \Delta t \left(\frac{\omega_s}{2\pi} \operatorname{sinc}\left(\frac{t\omega_s}{2\pi}\right) \right) = \operatorname{sinc}\left(t\frac{1}{\Delta t}\right), \quad (4.10)$$

which equals zero for all times t equal to $m\Delta t$ (except $m=0$).² Note that $r(0)=1$.

Multiplication of the signal frequency-domain description $Z(\omega)$ with the ideal reconstruction filter $R(\omega)$ yields the original spectrum (assuming that the sampling frequency was high enough, and no aliasing occurs):

$$\begin{aligned} R(\omega)Z(\omega) &= \Delta t \Pi\left(\frac{\omega}{\omega_s}\right) \cdot \frac{1}{\Delta t} \sum_{k=-\infty}^{\infty} X(\omega - k\omega_s) \\ &= X(\omega) \end{aligned} \quad (4.11)$$

Multiplication in the frequency domain is equivalent to a *convolution* in the time domain. So, convolving the sampled signal $z(t)$ with the sinc-function $r(t)$ results in the original signal $x(t)$:

$$z(t) * r(t) = x(t), \quad (4.12)$$

where:

$$z(t) = \sum_{n=-\infty}^{\infty} z(n\Delta t)\delta(t - n\Delta t), \quad (4.13)$$

so $z(n\Delta t) = x(n\Delta t)$. Convolution of a sinc-function, Eq. (4.10), with a Dirac function located at $t = n\Delta t$ yields a copy of that sinc-function located at that particular time instant:

$$x(t) = \sum_{n=-\infty}^{\infty} z(n\Delta t)\operatorname{sinc}((t - n\Delta t)/\Delta t). \quad (4.14)$$

In other words, $x(t)$ can be reconstructed by multiplying each sample $z(n\Delta t)$ with a continuous-time sinc-function and then adding-up the result. For each sample, the sinc-function is oriented around that sample at $n\Delta t$ and is *scaled* with the value of the sample $z(n\Delta t)$ which equals $x(n\Delta t)$. The fact that the sinc-function has its zeros at $t = m\Delta t$

²Where the ‘running variable’ m is used to avoid confusion with n which is commonly used for the sample index.

for all m except at $m = 0$ means that each copy of the sinc-function has its zeros at $t = (n + m)\Delta t$ except at $t = n\Delta t$. Hence, all sample values except for $n\Delta t$ coincide with the zeros of the sinc-function, for all values of n !

The procedure above is known as *ideal* signal reconstruction, and requires an ideal low-pass filter which is not causal. Ideal signal reconstruction would require knowledge of all future and past samples and therefore cannot be used in real-time, online applications where we have no knowledge of the future of the signal. Therefore, simpler and more practical signal reconstruction methods have been developed to make a discrete-time signal ‘continuous’ again, like the Zero-Order Hold (ZOH) filter, the first-order hold filter, etc.

In the zero-order hold filter, the signal between the samples is simply kept constant; that is, when $z(n\Delta t)$ is the sample at $t = n\Delta t$, then the ‘reconstructed’ or continuous-time signal after the ZOH filter, $x_r(t)$ equals $z(n\Delta t)$ for $n\Delta t \leq t < (n + 1)\Delta t$. Of course, the resulting signal reconstruction will not be exactly equal to the continuous time signal $x(t)$ that was sampled. Only with the ideal signal reconstruction do we obtain the *exact* continuous-time original signal $x(t)$.

4.3 The Discrete-time Fourier Transform

In Section 4.2 the theoretical model of sampling has been discussed. Our model of the sampled signal boils down to an infinite set of Dirac functions, scaled with the values of the continuous-time signal at $n\Delta t$. Naturally, in our computers we don’t have sets of impulses, we just have numbers x as a function of another number n , $x[n]$. Typically, $x \in \mathcal{R}$ and $n \in \mathcal{Z}$. Figure 4.7 illustrates that one step still needs to be made; we need to somehow map the continuous-time impulse train $z(n\Delta t)$ signal to the discrete time series $x[n]$.

The Discrete-time Fourier Transform

We have seen that the CTFT of $z(n\Delta t)$ equals:

$$Z(\omega) = \frac{1}{\Delta t} \sum_{k=-\infty}^{\infty} X(\omega - k\omega_s),$$

where $z(t)$ can be described as an impulse train with the weights of the impulses scaled to the values of the samples of $x(t)$ at discrete times $n\Delta t$:

$$z(t) = \sum_{n=-\infty}^{\infty} x(t) \delta(t - n\Delta t)$$

Directly CT Fourier transforming this signal yields:

$$Z(\omega) = \mathcal{F}\{z(n\Delta t)\} = \sum_{n=-\infty}^{\infty} x(n\Delta t) e^{-j\omega\Delta t n} \quad (4.15)$$

The **Discrete-time Fourier transform** (DTFT) of a time series $x[n]$ is defined as:

$$X(\Omega) = \sum_{n=-\infty}^{\infty} x[n] e^{-j \Omega n}, \quad (4.16)$$

with Ω the ‘discrete frequency’, a *continuous* variable, $\Omega \in [0, 2\pi]$. Note the range of n in this definition, we deal with infinite observation times, like the CTFT.

Because $x[n]$ must be equal to $x(n\Delta t)$:

$$X(\Omega) = \sum_{n=-\infty}^{\infty} x(n\Delta t) e^{-j \Omega n} \quad (4.17)$$

Comparing Eq. (4.15) with Eq. (4.17), we see that $X(\Omega)$ – the DTFT of the discrete-time sequence $x[n]$ – and $Z(\omega)$ – which is the CTFT of the continuous-time impulse train $z(n\Delta t)$ – are related through:

$$X(\Omega) = Z(\omega = \frac{\Omega}{\Delta t}), \quad (4.18)$$

in other words, we can just substitute $\frac{\Omega}{\Delta t}$ for ω .

Hence, the discrete frequency Ω equals $\omega\Delta t$. It is periodic with 2π , i.e.: $\Omega + 2\pi = \Omega$.

It is as if for the discrete-time equivalent of the CTFT, the CT frequency ω is *multiplied* with Δt , and therefore the CTFT *time* t is *divided* with Δt , mapping the time axis t (in seconds) to a DT index, just a number. That is, the sequence:

$$t \in \{..., -3\Delta t, -2\Delta t, -1\Delta t, 0\Delta t, 1\Delta t, 2\Delta t, 3\Delta t, ...\}$$

is mapped to:

$$n \in \{..., -3, -2, -1, 0, 1, 2, 3, ...\}$$

We are normalizing the time axis t with Δt to get to the ‘number’ or ‘index’-space n , numbers in a computer as a function of other numbers (the index n).

Sampling overview #2: Sampling complete

Figure 4.8 illustrates the final step that we have taken. Because of normalizing the time axis with Δt , to get from time space $n\Delta t$ to the ‘index’-space n , the frequency axes needed to be changed as well, from radial frequency ω -space in rad/s, to digital frequency space Ω which has no dimension at all! This makes a lot of sense, as in a computer ‘time’ and ‘frequency’ do not matter, we just get numbers as a function of other numbers, and discrete-time Fourier transforming the time series yields the frequency series, a new set of (complex) numbers as a function of other numbers as well.

Table 4.1 provides an overview of the main continuous-time and discrete-time transforms, with the DTFT the counterpart of the CTFT. Whereas the Laplace transform encapsulates the Fourier transform in continuous time, the z -transform encapsulates the DTFT in discrete time. When looking at the definitions one can see that all transforms assume an infinite observation time. In the next section, discussing the discrete Fourier transform (DFT) – which is not the same as the DTFT – we will introduce the reader to the consequences of taking a finite observation time. Before we continue with the DFT discussion, we will first briefly elaborate on the discrete frequency Ω .

Discrete frequency

The discrete frequency Ω has a number of peculiar properties that may be a little counter-intuitive at first sight. To stress the difference with continuous frequency ω we will state some very obvious properties of the latter first.

Consider a harmonic function $e^{j\omega_1 t}$ in continuous time, a rotating complex exponential with frequency ω_1 . First, for all ω_1 except $\omega_1 = 0$ the function will be periodic: at some time the function will repeat itself exactly. Second, when ω_1 increases, the higher the rate of the oscillation.

How different are these properties for discrete or digital frequency! Consider a harmonic function $e^{j\Omega_1 n}$ in discrete time, illustrated in Figure 4.9(a). Because n is not continuous but an index number ($n \in \mathbb{Z}$), the complex vector will rotate in *discrete steps*, with angle Ω_1 . This explains why discrete frequency $\Omega \in [0, 2\pi]$, and has dimension of [radians]. Now, first, contrary to continuous frequency, the complex exponentials are *only* periodic – with period N samples – when $\Omega/(2\pi)$ is a rational number:

$$e^{j\Omega n} = e^{j\Omega(n+N)} = e^{j\Omega n} e^{j\Omega N},$$

which only equals $e^{j\Omega n}$ when $\Omega N = m2\pi$, or when:

$$\frac{\Omega}{2\pi} = \frac{m}{N}.$$

In all other cases, the discrete-time oscillation will *not* be periodic, as none of the samples will ever repeat itself (π is an *irrational* number, remember?).

Second, we study the effects of increasing Ω as illustrated in Figure 4.9(b), when considering the sine-component (that is, the imaginary part) of the rotating complex exponential. We can see that from $\Omega = 0$ to π , oscillations go faster, then from π to 2π the oscillations appear to go slower again! In fact, the oscillations for $\Omega = \frac{2\pi \cdot 1}{16}$ and $\Omega = \frac{2\pi \cdot 15}{16}$ are opposite. It appears as if for $\Omega = \frac{2\pi \cdot 15}{16}$ the sine moves in the ‘other direction’ relative to the sine at frequency $\Omega = \frac{2\pi \cdot 1}{16}$. The same holds for the pairs $(\Omega = \frac{2\pi \cdot 1}{8}, \Omega = \frac{2\pi \cdot 7}{8})$ and $(\Omega = \frac{2\pi \cdot 1}{4}, \Omega = \frac{2\pi \cdot 3}{4})$, etc. This explains why we can refer to the left column as the ‘positive frequencies’ and to the right column as the ‘negative frequencies’. One could say

that the maximum frequency is $\Omega = \pi$. The rotation can still go faster, but we could regard that faster rotation beyond π also as a *slower* rotation, but in the other direction.

The third and final characteristic of the discrete frequency Ω is that it is *periodic* with 2π :

$$e^{j(\Omega+2\pi)n} = e^{j\Omega n}e^{j2\pi n} = e^{j\Omega n},$$

so an oscillation with frequency $\Omega + m2\pi$ will be exactly the same as an oscillation with frequency Ω ($\forall \Omega$ and $\forall m$). This result gives an alternative and perhaps also insightful view of why in discrete time the Fourier spectra are *periodic* with 2π .

4.4 The Discrete Fourier Transform

4.4.1 Definition of the DFT

Assume that we have sampled a continuous time signal $x(t)$ with a sufficiently high sampling frequency ($\frac{1}{\Delta t}$), yielding N samples $x[n]$ that are equally spaced at Δt seconds.

The **Discrete Fourier Transform** (DFT) is then defined as:

$$X[k] = \sum_{n=0}^{N-1} x[n]e^{-jk\frac{2\pi}{N}n}$$

(4.19)

with $k\frac{2\pi}{N}$ the k -th discrete frequency.

The inverse discrete Fourier transform is defined as:

$$x[n] = \frac{1}{N} \sum_{k=0}^{N-1} X[k]e^{jn\frac{2\pi}{N}k}$$

(4.20)

We see that the N real numbers $x[n]$ in discrete time become N complex numbers, the Fourier coefficients in discrete time. It may seem then as if we get twice the information in the frequency domain as that we had in the time domain. $X[k]$ repeats itself, however, for the positive and negative frequencies that we have seen in the previous section: $X[k]$ for $k = 0, \dots, \frac{N}{2} - 1$ has all the information.

The DFT bears a great resemblance with the continuous-time Fourier Series (CTFS). In the CTFS, $\frac{2\pi}{T}$ is the fundamental frequency, the frequency of the slowest sinusoidal function that first exactly one period in T seconds. In the DFT, $\frac{2\pi}{N}$ is the fundamental frequency, the smallest *digital* frequency that one can have with N samples.³

³When we would state that $\Omega_{smallest} = \frac{2\pi}{N}$, and $\omega_{smallest} = \Omega_{smallest}/\Delta t$, then it can be easily shown that $\omega_{smallest} = \frac{2\pi}{N\Delta t} = \frac{2\pi}{T}$!

The smallest change in natural frequency (Hz) equals $1/T = 1/(N\Delta t) = f_s/N$. This important number is known as the **frequency resolution** of the DFT. When f_s increases, but the observation time T remains the same, the resolution in time will increase, but the frequency resolution in the DFT will be equal. The frequency resolution can *only* be increased through having a longer observation time, i.e., take more samples N . The smallest frequency that we can ‘look at’ in the DFT therefore really behaves as a ‘fundamental frequency’.

4.4.2 Properties of the DFT

The DFT has some remarkable properties, some of which will be stated below. First of all, the DFT is *periodic*: $X[k+N] = X[k]$, which is simply because of the periodic character of the digital frequency:

$$e^{j(k+N)\frac{2\pi}{N}} = e^{jk\frac{2\pi}{N}} \cdot e^{jN\frac{2\pi}{N}} = e^{jk\frac{2\pi}{N}}.$$

The discrete-time sequence $x[n]$ is therefore ‘interpreted’ by the DFT as a realization of a single cycle of a *periodic* series, even when $[n]$ is not periodic at all! This has an important consequence, which will be discussed in the next subsection.

The ‘zero frequency’ in the DFT, $X[0]$ is a real number that equals the sum of all samples. The DFT at $k = \frac{N}{2}$ is also a real number and equals the sum of all even samples minus the sum of all odd samples.

It is relatively easy to show that the complex conjugate of $X[k]$ equals $X[k]$ for negative frequencies:

$$X^*[k] = X[-k]$$

Moreover:

$$X[N-k] = X[-k] = X^*[k]$$

In other words: $X[N-1] = X^*[1]$, $X[N-2] = X^*[2]$, … $X[N-(N/2-1)] = X^*[N/2-1]$, or, the DFT-values for $k = N/2 + 1$ until $k = N - 1$ equal the complex conjugates of the DFT-values for $k = N/2 - 1$ until $k = 1$. This is illustrated in Figure 4.10. Remember, this is simply a property of the discrete frequency!

A possible (and recommended) interpretation is that $X[k]$ from $k = 1$ to $k = N/2 - 1$ contains the positive frequency components of the DFT, whereas $X[k]$ from $k = N/2 + 1$ to $k = N - 1$ contains the negative frequency components of the DFT. This is further exemplified by Figure 4.11 which shows the ‘view’ of the DFT on the total discrete-time signal spectrum. Compare this figure with Figure 4.3, and notice that, apparently, the DFT provides information about the right-hand side of the copy of $X(\omega)$ at $0 \cdot \omega_s$ (the positive frequencies) and the left-hand side of the copy of $X(\omega)$ at $1 \cdot \omega_s$ (the negative

frequencies). Note that the DFT works with digital frequency Ω , not continuous like the DTFT, but *only* at discrete frequency points, namely $k\frac{2\pi}{N}$. This again illustrates the ‘Fourier series character’ of the DFT.

4.4.3 Leakage

Suppose we would be interested in obtaining the DFT of a discrete-time cosine function $x[n] = \cos(2\pi f_c n \Delta t)$. Assume that $f_c = 2.5$ Hz, and we observe the cosine for $T = 2$ seconds, then sample the signal with $f_s = 10$ Hz. Then $N = 2 \cdot 10 = 20$ and the DFT frequency resolution would be $f_s/N = 10/20 = 0.5$ Hz. The left-hand side of Figure 4.12 shows the result, after proper ‘book-keeping’ the outcome of the DFT. As is shown in the Examples in Section 4.8 the book-keeping boils down to: 1) properly defining the frequency axis which basically means to multiply the k ’s with the frequency resolution, and 2) taking the ‘negative frequencies’ from $k = N/2 + 1$ to $k = N - 1$ and bring them to the left-hand side of the frequency axis.

Now, as expected, the left figure in Figure 4.12 shows the magnitude of the DFT coefficients, $|X[k]|$, having one peak at $f_c = 2.5$ Hz and one at $-f_c = -2.5$ Hz, the magnitude of the peaks equals 10, or $N/2$, which shows that the DFT basically ‘integrates’ (crudely sums up) the cosine function $x[n]$ multiplied with the complex exponential function running at the same frequency, i.e., a cosine-squared. The end-result is just perfect.

The right-hand side of Figure 4.12, however, shows what happens if the frequency of the cosine function equals 2.3 Hz. The DFT of this function looks like a big mess and illustrates an important consequence of the basic DFT assumption that the signal it is transforming is periodic: **leakage**. Spectral leakage, or leakage for short, makes the application of the DFT a tedious one.

There are a number of ways to look at the problem; they all boil down to the same, however. In our example, leakage occurs when the frequency f_c of the cosine is not an integer multiple of the frequency resolution. In other words, the cosine function does not ‘fit’ an integer number of periods in the measurement period T . Apparently, when $f_c = 2.5$ Hz we get the 9th frequency component of the DFT, but when $f_c = 2.3$ Hz, we need to use the DFT components ‘around’ the 2.3 Hz to ‘fit’ the DFT.

To better understand the cause of leakage, we need to consider the relation between the DTFT and the DFT once more. Recall that the DTFT was defined as the discrete-time Fourier transform of a sequence $x[n]$ of infinite length. The DFT, on the other hand, is used for measured sequences $y[n]$ that only have limited length N .

Now, one may consider $y[n]$ to be the same as $x[n]$ but multiplied with a **time window**

$w[n]$, defined as:

$$w[n] = \begin{cases} 1 & n = 0, 1, \dots, N-1 \\ 0 & \text{other } n \end{cases}$$

Then, it can be shown that the DTFT of $y[n]$ ($= w[n] \cdot x[n]$) equals the DFT of $x[n]$ at the discrete set of frequencies of the DFT.

The DFT of $x[n]$ is defined as:

$$X[k] = \sum_{n=0}^{N-1} x[n] e^{-jk\frac{2\pi}{N}n},$$

for the discrete set of frequencies $\Omega_k = k\frac{2\pi}{N}$.

For the continuous discrete frequency Ω , the DTFT of $y[n]$ equals:

$$\begin{aligned} Y(\Omega) &= \sum_{n=-\infty}^{\infty} w[n] x[n] e^{-j\Omega n} \\ &= \sum_{n=0}^{N-1} x[n] e^{-j\Omega n} \end{aligned}$$

At the discrete set of frequencies of the DFT, $\Omega = \Omega_k = k\frac{2\pi}{N}$ we obtain:

$$\begin{aligned} Y(\Omega_k) &= \sum_{n=0}^{N-1} x[n] e^{-j\Omega_k n} \\ &= \sum_{n=0}^{N-1} x[n] e^{-jk\frac{2\pi}{N}n} \\ &= X[k] \end{aligned}$$

Multiplication of $w[n]$ and $x[n]$ in the time domain means that we have a **convolution** of the DTFTs $W(\Omega)$ and $X(\Omega)$ in the frequency domain. It can be shown that:

$$W(\Omega) = \frac{\sin(\frac{N}{2}\Omega)}{\sin(\frac{1}{2}\Omega)} e^{-j(N-1)\Omega/2},$$

which is a ‘sinc-like’ function: $W(\Omega)$ is zero when $\frac{N}{2}\Omega = m\pi$, i.e., when $\Omega = m\frac{2\pi}{N}$ for integer $m \in \mathbb{Z}, m \neq 0$. With $\omega = \Omega/\Delta t$ and $f = \omega/(2\pi)$ we see that the function passes zero for $f = m\frac{f_s}{N}$, i.e., *exactly* at integer multiples of the frequency resolution of the DFT.⁴

Returning to our cosine-function example, the DTFT of $x[n] = \cos(2\pi f_c n \Delta t)$ equals:

$$X(\Omega) = \frac{\pi}{\Delta t} (\delta(\Omega - 2\pi f_c \Delta t) + \delta(\Omega + 2\pi f_c \Delta t)) \quad (4.21)$$

Convolving $W(\Omega)$ with $X(\Omega)$ means (because we are dealing with Dirac functions in $X(\Omega)$) that in order to get the DTFT of $Y(\Omega)$ we must add the ‘copy’ of $W(\Omega)$ centered at the

⁴Note that $f = \frac{\omega}{2\pi} = \frac{\Omega}{\Delta t} \frac{1}{2\pi} = m\frac{2\pi}{N} \frac{1}{\Delta t} \frac{1}{2\pi} = m\frac{f_s}{N}$.

positive frequency $\Omega = 2\pi f_c \Delta t$ and the copy of $W(\Omega)$ centered at the negative frequency $\Omega = -2\pi f_c \Delta t$.

Then, since $W(\Omega)$ is zero at $\Omega = m \frac{2\pi}{N}$ ($m \in \mathcal{Z}$, $m \neq 0$), $Y(\Omega)$ will be zero at frequencies Ω equal to $2\pi f_c \Delta t + m \frac{2\pi}{N}$, or, equivalently, with $f = \omega/(2\pi) = \Omega/(\Delta t 2\pi)$, at f equal to $f_c + m \frac{1}{N \Delta t} = f_c + m \frac{f_s}{N}$ ($m \in \mathcal{Z}$, $m \neq 0$).

When the DFT frequency resolution f_s/N ‘fits’ an integer number ℓ in f_c (i.e., $f_c = \ell \frac{f_s}{N}$), the locations of the zeros in the ‘sinc-like’ function become $(\ell + m) \frac{f_s}{N}$. That is, they do not change at all, and no leakage appears; this is illustrated in the left-hand figure of Figure 4.13, with the absolute value of the DTFT (the sinc-function Eq. (4.21)) shown in green, for $f_c = 2.5$ Hz

When this is not the case, however, the zeros of the ‘sinc-like’ function will not coincide with the frequency bins of the DFT, and spectral leakage will appear; this is illustrated in the right-hand figure of Figure 4.13, for $f_c = 2.3$ Hz.

In most practical situations, the probability that an arbitrary measured signal is periodical and exactly fits an integer number of periods in the measurement time T , is zero. Except in the case we can construct a signal ourselves (which often occurs in system identification applications), we will generally have leakage in the DFT.

One way to investigate the effects of leakage is to use **windowing** techniques. Recall that the finite observation of N samples can be considered as the complete ‘infinite-time’ observation, but multiplied with a rectangular window $w[n] = 1$ ($n = 0, \dots, N-1$) in the time domain. We could define a window function operating on the finite observation sequence that tries to make the observation more ‘periodic’, e.g., by putting the values of the samples close to the bounds of the observation interval to zero, while maintaining the values in the middle as much as possible. Examples are the Bartlett, Hanning, Hamming and Chebyshev windows.

4.5 The Fast Fourier Transform

The fast Fourier transform, or FFT for short, is an efficient computer algorithm for calculating the discrete Fourier transform (DFT) (Brigham, 1974).

We have seen in the previous section how the discrete Fourier transform of a finite sequence $x[n]$, $n = 0, 1, \dots, N-1$ can be calculated. Interpreting the discrete series $x[n]$ as a realization of a single cycle of a *periodic* series, the DFT has been shown to equal:

$$X[k] = \sum_{n=0}^{N-1} x[n] e^{-jk \frac{2\pi}{N} n} \quad k = 0, 1, 2, \dots, N-1$$

Computing the values of $X[k]$ by a direct approach, we will have to perform N^2 multiplications and $N(N - 1)$ complex additions, or, we need $\mathcal{O}(N^2)$ calculations. The very efficient FFT algorithm reduces this number to $\mathcal{O}(N^2 \log N)$ operations. Especially for long sequences an enormous reduction in computer time can be achieved in this way.

As an example, let's take a 40.96 seconds time series sampled at 100 Hz; we have $N=4,096$ samples. Here, $N = 2^m$ with $m=12$. The DFT would take $N^2 = 2^{2m} = 16,777,216$ multiplications, the FFT would take $N^2 \log N = 2^m m = 49,152$ multiplications; 341 times less! Try to imagine what this meant in the 1960s, when the FFT was developed, with the digital computers one used at that time.

Basically, the FFT works by partitioning the full data sequence $x[n]$ into a number of shorter sequences. Rather than calculating the DFT of the original sequence, only the DFT's of these shorter sequences are elaborated; these are then combined to yield the full DFT of $x[n]$. In the following we shall see how the logic behind the FFT works.

Suppose that the original sequence $x[n]$, $n = 0, 1, \dots, N - 1$, where N is an even number, is partitioned into two shorter sequences, each consisting of $N/2$ samples:

$$x[n] : \quad y[r] = x[2r], \quad (4.22)$$

and:

$$x[n] : \quad z[r] = x[2r + 1], \quad (4.23)$$

for $r = 0, 1, 2, \dots, \frac{N}{2} - 1$.

The DFT's of these two shorter sequences are referred to as $Y[k]$ and $Z[k]$, respectively:

$$Y[k] = \sum_{r=0}^{N/2-1} y[r] e^{-jk\frac{2\pi}{N/2}r} \quad (4.24)$$

$$Z[k] = \sum_{r=0}^{N/2-1} z[r] e^{-jk\frac{2\pi}{N/2}r} \quad (4.25)$$

for $k = 0, 1, 2, \dots, \frac{N}{2} - 1$. Now, $X[k]$ is periodical with period N ($X[k+N] = X[k]$), then $Y[k]$ and $Z[k]$ are periodic with period $N/2$. This can also be seen in Eqs. 4.24 and 4.25, where the smallest digital frequency now equals $2\frac{2\pi}{N}$, i.e., twice as large (faster), so the period is twice as small (shorter).

Returning to the DFT of the original sequence $x[n]$, we see how a similar rearrangement into odd and even terms comes about:

$$X[k] = \sum_{r=0}^{N-1} x[r] e^{-jk\frac{2\pi}{N}r}$$

$$\begin{aligned}
&= \sum_{r=0}^{N/2-1} x[2r] e^{-jk\frac{2\pi}{N}(2r)} + \sum_{r=0}^{N/2-1} x[2r+1] e^{-jk\frac{2\pi}{N}(2r+1)} \\
&= \sum_{r=0}^{N/2-1} y[r] e^{-jk\frac{2\pi}{N/2}r} + e^{-jk\frac{2\pi}{N}} \sum_{r=0}^{N/2-1} z[r] e^{-jk\frac{2\pi}{N/2}r} \\
&= Y[k] + e^{-jk\frac{2\pi}{N}} Z[k]
\end{aligned} \tag{4.26}$$

This equation holds for $k = 0, 1, 2, \dots, \frac{N}{2} - 1$ as only for these k 's the DFT of $y[r]$ and $z[r]$ are defined.

It is clear that the DFT of the original sequence $x[n]$ can be obtained directly from the DFT's of the two half sequences $y[r]$ and $z[r]$. If the original number of samples N in the sequence $x[n]$ is a power of 2, then the half sequences $y[r]$ and $z[r]$ may themselves also be partitioned into quarter sequences, etcetera, etcetera. The last two half sub-sequences will have only one term each.

The recipe derived above only applies for half the coefficients of the $X[k]$ series, i.e., $k = 0, 1, \dots, N/2 - 1$. Advantage can be taken, however, from the property that $Y[k]$ and $Z[k]$ are periodic with period $N/2$:

$$Y[k] = Y[k - N/2], \quad k = N/2, \dots, N - 1 \tag{4.27}$$

$$Z[k] = Z[k - N/2], \quad k = N/2, \dots, N - 1 \tag{4.28}$$

The full computational recipe for calculating the FFT is therefore:

$$X[k] = Y[k] + e^{-jk\frac{2\pi}{N}} Z[k], \quad k = 0, 1, 2, \dots, \frac{N}{2} - 1$$

$$X[k] = Y[k - N/2] + e^{-jk\frac{2\pi}{N}} Z[k - N/2], \quad k = N/2, \dots, N - 1$$

or, when taking k from 0 to $\frac{N}{2} - 1$:

$$X[k] = Y[k] + e^{-jk\frac{2\pi}{N}} Z[k] \tag{4.29}$$

$$X[k + N/2] = Y[k] - e^{-jk\frac{2\pi}{N}} Z[k] \tag{4.30}$$

The mechanism of the FFT algorithm is further explained by Example 4.2 in Section 4.6.

We have spent some time discussing the basic theory of the FFT, which is actually nothing more than an efficient algorithm for calculating the DFT. The reason for going into such detail is the important role which the FFT plays in spectral analysis. Since 1965, when the FFT was first developed, it has had a great impact on our approach to digital spectral analysis. In the next section we will turn to this latter subject in some more detail.

4.6 The calculation of spectral estimates

In this section we will see how the DFT is used to calculate a *direct* estimate of the spectral density of a random process, *without* the need for calculating covariance functions first.

4.6.1 The periodogram as an estimate for the discrete-time power spectral density

In Chapter 3, spectral densities were introduced as Fourier transforms of their corresponding covariance functions, Eq. (3.27):⁵

$$S_{\bar{x}\bar{y}}(\omega) = \mathcal{F}\{C_{\bar{x}\bar{y}}(\tau)\} = \int_{-\infty}^{+\infty} C_{\bar{x}\bar{y}}(\tau) e^{-j\omega\tau} d\tau$$

For simplicity we will only consider auto spectral density functions in the following; the same holds, however, for cross power spectral density functions.

Suppose that we have the random discrete time series $\bar{x}[n]$ which extends from $n = 0$ until $n = N - 1$. A necessary assumption is that $\bar{x}[n]$ is considered to be a *periodic* function of which only a single cycle is available for analysis. We can then calculate the DFT $\bar{X}[k]$ according to Eq. (4.19):

$$\bar{X}[k] = \sum_{n=0}^{N-1} \bar{x}[n] e^{-jk\frac{2\pi}{N}n},$$

for $k = 0, 1, 2, \dots, N - 1$.

Consider calculating the auto-covariance function of $\bar{x}[n]$. Clearly, we can only estimate this for time lags τ that are integer multiples of the sampling time Δt , i.e., $\tau = r\Delta t$. Using $\bar{C}[r]$ as an *estimate* of the covariance function then we can define:

$$\bar{C}[r] = \frac{1}{N} \sum_{s=0}^{N-1} \bar{x}[s] \bar{x}[s+r], \quad (4.31)$$

for $r = 0, 1, 2, \dots, N - 1$. This equation represents a *circular* product function which, as we consider the stochastic variables to have zero mean, equals the circular auto-covariance function. Remember that $\bar{x}[n]$ is assumed to be periodic:

$$\bar{x}[s+r] = \bar{x}[s+r-N] \quad (4.32)$$

for $s+r \geq N$.

Note that this way of processing the data does *not* faithfully represent the true covariance function, since the actual discrete time series are (usually) not periodic and the true values

⁵Note that we assume zero-mean stochastic processes in the following.

of $\bar{x}[s+r]$ differ from $\bar{x}[s+r-N]$ for $s+r \geq N$. To deal with this problem, we will consider the (periodical) circular covariance function $\bar{C}[r]$ as the ‘best available’ estimate for the true covariance function (which may not be periodic at all).

Since the circular covariance function is periodic with period N , its Fourier transform is a Fourier series, with values only at discrete frequencies being the integer multiple of the fundamental frequency, which in turn depends on the observation time. This **periodogram** is assumed to be the best available *estimate* of the discrete-time power spectral density $S_{\bar{x}\bar{x}}[k]$:

$$I_{N_{\bar{x}\bar{x}}}[k] = \sum_{r=0}^{N-1} \bar{C}[r] e^{-jk\frac{2\pi}{N}r} = \hat{S}_{\bar{x}\bar{x}}[k] \quad (4.33)$$

We shall show that $I_{N_{\bar{x}\bar{x}}}[k]$ is directly related to the DFT $\bar{X}[k]$:

$$I_{N_{\bar{x}\bar{x}}}[k] = \frac{1}{N} \bar{X}^*[k] \bar{X}[k] = \frac{1}{N} |\bar{X}[k]|^2, \quad (4.34)$$

where the symbol * denotes the complex conjugate. The proof is as follows:

$$\begin{aligned} I_{N_{\bar{x}\bar{x}}}[k] &= \sum_{r=0}^{N-1} \bar{C}[r] e^{-jk\frac{2\pi}{N}r} \\ &= \sum_{r=0}^{N-1} \left(\frac{1}{N} \sum_{s=0}^{N-1} \bar{x}[s] \bar{x}[s+r] \right) e^{-jk\frac{2\pi}{N}r} \quad (\text{definition of } \bar{C}[r]) \\ &= \frac{1}{N} \sum_{r=0}^{N-1} \sum_{s=0}^{N-1} \bar{x}[s] e^{jk\frac{2\pi}{N}s} \bar{x}[s+r] e^{-jk\frac{2\pi}{N}(s+r)} \quad (\text{rearranging terms}) \\ &= \frac{1}{N} \sum_{s=0}^{N-1} \bar{x}[s] e^{jk\frac{2\pi}{N}s} \left(\sum_{r=0}^{N-1} \bar{x}[s+r] e^{-jk\frac{2\pi}{N}(s+r)} \right) \quad (\text{rearranging terms}) \\ &= \frac{1}{N} \sum_{s=0}^{N-1} \bar{x}[s] e^{jk\frac{2\pi}{N}s} \left(\sum_{u=s}^{(N-1)+s} \bar{x}[u] e^{-jk\frac{2\pi}{N}u} \right) \quad (\text{substitute } u = s + r) \\ &= \frac{1}{N} \bar{X}^*[k] \bar{X}[k] = \frac{1}{N} |\bar{X}[k]|^2 \quad (\text{use : } \bar{X}[-k] = \bar{X}^*[k]) \end{aligned}$$

4.6.2 Properties of the periodogram

We will now go into some depth in discussing the relationship between the periodogram $I_{N_{\bar{x}\bar{x}}}[k]$, the spectrum *estimate*, and the *true* power spectral density $S_{\bar{x}\bar{x}}[k]$.

As will be shown, for long observation times the periodogram is an unbiased estimate of the true power spectral density. The periodogram is not a consistent estimate of the power spectral density, however, as the variance of $I_{N_{\bar{x}\bar{x}}}[k]$ will not approach zero as the

number of samples N , increases (not even for $N \rightarrow \infty$). A practical expression for the variance of the periodogram $I_{N_{\bar{x}\bar{x}}}[k]$ will be derived.

Note that in practice, only a finite record length is available, and therefore the periodogram is only an *estimate* for the true power spectral density:

$$\lim_{N \rightarrow \infty} E\{I_{N_{\bar{x}\bar{x}}}[k]\} = S_{\bar{x}\bar{x}}[k] \quad (\text{unbiased}) \quad (4.35)$$

$$\lim_{N \rightarrow \infty} \text{var}\{I_{N_{\bar{x}\bar{x}}}[k]\} \neq 0 \quad (\text{not consistent}) \quad (4.36)$$

Let us first assume a data sequence, $\bar{x}[n]$, with $0 \leq n \leq N - 1$, to be a white, zero-mean process with Gaussian probability density function. The periodogram $I_{N_{\bar{x}\bar{x}}}[k]$ of this process can be expressed by:

$$I_{N_{\bar{x}\bar{x}}}[k] = \frac{1}{N} |\bar{X}[k]|^2 = \frac{1}{N} \sum_{l=0}^{N-1} \sum_{m=0}^{N-1} \bar{x}[l] \bar{x}[m] e^{jk\frac{2\pi}{N}l} e^{-jk\frac{2\pi}{N}m}$$

Before we derive an expression for the variance of the periodogram $I_{N_{\bar{x}\bar{x}}}$, we shall first evaluate the expression for the covariance of the periodogram. We first consider the expectation of $I_N[k]$ ⁶ at two different frequencies k_1 and k_2 :

$$\begin{aligned} E\{I_N[k_1] I_N[k_2]\} &= \\ &= \frac{1}{N^2} \sum_{p=0}^{N-1} \sum_{q=0}^{N-1} \sum_{r=0}^{N-1} \sum_{s=0}^{N-1} E\{\bar{x}[p] \bar{x}[q] \bar{x}[r] \bar{x}[s]\} e^{j[k_1 \frac{2\pi}{N}(p-q) + k_2 \frac{2\pi}{N}(r-s)]} \end{aligned} \quad (4.37)$$

Eq. (4.37) must be simplified to obtain a useful result. If $\bar{x}[n]$ is a white, Gaussian, zero-mean process, it can be shown that:

$$\begin{aligned} E\{\bar{x}[p] \bar{x}[q] \bar{x}[r] \bar{x}[s]\} &= E\{\bar{x}[p] \bar{x}[q]\} E\{\bar{x}[r] \bar{x}[s]\} + \\ &+ E\{\bar{x}[p] \bar{x}[r]\} E\{\bar{x}[q] \bar{x}[s]\} + \\ &+ E\{\bar{x}[p] \bar{x}[s]\} E\{\bar{x}[q] \bar{x}[r]\} \end{aligned}$$

Hence:

$$E\{\bar{x}[p] \bar{x}[q] \bar{x}[r] \bar{x}[s]\} = \begin{cases} \sigma_{\bar{x}}^4 & p = q \text{ and } r = s \\ & \text{or } p = r \text{ and } q = s \\ & \text{or } p = s \text{ and } q = r \\ 0 & \text{else} \end{cases}, \quad (4.38)$$

with $\sigma_{\bar{x}}^2$ the variance of $\bar{x}[n]$. For other than Gaussian joint density functions, the result may not be this simple. However, here we only aim to give some insight into problems

⁶For brevity's sake, we will for the time being dismiss the $\bar{x}\bar{x}$ subscript of $I_N[k]$ in the following.

of spectrum estimation rather than to give a general formula with wide validity. Such a formula could also be difficult to interpret.

If we now substitute Eq. (4.38) into Eq. (4.37), we obtain:

$$\text{E}\{I_N[k_1], I_N[k_2]\} = \frac{\sigma_{\bar{x}}^4}{N^2} \left\{ N^2 + \sum_{p=0}^{N-1} \sum_{q=0}^{N-1} e^{j \frac{2\pi(k_1+k_2)(p-q)}{N}} + \sum_{p=0}^{N-1} \sum_{q=0}^{N-1} e^{j \frac{2\pi(k_1-k_2)(p-q)}{N}} \right\} \quad (4.39)$$

where the first term between the brackets on the right hand side (N^2) is for the case $p = q \wedge r = s$, the second term for the case $p = r \wedge q = s$ and the third term for the case $p = s \wedge q = r$. This equation can also be written as:

$$\text{E}\{I_N[k_1] I_N[k_2]\} = \sigma_{\bar{x}}^4 \left\{ 1 + \left(\frac{\sin(\pi(k_1 + k_2))}{N \sin(\pi(k_1 + k_2)/N)} \right)^2 + \left(\frac{\sin(\pi(k_1 - k_2))}{N \sin(\pi(k_1 - k_2)/N)} \right)^2 \right\} \quad (4.40)$$

The covariance of the periodogram is:

$$\begin{aligned} \text{cov}\{I_N[k_1], I_N[k_2]\} &= \text{E}\{(I_N[k_1] - \text{E}\{I_N[k_1]\})(I_N[k_2] - \text{E}\{I_N[k_2]\})\} = \\ &= \text{E}\{I_N[k_1] I_N[k_2]\} - \text{E}\{I_N[k_1]\} \text{E}\{I_N[k_2]\} \end{aligned} \quad (4.41)$$

And since:

$$\text{E}\{I_N[k_1]\} = \text{E}\{I_N[k_2]\} = \sigma_{\bar{x}}^2,$$

we can write:

$$\text{cov}\{I_N[k_1], I_N[k_2]\} = \text{E}\{I_N[k_1] I_N[k_2]\} - \sigma_{\bar{x}}^4$$

Hence, using Eq. (4.40):

$$\text{cov}\{I_N[k_1], I_N[k_2]\} = \sigma_{\bar{x}}^4 \left\{ \left(\frac{\sin(\pi(k_1 + k_2))}{N \sin(\pi(k_1 + k_2)/N)} \right)^2 + \left(\frac{\sin(\pi(k_1 - k_2))}{N \sin(\pi(k_1 - k_2)/N)} \right)^2 \right\} \quad (4.42)$$

The covariance, Eq. (4.42), at a particular frequency $k = k_1 = k_2$ is equal to the variance of the periodogram at that frequency k , $\text{E}\{I_N[k] I_N[k]\} = \sigma_{I_N}^2$:

$$\text{E}\{I_N[k] I_N[k]\} = \text{cov}\{I_N[k], I_N[k]\} = \sigma_{\bar{x}}^4 \left\{ \left(\frac{\sin[2\pi k]}{N \sin[\frac{2\pi k}{N}]} \right)^2 + 1 \right\} \quad (4.43)$$

Clearly the variance of $I_N[k]$ does not approach zero for any N ($N \rightarrow \infty$):

$$\lim_{N \rightarrow \infty} \text{var}\{I_N[k]\} = \sigma_{I_N}^2 = \sigma_{\bar{x}}^4 \neq 0 \quad (4.44)$$

In fact the variance of $I_N[k]$ is of order $\sigma_{\bar{x}}^4$ no matter how large N (and with that the observation time) is chosen.

Note that we will not further study the cross power spectral density estimate, $I_{N_{\bar{x}\bar{y}}}[k] = \frac{1}{N} \bar{X}^*[k] \bar{Y}[k]$, since the results for the auto power spectral density estimate (periodogram)

are also applicable here.

Although the power spectral density estimate $I_{N_{\bar{x}\bar{x}}}[k]$ is not a consistent estimate of the true power spectral density $S_{\bar{x}\bar{x}}[k]$, many researchers still use it as a first estimate, simply because of its computational simplicity.

4.6.3 The periodogram as an estimate for the continuous-time power spectral density

In most of our applications we intend to study *continuous-time* signals and systems, based on *discrete-time* samples that we have in a computer, a time series $x[n]$. From the above it is clear that we use the periodogram to obtain an estimate of the discrete-time spectral density, $S_{\bar{x}\bar{x}}[k]$, the Fourier transform of the discrete-time covariance function.

Now, this estimate is not the same as the continuous-time spectral density $S_{\bar{x}\bar{x}}(\omega)$. Rather, consider Figure 4.8, where we can clearly see that the discrete-time transform $X(\Omega)$ equals the continuous-time transform, $X(\omega)$ but scaled with $1/\Delta t$. In other words, in order to obtain an estimate of the continuous-time power spectrum we simply need to multiply the discrete-time spectrum with Δt :

$$\boxed{S_{\bar{x}\bar{x}}(\omega) = \Delta t \cdot S_{\bar{x}\bar{x}}[k]} \quad (4.45)$$

This may seem (and in fact is) an almost trivial point, but the literature (and many textbooks) has countless examples where one ‘forgets’ this scaling. Please also carefully study the Matlab files included in these lecture notes, where it is shown that apart from scaling one also needs to account for the DFT book-keeping tasks.

4.6.4 Conclusions

Rather than estimating the signal spectrum by first determining the signal covariance function and then calculating its Fourier transform, a faster way is to calculate the spectral estimate directly from FFT-ing the original time series (Jenkins & Watts, 1968). Even if we would only be interested in the (circular) covariance function it would still be faster to calculate the spectrum first and inverse fast Fourier transform (IFFT) it to obtain the covariance function. Smoothed estimators for power spectral densities will be discussed in the next section.

4.7 Smoothed estimators for power spectral densities

Since the periodogram is not a consistent estimate of the power spectral density and since its behaviour is highly undesirable (see Figure 4.21), it is necessary to study modifications that give better results. A standard approach in reducing the variance of the periodogram

is to average over a number of independent estimates, also known as Bartlett's procedure (Oppenheim & Schafer, 1975; Priestley, 1981).

4.7.1 Bartlett's procedure

In this approach, a data sequence $\bar{x}[n]$, $0 \leq n \leq N - 1$, is divided into K segments of M samples each, so that $N = KM$:

$$\bar{x}^{(i)}[n] = \bar{x}[n + iM - M] \quad 0 \leq n \leq M - 1, \quad 1 \leq i \leq K \quad (4.46)$$

and compute the K periodograms:

$$I_M^{(i)}[k] = \frac{1}{M} \left| \sum_{n=0}^{M-1} \bar{x}^{(i)}[n] e^{-j\frac{2\pi k}{M} n} \right|^2 \quad 0 \leq i \leq K \quad (4.47)$$

The smoothed estimate of the power spectral density of $\bar{x}[n]$ is then defined as:

$$\hat{S}_{xx}[k] = \frac{1}{K} \sum_{i=1}^K I_M^{(i)}[k], \quad (4.48)$$

or, simply taking the average of the K periodograms. The variance of $\hat{S}_{xx}[k]$ is then:

$$\text{var} \left\{ \hat{S}_{xx}[k] \right\} = \frac{1}{K} \text{var} \{ I_M[k] \} \quad (4.49)$$

For a fixed record length N , as the number of periodograms K increases, the variance decreases but also M decreases, the number of samples available per periodogram, and therefore the spectrum *resolution* decreases. Remember that in a DFT, the frequency resolution equals f_s/N , for N samples and sampling frequency f_s . So for a subsequence of M samples, with $M < N$, the resolution of the DFT reduces. Hence, a tradeoff exists between, on the one hand, spectrum resolution and, on the other hand, the variance of the estimate in Bartlett's procedure.

The actual choice of M for a given time series measurement with N samples will generally be guided by prior knowledge of the signal under consideration. For example, if we know that the spectrum has a very narrow 'peak', and when it is important to accurately resolve this peak, we must choose M large enough to maintain the desired frequency resolution. From the expression for the variance we can then determine the record length $N = KM$ for an acceptable variance of the spectrum estimate.

4.7.2 Window functions: the 'indirect' and 'direct' method

Another approach to 'smooth' the periodogram is to use an appropriate **window**, i.e.:

$$\hat{S}_{xx}[k] = \sum_{n=0}^{M-1} q[n] \bar{C}[n] e^{-jk\frac{2\pi}{M} n} \quad M < N - 1 \quad (4.50)$$

with $\bar{C}[n]$ the circular covariance function. The window sequence $q[n]$ is called a lag window, which works on the time series samples.

This method is called the **indirect method** because we first calculate the circular covariance and then estimate the power spectral density $\hat{S}_{xx}[k]$ using a finite duration window sequence of length M . Using convolution, Eq. (4.50) can also be written as:

$$\hat{S}_{xx}[k] = \int_{-\frac{N}{2}}^{\frac{N}{2}} Q[k] I_N[k - \lambda] d\lambda = \int_{-\frac{N}{2}}^{\frac{N}{2}} Q[k - \lambda] I_N[\lambda] d\lambda, \quad (4.51)$$

where $Q[k]$ is the discrete Fourier transform of $q[n]$:

$$Q[k] = \sum_{n=0}^{M-1} q[n] e^{-jk\frac{2\pi}{M}n} \quad (4.52)$$

$Q[k]$ is called a spectrum window.

From Eq. (4.51) it can be seen that the estimate of the power spectral density $\hat{S}_{xx}[k]$ is just a result of putting the periodogram $I_N[k]$ through a discrete-time filter with impulse-response function $Q[k]$. The expectation of the estimate is then, using Eq. (4.51):

$$E \left\{ \hat{S}_{xx}[k] \right\} = \int_{-\frac{N}{2}}^{\frac{N}{2}} Q[\lambda] E \{ I_N[k] \} d\lambda \quad (4.53)$$

Since $I_N[k]$ is the unbiased estimate of the ‘true’ spectral density $S_{xx}[k]$ for $N \rightarrow \infty$, the expectation of $\hat{S}_{xx}[k]$ can be written as:

$$E \left\{ \hat{S}_{xx}[k] \right\} \cong \int_{-\frac{N}{2}}^{\frac{N}{2}} Q[\lambda] S_{xx}[k - \lambda] d\lambda \quad (4.54)$$

when N is large enough.

The variance of $\hat{S}_{xx}[k]$ in this method is:

$$var \left\{ \hat{S}_{xx}[k] \right\} \cong \left(\frac{1}{N} \sum_{n=0}^{M-1} q^2[n] \right) var \{ I_N[k] \} \quad (4.55)$$

Welch (Oppenheim & Schafer, 1975) introduced a method to modify the procedure of Bartlett discussed at the beginning of this subsection. This procedure is particularly well suited for the direct computation of a power spectral density estimate using the FFT. This method is called the **direct method** as compared to the indirect method discussed above.

In the Welch method, the data record is again partitioned into K segments of M samples, see Eq. (4.46). The window $w[n]$ is applied directly to the *data sequence* segment before computating the periodogram. Welch defined K modified periodograms as:

$$I_M^{(i)}[k] = \frac{1}{MU} \left| \sum_{n=0}^{M-1} \bar{x}^{(i)}[n] w[n] e^{-jk\frac{2\pi}{M}n} \right|^2 \quad i = 1, 2, \dots, K \quad (4.56)$$

where:

$$U = \frac{1}{M} \sum_{n=0}^{M-1} w^2[n] \quad (4.57)$$

and the spectrum estimate is then, see Eq. (4.48):

$$\hat{S}_{xx}[k] = \frac{1}{K} \sum_{i=1}^K I_M^{(i)}[k] \quad (4.58)$$

The variance of $\hat{S}_{xx}[k]$ in this procedure is also reduced with respect to the variance of the periodogram $I_N[k]$, Eq. (4.49):

$$\text{var} \left\{ \hat{S}_{xx}[k] \right\} = \frac{1}{K} \text{var} \{ I_M[k] \},$$

The normalizing factor U is required for the estimate $\hat{S}_{xx}[k]$ to be asymptotically unbiased.

The window sequence $w[n]$ in Eq. (4.56) and Eq. (4.57) is called the data window compared to the spectrum window in the indirect method. The relation between the two windows is:

$$q[r] = \frac{1}{N} \sum_{n=0}^{N-1} w[n] w[n+r] \quad (4.59)$$

Then:

$$\begin{aligned} Q[k] &= \sum_{r=0}^{N-1} q[r] e^{-jk\frac{2\pi}{N}r} \\ &= \frac{1}{N} \sum_{r=0}^{N-1} \sum_{n=0}^{N-1} w[n] w[n+r] e^{-jk\frac{2\pi}{N}r} \\ &= \frac{1}{N} \sum_{n=0}^{N-1} w[n] e^{jk\frac{2\pi}{N}n} \sum_{r=0}^{N-1} w[n+r] e^{-jk\frac{2\pi}{N}(n+r)} \\ &= \frac{1}{N} W^*[k] W[k] \\ &= \frac{1}{N} |W[k]|^2 \end{aligned}$$

where $W[k]$ is the Fourier transform of $w[n]$ and is called the ‘frequency window’.

Note that there are many more applicable windows, studied and proposed by different authors. In Example 4.4 the Welch method is used and original data is Hanning-windowed for the calculation of the power spectral density estimate (Ljung, 1987).

The Hanning window function in MATLAB according to Ljung (Ljung, 1987) is given by the following, using a MATLAB notation:

$$w[n] = 0.5 \left(1 - \cos \left(\frac{2\pi(1:n)'}{N+1} \right) \right). \quad (4.60)$$

Exactly the same results are obtained by the window:

$$w[n] = 0.5 \left(1 + \cos \left(\frac{2\pi \left(2(-\frac{n}{2} : \frac{n}{2} - 1) + 1 \right)'}{2(N+1)} \right) \right),$$

which is also called a Hanning window.

The definition of the windows is summarized in Table 4.2.

4.8 Examples and problems

4.8.1 Example 4.1: the DFT

In order to illustrate the DFT algorithm we consider a simple case in which the original sequence $x[n]$, $n = 0, 1, \dots, N - 1$ has only a few terms, and work through the whole calculation. Suppose $x[n]$ has only four terms ($N=4$):

$$x[n] = (x_0, x_1, x_2, x_3)$$

We will use the basic definition of the DFT, Eq. (4.19):

$$X[k] = \sum_{n=0}^{N-1} x[n] e^{-jk\frac{2\pi}{N}n}, \quad k = 0, 1, \dots, N - 1$$

Because $N=4$ this definition becomes, for our ultra short sequence:

$$X[k] = \sum_{n=0}^3 x[n] e^{-jk\frac{\pi}{2}n}, \quad k = 0, 1, \dots, 3$$

We obtain for $k=0$:

$$\begin{aligned} X[0] &= \sum_{n=0}^3 x[n] e^{-j0\frac{\pi}{2}n} \\ &= x_0 + x_1 + x_2 + x_3 \\ &= (x_0 + x_2) + (x_1 + x_3). \end{aligned}$$

For $k=1$ we obtain:

$$\begin{aligned} X[1] &= \sum_{n=0}^3 x[n] e^{-j1\frac{\pi}{2}n} \\ &= x_0 - jx_1 - x_2 + jx_3 \\ &= (x_0 - x_2) - j(x_1 - x_3). \end{aligned}$$

For $k=2$ we obtain:

$$\begin{aligned} X[2] &= \sum_{n=0}^3 x[n] e^{-j2\frac{\pi}{2}n} \\ &= x_0 - x_1 + x_2 - x_3 \\ &= (x_0 + x_2) - (x_1 + x_3). \end{aligned}$$

And for $k=3$ we obtain:

$$\begin{aligned} X[3] &= \sum_{n=0}^3 x[n] e^{-j3\frac{\pi}{2}n} \\ &= x_0 + jx_1 - x_2 - jx_3 \\ &= (x_0 - x_2) + j(x_1 - x_3). \end{aligned}$$

These calculations confirm some of the properties of the DFT, discussed in Section 4.4.2. $X[0]$ is a real number that equals the sum of all samples; $X[\frac{N}{2}] = X[2]$ is also a real number and equals the sum of even samples minus the sum of all odd samples (it reflects sampling at the Nyquist frequency); we also see that $X[3] = X^*[1]$, the complex conjugate.

4.8.2 Example 4.2: the FFT

To illustrate the FFT algorithm we will again consider the sequence $x[n]$ used in Example 4.1. This sequence can be partitioned into two shorter sequences, see Eq. (4.22) and Eq. (4.23),

$$x[n] = \begin{cases} y[r] &= (x_0, x_2) \\ z[r] &= (x_1, x_3) \end{cases} \quad r = 0, 1$$

Subdividing until every sub-sequence only has one term, yields:

$$x[n] = \begin{cases} y[r] &= (x_0, x_2) \\ z[r] &= (x_1, x_3) \end{cases} \quad \begin{cases} t[r] &= (x_0) \\ u[r] &= (x_2) \\ v[r] &= (x_1) \\ w[r] &= (x_3) \end{cases} \quad r = 0 \quad (4.61)$$

If we consider the basic definition of the DFT, Eq. (4.19),

$$X[k] = \sum_{n=0}^{N-1} x[n] e^{-jk\frac{2\pi}{N}n}, \quad k = 0, 1, \dots, N-1,$$

it is evident that the DFT of a single term ($N = 1, n = 0, k = 0$) is equal to the term itself, and therefore we know the DFT's of the 'quarter'-sequences Eq. (4.61).

We will be combining the DFT's in two stages and use the 'rearranging' formulae Eq. (4.29) and Eq. (4.30):

$$\begin{aligned} X[k] &= Y[k] + e^{-jk\frac{2\pi}{N}} Z[k] \\ X[k + \frac{N}{2}] &= Y[k] - e^{-jk\frac{2\pi}{N}} Z[k] \end{aligned}$$

In the first stage, we move from the quarter sequences ($t[r], u[r], v[r], w[r]$, $N=1$) to the half-sequences ($y[r], z[r]$), and then in the second stage we move from these half-sequences to the final sequence $x[n]$.

In the first stage, we use the DFT's of the quarter-sequences which are the same as the sample values, and combine these DFT's into the DFT of the half-sequence. Because $N = 2$, $e^{-jk\frac{2\pi}{N}} = e^{-jk\pi}$, and we obtain for $k = 0$ ($e^{-j0\pi} = 1$) and $k = 1$ ($e^{-j1\pi} = -1$):

$$\left. \begin{array}{lcl} t[r] &= (x_0) &\rightarrow T[k] = x_0 \\ u[r] &= (x_2) &\rightarrow U[k] = x_2 \\ v[r] &= (x_1) &\rightarrow V[k] = x_1 \\ w[r] &= (x_3) &\rightarrow W[k] = x_3 \end{array} \right] \quad \begin{array}{l} Y[k] = \{(x_0 + x_2), (x_0 - x_2)\} = \{Y[0], Y[1]\} \\ Z[k] = \{(x_1 + x_3), (x_1 - x_3)\} = \{Z[0], Z[1]\} \end{array}$$

In the second stage we combine the DFT's of the half sequence into the DFT of the full sequence. Here, $N = 4$, so $e^{-jk\frac{2\pi}{4}} = e^{-jk\frac{\pi}{2}}$, so that:

$k = 0 :$

$$\begin{aligned} X[k] &= X[0] = Y[0] + e^{-j0\frac{\pi}{2}} Z[0] = Y[0] + Z[0] \\ X[k + \frac{N}{2}] &= X[2] = Y[0] - e^{-j0\frac{\pi}{2}} Z[0] = Y[0] - Z[0] \end{aligned}$$

$k = 1 :$

$$\begin{aligned} X[k] &= X[1] = Y[1] + e^{-j1\frac{\pi}{2}} Z[1] = Y[1] - jZ[1] \\ X[k + \frac{N}{2}] &= X[3] = Y[1] - e^{-j1\frac{\pi}{2}} Z[1] = Y[1] + jZ[1] \end{aligned}$$

or:

$$\begin{aligned} X[0] &= (x_0 + x_2) + (x_1 + x_3) \\ X[1] &= (x_0 - x_2) - j(x_1 - x_3) \\ X[2] &= (x_0 + x_2) - (x_1 + x_3) \\ X[3] &= (x_0 - x_2) + j(x_1 - x_3) \end{aligned}$$

Of course this is exactly equals the result of Example 4.1 where we simply substituted $x[n]$ in Eq. (4.19).

4.8.3 Example 4.3

The differences between covariance functions and power spectral densities, determined analytically in continuous time, and calculated using a computer in discrete time, will be demonstrated by determining these functions for the sine and noise signals.

In the continuous-time case (Examples 2.2, 2.3, 3.1 and 3.2) the covariance functions and power spectral densities have been obtained using the statistical properties of the stochastic processes, and by using the fact that these stochastic processes were considered to be ergodic. In the discrete-time case, the covariance functions and power spectral densities will be computed, based on finite-length discrete time histories, implying again that the stochastic processes are considered to be ergodic.

Sine wave with mean one

The first ‘stochastic’ process \bar{x} , discussed in Examples 2.2 and 3.2, consists of a sine wave with amplitude and mean value one, and a frequency of 1 Hz ($\bar{x}(t) = 1 + \sin(2\pi t)$). A sample of \bar{x} has been created with a sample frequency of 20 Hz and a duration of 20 seconds, Figure 4.14. The covariance function $C_{\bar{x}\bar{x}}(\tau)$ has been computed using MATLAB; it has the form of a cosine with amplitude 0.5, just as in the continuous time case.

There are, however, two differences. First, $C_{\bar{x}\bar{x}}(\tau)$ consists of only a limited number of discrete τ -points. Secondly, the amplitude of $C_{\bar{x}\bar{x}}(\tau)$ decreases as the absolute value of τ increases. The reason for this can be understood when regarding the integral $\int \bar{x}(t)\bar{x}(t-\tau)dt$, that has to be computed for the computation of $C_{\bar{x}\bar{x}}(\tau)$.

The range of t -values, for which $\bar{x}(t)$ is given, is limited due to the finite length of the time series $\bar{x}(t)$. As $|\tau|$ increases, the number of sample points which can be used for the computation of the above integral will become smaller, resulting in a decreasing amplitude of $C_{\bar{x}\bar{x}}(\tau)$. The rate of decrease depends on the ratio between the maximum value of τ , for which $C_{\bar{x}\bar{x}}(\tau)$ is computed, and the maximum value T of t , for which $\bar{x}(t)$ is given, the observation time. This effect is often accounted for by multiplying the integral with a factor $\frac{1}{T-\tau}$.

When regarding the power spectral density $S_{\bar{x}\bar{x}}(\omega)$ of \bar{x} as numerically calculated using MATLAB, Figure 4.15, it can be seen that the peaks at $\omega = \pm 2\pi$ rad/s (1 Hz) are an approximation of the Dirac-pulses that were found in the theoretical case (see Example 3.2 and Figure 3.10). The numerically calculated ‘pulses’ that we obtain with the DFT appear to have a ‘finite width’ and only a limited height.

Note, however, that Figure 4.14 and Figure 4.15 are drawn ‘as if’ we show a continuous time example. We are working in discrete time, with a discrete time series of finite length

N , and for the sake of this example it would be better to show the time series and all the calculations we do as a discrete time procedure.

Figure 4.16 and Figure 4.17 show the discrete values of the time series and our calculations. In the time domain we only have information at the integer multiples of our sample time Δt ; in the frequency domain we only have information at integer multiples of our frequency resolution f_s/N . The frequency resolution can be directly seen, it is just the (frequency-)value of the first frequency point, $f_s/N=20/400=0.05$ Hz in this example.

The ‘pulses’ that we expected in the PSD appear as non-zero *numbers* at exactly the right frequency, 1 Hz; these pulses have no ‘width’, they are just numbers at ± 1 Hz. Their height is a function of the number of samples N (or, equivalently, the observation time T , which is $N\Delta t$); the DFT algorithm simply ‘integrates’ over N samples, so in order to obtain the right values for the peaks (or numbers) we can simply divide by N .

Finally, note that because the frequency of the sinusoid, 1 Hz, fits exactly in the frequency resolution 0.05 Hz, we have no leakage in the spectrum calculation. This is equivalent to saying that the period of the sinusoid (1 seconds) fits an integer multiple in the observation time T (20 seconds). When this is not the case, leakage will occur in the spectrum.

Note that in the following, as is conventional, the time series and spectra are shown using *continuous* lines, ‘connecting’ the discrete-time points which may lead to the illusion of considering a continuous-time process. Don’t forget, in discrete time we deal with discrete numbers only!

White noise with mean zero

The second stochastic process discussed in previous examples is zero mean stationary white noise $\bar{w}(t)$. As mentioned before, white noise cannot exist physically. The usual way to approximate white noise is to generate a series of random numbers. In this example a noise signal w , consisting of 400 numbers with sample time 0.05 seconds (intensity 1) has been obtained using the MATLAB random number generator.

A realization of the stochastic process \bar{w} is plotted in Figure 4.18, together with its discrete-time covariance function $C_{\bar{w}\bar{w}}(\tau)$, which is an approximation of the covariance function that has been derived analytically in the continuous time case, due to the limited number of sample-points that has been taken into account. The peak at $\tau = 0$ s again has finite ‘width’ and height and also values for $\tau \neq 0$ are not equal to zero. See also Figure 2.15. Again, $C_{\bar{w}\bar{w}}$ is a discrete-time function with a limited number of τ -points, $\tau = k\Delta t$.

For the power spectral density function $S_{\bar{w}\bar{w}}(f)$ (Figure 4.19), it appears that the stochastic signal \bar{w} contains power at all frequencies. The power, however, is not distributed

equally over all frequencies as was theoretically proven to be the case in continuous time, see Figure 3.7, but it varies along the frequency axis, showing peaks for some values of f and being almost zero for other values. Note that the horizontal dashed line shows the ‘theoretical’ auto-PSD of the white noise signal.

From Figure 4.18 and Figure 4.19 it can be concluded that the signal \bar{w} from Figure 4.18 is only an approximation of white noise. This approximation can be improved by taking a higher sample rate and taking longer observation times. The more the covariance function resembles a Dirac-pulse and the more the power spectral density function tends to a constant value, the better the approximation will be.

A MATLAB .m-file that produces the plots in this example is given below. Using a sample frequency of 20 Hz and a 20 seconds observation time, Figures 4.14 to 4.19 can be created.

Listing 4.1: Example 4.3

```
% Examp143.m
%
% Chapter 4 of lecture notes ae4-304
%
% Digital calculation of covariance function and
% auto power spectral density.

% Program revised 1995, February 2004 [MM], October 2014 [M Rodriguez]

clear all; close all; clc;

disp(' Example 4.3');
disp(' Digital calculation of covariance function and');
disp(' auto power spectral density of a stochastic signal x(t).');
disp('');
disp(' This program can produce Figures 4-14 to 4-19 of the lecture');
disp(' notes: Aircraft Responses to Atmospheric Turbulence.');
disp('');

fs = input(' Enter sample frequency f (Hz) : ');
T = input(' Enter time T_end (s) : ');
dt=1/fs; N=T*fs; t=[dt:dt:T];

x = input(' Enter function definition x(t)= : ');
int = input(' Enter noise intensity : ');

% generate DT white noise sequence
x = x + sqrt(int)*randn(1,N);

% compute the auto covariance function
Cxx = xcov(x,'biased');

% compute the Fast Fourier Transform
X = fft(x);
```

```
% calculate the DT power spectral density estimate
Sxx=X.*conj(X)/N;

% define the frequency axis
f=(fs/N)*(0:N/2-1);

% properly assign positive and negative frequencies
for i=1:N/2
    fg(i) = -f(N/2+1-i);
    Sx(i) = Sxx(N/2+1-i);
end
f = [fg f];
Sxx = [Sx Sxx(1:N/2)];

% reference for white noise PSD
Refw= int*ones(1,N/2);

% PLOTTING THE RESULTS
figure
subplot(2,1,1);
plot(t,x);
xlabel('time [s]');
ylabel('x (t)');
title('SIGNAL');

subplot(2,1,2);
plot(t-T/2,Cxx(2*N/4+1:6*N/4));
xlabel('tau [s]');
ylabel('Cxx (tau)');
title('Auto Covariance Function');

figure
subplot(2,1,1);
plot(f,Sxx);
xlabel('frequency [Hz]');
ylabel('Sxx');
title('Auto Power Spectral Density (linear scales)');

subplot(2,1,2);
loglog(f(N/2:N-1),Sxx(N/2:N-1),f(N/2:N-1),Refw,'--');
xlabel('frequency [Hz]');
ylabel('Sxx');
title('Auto Power Spectral Density (loglog Scales)');

% EOF
```

4.8.4 Example 4.4

In order to demonstrate again the difference between theory and practice, the continuous-time power spectral densities that have been discussed in Example 3.3 will now be com-

puted, based on a simulated *discrete* input signal and a digitally calculated discrete output signal. We will again use MATLAB.

A time history of the input signal $\bar{u}(t)$, being the runway surface irregularities with power spectral density, Eq. (3.72):

$$S_{\bar{u}\bar{u}}(\omega) = \frac{K^2}{(1 + \tau_1^2\omega^2)(1 + \tau_2^2\omega^2)},$$

with $K^2 = 6.3 \cdot 10^{-4}/V$, $\tau_1 = 0.4/V$, $\tau_2 = 7/V$, can be obtained by filtering white noise with an appropriate filter. When the filter is taken to be a second order system with frequency response function:

$$H_f(\omega) = \frac{K}{(1 + j\omega\tau_1)(1 + j\omega\tau_2)}, \quad (4.62)$$

and when white noise with power spectral density:

$$S_{\bar{w}\bar{w}}(\omega) = 1,$$

is used as input signal to the filter, then the output signal has a power spectral density:

$$\begin{aligned} S_{\bar{u}\bar{u}}(\omega) &= |H_f(\omega)|^2 S_{\bar{w}\bar{w}}(\omega) = H_f(\omega) H_f(-\omega) S_{\bar{w}\bar{w}}(\omega) = \\ &= \frac{K}{(1 + j\omega\tau_1)(1 + j\omega\tau_2)} \frac{K}{(1 - j\omega\tau_1)(1 - j\omega\tau_2)} = \\ &= \frac{K^2}{(1 + \tau_1^2\omega^2)(1 + \tau_2^2\omega^2)}, \end{aligned} \quad (4.63)$$

which equals the power spectral density, Eq. (3.72) of the ‘runway rumble’.

A noise signal, consisting of 600 numbers with sample time 0.01 seconds, has been obtained using the MATLAB random generator, see Figure 4.20(a). This signal has been filtered by the filter given by the frequency response function Eq. (4.62) resulting in a time history of the input signal $\bar{u}(t)$ (see Figure 4.20(b)) to the landing gear suspension system, a second order mass-spring-damper system with a frequency response function, Eq. (3.74):

$$H_{\bar{y}\bar{u}}(\omega) = \frac{cj\omega + k}{-m\omega^2 + cj\omega + k},$$

where the coefficients m , c and k are taken as in Example 3.3 yielding a time history of $\bar{y}(t)$, the vertical displacement of the aircraft above a horizontal datum, see Figure 4.20. Comparing Figure 4.20(b) with Figure 4.20(c), we see that the suspension system is rather stiff: only the very high frequencies are filtered out of the input signal $\bar{u}(t)$.

The discrete power spectral densities of signals \bar{w} , \bar{u} and \bar{y} can be computed using Eq. (4.34):

$$S_{\bar{x}\bar{y}}[k] = \frac{1}{N} X[k]^* Y[k],$$

where an auto power spectral density is obtained substituting $Y[k] = X[k]$.

The *continuous* power spectral densities of signals follow from Eq. (4.45):

$$S_{\bar{x}\bar{y}}(\omega) = \Delta t S_{\bar{x}\bar{y}}[k]$$

and can be compared with the analytically determined spectra shown in Figure 3.14. These analytical spectra are plotted with a dashed line and the digitally calculated (estimated) spectra with a continuous line in Figure 4.21.

The frequency response function of the suspension system, $H_{\bar{y}\bar{u}}(\omega)$ can be reconstructed by using two of the power spectral densities, Eq. (3.53):

$$\hat{H}_{\bar{y}\bar{u}}(\omega) = \frac{S_{\bar{u}\bar{y}}(\omega)}{S_{\bar{u}\bar{u}}(\omega)}$$

In this case the estimate of the power spectral density is not consistent and its behaviour is highly undesirable especially at higher frequencies, since we only use the definition of the periodogram Eq. (4.34) to estimate the power spectral density.

A MATLAB .m file is given below. Figure 4.20 and Figure 4.21 result when for the speed $V = 10$ m/s, sampling frequency $f_s = 100$ Hz, observation time 60 s, white noise intensity $W = 1$ and aircraft mass $m = 2290$ kg is substituted; the damping and stiffness are set at $c = 20000$ Ns/m and $k = 183000$ N/m, respectively.

Listing 4.2: Example 4.4

```
% Examp144.m
%
% Chapter 4 of lecture notes ae4-304
%
% Calculates digitally the spectral densities of displacement and
% acceleration as a result of runway surface irregularities.
% The results are compared with the analytical solutions
% as found in Example 3.3.

% Program revised August 1992, February 2004 [MM], October 2014 [M
% Rodriguez]

clc; clear all; close all;

disp(' Example 4.4');
disp(' Compares the digitally calculated spectral densities');
disp(' of displacement and acceleration as a result of runway');
disp(' surface irregularities with the analytical solutions');
disp(' found in Example 3.3. The landing gear is modelled as a');
disp(' second order 1-DOF mass-spring-damper system, the input');
disp(' power spectral density is taken from AGARD-R-632.');
disp(' The output power spectral density is calculated with');
disp('');
```

```

disp('           Syy(w) = |H(w)|^2 * Suu(w)      (analytical)');
disp('           Syy(w) = conj(Y[k]).Y[k]/N      (numerical)');
disp(' ');
disp(' while the power spectral density for the acceleration');
disp(' is found with');
disp(' ');
disp('           Saa(w) = w^4 Syy(w)');
disp(' ');
disp(' This program can produce Figures 4-20 and 4-21 of the lecture');
disp(' notes: Aircraft Responses to Atmospheric Turbulence.');

V = input(' Enter ground speed V [m/s] : ');
fs = input(' Enter sample frequency [Hz] : ');
T = input(' Enter time T_end   (s) : ');
Wn = input(' Enter noise intensity : ');
m = input(' Enter aircraft mass [kg] : ');

dt = 1/fs;      % sample time
N = T/dt;       % Number of samples
t=[0:dt:T-dt]; % time axis

tau1=0.4/V; tau2=7/V;

% LANDING GEAR PARAMETERS
c = 20000;      % damping constant
k = 183000;     % spring constant

% DIGITAL CALCULATION OF INPUT SIGNAL
% the shaping filter ('rumble' filter definition)
num1= (6.3e-4)/V; den = [tau1*tau2 tau1+tau2 1];
sys = tf(sqrt(num1),den);

% create CT white noise
w = sqrt(Wn).*randn(1,N);
% filter it before you use it as an input to Matlab's lsim
[B,A]=butter(3,0.99); w = filter(B,A,w);

% Note that lsim 'internally' works in DT, so we need to 'scale'
% the CT white noise intensity with dt, or the signal with sqrt(1/dt)
% this explained in detail in Chapter 5 of the lecture notes
w = w/sqrt(dt);

% Then compute response of the rumble filter to "white noise",
% this yields the colored noise signal u
u = lsim(sys,w,t,'zoh');

% DIGITAL CALCULATION OF OUTPUT SIGNAL
% the suspension system (with known transfer function H(s))
num=[c k]; den=[m c k];
sys = tf(num,den);

% compute response of the suspension system to the

```

```
% colored noise u
y = lsim(sys,u,t,'zoh');

% plot the results
figure
subplot(3,1,1)
plot(t,w);
vv=axis; vv(1,1)=0; vv(1,2)=T; axis(vv);
xlabel('time [sec]'); ylabel('w(t)'); title('White Noise w(t)');

subplot(3,1,2)
plot(t,u);
vv=axis; vv(1,1)=0; vv(1,2)=T; axis(vv);
xlabel('time [sec]'); ylabel('u(t)'); title('Surface irregularity u(t)');

subplot(3,1,3)
plot(t,y);
vv=axis; vv(1,1)=0; vv(1,2)=T; axis(vv);
xlabel('time [sec]'); ylabel('y(t)');
title('Suspension system output y(t)');
pause(5)

% TRANSFORM ALL TO THE FREQUENCY DOMAIN
U = fft(u,N);
W = fft(w,N);
Y = fft(y,N);

% ESTIMATE THE DT POWER SPECTRA (PERIODOGRAM)
Suucalc = U.*conj(U)/N;
Swwcalc = W.*conj(W)/N;
Syycalc = Y.*conj(Y)/N;

Suycalc = conj(U(1:N)).*Y(1:N)/N;

% COMPUTE THE CT POWER SPECTRA
Suucalc = dt*Suucalc;
Swwcalc = dt*Swwcalc;
Syycalc = dt*Syycalc;
Suycalc = dt*Suycalc;

% define frequency axis
freqHz = (fs/N)*(1:N/2)';
omega = 2*pi*freqHz;

% ANALYTICAL EXPRESSIONS FOR INPUT POWER SPECTRAL DENSITIES
for i=1:N/2
    Swwanal(i,1) = Wn;
    Suuanal(i,1) = num1/((1+tau1^2*omega(i)^2)*(1+tau2^2*omega(i)^2))*Swwanal(i);
end
% compute the accelerations
Saacalc = (omega.^4).*Syycalc(1:N/2);
```

```
% ANALYTICAL EXPRESSIONS FOR OUTPUT POWER SPECTRAL DENSITIES
h = freqs(num, den, omega);
maganal = abs(h);
phaseanal = 180*angle(h)/pi;

Suyanal = h.*Suuanal;
Syyanal = (maganal.^2).*Suuanal;
Saaanal = (omega.^4).*Syyanal;

% ESTIMATION OF FREQUENCY RESPONSE FUNCTION FROM
% POWER SPECTRAL DENSITY RATIO
hcalc = Suycalc./Suucalc;

magcalc = abs(hcalc);
phasecalc = 180*angle(hcalc)/pi;

% PLOT THE RESULTS
figure
subplot(2,2,1);
loglog(freqHz, Swwanal, freqHz, Swwcalc(1:N/2), '--');
vv=axis; vv=[0.001 10 0.001 10]; axis(vv);
xlabel('frequency [Hz]'); ylabel('Sww');
title('PSD White Noise');

subplot(2,2,2);
loglog(freqHz, Suuanal, freqHz, Suucalc(1:N/2), '--');
vv=axis; vv=[0.001 10 10^(-10) 0.1]; axis(vv);
xlabel('frequency [Hz]'); ylabel('Suu');
title('PSD Forming Filter Output');

subplot(2,2,3);
loglog(freqHz, abs(real(Suyanal)), freqHz, abs(real(Suycalc(1:N/2))), '--');
vv=axis; vv=[0.001 10 10^(-11) 0.01]; axis(vv);
xlabel('frequency [Hz]'); ylabel('Re (Suy)');
title('Cross PSD w-u');

subplot(2,2,4);
semilogx(freqHz, imag(Suyanal), freqHz, imag(Suycalc(1:N/2)), '--');
xlabel('frequency [Hz]'); ylabel('Im (Suy)');
pause(5)

figure
subplot(2,2,1);
loglog(freqHz, Syyanal, freqHz, Syycalc(1:N/2), '--');
xlabel('frequency [Hz]'); ylabel('Syy');
title('PSD Model Output');

subplot(2,2,2);
loglog(freqHz, Saaanal, freqHz, Saacalc(1:N/2), '--');
xlabel('frequency [Hz]'); ylabel('Saa');
title('PSD Normal Acceleration');
```

```

subplot(2,2,3);
loglog(freqHz ,maganal ,freqHz ,magcalc(1:N/2) , '--' );
xlabel('frequency [Hz]'); ylabel('gain (H)');
title('Frequency Response Function');

subplot(2,2,4);
semilogx(freqHz ,phaseanal ,freqHz ,phasescalc(1:N/2) , '--' );
xlabel('frequency [Hz]'); ylabel('phase angle (H)');

% EOF

```

4.8.5 Example 4.5

As can be seen in Figure 4.21, the spectral densities or periodograms are rather ‘noisy’, especially at higher frequencies. The next MATLAB program uses the .m file `pwelch.m` for the estimation of the autospectra for \bar{w} , \bar{u} and \bar{y} (results shown in blue). The example also includes another approach by means of simply *smoothing* the raw periodograms, i.e., directly in the frequency domain, using `smooth.m` (results are shown in red). For comparison, the analytical spectra and results are also drawn through the dashed lines. All data are illustrated in Figure 4.22 and the accompanying MATLAB program is given below; to obtain similar figures, insert for the speed $V = 10$ m/s, sampling frequency $f_s = 100$ Hz, observation time 100 s and white noise intensity $W = 1$.

The top row in Figure 4.23 shows the real and imaginary parts of the cross power spectral density $S_{\bar{u}\bar{y}}(f)$ using the same three methods as in Figure 4.22; the bottom row shows estimates of the frequency response function $H_{\bar{y}\bar{u}}(f)$ using its magnitude and phase.

Clearly, the estimates become less noisy and better approximate the analytical values, especially at the lower frequencies. At higher frequencies, the estimates are better than before although deteriorate for the highest frequencies. The reader is encouraged to experiment with higher sample frequencies and higher observation times and study what happens. Remember that often an estimate is needed for a limited range of frequencies only, say up to 10 Hz. What should the experimenter do to obtain a better estimate, do we just need more samples or would it just be the observation time that matters?

Listing 4.3: Example 4.5

```

% Exempl45.m
%
% Chapter 4 of the lecture notes ae4-304
%
% Calculates digitally the spectral densities of displacement
% and acceleration as a result of runway surface irregularities.
% The results are compared with the analytical solutions as
% found in Example 3.3.

```

```
% Program revised August 1992, February 2004 [MM], December 2014 [M
% Rodriguez]

%%
clear all; close all; clc;

disp(' Example 4.5');
disp(' Compares the digitally calculated spectral densities of' );
disp(' displacement and acceleration as a result of runway surface' );
disp(' irregularities with the analytical solutions found in' );
disp(' Example 3.3. The landing gear is modelled as a second order' );
disp(' 1-DOF mass-spring-damper system, the input power spectral' );
disp(' density is taken from AGARD-R-632.' );
disp(' ');
disp(' The output power spectral density is calculated with:' );
disp(' ');
disp(' Syy(w) = |H(w)|^2 * Suu(w) (analytical)' );
disp(' ');
disp(' and it is computed using either the pwelch.m routine, or' );
disp(' using periodograms and then smoothed with smooth.m.' );
disp(' ');
disp(' The program also obtains estimates for the cross PSD' );
disp(' between u and y, Suy, and the frequency response between' );
disp(' colored noise (u) and the suspension displacement.' );
disp(' ');
disp(' The power spectral density of the acceleration' );
disp(' is found with' );
disp(' ');
disp(' Saa(w) = w^4 Syy(w)' );
disp(' ');
disp(' This program produces Figures 4.22 and 4.23 of the lecture' );
disp(' notes: Aircraft Responses to Atmospheric Turbulence.' );

V = input(' Enter ground speed V [m/s] : ');
fs = input(' Enter sample frequency [Hz] : ');
T = input(' Enter time T_end (s) : ');
Wn = input(' Enter noise intensity : ');

% create time axis
dt = 1/fs; % sampling time
N = T/dt; % number of samples
t = [0:dt:T-dt]; % time axis

% create frequency axis
fres = fs/N; % frequency resolution in Hz
f = fres*[1:1:N/2]; % frequency axis, in Hz
omega= f*2*pi; % frequency axis, in rad/s

%%%%%%%%%%%%%
% RUNWAY RUMBLE
%%%%%%%%%%%%%
% DEFINE DYNAMICS
```

```
% shaping filter parameters
tau1 = 0.4/V; tau2 = 7/V;
% system dynamics
num = sqrt((6.3e-4)/V); % 'runway rumble' shaping filter dynamics
den = [tau1*tau2 tau1+tau2 1];
sys = tf(num,den);
% frequency response, in rad/s
hrr = freqs(num,den,omega);
% CALCULATE 'runway rumble' SYSTEM RESPONSE TO WHITE NOISE
% create white noise input, intensity Wn
% because lsim 'internally' works as a discrete-time simulation,
% the white noise intensity needs to scaled first (Chapter 5)
w = sqrt(Wn/dt)*randn(1,N);
% calculate runway rumble response to white noise
u = lsim(sys,w,t);

%%%%%%%%%%%%%
% SUSPENSION SYSTEM
%%%%%%%%%%%%%
% DEFINE DYNAMICS
% landing gear parameters
m = 2290; % aircraft mass m [kg]
c = 20000; % damping constant
k = 183000; % spring constant
% system dynamics
num = [c k]; % 'suspension system' dynamics
den = [m c k];
sys = tf(num,den);
% frequency response, in rad/s
hss = freqs(num,den,omega);
% CALCULATE 'suspension system' SYSTEM RESPONSE TO 'runway rumble'
y = lsim(sys,u,t);

%%%%%%%%%%%%%
% ANALYTICAL EXPRESSIONS FOR POWER SPECTRAL DENSITIES
%%%%%%%%%%%%%
% Note that these spectra are continuous-time, as our system dynamics
% above are defined as continuous-time transfer functions H(s). So when
% comparing these analytical spectra with what we will calculate with
% the simulated time series, which are discrete time, we need to multiply
% the spectra that we estimate with dt (Chapter 4).
% And also note that these analytical spectra are computed as a function
% of frequency in rad/s (omega).

% white noise has a spectrum that equals Wn at all frequencies
for i=1:N/2
    Swwanal(i,1) = Wn;
end
% the colored noise has an auto-spectrum that equals Wn * |Hrr|^2
% with Hr the runway rumble frequency response
hrrmag = abs(hrr)';
Suuanal = (hrrmag.^2).*Swwanal;
```

```
% the suspension system has an auto-spectrum that equals Suuanal * |Hss|^2
% with Hss the suspension system frequency response
hssmag = abs(hss)';
Syyanal = (hssmag.^2).*Suuanal;
% the analytical cross PSD between u and y equals Hss * Suuanal
Suyanal = hss.*Suuanal';
% the auto PSD of the acceleration comes from double differentiating
% the position, which in the frequency domain becomes
Saaanal = (omega.^4).*Syyanal;

%%%%%%%%%%%%%
% CALCULATE THE RAW PERIODOGRAMS
%%%%%%%%%%%%%
% white noise PSD estimate
WN = fft(w,N);
Sww = WN.*conj(WN)/N;
Sww = Sww(1:N/2); % only take positive frequencies
% runway rumble PSD estimate
U = fft(u,N);
Suu = U.*conj(U)/N;
Suu = Suu(1:N/2); % only take positive frequencies
% suspension system PSD estimate
Y = fft(y,N);
Syy = Y.*conj(Y)/N;
Syy = Syy(1:N/2); % only take positive frequencies
% cross PSD function Suy estimate
Suy = Y.*conj(U)/N;
Suy = Suy(1:N/2); % only take positive frequencies
% acceleration PSD estimate
Saa = (omega.^4).*Syy;
% correct for the fact that we want estimates of continuous-time
% spectra, so multiply with dt (Chapter 4)
Sww = Sww*dt;
Suu = Suu*dt;
Suy = Suy*dt;
Syy = Syy*dt;
Saa = Saa*dt;

%%%%%%%%%%%%%
% CALCULATE THE SMOOTHED PERIODOGRAMS USING pwelch.m
%%%%%%%%%%%%%
% To properly use pwelch (or any algorithm for that matter) we first
% need to state some of the algorithm's properties:
% - it gives us the estimate of the discrete-time spectrum,
%   but already multiplied with dt
% - it returns the frequency in Hz, starting with the zero frequency,
%   so we need to 'align' the frequency axis with our frequency axis
% - we can only compute autospectra with pwelch
% - it uses windows (here 100 samples) and overlap between these
%   windows (here set at 10 samples)
% - with one-sided the spectrum estimate needs to be divided by 2
%   to also take into account the negative frequencies
```

```
% smoothed periodogram of the white noise signal
[Swwspct fw] = pwelch(w,100,10,N,fs , 'onesided');
Swwspct = Swwspct/2; % adjust power for negative frequencies
Swwspct = Swwspct(2:N/2+1); % get rid of the zero frequency, to align
% smoothed periodogram of runway rumble response
[Suuspct fw] = pwelch(u,100,10,N,fs , 'onesided');
Suuspct = Suuspct/2;
Suuspct = Suuspct(2:N/2+1);
% smoothed periodogram of suspension system response
[Syyspct fw] = pwelch(y,100,10,N,fs , 'onesided');
Syyspct = Syyspct/2;
Syyspct = Syyspct(2:N/2+1);
fw = fw(2:N/2+1);
% smoothed periodogram of acceleration
Saaspct = (omega.^4) .* Syyspct;

%%%%%%%%%%%%%
% A SIMPLER ALTERNATIVE TO SMOOTH THE RAW PERIODOGRAMS
%%%%%%%%%%%%%
% Basically we smoothen the periodogram in the frequency domain
% with a 'moving average' (the algorithm's default) of 100 samples
Swws = smooth(Sww,100);
Suus = smooth(Suu,100);
Syys = smooth(Syy,100);
Saas = smooth(Saa,100);
% Suy is complex
Suys = smooth(Suy,100);
Suyrs= smooth(real(Suy),100); % smooth real part of Suy
Suyis= smooth(imag(Suy),100); % smooth imaginary part of Suy

%%%%%%%%%%%%%
% ESTIMATE THE suspension dynamics FREQUENCY RESPONSE FUNCTION
%%%%%%%%%%%%%
% We can now obtain estimates of the frequency response function
% of the suspension system dynamics, in two ways
% 1) using the raw periodograms
hss_raw = Suy./Suu;
mss_raw = abs(hss_raw);
pss_raw = (180/pi)*phase(hss_raw)';
% 2) using the smoothed periodograms with pwelch
hss_sm = Suys./Suus;
mss_sm = abs(hss_sm);
pss_sm = (180/pi)*phase(hss_sm)';
% the analytic frequency response
mss_anal = abs(hss);
pss_anal = (180/pi)*phase(hss)';

%%%%%%%%%%%%%
% PLOTTING THE RESULTS
%%%%%%%%%%%%%
% FIRST THE AUTOSPECTRA and the smoothed ways to compute them
figure(1)
```

```

subplot(2,2,1)
loglog(f,Swwspect,f,Swws,'r- ',f,Swwanal,'g--')
xlabel('frequency [Hz]'); ylabel('Sww(f)');
title('PSD White Noise and Smoothed PSDs');

subplot(2,2,2)
loglog(f,Suspect,f,Suus,'r- ',f,Suanal,'g--')
xlabel('frequency [Hz]'); ylabel('Suu(f)');
title('PSD Forming Filter Output and Smoothed PSDs');

subplot(2,2,3)
loglog(f,Syyspect,f,Syys,'r- ',f,Syyanal,'g--')
xlabel('frequency [Hz]'); ylabel('Syy(f)');
title('PSD Damper Output and Smoothed PSDs');

subplot(2,2,4)
loglog(f,Saspct,f,Saas,'r- ',f,Saaanal,'g--')
xlabel('frequency [Hz]'); ylabel('Syy(f)');
title('PSD Acceleration and Smoothed PSDs');

%% THEN THE crossSPECTRUM, in two ways (raw & smoothed vs. analytic)
% note that we take the absolute values of the real and imaginary parts
% as these may be very small and negative
figure(2)
subplot(2,2,1)
loglog(f,abs(real(Suy)),f,abs(Suyrs),'r- ', f,abs(real(Suyanal)),'g--')
xlabel('frequency [Hz]'); ylabel('Real Suy(f)');
title('Real part cross PSDs Suy');

subplot(2,2,2)
loglog(f,abs(imag(Suy)),f,abs(Suyis),'r- ', f,abs(imag(Suyanal)),'g--')
xlabel('frequency [Hz]'); ylabel('Imag Suy(f)');
title('Imaginary part cross PSDs Suy');

%% AND the estimated frequency response, in two ways
%% (raw & smoothed vs. analytic)
subplot(2,2,3)
loglog(f,mss_raw,f,mss_sm,'r- ',f,mss_anal,'g--')
xlabel('frequency [Hz]'); ylabel('|Hyu|');
title('Frequency response function Hyu (gain)');

subplot(2,2,4)
semilogx(f,pss_raw,f,pss_sm,'r- ',f,pss_anal,'g--')
vv=axis; vv(1,3)=-180; vv(1,4)=45; axis(vv);
xlabel('frequency [Hz]'); ylabel('<Hyu, deg');
title('Frequency response function Hyu (phase)');

% EOF

```

4.8.6 Problem 4.1

Calculate the DFT's of the discrete time series:

$$x_1[n] = \left\{ 0, \frac{1}{2}\sqrt{2}, 1, \frac{1}{2}\sqrt{2}, 0, -\frac{1}{2}\sqrt{2}, -1, -\frac{1}{2}\sqrt{2} \right\},$$

and

$$x_2[n] = \left\{ 1, \frac{1}{2}\sqrt{2}, 0, -\frac{1}{2}\sqrt{2}, -1, -\frac{1}{2}\sqrt{2}, 0, \frac{1}{2}\sqrt{2} \right\},$$

and compare the results with the (continuous) Fourier transforms of the periodic functions $\sin(\frac{2\pi t}{T})$ and $\cos(\frac{2\pi t}{T})$.

4.8.7 Problem 4.2

Compare the variances of the runway surface irregularities with a power spectral density given by Eq. (3.72) using three different methods. Use MATLAB where necessary.

- In the frequency domain using the filter given by Eq. (4.62) driven by white noise with intensity 1 and the standard integrals from Tables 3.5 and 3.6:

$$\sigma_{\bar{u}}^2 = \frac{1}{\pi} \int_0^{+\infty} |H(\omega)|^2 S_{\bar{w}\bar{w}}(\omega) d\omega$$

- In the time domain using a time history like in Figure 4.20, with:

$$\sigma_{\bar{u}}^2 = \frac{1}{N-1} \sum_{i=1}^N (u[i] - \mu_{\bar{u}})^2$$

- In the frequency domain by numerically integrating the output power spectral density Eq. (4.63):

$$\sigma_{\bar{u}}^2 = \frac{1}{\pi} \int_0^{+\infty} S_{\bar{u}\bar{u}}(\omega) d\omega$$

4.9 Summary

In this chapter we presented the theory of spectral analysis for discrete-time stochastic processes. The discrete Fourier transform (DFT) and the calculation of spectral estimates have extensively been discussed. As an estimate for the power spectral density functions the periodogram has been introduced. The periodogram is a simple tool for calculating the power spectral density functions using time-domain data. Smoothed estimators for power spectral densities have been discussed as well.

continuous time	discrete time
CTFT	DTFT
$X(\omega) = \mathcal{F}\{x(t)\} = \int_{-\infty}^{\infty} x(t)e^{-j\omega t} dt$	$X(\Omega) = \mathcal{F}\{x[n]\} = \sum_{n=-\infty}^{\infty} x[n]e^{-j\Omega n}$
$x(t) = \mathcal{F}^{-1}\{X(\omega)\} = \frac{1}{2\pi} \int_{-\infty}^{\infty} X(\omega)e^{j\omega t} d\omega$	$x[n] = \mathcal{F}^{-1}\{X(\Omega)\} = \frac{1}{2\pi} \int_0^{2\pi} X(\Omega)e^{j\Omega n} d\Omega$
Laplace transform	z -transform
$X(s) = \mathcal{L}\{x(t)\} = \int_{-\infty}^{\infty} x(t)e^{-st} dt$	$X(z) = \mathcal{Z}\{x[n]\} = \sum_{n=-\infty}^{\infty} x[n]z^{-n}$
$x(t) = \mathcal{L}^{-1}\{X(s)\} = \frac{1}{2\pi j} \int_{\sigma-j\infty}^{\sigma+j\infty} X(s)e^{st} ds$	$x[n] = \mathcal{F}^{-1}\{X(z)\} = \frac{1}{2\pi j} \oint X(z)z^{n-1} dz$

Table 4.1: Relations between continuous-time and discrete-time transforms.

Time domain	Frequency domain
Data window $w[n]$	Frequency window $W[k]$
Lag window $q[n]$	Spectrum window $Q[k]$

Table 4.2: Examples of time- and frequency-domain windows

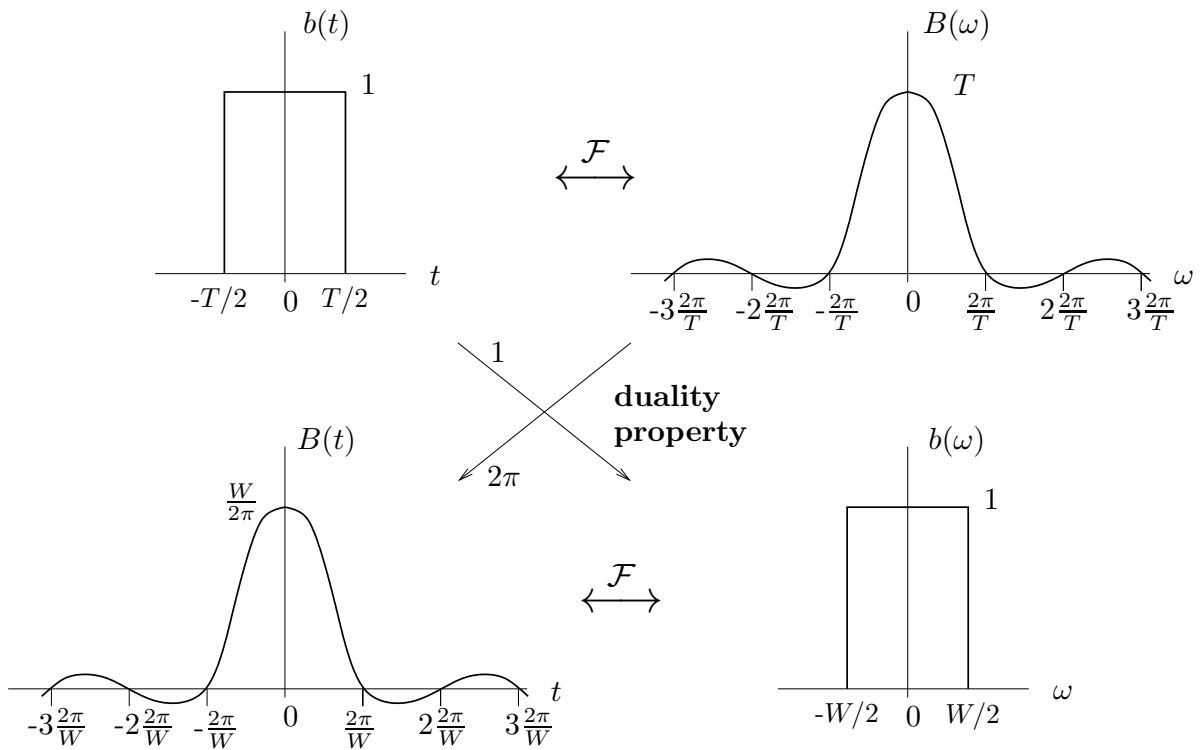


Figure 4.1: Duality of the block transformation.

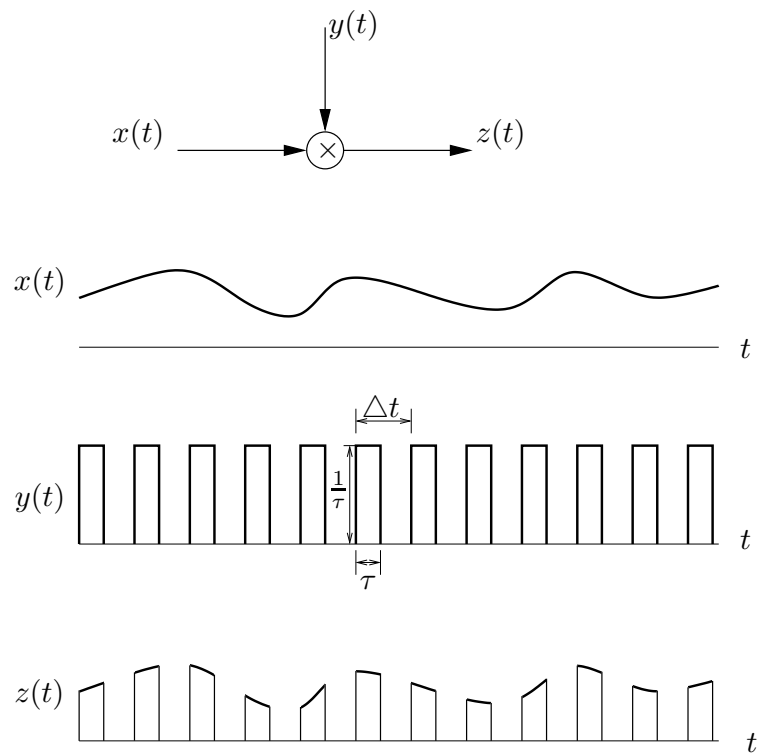


Figure 4.2: The sampling process.

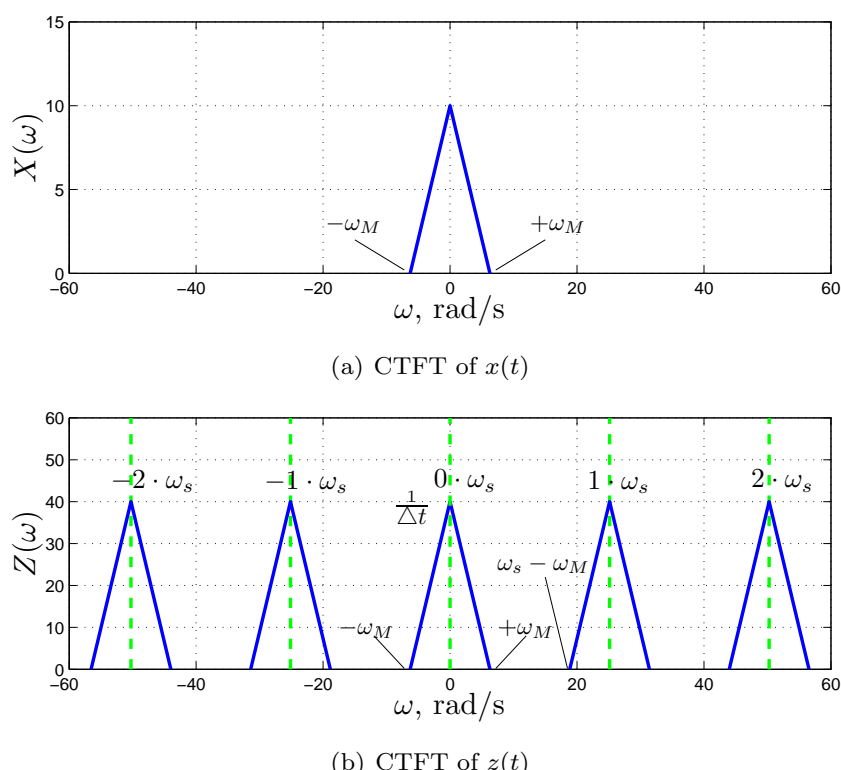
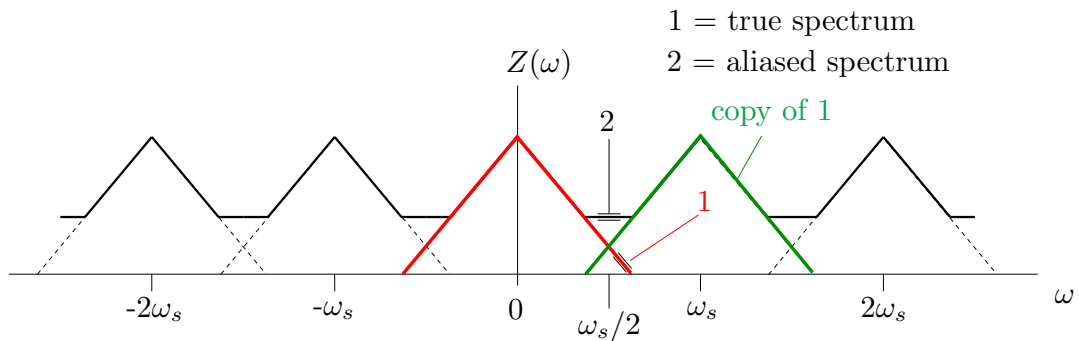
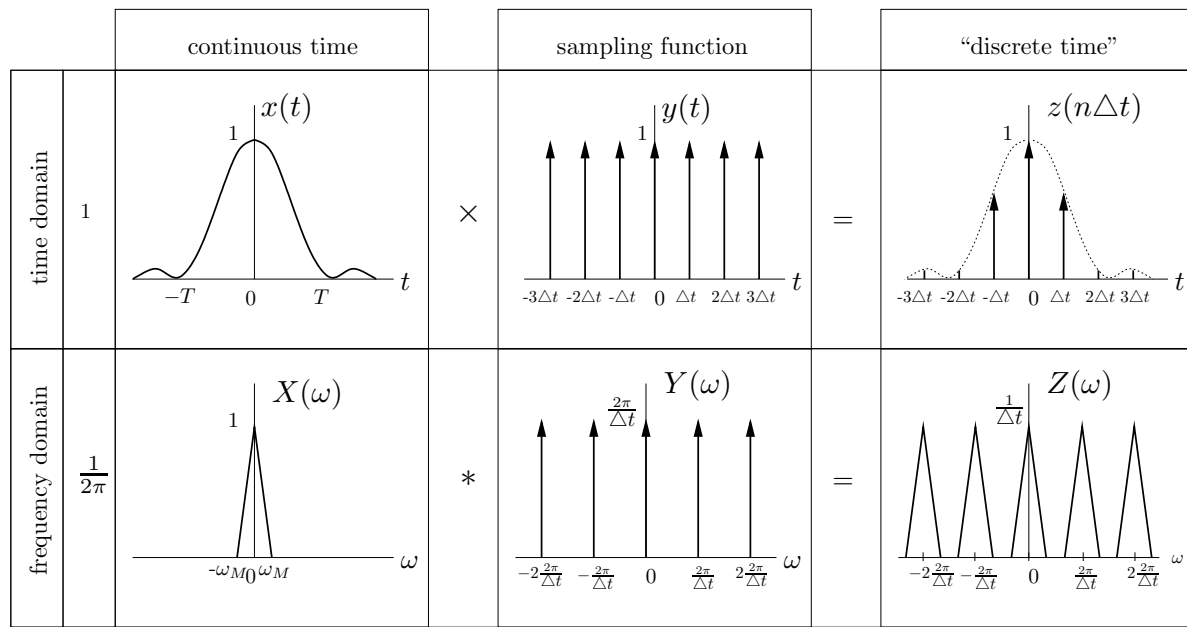


Figure 4.3: Example of impulse-train sampled spectrum

**Figure 4.4:** Illustration of the aliasing effect.**Figure 4.5:** Impulse-train sampling overview 1.

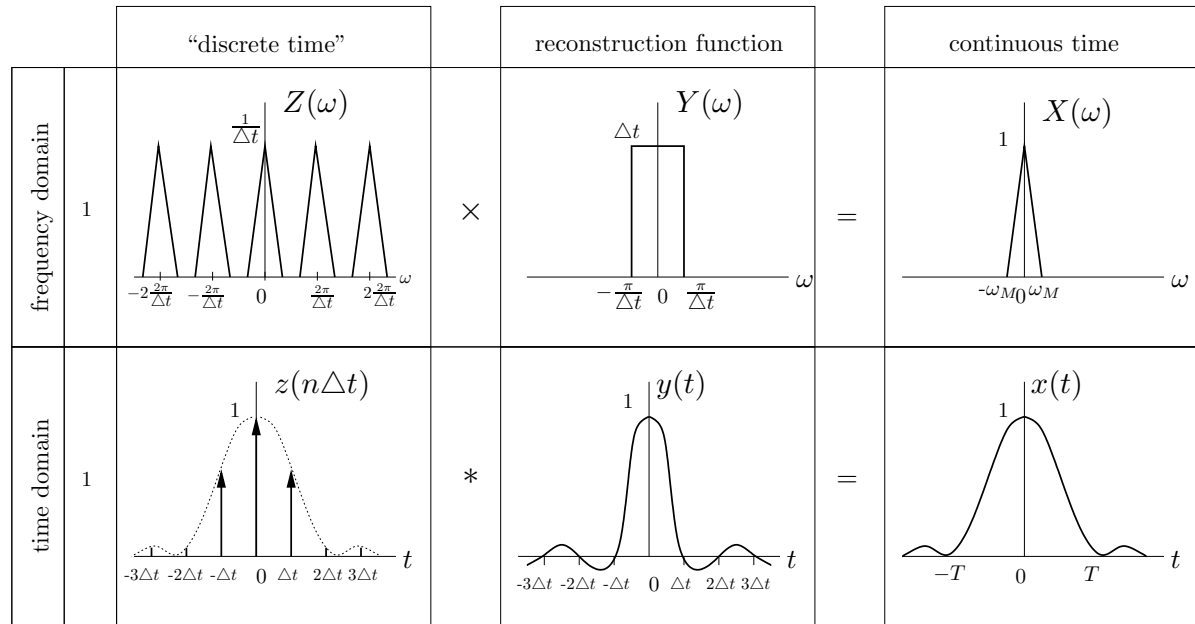


Figure 4.6: Ideal signal reconstruction scheme.

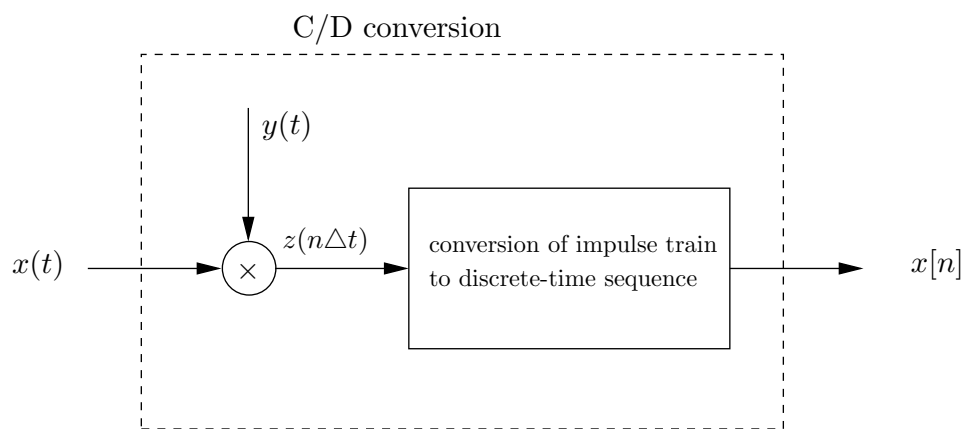


Figure 4.7: Conversion of the CT pulse train model $z(n\Delta t)$ to a discrete time series $x[n]$.

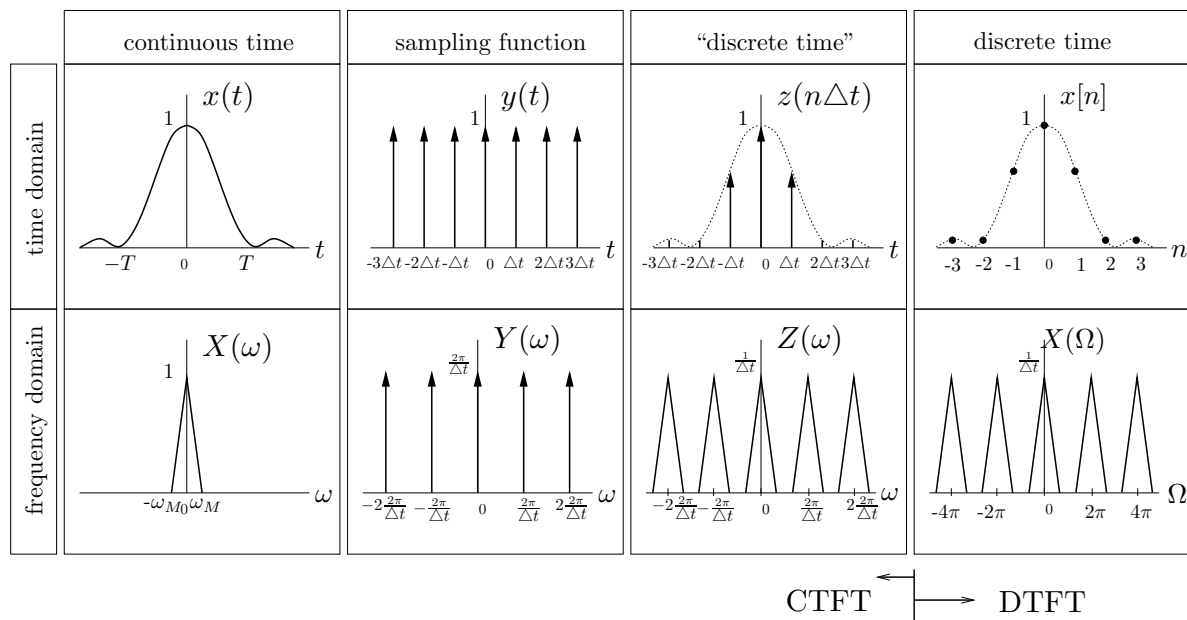
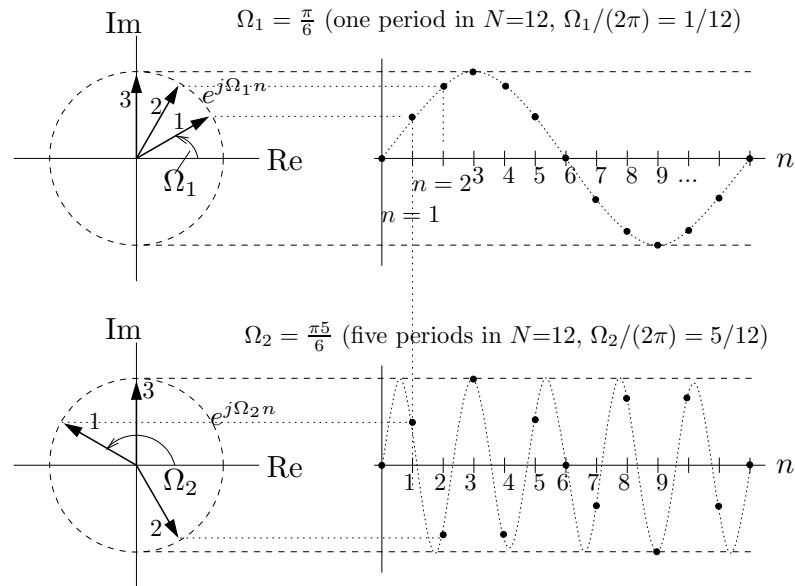
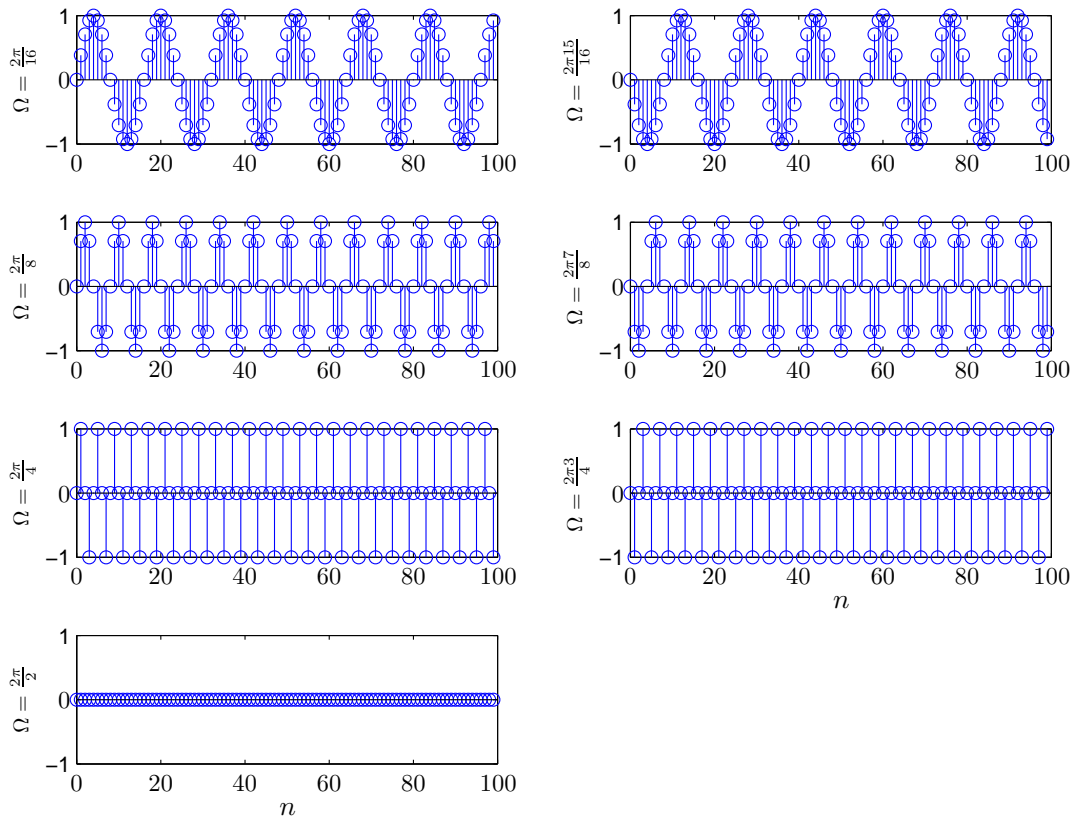


Figure 4.8: Impulse-train sampling overview 2: sampling complete.



(a) Rotating complex exponential function in discrete time.

(b) The 'sine'-component of the complex exponential, for various discrete frequencies Ω .**Figure 4.9:** Frequency in discrete time.

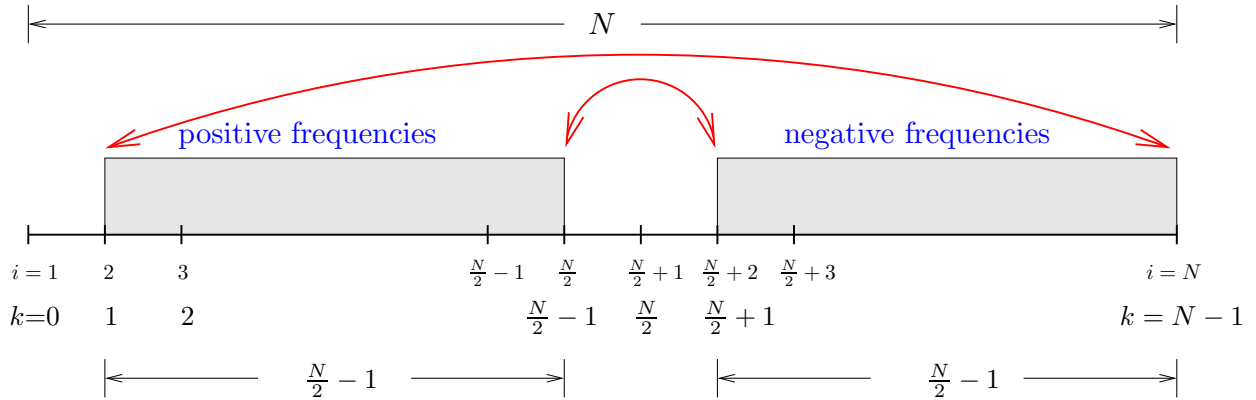


Figure 4.10: The Discrete Fourier Transform; positive and negative frequencies.

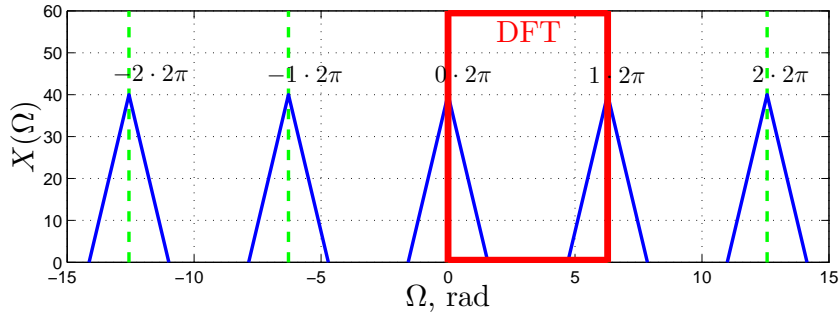


Figure 4.11: The ‘view’ of the DFT on the discrete-time spectrum.

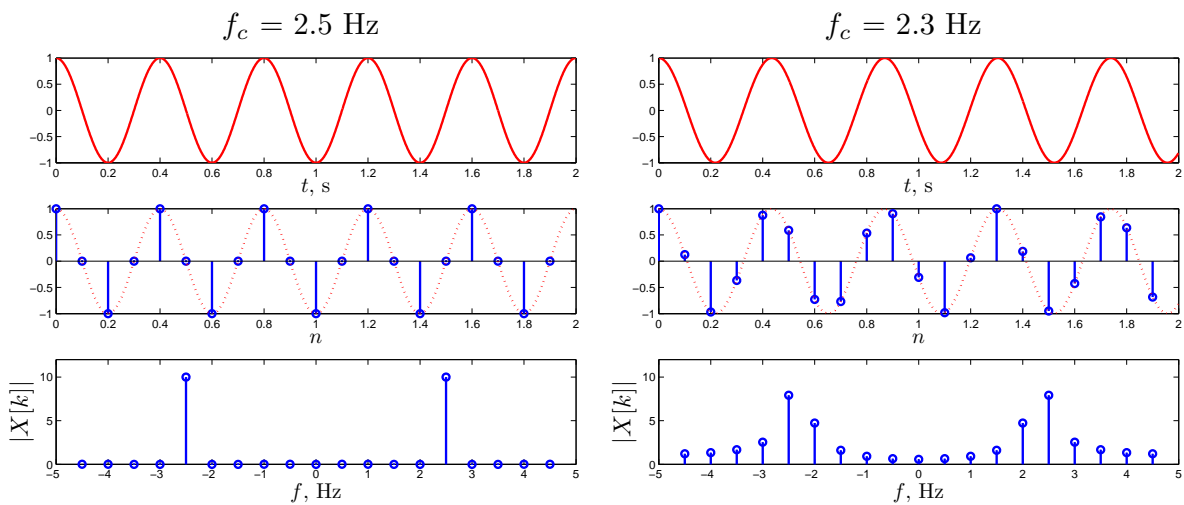


Figure 4.12: Illustration of the ‘leakage’ phenomenon (right).

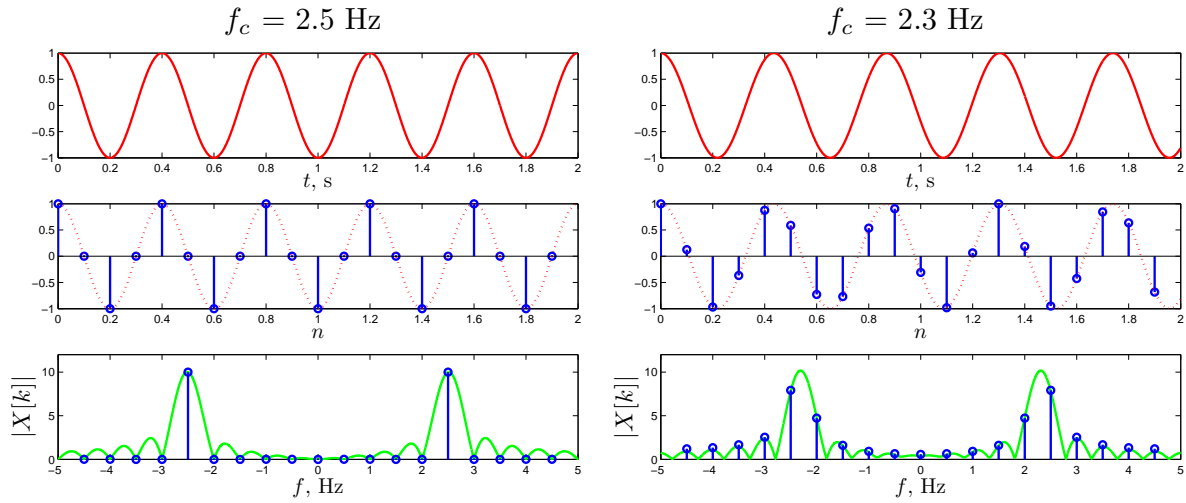


Figure 4.13: Second illustration of the ‘leakage’ phenomenon.

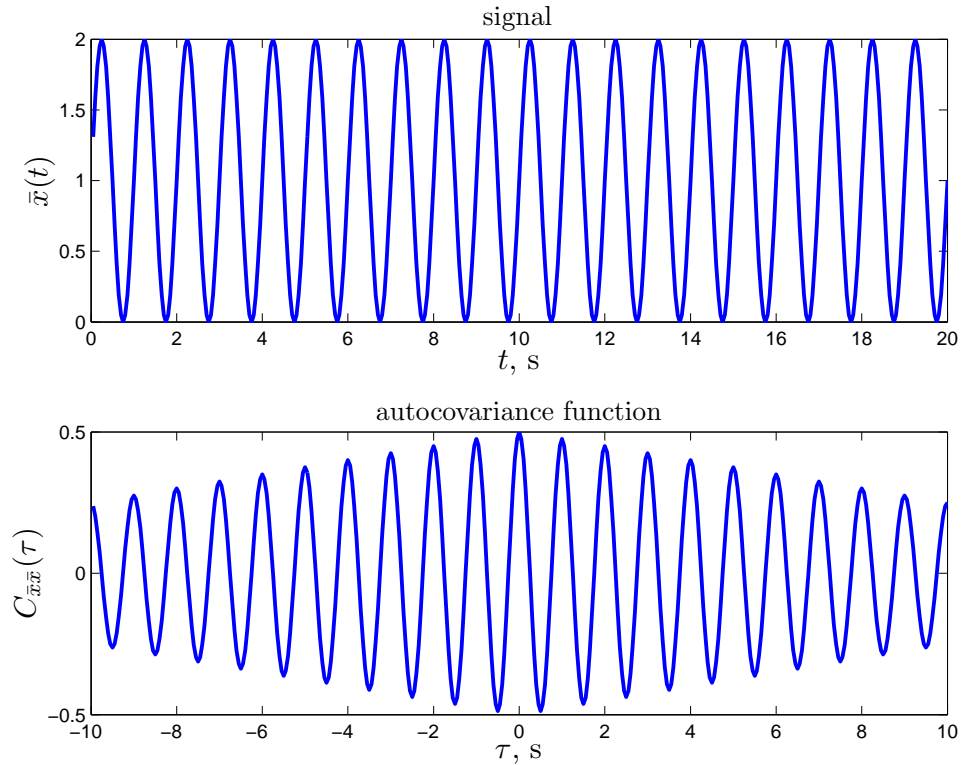


Figure 4.14: A discrete sample of $\bar{x}(t)$ and the resulting auto-covariance function, drawn in MATLAB as a continuous line.

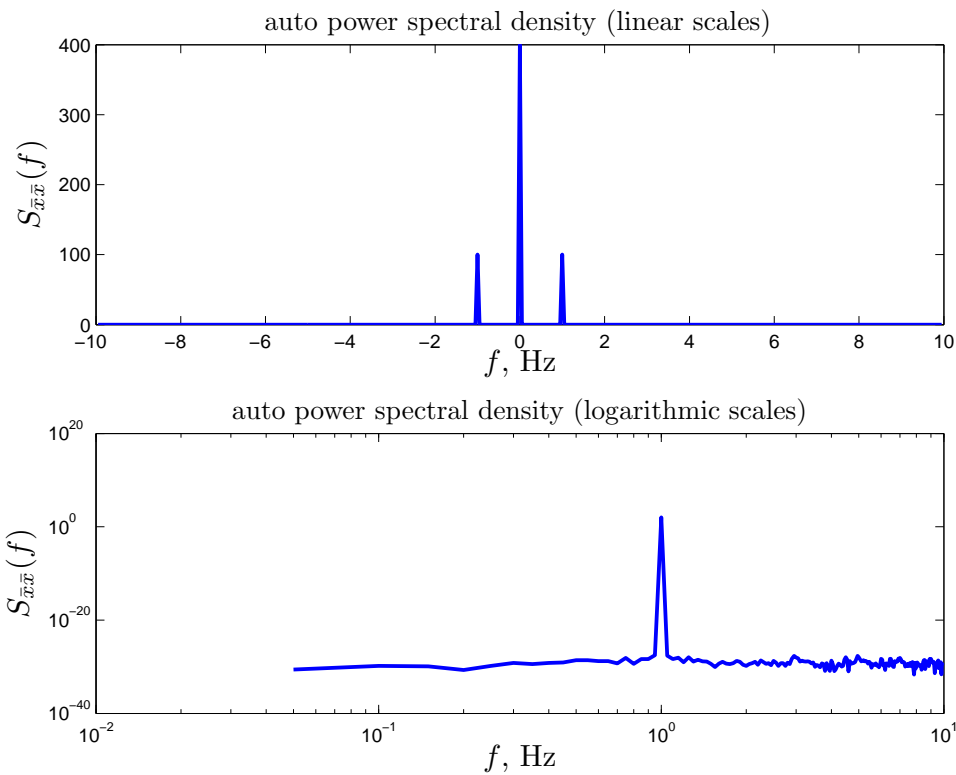


Figure 4.15: Auto spectral density function of $\bar{x}(t)$, drawn in MATLAB as a continuous line.

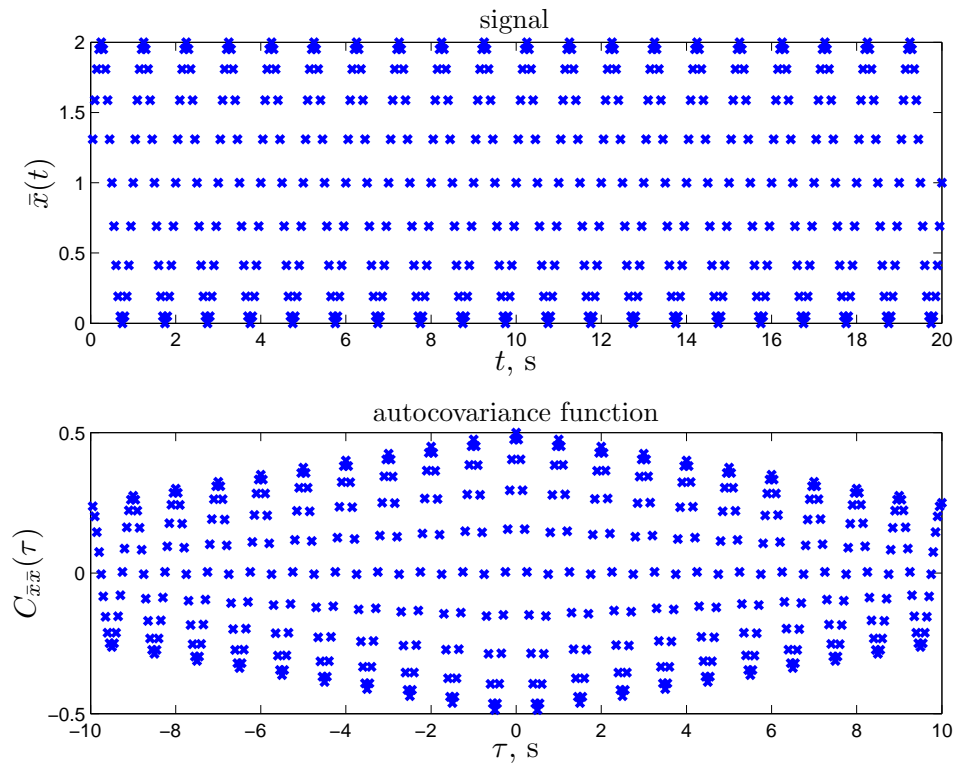


Figure 4.16: A discrete sample of $\bar{x}(t)$ and the resulting auto-covariance function, drawn in MATLAB as discrete samples.

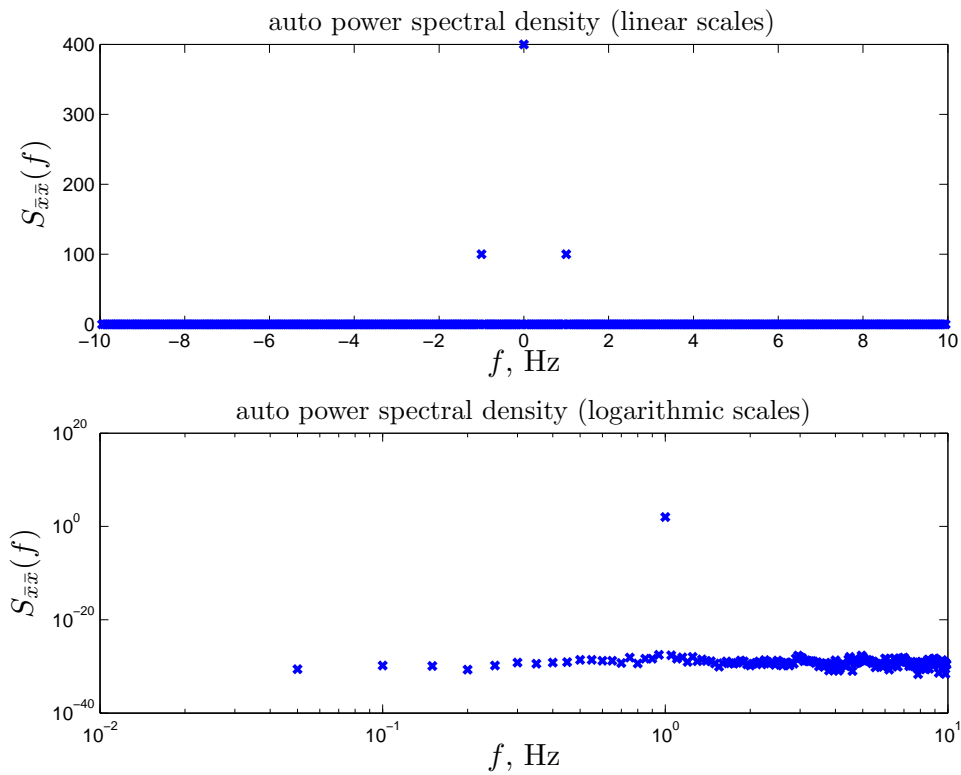


Figure 4.17: Auto spectral density function of $\bar{x}(t)$, drawn in MATLAB as discrete samples.

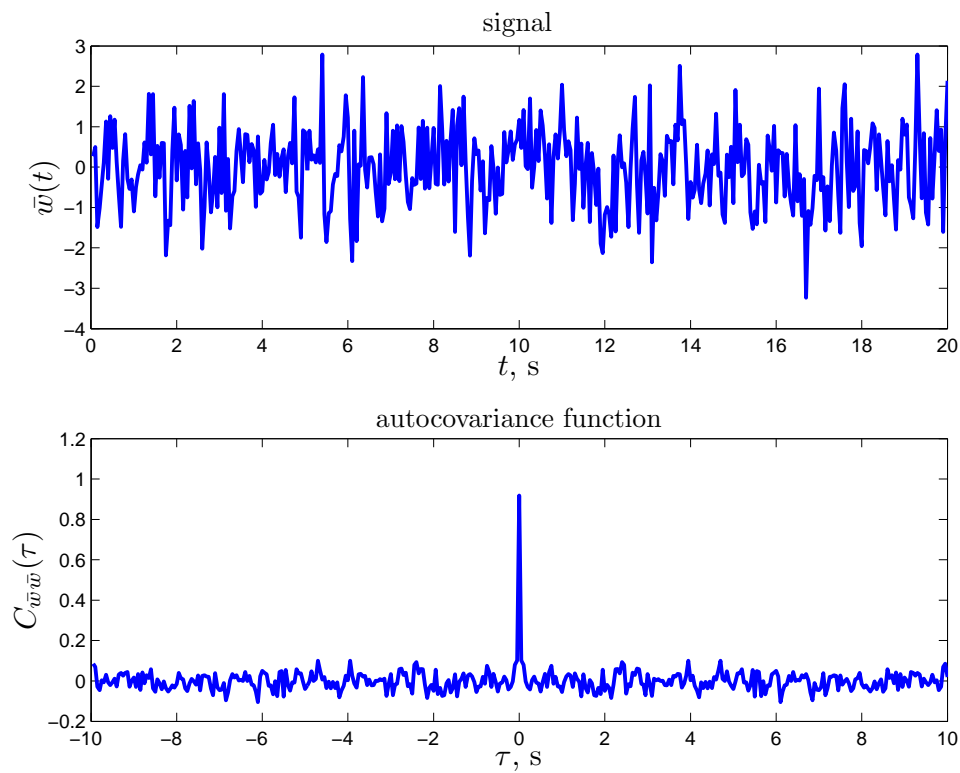


Figure 4.18: A discrete-time sample of $\bar{w}(t)$ and the resulting auto-covariance function.

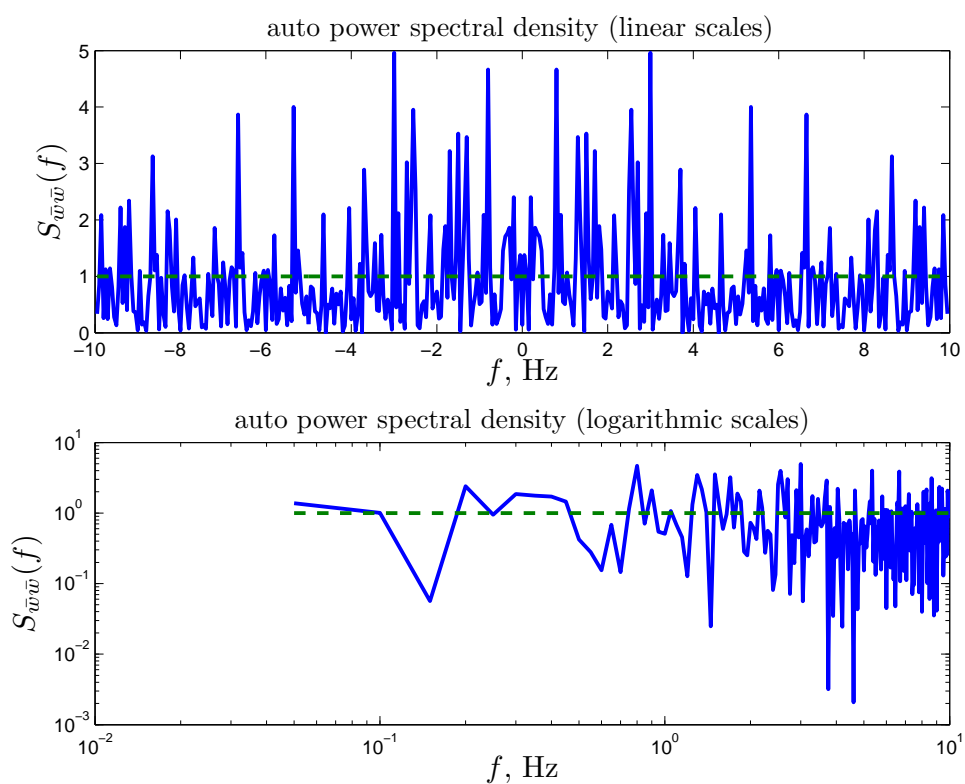


Figure 4.19: Auto spectral density function of $\bar{w}(t)$.

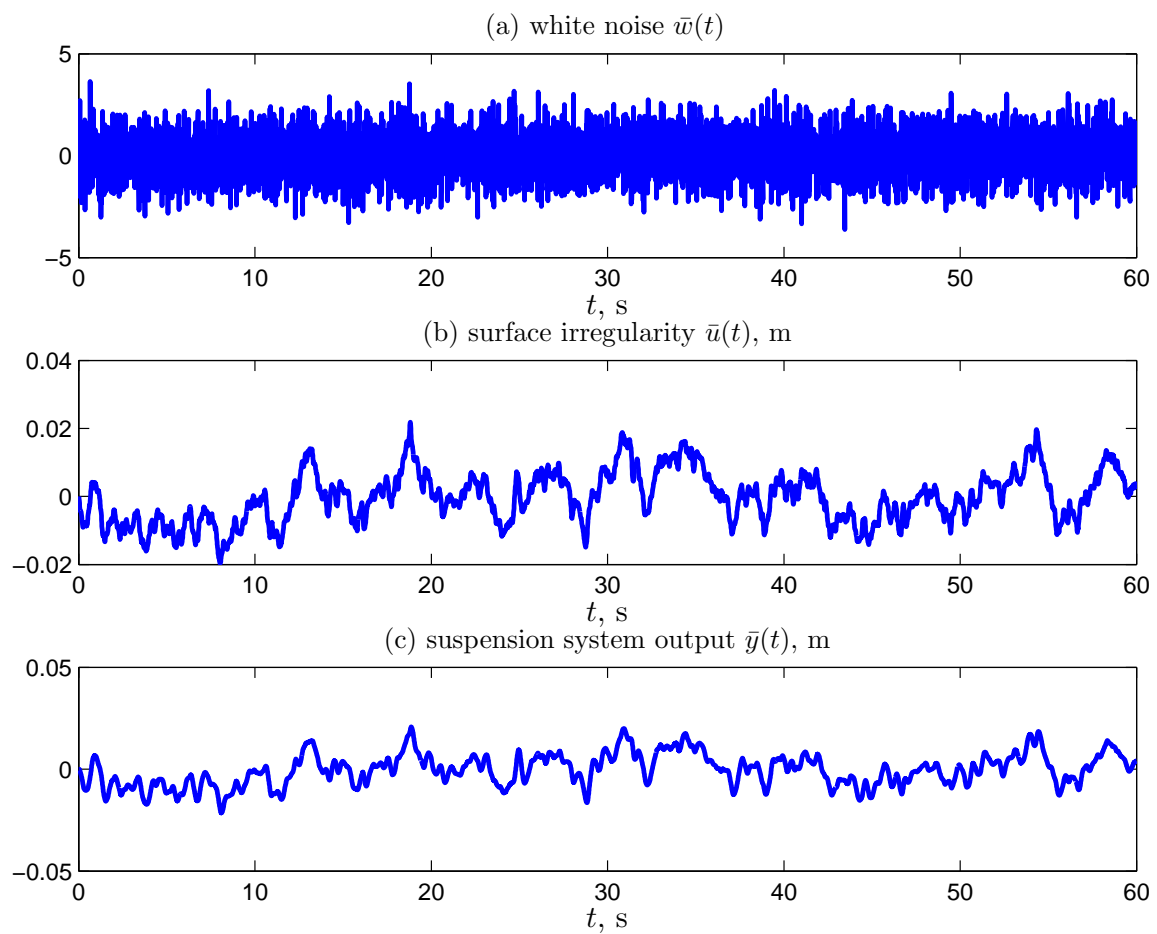


Figure 4.20: Filter input ‘white’ noise signal $\bar{w}(t)$ (a), resulting input signal of surface irregularities $\bar{u}(t)$ (b) and suspension system output signal $\bar{y}(t)$ (c).

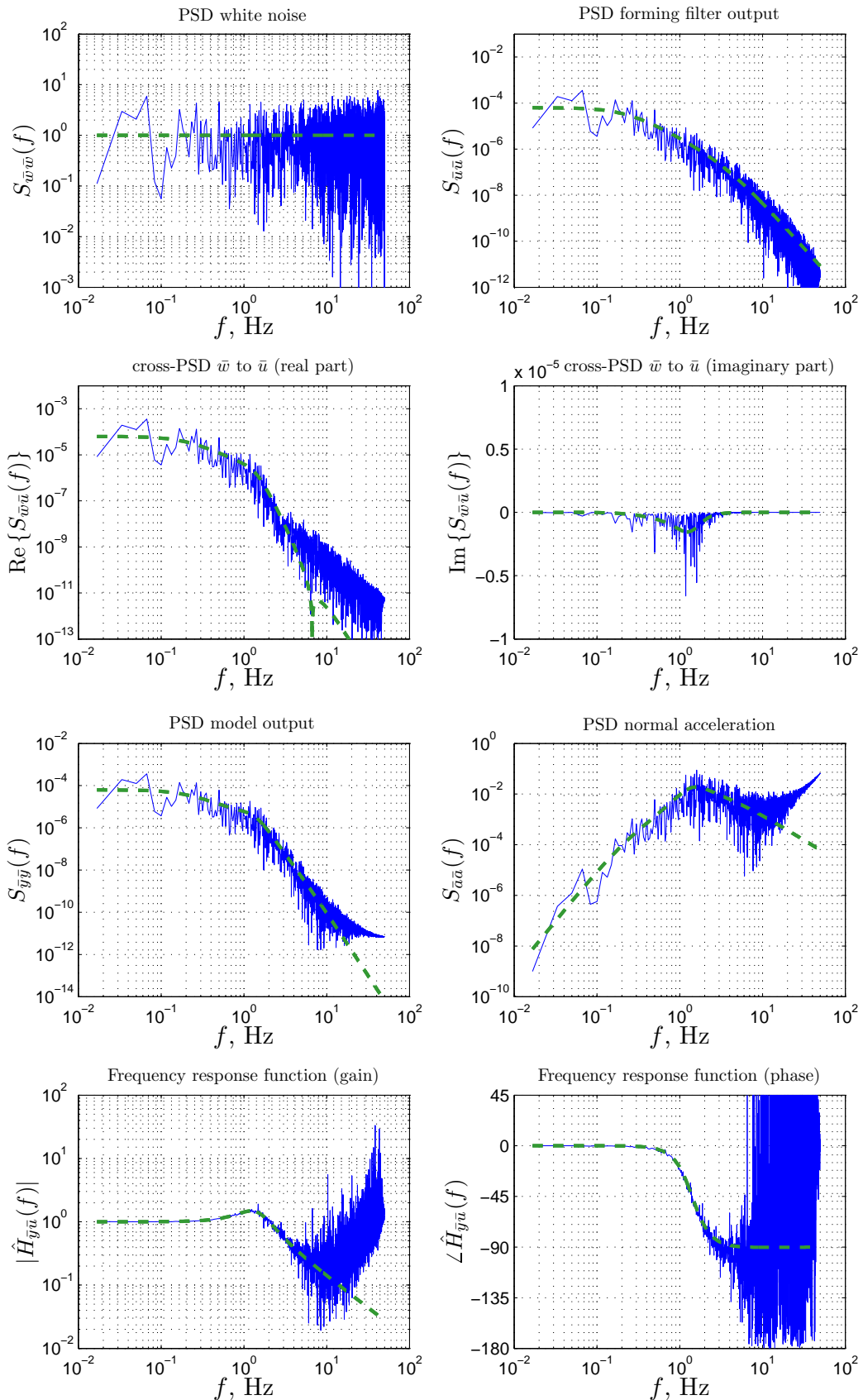


Figure 4.21: Digitally calculated power spectral density functions, compared to analytically derived power spectral density functions (dashed lines).

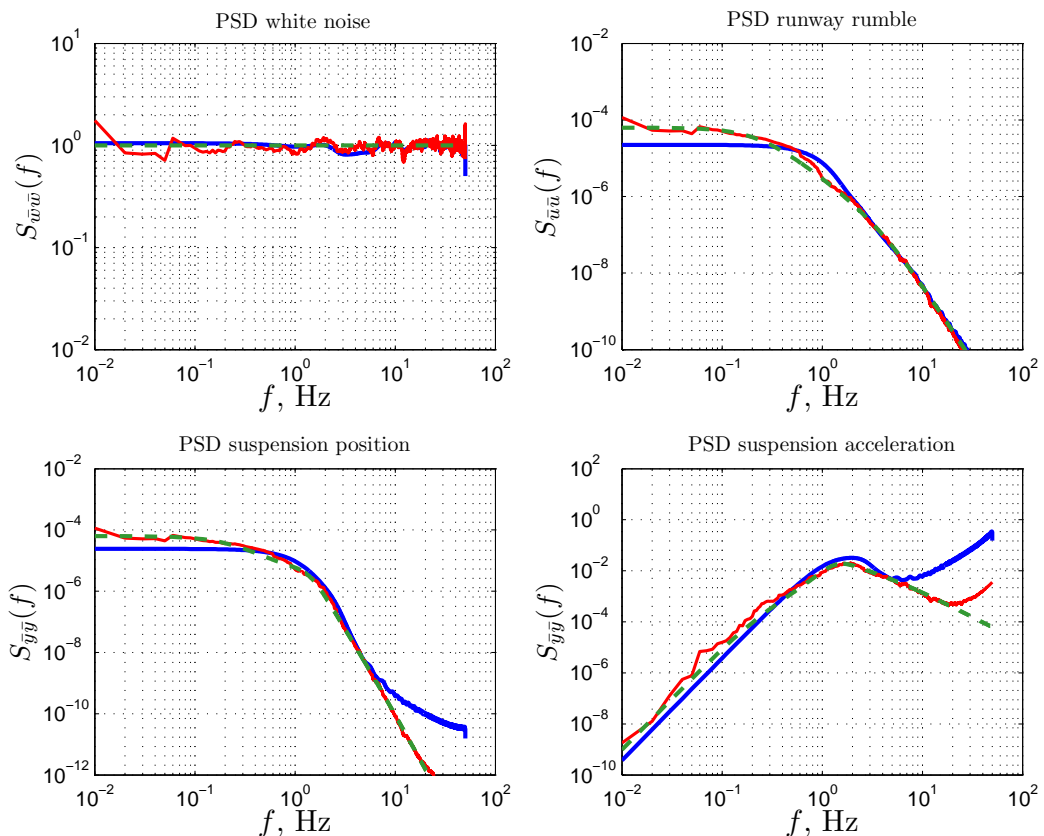


Figure 4.22: Digitally calculated auto power spectral density functions (using `pwelch.m`: blue, using `smooth.m`: red), compared to the analytically derived power spectral density functions (dashed green lines).

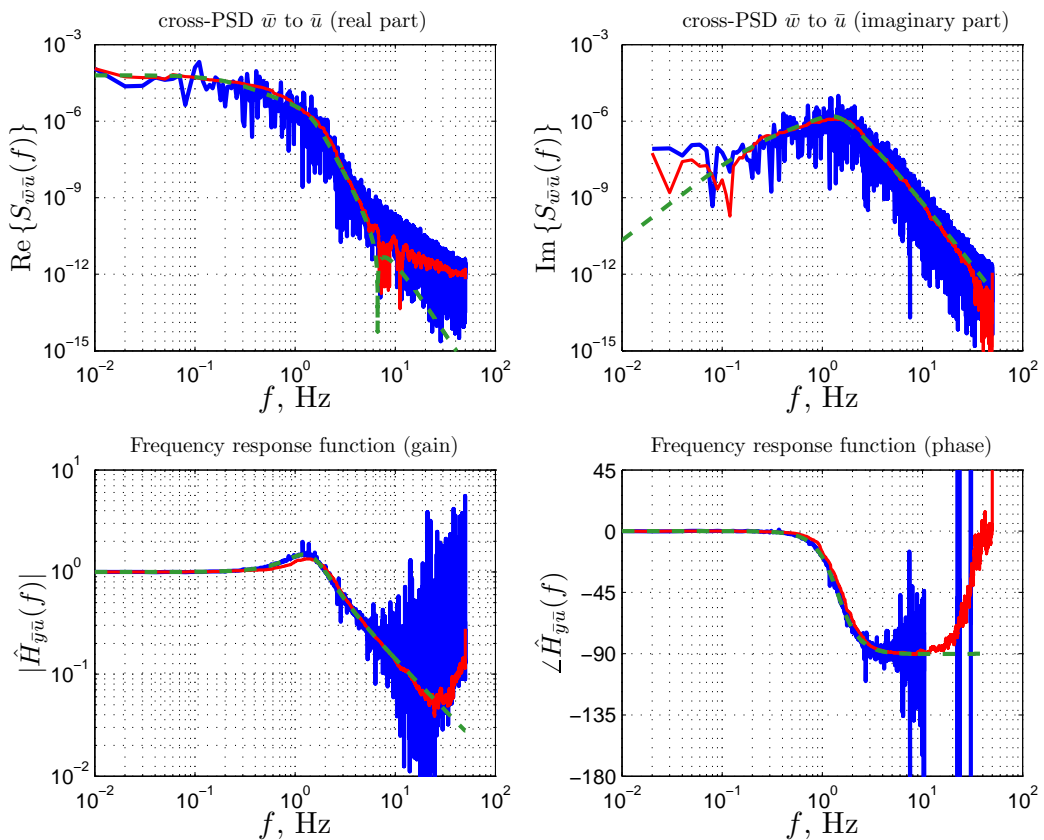


Figure 4.23: Digitally calculated results (using `pwelch.m`: blue, using `smooth.m`: red), compared to the analytically derived reference (dashed green lines).

Chapter 5

Multivariable Stochastic Processes

5.1 Introduction

In the preceding chapters a number of fundamental properties of scalar stochastic processes were introduced. In this chapter the discussion will be extended to multivariable stochastic processes where the stochastic processes will be vectors rather than scalars.

In this chapter we will use elements of linear system theory. Linear systems play an important role in system analysis and design, in part due to the fact that many physical systems encountered in nature can be successfully modelled as linear, or linearized about an equilibrium. Furthermore, linear systems are interesting from the mathematical point of view because the principle of superposition holds. This implies we can consider how each output variable responds to a single input variable alone and by just adding together the separate responses, the response of the combined excitation is obtained.

A description of linear systems in the time domain is supplied by the state-space model:

- continuous time:

$$\dot{\underline{x}}(t) = A \underline{x}(t) + B \underline{u}(t) \quad (5.1)$$

$$\underline{y}(t) = C \underline{x}(t) + D \underline{u}(t) \quad (5.2)$$

- discrete time:

$$\underline{x}[k+1] = \Phi \underline{x}[k] + \Gamma \underline{u}[k] \quad (5.3)$$

$$\underline{y}[k] = C \underline{x}[k] + D \underline{u}[k] \quad (5.4)$$

The main question to be answered in this chapter is: what will happen to the state vector \underline{x} and output vector \underline{y} if a stochastic input vector \underline{u} acts on the system? Under the assumption we have made in Chapter 2, that the stochastic processes considered have a Gaussian distribution, this question means finding the mean and variance as these parameters then completely describe the process. Because of the close relationship between continuous time and discrete time systems both types of systems will be treated in parallel so both similarities and differences will become more clear.

5.2 Probability distribution, probability density, mean value and covariance

As a starting point for the discussion of multivariable stochastic processes, the n -dimensional stochastic variable, column vector $\bar{\underline{x}}$, is introduced:

$$\bar{\underline{x}} = \begin{bmatrix} \bar{x}_1 \\ \bar{x}_2 \\ \vdots \\ \bar{x}_n \end{bmatrix} = [\bar{x}_1, \bar{x}_2, \dots, \bar{x}_n]^T \quad (5.5)$$

This vector $\bar{\underline{x}}$ consists of n stochastic elements \bar{x}_i , $i = 1..n$, in which each element can have a random value x_i . Quite similar to scalar stochastic processes we can define the probability distribution function and the probability density function, respectively, as:

$$F_{\bar{\underline{x}}}(\bar{x}) = Prob\{\bar{x}_1 \leq x_1, \bar{x}_2 \leq x_2, \dots, \bar{x}_n \leq x_n\} \quad (5.6)$$

$$f_{\bar{\underline{x}}}(\bar{x}) = \frac{\partial^n F_{\bar{\underline{x}}}(\bar{x})}{\partial x_1 \partial x_2 \dots \partial x_n} \quad (5.7)$$

comparable to (2.1) and (2.2) for the scalar case.

If all the elements \bar{x}_i of the stochastic vector $\bar{\underline{x}}$ are independent, the probability density function (5.7) reduces to:

$$f_{\bar{\underline{x}}}(\bar{x}) = \prod_{i=1}^n f_{\bar{x}_i}(x_i) \quad (5.8)$$

In general, the probability functions (5.6) and (5.7) of a vectorial stochastic process cannot be determined explicitly. Using the expectation operator $E\{\}$, we may concentrate on parameters related to the density function.

The mean or average of a stochastic vector is defined as:

$$E\{\bar{\underline{x}}\} = \begin{bmatrix} E\{\bar{x}_1\} \\ E\{\bar{x}_2\} \\ \vdots \\ E\{\bar{x}_n\} \end{bmatrix} = [E\{\bar{x}_1\}, E\{\bar{x}_2\}, \dots, E\{\bar{x}_n\}]^T = \mu_{\bar{\underline{x}}} \quad (5.9)$$

5.2 Probability distribution, probability density, mean value and covariance 53

Or: the expectation operator $E\{ \}$ applied to a stochastic vector $\underline{\bar{x}}$ simply yields a vector with the expected values of each of the n stochastic elements \bar{x}_i .

The covariance $C_{\bar{x}\bar{y}}$ and the correlation $K_{\bar{x}\bar{y}}$ introduced in Section 2.8 were based on two stochastic variables \bar{x} and \bar{y} . We will now use these notations to characterize the coherence between elements within the stochastic vectors $\underline{\bar{x}} = (\bar{x}_1, \bar{x}_2, \dots, \bar{x}_n)^T$ and $\underline{\bar{y}} = (\bar{y}_1, \bar{y}_2, \dots, \bar{y}_m)^T$. For that purpose consider the $n \times m$ matrix product,

$$(\underline{\bar{x}} - E\{\underline{\bar{x}}\}) \cdot (\underline{\bar{y}} - E\{\underline{\bar{y}}\})^T$$

for which the element (i, j) (scalar) can be written as:

$$(\bar{x}_i - E\{\bar{x}_i\}) \cdot (\bar{y}_j - E\{\bar{y}_j\})$$

for: $i = 1, 2, \dots, n$ and $j = 1, 2, \dots, m$. If we now define the expected value of a matrix as a matrix of the expected values of its elements, we can define the cross covariance matrix $C_{\underline{\bar{x}}\bar{y}}$ as:

$$\begin{aligned} C_{\underline{\bar{x}}\bar{y}} &= E\{(\underline{\bar{x}} - E\{\underline{\bar{x}}\}) \cdot (\underline{\bar{y}} - E\{\underline{\bar{y}}\})^T\} \\ &= \begin{bmatrix} E\{(\bar{x}_1 - E\{\bar{x}_1\}) \cdot (\bar{y}_1 - E\{\bar{y}_1\})\} \dots & E\{(\bar{x}_1 - E\{\bar{x}_1\}) \cdot (\bar{y}_m - E\{\bar{y}_m\})\} \\ E\{(\bar{x}_2 - E\{\bar{x}_2\}) \cdot (\bar{y}_1 - E\{\bar{y}_1\})\} \dots & E\{(\bar{x}_2 - E\{\bar{x}_2\}) \cdot (\bar{y}_m - E\{\bar{y}_m\})\} \\ \vdots & \vdots \\ E\{(\bar{x}_n - E\{\bar{x}_n\}) \cdot (\bar{y}_1 - E\{\bar{y}_1\})\} \dots & E\{(\bar{x}_n - E\{\bar{x}_n\}) \cdot (\bar{y}_m - E\{\bar{y}_m\})\} \end{bmatrix} \end{aligned} \quad (5.10)$$

Taking the special case of $\underline{\bar{x}} = \underline{\bar{y}}$ yields the auto covariance matrix,

$$\begin{aligned} C_{\underline{\bar{x}}\bar{x}} &= E\{(\underline{\bar{x}} - E\{\underline{\bar{x}}\}) \cdot (\underline{\bar{x}} - E\{\underline{\bar{x}}\})^T\} \\ &= \begin{bmatrix} E\{(\bar{x}_1 - E\{\bar{x}_1\})^2\} \dots & E\{(\bar{x}_1 - E\{\bar{x}_1\}) \cdot (\bar{x}_n - E\{\bar{x}_n\})\} \\ E\{(\bar{x}_2 - E\{\bar{x}_2\}) \cdot (\bar{x}_1 - E\{\bar{x}_1\})\} \dots & E\{(\bar{x}_2 - E\{\bar{x}_2\}) \cdot (\bar{x}_n - E\{\bar{x}_n\})\} \\ \vdots & \vdots \\ E\{(\bar{x}_n - E\{\bar{x}_n\}) \cdot (\bar{x}_1 - E\{\bar{x}_1\})\} \dots & E\{(\bar{x}_n - E\{\bar{x}_n\})^2\} \end{bmatrix} \end{aligned} \quad (5.11)$$

The term 'auto' is used to denote that both stochastic variables \bar{x}_i and \bar{x}_j belong to the same stochastic vector $\underline{\bar{x}}$. If we examine (2.15) of Section 2.8 we see that the ij^{th} element of the auto covariance matrix $C_{\underline{\bar{x}}\bar{x}}$ is simply the cross covariance of two stochastic variables \bar{x}_i and \bar{x}_j . The elements on the main diagonal of $C_{\underline{\bar{x}}\bar{x}}$ are the variances of the stochastic variables $\bar{x}_1, \bar{x}_2, \dots, \bar{x}_n$. Another interpretation of the auto covariance matrix is therefore:

$$C_{\underline{\bar{x}}\bar{x}} = \begin{bmatrix} \sigma_{\bar{x}_1}^2 & C_{\bar{x}_1\bar{x}_2} & \dots & C_{\bar{x}_1\bar{x}_n} \\ C_{\bar{x}_2\bar{x}_1} & \sigma_{\bar{x}_2}^2 & \dots & C_{\bar{x}_2\bar{x}_n} \\ \vdots & \vdots & & \vdots \\ C_{\bar{x}_n\bar{x}_1} & C_{\bar{x}_n\bar{x}_2} & \dots & \sigma_{\bar{x}_n}^2 \end{bmatrix} \quad (5.12)$$

As $C_{\bar{x}_i \bar{x}_j} = C_{\bar{x}_j \bar{x}_i}$, we can see that the auto covariance matrix $C_{\bar{x}\bar{x}}$ is symmetric. If we are interested in the correlations between the different elements of the stochastic vector $\underline{\bar{x}}$ we may scale the auto covariance matrix and introduce the auto correlation matrix $K_{\bar{x}\bar{x}}$ as:

$$K_{\bar{x}\bar{x}} = \begin{bmatrix} 1 & \frac{C_{\bar{x}_1 \bar{x}_2}}{\sigma_{\bar{x}_1} \sigma_{\bar{x}_2}} & \dots & \frac{C_{\bar{x}_1 \bar{x}_n}}{\sigma_{\bar{x}_1} \sigma_{\bar{x}_n}} \\ \frac{C_{\bar{x}_1 \bar{x}_2}}{\sigma_{\bar{x}_1} \sigma_{\bar{x}_2}} & 1 & \dots & \frac{C_{\bar{x}_2 \bar{x}_n}}{\sigma_{\bar{x}_2} \sigma_{\bar{x}_n}} \\ \vdots & \vdots & \ddots & \vdots \\ \frac{C_{\bar{x}_1 \bar{x}_n}}{\sigma_{\bar{x}_1} \sigma_{\bar{x}_n}} & \frac{C_{\bar{x}_2 \bar{x}_n}}{\sigma_{\bar{x}_2} \sigma_{\bar{x}_n}} & \dots & 1 \end{bmatrix} \quad (5.13)$$

Notice that the off-diagonal elements of $K_{\bar{x}\bar{x}}$ contain the scalar correlation coefficients $K_{\bar{x}_i \bar{x}_j}$ as defined by (2.17). If the elements of the stochastic vector are uncorrelated, i.e. if:

$$C_{\bar{x}_i \bar{x}_j} = K_{\bar{x}_i \bar{x}_j} = 0 \quad \text{for } i \neq j$$

then all non-diagonal elements of the covariance matrix $C_{\bar{x}\bar{x}}$ and the correlation matrix $K_{\bar{x}\bar{x}}$ are zero.

5.3 Linear transformations

Stochastic vector processes will often be submitted to linear transformations. For example, the output equation of the state-space description, Equation (5.2):

$$\underline{\bar{y}}(t) = C \underline{\bar{x}}(t) + D \underline{\bar{u}}(t)$$

is a linear transformation. Another example is a transformation from one frame of reference to another, for instance from aircraft body-fixed axes to stability- or wind axes.

In this section we will investigate the mean and the covariance matrix of a stochastic vector $\underline{\bar{y}}$ given by:

$$\underline{\bar{y}} = A \underline{\bar{x}}$$

or:

$$\begin{bmatrix} y_1 \\ y_2 \\ \vdots \\ y_m \end{bmatrix} = \begin{bmatrix} a_{11} & \dots & a_{1n} \\ \vdots & & \vdots \\ a_{m1} & \dots & a_{mn} \end{bmatrix} \begin{bmatrix} x_1 \\ x_2 \\ \vdots \\ x_n \end{bmatrix} \quad (5.14)$$

If we know the mean $E\{\underline{\bar{x}}\}$ of vector $\underline{\bar{x}}$, we find for the mean of vector $\underline{\bar{y}}$:

$$E\{\underline{\bar{y}}\} = E\{A\underline{\bar{x}}\} = A E\{\underline{\bar{x}}\} \quad (5.15)$$

In the case that $n=2$ and $m=2$, we can expand this as follows:

$$\begin{aligned} E\{\underline{\bar{y}}\} &= \begin{bmatrix} E\{\bar{y}_1\} \\ E\{\bar{y}_2\} \end{bmatrix} = \begin{bmatrix} E\{a_{11}\bar{x}_1 + a_{12}\bar{x}_2\} \\ E\{a_{21}\bar{x}_1 + a_{22}\bar{x}_2\} \end{bmatrix} = \begin{bmatrix} a_{11}E\{\bar{x}_1\} + a_{12}E\{\bar{x}_2\} \\ a_{21}E\{\bar{x}_1\} + a_{22}E\{\bar{x}_2\} \end{bmatrix} = \\ &= \begin{bmatrix} a_{11} & a_{12} \\ a_{21} & a_{22} \end{bmatrix} \begin{bmatrix} E\{\bar{x}_1\} \\ E\{\bar{x}_2\} \end{bmatrix} = A E\{\underline{\bar{x}}\} \end{aligned}$$

For the auto covariance matrix $C_{\bar{y}\bar{y}}$ of vector $\underline{\bar{y}}$ the following result is found:

$$C_{\bar{y}\bar{y}} = A C_{\bar{x}\bar{x}} A^T \tag{5.16}$$

which is straightforward to prove,

$$\begin{aligned} C_{\bar{y}\bar{y}} &= E\{(\underline{\bar{y}} - E\{\underline{\bar{y}}\})(\underline{\bar{y}} - E\{\underline{\bar{y}}\})^T\} \\ &= E\{(A\underline{\bar{x}} - E\{A\underline{\bar{x}}\})(A\underline{\bar{x}} - E\{A\underline{\bar{x}}\})^T\} \\ &= E\{A(\underline{\bar{x}} - E\{\underline{\bar{x}}\})(\underline{\bar{x}} - E\{\underline{\bar{x}}\})^T A^T\} \\ &= A E\{(\underline{\bar{x}} - E\{\underline{\bar{x}}\})(\underline{\bar{x}} - E\{\underline{\bar{x}}\})^T\} A^T \\ &= A C_{\bar{x}\bar{x}} A^T \end{aligned}$$

5.4 The covariance function matrix and the spectral density matrix

The concept of covariance functions introduced in Section 2.10, expressing the coherence between stochastic variable \bar{x} at time t and the stochastic variable \bar{y} at time $t + \tau$ can easily be extended to the multivariable case, yielding matrices of functions rather than a scalar function of the time delay τ . If we take the covariance matrix $C_{\bar{x}\bar{y}}$ as defined by (5.10),

$$C_{\bar{x}\bar{y}} = E\{(\underline{\bar{x}} - E\{\underline{\bar{x}}\})(\underline{\bar{y}} - E\{\underline{\bar{y}}\})^T\}$$

and consider two stationary stochastic vector processes which are a function of time, say $\underline{\bar{x}}(t_1)$ and $\underline{\bar{y}}(t_2)$, defining $\tau = t_2 - t_1$ we can write (2.28) in the multivariable case as:

$$C_{\bar{x}\bar{y}}(\tau) = E\{(\underline{\bar{x}}(t) - E\{\underline{\bar{x}}(t)\})(\underline{\bar{y}}(t + \tau) - E\{\underline{\bar{y}}(t + \tau)\})^T\} \tag{5.17}$$

Assuming the processes are zero mean or corrected for an offset (regarding the stochastic variable $(\underline{\bar{x}} - E\{\underline{\bar{x}}\})$ rather than $\underline{\bar{x}}$) we can write (5.17) as:

$$C_{\bar{x}\bar{y}}(\tau) = R_{\bar{x}\bar{y}}(\tau) = E\{\underline{\bar{x}}(t) \underline{\bar{y}}^T(t + \tau)\} \tag{5.18}$$

The spectral density function was defined by (3.27) as the Fourier transform of the covariance function. If we define the Fourier transform of a matrix as a matrix with the Fourier transforms of the elements, we can write for the multi-dimensional spectral density matrix:

$$\begin{aligned} S_{\underline{\bar{x}}\underline{\bar{y}}}(\omega) &= F\{C_{\underline{\bar{x}}\underline{\bar{y}}}(\tau)\} \\ S_{\underline{\bar{x}}\underline{\bar{y}}}(\omega) &= \begin{bmatrix} F\{C_{\bar{x}_1\bar{y}_1}(\tau)\} & F\{C_{\bar{x}_1\bar{y}_2}(\tau)\} & \dots & F\{C_{\bar{x}_1\bar{y}_m}(\tau)\} \\ F\{C_{\bar{x}_2\bar{y}_1}(\tau)\} & F\{C_{\bar{x}_2\bar{y}_2}(\tau)\} & \dots & F\{C_{\bar{x}_2\bar{y}_m}(\tau)\} \\ \vdots & \vdots & & \vdots \\ F\{C_{\bar{x}_n\bar{y}_1}(\tau)\} & F\{C_{\bar{x}_n\bar{y}_2}(\tau)\} & \dots & F\{C_{\bar{x}_n\bar{y}_m}(\tau)\} \end{bmatrix} \\ S_{\underline{\bar{x}}\underline{\bar{y}}}(\omega) &= \begin{bmatrix} S_{\bar{x}_1\bar{y}_1}(\omega) & S_{\bar{x}_1\bar{y}_2}(\omega) & \dots & S_{\bar{x}_1\bar{y}_m}(\omega) \\ S_{\bar{x}_2\bar{y}_1}(\omega) & S_{\bar{x}_2\bar{y}_2}(\omega) & \dots & S_{\bar{x}_2\bar{y}_m}(\omega) \\ \vdots & \vdots & & \vdots \\ S_{\bar{x}_n\bar{y}_1}(\omega) & S_{\bar{x}_n\bar{y}_2}(\omega) & \dots & S_{\bar{x}_n\bar{y}_m}(\omega) \end{bmatrix} \end{aligned} \quad (5.19)$$

If the special case of $\underline{\bar{x}} = \underline{\bar{y}}$ is considered, the spectral density matrix is square and the diagonal elements contain the auto spectral density functions of the stochastic elements of vector $\underline{\bar{x}} = [\bar{x}_1, \bar{x}_2, \dots, \bar{x}_n]^T$.

5.5 Dynamic multivariable system analysis in the frequency domain

In the multi-dimensional case, systems in general have more than one input and several outputs (multiple input-multiple output (MIMO) systems) contrasting the single input-single output (SISO) case. The dynamics of such a system can be studied by examining the power spectral density matrix $S_{\underline{\bar{y}}\underline{\bar{y}}}(\omega)$ of the system output vector $\underline{\bar{y}}$, applying an input vector $\underline{\bar{u}}$ with power spectral density matrix $S_{\underline{\bar{u}}\underline{\bar{u}}}(\omega)$.

Suppose that the relation between input signal $\underline{\bar{u}}$ and output signal $\underline{\bar{y}}$ is given by the impulse response function matrix $h_{\underline{\bar{y}}\underline{\bar{u}}}(t)$, considering m output and n input variables,

$$\underline{\bar{y}}(t) = h_{\underline{\bar{y}}\underline{\bar{u}}}(t) * \underline{\bar{u}}(t) \quad (5.20)$$

or:

$$\begin{bmatrix} y_1(t) \\ y_2(t) \\ \vdots \\ y_m(t) \end{bmatrix} = \begin{bmatrix} h_{11}(t) & \dots & h_{1n}(t) \\ \vdots & & \vdots \\ h_{m1}(t) & \dots & h_{mn}(t) \end{bmatrix} * \begin{bmatrix} u_1(t) \\ u_2(t) \\ \vdots \\ u_n(t) \end{bmatrix} \quad (5.21)$$

where $*$ denotes a convolution, or in the frequency-domain:

$$\begin{bmatrix} Y_1(\omega) \\ Y_2(\omega) \\ \vdots \\ Y_m(\omega) \end{bmatrix} = \begin{bmatrix} H_{11}(\omega) & \dots & H_{1n}(\omega) \\ \vdots & & \vdots \\ H_{m1}(\omega) & \dots & H_{mn}(\omega) \end{bmatrix} \cdot \begin{bmatrix} U_1(\omega) \\ U_2(\omega) \\ \vdots \\ U_n(\omega) \end{bmatrix} \quad (5.22)$$

In order to find a relation between the input power spectral density matrix $S_{\bar{u}\bar{u}}(\omega)$ and the output power spectral density matrix $S_{\bar{y}\bar{y}}(\omega)$, we will first consider the covariance matrices $C_{\bar{u}\bar{y}}(\tau)$, $C_{\bar{y}\bar{u}}(\tau)$ and $C_{\bar{y}\bar{y}}(\tau)$, writing for the impulse response function matrix $h(t)$ instead of $h_{\bar{y}\bar{u}}(t)$,

$$\begin{aligned} C_{\bar{u}\bar{y}}(\tau) &= E \left\{ \bar{u}(t) \cdot \bar{y}^T(t + \tau) \right\} \\ &= E \left\{ \bar{u}(t) \cdot \left(\int_{-\infty}^{+\infty} h(\theta) \bar{u}(t + \tau - \theta) d\theta \right)^T \right\} \\ &= E \left\{ \bar{u}(t) \cdot \int_{-\infty}^{+\infty} \bar{u}^T(t + \tau - \theta) h^T(\theta) d\theta \right\} \\ &= E \left\{ \int_{-\infty}^{+\infty} \bar{u}(t) \bar{u}^T(t + \tau - \theta) h^T(\theta) d\theta \right\} \\ &= \int_{-\infty}^{+\infty} E \left\{ \bar{u}(t) \bar{u}^T(t + \tau - \theta) \right\} h^T(\theta) d\theta \\ &= \int_{-\infty}^{+\infty} C_{\bar{u}\bar{u}}(\tau - \theta) h^T(\theta) d\theta \\ &= C_{\bar{u}\bar{u}}(\tau) * h^T(\tau) \end{aligned} \quad (5.23)$$

$$\begin{aligned} C_{\bar{y}\bar{u}}(\tau) &= E \left\{ \bar{y}(t) \cdot \bar{u}^T(t + \tau) \right\} \\ &= E \left\{ \left(\int_{-\infty}^{+\infty} h(\theta) \bar{u}(t - \theta) d\theta \right) \cdot \bar{u}^T(t + \tau) \right\} \\ &= E \left\{ \int_{-\infty}^{+\infty} h(\theta) \bar{u}(t - \theta) \bar{u}^T(t + \tau) d\theta \right\} \\ &= \int_{-\infty}^{+\infty} h(\theta) E \left\{ \bar{u}(t - \theta) \bar{u}^T(t + \tau) \right\} d\theta \end{aligned}$$

$$\begin{aligned}
&= \int_{-\infty}^{+\infty} h(\theta) C_{\bar{u}\bar{u}}(\tau + \theta) d\theta \\
&= \int_{\xi=-\infty}^{\xi=-\infty} h(-\xi) C_{\bar{u}\bar{u}}(\tau - \xi) d(-\xi) \\
&= \int_{\xi=+\infty}^{\xi=+\infty} h(-\xi) C_{\bar{u}\bar{u}}(\tau - \xi) d\xi \\
&= h(-\tau) * C_{\bar{u}\bar{u}}(\tau)
\end{aligned} \tag{5.24}$$

$$\begin{aligned}
C_{\bar{y}\bar{y}}(\tau) &= E \{ \bar{y}(t) \cdot \bar{y}^T(t + \tau) \} \\
&= E \left\{ \left(\int_{-\infty}^{+\infty} h(\theta) \bar{u}(t - \theta) d\theta \right) \cdot \bar{y}^T(t + \tau) \right\} \\
&= E \left\{ \int_{-\infty}^{+\infty} h(\theta) \bar{u}(t - \theta) \bar{y}^T(t + \tau) d\theta \right\} \\
&= \int_{-\infty}^{+\infty} h(\theta) E \{ \bar{u}(t - \theta) \bar{y}^T(t + \tau) \} d\theta \\
&= \int_{-\infty}^{+\infty} h(\theta) C_{\bar{u}\bar{y}}(\tau + \theta) d\theta \\
&= \int_{\xi=-\infty}^{\xi=-\infty} h(-\xi) C_{\bar{u}\bar{y}}(\tau - \xi) d(-\xi) \\
&= \int_{\xi=+\infty}^{\xi=+\infty} h(-\xi) C_{\bar{u}\bar{y}}(\tau - \xi) d\xi \\
&= h(-\tau) * C_{\bar{u}\bar{y}}(\tau) \\
&= h(-\tau) * C_{\bar{u}\bar{u}}(\tau) * h^T(\tau)
\end{aligned} \tag{5.25}$$

From Section 5.4 we know how to obtain the spectral density matrix by taking the Fourier transform of the elements of the covariance matrix. Applying the rule that a convolution in the time domain corresponds to a multiplication in the frequency domain, we get,

$$S_{\bar{u}\bar{y}}(\omega) = F\{C_{\bar{u}\bar{y}}(\tau)\} = S_{\bar{u}\bar{u}}(\omega) H_{\bar{y}\bar{u}}^T(\omega) \tag{5.26}$$

$$S_{\bar{y}\bar{u}}(\omega) = F\{C_{\bar{y}\bar{u}}(\tau)\} = H_{\bar{y}\bar{u}}(-\omega) S_{\bar{u}\bar{u}}(\omega) \tag{5.27}$$

$$S_{\bar{y}\bar{y}}(\omega) = F\{C_{\bar{y}\bar{y}}(\tau)\} = H_{\bar{y}\bar{u}}(-\omega) S_{\bar{u}\bar{u}}(\omega) H_{\bar{y}\bar{u}}^T(\omega) \tag{5.28}$$

It is easy to see that in the scalar case Equation (5.28) equals Equation (3.44):

$$S_{\bar{y}\bar{y}}(\omega) = H_{yu}(-\omega) S_{\bar{u}\bar{u}}(\omega) H_{yu}(\omega) = |H_{yu}(\omega)|^2 S_{\bar{u}\bar{u}}(\omega)$$

5.6 Dynamic multivariable system analysis in the time domain

In the previous section the classical multivariable system analysis in the frequency domain was considered, based on the frequency response function matrix $H_{yu}(\omega)$. A description of dynamic processes is, however, also often based on linear differential- (continuous time) or difference equations (discrete time) in the time domain. The state equation (Equations (5.1) to (5.4)),

- continuous time:

$$\begin{aligned}\dot{\underline{x}}(t) &= A \underline{x}(t) + B \underline{u}(t) \\ \underline{y}(t) &= C \underline{x}(t) + D \underline{u}(t)\end{aligned}$$

- discrete time:

$$\begin{aligned}\underline{x}[k+1] &= \Phi \underline{x}[k] + \Gamma \underline{u}[k] \\ \underline{y}[k] &= C \underline{x}[k] + D \underline{u}[k]\end{aligned}$$

of the general state-space equation is one example. In this section we will consider a dynamic system with a stochastic input vector $\underline{u}(t)$. Our main interest is focussed on the statistical properties of the state vector \underline{x} as a function of time.

Note, that when a linear system is driven by a stochastic signal, all other signals are stochastic as well, i.e. the state and output vectors become stochastic variables \bar{x} and \bar{y} . In many, if not all, practical applications this means that we are always dealing with stochastic processes. I.e. all outcomes of a particular “experiment” or “trial” or “test” are in fact realizations.

First the continuous-time case will be discussed, followed by a description of the discrete-time case. It will be shown that there are differences in both situations and we have to be very cautious about our simulations, which are generally, because we use computers and software like Matlab, in discrete-time (even when considering physical systems like aircraft which are of course continuous-time).

5.6.1 Continuous time

Let the system under consideration be described by the following linear vector differential equation, Equation (5.1),

$$\dot{\underline{x}}(t) = A \underline{x}(t) + B \underline{u}(t)$$

Solving this equation yields (see (Kwakernaak & Sivan, 1972; Ogata, 2002))

$$\underline{x}(t) = \Phi(t, t_0) \underline{x}(0) + \int_{t_0}^t \Phi(t, \tau) B \underline{u}(\tau) d\tau \quad (5.29)$$

with,

$$\Phi(t, t_0) = e^{A(t-t_0)} = I + A(t - t_0) + \frac{1}{2!} A^2(t - t_0)^2 + \dots \quad (5.30)$$

This result can be verified by substitution of (5.29) and (5.30) in (5.1). First consider the solution of the homogeneous part of the differential equation (5.1):

$$\underline{x}(t) = \Phi(t, t_0) \underline{x}(0) \quad (\text{start with (5.29)})$$

$$\dot{\underline{x}}(t) = \dot{\Phi}(t, t_0) \underline{x}(0) \quad (\text{differentiate})$$

$$\dot{\underline{x}}(t) = A e^{A(t-t_0)} \underline{x}(0) \quad (\text{differentiate (5.30) and substitute})$$

$$\dot{\underline{x}}(t) = A \Phi(t, t_0) \underline{x}(0) \quad (\text{substitute (5.30)})$$

$$\dot{\underline{x}}(t) = A \underline{x}(t) \quad (\text{substitute (5.29)})$$

Next, consider the total solution (5.29),

$$\underline{x}(t) = \Phi(t, t_0) \underline{x}(0) + \int_{t_0}^t \Phi(t, \tau) B \underline{u}(\tau) d\tau$$

$$\dot{\underline{x}}(t) = \dot{\Phi}(t, t_0) \underline{x}(0) + \Phi(t, t) B \underline{u}(t) \quad (\text{differentiate})$$

$$\dot{\underline{x}}(t) = \dot{\Phi}(t, t_0) \underline{x}(0) + B \underline{u}(t) \quad (\Phi(t, t) = I, \text{ Equation(5.30)})$$

$$\dot{\underline{x}}(t) = A \underline{x}(t) + B \underline{u}(t)$$

This result can also be proven analytically¹.

Now consider the stochastic problem where the input vector $\underline{u}(t)$ is chosen to be white noise $\bar{u}(t)$ with mean,

$$E\{\bar{u}(t)\} = 0 \quad (5.31)$$

and auto covariance matrix

$$C_{\bar{w}\bar{w}}(\tau) = W \delta(\tau) \quad (5.32)$$

where W denotes the noise intensity matrix. Equation (5.32) is the multivariable equivalent of (2.31).

We want to find the mean of the state vector $\underline{\bar{x}}$ and the auto covariance matrix as a function of time. For the average value we find:

$$\begin{aligned} E\{\underline{\bar{x}}(t)\} &= E \left\{ \Phi(t, t_0) \underline{\bar{x}}(0) + \int_{t_0}^t \Phi(t, \tau) B \underline{\bar{w}}(\tau) d\tau \right\} \\ &= \Phi(t, t_0) E\{\underline{\bar{x}}(0)\} + \int_{t_0}^t \Phi(t, \tau) B E\{\underline{\bar{w}}(\tau)\} d\tau \end{aligned}$$

with $E\{\underline{\bar{w}}(t)\} = 0$ we find:

$$E\{\underline{\bar{x}}(t)\} = \Phi(t, t_0) E\{\underline{\bar{x}}(0)\} \quad (5.33)$$

The auto covariance matrix of the state vector $\underline{\bar{x}}$ is found to be:

$$\begin{aligned} E\{\underline{\bar{x}}(t_1) \underline{\bar{x}}^T(t_2)\} &= E \left\{ \left(\Phi(t_1, t_0) \underline{\bar{x}}(0) + \int_{t_0}^{t_1} \Phi(t_1, \tau_1) B \underline{\bar{w}}(\tau_1) d\tau_1 \right) \right. \\ &\quad \cdot \left. \left(\Phi(t_2, t_0) \underline{\bar{x}}(0) + \int_{t_0}^{t_2} \Phi(t_2, \tau_2) B \underline{\bar{w}}(\tau_2) d\tau_2 \right)^T \right\} \end{aligned}$$

¹Proof

Use the following property (Chen, 1998):

$$\frac{\partial}{\partial t} \int_{t_0}^t f(t, \tau) d\tau = f(t, \tau)|_{\tau=t} + \int_{t_0}^t \frac{\partial}{\partial t} f(t, \tau) d\tau$$

Then, differentiate (5.29):

$$\begin{aligned} \dot{\underline{x}}(t) &= \dot{\Phi}(t, t_0) \underline{x}(0) + \frac{\partial}{\partial t} \int_{t_0}^t \Phi(t, \tau) B \underline{u}(\tau) d\tau \\ &= A \cdot \Phi(t, t_0) \underline{x}(0) + \Phi(t, t) B \underline{u}(t) + \int_{t_0}^t \frac{\partial}{\partial t} \Phi(t, \tau) B \underline{u}(\tau) d\tau \\ &= A \cdot \Phi(t, t_0) \underline{x}(0) + B \underline{u}(t) + \int_{t_0}^t A \Phi(t, \tau) B \underline{u}(\tau) d\tau \\ &= A \cdot \Phi(t, t_0) \underline{x}(0) + B \underline{u}(t) + A \cdot \left(\int_{t_0}^t \Phi(t, \tau) B \underline{u}(\tau) d\tau \right) \\ &= A \cdot \left(\Phi(t, t_0) \underline{x}(0) + \int_{t_0}^t \Phi(t, \tau) B \underline{u}(\tau) d\tau \right) + B \underline{u}(t) \\ &= A \underline{x}(t) + B \underline{u}(t) \end{aligned}$$

q.e.d.

Writing out the multiplication yields the following expression:

$$\begin{aligned}
 E\{\bar{x}(t_1) \bar{x}^T(t_2)\} &= E\{\Phi(t_1, t_0) \bar{x}(0) \bar{x}^T(0) \Phi^T(t_2, t_0)\} + \\
 &+ E\left\{\Phi(t_1, t_0) \bar{x}(0) \int_{t_0}^{t_2} \bar{w}^T(\tau_2) B^T \Phi^T(t_2, \tau_2) d\tau_2\right\} + \\
 &+ E\left\{\int_{t_0}^{t_1} \Phi(t_1, \tau_1) B \bar{w}(\tau_1) d\tau_1 \cdot \bar{x}^T(0) \Phi^T(t_2, t_0)\right\} + \\
 &+ E\left\{\int_{t_0}^{t_1} \Phi(t_1, \tau_1) B \bar{w}(\tau_1) d\tau_1 \cdot \int_{t_0}^{t_2} \bar{w}^T(\tau_2) B^T \Phi^T(t_2, \tau_2) d\tau_2\right\}
 \end{aligned}$$

In order to get an expression for the behaviour of the auto covariance matrix as a function of time we set $t_1 = t_2 = t$,

$$\begin{aligned}
 C_{\bar{x}\bar{x}}(t) &= \Phi(t, t_0) E\{\bar{x}(0) \bar{x}^T(0)\} \Phi^T(t, t_0) + \\
 &+ \Phi(t, t_0) \int_{t_0}^t E\{\bar{x}(0) \bar{w}^T(\tau)\} B^T \Phi^T(t, \tau) d\tau + \\
 &+ \int_{t_0}^t \Phi(t, \tau) B E\{\bar{w}(\tau) \bar{x}^T(0)\} d\tau \cdot \Phi^T(t, t_0) + \\
 &+ \int_{t_0}^t \int_{t_0}^t \Phi(t, \tau_1) B E\{\bar{w}(\tau_1) \bar{w}^T(\tau_2)\} B^T \Phi^T(t, \tau_2) d\tau_2 d\tau_1
 \end{aligned}$$

with,

$$\begin{aligned}
 E\{\bar{x}(0) \bar{w}^T(\tau)\} &= 0 \\
 E\{\bar{w}(\tau) \bar{x}^T(0)\} &= 0 \\
 E\{\bar{w}(\tau_1) \bar{w}^T(\tau_2)\} &= W \delta(\tau_2 - \tau_1)
 \end{aligned} \tag{5.34}$$

we find,

$$C_{\bar{x}\bar{x}}(t) = \Phi(t, t_0) C_{\bar{x}\bar{x}}(0) \Phi^T(t, t_0) + \int_{t_0}^t \Phi(t, \tau) B W B^T \Phi^T(t, \tau) d\tau \tag{5.35}$$

Together with (5.33) the above result describes the behaviour of a dynamic system driven by white noise in continuous time. Equation (5.35) is not very practical to compute the growth in time of the covariance matrix because both the Taylor expansion for Φ and the integration in the second right hand term must be evaluated as a function of time. In Section 5.7 we will return to the above result (5.35) to derive a method for calculating the variance of a stochastic variable \bar{x}_i as a function of time where use is made of Equation (5.35). For most practical purposes, however, we are mainly interested in the covariance

matrix of the steady-state after the transient behaviour has died out.

Considering the time-invariant case, where A , B and W are constant matrices, we can find the asymptote of $C_{\bar{x}\bar{x}}(t)$ by taking the limit of (5.35) for $t \rightarrow \infty$ and substituting (5.30) for $\Phi(t, t_0)$:

$$\begin{aligned} C_{\bar{x}\bar{x},ss} &= \lim_{t \rightarrow \infty} C_{\bar{x}\bar{x}}(t) = \lim_{t_0 \rightarrow -\infty} C_{\bar{x}\bar{x}}(t) = \\ &= \lim_{t_0 \rightarrow -\infty} \left\{ e^{A(t-t_0)} C_{\bar{x}\bar{x}}(0) e^{A^T(t-t_0)} + \int_{t_0}^t e^{A(t-\tau)} B W B^T e^{A^T(t-\tau)} d\tau \right\} \end{aligned}$$

If, and only if, A is asymptotically stable (all eigenvalues have strictly negative parts), the first right hand term tends to zero for arbitrary $C_{\bar{x}\bar{x}}(0)$ and we can write:

$$C_{\bar{x}\bar{x},ss} = \int_0^\infty e^{A\tau} B W B^T e^{A^T\tau} d\tau \quad (5.36)$$

This is the unique solution of an algebraic matrix equation obtained by first differentiating (5.35) with respect to t from a steady-state t_0 , where we get:

$$\begin{aligned} \dot{C}_{\bar{x}\bar{x},ss} &= \dot{\Phi}(t, t_0) C_{\bar{x}\bar{x},ss} \Phi^T(t, t_0) + \Phi(t, t_0) \dot{C}_{\bar{x}\bar{x},ss} \Phi^T(t, t_0) + \\ &+ \Phi(t, t_0) C_{\bar{x}\bar{x},ss} \dot{\Phi}^T(t, t_0) + \frac{d}{dt} \int_{t_0}^t \Phi(t, \tau) B W B^T \Phi^T(t, \tau) d\tau \end{aligned}$$

substituting $\dot{\Phi}(t, t_0) = A\Phi(t, t_0)$ and $\dot{C}_{\bar{x}\bar{x},ss} = 0$, leads to:

$$\begin{aligned} 0 &= A \Phi(t, t_0) C_{\bar{x}\bar{x},ss} \Phi^T(t, t_0) + \Phi(t, t_0) C_{\bar{x}\bar{x},ss} \Phi^T(t, t_0) A^T + \\ &+ \frac{d}{dt} \int_{t_0}^t \Phi(t, \tau) B W B^T \Phi^T(t, \tau) d\tau \end{aligned}$$

This differential equation has to obey the initial condition $t = t_0$, yielding:

$$0 = AC_{\bar{x}\bar{x},ss} + C_{\bar{x}\bar{x},ss} A^T + BWB^T \quad (5.37)$$

Although Equation (5.37) is a linear algebraic equation in $C_{\bar{x}\bar{x},ss}$, its solution cannot be directly obtained by simple matrix inversion. Equations in the form of (5.37) are known as Lyapunov equations. A unique solution exists if A is asymptotically stable (Bryson Jr. & Ho, 1975), and the solution is given by Equation (5.36).

5.6.2 Discrete time

Instead of a linear differential equation as was the case in continuous time, a linear dynamic system in discrete time is given by a linear difference equation, e.g. Equation (5.3),

$$\underline{x}[k+1] = \Phi \underline{x}[k] + \Gamma \underline{u}[k]$$

The relation between the continuous time matrices A and B and their discrete time counterparts Φ and Γ is most conveniently expressed in a Taylor series expansion form:

$$\Phi = I + \Delta t A + \frac{\Delta t^2}{2!} A^2 + \frac{\Delta t^3}{3!} A^3 + \dots \quad (5.38)$$

$$\Gamma = \Delta t B + \frac{\Delta t^2}{2!} AB + \frac{\Delta t^3}{3!} A^2 B + \dots \quad (5.39)$$

where Δt is the sampling time.

Equation (5.38) is recognized as a special case of (5.30) where the discrete time system matrix Φ is expressed as, Equation (5.38),

$$\Phi = \Phi(t_{k+1}, t_k) = e^{A \cdot \Delta t} = I + \Delta t A + \frac{\Delta t^2}{2!} A^2 + \dots$$

The discrete time input matrix Γ in Equation (5.39) can be derived from the last term in (5.29),

$$\Gamma \underline{u}[k] = \int_{t_k}^{t_{k+1}} \Phi(t_{k+1}, t) B \underline{u}[k] dt = \underline{u}[k] \int_{t_k}^{t_{k+1}} \Phi(t_{k+1}, t) B dt$$

$$\begin{aligned} \Gamma &= \int_{t_k}^{t_{k+1}} \left\{ I + A(t_{k+1} - t) + \frac{1}{2!} A^2(t_{k+1} - t)^2 + \dots \right\} B dt = \\ &= - \left[(t_{k+1} - t) + \frac{1}{2!} A(t_{k+1} - t)^2 + \frac{1}{3!} A^2(t_{k+1} - t)^3 + \dots \right]_{t_k}^{t_{k+1}} B = \\ &= \Delta t B + \frac{\Delta t^2}{2!} AB + \frac{\Delta t^3}{3!} A^2 B + \dots \end{aligned}$$

Just as in the continuous time case (Section 5.6.1) we will now develop expressions for the average value and the auto covariance matrix of the system state \bar{x} at time t_k when the system input signal $\underline{u}[k]$ is white noise $\underline{w}[k]$.

The average value of \bar{x} is calculated according to,

$$E\{\bar{x}[k+1]\} = E\{\Phi \bar{x}[k] + \Gamma \underline{w}[k]\} = \Phi E\{\bar{x}[k]\} + \Gamma E\{\underline{w}[k]\}$$

with,

$$E\{\underline{w}[k]\} = 0$$

the following recursive expression results:

$$E\{\underline{\bar{x}}[k+1]\} = \Phi E\{\underline{\bar{x}}[k]\} \quad (5.40)$$

Notice, that the average value $E\{\underline{\bar{x}}[k]\}$ will remain zero for all k if the initial expected state vector $E\{\underline{\bar{x}}[0]\}$ equals zero.

Assuming $E\{\underline{\bar{x}}[0]\} = 0$, the auto covariance matrix of $\underline{\bar{x}}$ is calculated according to:

$$\begin{aligned} C_{\underline{\bar{x}}\underline{\bar{x}}}[k+1] &= E\{\underline{\bar{x}}[k+1] \underline{\bar{x}}^T[k+1]\} \\ &= E\{(\Phi \underline{\bar{x}}[k] + \Gamma \underline{\bar{w}}[k])(\Phi \underline{\bar{x}}[k] + \Gamma \underline{\bar{w}}[k])^T\} = \\ &= E\{\Phi \underline{\bar{x}}[k] \underline{\bar{x}}^T[k] \Phi^T + \Phi \underline{\bar{x}}[k] \underline{\bar{w}}^T[k] \Gamma^T + \\ &\quad + \Gamma \underline{\bar{w}}[k] \underline{\bar{x}}^T[k] \Phi^T + \Gamma \underline{\bar{w}}[k] \underline{\bar{w}}^T[k] \Gamma^T\} \end{aligned}$$

with,

$$\begin{aligned} E\{\underline{\bar{x}}[k] \underline{\bar{w}}^T[k]\} &= 0 \\ E\{\underline{\bar{w}}[k] \underline{\bar{x}}^T[k]\} &= 0 \end{aligned}$$

it follows that,

$$C_{\underline{\bar{x}}\underline{\bar{x}}}[k+1] = \Phi C_{\underline{\bar{x}}\underline{\bar{x}}}[k] \Phi^T + \Gamma C_{\underline{\bar{w}}\underline{\bar{w}}}[k] \Gamma^T \quad (5.41)$$

There is one last problem to be solved. In Equation (5.41) the unknown term $C_{\underline{\bar{w}}\underline{\bar{w}}}[k]$ appears, the auto covariance matrix of the discrete time white noise signal. If the system under consideration is a truly discrete system, that is, the state vector $\underline{\bar{x}}$ is only defined at time $t = k\Delta t$, the matrix $C_{\underline{\bar{w}}\underline{\bar{w}}}[k]$ simply reflects the variances of the discrete time white noise signals which might be known a priori. However, if the discrete time system (5.3) and (5.4) are a discrete model of a continuous time physical process (using (5.38) and (5.39) to obtain the discretized system- and input matrices), the choice for the $C_{\underline{\bar{w}}\underline{\bar{w}}}[k]$ matrix is no longer evident. Given (5.35) and (5.41),

$$C_{\underline{\bar{x}}\underline{\bar{x}}}(t) = \Phi(t, t_0) C_{\underline{\bar{x}}\underline{\bar{x}}}(0) \Phi^T(t, t_0) + \int_{t_0}^t \Phi(t, \tau) B W B^T \Phi^T(t, \tau) d\tau$$

$$C_{\underline{\bar{x}}\underline{\bar{x}}}[k+1] = \Phi C_{\underline{\bar{x}}\underline{\bar{x}}}[k] \Phi^T + \Gamma C_{\underline{\bar{w}}\underline{\bar{w}}}[k] \Gamma^T$$

where the increase of the variance $C_{\underline{\bar{x}}\underline{\bar{x}}}[k]$ of the state vector $\underline{\bar{x}}$ as a function of time is calculated in continuous- or discrete time when the input is white noise $\underline{\bar{w}}$ with an intensity matrix W .

The question is: how to choose $C_{\underline{\bar{w}}\underline{\bar{w}}}[k]$ of the discrete noise signal in order to truly

simulate the continuous time situation. An equal increase in the co-variance matrix $C_{\bar{x}\bar{x}_{con}}(t) = C_{\bar{x}\bar{x}_{dis}}(k\Delta t)$ should then be obtained in the continuous time situation and the equivalent discrete time system.

Calculating the increase of $C_{\bar{x}\bar{x}}[k]$ from $t = k\Delta t$ to $t = (k + 1)\Delta t$ in discrete time:

$$\Delta C_{\bar{x}\bar{x}_{dis}} = C_{\bar{x}\bar{x}}[k + 1] - C_{\bar{x}\bar{x}}[k] = \Phi C_{\bar{x}\bar{x}}[k] \Phi^T + \Gamma C_{\bar{w}\bar{w}}[k] \Gamma^T - C_{\bar{x}\bar{x}}[k] \quad (5.42)$$

In continuous time this increase of the covariance matrix is:

$$\begin{aligned} \Delta C_{\bar{x}\bar{x}_{con}} &= C_{\bar{x}\bar{x}}(t_k + \Delta t) - C_{\bar{x}\bar{x}}(t_k) = \\ &= \Phi(t_k + \Delta t, t_k) C_{\bar{x}\bar{x}}(t_k) \Phi^T(t_k + \Delta t, t_k) + \\ &+ \int_{t_k}^{t_k + \Delta t} \Phi(t_k + \Delta t, \tau) B W B^T \Phi^T(t_k + \Delta t, \tau) d\tau - C_{\bar{x}\bar{x}}(t_k) \end{aligned} \quad (5.43)$$

If the discrete time system is used to correctly model the continuous system, the increases in Equation (5.42) and (5.43) must be the same. From the Taylor expansion of the discrete time state matrix Φ , Equation (5.38), it is clear that the first and last terms in (5.42) and (5.43) indeed are the same. Therefore the middle terms of (5.42) and (5.43) should be equal,

$$\Gamma C_{\bar{w}\bar{w}}[k] \Gamma^T = \int_{t_k}^{t_k + \Delta t} \Phi(t_k + \Delta t, \tau) B W B^T \Phi^T(t_k + \Delta t, \tau) d\tau \quad (5.44)$$

with $\Gamma \approx B\Delta t$ and $\Phi(t_k + \Delta t, \tau) \approx I$ on the interval $[t_k, t_k + \Delta t]$ we can write for (5.44):

$$\Delta t^2 B C_{\bar{w}\bar{w}} B^T = B W B^T \Delta t$$

or:

$$C_{\bar{w}\bar{w}} = \frac{W}{\Delta t} \quad (5.45)$$

Summarizing, we can say that when an actual continuous time physical stochastic process driven by white noise with a noise intensity matrix W is to be modelled by a discrete time model, the discrete time system should be driven by a random time series with covariance matrix $\frac{W_{con}}{\Delta t}$. The recursive equation for calculating the state vector covariance matrix then is, Equation (5.41):

$$C_{\bar{x}\bar{x}}[k + 1] = \Phi C_{\bar{x}\bar{x}}[k] \Phi^T + \Gamma \frac{W_{con}}{\Delta t} \Gamma^T$$

Based on these results we may conclude that for dynamic systems subject to stochastic input signals the auto covariance matrix $C_{\bar{x}\bar{x}}(t)$ will not remain constant in time. This contradicts the result found for linear transformations, see Section 5.3 Equation (5.16)

which yielded a constant auto covariance matrix $C_{\bar{y}\bar{y}}$ of the system output. Due to the non-stationary character of the auto covariance matrix for dynamic systems with stochastic inputs, the process state- and output vectors will generally not be ergodic. It should therefore be realized that the auto covariance matrix is an ensemble average rather than a time average.

Notice that the discrete time method for the calculation of the auto covariance matrix (Equation (5.41)) is a very powerful mathematical tool. It allows treatment of virtually all possible situations since the input auto covariance $C_{\bar{w}\bar{w}}$ as well as the system matrices Φ , Γ , C and D are not restricted to be time-invariant. As mentioned in Section 5.6.1, the covariance matrix tends towards a constant matrix $C_{\bar{x}\bar{x},ss}$ for $t \rightarrow \infty$. In the steady-state condition we can write (5.41) as:

$$C_{\bar{x}\bar{x},ss} = \Phi C_{\bar{x}\bar{x},ss} \Phi^T + \Gamma \frac{W_{con}}{\Delta t} \Gamma^T \quad (5.46)$$

which is a discrete matrix Lyapunov equation. A method to obtain the steady-state covariance matrix is to transform (Φ, Γ) to the continuous form (A, B) and solve Equation (5.36) (Kwakernaak & Sivan, 1972). A more practical approach is to run (5.43) until

$$C_{\bar{x}\bar{x}}[k+1] - C_{\bar{x}\bar{x}}[k] < \epsilon \quad (5.47)$$

With the increased use of digital computers for system analysis, continuous time systems (A, B) are usually converted to their discrete time counterpart (Φ, Γ) using Equations (5.38), (5.39) and (5.45) after which the growth in time of the auto covariance matrix $C_{\bar{x}\bar{x}}$ is calculated with (5.41). Another method for the calculation of the growth of the auto covariance matrix of continuous time systems, particularly useful with analogue computers, will, for the sake of completeness, be presented in the next paragraph.

An extension to cross covariance matrices, e.g. $C_{\bar{u}\bar{y}}$, $C_{\bar{y}\bar{u}}$ or $C_{\bar{x}\bar{y}}$ is possible and straightforward in its derivation. They are, however, seldomly used and therefore considered to be outside the scope of this chapter.

5.7 The impulse response method

In the case of continuous time control systems perturbed by stochastic signals, it is often necessary to know the probability of a stochastic variable $\underline{x}(t)$ exceeding a certain value. Thus the probability distribution function $F_{\underline{x}}(\underline{x})$ or the probability density function $f_{\underline{x}}(\underline{x})$ is to be known. Under the assumption the stochastic variable has a Gaussian distribution the first and second central moments completely determine the probability density function (see Section 2.5.2). In the multidimensional case, it therefore suffices to obtain the average of $\underline{x}(t)$ and the auto covariance matrix $C_{\bar{x}\bar{x}}$ of \underline{x} . When dealing with deviations of \underline{x} from a certain datum, as often is the case, the average of \underline{x} is zero and only $C_{\bar{x}\bar{x}}$ needs to be obtained. As seen, in practice this can be done in a number of ways, recapitulating the foregoing,

- In the time domain, under the assumption the stochastic process is ergodic, the auto covariance matrix can be obtained by the sampling of a realization:

$$C_{\bar{x}\bar{x}}[i] = \frac{1}{N-1} \sum_{i=1}^N (\bar{x}[i] - \mu_{\bar{x}})(\bar{x}[i] - \mu_{\bar{x}})^T$$

this method, sometimes referred to as the 'Monte Carlo method', yields acceptable results only for a large number of samples ($N \rightarrow \infty$) and can therefore practically only be used for the determination of the steady-state auto covariance matrix.

- Another possible method for stationary Gaussian processes is integrating the auto power spectral density matrix of \underline{x} ,

$$\begin{aligned} C_{\bar{x}\bar{x}}(\tau) &= F^{-1} \{ S_{\bar{x}\bar{x}}(\omega) \} \\ C_{\bar{x}\bar{x}}(\tau = 0) &= \frac{1}{2\pi} \int_{-\infty}^{+\infty} S_{\bar{x}\bar{x}}(\omega) d\omega \end{aligned}$$

This method also only yields the steady-state auto covariance matrix of the stationary stochastic process.

- In continuous time the covariance matrix as function of time is given by Equation (5.35),

$$C_{\bar{x}\bar{x}}(t) = \Phi(t, t_0) C_{\bar{x}\bar{x}}(0) \Phi^T(t, t_0) + \int_{t_0}^t \Phi(t, \tau) B W B^T \Phi^T(\tau, t) d\tau$$

The steady state covariance matrix is the solution of the Lyapunov equation,

$$A C_{\bar{x}\bar{x},ss} + C_{\bar{x}\bar{x},ss} A^T = -B W B^T$$

and is given by Equation (5.36).

- In Section 5.6 a computational powerful method was given by discretizing the continuous time system and computing the growth in time of the covariance matrix $C_{\bar{x}\bar{x}}$ with Equation (5.41),

$$C_{\bar{x}\bar{x}}[k+1] = \Phi C_{\bar{x}\bar{x}}[k] \Phi^T + \Gamma \frac{W_{con}}{\Delta t} \Gamma^T$$

The subject of this section is still another and rather different method for calculating the auto covariance matrix $C_{\bar{x}\bar{x}}(t)$. It will be shown that the growth in time of the auto covariance matrix can be calculated by integrating the squared impulse responses of the system (Van der Vaart, 1975; Etkin, 1960).

For a given constant linear system, the solution of the state Equation (5.1) is given by Equation (5.29),

$$\underline{x}(t) = \Phi(t, t_0) \underline{x}(0) + \int_{t_0}^t \Phi(t, \tau) B \underline{u}(\tau) d\tau$$

The first term on the right hand side of Equation (5.29) is the system's response to a set of initial conditions $\underline{x}(0)$, the second term is the response to a set of input signals $\underline{u}(t)$. Now consider the case where all the elements of $\underline{u}(t)$ are zero except one, for instance the i -th element u_i of $\underline{u}(t)$. The matrix B then reduces to one column, pertaining the vector \underline{B}_i . If in addition the initial conditions $\underline{x}(0)$ are zero, then $\underline{x}(t)$ is given by:

$$\underline{x}(t) = \int_{t_0}^t \Phi(t, \tau) \underline{B}_i u_i(\tau) d\tau \quad (5.48)$$

Now let u_i be a unit impulse at $\tau = 0$. Substitution of $u_i = \delta(0)$ into (5.48) yields the impulse response of the system:

$$\underline{x}(t) = \Phi(t, t_0) \underline{B}_i = h_i(t) \quad (5.49)$$

The subscript i in $h_i(t)$ denotes the impulse response to $u_i = \delta(0)$. Comparing Equations (5.29) and (5.49) it is apparent that the impulse response is identical with a response to an initial condition,

$$\underline{x}(0) = \underline{B}_i \quad (5.50)$$

Next a similar system is considered driven by a number of uncorrelated zero-mean white noise input signals, a vector $\bar{\underline{w}}(t)$, with an intensity matrix W , Equation (5.32),

$$C_{\bar{\underline{w}}\bar{\underline{w}}}(\tau) = W \delta(\tau)$$

In Section 5.6.1 it was shown that the auto covariance matrix $C_{\bar{\underline{x}}\bar{\underline{x}}}(t)$ of the state vector $\bar{\underline{x}}$ of a constant linear system driven by a noise vector $\bar{\underline{w}}$ is given by, Equation (5.35),

$$C_{\bar{\underline{x}}\bar{\underline{x}}}(t) = \Phi(t, t_0) C_{\bar{\underline{x}}\bar{\underline{x}}}(0) \Phi^T(t, t_0) + \int_{t_0}^t \Phi(t, \tau) B W B^T \Phi^T(\tau, t) d\tau$$

If all the variances and covariances of the system's state vector are zero at $t = 0$, so $C_{\bar{\underline{x}}\bar{\underline{x}}}(0) = 0$, then the first right hand term in (5.35) disappears. Now suppose that all white noise input signals are zero except one element $\bar{w}_i(t)$ of vector $\bar{\underline{w}}(t)$, with intensity,

$$C_{\bar{w}_i\bar{w}_i} = \sigma_{\bar{w}_i}^2 = 1$$

The matrix B now again reduces to \underline{B}_i and Equation (5.35) can be written as, taking $t_0 = 0$:

$$C_{\bar{\underline{x}}\bar{\underline{x}}}(t) = \int_0^t \Phi(t, \tau) \underline{B}_i \underline{B}_i^T \Phi^T(\tau, t) d\tau = \int_0^t \Phi(t, \tau) \underline{B}_i (\Phi(t, \tau) \underline{B}_i)^T d\tau \quad (5.51)$$

Substituting $\nu = t - \tau$:

$$C_{\bar{x}\bar{x}}(t) = - \int_t^0 \Phi(t, \nu) \underline{B}_i (\Phi(t, \nu) \underline{B}_i)^T d\nu = \int_0^t \Phi(t, t_0) \underline{B}_i (\Phi(t, t_0) \underline{B}_i)^T dt$$

and comparing with (5.49) it appears that for the time response of the covariance matrix $C_{\bar{x}\bar{x}}(t)$ due to input i of the state-space model, according to Equation (5.1):

$$\dot{\underline{x}}(t) = A \underline{x}(t) + B \underline{u}(t) = A \underline{x}(t) + [\underline{B}_1 \underline{B}_2 \cdots \underline{B}_m] \begin{bmatrix} u_1 \\ u_2 \\ \vdots \\ u_m \end{bmatrix}$$

one can write for the response of the state vector $\bar{x}(t)$ due to input i ,

$$C_{\bar{x}\bar{x}}(t) = \int_0^t \underline{h}_i(\nu) \cdot \underline{h}_i^T(\nu) d\nu \quad (5.52)$$

In particular, a diagonal element $\sigma_{\bar{x}_j}^2(t)$ of $C_{\bar{x}\bar{x}}(t)$ is according to (5.52),

$$\sigma_{\bar{x}_j}^2(t) = \int_0^t h_{ji}^2(\nu) d\nu \quad (5.53)$$

with h_{ji} the j -th element of vector \underline{h}_i . An off-diagonal element of the covariance matrix $C_{\bar{x}\bar{x}}(t)$ is then:

$$C_{\bar{x}_j \bar{x}_k}(t) = \int_0^t h_{ji}(\nu) \cdot h_{ki}(\nu) d\nu \quad (5.54)$$

Remember that the impulse response vector \underline{h} due to input i is equal to,

$$\underline{h}_i = \begin{bmatrix} h_{1i} \\ h_{2i} \\ \vdots \\ h_{ni} \end{bmatrix}$$

assuming n state variables. The dot-product $\underline{h}_i \cdot \underline{h}_i^T$ becomes,

$$\underline{h}_i \cdot \underline{h}_i^T = \begin{bmatrix} h_{1i} \\ h_{2i} \\ \vdots \\ h_{ni} \end{bmatrix} \cdot [h_{1i} \ h_{2i} \ \cdots \ h_{ni}] = \begin{bmatrix} h_{1i}^2 & h_{1i} \cdot h_{2i} & \cdots & h_{1i} \cdot h_{ni} \\ h_{2i} \cdot h_{1i} & h_{2i}^2 & \cdots & h_{2i} \cdot h_{ni} \\ \vdots & \vdots & & \vdots \\ h_{ni} \cdot h_{1i} & h_{ni} \cdot h_{2i} & \cdots & h_{ni}^2 \end{bmatrix}$$

According to (5.53) and (5.54) the growth in time of the variance of an output signal $\bar{x}_j(t)$ of a system perturbed from $t = 0$ onwards by a single white noise signal can be obtained

by integrating the square of the system's impulse response with respect to time, while the covariance of two output signals is obtained by integrating the product of the impulse response functions. For practical calculations the impulse response is usually obtained as the response to properly chosen initial conditions, Equation (5.50):

$$\underline{x}(0) = \underline{B}_i$$

The variances and covariances caused by all m white noise input signals acting simultaneously from $t = 0$ onwards, can, still assuming uncorrelated white noise signals and system linearity, be obtained by summing the results (5.53) and (5.54) for all m input signals:

$$C_{\bar{x}\bar{x}}(t) = \sum_{i=1}^m \int_0^t \underline{h}_i(\nu) \cdot \underline{h}_i^T(\nu) d\nu \quad (5.55)$$

with,

$$\sigma_{\bar{x}_j}^2(t) = \sum_{i=1}^m \int_0^t h_{ji}^2(\nu) d\nu \quad (5.56)$$

and,

$$C_{\bar{x}_j \bar{x}_k}(t) = \sum_{i=1}^m \int_0^t h_{ji}(\nu) \cdot h_{ki}(\nu) d\nu \quad (5.57)$$

It is worth while noting that it is possible to calculate the covariance matrix of a system perturbed by a stochastic signal by integrating a deterministic function.

5.8 Examples and problems

5.8.1 Example 5.1

In Section 5.6.2, it was shown that when a continuous time (CT) physical stochastic process driven by continuous time white noise with a noise intensity matrix W was to be modelled by a discrete-time (DT) model, then the discrete time system should be driven by a discrete-time random time series with auto covariance matrix $\frac{W}{\Delta t}$ (Equation (5.45)).

In this example, it will be shown that, in MATLAB, when using `lsim` to compute the response of a continuous time system model to a (inevitably discrete) noise input signal, the covariance matrix of the input signal should also be $\frac{W}{\Delta t}$. This is caused by the fact that, internally (i.e., hidden for the user) MATLAB transforms the CT system to DT, and therefore to get the right response to the noise, the intensity needs to be divided by Δt .

Consider a first order continuous LTI system with gain $K = 2$ and time constant $\tau = 0.5$ s, Figure 5.1. The system is driven by a white noise input signal with intensity $W = 2$ and

is simulated with a time step $\Delta t = 0.01$ s. Figure 5.2(a) shows the estimated mean, the variance of the covariance of 500 white noise realizations and the analytical covariance. Figure 5.2(b) shows the mean and the variance of the covariance of the response to the discrete time white noise input signal without using $\frac{W}{\Delta t}$. It shows that the mean of the output covariance does not approximate the analytical covariance. However, when using $\frac{W}{\Delta t}$ to generate the discrete white noise input signal driving the system, the estimated mean covariance of the output signal approximates the analytical covariance of the output, Figure 5.2(c).

Listing 5.1: Example 5.1

```
% Exampl51 shows the response of a CT first order linear system to a white
% noise input signal and examine the statistical properties
% of the response for a large number of realizations.
%
% Check the outcome with the result that can be
% analytically obtained through Tables 3.5 and 3.6.
%
% Chapter 5 of lecture notes ae4-304.
%
% (c) MM 2004 Revised: November 2014, [M Rodriguez]
%%
clc; close all; clear all;

disp(' Example 5.1 ');
disp(' ');
disp(' Simulation of a continuous time first order system response ');
disp(' to a white noise input signal and examine the mean and ');
disp(' standard deviation of the response for a large number ');
disp(' of realizations ');
disp(' ');
disp(' The outcome can be verified with the result obtained ');
disp(' analytically using Tables 3.5 and 3.6 ');
disp(' ');
disp(' This program can produce Figure 5.2 of the lecture ');
disp(' notes: Aircraft Responses to Atmospheric Turbulence. ');
disp(' ');

% SYSTEM DYNAMICS
%
% Assume we have a CT system, a first order low-pass filter K/(1+s tau)
%
K = 2.00;           % system gain      [-]
tau = 0.50;          % system time lag [s]

num = K; den = [tau 1];    % system dynamics in rational polynomial form

sys = tf(num,den);       % Matlab LTI system

% TIME DEFINITION
fs = 100;              % sample rate [Hz], 100 Hz is very common.
```

```

dt = 1/fs; % sample time [s]
t = 0:dt:60; % 60 seconds of data
NT = length(t); % the number of time samples

% WHITE NOISE DEFINITION
Wn = 2; % intensity of the white noise

w = sqrt(Wn)*randn(NT,1); % random, normally distributed white
                           % noise with intensity Wn
%
% COMPUTE SYSTEM TIME RESPONSE

% REPEAT THE SYSTEM RESPONSE N TIMES AND LOOK AT VARIANCES
% OF INPUT AND OUTPUT SIGNALS
% DO NOT FORGET TO SKIP THE TRANSIENT PART OF THE RESPONSE!
N = 500; % the number of realizations

Var_in = zeros(N,1);
Var_out = zeros(N,1);
Var_out_e = zeros(N,1);

% skip the first part of the response, because of the transient
% in this case this only depends on the value of tau, but let's be
% safe and skip the first 33% anyway
stationary_part = (floor(NT/3)+1):1:NT;

for kk=1:N
%
% create white noise input
w = sqrt(Wn)*randn(NT,1);
% compute system output
y = lsim(sys,w/sqrt(dt),t,'zoh'); % Correct: DIVISION of Wn by dt!
y_e = lsim(sys,w,t,'zoh'); % Wrong: NO DIVISION of Wn by dt!
% compute variance of input and output
Var_in(kk,1) = cov(w(stationary_part,1));
Var_out(kk,1) = cov(y(stationary_part,1));
Var_out_e(kk,1) = cov(y_e(stationary_part,1));
%
end

% NOW, NOTE THAT WE ARE INTERESTED IN THE VARIANCE OF
% THE WHITE NOISE INPUT SIGNAL AND THE VARIANCE OF THE SYSTEM
% OUTPUT SIGNAL. FOR EACH REALIZATION, THESE ARE DIFFERENT:
% THEY CAN BE CONSIDERED STOCHASTIC VARIABLES THEMSELVES!!!
%
% SO, if var(w; realization i) = vw_i    i = 1, ... N
% and var(y; realization i) = vy_i      i = 1, ... N
%
% WE CAN THEN COMPUTE THE MEAN AND THE VARIANCES OF
% THESE SVs:
%
%       mean(vw_i, for all i) and std(vw_i, for all i)

```

```

%
% mean(vy_i, for all i) and std(vy_i, for all i)
%
% AND THE MEANS SHOULD IN PRINCIPLE (for a large number of
% realizations N) BE IDENTICAL TO THE ANALYTICAL VALUES
% REPRESENTING THE ENSEMBLE.
%
% REMEMBER: AVERAGING OVER THE REALIZATIONS MEANS THAT WE
% ARE ESTIMATING THE ENSEMBLE AVERAGE. WHEN THE
% NUMBER OF REALIZATIONS INCREASES (N -> infinity)
% THE ESTIMATIONS SHOULD CONVERGE TO THE ENSEMBLE
% AVERAGE. IT CAN BE SHOWN THAT THE ESTIMATOR
% FOR THE MEAN AND THE ESTIMATOR FOR THE VARIANCE
% ARE UNBIASED AND ASYMPTOTICALLY RIGHT
%
% (check in Matlab: help mean
%                      help var  )
%
mean_var_in      = mean(Var_in);
mean_var_out     = mean(Var_out);
mean_var_out_e   = mean(Var_out_e);
var_var_in       = var(Var_in);
var_var_out      = var(Var_out);
var_var_out_e    = var(Var_out_e);

%
% THE ANALYTICAL VALUE OF THE SYSTEM OUTPUT SIGNAL VARIANCE
% CAN BE OBTAINED WITH TABLE 3.5
%
% For this system it is equal to:
%      K^2
%      W----- with: W : the CT white noise intensity
%      2*tau          K : the system gain
%                          tau : the system lag time constant
%
var_out_analytic = Wn*K*K/(2*tau);

% THE ANALYTICAL VALUE OF THE WHITE NOISE INPUT VARIANCE
% JUST EQUALS THE INTENSITY
var_in_analytic = Wn;

% PLOT THE RESULTS
figure(1)
% first the white noise input
subplot(3,1,1)
% show the values for each realization
plot([1:1:N],Var_in)
hold on
% show the mean +- var of the average over
% all realizations in green
plot([1 N],mean_var_in*[1 1],'g');
plot([1 N],mean_var_in*[1 1]+var_var_in,'g--');
% show the analytical value (the ensemble average) in red

```

```

plot([1 N],var_in_analytic*[1 1],'r');
% plot the other var line here, otherwise it is
% redundant in the legend
plot([1 N],mean_var_in*[1 1]-var_var_in,'g--');
hold off
title('variance of CT white noise input signal')
axis('tight')
ylabel('var(w)')
xlabel('realization')
legend('estimated','mean','variance','analytic')

% the system output without division of Wn by dt
subplot(3,1,2)
% show the values for each realization
plot([1:1:N],Var_out_e)
hold on
% show the mean +- var of the average over
% all realizations in green
plot([1 N],mean_var_out_e*[1 1],'g');
plot([1 N],mean_var_out_e*[1 1]+var_var_out_e,'g--');
% show the analytical value (the ensemble average) in red
plot([1 N],var_out_analytic*[1 1],'r');
% plot the other var line here, otherwise it is
% redundant in the legend
plot([1 N],mean_var_out_e*[1 1]-var_var_out_e,'g--');
hold off
title('variance of system output signal no dt')
ylabel('var(y)')
xlabel('realization')
legend('estimated','mean','var','analytic')

% the system output with Wn/dt
subplot(3,1,3)
% show the values for each realization
plot([1:1:N],Var_out)
hold on
% show the mean +- var of the average over
% all realizations in green
plot([1 N],mean_var_out*[1 1],'g');
plot([1 N],mean_var_out*[1 1]+var_var_out,'g--');
% show the analytical value (the ensemble average) in red
plot([1 N],var_out_analytic*[1 1],'r');
% plot the other var line here, otherwise it is
% redundant in the legend
plot([1 N],mean_var_out*[1 1]-var_var_out,'g--');
hold off
title('variance of system output signal')
axis('tight')
ylabel('var(y)')
xlabel('realization')
legend('estimated','mean','variance','analytic')
% EOF

```

5.8.2 Example 5.2

In this example the response of the covariance matrix of a second order system (see Figure 5.3) driven by a white noise input will be calculated using the method introduced in Section 5.6.2, see also (Jonkers, Kappetijn, & Van der Vaart, 1981).

The equation of motion for the one-degree-of-freedom system depicted in Figure 5.3 is given by:

$$m\ddot{y}(t) + c\dot{y}(t) + ky(t) = \bar{u}(t) \quad (5.58)$$

where $y(t)$ is the displacement from a datum and $\bar{u}(t)$ a white noise force input signal. Taking the Laplace-transform of Equation (5.58) yields the transfer function of the system:

$$H(s) = \frac{Y(s)}{U(s)} = \frac{1}{ms^2 + cs + k} \quad (5.59)$$

or substituting $s = j\omega$ in (5.59) to obtain the frequency response function:

$$H(\omega) = \frac{1}{-m\omega^2 + cj\omega + k} \quad (5.60)$$

If we define,

$$\omega_0 = \sqrt{\frac{k}{m}} \text{ and } \zeta = \frac{c}{2m\omega_0} \quad (5.61)$$

where ω_0 is the undamped natural frequency and ζ the damping ratio, we can write (5.60) as:

$$H(\omega) = \frac{\frac{1}{k}}{1 + 2\zeta\frac{j\omega}{\omega_0} + \left(\frac{j\omega}{\omega_0}\right)^2} \quad (5.62)$$

A state-space description can be obtained by taking $\underline{y}(t) = [y(t) \ \dot{y}(t)]^T$ as state vector:

$$\begin{aligned} \frac{d}{dt} \begin{bmatrix} y(t) \\ \dot{y}(t) \end{bmatrix} &= \begin{bmatrix} 0 & 1 \\ -\frac{k}{m} & -\frac{c}{m} \end{bmatrix} \begin{bmatrix} y(t) \\ \dot{y}(t) \end{bmatrix} + \begin{bmatrix} 0 \\ \frac{1}{m} \end{bmatrix} \bar{u}(t) \\ y(t) &= [1 \ 0] \begin{bmatrix} y(t) \\ \dot{y}(t) \end{bmatrix} \end{aligned} \quad (5.63)$$

The covariance matrix is then:

$$C_{\underline{y}\underline{y}}(t) = \begin{bmatrix} \sigma_y^2(t) & C_{\bar{y}\bar{y}}(t) \\ C_{\bar{y}\bar{y}}(t) & \sigma_{\dot{y}}^2(t) \end{bmatrix} \quad (5.64)$$

The steady-state variance $\sigma_{\bar{y}}^2$ of the displacement of the second order system driven by white noise is found to be using Tables 3.5 and 3.6:

$$\sigma_{\bar{y}}^2 = \frac{\omega_0}{4\zeta} \quad (5.65)$$

The response of $C_{\bar{y}\bar{y}}(t)$ is calculated in this example by discretizing (5.63) and applying Equation (5.41),

$$C_{\bar{y}\bar{y}}[k+1] = \Phi C_{\bar{y}\bar{y}}[k] \Phi^T + \Gamma \frac{W_{con}}{\Delta t} \Gamma^T$$

where W is the intensity of the white noise input $\bar{u}(t)$, Equation (2.31),

$$\sigma_{\bar{u}}^2(\tau) = W \delta(\tau)$$

A MATLAB program to calculate the growth in time of $C_{\bar{y}\bar{y}}$ is given below. For the used values of the necessary input variables we refer to the Figures 5.4 to 5.8.

Listing 5.2: Example 5.2

```
% Example52 Calculates covariance matrix as function of time for a
% second order mass-spring-damper system perturbed by white
% noise, using the discrete-time recursive calculation method.
%
% Chapter 5 of lecture notes ae4-304
%
% Program revised August 1992, February 2004 [MM], November 2014 [M
% Rodriguez]
%%
clc; close all; clear;

disp(' Example 5.2');
disp(' Calculation of the growth in time of the covariance');
disp(' matrix of a second order mass-spring-damper system');
disp(' perturbed by white noise. The covariance matrix C');
disp(' is calculated in time with:');
disp(' ');
disp(' C(k+1) = PHI(k) C(k) PHI(k)^T + GAMMA(k) C(k) GAMMA(k)^T');
disp(' xx xx ww');
disp(' ');
disp(' This program can produce Figures 5.4 to 5.8 of the lecture');
disp(' notes: Aircraft Responses to Atmospheric Turbulence.');
disp(' ');
disp(' 2nd Order Model Definition:');
disp(' ');

% CT SYSTEM DYNAMICS
w0 = input(' Give undamped natural frequency [rad/s] : ');
zeta = input(' Give damping ratio : ');

m = 1; k = w0^2;
c = zeta*2*m*w0;

A=[0 1;-k/m -c/m]; % state-space representation of second
B=[0 1/m]; % order system
```

```

C=[1 0];
D=[0];

% DEFINE TIME AXIS
dt= 0.01; % sample time 0.1 seconds
t = [dt:dt:15]; % time axis
N = 15/dt; % number of samples

% DISCRETIZE SYSTEM MATRICES
[Phi, Gamma]=c2d(A,B, dt); % discretizing using MATLAB c2d command

% DEFINE WHITE NOISE CHARACTERISTICS
Wc = input(' Enter CT white noise intensity : ');
answ = input(' Stepwise change of noise intensity ? (y/n) : ', 's');

W = zeros(N,1);

if answ=='y',
    Q = input(' Enter Q (0<Q<1) : ');
    answ1 = input(' Noise intensity W=0 after t=T(1-Q) (y/n) : ', 's');
    answ2 = input(' Noise intensity W=2*Wc after t=T(1-Q) (y/n) : ', 's');
    M=Q*N;

    %for k=1:N-M;
    %    W(1:N-M)=Wc/dt; % always apply equation (5.45)
    %end

    for k=N-M+1:N;
        if answ1=='y',
            W(k)=0;
        end
        if answ2=='y',
            W(k)=2*Wc/dt;
        end
    end
end
if answ=='n';
    for k=1:N;
        W(k)=Wc/dt;
    end
end

% DEFINE INITIAL CONDITIONS
Cx1x1 = zeros(N,1);
Cx1x2 = zeros(N,1);
Cx2x2 = zeros(N,1);

Cx1x1(1)= input(' Give initial value of Cyy(1,1) : ');
Cx1x2(1)= input(' Give initial value of Cyy(1,2)=C(2,1) : ');
Cx2x2(1)= input(' Give initial value of Cyy(2,2) : ');
Cxx=[Cx1x1(1) Cx1x2(1);Cx1x2(1) Cx2x2(1)];

```

```
% DISCRETE SOLUTION Cxx(k+1)=Phi*Cxx(k)*Phi' + Gamma*W*Gamma';
for k=1:N-1;
    Cxx      = Phi*Cxx*Phi'+Gamma*W(k)*Gamma';
    Cx1x1(k+1) = Cxx(1,1);
    Cx1x2(k+1) = Cxx(2,1);
    Cx2x2(k+1) = Cxx(2,2);
end

ref=zeros(1,N);

% PLOT RESULTS
subplot(221);
axis([0 15 -0.5 1.5]);
plot(t,Cx1x1,'-',t,ref,'-');
xlabel('time [s]'); ylabel('Cx1x1 (t)');

subplot(222);
plot(t,Cx1x2,'-',t,ref,'-');
xlabel('time [s]'); ylabel('Cx1x2 (t)');

subplot(224);
plot(t,Cx2x2,'-',t,ref,'-');
xlabel('time [s]'); ylabel('Cx2x2 (t)');

% EOF
```

Figure 5.4 shows the response of each element of $C_{\bar{y}\bar{y}}(t)$ as given by (5.64) caused by a white noise signal acting as an input to the second order system from $t = 0$ onwards, all initial conditions zero, for three different values of the damping ratio. That the covariance $C_{\bar{y}\bar{y}}(t)$ is zero in the steady-state is to be expected, because in this case the second element of the state vector is the time derivative of the first element. Figure 5.5 shows the response to an initial condition only,

$$C_{\bar{y}\bar{y}}(0) = \begin{bmatrix} 1 & 0 \\ 0 & 1 \end{bmatrix}$$

where with increase in time the covariance matrix tends to 0. Because the system is linear, we can superimpose Figures 5.4 and 5.5 to get the response from a white noise input and initial conditions. The result is plotted in Figure 5.6.

That this way of calculating the covariance matrix as a function of time is such a powerful method, can be illustrated with Figures 5.7 and 5.8, where the response of the second order system to a white noise input is given when the statistical properties of the input signal change in time. The processes are no longer stationary but if it is known how these properties change in time, the response can be determined.

5.8.3 Example 5.3

The propagation in time of the variance of the displacement of the second order system from the previous example can also be determined by the 'impulse response method' as introduced in Section 5.7. There it was shown that the impulse response due to input i of a system with one white noise input is identical with a response to an initial condition, Equation (5.50),

$$\underline{x}(0) = \underline{B}_i$$

Using MATLAB, $\sigma_y^2(t)$ is computed for a white noise input with intensity 1 for three different damping ratios of the second order system Equation (5.62) or (5.63). and plotted in Figure 5.9 where the used values for the program's input variables have been stated as well.

Listing 5.3: Example 5.3

```
% Exempl53      Calculates covariance matrix as function of time for a
%               second order mass-spring-damper system perturbed by white
%               noise using the impulse response method.
%
% Chapter 5 of lecture notes ae4-304
%
% Program revised August 1992, February 2004 [MM], November 2014 [M
% Rodriguez]
%%
clc; close all; clear all;

disp('    Example 5.3          ');
disp('
disp('    Calculation of the growth in time of the covariance      ');
disp('    matrix of a second order mass-spring-damper system        ');
disp('    perturbed by white noise using the impulse response method:');
disp('
disp('           _ t
disp('           |           T
disp('           C (k) = | h(v).h(v)   dv
disp('           xx     - |
disp('           0
disp('
disp('    This program can produce Figure 5.9 of the lecture notes:  ');
disp('    Aircraft Responses to Atmospheric Turbulence.
disp('
disp('
disp('    2nd Order Model Definition:
disp('

% CT SYSTEM DYNAMICS
w0      = input('    Give undamped natural frequency [rad/s] : ');
zeta   = input('    Give damping ratio :');
```

```

m = 1;                                % mass
k = w0^2;                             % spring constant
c = zeta*2*m*w0;                      % damping constan

A=[0 1;-k/m -c/m];                   % state-space representation of a CT second
B=[0 1/m]';                           % order system
C=[1 0];
D=[0];

% TIME AXIS
dt=.1; T=15; t=[0:dt:T]; N=length(t);

% COMPUTE CT SYSTEM IMPULSE RESPONSE
u = zeros(1,N);                      % zero input
x0 = B;                               % initial condition
h = lsim(A,B,C,D,u,t,x0);           % calculation impulse response as a resonse
                                      % to an initial condition.

% SQUARE IMPULSE RESPONSE
hsq=h.*h;                            % squared impulse response

% INTEGRATE THE SQUARED IMPULSE RESPONSE
% done rather crudely here
vary = zeros(N,1);
for i=1:N-1
    vary(i+1) = vary(i) + hsq(i)*dt;   % integrated squared impulse response
end

% PLOT RESULTS
subplot(2,2,1)
axis([0 15 -.5 1.5]);
plot(t,h,'-');
xlabel('time [s]'); ylabel('h (t)'); title('Impulse Response');

subplot(2,2,2)
plot(t,hsq,'-');
xlabel('time [s]'); ylabel('h^2 (t)'); title('Squared Impulse Response');
axis([0 15 -.5 1.5]);

subplot(2,2,3)
plot(t,vary,'-'); xlabel('time [s]'); ylabel('Cx1x1 (t)');
title('Variance');

% EOF

```

Figure 5.9 can be compared with Figure 5.4 of Example 5.2.

5.8.4 Example 5.4

In the following example, the covariance matrix is calculated using time domain responses of simulations. Results are plotted in Figures 5.10 to 5.12. The examples are given for an

undamped frequency of 1 rad/s, damping ratio of 0.7, white noise intensity of 1, sample time of 0.01 seconds and a final time of 5 seconds. The number of replications is stated in the caption of the figures.

In the following MATLAB program we try to calculate the variance of the motion variables by doing more than one simulation; for the average we do not use a time average for the estimate of $\mu_{\bar{x}}$ but an ensemble average. We calculate the time response of the system (5.63) for several (N is now the number of experiments) white noise inputs, using these responses for the calculation of the ensemble variable x and ensemble average $\mu_{\bar{x}}$. The variances are calculated by the estimate, using the ensemble variable x and ensemble average $\mu_{\bar{x}}$,

$$C_{\bar{x}\bar{x}} = \frac{1}{N-1} \sum_{i=1}^N (x[i] - \mu_{\bar{x}}) (x[i] - \mu_{\bar{x}})^T \quad (5.66)$$

Listing 5.4: Example 5.4

```
% Example54 Calculates covariance matrix of a second order mass-spring-damper
% system perturbed by white noise, using the Monte Carlo
% method (ensemble average = average over all realizations)
%
% Chapter 5 of lecture notes ae4-304
%
% Program revised August 1992, February 2004 [MM], November 2014 [M
% Rodriguez]
%%
clc; close all; clear all;

disp(' Example 5.4');
disp(' Calculation of the Covariance matrix of a second order');
disp(' mass-spring-damper system perturbed by white noise using');
disp(' Monte Carlo Method.');
disp(' The covariance matrix C is calculated with:');
disp(' ');
disp('      1   N          T');
disp('      C = --- SUM (x(i)-m )(x(i)-m )');
disp('      xx   N-1 i=1      x       x');
disp(' ');
disp(' This program can produce Figures 5.10-5.12 in the lecture');
disp(' notes: Aircraft Responses to Atmospheric Turbulence.');
disp(' ');
disp(' 2nd order dynamic model Definition:');
disp(' ');

% DEFINE CT SYSTEM DYNAMICS
w0 = input(' Give undamped natural frequency [rad/s] : ');
zeta = input(' Give damping ratio : '');
```

```

m = 1;                                % mass
k = w0^2;                             % spring constant
c = zeta*2*m*w0;                      % damping coefficient

A=[0 1;-k/m -c/m];
B=[0 1/m]';

% SET TIME AXIS
dt = input(' Give sampling time interval dt      : ');
T = input(' Give total time interval T      : ');
t=[0:dt:T-dt];
N=T/dt;

% COMPUTE DT EQUIVALENT
[Phi,Gamma]=c2d(A,B,dt);

% DEFINE CT WHITE NOISE CHARACTERISTICS
Wc = input(' Give CT white noise intensity      : ');

Wd = Wc/dt;    % NOTE: divide by sample time dt, this was not done
                % correctly in the lecture notes ae4-404, May 1998
                % and earlier!! (Figures 5.8, 5.9
                % and 5.10 are now correct)

% DEFINE # of EXPERIMENTS (MONTE CARLO METHOD)
NN = input(' Give number of experiments      : ');

w = sqrt(Wd).*randn(N,NN);    % generate realizations of the random noise

% Initialize variables
x1 = zeros(N,NN);
x2 = zeros(N,NN);
x = [x1(1,:);x2(1,:)];
w1 = zeros(2,1);
xx = zeros(2,1);

for j = 1:NN;
    for l = 1:2;
        xx(l,1) = x(l,j);
    end

    for i = 1:N-1;
        for k = 1:2;
            w1(k,1) = Gamma(k,1)*w(i,j);          % response to noise
        end

        xx = Phi*xx + w1;
        x1(i+1,j) = xx(1,1);
        x2(i+1,j) = xx(2,1);
    end
end

```

```

mean1 = zeros(N,1);
mean2 = zeros(N,1);

for i=1:N;
    for j=1:NN;
        mean1(i,1) = mean1(i,1) + x1(i,j);
        mean2(i,1) = mean2(i,1) + x2(i,j);
    end
end

mean1 = (1/NN).*mean1;
mean2 = (1/NN).*mean2;

Cx1x1 = zeros(N,1);
Cx1x2 = zeros(N,1);
Cx2x2 = zeros(N,1);

for i = 1:N;
    for j = 1:NN;
        Cx1x1(i,1) = Cx1x1(i,1)+(x1(i,j)-mean1(i,1))*(x1(i,j)-mean1(i,1));
        Cx1x2(i,1) = Cx1x2(i,1)+(x1(i,j)-mean1(i,1))*(x2(i,j)-mean2(i,1));
        Cx2x2(i,1) = Cx2x2(i,1)+(x2(i,j)-mean2(i,1))*(x2(i,j)-mean2(i,1));
    end
end

Cx1x1(i,1) = Cx1x1(i,1)/(NN-1);
Cx1x2(i,1) = Cx1x2(i,1)/(NN-1);
Cx2x2(i,1) = Cx2x2(i,1)/(NN-1);
end

% PLOT RESULTS
figure
subplot(2,1,1);
plot(t,mean1); xlabel('time (s)'); ylabel('mean1(t)');
subplot(2,1,2);
plot(t,mean2); xlabel('time (s)'); ylabel('mean2(t)');
pause

% ANALYTICAL CALCULATIONS
Cy1y1(1) = Cx1x1(1,1); Cy1y2(1) = Cx1x2(1,1); Cy2y2(1) = Cx2x2(1,1);
Cyy = [0 0; 0 0];
for i=1:N-1;
    Cyy = Phi*Cyy*Phi' + Gamma*Wd*Gamma';
    Cy1y1(i+1) = Cyy(1,1);
    Cy1y2(i+1) = Cyy(1,2);
    Cy2y2(i+1) = Cyy(2,2);
end

% SHOW ANALYTICAL CALCULATIONS AND "MONTE-CARLO" DATA
figure
subplot(2,2,1);
plot(t,Cx1x1,'--',t,Cy1y1); xlabel('time (s)'); ylabel('Cx1x1(t)');

```

```

subplot(2,2,2);
plot(t,Cx1x2,'--',t,Cy1y2); xlabel('time (s)'); ylabel('Cx1x2(t)');
subplot(2,2,4);
plot(t,Cx2x2,'--',t,Cy2y2); xlabel('time (s)'); ylabel('Cx2x2(t)');
% EOF

```

We can conclude that this procedure may be used for estimating the variance of a stochastic variable, especially for the number of samples $N \rightarrow \infty$. However, the procedure is very time consuming.

5.8.5 Problem 5.1

For the second order system of Example 5.2, find a damping ratio ζ such that the displacement of the system falls with a 99.7% probability in the range [-0.5 0.5] (m).

5.8.6 Problem 5.2

In the Examples 5.2 and 5.3 the influence of the damping ratio on the covariance matrix of a second order system was investigated. Adapting the MATLAB programs, make plots similar to the Figures 5.4 to 5.8 with different sample rates and total time. What happens if the sample frequency approaches the undamped natural frequency of the system under consideration?

5.9 Summary

In this chapter we presented the general theory for multivariable stochastic processes. The probability distribution - and density function have been introduced as well as the definitions of the mean value and covariance functions for multivariable processes. Several ways for calculating the time-dependent and steady state covariance matrix functions have been introduced: solutions for continuous time, such as the solution of the Lyapunov equation and the impulse response method, and solutions for discrete time, such as the calculation of the covariance matrix function by a derived recursive equation, have been discussed.

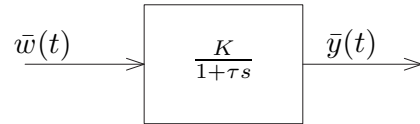


Figure 5.1: A first order continuous LTI system driven by a white noise input signal.

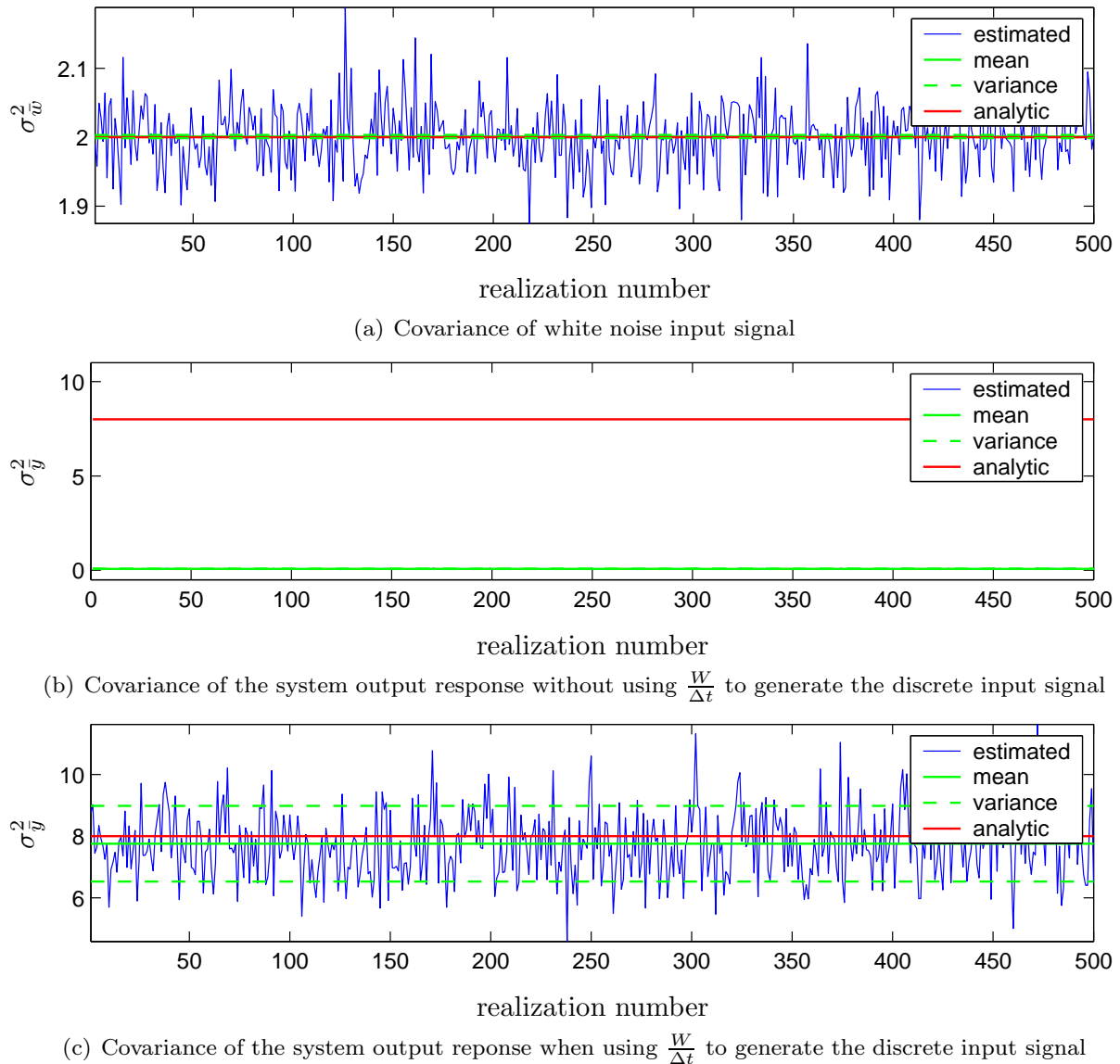


Figure 5.2: Covariance of discrete white noise input signals and output signals of a continuous system simulated with MATLAB's `lsim` function, driven by the discrete input signals.

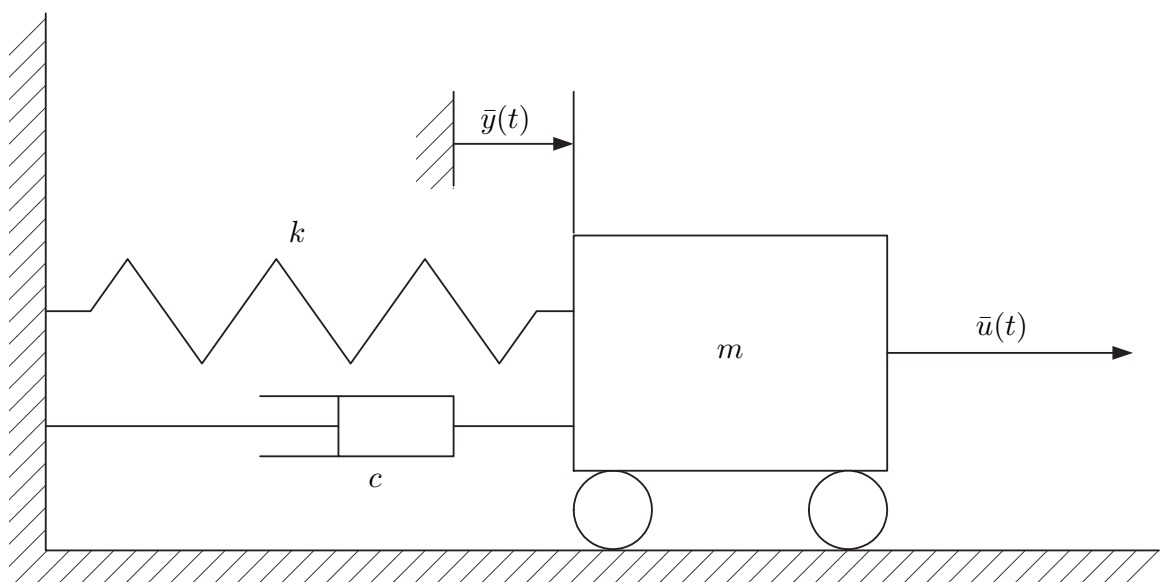


Figure 5.3: 1 DOF mass-spring-damper system.

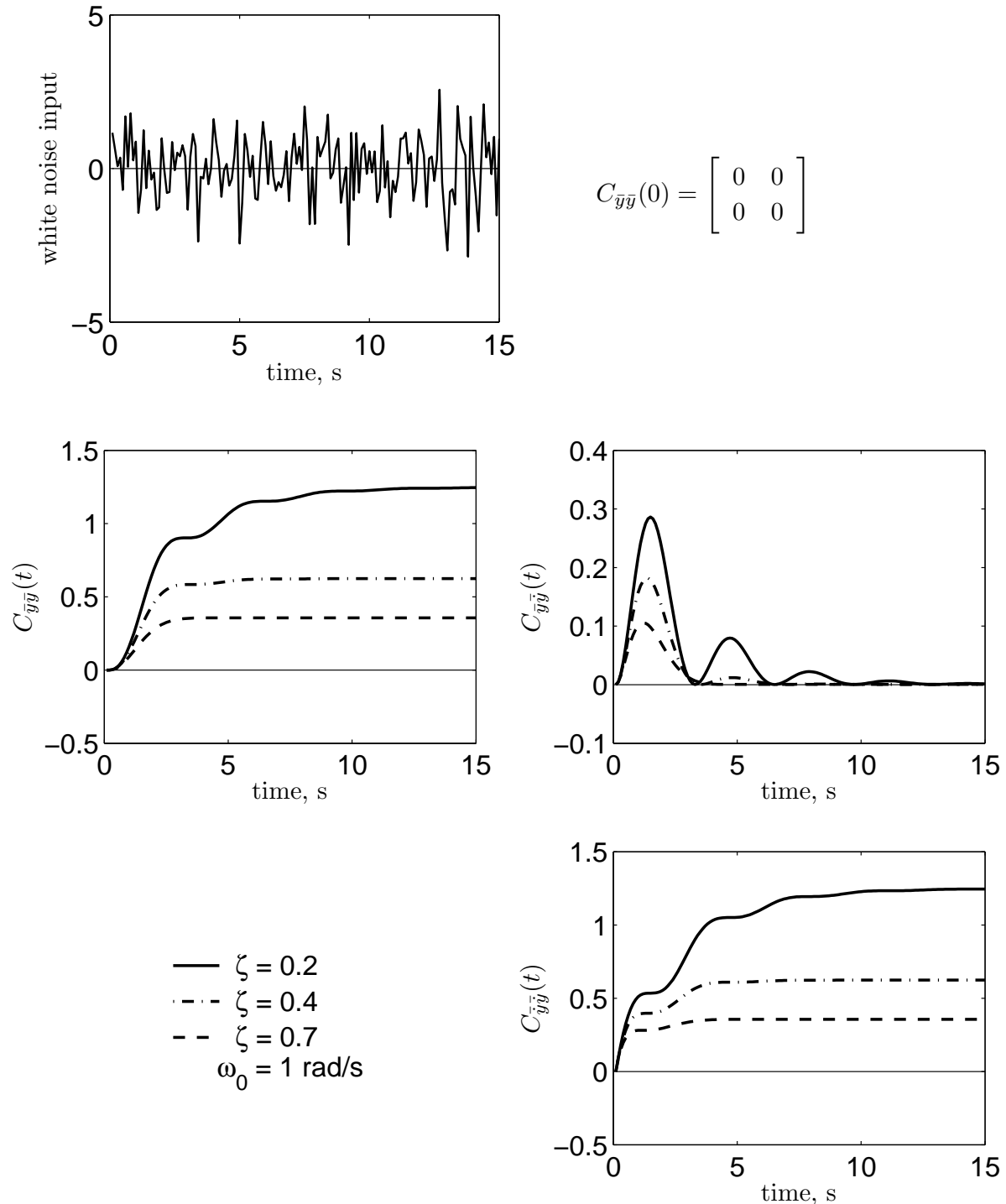


Figure 5.4: Responses of the elements of the covariance matrix to a white noise input signal. Second order system, initial conditions zero.

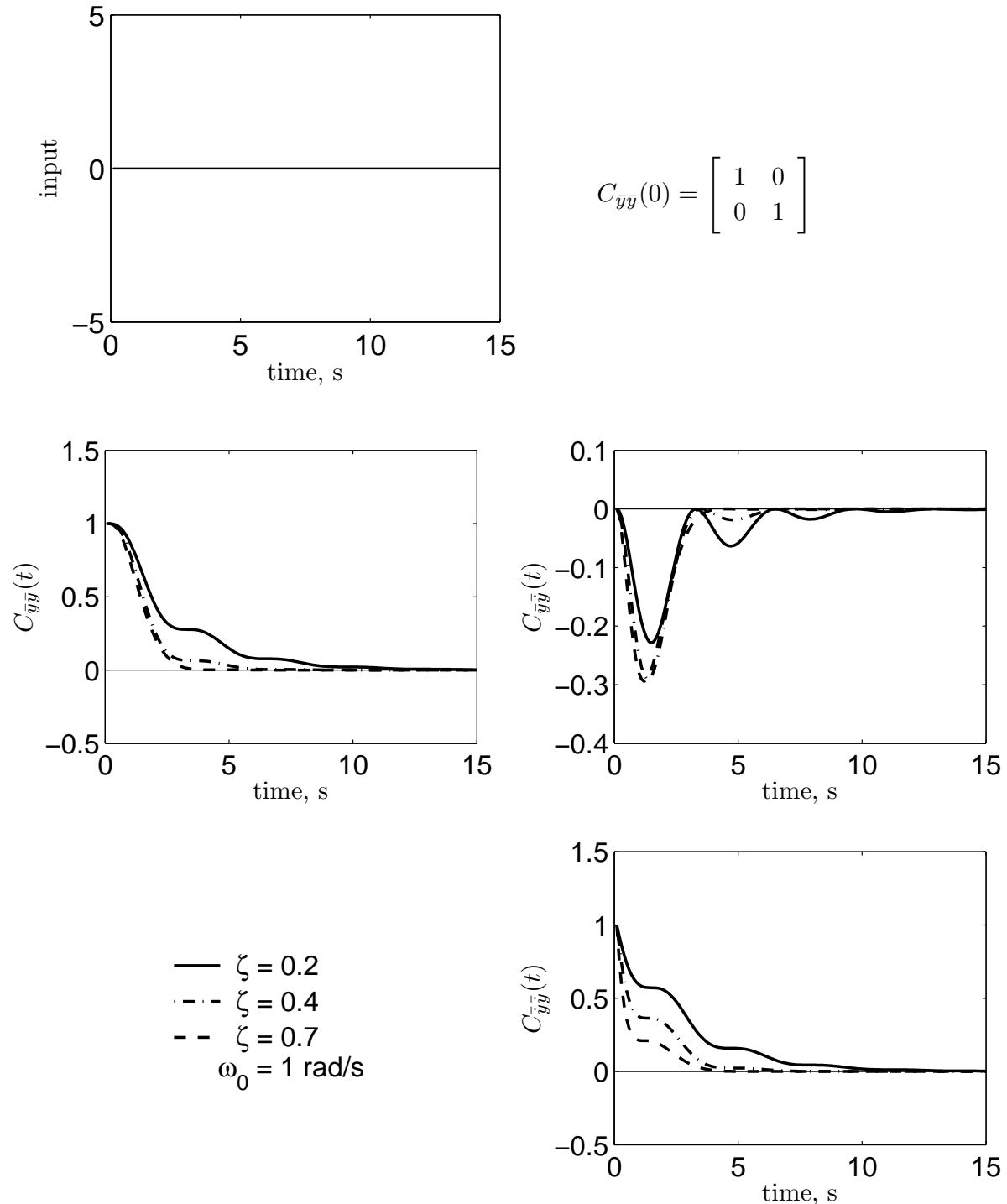


Figure 5.5: Responses of the elements of the covariance matrix to initial conditions. Second order system, no noise input signal.

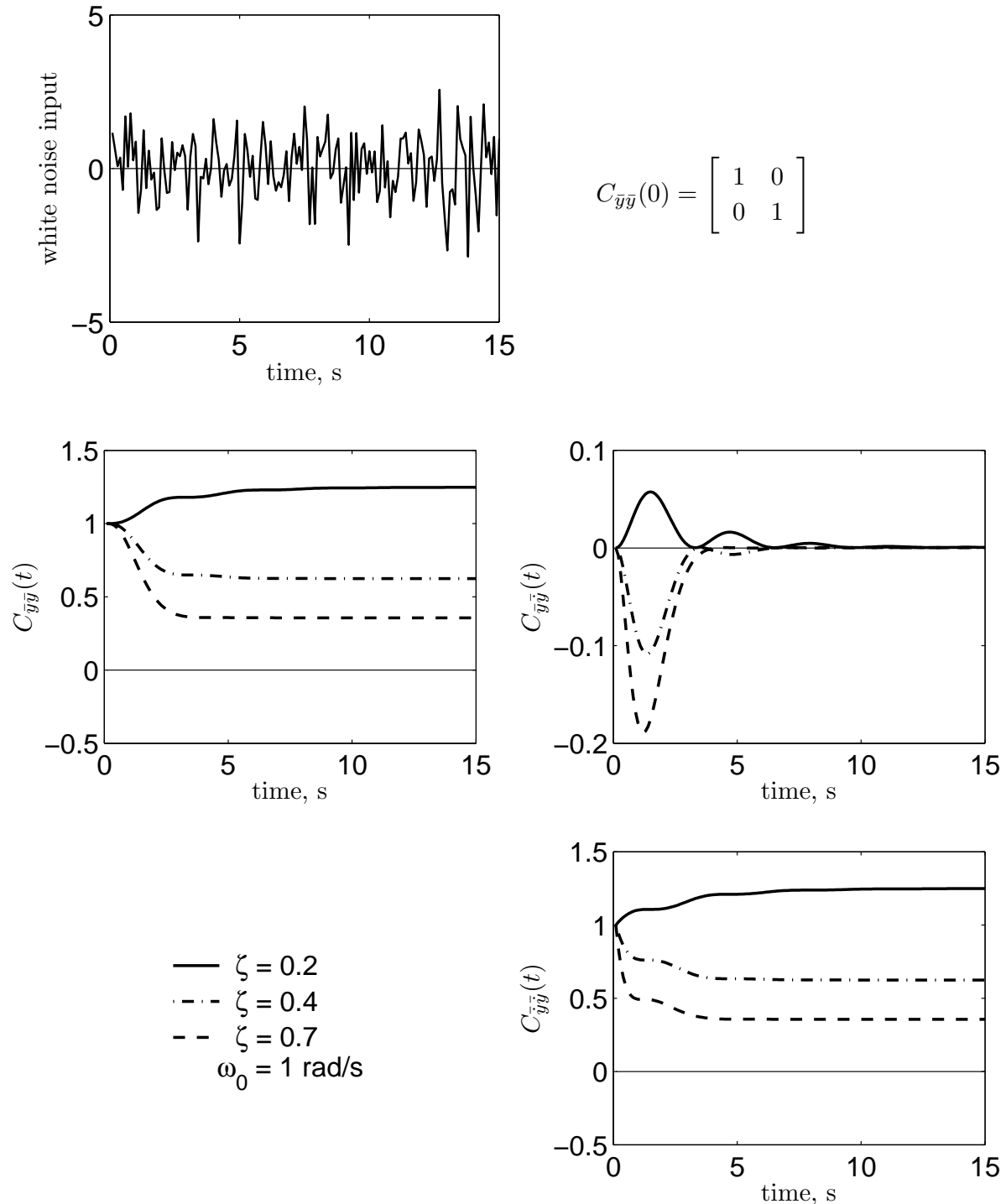


Figure 5.6: Responses of the elements of the covariance matrix to white noise input and initial conditions. Second order system.

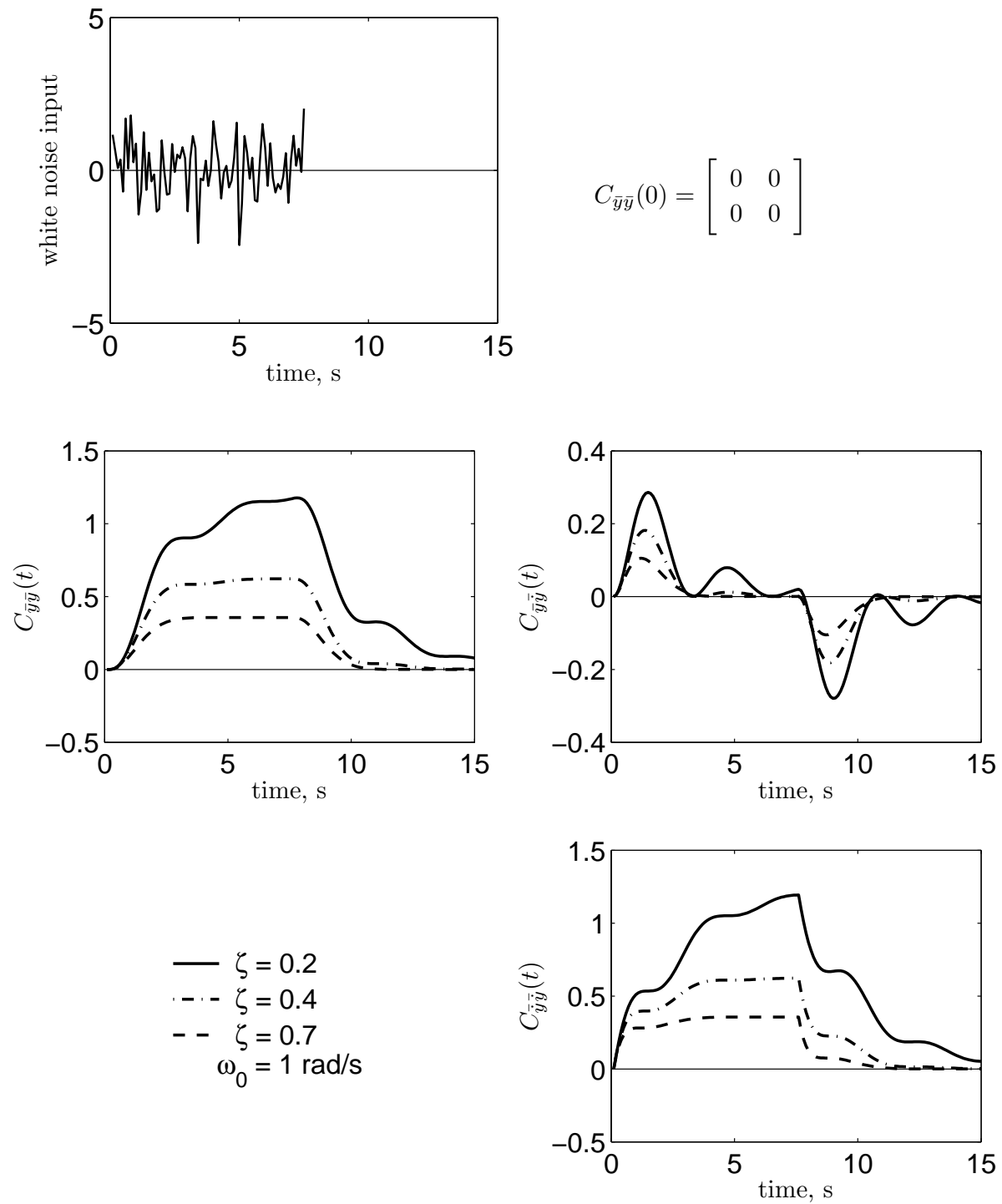


Figure 5.7: Response to a white noise input signal of limited duration.

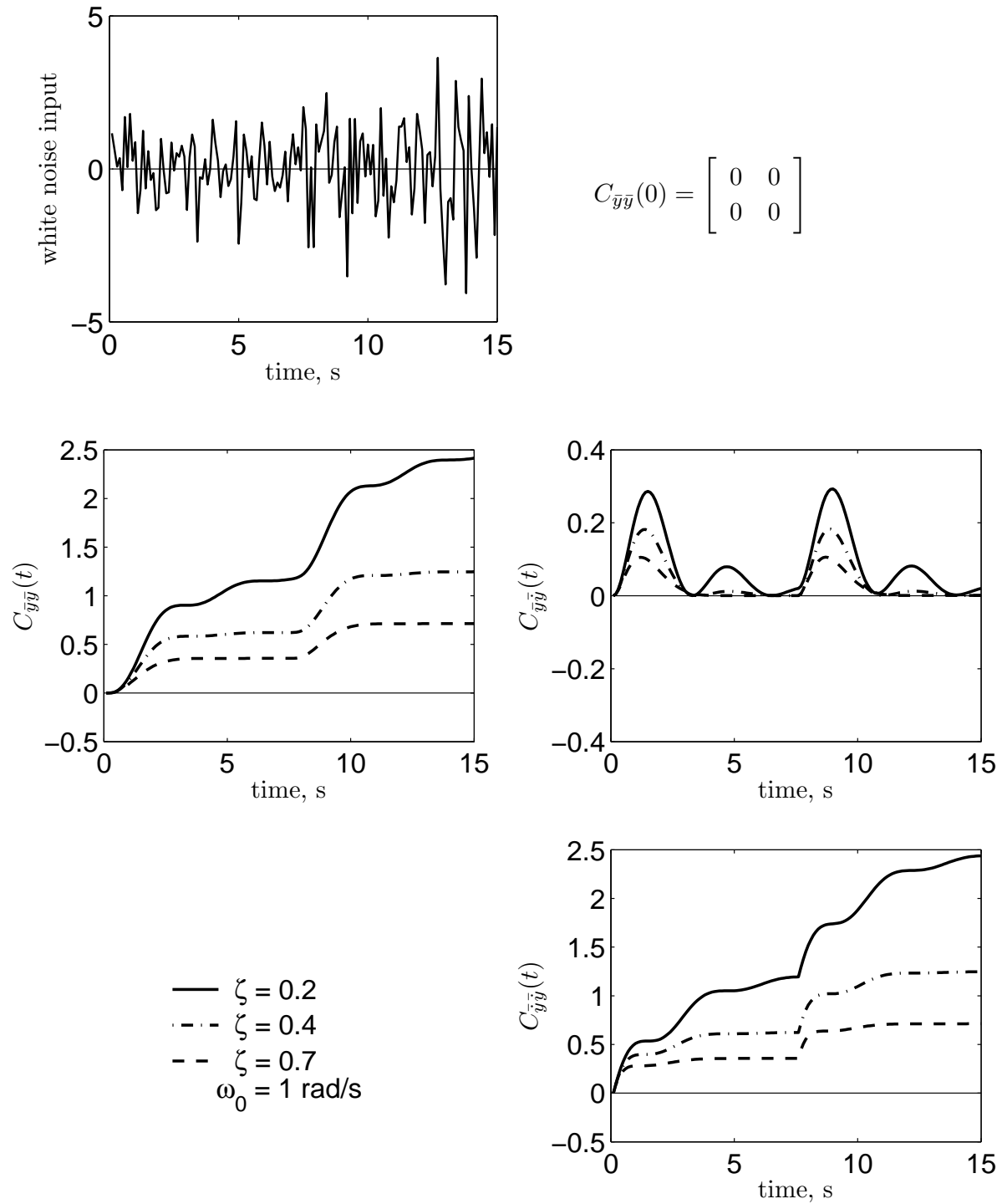


Figure 5.8: The effect of a stepwise change in white noise input intensity.

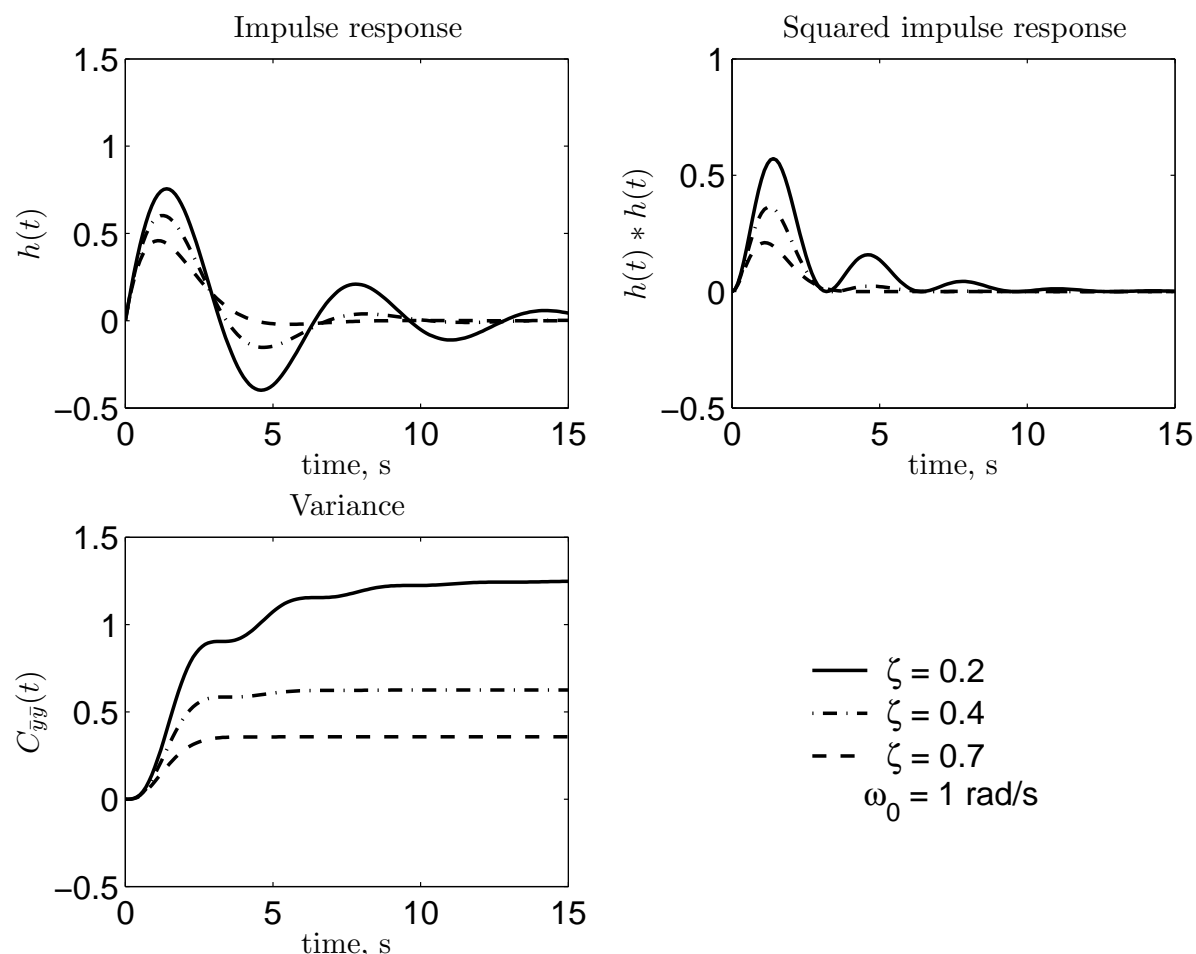


Figure 5.9: The response of the variance of the displacement to a white noise input signal calculated using the impulse response method. Second order system.

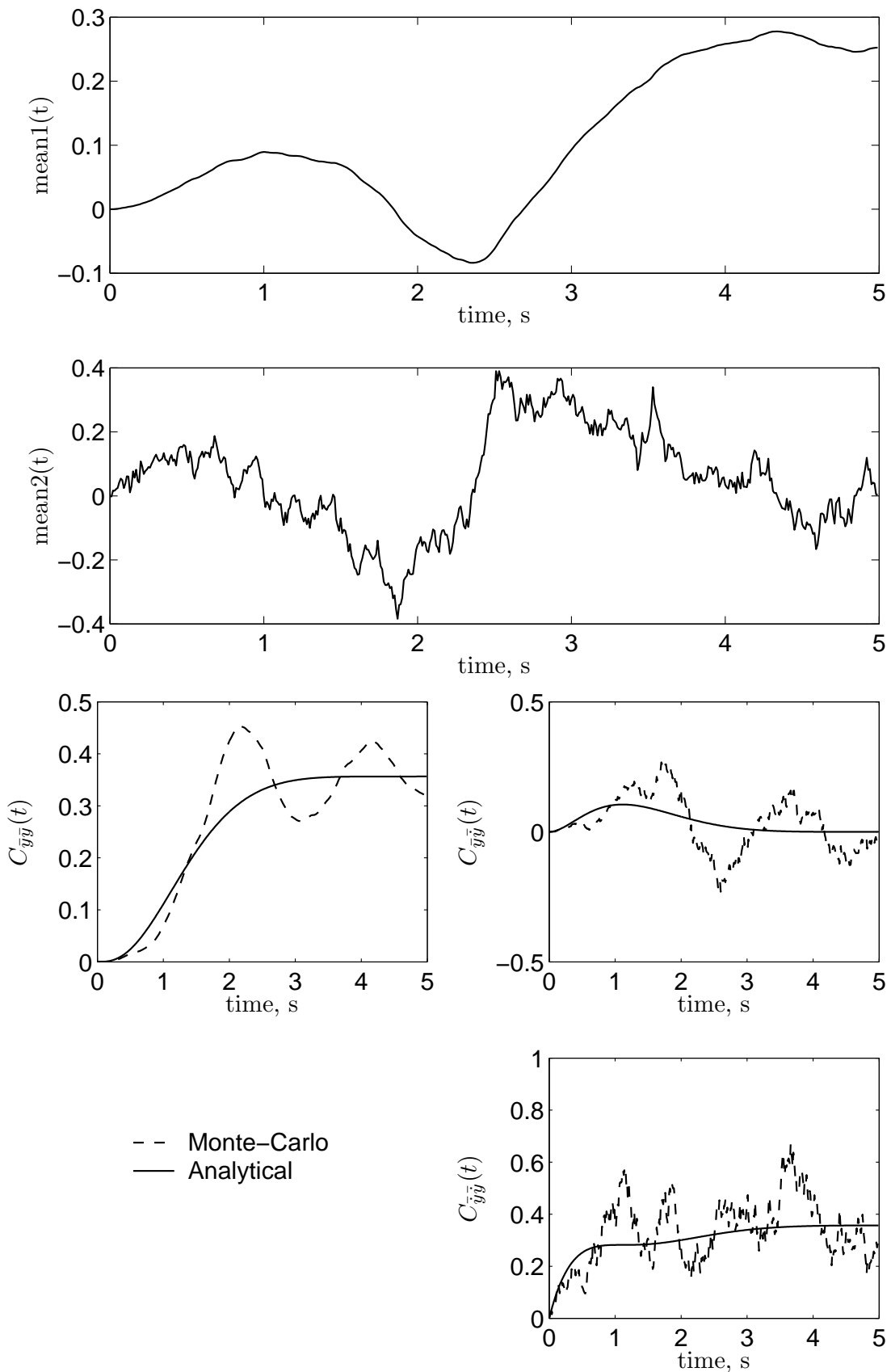


Figure 5.10: The response of the ensemble variable $x(t)$ and variances of the second order system to a white noise input signal calculated using time responses. The number of replications is 15.

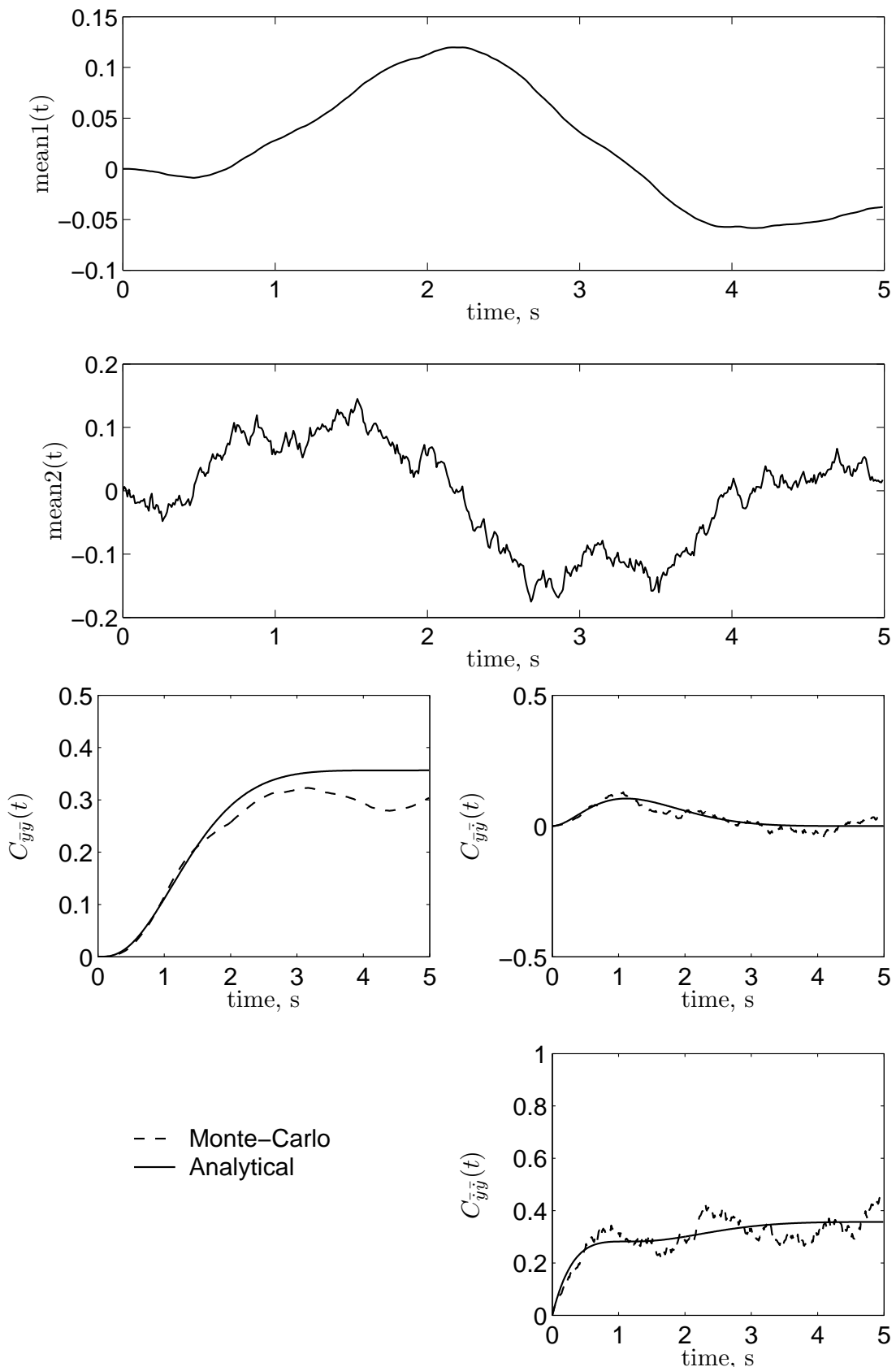


Figure 5.11: The response of the ensemble variable $x(t)$ and variances of the second order system to a white noise input signal calculated using time responses. The number of replications is 150.

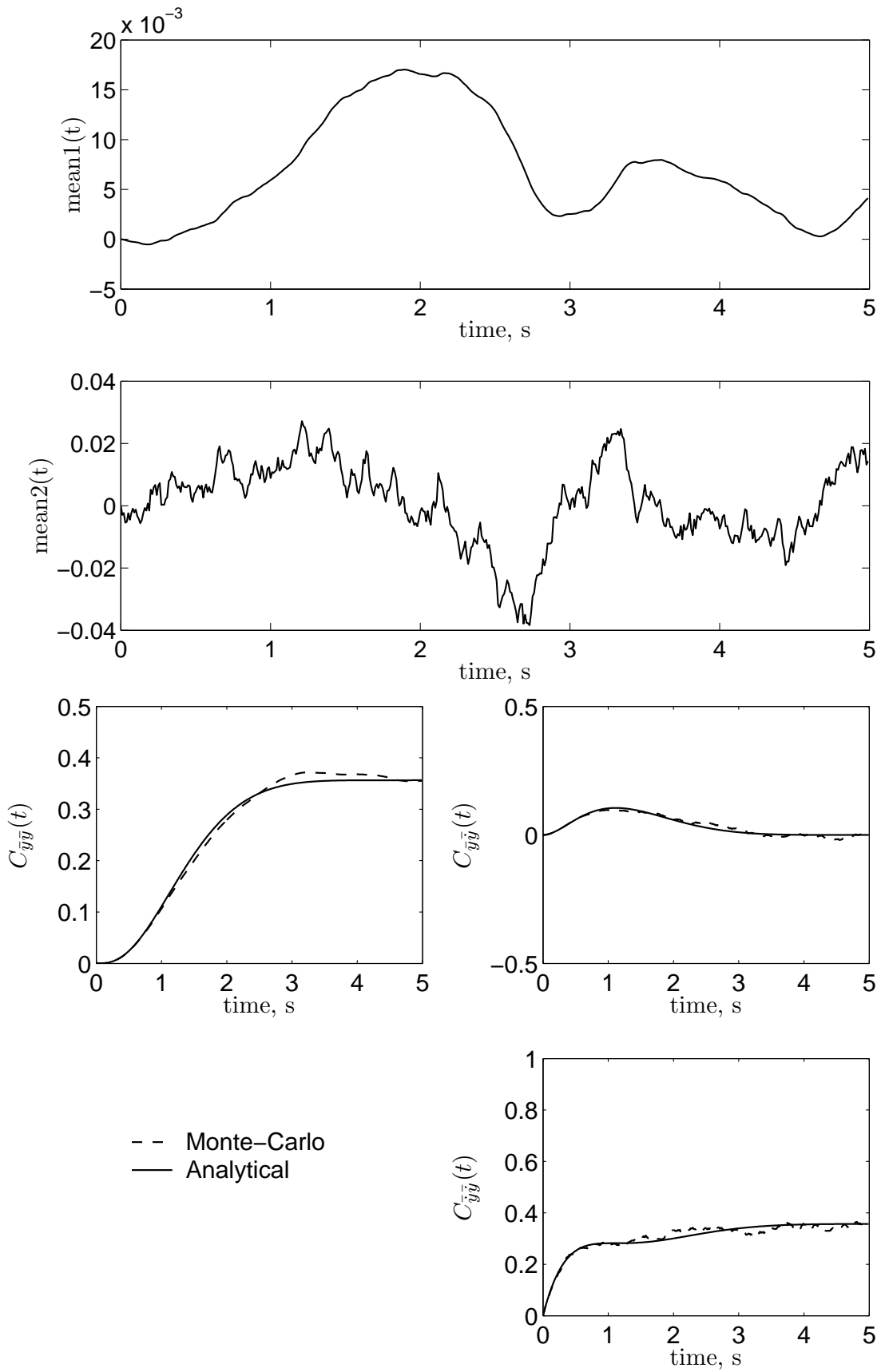


Figure 5.12: The response of the ensemble variable $x(t)$ and variances of the second order system to a white noise input signal calculated using time responses. The number of replications is 1500.

Chapter 6

Description of Atmospheric Turbulence

6.1 Introduction

After a few introductory chapters on the general theory of stochastic processes, we will now proceed with the analysis of aircraft behaviour in turbulent air. We are thus concerned with an input-output system where the input consists of atmospheric turbulence which acts on the aircraft yielding the output, the aircraft responses. Figure 6.1 illustrates this system.

In the analysis of the motions of an aircraft flying in turbulent air, the turbulence velocity vector is normally decomposed in three perpendicular components in the stability reference frame, a vertical gust velocity \bar{w}_g positive upwards, a side gust velocity \bar{v}_g positive to the left and a longitudinal component \bar{u}_g positive backwards.

The components of turbulence that are of prime interest are the components that are normal to the flight path, i.e. the vertical and side gust components \bar{w}_g and \bar{v}_g . The component \bar{w}_g gives rise both to large normal aerodynamic forces, which accelerate the aircraft vertically, and induce pitching moments. The \bar{v}_g or side component of turbulence gives rise mainly to aerodynamic forces on the vertical tail and fuselage, which in turn result in yawing and rolling motions. These motions can on occasion become so violent that its effect can produce fatigue on both the pilot and structure, give an uncomfortable ride for the passengers, and may interfere with the precise control of the aircraft.

The longitudinal component of turbulence \bar{u}_g is usually less significant although under some conditions, such as low-speed flights in ground proximity, it may require special attention.

The airplane responses that are of interest include both linear and angular velocities and accelerations. In order to understand and analyse these responses we dissect the total phenomenon into two separate parts, see Figure 6.1. The first is the description of

atmospheric turbulence itself, i.e. the velocity field in which the aircraft is immersed. Next it is necessary to determine how these velocity fields induce aerodynamic force and moment variations, which in turn drive the aircraft's equations of motion. The first topic of how to model atmospheric turbulence will be presented in this chapter. The development of the mathematical models for aircraft dynamics in atmospheric turbulence, will be the aim of Chapter 7 for the symmetric aircraft motions, and Chapter 8 for the asymmetric aircraft motions.

6.2 Meteorological aspects of atmospheric turbulence

This section provides a somewhat fundamental introduction to atmospheric turbulence. Since atmospheric turbulence is essentially a meteorological phenomenon, a few meteorological aspects will be introduced.

6.2.1 Vertical stability

A decisive factor in the occurrence of turbulence is the geometric temperature lapse rate $\lambda = \frac{dT}{dh}$. In order to illustrate the importance of this parameter, first consider a parcel of air undergoing an adiabatic ascent. The rate at which the temperature decreases during an adiabatic ascent, for dry air, is $\beta_{dry} = -0.0098 \text{ } ^\circ/\text{m}$ and slightly less for unsaturated air, see (Iribarne & Cho, 1980) or (Ruygrok, 1970). For saturated air under ascent, this rate varies with temperature and pressure but is always less than β_{dry} and β can be as low as $0.0030 \text{ } ^\circ/\text{m}$, see (Ruygrok, 1970).

Next, regard a parcel of air at height h in an atmospheric condition where at the time the geometric lapse rate λ , the actual vertical temperature stratification, is larger than the process lapse rate β , the change in temperature with height when a parcel rises or descends, so $|\lambda| > |\beta|$. If we submit this parcel of air to a virtual infinitesimal vertical displacement Δh we will have the situation of Figure 6.2. Virtually, the parcel of air at $h + \Delta h$ will have a temperature $T = T_0 + \lambda \Delta h$. Following an adiabatic ascent, however, the parcel of air when rising from h to $h + \Delta h$ will obtain a temperature $T' = T_0 + \beta \Delta h > T_0 + \lambda \Delta h$. Because the pressure at $h + \Delta h$ will be equal for parcel and environment, the density ρ' will be smaller than the density ρ of the environment and the parcel will experience a positive buoyancy, i.e. an upward force. Because the parcel will tend to continue to rise after the virtual displacement this is clearly an unstable situation.

If $|\lambda| < |\beta|$ an inverse argument holds. Then the buoyancy is negative so the virtually displaced parcel will tend to return to the original level h . This is a stable situation.

The conditions for vertical stability are summarized in Figure 6.3. If the geometric lapse rate λ lies to the right of β_{sat} the atmosphere is absolutely stable, if it lies left of β_{dry} it is absolutely unstable. If λ lies between β_{dry} and β_{sat} it is said to be conditionally stable, meaning that it is stable if the air is not saturated but unstable if the air is saturated.

In the ICAO Standard Atmosphere, for altitudes up to 11 km, the temperature lapse rate

is:

$$\lambda_{ICAO} = -0.0065^\circ/m, \quad (6.1)$$

with,

$$T(h) = T(0) + \lambda h.$$

Heat convection is believed to be the driving force in the occurrence of atmospheric turbulence. Over land, near the ground, the air is usually unstable during sunny days and stable during clear nights. On windy, cloudy days, the air is essentially neutral. Over water, the stability near the water depends on the water temperature and the temperature of the surface on which the air was previously located. At larger altitudes, the geometric temperature gradient λ usually is adiabatic.

6.2.2 Windshear

Windshear is another important factor in the occurrence of atmospheric turbulence. Horizontal windshear is the magnitude of the rate of change of the windvector in the horizontal plane ($\partial V_w / \partial x$, $\partial V_w / \partial y$), while vertical wind-shear ($\partial V / \partial h$) indicates the rate of change in the vertical direction. Figure 6.4 illustrates the difference.

The larger the windshear, the more turbulence is created due to ‘mechanical friction’ between layers of air.

6.3 Different kinds of turbulence

In order to qualitatively understand the conditions under which turbulence occurs in the atmosphere, the so called ‘eddy energy equation’ will now be introduced,

$$\frac{dE}{dt} = S + H + B - D \quad (6.2)$$

where,

- E = the turbulent kinetic energy
- S = a positive term related to vertical windshear
- H = a positive term related to horizontal windshear
- B = a term related to the stability of the air,
positive valued for unstable air, $dT/dh < -0.0065^\circ/m$
negative valued for stable air, $dT/dh > -0.0065^\circ/m$
- D = a term related to the rate at which turbulent energy is
dissipated into heat. It is always positive. The value
of D depends on the actual level of turbulent kinetic
energy E .

If the dissipation term D in Equation (6.2) is proportional to the energy E , it follows that the energy E itself is the low-pass filtered sum of S , H and B . Therefore, turbulent energy can be expected to be large in regions of large wind shear and in ‘unstable’ air.

We will now see how we can use Equation (6.2) in explaining the driving mechanism behind different kinds of turbulence.

6.3.1 Turbulence near the ground

Conditions near the ground have an important characteristic not necessarily found elsewhere. The wind shear term S decreases rapidly upward and is positive. The temperature gradient term B tends to be positive at day-time and negative at night with clear sky, and is nearly invariant with height. As a result, the effect of wind shear is dominant close to the ground while the effect of stability or instability increases upward.

6.3.2 Turbulence in clouds

Inside of cumulus clouds the air is saturated and is unstable so that the B term is positive. Thus turbulence is usually found in cumulus clouds, increasing with height to large intensities near the top. Typical variances of vertical turbulence velocity in ordinary cumulus clouds rate $1 \text{ m}^2/\text{sec}^2$ with much larger values in cumulonimbus clouds.

Although the term B sets up the general circulation in clouds, once such a circulation has developed the shear terms do become important. Particularly, in the boundary layer between the general updraft in a cumulonimbus cloud and the rain-producing downdrafts, turbulence intensities are likely to be severe. As a consequence, cumulus-type clouds from which rain is falling are more turbulent than those from which precipitation has stopped or has not yet started.

6.3.3 Clear-air turbulence

The term clear-air turbulence is used to describe turbulence in the free atmosphere, away from the ground and not in clouds. An example of this type of turbulence occurs in the general region of the jet stream at altitudes of 10.000 to 12.000 meters. In general, the turbulence encountered appears to be of light to moderate intensity.

Figure 6.5 (Endlich & McLean, 1957) shows the probability distribution of clear-air turbulence associated with jet streams. According to Figure 6.5, the probability of turbulence is largest on the north side of strong jets, about 150 nautical miles from the core and 1000 meters below the region of the strongest winds. In this position, particularly the shear term H in Equation (6.2) is large and turbulence due to ‘mechanical friction’ is likely. It should be noted that all regions of large probability of strong turbulence lie in the troposphere. There the temperature gradient is usually adiabatic and hence the B term in Equation (6.2) is too small to offset the wind shear terms.

6.3.4 Mountain wave turbulence

Some of the strongest turbulence occurs in connection with mountain waves. Basically, when a rapid air current crosses a mountain at the right angle, and if the mountain is steep on its lee side, the air flow will be perturbed for a long distance downstream the mountain, see Figure 6.6 (Kuettner & Jenkins, 1953).

Severe turbulence may be encountered in the ‘rotor’ cloud which is formed downstream of the mountain. The mechanism for this kind of turbulence is presumably that the steady currents are such as to set up huge vertical windshears.

6.4 Statistical aspects of atmospheric turbulence

6.4.1 Introduction

It is sometimes a bit misleading to say that turbulent flow is ‘random’ since its evolution must be governed by the general Navier-Stokes Equations (which are a set of deterministic, nonlinear, coupled partial differential equations), even if the birth of an eddy out of an instability somewhere in the flow field is just a matter of ‘chance’. There are circumstances in which a statistical treatment will not be sufficient, for instance in studies in the atmosphere’s general motion, weather forecasting etc.

Our approach will not consider such questions. In effect, we accept a priori that the predictability of turbulent flows is limited to relatively short time intervals, no matter how well the initial conditions are known. If we are interested in time intervals beyond the limits of predictability for individual realizations, we simply have to adopt stochastic methods.

The basic flow equations, the Navier-Stokes equations, will be discussed in the next section.

6.4.2 The Navier-Stokes equations

Considering an infinitesimal particle of air and applying the conservation of mass, impulse and energy, the Navier-Stokes equations can be derived,

$$\frac{\partial}{\partial t} \begin{bmatrix} \rho \\ \rho \vec{v} \\ \rho E \end{bmatrix} + \vec{\nabla} \cdot \begin{bmatrix} \rho \vec{v} \\ \rho \vec{v} \otimes \vec{v} + p \bar{\bar{I}} - \bar{\tau} \\ \rho \vec{v} H - \bar{\tau} \cdot \vec{v} - k \vec{\nabla} T \end{bmatrix} = \begin{bmatrix} 0 \\ \rho \vec{f}_e \\ W_f + q_H \end{bmatrix} \quad (6.3)$$

with,

ρ	: air density
\vec{v}	$(u \ v \ w)^T$
u	velocity 'in X -direction'
v	velocity 'in Y -direction'
w	velocity 'in Z -direction'
p	pressure
E	total internal energy $E = e + \frac{\vec{v}^2}{2} = C_V T + \frac{1}{2}(u^2 + v^2 + w^2) = \frac{1}{\gamma-1} \frac{p}{\rho} + (u^2 + v^2 + w^2)$
H	total enthalpy $H = E + \frac{p}{\rho} = h + \frac{\vec{v}^2}{2} = C_p T + \frac{1}{2}(u^2 + v^2 + w^2) = \frac{\gamma}{\gamma-1} \frac{p}{\rho} + (u^2 + v^2 + w^2)$
T	temperature
\vec{f}_e	volume (e.g. gravity) forces
W_f	work of external volume forces $\rho \vec{f}_e \cdot \vec{v}$
k	thermal conductivity coefficient
q_H	heat sources other than conduction (i.e. radiation, chemical reactions)
γ	$\frac{C_p}{C_V}$
C_P	$\frac{\gamma}{\gamma-1} R$
R	$\frac{p}{\rho T}$
$\bar{\tau}$	shear tensor
\bar{I}	unity tensor
\otimes	tensor product
$\vec{\nabla}$	$\left(\frac{\partial}{\partial x} \ \frac{\partial}{\partial y} \ \frac{\partial}{\partial z} \right)^T$

Another representation of Equation (6.3) is,

$$\frac{\partial U}{\partial t} + \frac{\partial F}{\partial x} + \frac{\partial G}{\partial y} + \frac{\partial H}{\partial z} = Q \quad (6.4)$$

with,

$$U = \begin{bmatrix} \rho \\ \rho u \\ \rho v \\ \rho w \\ \rho E \end{bmatrix} \quad (6.5)$$

$$F = \begin{bmatrix} \rho u \\ \rho u^2 + p - \tau_{xx} \\ \rho uv - \tau_{xy} \\ \rho uw - \tau_{xz} \\ \rho uH - (\bar{\tau} \cdot \vec{v})_x - k \frac{\partial T}{\partial x} \end{bmatrix} \quad (6.6)$$

$$G = \begin{bmatrix} \rho v \\ \rho vu - \tau_{yx} \\ \rho v^2 + p - \tau_{yy} \\ \rho vw - \tau_{yz} \\ \rho vH - (\bar{\tau} \cdot \vec{v})_y - k \frac{\partial T}{\partial y} \end{bmatrix} \quad (6.7)$$

$$H = \begin{bmatrix} \rho w \\ \rho wu - \tau_{zx} \\ \rho wv - \tau_{zy} \\ \rho w^2 + p - \tau_{zz} \\ \rho wH - (\bar{\tau} \cdot \vec{v})_z - k \frac{\partial T}{\partial z} \end{bmatrix} \quad (6.8)$$

$$Q = \begin{bmatrix} 0 \\ \rho \vec{f}_e \\ W_f + q_H \end{bmatrix} \quad (6.9)$$

In the above equations the $()_i$ terms represent the i -th component of the term between parentheses.

The Navier-Stokes equations describe the fluid flow of a viscous, compressible flow around a body or in a volume. The Navier-Stokes equations need to be supplemented by boundary conditions such as prescribed pressure -, velocity -, density - or energy distributions. Remember that the Navier-Stokes equations describe the flow around a bicyclist, but also around an airliner flying at transonic speeds. Basically, the Navier-Stokes equations hold for a wide speed range, even up to the hypersonic speeds (although the perfect gas model should then be replaced by a real gas model).

As was said, the Navier-Stokes equations ‘almost exactly’ model the fluid flow of arbitrary fluids. In fact the only assumptions in Equation (6.4) are the function relating density, temperature and pressure: the perfect gas law and the functions describing the shear terms in Equations (6.6) to (6.8). If the fluid is assumed to be Newtonian, the shear terms can be assumed to be functions of u , v , w and the spatial derivatives of u , v and w according to Stokes (1845).

The reason for mentioning the theory of fluid dynamics, is the conformity between turbulence in boundary layers and atmospheric turbulence, which both are described by the Navier-Stokes equations.

The Navier-Stokes equations are a set of coupled partial differential equations and appear to be a deterministic set of equations; there are no stochastic variables in this set of equations. Any stochastic phenomena have to be brought into the equations explicitly by,

$$\begin{aligned} u &= u' + \bar{u} &= u' + \bar{u}_g \\ v &= v' + \bar{v} &= v' + \bar{v}_g \\ w &= w' + \bar{w} &= w' + \bar{w}_g \\ \rho &= \rho' + \bar{\rho} &= \rho' + \bar{\rho}_g \\ p &= p' + \bar{p} &= p' + \bar{p}_g \\ &&etc. \end{aligned} \quad (6.10)$$

where the parameters ...' represent the mean value, while the parameters ... represent the stochastic variations.

The flow equations hold for a turbulent flow in a boundary layer near a solid boundary (e.g. a wing's boundary layer) but also describe the flow of a turbulent atmosphere. The only difference between the two flows is the scale of turbulence.

From this discussion it follows that nature is hard to describe analytically without making assumptions. The Navier-Stokes equations are solved numerically at research institutes and meteorologic centers.

6.4.3 A general statistical description

As discussed in the previous section, we can consider the total velocity field of the atmosphere to be variable in both space and time, composed of a mean value and variations from it. The mean wind is a problem primarily for navigation and guidance and is not of interest here. We could eliminate it by choosing as our reference frame some kind of 'atmosphere fixed frame of reference F_a ' relative to which the mean motion is zero. Let the velocity vector of the air at position $\underline{r} = (x_1, x_2, x_3)^T$ and time t be,

$$\bar{\underline{u}}(\underline{r}, t) = (\bar{u}_1, \bar{u}_2, \bar{u}_3)^T \quad (6.11)$$

Then $\bar{\underline{u}}(\underline{r}, t)$ is a random function of both space and time, so we have to deal with the statistics of a random vector composed of 3 elements, each depending on four variables (x_1, x_2, x_3, t) .

The definition of the statistical correlation function as introduced in earlier chapters, could in principle be applied on the speed vector $\bar{\underline{u}}$ as well. When applying these ideas some care is required. Instead of dealing with the usual time separation τ only, we now have to consider the scalar time separation τ as well as the 3 dimensional separation distance vector $\xi = (\xi_1, \xi_2, \xi_3)^T$. Such processes are sometimes denoted as 'multivariable multidimensional processes'. Here the term 'multivariable' is used to indicate that more than one variable is involved in the process (c.f. $\bar{\underline{u}} = (\bar{u}_1, \bar{u}_2, \bar{u}_3)^T$) while the term 'multidimensional' indicates that each element of the process vector depends on more than one dimension (c.f. $\bar{u}_g = f(x_1, x_2, x_3, t)$). The covariance matrix of atmospheric turbulence is now formally introduced as,

$$C_{\bar{\underline{u}}\bar{\underline{u}}}(\underline{r}, t; \underline{r} + \xi, t + \tau) = E \{ \bar{\underline{u}}(\underline{r}, t) \cdot \bar{\underline{u}}(\underline{r} + \xi, t + \tau) \} = \quad (6.12)$$

$$= \begin{bmatrix} E \{ \bar{u}_1(\underline{r}, t) \cdot \bar{u}_1(\underline{r} + \xi, t + \tau) \} & E \{ \bar{u}_1(\underline{r}, t) \cdot \bar{u}_2(\underline{r} + \xi, t + \tau) \} & E \{ \bar{u}_1(\underline{r}, t) \cdot \bar{u}_3(\underline{r} + \xi, t + \tau) \} \\ E \{ \bar{u}_2(\underline{r}, t) \cdot \bar{u}_1(\underline{r} + \xi, t + \tau) \} & E \{ \bar{u}_2(\underline{r}, t) \cdot \bar{u}_2(\underline{r} + \xi, t + \tau) \} & E \{ \bar{u}_2(\underline{r}, t) \cdot \bar{u}_3(\underline{r} + \xi, t + \tau) \} \\ E \{ \bar{u}_3(\underline{r}, t) \cdot \bar{u}_1(\underline{r} + \xi, t + \tau) \} & E \{ \bar{u}_3(\underline{r}, t) \cdot \bar{u}_2(\underline{r} + \xi, t + \tau) \} & E \{ \bar{u}_3(\underline{r}, t) \cdot \bar{u}_3(\underline{r} + \xi, t + \tau) \} \end{bmatrix}$$

Fourier transformation (c.f. Equation (3.16)) of each element of the 3x3 covariance matrix $C_{\bar{\underline{u}}\bar{\underline{u}}}(\underline{r}, t; \underline{r} + \xi, t + \tau)$ yields the spectral densities which can be grouped together in a 3x3

matrix $S_{\bar{u}\bar{u}}(\underline{r}, t; \underline{\Omega}, \omega)$,

$$S_{\bar{u}\bar{u}}(\underline{r}, t; \underline{\Omega}, \omega) = \int_{-\infty}^{+\infty} \int_{-\infty}^{+\infty} \int_{-\infty}^{+\infty} \int_{-\infty}^{+\infty} C_{\bar{u}\bar{u}}(\underline{r}, t; \underline{r} + \underline{\xi}, t + \tau) e^{-j(\underline{\Omega} \cdot \underline{\xi} + \omega \tau)} d\xi_1 d\xi_2 d\xi_3 d\tau \quad (6.13)$$

In Equation (6.13), four integrals appear due to the four variables $(\xi_1, \xi_2, \xi_3, \tau)$ we have to deal with. The spatial frequency vector $\underline{\Omega} = (\Omega_1, \Omega_2, \Omega_3)^T$, with $\Omega = \frac{2\pi}{\lambda}$ where λ is the wave length, naturally arises in the Fourier transformation as the dual of the circular frequency ω . Notice that the general expression for the spectral densities may differ from point to point and from time to time, and therefore it is actually a function of \underline{r} and t . A principle objective of research into atmospheric turbulence is to ascertain the statistics related to the vector $\bar{u}(\bar{r}, t)$ in the form of correlation and spectral density matrices. It will be obvious that this problem is far too complicated to be handled in general. Therefore, we will now consider a number of simplifying assumptions each of which helps to reduce the complexity of the general problem.

1. Atmospheric turbulence is a random process with Gaussian distribution

Although there is some evidence that atmospheric turbulence is not necessarily normal, or Gaussian, many researchers have concluded that this assumption indeed holds true in many practical situations. There are great gains in simplicity with this assumption since only the information of the covariance matrix, Equation (6.12), now suffices for a total statistical description of atmospheric turbulence.

2. Atmospheric turbulence is a stationary process

The most general case allows the turbulence statistics to vary from point to point and time to time (c.f. Equation (6.12)). A fact of great practical importance is, however, that the speed of an ‘air particle’ in the atmosphere is constrained to relatively slow fluctuations with time. Now suppose that an aircraft flies through turbulent atmosphere. It will then encounter the fluctuating components \bar{u}_1, \bar{u}_2 and \bar{u}_3 of the turbulence velocity. Aircraft usually fly at speeds large compared to the turbulence velocities. Thus a relatively large patch of turbulence can be traversed in a time so short that the turbulence velocities have not had time to change very much. This amounts to neglecting t in the argument of $\bar{u}(\underline{r}, t)$, Equation (6.12), i.e. treating the turbulence as a ‘frozen’ pattern in the atmosphere. This theory was first postulated by G.I. Taylor in 1938 and has become known as ‘Taylor’s hypothesis’. As a consequence, the general expression for the correlation- and spectral density matrices simplify to $C_{\bar{u}\bar{u}}(\underline{r}; \underline{r} + \underline{\xi})$ and $S_{\bar{u}\bar{u}}(\underline{r}; \underline{\Omega})$.

3. Atmospheric turbulence is homogeneous along the flight path

At high altitudes, turbulence appears to occur in large patches, each of which can reasonably be taken to be homogeneous but with differences from patch to patch. At low altitudes, near the ground there are fairly rapid changes in the turbulence with altitude (induced by vertical windshear). However, for aircraft in nearly horizontal flight, homogeneity along the flight path is a reasonable approximation. As a consequence of this assumption, the dependency of covariance- and spectral density matrices on \underline{r} vanishes. Thus we can now write $C_{\bar{u}\bar{u}}(\xi)$ and $S_{\bar{u}\bar{u}}(\Omega)$. Notice that when the turbulence is stationary and homogeneous it is also ergodic, so time averages may replace ensemble averages. A matter of no small importance in practical applications!

4. Atmospheric turbulence is an isotropic process

In general the statistical functions describing atmospheric turbulence depend on the directions of the axes of F_A . This is especially so in the earth's boundary layer. When this dependency is absent, and there is evidence that this is the case at high altitudes, the turbulence is isotropic, i.e. all statistical properties are independent of the orientation of the axes. In this case it follows that the three mean-square velocity components are equal,

$$\sigma_{\bar{u}_1}^2 = \sigma_{\bar{u}_2}^2 = \sigma_{\bar{u}_3}^2 = \sigma^2 \quad (6.14)$$

A typical value for σ^2 in high-altitude turbulence is $\sigma^2 = 1 \text{ m}^2/\text{sec}^2$.

So, the simplest model we can obtain is of Gaussian, frozen, homogeneous, isotropic turbulence. This is the model most commonly used for analysis of flight outside the earth's boundary layer. Unfortunately, the strong anisotropy of boundary layer turbulence makes the model less suitable for aircraft landing and take-off analysis. We will return to this problem in Section 6.7.

6.4.4 Two fundamental correlation functions

Due to the simplifications we have made, two fundamental correlation functions $f(\xi)$ and $g(\xi)$ can now be distinguished, viz. Figure 6.7. Note, ξ equals $\sqrt{\xi_1^2 + \xi_2^2 + \xi_3^2}$, or ξ equals $|\xi|$.

The correlation between the velocities parallel to a connecting line between two points is termed the 'longitudinal' correlation $f(\xi)$. The correlation between velocities normal to a line connecting the two points is termed the 'lateral' correlation $g(\xi)$. The functions $f(\xi)$ and $g(\xi)$ can be found theoretically, see (Batchelor, 1953), and have been shown to

be well-correlated with windtunnel experiments. A rough picture of the curves $f(\xi)$ and $g(\xi)$ is given in Figure 6.8. Based on these two fundamental correlation functions the complete covariance matrix of Equation (6.12) can now formally be written as (see also (Etkin, 1972)),

$$C_{ij}(\underline{\xi}) = \sigma^2 \left(\frac{f(|\underline{\xi}|) - g(|\underline{\xi}|)}{|\underline{\xi}|^2} \xi_i \xi_j + g(|\underline{\xi}|) \delta_{ij} \right) \quad (6.15)$$

where δ_{ij} is the Kronecker delta and σ^2 is given by Equation (6.14). Due to its formal notation, Equation (6.15) is not easy to comprehend. An example is given in Section 6.8.

6.4.5 The integral scale of turbulence

There is an intuitive notion for the scale of turbulence. Clearly there are significant differences of ‘size’ between the turbulence in the wing boundary layer, in the wake of the aircraft and in the atmosphere itself. These differences are quantified by a definition of the ‘integral scale of turbulence’ L_g , which is derived directly from the correlation functions $f(\xi)$ and $g(\xi)$ (with $\xi = \sqrt{\xi_1^2 + \xi_2^2 + \xi_3^2}$),

$$\text{longitudinal scale} : L_g = \int_0^\infty f(\xi) d\xi \quad (6.16)$$

$$\text{lateral scale} : L'_g = \int_0^\infty g(\xi) d\xi \quad (6.17)$$

The continuity condition for incompressible fluids imposes a direct relation between $f(\xi)$ and $g(\xi)$. It is due to this relation that the longitudinal scale L_g equals exactly twice the lateral scale L'_g ,

$$L_g = 2L'_g \quad (6.18)$$

Because the maximum ordinate of $f(\xi)$ is unity, L_g can be interpreted as the width of a rectangle that contains the same area as the correlation curve $f(\xi)$. Thus the scale length L_g is a measure of the spatial extent of significant correlation. A typical value for L_g in high-altitude turbulence is $L_g = 300$ meters.

6.5 The von Kármán spectra

Several authors suggest analytical functions for the turbulence spectra (6.13) from analytical data, see e.g. (Etkin, 1972) or (Houbolt, Steiner, & Pratt, 1964). The von Kármán functions yield spectra that seem to best fit the available theoretical and experimental data on atmospheric turbulence,

$$\text{longitudinal} : S(\Omega) = 2\sigma^2 L_g \frac{1}{[1 + (1.339 L_g \Omega)^2]^{5/6}} \quad (6.19)$$

$$\text{lateral} : S(\Omega) = \sigma^2 L_g \frac{1 + \frac{8}{3}(1.339 L_g \Omega)^2}{[1 + (1.339 L_g \Omega)^2]^{11/6}} \quad (6.20)$$

Figure 6.9 shows a graphical representation. Inverse Fourier transformation of the von Kármán spectra provides exact analytical expressions for the associated fundamental correlation functions $f(\xi)$ and $g(\xi)$,

$$f(\xi) = \frac{2^{\frac{2}{3}}}{\Gamma(\frac{1}{3})} \left(\frac{\xi}{1.339 L_g} \right)^{\frac{1}{3}} K_{\frac{1}{3}} \left(\frac{\xi}{1.339 L_g} \right) \quad (6.21)$$

$$g(\xi) = \frac{2^{\frac{2}{3}}}{\Gamma(\frac{1}{3})} \left(\frac{\xi}{1.339 L_g} \right)^{\frac{1}{3}} \left[K_{\frac{1}{3}} \left(\frac{\xi}{1.339 L_g} \right) - \frac{1}{2} \left(\frac{\xi}{1.339 L_g} \right) K_{\frac{2}{3}} \left(\frac{\xi}{1.339 L_g} \right) \right] \quad (6.22)$$

Again, ξ equals $\sqrt{\xi_1^2 + \xi_2^2 + \xi_3^2}$ and,

$$\underline{\xi} = (\xi_1, \xi_2, \xi_3)^T = (V \cdot \tau, 0, 0)^T$$

In Equations (6.21) and (6.22) Γ denotes the gamma function,

$$\Gamma(z) = \int_0^\infty t^{z-1} e^{-t} dt \quad (6.23)$$

which may be approximated by using the following series expansion,

$$\Gamma(z) = \lim_{n \rightarrow \infty} \frac{n!}{z(z+1)(z+2)\dots(z+n-1)} n^{z-1}$$

K denotes the modified Bessel function of the second kind (Korn & Korn, 1968),

$$K_m(z) = \frac{\pi/2}{\sin m\pi} [I_{-m}(z) - I_m(z)] \quad (6.24)$$

In this expression, I_m denotes the modified Bessel function of the first kind of order m ,

$$I_m(z) = j^{-m} J_m(jz)$$

where J_m is the standard Bessel function of the first kind, which may be approximated by,

$$J_m(z) = \left(\frac{z}{2} \right)^m \sum_{k=0}^{\infty} \frac{(-1)^k}{k! \Gamma(m+k+1)} \left(\frac{z}{2} \right)^{2k}$$

Please note: Because of the use of a different definition of the Fourier transform (the partition of the constant $\frac{1}{2\pi}$ may differ) some textbooks may use a scaled version of the spectra (6.19) and (6.20). However, an agreement on the correlation functions exists, because these originate from measured wind velocities.

So far we have considered an arbitrary frame of reference and a general separation distance vector $\underline{\xi}$. In the following we will restrict ourselves to a special case, i.e. we choose the

stability reference frame and select a separation distance vector along the aircraft's flight path. In this reference frame the turbulence velocities are denoted as $\underline{\bar{u}} = (\bar{u}_g, \bar{v}_g, \bar{w}_g)^T$ and the separation distance vector evolves with time as $\underline{\xi} = (V \cdot \tau, 0, 0)^T$. Figure 6.10 illustrates the situation.

The frozen field concept (Taylor's hypothesis) mentioned previously, implies that the circular frequency ω (rad/sec) encountered at the aircraft's centre of gravity is now directly related to the spatial frequency Ω (rad/m) according to,

$$\omega = \Omega \cdot V \quad (6.25)$$

Therefore, the covariance functions and spectral densities are transformed to functions of τ and ω as follows,

$$\begin{aligned} C(\tau) &= R(\xi = V \cdot \tau) \\ S(\omega) &= \frac{1}{V} S(\Omega = \frac{\omega}{V}) \end{aligned}$$

Notice the extra term of $\frac{1}{V}$ arising in the spectral density function. This is due to the fact that we now integrate over dt in the Fourier transform instead of the $d\xi$ variable used in Equations (6.13), (6.19) and (6.20).

In this special situation, the von Kármán spectra are,

$$\begin{aligned} S_{\bar{u}_g \bar{u}_g}(\omega) &= 2\sigma^2 \frac{L_g}{V} \frac{1}{\left[1 + \left(1.339 \frac{L_g \omega}{V}\right)^2\right]^{5/6}} \\ S_{\bar{v}_g \bar{v}_g}(\omega) &= \sigma^2 \frac{L_g}{V} \frac{1 + \frac{8}{3} \left(1.339 \frac{L_g \omega}{V}\right)^2}{\left[1 + \left(1.339 \frac{L_g \omega}{V}\right)^2\right]^{11/6}} \\ S_{\bar{w}_g \bar{w}_g}(\omega) &= \sigma^2 \frac{L_g}{V} \frac{1 + \frac{8}{3} \left(1.339 \frac{L_g \omega}{V}\right)^2}{\left[1 + \left(1.339 \frac{L_g \omega}{V}\right)^2\right]^{11/6}} \end{aligned} \quad (6.26)$$

The correlation functions C can be calculated by substituting Equations (6.21) and (6.22) in Equation (6.15). See also Chapter 9. Notice that in this special situation all cross-covariance functions $C_{\bar{u}_g \bar{v}_g}$, $C_{\bar{u}_g \bar{w}_g}$ etc. exactly equal zero. Consequently a similar situation arises for the cross-spectral density functions $S_{\bar{u}_g \bar{v}_g}$, $S_{\bar{u}_g \bar{w}_g}$ etc.

6.6 The Dryden spectra

The von Kármán spectra yield $S(\Omega) \sim \Omega^{-\frac{5}{3}}$ as $\Omega \rightarrow \infty$, a condition imposed by the rate at which the most energetic eddies of turbulence loose their kinetic energy. That energy is not lost immediately to viscosity but is transferred to smaller eddies (typically with a

spatial frequency Ω about an octave higher than the first), which in turn transfer energy to yet smaller eddies and so on. This transfer of energy occurs in a range called the ‘inertial subrange’, in which energy is neither fed into nor dissipated from the turbulence. This process continues until the last eddies become so small in size (i.e. large in spatial frequency Ω) that viscosity can annihilate them almost immediately.

A major drawback of the von Kármán spectral densities is, however, that they are not rational functions. Rational spectral density functions would greatly simplify analysis and computation in any application. To overcome this problem, the Dryden spectral form was introduced. The Dryden spectral densities mathematically have the same low-frequency asymptote as the von Kármán spectral densities. However, its high-frequency asymptote is directly proportional to the -2 power of frequency. The Dryden spectra are given as,

$$\begin{aligned} S_{\bar{u}_g \bar{u}_g}(\omega) &= 2\sigma^2 \frac{L_g}{V} \frac{1}{1 + (L_g \frac{\omega}{V})^2} \\ S_{\bar{v}_g \bar{v}_g}(\omega) &= \sigma^2 \frac{L_g}{V} \frac{1 + 3(L_g \frac{\omega}{V})^2}{\left[1 + (L_g \frac{\omega}{V})^2\right]^2} \\ S_{\bar{w}_g \bar{w}_g}(\omega) &= \sigma^2 \frac{L_g}{V} \frac{1 + 3(L_g \frac{\omega}{V})^2}{\left[1 + (L_g \frac{\omega}{V})^2\right]^2} \end{aligned} \quad (6.27)$$

The covariance or correlation functions C , Equation (6.15), may be calculated using the following longitudinal and lateral correlation functions f and g ,

$$\begin{aligned} f(\xi) &= e^{-\frac{\xi}{L_g}} \\ g(\xi) &= e^{-\frac{\xi}{L_g}} \left(1 - \frac{\xi}{2L_g}\right) \end{aligned} \quad (6.28)$$

Again, ξ equals $\sqrt{\xi_1^2 + \xi_2^2 + \xi_3^2}$ and,

$$\underline{\xi} = (\xi_1, \xi_2, \xi_3)^T = (V \cdot \tau, 0, 0)^T$$

See also Chapter 9.

Figures 6.11 and 6.12 show graphical representations of typical Dryden spectral densities and longitudinal and lateral correlation functions as compared to the von Kármán functions. There is every indication that, although the von Kármán form seems to fit the available experimental data somewhat better (see also Figure 6.13), both the von Kármán and the Dryden form yield much the same results for aircraft responses, see also (Houbolt et al., 1964).

The variance of the gust velocities is given by the parameter σ^2 in (6.27). To see this, apply (3.32) to (6.27):

$$\sigma_{\bar{u}_g}^2 = \frac{1}{2\pi} \int_{-\infty}^{+\infty} S_{\bar{u}_g \bar{u}_g}(\omega) d\omega = \frac{1}{2\pi} 2\sigma^2 \frac{L_g}{V} \int_{-\infty}^{+\infty} \frac{1}{1 + (L_g \frac{\omega}{V})^2} d\omega =$$

$$= \frac{\sigma^2}{\pi} \frac{L_g}{V} \frac{V}{L_g} \left[\arctan \left(L_g \frac{\omega}{V} \right) \right]_{-\infty}^{+\infty} = \frac{\sigma^2}{\pi} \left[\frac{\pi}{2} + \frac{\pi}{2} \right] = \sigma^2 = C_{\bar{u}_g \bar{u}_g}(\tau = 0)$$

Similar arguments hold for $\sigma_{\bar{v}_g}^2$ and $\sigma_{\bar{w}_g}^2$ giving Equation (6.14).

The motivation for developing the Dryden spectra was the search for approximate turbulence spectral densities that are rational functions of frequency. In order to illustrate some of the resulting simplifications, consider the following problem.

We want to model atmospheric turbulence with Dryden spectral densities as a white noise signal passing through a linear, rational filter, see Figure 6.13. We want to know the frequency response function $H(\omega)$, the transfer function $H(s)$ or the state-space description $\dot{\underline{x}} = A\underline{x} + B\underline{u}$ of the forming filter.

As a starting point in the derivation of the forming filter, let us consider Equation (3.44) once again,

$$S_{\bar{y}\bar{y}}(\omega) = |H(\omega)|^2 S_{\bar{u}\bar{u}}(\omega)$$

As the input signal we choose white noise with spectral density,

$$S_{\bar{u}\bar{u}}(\omega) = 1 \quad (6.29)$$

As the output signal consider both the longitudinal turbulence velocity \bar{u}_g and the lateral turbulence velocities \bar{v}_g and \bar{w}_g . The Dryden spectra for \bar{v}_g and \bar{w}_g are exactly equal and, therefore, we will only consider \bar{w}_g in the following. Remember that all expressions for \bar{w}_g derived hereafter, apply equally well to \bar{v}_g .

From the definitions of the Dryden spectra, Equation (6.27), we find,

$$2\sigma^2 \frac{L_g}{V} \frac{1}{1 + (L_g \frac{\omega}{V})^2} = |H_{\bar{u}_g w_1}(\omega)|^2 \quad (6.30)$$

$$\sigma^2 \frac{L_g}{V} \frac{1 + 3(L_g \frac{\omega}{V})^2}{\left[1 + (L_g \frac{\omega}{V})^2\right]^2} = |H_{\bar{w}_g w_3}(\omega)|^2 \quad (6.31)$$

Solving Equations (6.30) and (6.31) yields the following candidate functions for the frequency response functions $H_{\bar{u}_g w_1}(\omega)$ and $H_{\bar{w}_g w_3}(\omega)$,

$$H_{\bar{u}_g w_1}(\omega) = \frac{\bar{u}_g(\omega)}{\bar{w}_1(\omega)} = \sigma \sqrt{\frac{2L_g}{V}} \frac{1}{1 \pm \frac{L_g}{V} j\omega} \quad (6.32)$$

$$H_{\bar{w}_g w_3}(\omega) = \frac{\bar{w}_g(\omega)}{\bar{w}_3(\omega)} = \sigma \sqrt{\frac{L_g}{V}} \frac{1 \pm \sqrt{3} \frac{L_g}{V} j\omega}{\left(1 \pm \frac{L_g}{V} j\omega\right)^2} \quad (6.33)$$

Replacing the imaginary variable $j\omega$ by the more general complex variable s , the Laplace transform $H(s)$ is found to be,

$$H_{\bar{u}_g w_1}(s) = \frac{\bar{u}_g(s)}{\bar{w}_1(s)} = \sigma \sqrt{\frac{2L_g}{V}} \frac{1}{1 \pm \frac{L_g}{V} s} \quad (6.34)$$

$$H_{\bar{w}_g w_3}(s) = \frac{\bar{w}_g(s)}{\bar{w}_3(s)} = \sigma \sqrt{\frac{L_g}{V}} \frac{1 \pm \sqrt{3} \frac{L_g}{V} s}{\left(1 \pm \frac{L_g}{V} s\right)^2} \quad (6.35)$$

Choosing the minus sign in the denominator of $H_{\bar{u}_g w_1}(s)$ and $H_{\bar{w}_g w_3}(s)$ would lead to unstable filters and hence should be rejected for physical reasons. Notice that choosing the minus sign in the numerator of $H_{\bar{w}_g w_3}(s)$ would lead to a non-minimum phase system, see (Oppenheim et al., 1997). Therefore we use positive signs only in the numerator and denominator of both transfer functions. By substitution of $s = \frac{d}{dt}$, the differential equations for the turbulence filters are found to be, writing $u_g(t)$ and $w_g(t)$ rather than $\bar{u}_g(t)$ and $\bar{w}_g(t)$,

$$\frac{L_g}{V} \dot{u}_g(t) + u_g(t) = \sigma \sqrt{\frac{2L_g}{V}} w_1(t) \quad (6.36)$$

$$\frac{L_g^2}{V^2} \ddot{w}_g(t) + 2 \frac{L_g}{V} \dot{w}_g(t) + w_g(t) = \sigma \sqrt{\frac{L_g}{V}} w_3(t) + \sigma \frac{L_g}{V} \sqrt{\frac{3L_g}{V}} \dot{w}_3(t) \quad (6.37)$$

To obtain a state-space description for the forming filters, an auxiliary variable $w_g^*(t)$ is introduced as, see also Example 6.3,

$$w_g^*(t) = \dot{w}_g(t) - \sigma \sqrt{\frac{3V}{L_g}} w_3(t) \quad (6.38)$$

The general state-space description for the forming filters can now be written as,

$$\dot{u}_g(t) = -\frac{V}{L_g} u_g(t) + \sigma \sqrt{\frac{2V}{L_g}} w_1(t) \quad (6.39)$$

$$\begin{bmatrix} \dot{v}_g(t) \\ \dot{v}_g^*(t) \end{bmatrix} = \begin{bmatrix} 0 & 1 \\ -\frac{V^2}{L_g^2} & -2\frac{V}{L_g} \end{bmatrix} \begin{bmatrix} v_g(t) \\ v_g^*(t) \end{bmatrix} + \begin{bmatrix} \sigma \sqrt{\frac{3V}{L_g}} \\ (1 - 2\sqrt{3}) \sigma \sqrt{\left(\frac{V}{L_g}\right)^3} \end{bmatrix} w_2(t) \quad (6.40)$$

$$\begin{bmatrix} \dot{w}_g(t) \\ \dot{w}_g^*(t) \end{bmatrix} = \begin{bmatrix} 0 & 1 \\ -\frac{V^2}{L_g^2} & -2\frac{V}{L_g} \end{bmatrix} \begin{bmatrix} w_g(t) \\ w_g^*(t) \end{bmatrix} + \begin{bmatrix} \sigma \sqrt{\frac{3V}{L_g}} \\ (1 - 2\sqrt{3}) \sigma \sqrt{\left(\frac{V}{L_g}\right)^3} \end{bmatrix} w_3(t) \quad (6.41)$$

where $w_1(t)$, $w_2(t)$ and $w_3(t)$ are three independent white noise inputs driving the turbulence generating filters (6.39) - (6.41).

6.7 Quantitative description of turbulence parameters at low altitude

In Sections 6.4.3 and 6.4.5 variances $\sigma_{\bar{u}_g}$, $\sigma_{\bar{v}_g}$, $\sigma_{\bar{w}_g}$ and the integral scales of turbulence L_g and L'_g were mentioned which are to be inserted in the power spectra according to either

von Kármán or Dryden. The quantitative values of these variances and scales are based on experimental data, see for example (Pritchard, 1966). As might be expected, these experimental data show the variances and scales to be functions of height and mean wind velocity. In proximity of the ground the vertical component \bar{w}_g behaves differently from the horizontal components \bar{u}_g and \bar{v}_g and as a consequence turbulence at low altitudes is considered to be neither homogeneous nor isentropic. Although for heights > 500 m Equations (6.14) and (6.18) seem to hold, these relations must again be evaluated at lower altitudes to fit the available experimental data. Following (Pritchard, 1966) and (Gerlach & Schuring, 1970), the intensity and the scale of the vertical component \bar{w}_g are described first, then the corresponding characteristics of the horizontal components \bar{u}_g and \bar{v}_g are related to those of the vertical component \bar{w}_g .

6.7.1 The intensity of turbulence

The standard deviation of vertical gust velocity $\sigma_{\bar{w}_g}$ was experimentally found to be a function of height, atmospheric stability (as expressed by the temperature lapse rate λ see Section 6.2.1), wind velocity and a terrain factor, see (Pritchard, 1966).

Since the likely variations in terrain factor appear to be relatively small and the data concerned shows a large scatter, the external disturbances due to the atmosphere, acting on the aircraft at a certain altitude, are seen to depend primarily on the wind speed and on the stability of the atmosphere, see (Gerlach & Schuring, 1970).

With wind profiles (wind speed versus altitude) experimentally determined at different atmospheric stabilities, the standard deviation of atmospheric turbulence is dependent on the wind speed at a reference height (in meteorological experiments a reference height of 9.15 m (30 ft) is commonly seen), and the temperature lapse rate λ . In Figure 6.14 a wind speed at 9.15 m and a temperature lapse rate are needed to find $\sigma_{\bar{w}_g}$ at any altitude between 0 and 450 m. As was mentioned in Section 6.4.3, $\sigma_{\bar{u}_g}$ and $\sigma_{\bar{v}_g}$ are equal to $\sigma_{\bar{w}_g}$ in isentropic turbulence (c.f. Equation (6.14)). In (Pritchard, 1966) a set of expressions for $\sigma_{\bar{u}_g}$ and $\sigma_{\bar{v}_g}$ is suggested for different lapse rates and altitudes. In view of the considerable scatter in the data on which these expressions are based, (Gerlach & Schuring, 1970) combines the sets into the following relations for all stability conditions of the atmosphere:

$$\begin{aligned} \frac{\sigma_{\bar{u}_g}}{\sigma_{\bar{w}_g}} &= \frac{\sigma_{\bar{v}_g}}{\sigma_{\bar{w}_g}} = 2.5 & 0 \text{ m} \leq h < 15 \text{ m} \\ \frac{\sigma_{\bar{u}_g}}{\sigma_{\bar{w}_g}} &= \frac{\sigma_{\bar{v}_g}}{\sigma_{\bar{w}_g}} = 1.25 - 0.001 h & 15 \text{ m} \leq h < 250 \text{ m} \end{aligned} \quad (6.42)$$

and, Equation (6.14),

$$\frac{\sigma_{\bar{u}_g}}{\sigma_{\bar{w}_g}} = \frac{\sigma_{\bar{v}_g}}{\sigma_{\bar{w}_g}} = 1 \quad h > 250 \text{ m}$$

6.7.2 The scale of turbulence

The information available on L_g has been presented in Figure 6.15, see also Figure 2 of (Pritchard, 1966). For a given temperature lapse rate λ , L_g can be read directly as a function of altitude.

From the foregoing it can be concluded that the entire structure of the atmospheric turbulence at low altitudes (during approach and landing!) can be described according to the model just presented and plotted in Figures 6.14 and 6.15 by giving:

- the wind speed at some reference height, e.g. 9.15 m.
- the temperature lapse rate λ of the lower atmosphere.

6.8 Examples

6.8.1 Example 6.1

Suppose that we are interested in the correlation coefficients of the turbulence velocities at three different locations of a large transport aircraft, see the wing-fin system of Figure 6.16. The first point we choose is the middle of the right half wing (A), the second location we choose the middle of the left half wing (B) and as a third location the middle of the stabilizer (C).

Using the covariance functions according to Dryden, Equation (6.28), we find for the longitudinal- and lateral correlation functions:

$$f(\xi) = \sigma^2 e^{-\frac{\xi}{L_g}} \quad (6.43)$$

$$g(\xi) = \sigma^2 e^{-\frac{\xi}{L_g}} \left(1 - \frac{\xi}{2L_g}\right) \quad (6.44)$$

see also Figure 6.12. Using Equation (6.15),

$$K_{ij}(\underline{\xi}) = \frac{f(|\underline{\xi}|) - g(|\underline{\xi}|)}{|\underline{\xi}|^2} \xi_i \xi_j + g(|\underline{\xi}|) \delta_{ij} \quad (6.45)$$

we can calculate the correlation coefficients between the turbulence velocities given in Figure 6.16, where specific values for $f(\xi)$ and $g(\xi)$ are obtained by substitution in (6.43) and (6.44) using $L_g = 150$ m.

$$K_{u_{1A} u_{3B}}(0, -40, 0)^T = 0 \quad (\text{because } \xi_1 = 0)$$

$$K_{u_{1A} u_{3C}}(-40, -20, -10)^T = \frac{f(\sqrt{2100}) - g(\sqrt{2100})}{2100} (-40) \cdot (-10) = 0.0214$$

$$\begin{aligned} K_{u_{3B} u_{3C}}(-40, 20, -10)^T &= \frac{f(\sqrt{2100}) - g(\sqrt{2100})}{2100} (-10) \cdot (-10) + g(\sqrt{2100}) = \\ &= 0.6296 \end{aligned}$$

Intuitively, the correlation between turbulence velocities at two given points increases with an increase in scale length of the turbulence L_g . To demonstrate this, regard Figure 6.17 where $K_{u_3 B} u_{3C}$ has been plotted as a function of L_g . If $L_g \rightarrow \infty$ the correlation coefficient tends towards 1.

A MATLAB program to produce Figure 6.17 is given below. Inputting $\xi = [-40, 20, -10]^T$ for normal turbulence yields Figure 6.17.

Listing 6.1: Example 6.1

```
% Filename : examp161.m
%
% Calculation of correlation coefficients of turbulence
% velocities according to Batchelor using Dryden correlation
% functions at two points A and B.
%
% Chapter 6 of lecture notes ae4-304
%
% Revised November 2014 [M Rodriguez]
%%

clc; close all; clear all;

disp(' Example 6.1');
disp(' Calculates the correlation coefficient between velocity ');
disp(' vectors at two points as a function of the longitudinal ');
disp(' scale length L according to Batchelor using Dryden ');
disp(' correlation functions f(.) and g(.)');
disp(' ');
disp(' This program produces Figure 6-17 of the lecture notes: ');
disp(' Aircraft Responses to Atmospheric Turbulence. ');

x1 = input(' Give x-separation [m] between the two points (-40) : ');
x2 = input(' Give y-separation [m] between the two points ( 20) : ');
x3 = input(' Give z-separation [m] between the two points (-10) : ');
xi = [x1,x2,x3];

disp('');
disp(' Velocity directions:');
disp(' 1 --- Longitudinal');
disp(' 2 --- Lateral');
disp(' 3 --- Normal');
disp('');

uA = input(' Give velocity direction 1st point (3) : ');
uB = input(' Give velocity direction 2nd point (3) : ');

if uA < 1 | uA > 3 | uB < 1 | uB > 3
    error('Make a choice 1, 2 or 3')
end

% Turbulence velocity directions for calculation of correlation;
% 1: longitudinal;
% 2: lateral;
```

```
% 3: normal;

if uA == uB
    delta = 1;
else
    delta = 0;
end;

Lg = logspace(1,4,50); % running Lg from 10-10000m

% Specific functions f(xi) and g(xi) according to Dryden;
f = exp(-norm(xi)./Lg);
g = f.*((1-norm(xi)./(2*Lg)));

% Correlation according to Batchelor;
K = ((f-g)/norm(xi)^2)*xi(uA)*xi(uB)+delta*g;

% PLOTTING RESULTS
semilogx(Lg,K);
axis('square'); axis([10^1 10^4 -2 1]);
xlabel('scale length of turbulence Lg [m]');
ylabel('correlation coefficient K');
grid
```

6.8.2 Example 6.2

A time history of atmospheric turbulence can be obtained by filtering white noise with an appropriate filter. In this example, a signal describing vertical turbulence according to Dryden will be generated. The power spectral density function according to Dryden of this signal has been given in paragraph 6.6, Equation (6.27),

$$S_{\bar{w}_g \bar{w}_g}(\omega) = \sigma^2 \frac{L_g}{V} \frac{1 + 3 \left(L_g \frac{\omega}{V} \right)^2}{\left[1 + \left(L_g \frac{\omega}{V} \right)^2 \right]^2}$$

The state equation for the filter, that can be used to obtain a time history of \bar{w}_g , was found to be, Equation (6.41),

$$\begin{bmatrix} \dot{w}_g(t) \\ \dot{w}_g^*(t) \end{bmatrix} = \begin{bmatrix} 0 & 1 \\ -\frac{V^2}{L_g^2} & -2\frac{V}{L_g} \end{bmatrix} \begin{bmatrix} w_g(t) \\ w_g^*(t) \end{bmatrix} + \begin{bmatrix} \sigma \sqrt{\frac{3V}{L_g}} \\ (1 - 2\sqrt{3}) \sigma \sqrt{\left(\frac{V}{L_g}\right)^3} \end{bmatrix} w_3(t)$$

where $w_3(t)$ is the white noise signal driving the filter. In this example, the following values are used:

$$\sigma = 0.282 \text{ m/sec}$$

$$L_g = 150 \text{ m}$$

$$V = 35 \text{ m/sec}$$

corresponding to those at a height of 265 m in the atmospheric model according to Pritchard (Pritchard, 1966) for a neutral atmosphere, with an average windspeed at the reference height 9.15 m of 0.5 m/sec, see Figures 6.14 and 6.15. In order to gain some insight in the influence of the scale of turbulence L_g , a value of,

$$L_g = 1500 \text{ m}$$

will be considered as well.

The power spectral density functions, resulting from these values, are plotted in Figure 6.18. It can be seen that in the spectrum for the largest turbulence scale ($L_g = 1500 \text{ m}$), there is more power in the lower frequencies, and less power in the higher frequencies, compared to the spectrum for $L_g = 150 \text{ m}$. Of course the total surface underneath both curves equals the variance σ^2 and does not depend on the choice of L_g . Besides the turbulence scale L_g , the variance σ^2 has an influence on the turbulence as well, which is straightforward to see. By regarding the formula for the vertical Dryden spectrum (6.27), it can be seen that this spectrum is proportional to the variance σ^2 . Also the gust signal w_g is proportional to the standard deviation σ as follows from inspection of the forming filters (6.39)- (6.41).

Zero mean white noise with intensity 1 has been approximated by using the MATLAB random number generator. A time history of the ‘white noise’ input is plotted in Figure 6.19(a). Because the low undamped natural frequency of the filters (6.39)- (6.41), $\omega_0 = \frac{V}{L_g}$, the simulation must run for quite a considerable time interval for a representative filter output gust velocity. The resulting gust signal w_g has been plotted in Figure 6.19(b) for both $L_g = 150 \text{ m}$ and $L_g = 1500 \text{ m}$.

A MATLAB program to simulate the gust responses is straightforward.

Listing 6.2: Example 6.2

```
% Filename : examp162.m
%
% Simulation of atmospheric turbulence using Dryden model
%
% Chapter 6 of lecture notes ae4-304
%
% Revised: November 2014 [M Rodriguez]
%%

close all; clc, clear all;

disp(' Example 6.2 ') ;
disp(' Simulation of vertical gust velocity using Dryden model. ') ;
disp(' ') ;
disp(' This example produces Figure 6-19 of the lecture notes: ') ;
disp(' Aircraft Responses to Atmospheric Turbulence. ') ;
```

```

sigma = input(' Enter turbulence intensity sigma [m/s] (0.282) : ');
Lg1   = input(' Enter turbulence scale length Lg1 [m] ( 150) : ');
Lg2   = input(' Enter turbulence scale length Lg2 [m] ( 1500) : ');
V     = input(' Enter airspeed V [m/s] (    35) : ');

% Define time basis
dt = 0.1; T = 120;
t = [0:dt:T];
N = length(t);

% White noise input
w = randn(1,N)/sqrt(dt); % note: divide by sqrt(dt), with dt the sample time
                           % because of lsim characteristics

% Forming filter characteristics equation (6.41)
rat = V/Lg1;
A = [0 1;-rat^2 -2*rat];
B = sigma*[sqrt(3*rat);(1-2*sqrt(3))*sqrt((rat^3))];
C = [1 0];
D = [0];

% Output turbulence velocity
wg = lsim(A,B,C,D,w,t);

% Forming filter characteristics equation (6.41)
rat = V/Lg2;
A = [0 1;-rat^2 -2*rat];
B = sigma*[sqrt(3*rat);(1-2*sqrt(3))*sqrt((rat^3))];
C = [1 0];
D = [0];

% Output turbulence velocity
wgg = lsim(A,B,C,D,w,t);

% Plot the results
subplot(2,1,1)
plot(t,w);
xlabel('time [s]');
ylabel('w');
title('White Noise Filter Input');

subplot(2,1,2)
plot(t,wg,t,wgg,'--');
xlabel('time [s]');
ylabel('wg [m/s]');
title('Vertical Gust Velocity');
legend(['Lg = ' num2str(Lg1) 'm', ['Lg = ' num2str(Lg2) 'm']]);

```

6.8.3 Example 6.3

In this example the mathematics for transforming a transfer function to a model for the time-domain, the state space model, will be given.

Consider the second order differential equation,

$$\ddot{x} + a_1\dot{x} + a_2x = b_0\ddot{u} + b_1\dot{u} + b_2u \quad (6.46)$$

originating from the transfer function,

$$H(s) = \frac{b_0s^2 + b_1s + b_2}{s^2 + a_1s + a_2} \quad (6.47)$$

The new state space model will be written as (Ogata, 2002),

$$\begin{aligned} \dot{x}_1 &= x_2 + c_1u \\ \dot{x}_2 &= -a_2x_1 - a_1x_2 + c_2u \end{aligned} \quad (6.48)$$

or in state space form,

$$\begin{bmatrix} \dot{x}_1 \\ \dot{x}_2 \end{bmatrix} = \begin{bmatrix} 0 & 1 \\ -a_2 & -a_1 \end{bmatrix} \begin{bmatrix} x_1 \\ x_2 \end{bmatrix} + \begin{bmatrix} c_1 \\ c_2 \end{bmatrix} u \quad (6.49)$$

The original state x and the new state-variables x_1, x_2 are related by,

$$x = x_1 + c_0u \quad (6.50)$$

The parameters c_0, c_1, c_2 can be calculated by first considering the time-derivatives of Equation (6.50), using (6.48),

$$\dot{x} = \dot{x}_1 + c_0\dot{u} = x_2 + c_1u + c_0\dot{u} \quad (6.51)$$

It follows,

$$\ddot{x} = \dot{x}_2 + c_1\dot{u} + c_0\ddot{u} = -a_2x_1 - a_1x_2 + c_2u + c_1\dot{u} + c_0\ddot{u} \quad (6.52)$$

Equations (6.50), (6.51) and (6.52) are substituted in Equation (6.46), yielding,

$$\begin{aligned} (-a_2x_1 - a_1x_2 + c_2u + c_1\dot{u} + c_0\ddot{u}) + a_1(x_2 + c_1u + c_0\dot{u}) + a_2(x_1 + c_0u) &= \\ = b_0\ddot{u} + b_1\dot{u} + b_2u & \end{aligned} \quad (6.53)$$

or,

$$c_0\ddot{u} + (c_1 + a_1c_0)\dot{u} + (c_2 + a_1c_1 + a_2c_0)u = b_0\ddot{u} + b_1\dot{u} + b_2u \quad (6.54)$$

Hence,

$$c_0 = b_0 \quad (6.55)$$

$$c_1 + a_1 c_0 = b_1 \quad (6.56)$$

$$c_2 + a_1 c_1 + a_2 c_0 = b_2 \quad (6.57)$$

Hence,

$$c_0 = b_0 \quad (6.58)$$

$$c_1 = b_1 - a_1 b_0 \quad (6.59)$$

$$c_2 = b_2 - a_1 (b_1 - a_1 b_0) - a_2 b_0 \quad (6.60)$$

The initial conditions for Equation (6.46) become for the equivalent state space description,

$$x_1(0) = x(0) - c_0 u(0) \quad (6.61)$$

$$x_2(0) = \dot{x}(0) - c_1 u(0) - c_0 \dot{u}(0) \quad (6.62)$$

6.9 Summary

In Chapter 6 we described the mechanism of several kinds of atmospheric turbulence and presented several models for the power spectral densities of it. The Dryden spectra were discussed in detail because of the possibility of an equivalent time domain representation.

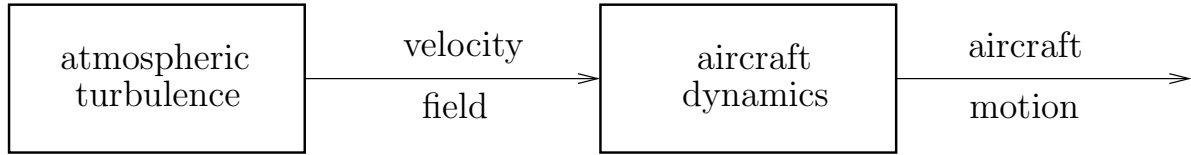


Figure 6.1: Breakdown of the ‘flight in atmospheric turbulence’ problem.

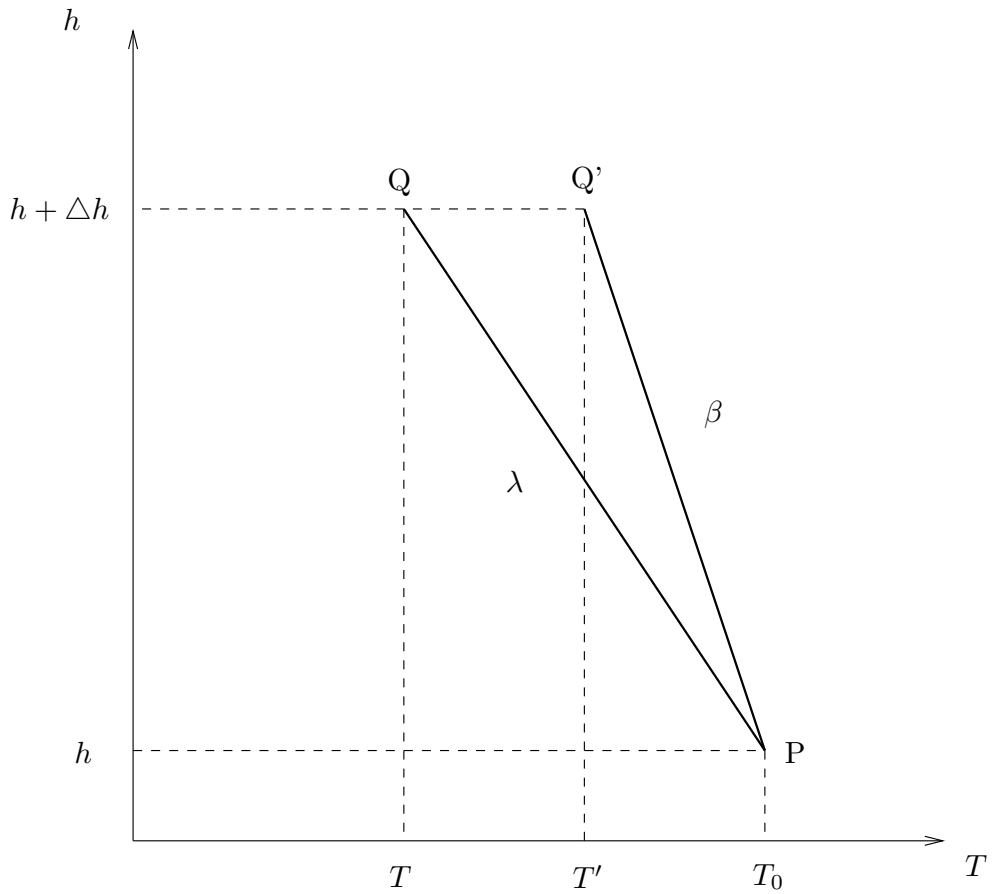


Figure 6.2: Vertical instability. If the geometric lapse rate $|\lambda|$ at height h is larger than $|\beta|$, a parcel rising Δh from P will have at Q' a temperature $T' > T$ where T is the temperature of the surrounding air (Q). It will tend to continue to rise.

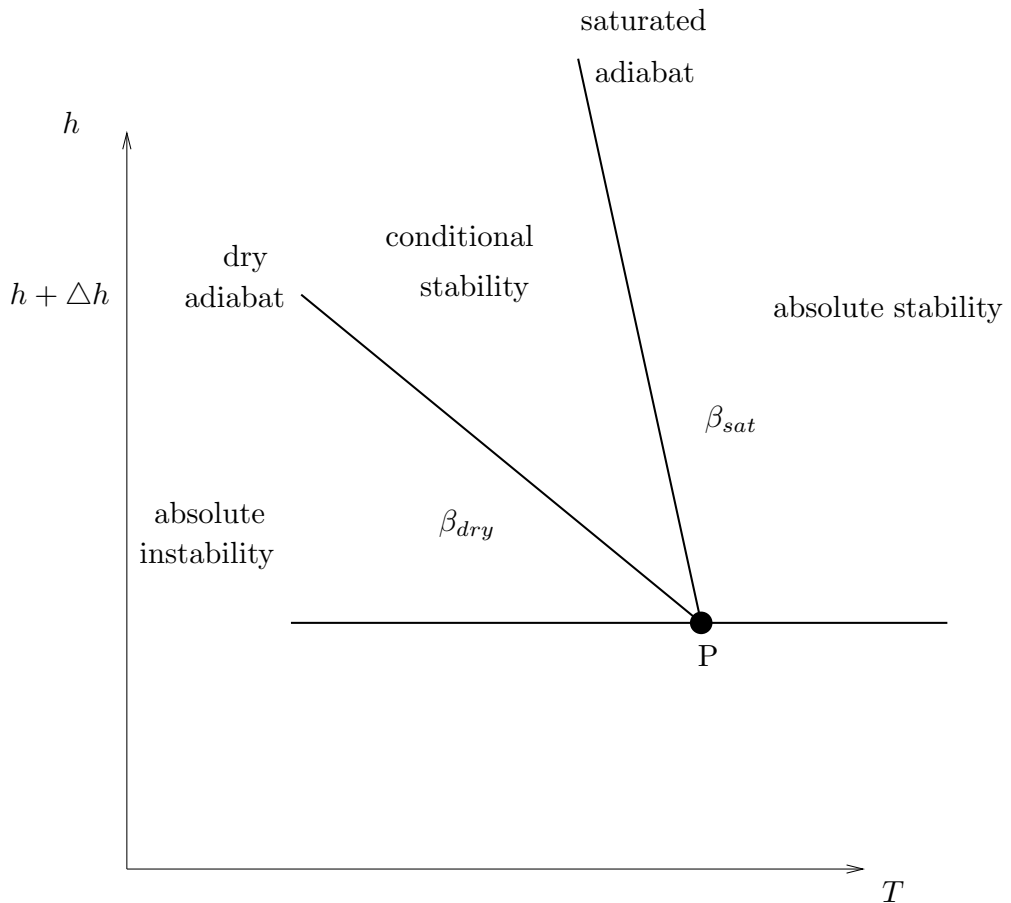


Figure 6.3: Conditions for vertical stability. The diagram summarizes the stability conditions for both unsaturated and saturated air.

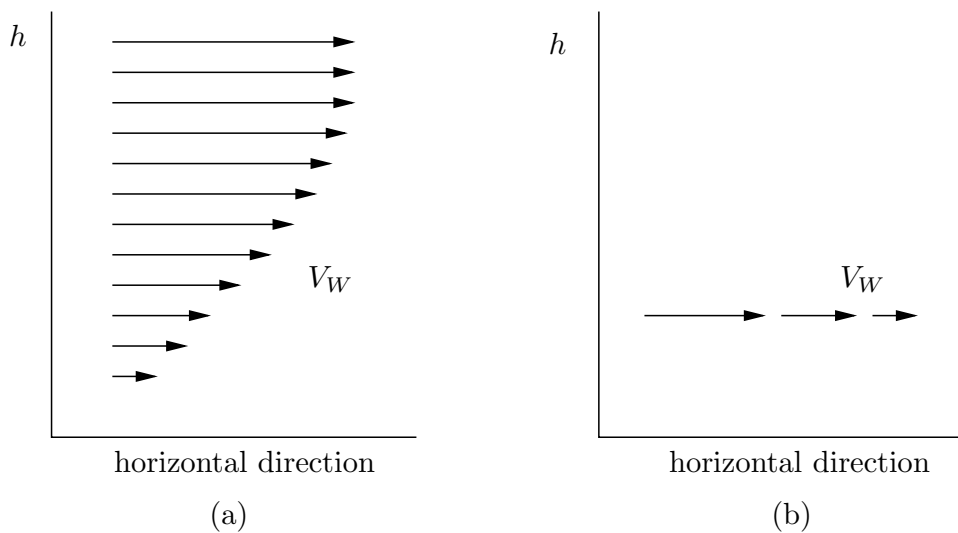


Figure 6.4: Definition of vertical (a) and horizontal (b) windshear.

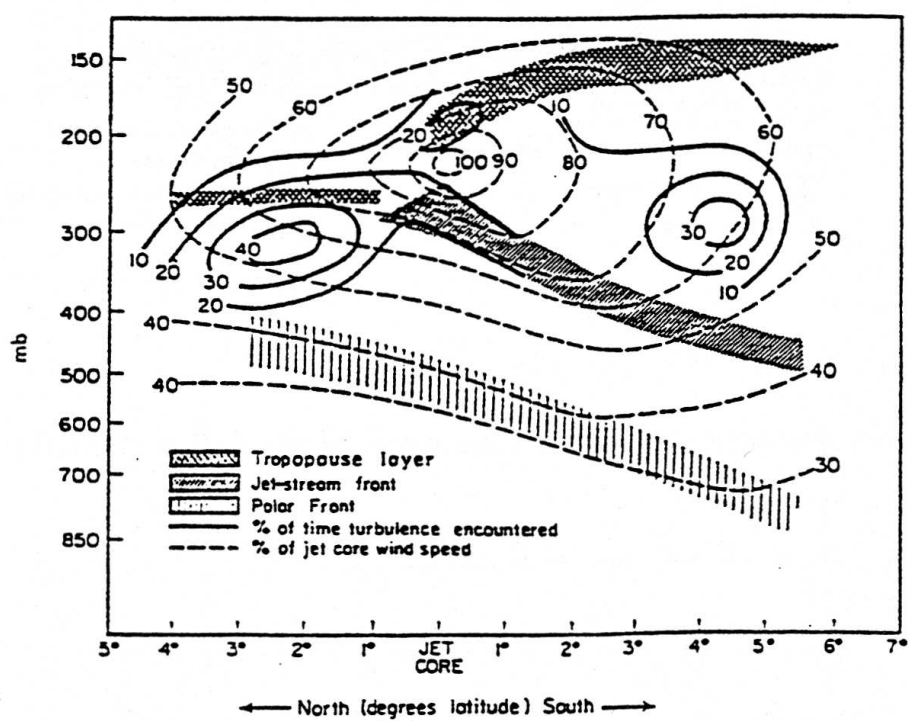


Figure 6.5: Percent of time clear-air turbulence reported by pilots with respect to jet-stream core (Endlich & McLean, 1957).

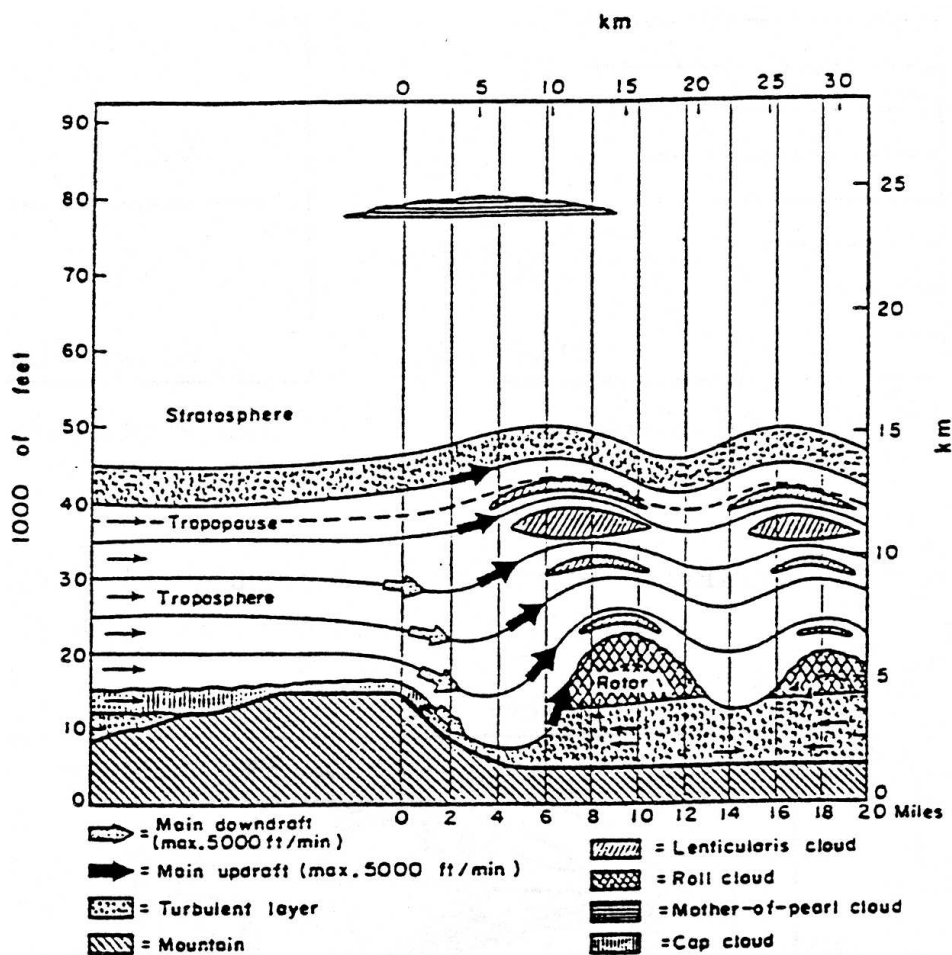


Figure 6.6: Cross-section of conditions associated with a typical mountain wave (Kuettner & Jenkins, 1953).

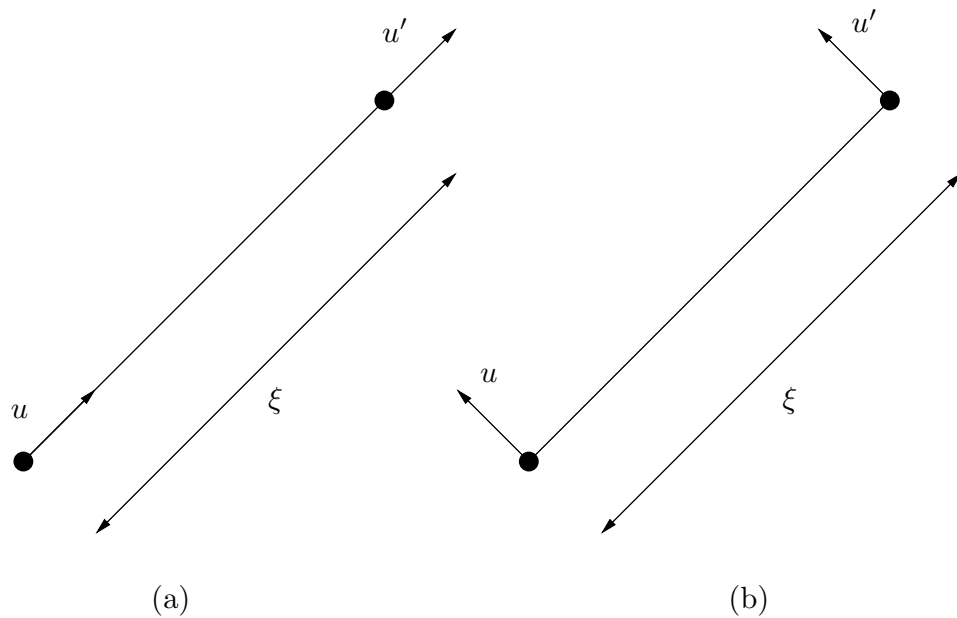


Figure 6.7: Correlations in isotropic turbulence a) Longitudinal correlation, $f(\xi)$ and b) Lateral correlation, $g(\xi)$.

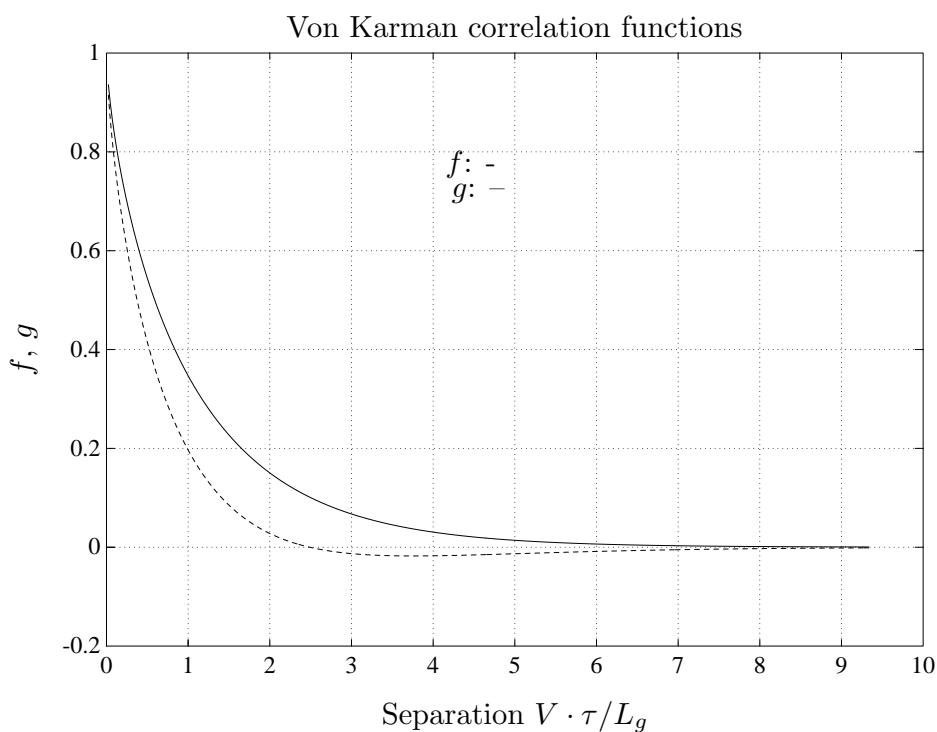


Figure 6.8: General shape of the correlation curves $f(\xi)$ and $g(\xi)$.

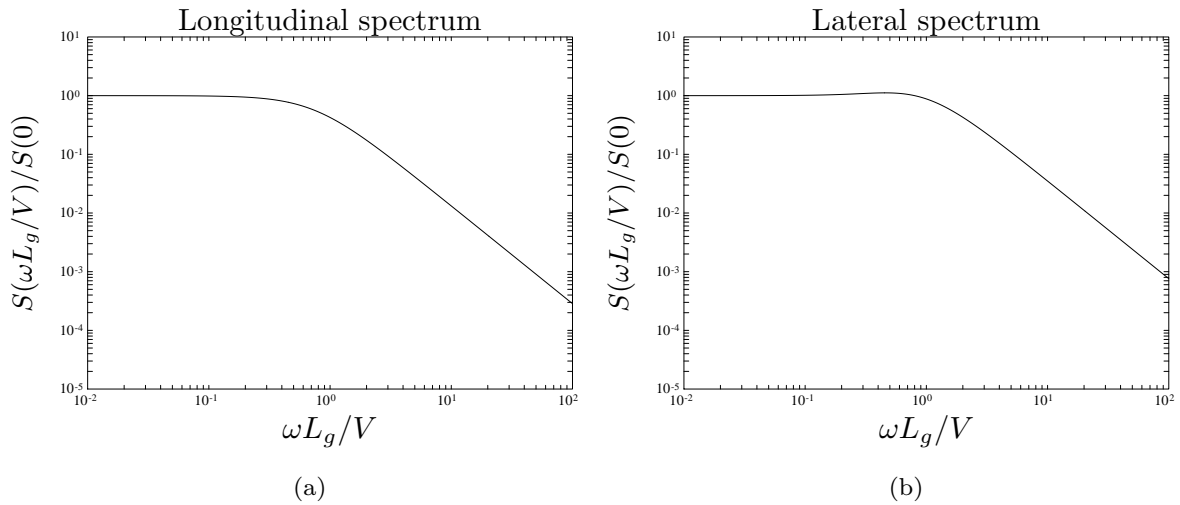


Figure 6.9: a) The longitudinal von Kármán spectrum, b) the lateral von Kármán spectrum.

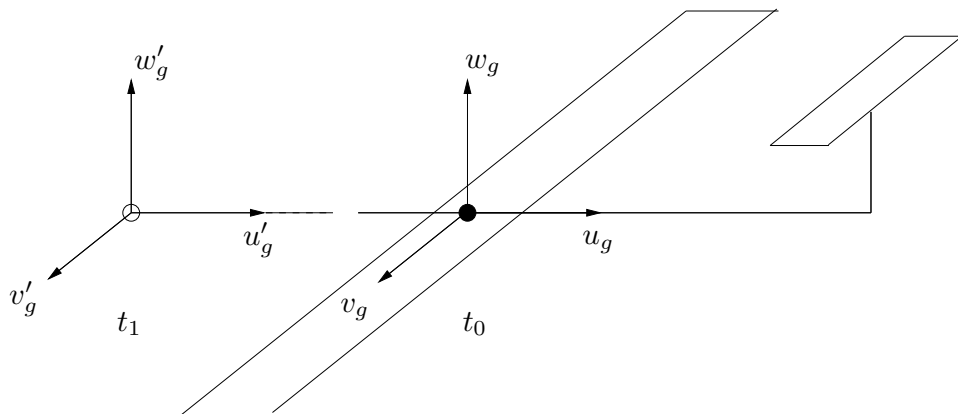


Figure 6.10: Reference frame and separation distance vector definition.

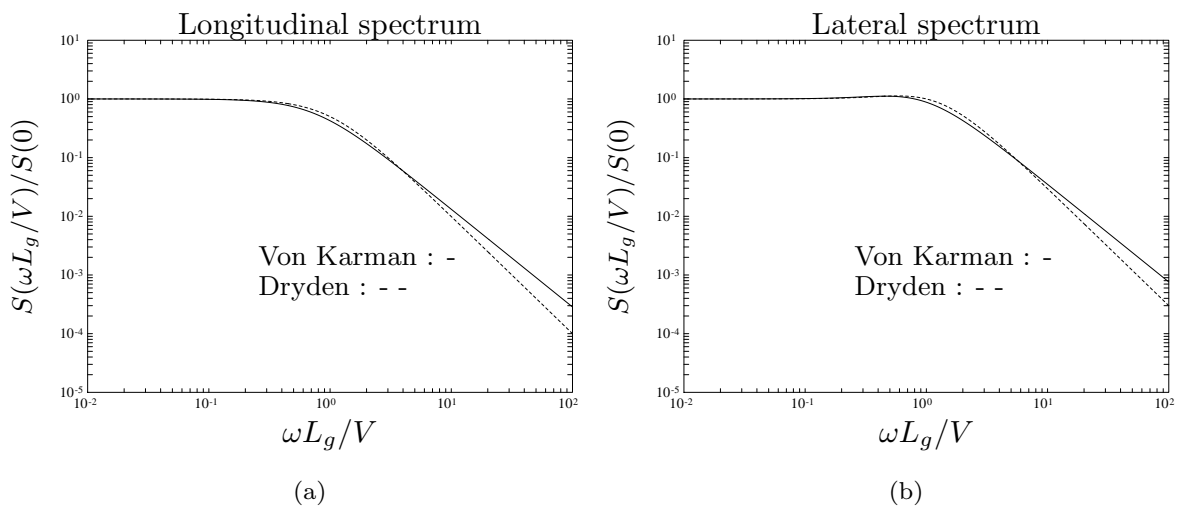


Figure 6.11: a) The longitudinal Dryden spectrum, b) the lateral Dryden spectrum.

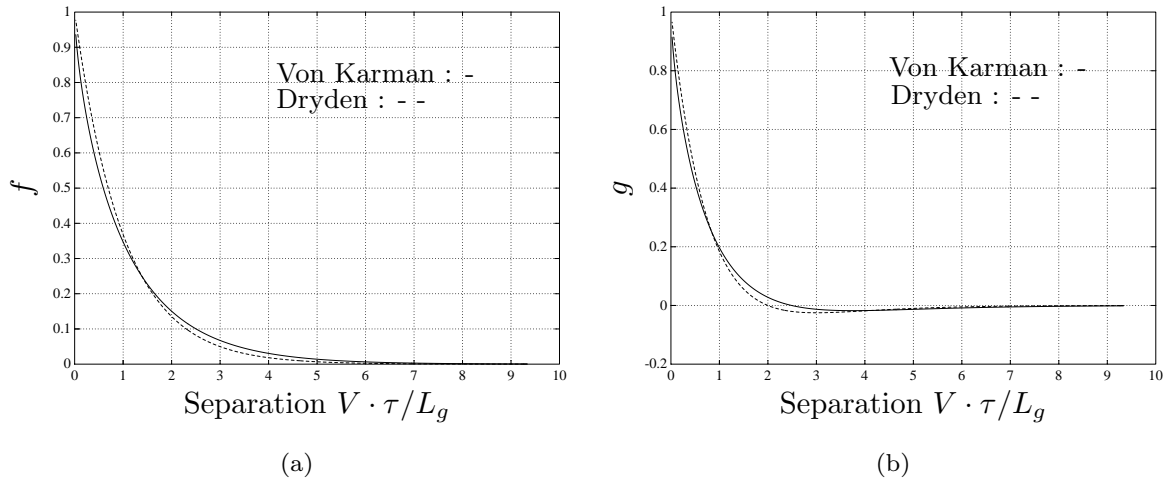


Figure 6.12: a) The longitudinal Dryden spectrum, b) the lateral Dryden spectrum.

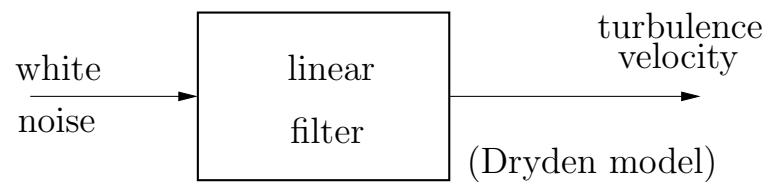


Figure 6.13: Modelling of atmospheric turbulence.

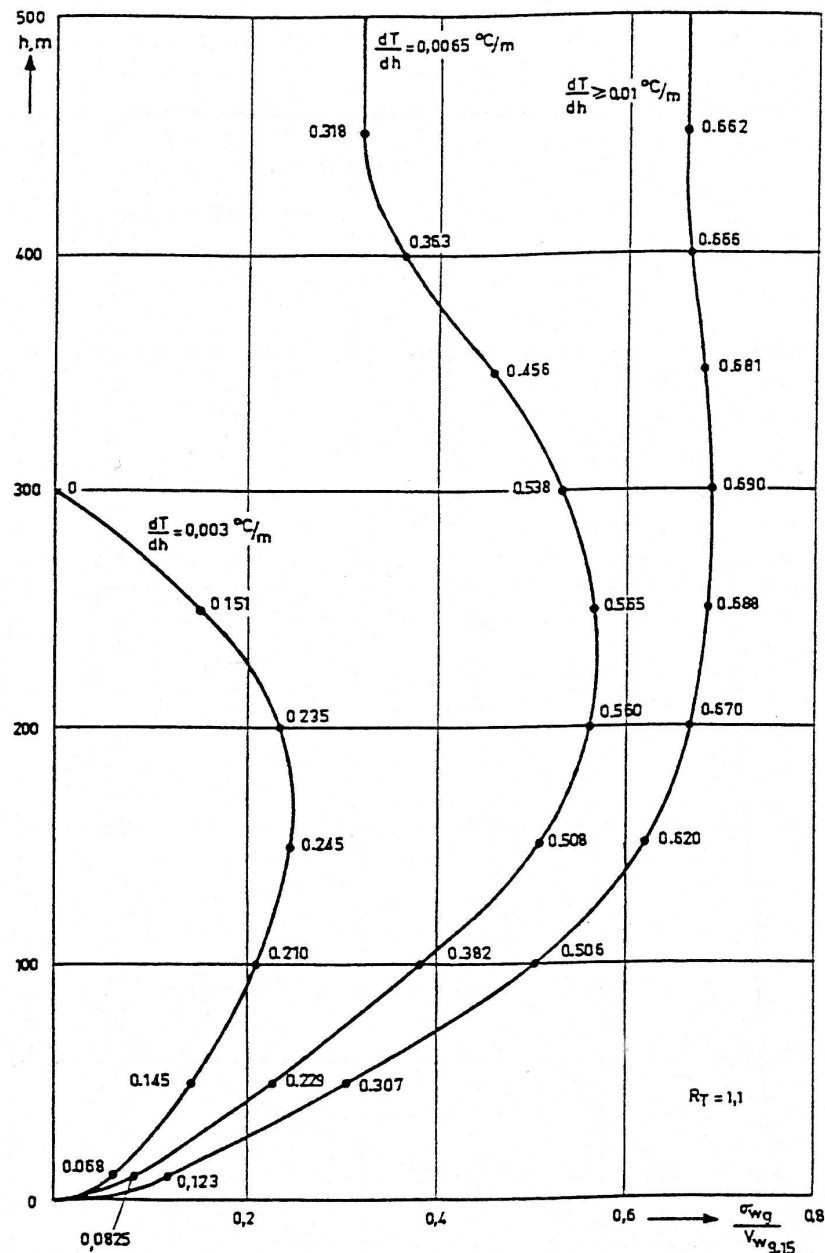


Figure 6.14: Standard deviation of vertical gust velocity as a function of altitude.

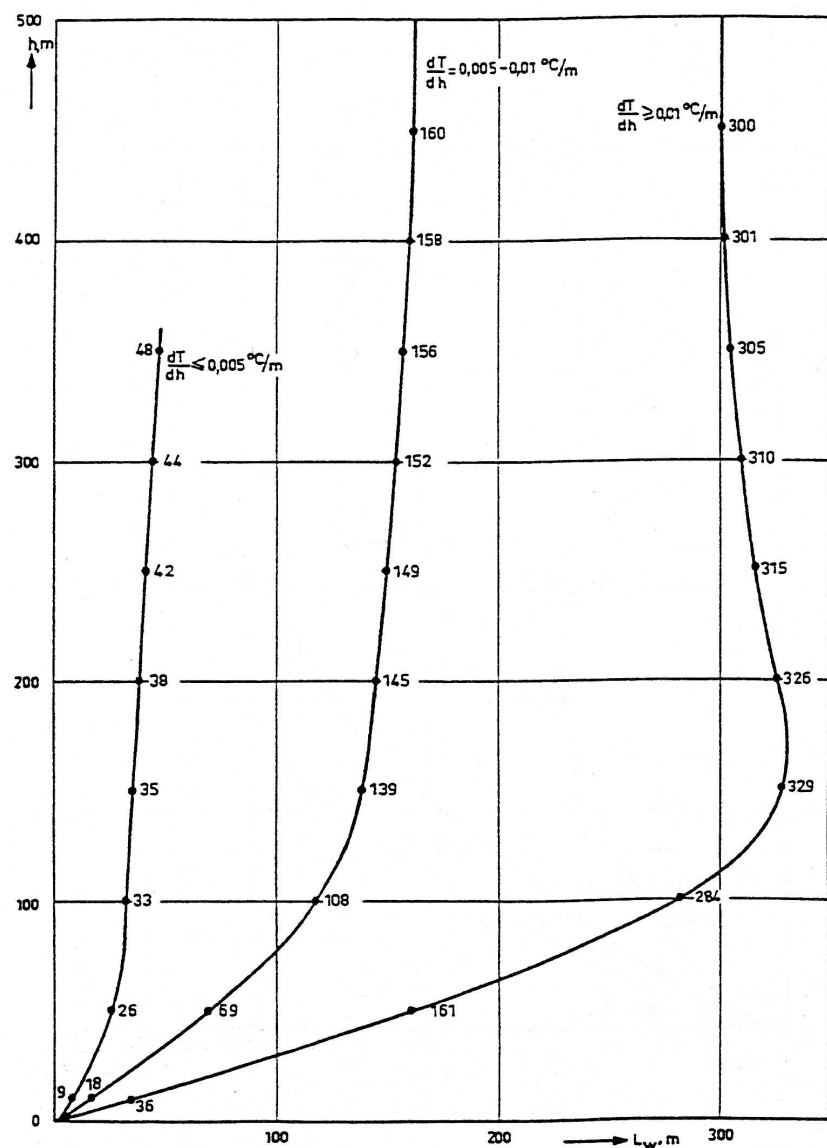


Figure 6.15: Scale of (longitudinal) turbulence as a function of altitude.

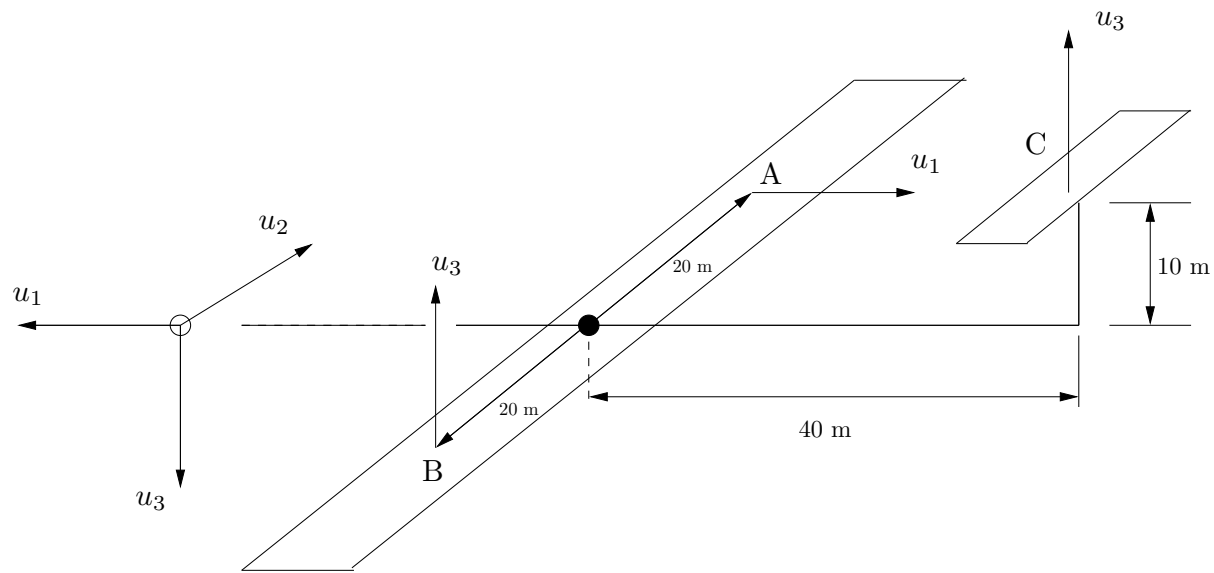


Figure 6.16: Schematic view of aircraft.

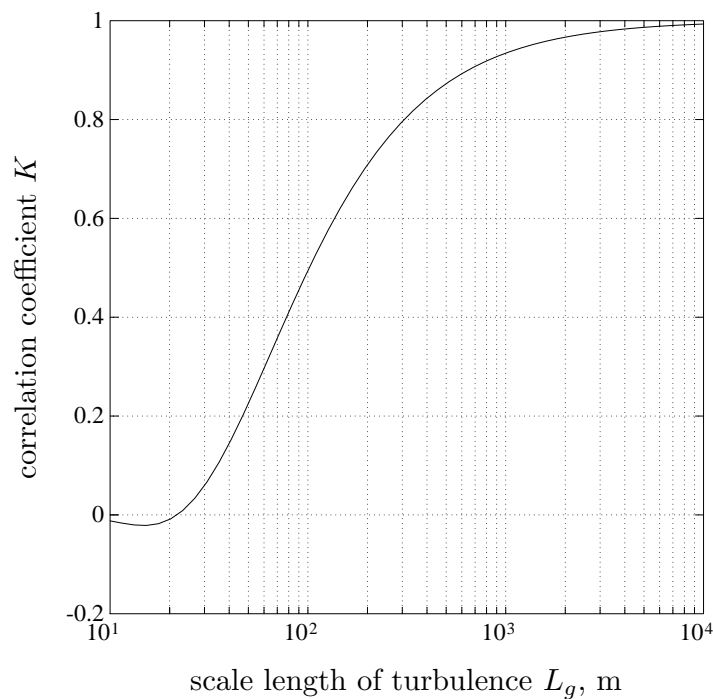


Figure 6.17: Correlation coefficient of turbulence velocity at two points as a function of scale length. Dryden turbulence model.

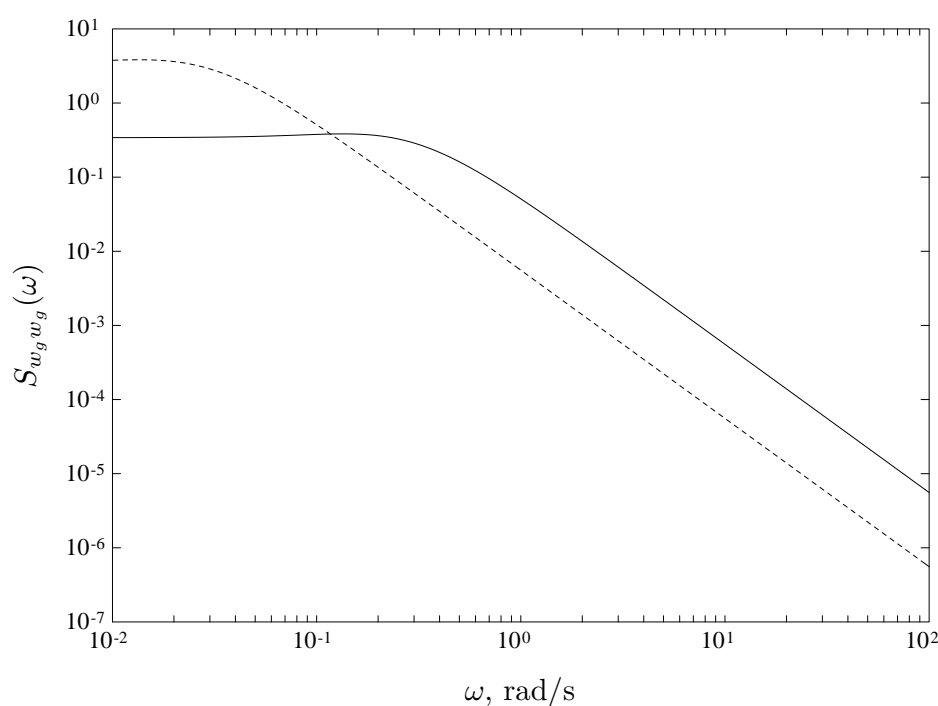


Figure 6.18: Dryden spectra for vertical turbulence for two values of L_g : Solid line: $L_g = 150$ m; dashed line $L_g = 1500$ m.

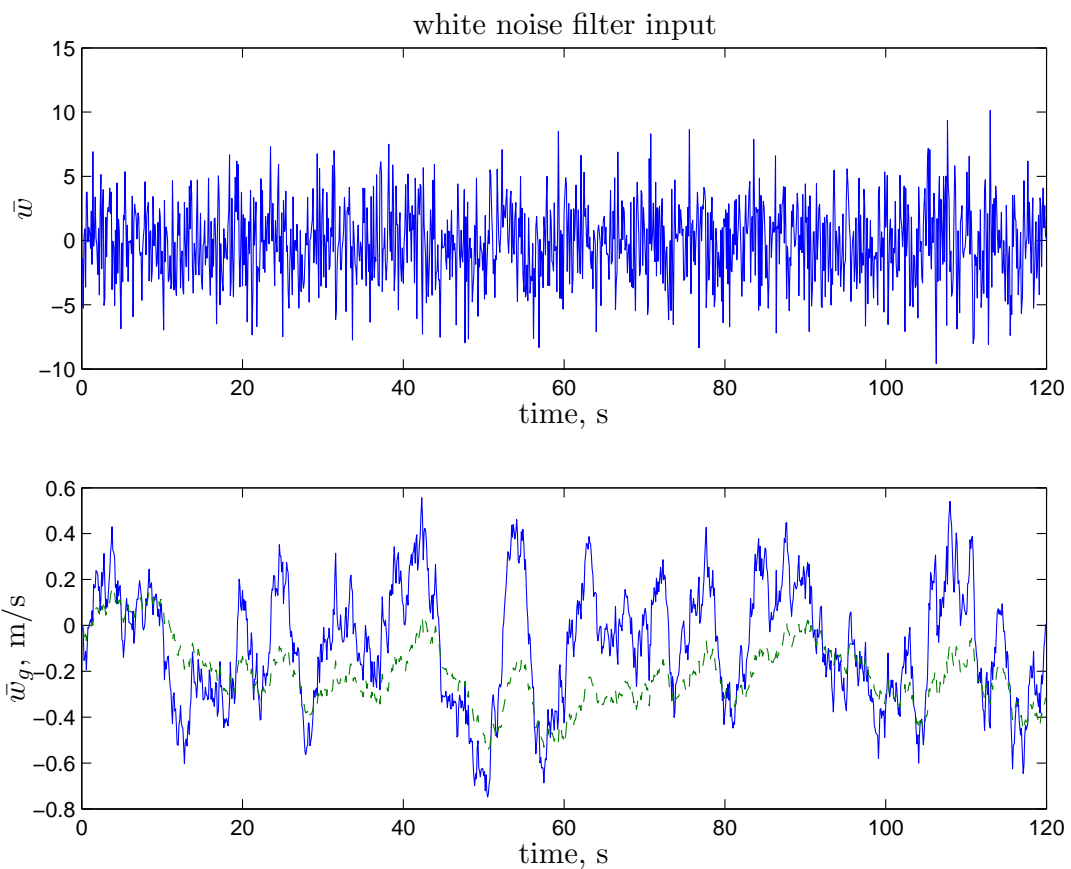


Figure 6.19: Approximated white noise \bar{w} (a), and resulting vertical turbulence signal \bar{w}_g for $L_g = 150 \text{ m}$ (continuous line) and $L_g = 1500 \text{ m}$ (dashed line) (b).

Chapter 7

Symmetric Aircraft Response to Atmospheric Turbulence

7.1 Introduction

In the preceding chapter a general description of the characteristics of atmospheric turbulence was presented. The description mainly covered meteorological and statistical issues, i.e. the physical sources of atmospheric turbulence, its temporal and spatial characteristics, its random nature and the related statistical description. Applying the available information to an analysis of aircraft behaviour in turbulent air clearly requires going into some depth into the topic of aerodynamics.

The goal of the present chapter is to extend the common mathematical models describing the aircraft motion such that it incorporates the effects of atmospheric turbulence. This model then provides a general tool for calculating responses of interest for any design or operational problem.

This chapter deals with the symmetric aircraft motions only. A similar method for calculating the aircraft's response in the asymmetric aircraft modes will be dealt with in the next chapter.

In order to simplify notations, gust velocities and aircraft responses, although they are assumed (Gaussian) distributed stochastic variables, will not be overstripped, and will be written as v_g instead of \bar{v}_g, \dots etc.

7.2 The symmetric aerodynamic forces and moments due to atmospheric turbulence

In calculations concerning the motion of aircraft, the atmospheric air usually is assumed to be in rest relative to the earth. In this chapter the air is supposed to perform non-

uniform motions relative to the earth. The aircraft's motions relative to the surrounding air determine the aerodynamic forces and moments acting on it. The aircraft's behaviour relative to the earth has to be considered for an assessment of its stability and control characteristics. If \underline{V} is the velocity of the aircraft's centre of gravity relative to the earth, \underline{V}_a the corresponding velocity relative to the air and \underline{V}_g the velocity of the air relative to the earth (the gust velocity) then, Figure 7.1,

$$\underline{V} = \underline{V}_a + \underline{V}_g \quad (7.1)$$

Variations of \underline{V}_g with time are disturbances which cause the aircraft to deviate from its intended flight path. It is assumed that the average of \underline{V}_g is zero. In order to simplify the calculation of the symmetric disturbed motions, variations of \underline{V}_g along the aircraft's wing in the spanwise direction will be neglected. Also the component v_g of \underline{V}_g along the aircraft's lateral axis need not to be considered. Only motions caused by the remaining horizontal component u_g and the vertical component w_g , both in the aircraft's plane of symmetry, have to be studied. As indicated in Figure 7.2 the positive directions of u_g , v_g and w_g are chosen along the negative stability reference frame axes.

As usual, the angle of pitch θ is the angle between the aircraft's X -axis and the horizontal plane; the flight path angle γ is the angle between \underline{V} and the horizontal plane. The angle of attack is now defined as the angle between \underline{V} and the X -axis. As a consequence the formula,

$$\alpha = \theta - \gamma \quad (7.2)$$

holds also when the air performs a non-horizontal motion relative to the earth's surface. The angle α_g between \underline{V} and \underline{V}_a is called the 'gust angle of attack'. If u_g and w_g are small relative to \underline{V} , α_g is expressed by,

$$\alpha_g = \frac{w_g}{V} \quad (7.3)$$

The angle between \underline{V}_a and the aircraft X -axis is called the 'total angle of attack' α_{tot} . Based on these definitions, α , α_g and α_{tot} are related by,

$$\alpha_{tot} = \alpha + \alpha_g \quad (7.4)$$

Provided α_g and γ are small, the relation between the x -components of \underline{V}_a and \underline{V} and u_g is,

$$V_a = V + u_g \quad (7.5)$$

Introduction of a non-dimensional gust velocity \hat{u}_g ,

$$\hat{u}_g = \frac{u_g}{V} \quad (7.6)$$

leads to,

$$V_a = V (1 + \hat{u}_g) \quad (7.7)$$

The longitudinal aerodynamic forces and the moment acting on the aircraft due to turbulence are written as X , Z and M to which the subscript g is added: X_g , Z_g and M_g . These three variables are functions of the gust velocities u_g and w_g or their non-dimensional equivalents \hat{u}_g and α_g and the time derivatives of \hat{u}_g and α_g .

Using a series expansion, X_g for example can be expressed as,

$$\begin{aligned} X_g &= \frac{\partial X_g}{\partial \hat{u}_g} \hat{u}_g + \frac{\partial X_g}{\partial \frac{\dot{\hat{u}}_g \bar{c}}{V}} \frac{\dot{\hat{u}}_g \bar{c}}{V} + \frac{\partial X_g}{\partial \frac{\ddot{\hat{u}}_g \bar{c}^2}{V^2}} \frac{\ddot{\hat{u}}_g \bar{c}^2}{V^2} + \dots \\ &+ \frac{\partial X_g}{\partial \alpha_g} \alpha_g + \frac{\partial X_g}{\partial \frac{\dot{\alpha}_g \bar{c}}{V}} \frac{\dot{\alpha}_g \bar{c}}{V} + \frac{\partial X_g}{\partial \frac{\ddot{\alpha}_g \bar{c}^2}{V^2}} \frac{\ddot{\alpha}_g \bar{c}^2}{V^2} + \dots \\ &+ \frac{1}{2!} \left(\text{2nd order terms with respect to } \hat{u}_g, \alpha_g, \frac{\dot{\hat{u}}_g \bar{c}}{V}, \frac{\dot{\alpha}_g \bar{c}}{V}, \dots \right) + \\ &+ \frac{1}{3!} (\dots \dots \dots) + \dots \text{etc.} \end{aligned} \quad (7.8)$$

This expression for the force X_g holds for any reference state of equilibrium and equals the force X_g if the expansion is extended towards an infinite number of derivatives. However, due to the assumption that \hat{u}_g and α_g remain sufficiently small (i.e. of the same order of magnitude as \hat{u} and α) only the linear terms in the above series have to be maintained. Also the derivatives with respect to $\frac{\ddot{\hat{u}}_g \bar{c}^2}{V^2}$, $\frac{\ddot{\alpha}_g \bar{c}^2}{V^2}$, ... are omitted, like the corresponding stability derivatives. The resulting expression for X_g then becomes,

$$X_g = \frac{\partial X_g}{\partial \hat{u}_g} \hat{u}_g + \frac{\partial X_g}{\partial \frac{\dot{\hat{u}}_g \bar{c}}{V}} \frac{\dot{\hat{u}}_g \bar{c}}{V} + \frac{\partial X_g}{\partial \alpha_g} \alpha_g + \frac{\partial X_g}{\partial \frac{\dot{\alpha}_g \bar{c}}{V}} \frac{\dot{\alpha}_g \bar{c}}{V} \quad (7.9)$$

It is possible to express the forces X_g , Z_g and the moment M_g in non-dimensional coefficients,

$$\begin{aligned} C_{X_g} &= \frac{X_g}{\frac{1}{2} \rho V^2 S} \\ C_{Z_g} &= \frac{Z_g}{\frac{1}{2} \rho V^2 S} \\ C_{m_g} &= \frac{M_g}{\frac{1}{2} \rho V^2 S \bar{c}} \end{aligned} \quad (7.10)$$

The expression for C_{X_g} then reads,

$$\begin{aligned} C_{X_g} &= \frac{1}{\frac{1}{2} \rho V^2 S} \frac{\partial X_g}{\partial \hat{u}_g} \hat{u}_g + \frac{1}{\frac{1}{2} \rho V^2 S} \frac{\partial X_g}{\partial \frac{\dot{\hat{u}}_g \bar{c}}{V}} \frac{\dot{\hat{u}}_g \bar{c}}{V} + \\ &+ \frac{1}{\frac{1}{2} \rho V^2 S} \frac{\partial X_g}{\partial \alpha_g} \alpha_g + \frac{1}{\frac{1}{2} \rho V^2 S} \frac{\partial X_g}{\partial \frac{\dot{\alpha}_g \bar{c}}{V}} \frac{\dot{\alpha}_g \bar{c}}{V} \end{aligned} \quad (7.11)$$

or, in an abbreviated notation,

$$C_{X_g} = C_{X_{u_g}} \hat{u}_g + C_{X_{\dot{u}_g}} \frac{\dot{\hat{u}}_g \bar{c}}{V} + C_{X_{\alpha_g}} \alpha_g + C_{X_{\dot{\alpha}_g}} \frac{\dot{\alpha}_g \bar{c}}{V} \quad (7.12)$$

In the same way C_{Z_g} and C_{m_g} can be written as,

$$C_{Z_g} = C_{Z_{u_g}} \hat{u}_g + C_{Z_{\dot{u}_g}} \frac{\dot{\hat{u}}_g \bar{c}}{V} + C_{Z_{\alpha_g}} \alpha_g + C_{Z_{\dot{\alpha}_g}} \frac{\dot{\alpha}_g \bar{c}}{V} \quad (7.13)$$

$$C_{m_g} = C_{m_{u_g}} \hat{u}_g + C_{m_{\dot{u}_g}} \frac{\dot{\hat{u}}_g \bar{c}}{V} + C_{m_{\alpha_g}} \alpha_g + C_{m_{\dot{\alpha}_g}} \frac{\dot{\alpha}_g \bar{c}}{V} \quad (7.14)$$

The partial derivatives, $C_{X_{u_g}}$, $C_{X_{\dot{u}_g}}$, etc. will be called ‘*gust derivatives*’.

7.3 Derivation of the gust derivatives for longitudinal aircraft motion

7.3.1 Introduction

Let us assume that the longitudinal forces and the moment due to atmospheric turbulence are represented by the equations,

$$\begin{aligned} C_{X_g} &= C_{X_{u_g}} \hat{u}_g + C_{X_{\dot{u}_g}} \frac{\dot{\hat{u}}_g \bar{c}}{V} + C_{X_{\alpha_g}} \alpha_g + C_{X_{\dot{\alpha}_g}} \frac{\dot{\alpha}_g \bar{c}}{V} \\ C_{Z_g} &= C_{Z_{u_g}} \hat{u}_g + C_{Z_{\dot{u}_g}} \frac{\dot{\hat{u}}_g \bar{c}}{V} + C_{Z_{\alpha_g}} \alpha_g + C_{Z_{\dot{\alpha}_g}} \frac{\dot{\alpha}_g \bar{c}}{V} \\ C_{m_g} &= C_{m_{u_g}} \hat{u}_g + C_{m_{\dot{u}_g}} \frac{\dot{\hat{u}}_g \bar{c}}{V} + C_{m_{\alpha_g}} \alpha_g + C_{m_{\dot{\alpha}_g}} \frac{\dot{\alpha}_g \bar{c}}{V} \end{aligned} \quad (7.15)$$

For each of the components u_g and w_g the atmospheric field of turbulence can be thought of as a superposition of infinitely many ‘elementary fields’. In each of these elementary fields the magnitude of the gust velocity u_g or w_g varies sinusoidally along the X -axis, as given by the real part of,

$$u_g = u_{g_{max}} e^{j\Omega x} = u_{g_{max}} e^{j\frac{\omega x}{V}} \quad (7.16)$$

$$w_g = w_{g_{max}} e^{j\Omega x} = w_{g_{max}} e^{j\frac{\omega x}{V}} \quad (7.17)$$

The gust velocities u_g and w_g are within the aircraft dimensions assumed to be invariant in the Y - and Z -directions (Figure 7.3). The wavelength in such an elementary field is given by,

$$\lambda = \frac{2\pi}{\Omega} \quad (7.18)$$

In these fields the following holds for the non-dimensional gust velocities,

$$\hat{u}_g = \hat{u}_{g_{max}} e^{j\Omega x} \quad (7.19)$$

or with,

$$s_c = \frac{x}{\bar{c}} = \frac{Vt}{\bar{c}} \quad (7.20)$$

and with the definition of the reduced frequency k_c ,

$$k_c = \Omega \bar{c} = \frac{\omega \bar{c}}{V} \quad (7.21)$$

is,

$$\hat{u}_g = \hat{u}_{g_{max}} e^{jk_c s_c} \quad (7.22)$$

Hence,

$$\frac{\dot{\hat{u}}_g \bar{c}}{V} \equiv j k_c \hat{u}_g \quad (7.23)$$

and,

$$\frac{\dot{\alpha}_g \bar{c}}{V} \equiv j k_c \alpha_g \quad (7.24)$$

Hence, in an elementary field C_{X_g} , C_{Z_g} and C_{m_g} can be expressed as,

$$C_{X_g} = \left(C_{X_{u_g}} + C_{X_{\dot{u}_g}} j k_c \right) \hat{u}_g + \left(C_{X_{\alpha_g}} + C_{X_{\dot{\alpha}_g}} j k_c \right) \alpha_g \quad (7.25)$$

$$C_{Z_g} = \left(C_{Z_{u_g}} + C_{Z_{\dot{u}_g}} j k_c \right) \hat{u}_g + \left(C_{Z_{\alpha_g}} + C_{Z_{\dot{\alpha}_g}} j k_c \right) \alpha_g \quad (7.26)$$

$$C_{m_g} = \left(C_{m_{u_g}} + C_{m_{\dot{u}_g}} j k_c \right) \hat{u}_g + \left(C_{m_{\alpha_g}} + C_{m_{\dot{\alpha}_g}} j k_c \right) \alpha_g \quad (7.27)$$

The aerodynamic forces and the moment as described above represent the complex forces and the moment if deterministic elementary harmonic gust-oscillations are encountered. The complex numbers as described above, can be represented by a gain and phase, for example,

$$C_{X_g} = \hat{C}_{X_g} e^{j\phi} \quad (7.28)$$

The pairs of gust derivatives such as $C_{X_{\alpha_g}}$ and $C_{X_{\dot{\alpha}_g}}$, describe the force- and moment buildup as a result of turbulence. This force- and moment buildup is caused by unsteady aerodynamic effects or by other aerodynamic lags such as time-delays. One aerodynamic lag caused by time-delays is called the '*gust penetration effect*' of atmospheric turbulence which is a result of the finite dimensions of an aircraft. It will be described in detail in the following sections. In the following sections we will assume that the aircraft may be considered as a wing/fuselage-horizontal tailplane combination. In that case, it is possible to derive some analytical expressions for the gust derivatives.

7.3.2 Derivation of gust derivatives with respect to \hat{u}_g

The expression for the aerodynamic forces and moment caused by an elementary field of symmetric horizontal longitudinal turbulence is,

$$C_{X_g} = \left(C_{X_{u_g}} + C_{X_{\dot{u}_g}} j k_c \right) \hat{u}_g \quad (7.29)$$

$$C_{Z_g} = \left(C_{Z_{u_g}} + C_{Z_{\dot{u}_g}} j k_c \right) \hat{u}_g \quad (7.30)$$

$$C_{m_g} = \left(C_{m_{u_g}} + C_{m_{\dot{u}_g}} j k_c \right) \hat{u}_g \quad (7.31)$$

Considering for the moment a constant horizontal gust velocity only (the elementary field has a (reduced) frequency equal to zero, hence $k_c = 0$), the variation in C_X due to u_g is,

$$C_{X_g} = C_{X_{u_g}} \hat{u}_g \quad (7.32)$$

It makes no difference to the aerodynamic force on the aircraft, whether the velocity of the aircraft relative to the earth has changed a certain amount u , or whether the velocity of the air relative to the earth has changed an equally large amount u_g . The finite airplane flies in an atmosphere with no changes in the velocity u_g over its dimensions: consequently an elementary gust-field of reduced frequency equal to zero, leads to the same aerodynamic effects due to changes in airspeed u ! Hence,

$$C_{X_{u_g}} = C_{X_u} \quad (7.33)$$

and also,

$$C_{Z_{u_g}} = C_{Z_u} \quad (7.34)$$

$$C_{m_{u_g}} = C_{m_u} \quad (7.35)$$

The above parameters will be called the *steady gust derivatives*, whilst the gust derivatives with respect to the time derivative of \hat{u}_g are called the *unsteady gust derivatives*.

Variations in C_X mainly have an influence on changes in airspeed, occurring at very low frequencies (phugoid motion). This means that fast fluctuations of C_X are only of secondary importance to the aircraft's behaviour. It seems to be justified, therefore, to neglect the terms $j k_c C_{X_{\dot{u}_g}}$ and $j k_c C_{X_{\ddot{\alpha}_g}}$. Moreover, a simple method to calculate $C_{X_{\dot{u}_g}}$ cannot be given. In the remaining part of this chapter, $C_{X_{u_g}}$ (and for that matter $C_{X_{\dot{u}_g}}$) will be equaled to zero. The remaining two unsteady gust derivatives $C_{Z_{u_g}}$ and $C_{m_{u_g}}$ will be studied next.

As for the derivation of some analytical expressions for the unsteady gust derivatives with respect to u_g , the finite dimensions of the aircraft come into effect. The unsteady gust derivatives describe the aerodynamic effect of a gust hitting the wing first, before it reaches the horizontal tailplane. It is possible to derive some analytical expressions for the unsteady gust derivatives only if the aircraft is considered to be a wing/fuselage-horizontal tailplane combination.

We emphasize that the lift or moment of an airfoil is proportional to the 'deflection' of the state variables, i.e. the angle of attack etc.. The aerodynamic model acts like a spring: aerodynamic forces and moments are proportional to the variations of the motion variables, e.g. $C_X = C_{X_\alpha} \alpha$ etc.!

Let us consider a gust reaching the wing at time instant t . After the gust is first attenuated by the downwash, it hits some instant in time later the horizontal tailplane, causing the lag

in buildup of the aerodynamic forces and moment. This instant in time, when the gust is travelling from the wing to the horizontal tailplane combination, is equal to the taillength l_h divided by the airspeed V . This aerodynamic effect is called the *gust penetration effect*. In the following, two methods will be presented for calculating the steady- and unsteady gust derivatives since the derivation of these two mentioned derivatives are coupled when the aircraft is considered to be a wing/fuselage-horizontal tailplane combination.

Method I

In the calculation of the gust derivatives $C_{Z_{\hat{u}_g}}$ and $C_{m_{\hat{u}_g}}$ given below, the magnitude and phase-difference of the gust velocity is required in a point P differing from the aircraft's centre of gravity. This subject will be discussed first, considering a discrete gust field of flow. Let the abscissa of P in a frame of reference fixed relative to the aircraft be x , the abscissa of the aerodynamic centres of the wing/fuselage and horizontal tailplane w and h and the abscissa of the centre of gravity cg , see Figure 7.4. The non-dimensional gust velocity in P is \hat{u}_{g_w} . If the centre of gravity is located between the aerodynamic centres of the wing and the horizontal tailplane, the discrete gust travels during a time $\frac{x_{cg}-x_w}{V}$ from the aerodynamic centre of the wing to the position of the centre of gravity and it takes the gust an additional time, equal to $\frac{x_h-x_{cg}}{V}$, to reach the aerodynamic centre of the horizontal tailplane. In the discrete gust field the horizontal velocity of the air at the aerodynamic centre of the wing is,

$$V_{a_w} = V + u_{g_w} = V(1 + \hat{u}_{g_w}) \quad (7.36)$$

from which follows,

$$V_{a_w}^2 = V^2 (1 + \hat{u}_{g_w})^2 \approx V^2 (1 + 2 \hat{u}_{g_w}) \quad (7.37)$$

and in the same way,

$$V_{a_h}^2 \approx V^2 (1 + 2 \hat{u}_{g_h}) \quad (7.38)$$

The non-dimensional gust velocity at the aerodynamic centre of the wing is leading in phase as compared to the non-dimensional gust velocity at the centre of gravity. The gust velocity is written in the frequency domain as,

$$\hat{u}_{g_w} = \hat{u}_g e^{j\omega\tau_1} = \hat{u}_g e^{j\omega \frac{x_{cg}-x_w}{V}} \quad (7.39)$$

The gust velocity \hat{u}_g is the gust velocity at the position of the centre of gravity. The time constants are positive. In the same way, the non-dimensional gust velocity at the horizontal tailplane can be written as,

$$\hat{u}_{g_h} = \hat{u}_g e^{-j\omega\tau_2} = \hat{u}_g e^{j\omega \frac{x_{cg}-x_h}{V}} \hat{u}_g e^{-j\omega \frac{x_h-x_{cg}}{V}} \quad (7.40)$$

The gust velocity at the horizontal tailplane is lagging in phase as compared to the gust velocity at the centre of gravity (only if the wavelength λ of the turbulence is greater than the taillength l_h . If not, the gust velocity at the horizontal tailplane will be leading in phase as compared to the gust velocity at the centre of gravity!). The aerodynamic force along the Z -axis consists of two parts: a contribution of the wing/fuselage and a contribution of the horizontal tailplane,

$$\begin{aligned} Z_w &= C_{Z_w} \frac{1}{2} \rho V^2 S \\ Z_h &= C_{Z_h} \frac{1}{2} \rho V^2 S \end{aligned} \quad (7.41)$$

The increase Z_g of the aerodynamic force Z due to the gust velocity can now, with Equations (7.37) and (7.38), be written as,

$$Z_g = C_{Z_w} \frac{1}{2} \rho V^2 S 2\hat{u}_{g_w} + C_{Z_h} \frac{1}{2} \rho V^2 S 2\hat{u}_{g_h} \quad (7.42)$$

With the expressions for the gust velocities at the aerodynamic centres of the wing and the horizontal tailplane, the increase in Z_g can now be written as,

$$Z_g(\omega) = C_{Z_w} \frac{1}{2} \rho V^2 S 2\hat{u}_g e^{j\omega\tau_1} + C_{Z_h} \frac{1}{2} \rho V^2 S 2\hat{u}_g e^{-j\omega\tau_2} \quad (7.43)$$

With the definition of the time constants, the expression becomes,

$$Z_g(\omega) = C_{Z_w} \frac{1}{2} \rho V^2 S 2\hat{u}_g e^{j\omega \frac{x_{cg} - x_w}{V}} + C_{Z_h} \frac{1}{2} \rho V^2 S \hat{u}_g e^{-j\omega \frac{x_h - x_{cg}}{V}} \quad (7.44)$$

The corresponding non-dimensional coefficient is,

$$C_{Z_g}(\omega) = C_{Z_w} 2\hat{u}_g e^{j\omega\tau_1} + C_{Z_h} 2\hat{u}_g e^{-j\omega\tau_2} \quad (7.45)$$

Remember that over a moderate frequency range, the time shift expressions, may be written as,

$$e^{-j\omega\tau} \approx 1 - j\omega\tau \quad (7.46)$$

Hence, the non-dimensional aerodynamic force may be written as,

$$\begin{aligned} C_{Z_g}(\omega) &= C_{Z_w} 2\hat{u}_g \left(1 + j\omega \frac{x_{cg} - x_w}{V} \right) + C_{Z_h} 2\hat{u}_g \left(1 + j\omega \frac{x_{cg} - x_h}{V} \right) \\ &= 2(C_{Z_w} + C_{Z_h}) \hat{u}_g + 2 \left(C_{Z_w} \frac{x_{cg} - x_w}{V} + C_{Z_h} \frac{x_{cg} - x_h}{V} \right) j\omega \hat{u}_g \\ &= 2(C_{Z_w} + C_{Z_h}) \hat{u}_g + 2 \left(C_{Z_w} \frac{x_{cg} - x_w}{\bar{c}} + C_{Z_h} \frac{x_{cg} - x_h}{\bar{c}} \right) \frac{j\omega \bar{c}}{V} \hat{u}_g \end{aligned} \quad (7.47)$$

For the time domain the expression becomes (the coefficients are considered to be constants),

$$\begin{aligned} C_{Z_g} &= 2(C_{Z_w} + C_{Z_h}) \hat{u}_g + 2 \left(C_{Z_w} \frac{x_{cg} - x_w}{\bar{c}} + C_{Z_h} \frac{x_{cg} - x_h}{\bar{c}} \right) \frac{\dot{\hat{u}}_g \bar{c}}{V} \\ &= C_{Z_{\hat{u}_g}} \hat{u}_g + C_{Z_{\dot{\hat{u}}_g}} \frac{\dot{\hat{u}}_g \bar{c}}{V} \end{aligned} \quad (7.48)$$

Hence,

$$C_{Z_{\dot{u}_g}} = 2 \left(C_{Z_w} \frac{x_{cg} - x_w}{\bar{c}} + C_{Z_h} \frac{x_{cg} - x_h}{\bar{c}} \right) \quad (7.49)$$

And remember that,

$$C_{Z_{\dot{u}_g}} = C_{Z_u} = 2(C_{Z_w} + C_{Z_h}) \approx -2 C_L \quad (7.50)$$

In steady flight the moment along the Y -axis, neglecting the contribution of forces along the X -axis, is,

$$C_m = C_{m_{ac}} - C_{Z_w} \frac{x_{cg} - x_w}{\bar{c}} - C_{Z_h} \frac{x_{cg} - x_h}{\bar{c}} = 0 \quad (7.51)$$

Combining Equations (7.49) and (7.51), $C_{Z_{\dot{u}_g}}$ can be written as,

$$C_{Z_{\dot{u}_g}} = 2 C_{m_{ac}} \quad (7.52)$$

In a manner analogous to the derivation of $C_{Z_{\dot{u}_g}}$, $C_{m_{\dot{u}_g}}$ is found to be,

$$C_{m_{\dot{u}_g}} = 2 \left(C_{m_w} \frac{x_{cg} - x_w}{\bar{c}} + C_{m_h} \frac{x_{cg} - x_h}{\bar{c}} \right) \quad (7.53)$$

In steady flight $C_m = 0$, hence,

$$C_{m_w} = -C_{m_h} \quad (7.54)$$

or,

$$C_{m_{\dot{u}_g}} = 2 \left(-C_{m_h} \frac{x_{cg} - x_w}{\bar{c}} + C_{m_h} \frac{x_{cg} - x_h}{\bar{c}} \right) \quad (7.55)$$

Using the taillength $l_h = x_h - x_w$, the resulting unsteady gust derivative $C_{m_{\dot{u}_g}}$ becomes,

$$C_{m_{\dot{u}_g}} = -2 C_{m_h} \frac{l_h}{\bar{c}} \quad (7.56)$$

Method II

Let us consider a discrete symmetric horizontal longitudinal gust reaching the wing. When the gust has reached the wing, it will induce a change in speed which will be denoted by Δu (this parameter is equivalent to the downwash angle due to a change in angle of attack). After a certain instant in time, $\tau = \frac{l_h}{V}$, the change in speed Δu will reach the horizontal tailplane, inducing a change in the aerodynamic force on it. The gust itself will reach the horizontal tailplane after the same amount of time.

Note: in contrast with the previous method we will now for simplicity's sake assume that the positions of the centre of gravity and the aerodynamic centre of the wing/fuselage coincide (see also Section 7.5). The gust velocity at the aerodynamic centre of the wing/fuselage equals in gain and phase (which is now zero degrees) the gust velocity at the centre of gravity.

The second method for calculating the gust-derivatives will describe the influence of the change in speed on the aerodynamic forces and the moment using stability derivatives with respect to u . This is a completely different approach compared to the previous method where the influence of the change in speed on the aerodynamic forces and moment was described by a change in dynamic pressure.

The total aerodynamic force along the Z -axis can be written as,

$$Z_g = C_{Z_{w_u}} \frac{1}{2} \rho V^2 S \hat{u}_g + C_{Z_{h_u}} \frac{1}{2} \rho V_h^2 S_h \hat{u}_{h_g} \quad (7.57)$$

With, in the frequency domain,

$$\hat{u}_{h_g}(\omega) = \hat{u}_g e^{-j\omega\tau} - \frac{\partial \Delta u}{\partial \hat{u}} e^{-j\omega\tau} \hat{u}_g = \left(1 - \frac{\partial \Delta u}{\partial \hat{u}}\right) e^{-j\omega\tau} \hat{u}_g = \left(1 - \frac{\partial \Delta u}{\partial \hat{u}}\right) e^{-j\omega \frac{l_h}{V}} \hat{u}_g \quad (7.58)$$

The aerodynamic force along the Z -axis can now be written as,

$$C_{Z_g}(\omega) = C_{Z_{w_u}} \hat{u}_g + C_{Z_{h_u}} \left(\frac{V_h}{V}\right)^2 \frac{S_h}{S} \left(1 - \frac{\partial \Delta u}{\partial \hat{u}}\right) e^{-j\omega \frac{l_h}{V}} \hat{u}_g \quad (7.59)$$

or,

$$\frac{C_{Z_g}}{\hat{u}_g}(\omega) = C_{Z_{w_u}} + C_{Z_{h_u}} \left(\frac{V_h}{V}\right)^2 \frac{S_h}{S} \left(1 - \frac{\partial \Delta u}{\partial \hat{u}}\right) e^{-j\omega \frac{l_h}{V}} \quad (7.60)$$

Equation (7.60) is called an '*aerodynamic frequency response function*'. For the aerodynamic moment along the Y -axis the expression becomes, neglecting the moment generated by the horizontal tail according to $C_{m_{h_u}} \left(\frac{V_h}{V}\right)^2 \frac{S_h}{S} \left(1 - \frac{\partial \Delta u}{\partial \hat{u}}\right) e^{-j\omega \frac{l_h}{V}}$,

$$\frac{C_{m_g}}{\hat{u}_g}(\omega) = C_{m_{w_u}} + C_{Z_{h_u}} \left(\frac{V_h}{V}\right)^2 \frac{S_h l_h}{S c} \left(1 - \frac{\partial \Delta u}{\partial \hat{u}}\right) e^{-j\omega \frac{l_h}{V}} \quad (7.61)$$

For the sake of completeness, the aerodynamic frequency response function for the aerodynamic force along the X -axis is also given,

$$\frac{C_{X_g}}{\hat{u}_g}(\omega) = C_{X_{w_u}} + C_{X_{h_u}} \left(\frac{V_h}{V}\right)^2 \frac{S_h}{S} \left(1 - \frac{\partial \Delta u}{\partial \hat{u}}\right) e^{-j\omega \frac{l_h}{V}} \quad (7.62)$$

Remember that,

$$e^{-j\omega\tau} \approx 1 - j\omega\tau = 1 - j\omega \frac{l_h}{V} \quad (7.63)$$

With Equation (7.63), the aerodynamic frequency response functions become,

$$\frac{C_{X_g}}{\hat{u}_g}(\omega) = C_{X_{w_u}} + C_{X_{h_u}} \left(\frac{V_h}{V}\right)^2 \frac{S_h}{S} \left(1 - \frac{\partial \Delta u}{\partial \hat{u}}\right) \left(1 - j\omega \frac{l_h}{V}\right) \quad (7.64)$$

$$\frac{C_{Z_g}}{\hat{u}_g}(\omega) = C_{Z_{w_u}} + C_{Z_{h_u}} \left(\frac{V_h}{V} \right)^2 \frac{S_h}{S} \left(1 - \frac{\partial \Delta u}{\partial \hat{u}} \right) \left(1 - j\omega \frac{l_h}{V} \right) \quad (7.65)$$

$$\frac{C_{m_g}}{\hat{u}_g}(\omega) = C_{m_{w_u}} + C_{Z_{h_u}} \left(\frac{V_h}{V} \right)^2 \frac{S_h l_h}{S \bar{c}} \left(1 - \frac{\partial \Delta u}{\partial \hat{u}} \right) \left(1 - j\omega \frac{l_h}{V} \right) \quad (7.66)$$

As an example the gust derivatives for the aerodynamic force along the Z -axis will be expanded,

$$\begin{aligned} \frac{C_{Z_g}}{\hat{u}_g}(\omega) &= C_{Z_{w_u}} + C_{Z_{h_u}} \left(\frac{V_h}{V} \right)^2 \frac{S_h}{S} \left(1 - \frac{\partial \Delta u}{\partial \hat{u}} \right) \left(1 - j\omega \frac{l_h}{V} \right) \\ &= C_{Z_{w_u}} + C_{Z_{h_u}} \left(\frac{V_h}{V} \right)^2 \frac{S_h}{S} \left(1 - \frac{\partial \Delta u}{\partial \hat{u}} \right) - C_{Z_{h_u}} \left(\frac{V_h}{V} \right)^2 \frac{S_h}{S} \left(1 - \frac{\partial \Delta u}{\partial \hat{u}} \right) j\omega \frac{l_h}{V} \\ &= \left(C_{Z_{w_u}} + C_{Z_{h_u}} \left(\frac{V_h}{V} \right)^2 \frac{S_h}{S} \left(1 - \frac{\partial \Delta u}{\partial \hat{u}} \right) \right) + \left(-C_{Z_{h_u}} \left(\frac{V_h}{V} \right)^2 \frac{S_h l_h}{S \bar{c}} \left(1 - \frac{\partial \Delta u}{\partial \hat{u}} \right) \right) \frac{\bar{c}}{V} j\omega \\ &= C_{Z_{u_g}} + C_{Z_{\dot{u}_g}} \frac{\bar{c}}{V} j\omega \end{aligned} \quad (7.67)$$

Multiplying by \hat{u}_g yields the equivalent expression for the time domain,

$$C_{Z_g} = C_{Z_{u_g}} \hat{u}_g + C_{Z_{\dot{u}_g}} \frac{\dot{\hat{u}}_g \bar{c}}{V} \quad (7.68)$$

With in Equation (7.67) and (7.68),

$$C_{Z_{u_g}} = C_{Z_u} = C_{Z_{w_u}} + C_{Z_{h_u}} \left(\frac{V_h}{V} \right)^2 \frac{S_h}{S} \left(1 - \frac{\partial \Delta u}{\partial \hat{u}} \right) \quad (7.69)$$

$$C_{Z_{\dot{u}_g}} = -C_{Z_{h_u}} \left(\frac{V_h}{V} \right)^2 \frac{S_h l_h}{S \bar{c}} \left(1 - \frac{\partial \Delta u}{\partial \hat{u}} \right) \quad (7.70)$$

The expressions for the gust derivatives regarding the aerodynamic force along the X -axis and moment along the Y - axis, can be derived in a similar way. The results are,

$$C_{X_g} = C_{X_{u_g}} \hat{u}_g + C_{X_{\dot{u}_g}} \frac{\dot{\hat{u}}_g \bar{c}}{V} \quad (7.71)$$

$$C_{m_g} = C_{m_{u_g}} \hat{u}_g + C_{m_{\dot{u}_g}} \frac{\dot{\hat{u}}_g \bar{c}}{V} \quad (7.72)$$

With in the Equations (7.71) and (7.72),

$$C_{X_{u_g}} = C_{X_u} = C_{X_{w_u}} + C_{X_{h_u}} \left(\frac{V_h}{V} \right)^2 \frac{S_h}{S} \left(1 - \frac{\partial \Delta u}{\partial \hat{u}} \right) \quad (7.73)$$

$$C_{X_{\dot{u}_g}} = -C_{X_{h_u}} \left(\frac{V_h}{V} \right)^2 \frac{S_h l_h}{S \bar{c}} \left(1 - \frac{\partial \Delta u}{\partial \hat{u}} \right) \quad (7.74)$$

$$C_{m_{u_g}} = C_{m_u} = C_{m_{w_u}} + C_{Z_{h_u}} \left(\frac{V_h}{V} \right)^2 \frac{S_h l_h}{S \bar{c}} \left(1 - \frac{\partial \Delta u}{\partial \hat{u}} \right) \quad (7.75)$$

$$C_{m_{\dot{u}_g}} = -C_{Z_{h_u}} \left(\frac{V_h}{V} \right)^2 \frac{S_h l_h^2}{S \bar{c}^2} \left(1 - \frac{\partial \Delta u}{\partial \hat{u}} \right) \quad (7.76)$$

In the previous two methods we considered the aircraft to be a wing/fuselage-horizontal tailplane combination and the aerodynamics to be steady. Unsteady aerodynamic effects were not incorporated in the derivation of the steady and the unsteady gust derivatives. The unsteady gust derivatives owe their existence to the fact that an aircraft has finite dimensions. The reason why we called the gust derivatives ‘unsteady’ has nothing to do with the unsteadiness of the aerodynamics. Keep in mind that the unsteady gust derivative of the aerodynamic force along the X -axis with respect to the time derivative of the speed induced gust, \dot{u}_g , is usually set equal to zero!

7.3.3 Derivation of gust derivatives with respect to α_g

Let us consider a discrete symmetrical vertical gust reaching the wing. When the gust has reached the wing, it will induce a change in downwash which will be denoted by ϵ . After a certain instant in time, $\tau = \frac{l_h}{V}$, the change in angle of attack will reach the horizontal tailplane, inducing a change in the aerodynamic force on it. The gust itself will reach the horizontal tailplane after the same amount of time.

Again, we will assume the positions of the aerodynamic centre of the wing/fuselage and centre of gravity to coincide.

The total aerodynamic force along the Z -axis can be written as,

$$Z_g = C_{Z_{w\alpha}} \frac{1}{2} \rho V^2 S \alpha_g + C_{Z_{h\alpha}} \frac{1}{2} \rho V_h^2 S_h \alpha_{h_g} \quad (7.77)$$

With, in the frequency domain,

$$\alpha_{h_g}(\omega) = \alpha_g e^{-j\omega\tau} - \frac{\partial\epsilon}{\partial\alpha} e^{-j\omega\tau} \alpha_g = \left(1 - \frac{\partial\epsilon}{\partial\alpha}\right) e^{-j\omega\tau} \alpha_g = \left(1 - \frac{\partial\epsilon}{\partial\alpha}\right) e^{-j\omega\frac{l_h}{V}} \alpha_g \quad (7.78)$$

The aerodynamic force along the Z -axis can now be written as,

$$C_{Z_g}(\omega) = C_{Z_{w\alpha}} \alpha_g + C_{Z_{h\alpha}} \left(\frac{V_h}{V}\right)^2 \frac{S_h}{S} \left(1 - \frac{\partial\epsilon}{\partial\alpha}\right) e^{-j\omega\frac{l_h}{V}} \alpha_g \quad (7.79)$$

or,

$$\frac{C_{Z_g}}{\alpha_g}(\omega) = C_{Z_{w\alpha}} + C_{Z_{h\alpha}} \left(\frac{V_h}{V}\right)^2 \frac{S_h}{S} \left(1 - \frac{\partial\epsilon}{\partial\alpha}\right) e^{-j\omega\frac{l_h}{V}} \quad (7.80)$$

For the aerodynamic moment along the Y -axis, the aerodynamic frequency response function becomes, again neglecting the horizontal tailplane contribution according to

$$C_{m_{h\alpha}} \left(\frac{V_h}{V}\right)^2 \frac{S_h}{S} \left(1 - \frac{\partial\epsilon}{\partial\alpha}\right) e^{-j\omega\frac{l_h}{V}},$$

$$\frac{C_{m_g}}{\alpha_g}(\omega) = C_{m_{w\alpha}} + C_{Z_{h\alpha}} \left(\frac{V_h}{V}\right)^2 \frac{S_h l_h}{S c} \left(1 - \frac{\partial\epsilon}{\partial\alpha}\right) e^{-j\omega\frac{l_h}{V}} \quad (7.81)$$

For the sake of completeness, the aerodynamic frequency response function for the aerodynamic force along the X -axis is equal to,

$$\frac{C_{X_g}}{\alpha_g}(\omega) = C_{X_{w\alpha}} + C_{X_{h\alpha}} \left(\frac{V_h}{V}\right)^2 \frac{S_h}{S} \left(1 - \frac{\partial\epsilon}{\partial\alpha}\right) e^{-j\omega\frac{l_h}{V}} \quad (7.82)$$

As an example, the aerodynamic frequency response function for the force along the Z -axis with respect to the angle of attack induced by the gust, α_g , will be expanded. The time-delay will be written as a first order Taylor polynomial,

$$\begin{aligned}\frac{C_{Z_g}}{\alpha_g}(\omega) &= C_{Z_{w\alpha}} + C_{Z_{h\alpha}} \left(\frac{V_h}{V} \right)^2 \frac{S_h}{S} \left(1 - \frac{\partial \epsilon}{\partial \alpha} \right) \left(1 - j\omega \frac{l_h}{V} \right) \\ &= C_{Z_{w\alpha}} + C_{Z_{h\alpha}} \left(\frac{V_h}{V} \right)^2 \frac{S_h}{S} \left(1 - \frac{\partial \epsilon}{\partial \alpha} \right) - C_{Z_{h\alpha}} \left(\frac{V_h}{V} \right)^2 \frac{S_h}{S} \left(1 - \frac{\partial \epsilon}{\partial \alpha} \right) \frac{l_h}{V} j\omega \\ &= \left(C_{Z_{w\alpha}} + C_{Z_{h\alpha}} \left(\frac{V_h}{V} \right)^2 \frac{S_h}{S} \left(1 - \frac{\partial \epsilon}{\partial \alpha} \right) \right) + \left(-C_{Z_{h\alpha}} \left(\frac{V_h}{V} \right)^2 \frac{S_h l_h}{S \bar{c}} \left(1 - \frac{\partial \epsilon}{\partial \alpha} \right) \right) \frac{\bar{c}}{V} j\omega \\ &= C_{Z_{\dot{\alpha}_g}} + C_{Z_{\dot{\alpha}_g}} \frac{\bar{c}}{V} j\omega\end{aligned}\quad (7.83)$$

with,

$$C_{Z_{\dot{\alpha}_g}} = C_{Z_{\dot{\alpha}}} = C_{Z_{w\alpha}} + C_{Z_{h\alpha}} \left(\frac{V_h}{V} \right)^2 \frac{S_h}{S} \left(1 - \frac{\partial \epsilon}{\partial \alpha} \right) \quad (7.84)$$

And,

$$\begin{aligned}C_{Z_{\dot{\alpha}_g}} &= -C_{Z_{h\alpha}} \left(\frac{V_h}{V} \right)^2 \frac{S_h l_h}{S \bar{c}} \left(1 - \frac{\partial \epsilon}{\partial \alpha} \right) = C_{Z_{h\alpha}} \left(\frac{V_h}{V} \right)^2 \frac{S_h l_h}{S \bar{c}} \frac{\partial \epsilon}{\partial \alpha} - C_{Z_{h\alpha}} \left(\frac{V_h}{V} \right)^2 \frac{S_h l_h}{S \bar{c}} = \\ &= C_{Z_{\dot{\alpha}}} - C_{Z_q}\end{aligned}\quad (7.85)$$

In the above equation is,

$$C_{Z_{\dot{\alpha}}} = C_{Z_{h\alpha}} \left(\frac{V_h}{V} \right)^2 \frac{S_h l_h}{S \bar{c}} \frac{\partial \epsilon}{\partial \alpha} \quad (7.86)$$

$$C_{Z_q} = C_{Z_{h\alpha}} \left(\frac{V_h}{V} \right)^2 \frac{S_h l_h}{S \bar{c}} \quad (7.87)$$

which are the theoretical horizontal tailplane contributions to the stability derivatives $C_{Z_{\dot{\alpha}}}$ and C_{Z_q} , (Gerlach, 1966).

The expressions for the gust derivatives regarding the aerodynamic force along the X -axis and moment along the Y - axis, can be derived in a similar way. The results are,

$$C_{X_{\alpha_g}} = C_{X_\alpha} \quad (7.88)$$

$$C_{X_{\dot{\alpha}_g}} = C_{X_{\dot{\alpha}}} - C_{X_q} \quad (7.89)$$

$$C_{m_{\alpha_g}} = C_{m_\alpha} \quad (7.90)$$

$$C_{m_{\dot{\alpha}_g}} = C_{m_{\dot{\alpha}}} - C_{m_q} \quad (7.91)$$

In the previous we have considered the aircraft to be a wing/fuselage-horizontal tailplane combination and the aerodynamics of the wing and the horizontal tailplane to be steady. Unsteady aerodynamic effects were not incorporated in the derivation of the steady and unsteady gust derivatives. The unsteady gust derivatives owe their existance to the fact that an aircraft has finite dimensions. The reason why we called the gust derivatives ‘unsteady’ has nothing to do with the unsteadiness of the aerodynamics. Keep in mind

that the unsteady gust derivative of the aerodynamic force along the X -axis with respect to the time derivative of the, by the gust velocity induced angle of attack, α_g , is usually set equal to zero!

7.4 Equations for the symmetric motions of aircraft in atmospheric turbulence

7.4.1 Introduction

In this section the equations of motion for a rigid aircraft in a field of atmospheric turbulence will be presented. The equations of motion for a rigid aircraft in smooth atmospheric conditions have been derived in (Gerlach, 1966). The general aerodynamic forces and the moment due to atmospheric turbulence have been derived in the previous sections. As a recapitulation the general aerodynamic forces and the moment are in the frequency domain,

$$C_{X_g}(\omega) = \frac{C_{X_g}}{\hat{u}_g}(\omega) \hat{u}_g(\omega) + \frac{C_{X_g}}{\alpha_g}(\omega) \alpha_g(\omega) \quad (7.92)$$

$$C_{Z_g}(\omega) = \frac{C_{Z_g}}{\hat{u}_g}(\omega) \hat{u}_g(\omega) + \frac{C_{Z_g}}{\alpha_g}(\omega) \alpha_g(\omega) \quad (7.93)$$

$$C_{m_g}(\omega) = \frac{C_{m_g}}{\hat{u}_g}(\omega) \hat{u}_g(\omega) + \frac{C_{m_g}}{\alpha_g}(\omega) \alpha_g(\omega) \quad (7.94)$$

We represent the aerodynamic forces and the moment as a function of aerodynamic frequency response functions for the purpose of describing the gust penetration effect in one of the following sections. In the previous sections, however, we have assumed the aerodynamic frequency response functions may be described by,

$$C_{X_g}(\omega) = C_{X_{u_g}} \hat{u}_g(\omega) + C_{X_{\dot{u}_g}} \frac{j\omega \hat{u}_g(\omega) \bar{c}}{V} + C_{X_{\alpha_g}} \alpha_g(\omega) + C_{X_{\dot{\alpha}_g}} \frac{j\omega \alpha_g(\omega) \bar{c}}{V} \quad (7.95)$$

$$C_{Z_g}(\omega) = C_{Z_{u_g}} \hat{u}_g(\omega) + C_{Z_{\dot{u}_g}} \frac{j\omega \hat{u}_g(\omega) \bar{c}}{V} + C_{Z_{\alpha_g}} \alpha_g(\omega) + C_{Z_{\dot{\alpha}_g}} \frac{j\omega \alpha_g(\omega) \bar{c}}{V} \quad (7.96)$$

$$C_{m_g}(\omega) = C_{m_{u_g}} \hat{u}_g(\omega) + C_{m_{\dot{u}_g}} \frac{j\omega \hat{u}_g(\omega) \bar{c}}{V} + C_{m_{\alpha_g}} \alpha_g(\omega) + C_{m_{\dot{\alpha}_g}} \frac{j\omega \alpha_g(\omega) \bar{c}}{V} \quad (7.97)$$

or equivalently in the time domain, assuming constant parameters,

$$C_{X_g} = C_{X_{u_g}} \hat{u}_g + C_{X_{\dot{u}_g}} \frac{\dot{\hat{u}}_g \bar{c}}{V} + C_{X_{\alpha_g}} \alpha_g + C_{X_{\dot{\alpha}_g}} \frac{\dot{\alpha}_g \bar{c}}{V} \quad (7.98)$$

$$C_{Z_g} = C_{Z_{u_g}} \hat{u}_g + C_{Z_{\dot{u}_g}} \frac{\dot{\hat{u}}_g \bar{c}}{V} + C_{Z_{\alpha_g}} \alpha_g + C_{Z_{\dot{\alpha}_g}} \frac{\dot{\alpha}_g \bar{c}}{V} \quad (7.99)$$

$$C_{m_g} = C_{m_{u_g}} \hat{u}_g + C_{m_{\dot{u}_g}} \frac{\dot{\hat{u}}_g \bar{c}}{V} + C_{m_{\alpha_g}} \alpha_g + C_{m_{\dot{\alpha}_g}} \frac{\dot{\alpha}_g \bar{c}}{V} \quad (7.100)$$

Remember that the unsteady gust derivatives for the aerodynamic force along the X -axis are usually set to zero, hence Equation (7.98) becomes,

$$C_{X_g} = C_{X_{u_g}} \hat{u}_g + C_{X_{\alpha_g}} \alpha_g \quad (7.101)$$

In the following sections the equations of motion will be given.

7.4.2 The symmetric equations of motion for aircraft in atmospheric turbulence

The equations of motion for a rigid aircraft have been derived in (Gerlach, 1966) and (Etkin, 1972). These equations are valid for small deviations from steady horizontal flight. The equations are extended for flight in a turbulent atmosphere and can be written as follows (with $D_c = \frac{\bar{c}}{V} \frac{d}{dt}$),

$$\begin{bmatrix} C_{X_u} - 2\mu_c D_c & C_{X_\alpha} & C_{Z_0} & 0 \\ C_{Z_u} & C_{Z_\alpha} + (C_{Z_{\dot{\alpha}}} - 2\mu_c) D_c & -C_{X_0} & 2\mu_c + C_{Z_q} \\ 0 & 0 & -D_c & 1 \\ C_{m_u} & C_{m_\alpha} + C_{m_{\dot{\alpha}}} D_c & 0 & C_{m_q} - 2\mu_c K_Y^2 D_c \end{bmatrix} \begin{bmatrix} \hat{u} \\ \alpha \\ \theta \\ \frac{q\bar{c}}{V} \end{bmatrix} = \\ - \begin{bmatrix} C_{X_{\delta_e}} & C_{X_{u_g}} & 0 & C_{X_{\alpha_g}} & 0 \\ C_{Z_{\delta_e}} & C_{Z_{u_g}} & C_{Z_{\dot{u}_g}} & C_{Z_{\alpha_g}} & C_{Z_{\dot{\alpha}_g}} \\ 0 & 0 & 0 & 0 & 0 \\ C_{m_{\delta_e}} & C_{m_{u_g}} & C_{m_{\dot{u}_g}} & C_{m_{\alpha_g}} & C_{m_{\dot{\alpha}_g}} \end{bmatrix} \begin{bmatrix} \delta_e \\ \hat{u}_g \\ D_c \hat{u}_g \\ \alpha_g \\ D_c \alpha_g \end{bmatrix} \quad (7.102)$$

The general state-space representation,

$$\dot{\underline{x}} = A \underline{x} + B \underline{u} \quad (7.103)$$

can be obtained by rearranging Equation (7.102), see (Stevens & Lewis, 1992). The final result, in abbreviated notation, is,

$$\begin{bmatrix} \dot{u} \\ \dot{\alpha} \\ \dot{\theta} \\ \frac{\dot{q}\bar{c}}{V} \end{bmatrix} = \begin{bmatrix} x_u & x_\alpha & x_\theta & 0 \\ z_u & z_\alpha & z_\theta & z_q \\ 0 & 0 & 0 & \frac{V}{\bar{c}} \\ m_u & m_\alpha & m_\theta & m_q \end{bmatrix} \begin{bmatrix} \hat{u} \\ \alpha \\ \theta \\ \frac{q\bar{c}}{V} \end{bmatrix} + \begin{bmatrix} x_{\delta_e} & x_{u_g} & 0 & x_{\alpha_g} & 0 \\ z_{\delta_e} & z_{u_g} & z_{\dot{u}_g} & z_{\alpha_g} & z_{\dot{\alpha}_g} \\ 0 & 0 & 0 & 0 & 0 \\ m_{\delta_e} & m_{u_g} & m_{\dot{u}_g} & m_{\alpha_g} & m_{\dot{\alpha}_g} \end{bmatrix} \begin{bmatrix} \delta_e \\ \hat{u}_g \\ \dot{u}_g \\ \frac{\dot{q}\bar{c}}{V} \\ \alpha_g \\ \dot{\alpha}_g \end{bmatrix} \quad (7.104)$$

The definition of the newly introduced symbols are recapitulated in the Tables 7.1 and 7.2. The turbulence inputs are generated by turbulence filters as discussed in Chapter 6 (Dryden models),

$$\dot{u}_g = \left[-\frac{V}{L_g} \right] u_g + \left[\sigma_{u_g} \sqrt{\frac{2V}{L_g}} \right] w_1 \quad (7.105)$$

$$\begin{bmatrix} \dot{w}_g \\ \dot{w}_g^* \end{bmatrix} = \begin{bmatrix} 0 & 1 \\ -\frac{V^2}{L_g^2} & -2\frac{V}{L_g} \end{bmatrix} \begin{bmatrix} w_g \\ w_g^* \end{bmatrix} + \begin{bmatrix} \sigma_{w_g} \sqrt{\frac{3V}{L_g}} \\ (1 - 2\sqrt{3}) \sigma_{w_g} \sqrt{\left(\frac{V}{L_g}\right)^3} \end{bmatrix} w_3 \quad (7.106)$$

with w_1 and w_3 white noise inputs. The non-dimensional counterparts of these equations are,

$$\dot{\hat{u}}_g = \left[-\frac{V}{L_g} \right] \hat{u}_g + \left[\sigma_{\hat{u}_g} \sqrt{\frac{2V}{L_g}} \right] w_1 \quad (7.107)$$

$$\begin{bmatrix} \dot{\alpha}_g \\ \dot{\alpha}_g^* \end{bmatrix} = \begin{bmatrix} 0 & 1 \\ -\frac{V^2}{L_g^2} & -2\frac{V}{L_g} \end{bmatrix} \begin{bmatrix} \alpha_g \\ \alpha_g^* \end{bmatrix} + \begin{bmatrix} \sigma_{\alpha_g} \sqrt{\frac{3V}{L_g}} \\ (1 - 2\sqrt{3}) \sigma_{\alpha_g} \sqrt{\left(\frac{V}{L_g}\right)^3} \end{bmatrix} w_3 \quad (7.108)$$

If the turbulence filters Equations (7.107) and (7.108) are added to the equations of motion (7.104), it is possible to write,

$$\begin{bmatrix} \dot{\hat{u}} \\ \dot{\alpha} \\ \dot{\theta} \\ \dot{\frac{q\bar{c}}{V}} \\ \dot{\hat{u}}_g \\ \dot{\alpha}_g \\ \dot{\alpha}_g^* \end{bmatrix} = \begin{bmatrix} x_u & x_\alpha & x_\theta & 0 & x_{u_g} & x_{\alpha_g} & 0 \\ z_u & z_\alpha & z_\theta & z_q & z_{u_g} - z_{\hat{u}_g} \frac{V}{L_g} \frac{\bar{c}}{V} & z_{\alpha_g} & z_{\dot{\alpha}_g} \frac{\bar{c}}{V} \\ 0 & 0 & 0 & \frac{V}{\bar{c}} & 0 & 0 & 0 \\ m_u & m_\alpha & m_\theta & m_q & m_{u_g} - m_{\hat{u}_g} \frac{V}{L_g} \frac{\bar{c}}{V} & m_{\alpha_g} & m_{\dot{\alpha}_g} \frac{\bar{c}}{V} \\ 0 & 0 & 0 & 0 & -\frac{V}{L_g} & 0 & 0 \\ 0 & 0 & 0 & 0 & 0 & 0 & 1 \\ 0 & 0 & 0 & 0 & 0 & -\frac{V^2}{L_g^2} & -2\frac{V}{L_g} \end{bmatrix} \begin{bmatrix} \hat{u} \\ \alpha \\ \theta \\ \frac{q\bar{c}}{V} \\ \hat{u}_g \\ \alpha_g \\ \alpha_g^* \end{bmatrix} + \begin{bmatrix} x_{\delta_e} & 0 & 0 \\ z_{\delta_e} & z_{\hat{u}_g} \frac{\bar{c}}{V} \sigma_{\hat{u}_g} \sqrt{\frac{2V}{L_g}} & z_{\dot{\alpha}_g} \frac{\bar{c}}{V} \sigma_{\alpha_g} \sqrt{\frac{3V}{L_g}} \\ 0 & 0 & 0 \\ m_{\delta_e} & m_{\hat{u}_g} \frac{\bar{c}}{V} \sigma_{\hat{u}_g} \sqrt{\frac{2V}{L_g}} & m_{\dot{\alpha}_g} \frac{\bar{c}}{V} \sigma_{\alpha_g} \sqrt{\frac{3V}{L_g}} \\ 0 & \sigma_{\hat{u}_g} \sqrt{\frac{2V}{L_g}} & 0 \\ 0 & 0 & \sigma_{\alpha_g} \sqrt{\frac{3V}{L_g}} \\ 0 & 0 & (1 - 2\sqrt{3}) \sigma_{\alpha_g} \sqrt{\left(\frac{V}{L_g}\right)^3} \end{bmatrix} \begin{bmatrix} \delta_e \\ w_1 \\ w_3 \end{bmatrix} \quad (7.109)$$

Equation (7.109) is the general non-dimensional state-space model describing the symmetric motions of an aircraft flying in turbulent air.

7.5 Modeling the gust penetration effect

Because of the distinct contributions of the wing and the horizontal tailplane in the buildup of the aerodynamic forces and the moment, the term ‘gust penetration effect’ has been introduced. This aerodynamic phenomenon is caused by the finite dimensions of an aircraft: a gust hitting the wing will be attenuated by the downwash and will then travel over an instant in time, equal to the taillength l_h divided by the the airspeed V , till it reaches the horizontal tailplane. The concept of aerodynamic frequency response functions has been introduced in the previous sections and enables us to describe this aerodynamic

phenomenon exactly if the aircraft is to be considered a wing/fuselage-horizontal tailplane combination and other ‘unsteady’ aerodynamic effects are neglected. The aerodynamic frequency response functions, as derived in the previous sections, are, for symmetric horizontal longitudinal atmospheric turbulence,

$$\frac{C_{X_g}}{\hat{u}_g}(\omega) = C_{X_{w_u}} + C_{X_{h_u}} \left(\frac{V_h}{V} \right)^2 \frac{S_h}{S} \left(1 - \frac{\partial \Delta u}{\partial \hat{u}} \right) e^{-j\omega \frac{l_h}{V}} \quad (7.110)$$

$$\frac{C_{Z_g}}{\hat{u}_g}(\omega) = C_{Z_{w_u}} + C_{Z_{h_u}} \left(\frac{V_h}{V} \right)^2 \frac{S_h}{S} \left(1 - \frac{\partial \Delta u}{\partial \hat{u}} \right) e^{-j\omega \frac{l_h}{V}} \quad (7.111)$$

$$\frac{C_{m_g}}{\hat{u}_g}(\omega) = C_{m_{w_u}} + C_{Z_{h_u}} \left(\frac{V_h}{V} \right)^2 \frac{S_h l_h}{S \bar{c}} \left(1 - \frac{\partial \Delta u}{\partial \hat{u}} \right) e^{-j\omega \frac{l_h}{V}} \quad (7.112)$$

and for symmetric vertical atmospheric turbulence,

$$\frac{C_{X_g}}{\alpha_g}(\omega) = C_{X_{w_\alpha}} + C_{X_{h_\alpha}} \left(\frac{V_h}{V} \right)^2 \frac{S_h}{S} \left(1 - \frac{\partial \epsilon}{\partial \alpha} \right) e^{-j\omega \frac{l_h}{V}} \quad (7.113)$$

$$\frac{C_{Z_g}}{\alpha_g}(\omega) = C_{Z_{w_\alpha}} + C_{Z_{h_\alpha}} \left(\frac{V_h}{V} \right)^2 \frac{S_h}{S} \left(1 - \frac{\partial \epsilon}{\partial \alpha} \right) e^{-j\omega \frac{l_h}{V}} \quad (7.114)$$

$$\frac{C_{m_g}}{\alpha_g}(\omega) = C_{m_{w_\alpha}} + C_{Z_{h_\alpha}} \left(\frac{V_h}{V} \right)^2 \frac{S_h l_h}{S \bar{c}} \left(1 - \frac{\partial \epsilon}{\partial \alpha} \right) e^{-j\omega \frac{l_h}{V}} \quad (7.115)$$

In the following, two approximations of the full set of equations of motion will be given: an approximation for the phugoid and an approximation for the short period mode.

The approximation of the short period mode will be described in detail; the derivation of the equations for the approximation of the phugoid can be derived in an equivalent manner and is left for the interested reader.

As seen in the theoretical aerodynamic frequency response functions, an unpractical term for the time domain arises: the time-delay. How to cope with this factor will be described in the following. One can use the approximation for the time-delay by using a first order Taylor polynomial resulting in the derived steady and unsteady gust derivatives. For the frequency domain the time-delay can be used as such,

$$e^{j\omega\tau} = \cos \omega\tau + j \sin \omega\tau \quad (7.116)$$

Remember that for harmonic oscillations the Laplace variable s is equal to (with j the square-root of -1),

$$s = j\omega \quad (7.117)$$

Since we are deriving transfer functions for the aircraft concerned, this substitution is justified.

Let us assume that the airspeed will not change during the passage of a field of turbulent flow and that the reference state was steady horizontal flight. The full set of equations

of motion for a rigid aircraft can then be reduced to the set of equations for the Laplace domain,

$$\begin{bmatrix} C_{z_\alpha} + (C_{z_\dot{\alpha}} - 2\mu_c) \frac{\bar{c}}{V} s & C_{Z_q} + 2\mu_c \\ C_{m_\alpha} + C_{m_\dot{\alpha}} \frac{\bar{c}}{V} s & C_{m_q} - 2\mu_c K_y^2 \frac{\bar{c}}{V} s \end{bmatrix} \cdot \begin{bmatrix} \alpha(s) \\ \frac{q\bar{c}}{V}(s) \end{bmatrix} = \begin{bmatrix} -\frac{C_{Z_g}}{\alpha_g}(s) \\ -\frac{C_{m_g}}{\alpha_g}(s) \end{bmatrix} \alpha_g(s) \quad (7.118)$$

If the time-delays in the aerodynamic frequency response functions, which were given on the previous page, are approximated by a first order Taylor polynomial, the equations of motion become,

$$\begin{bmatrix} C_{z_\alpha} + (C_{z_\dot{\alpha}} - 2\mu_c) \frac{\bar{c}}{V} s & C_{Z_q} + 2\mu_c \\ C_{m_\alpha} + C_{m_\dot{\alpha}} \frac{\bar{c}}{V} s & C_{m_q} - 2\mu_c K_y^2 \frac{\bar{c}}{V} s \end{bmatrix} \cdot \begin{bmatrix} \alpha(s) \\ \frac{q\bar{c}}{V}(s) \end{bmatrix} = - \begin{bmatrix} C_{Z_{\alpha_g}} + C_{Z_{\dot{\alpha}_g}} \frac{\bar{c}}{V} s \\ C_{m_{\alpha_g}} + C_{m_{\dot{\alpha}_g}} \frac{\bar{c}}{V} s \end{bmatrix} \alpha_g(s) \quad (7.119)$$

or in the time domain,

$$\begin{bmatrix} C_{z_\alpha} + (C_{z_\dot{\alpha}} - 2\mu_c) D_c & C_{Z_q} + 2\mu_c \\ C_{m_\alpha} + C_{m_\dot{\alpha}} D_c & C_{m_q} - 2\mu_c K_y^2 D_c \end{bmatrix} \begin{bmatrix} \alpha \\ \frac{q\bar{c}}{V} \end{bmatrix} = - \begin{bmatrix} C_{Z_{\alpha_g}} & C_{Z_{\dot{\alpha}_g}} \\ C_{m_{\alpha_g}} & C_{m_{\dot{\alpha}_g}} \end{bmatrix} \begin{bmatrix} \alpha_g \\ D_c \alpha_g \end{bmatrix} \quad (7.120)$$

Equation (7.118) can be used to calculate transfer functions using Cramer's rule,

$$H_{\alpha\alpha_g}(s) = \frac{\text{num}_{\alpha\alpha_g}}{\text{den}} \quad (7.121)$$

$$H_{q\alpha_g}(s) = \frac{\text{num}_{q\alpha_g}}{\text{den}} \quad (7.122)$$

With,

$$\begin{aligned} \text{num}_{\alpha\alpha_g} &= 2\mu_c K_Y^2 \frac{C_{Z_g}}{\alpha_g}(s) \frac{\bar{c}}{V} s - C_{m_q} \frac{C_{Z_g}}{\alpha_g}(s) + (C_{Z_q} + 2\mu_c) \frac{C_{m_g}}{\alpha_g}(s) \\ \text{num}_{q\alpha_g} &= \left((2\mu_c - C_{Z_\dot{\alpha}}) \frac{C_{m_g}}{\alpha_g}(s) + C_{m_\dot{\alpha}} \frac{C_{Z_g}}{\alpha_g}(s) \right) \frac{\bar{c}}{V} s + C_{m_\alpha} \frac{C_{Z_g}}{\alpha_g}(s) - C_{Z_\alpha} \frac{C_{m_g}}{\alpha_g}(s) \\ \text{den} &= 2\mu_c K_Y^2 (2\mu_c - C_{Z_\dot{\alpha}}) \left(\frac{\bar{c}}{V} s \right)^2 + \\ &+ (C_{m_q} (C_{Z_\dot{\alpha}} - 2\mu_c) - 2\mu_c K_Y^2 C_{Z_\alpha} - (C_{Z_q} + 2\mu_c) C_{m_\dot{\alpha}}) \frac{\bar{c}}{V} s + \\ &+ C_{Z_\alpha} C_{m_q} - (C_{Z_q} + 2\mu_c) C_{m_\alpha} \end{aligned}$$

The expressions for the aerodynamic frequency response functions can be used in the above transfer functions if $j\omega$ is replaced by the Laplace variable s in the aerodynamic frequency response functions. However, approximations for the aerodynamic frequency response functions using a Padé- or first order Taylor approximation for the time-delay, can also be used,

$$e^{\tau s} = 1 + \tau s \quad (\text{Taylor}) \quad (7.123)$$

$$e^{\tau s} = \frac{1 + \frac{\tau}{2}s}{1 - \frac{\tau}{2}s} \quad (\text{Padé}) \quad (7.124)$$

For a time domain analysis only n^{th} -order Padé- or Taylor-polynomial approximations can be used, with n smaller than infinity. Remember that a time delay has a state space realization of infinite order.

For a phugoid approximation the equation similar to Equation (7.118) becomes,

$$\begin{bmatrix} C_{X_u} - 2\mu_c \frac{\bar{c}}{V} s & C_{Z_0} & 0 \\ C_{Z_u} & 0 & 2\mu_c \\ 0 & -\frac{\bar{c}}{V} s & 1 \end{bmatrix} \cdot \begin{bmatrix} \hat{u}(s) \\ \theta(s) \\ \frac{q\bar{c}}{V}(s) \end{bmatrix} = \begin{bmatrix} -\frac{C_{X_g}}{\hat{u}_g}(s) \\ -\frac{C_{Z_g}}{\hat{u}_g}(s) \\ 0 \end{bmatrix} \hat{u}_g(s) \quad (7.125)$$

This problem is left for the interested reader.

Note

In the previous sections (except for method I in subsection 7.3.2) we considered the positions of the aircraft's centre of gravity and aerodynamic centre of the wing/fuselage to coincide. As an example, the gust derivatives will now be determined for the aerodynamic force along the Z -axis due to a vertical gust, if the positions of the aircraft's centre of gravity and aerodynamic centre of the wing/fuselage do not coincide. Consider the position of the aircraft's centre of gravity located between the positions of the aerodynamic centres of the wing and the horizontal tailplane. If a gust reaches the aerodynamic centre of the wing, it will take the gust τ_1 seconds to reach the position of the aircraft's centre of gravity, which is the reference position in our calculations. The time constant is equal to $\tau_1 = \frac{x_{cg} - x_w}{V}$. The gust will reach the aerodynamic centre of the horizontal tailplane after an additional time, equal to τ_2 seconds. The time constant is equal to $\tau_2 = \frac{x_h - x_{cg}}{V}$. The downwash will reach the horizontal tailplane after $\tau = \tau_1 + \tau_2$ seconds (see Figure 7.5).

Now one can write for the aerodynamic force along the Z -axis due to a vertical gust:

$$C_{Z_g}(\omega) = C_{Z_{w\alpha}} \alpha_g e^{j\omega\tau_1} + C_{Z_{h\alpha}} \left(\frac{V_h}{V} \right)^2 \frac{S_h}{S} \alpha_{h_g} \quad (7.126)$$

with,

$$\alpha_{h_g}(\omega) = \alpha_g e^{-j\omega\tau_2} - \frac{\partial \epsilon}{\partial \alpha} \alpha_g e^{-j\omega\tau}$$

$$\begin{aligned}
&= \alpha_g e^{-j\omega\tau_2} - \frac{\partial\epsilon}{\partial\alpha}\alpha_g e^{-j\omega(\tau_1+\tau_2)} \\
&= \left(e^{-j\omega\tau_2} - \frac{\partial\epsilon}{\partial\alpha}e^{-j\omega(\tau_1+\tau_2)} \right) \alpha_g \\
&= \left(1 - \frac{\partial\epsilon}{\partial\alpha}e^{-j\omega\tau_1} \right) e^{-j\omega\tau_2} \alpha_g
\end{aligned} \tag{7.127}$$

The aerodynamic force along the Z -axis is:

$$C_{Z_g}(\omega) = C_{Z_{w_\alpha}} \alpha_g e^{j\omega\tau_1} + C_{Z_{h_\alpha}} \left(\frac{V_h}{V} \right)^2 \frac{S_h}{S} \left(1 - \frac{\partial\epsilon}{\partial\alpha}e^{-j\omega\tau_1} \right) e^{-j\omega\tau_2} \alpha_g \tag{7.128}$$

Or the aerodynamic frequency response function becomes:

$$\frac{C_{Z_g}}{\alpha_g}(\omega) = C_{Z_{w_\alpha}} e^{j\omega\tau_1} + C_{Z_{h_\alpha}} \left(\frac{V_h}{V} \right)^2 \frac{S_h}{S} \left(1 - \frac{\partial\epsilon}{\partial\alpha}e^{-j\omega\tau_1} \right) e^{-j\omega\tau_2} \tag{7.129}$$

The time delays are approximated by a first order Taylor polynomial:

$$\begin{aligned}
e^{j\omega\tau_1} &\approx 1 + j\omega\tau_1 \\
e^{-j\omega\tau_1} &\approx 1 - j\omega\tau_1 \\
e^{-j\omega\tau_2} &\approx 1 - j\omega\tau_2
\end{aligned} \tag{7.130}$$

The aerodynamic frequency response function becomes:

$$\frac{C_{Z_g}}{\alpha_g}(\omega) = C_{Z_{w_\alpha}} (1 + j\omega\tau_1) + C_{Z_{h_\alpha}} \left(\frac{V_h}{V} \right)^2 \frac{S_h}{S} \left(1 - \frac{\partial\epsilon}{\partial\alpha} (1 - j\omega\tau_1) \right) (1 - j\omega\tau_2) \tag{7.131}$$

Or:

$$\begin{aligned}
\frac{C_{Z_g}}{\alpha_g}(\omega) &= C_{Z_{w_\alpha}} + C_{Z_{h_\alpha}} \left(\frac{V_h}{V} \right)^2 \frac{S_h}{S} \left(1 - \frac{\partial\epsilon}{\partial\alpha} \right) + \\
&+ \left[\left(C_{Z_{w_\alpha}} + C_{Z_{h_\alpha}} \left(\frac{V_h}{V} \right)^2 \frac{S_h}{S} \frac{\partial\epsilon}{\partial\alpha} \right) \tau_1 - C_{Z_{h_\alpha}} \left(\frac{V_h}{V} \right)^2 \frac{S_h}{S} \left(1 - \frac{\partial\epsilon}{\partial\alpha} \right) \tau_2 \right] j\omega + \\
&+ \left[-C_{Z_{h_\alpha}} \left(\frac{V_h}{V} \right)^2 \frac{S_h}{S} \frac{\partial\epsilon}{\partial\alpha} \tau_1 \tau_2 \right] (j\omega)^2
\end{aligned} \tag{7.132}$$

With:

$$C_{Z_\alpha} = C_{Z_{w_\alpha}} + C_{Z_{h_\alpha}} \left(\frac{V_h}{V} \right)^2 \frac{S_h}{S} \left(1 - \frac{\partial\epsilon}{\partial\alpha} \right) \tag{7.133}$$

one can write for the aerodynamic frequency response function:

$$\frac{C_{Z_g}}{\alpha_g}(\omega) = C_{Z_\alpha} +$$

$$\begin{aligned}
& + \left[\left(C_{Z_{w\alpha}} + C_{Z_{h\alpha}} \left(\frac{V_h}{V} \right)^2 \frac{S_h}{S} \frac{\partial \epsilon}{\partial \alpha} \right) \tau_1 \frac{V}{\bar{c}} - C_{Z_{h\alpha}} \left(\frac{V_h}{V} \right)^2 \frac{S_h}{S} \left(1 - \frac{\partial \epsilon}{\partial \alpha} \right) \tau_2 \frac{V}{\bar{c}} \right] \frac{j\omega \bar{c}}{V} + \\
& + \left[-C_{Z_{h\alpha}} \left(\frac{V_h}{V} \right)^2 \frac{S_h}{S} \frac{\partial \epsilon}{\partial \alpha} \tau_1 \frac{V}{\bar{c}} \tau_2 \frac{V}{\bar{c}} \right] \left(\frac{j\omega \bar{c}}{V} \right)^2
\end{aligned} \tag{7.134}$$

Or:

$$\frac{C_{Z_g}}{\alpha_g}(\omega) = C_{Z_\alpha} + C_{Z_{\dot{\alpha}g}} \frac{j\omega \bar{c}}{V} + C_{Z_{\ddot{\alpha}g}} \left(\frac{j\omega \bar{c}}{V} \right)^2 \tag{7.135}$$

with:

$$C_{Z_{\alpha g}} = C_{Z_\alpha} = C_{Z_{w\alpha}} + C_{Z_{h\alpha}} \left(\frac{V_h}{V} \right)^2 \frac{S_h}{S} \left(1 - \frac{\partial \epsilon}{\partial \alpha} \right) \tag{7.136}$$

$$C_{Z_{\dot{\alpha}g}} = C_{Z_{w\alpha}} \tau_1 \frac{V}{\bar{c}} + C_{Z_{h\alpha}} \left(\frac{V_h}{V} \right)^2 \frac{S_h}{S} \frac{\partial \epsilon}{\partial \alpha} \tau_1 \frac{V}{\bar{c}} - C_{Z_{h\alpha}} \left(\frac{V_h}{V} \right)^2 \frac{S_h}{S} \left(1 - \frac{\partial \epsilon}{\partial \alpha} \right) \tau_2 \frac{V}{\bar{c}} \tag{7.137}$$

$$C_{Z_{\ddot{\alpha}g}} = -C_{Z_{h\alpha}} \left(\frac{V_h}{V} \right)^2 \frac{S_h}{S} \frac{\partial \epsilon}{\partial \alpha} \tau_1 \tau_2 \left(\frac{V}{\bar{c}} \right)^2 \tag{7.138}$$

Or:

$$C_{Z_{\alpha g}} = C_{Z_\alpha} = C_{Z_{w\alpha}} + C_{Z_{h\alpha}} \left(\frac{V_h}{V} \right)^2 \frac{S_h}{S} \left(1 - \frac{\partial \epsilon}{\partial \alpha} \right) \tag{7.139}$$

$$\begin{aligned}
C_{Z_{\dot{\alpha}g}} &= C_{Z_{w\alpha}} \frac{x_{cg} - x_w}{\bar{c}} + C_{Z_{h\alpha}} \left(\frac{V_h}{V} \right)^2 \frac{S_h}{S} \frac{\partial \epsilon}{\partial \alpha} \frac{x_{cg} - x_w}{\bar{c}} \\
&- C_{Z_{h\alpha}} \left(\frac{V_h}{V} \right)^2 \frac{S_h}{S} \left(1 - \frac{\partial \epsilon}{\partial \alpha} \right) \frac{x_h - x_{cg}}{\bar{c}}
\end{aligned} \tag{7.140}$$

$$C_{Z_{\ddot{\alpha}g}} = -C_{Z_{h\alpha}} \left(\frac{V_h}{V} \right)^2 \frac{S_h}{S} \frac{\partial \epsilon}{\partial \alpha} \frac{x_{cg} - x_w}{\bar{c}} \frac{x_h - x_{cg}}{\bar{c}} \tag{7.141}$$

Substituting $\tau_1 = 0$ and $\tau_2 = \tau$ (the positions of the aerodynamic centre of the wing/fuselage and the centre of gravity coincide: $x_w = x_{cg}$), yields the standard gust derivatives.

7.6 Examples and problems

7.6.1 Example 7.1

Once the equations of motion of an aircraft, flying in atmospheric turbulence, are known, the response of the motion variables can be determined. In this example, the response of a twin engined executive jet aircraft, the Cessna Ce-500 ‘Citation’, to vertical atmospheric turbulence will be determined. The turbulence, being the input signal to the aircraft, will be calculated using the Dryden model.

- Aircraft data:

V	=	59.9 m/s	m	=	4547.8 kg	\bar{c}	=	2.022 m
S	=	24.2 m ²	l_h	=	5.5 m	μ_c	=	102.7
K_Y^2	=	0.980	x_{cg}	=	0.30 \bar{c}			
C_{X_0}	=	0	C_{Z_0}	=	-1.1360			
C_{X_u}	=	-0.2199	C_{Z_u}	=	-2.2720	C_{m_u}	=	0
C_{X_α}	=	0.4653	C_{Z_α}	=	-5.1600	C_{m_α}	=	-0.4300
$C_{X_{\dot{\alpha}}}$	=	0	$C_{Z_{\dot{\alpha}}}$	=	-1.4300	$C_{m_{\dot{\alpha}}}$	=	-3.7000
C_{X_q}	=	0	C_{Z_q}	=	-3.8600	C_{m_q}	=	-7.0400
C_{X_δ}	=	0	C_{Z_δ}	=	-0.6238	C_{m_δ}	=	-1.5530

- Turbulence model:

$$\sigma_{w_g} = 1 \text{ m/s} \quad L_g = 150 \text{ m}$$

Because in the examples the matrices in Equation (7.109) will appear frequently, a MATLAB program, `cit2s.m`, will be used to define these matrices. Adapting this file makes it possible to perform the calculations for other aircraft or other atmospheric conditions by just changing the aerodynamic derivatives or turbulence parameters.

Listing 7.1: Symmetric aircraft response to atmospheric turbulence

```
% Filename: cit2s.m
%
% Calculation of state matrix and input matrix for calculation
% of symmetric aircraft response to atmospheric turbulence.
% The system model is in the form
%
%      .
%
%      x = Ax + Bu
%      - - -
%
```

```

% with
%     x = [u/V alpha theta qc/V u_g/V alpha_g alpha_g*] ,
% and
%     u = [delta_e w_1 w_3] .
%
% The turbulence filters are according to Dryden.

%
% Cessna Citation Ce-500, landing (1)
%

% INPUT TURBULENCE- AND AIRCRAFT PARAMETERS

% AIRCRAFT FLIGHT CONDITION 'LANDING'.
V      = 59.9;
m      = 4547.8;
twmuc = 2*102.7;
KY2    = 0.980;
c      = 2.022;
S      = 24.2;
lh     = 5.5;

% TURBULENCE PARAMETERS
disp(' ');
sigma = input(' Enter turbulence intensity sigma [m/s] ( 1) : ');
Lg    = input(' Enter turbulence scale length Lg [m] (150) : ');

sigmaug_V = sigma/V;
sigmaag   = sigma/V;

% AIRCRAFT SYMMETRIC AERODYNAMIC DERIVATIVES :
CX0 = 0.0000;      CZ0  = -1.1360;      Cm0  = 0.0000;
CXu = -0.2199;     CZu  = -2.2720;     Cmu  = 0.0000;
Cxa = 0.4653;      Cza  = -5.1600;     Cma  = -0.4300;
CXq = 0.0000;      CZq  = -3.8600;     Cmq  = -7.0400;
CXd = 0.0000;      CZd  = -0.6238;     Cmd  = -1.5530;
CXfa= 0.0000;      CZfa = -1.4300;     Cmfa = -3.7000;
                           CZfug= 0.0000;     Cmfug= -Cm0*lh/c ;
                           CZfag= CZfa-CZq;   Cmfag= Cmfa-Cmq;

% CALCULATION OF AIRCRAFT SYMMETRIC STABILITY DERIVATIVES
xu   = (V/c)*(CXu/twmuc);
xa   = (V/c)*(Cxa/twmuc);
xt   = (V/c)*(CZ0/twmuc);
xq   = 0;
xd   = (V/c)*(CXd/twmuc);
xug  = xu;
xfug = 0;
xag  = xa;
xflag = 0;

zu   = (V/c)*( CZu/(twmuc-CZfa));

```

```

za = (V/c)*( CZa/(twmuc-CZfa));
zt = (V/c)*(-CX0/(twmuc-CZfa));
zq = (V/c)*(( CZq+twmuc)/(twmuc-CZfa));
zd = (V/c)*( CZd/(twmuc-CZfa));
zug = zu;
zfug = (V/c)*( CZfug/(twmuc-CZfa));
zag = za;
zfag = (V/c)*( CZfag/(twmuc-CZfa));

mu = (V/c)*(( Cmu+CZu*Cmfa/(twmuc-CZfa))/(twmuc*KY2));
ma = (V/c)*(( Cma+CZa*Cmfa/(twmuc-CZfa))/(twmuc*KY2));
mt = (V/c)*((-CX0*Cmfa/(twmuc-CZfa))/(twmuc*KY2));
mq = (V/c)*(Cmq+Cmfa*(twmuc+CZq)/(twmuc-CZfa))/(twmuc*KY2);
md = (V/c)*((Cmd+CZd*Cmfa/(twmuc-CZfa))/(twmuc*KY2));
mug = mu;
mfug = (V/c)*(Cmfug+CZfug*Cmfa/(twmuc-CZfa))/(twmuc*KY2);
mag = ma;
mfag = (V/c)*(Cmfag+CZfag*Cmfa/(twmuc-CZfa))/(twmuc*KY2);

% STATE- AND INPUT MATRICES
A=[xu xa xt 0      xug          xag      0;
   zu za zt zq    zug-zfug*V/Lg*(c/V)  zag      zfag*(c/V);
   0   0   0   V/c  0           0         0;
   mu ma mt mq    mug-mfug*V/Lg*(c/V)  mag      mfag*(c/V);
   0   0   0   0    -V/Lg        0         0;
   0   0   0   0    0           0         1;
   0   0   0   0    0           -(V/Lg)^2 -2*V/Lg];

B=...
[ xd 0          0;
  zd zfug*(c/V)*sigmaaug_V*sqrt(2*V/Lg) zfag*(c/V)*sigmaag*sqrt(3*V/Lg);
  0  0          0;
  md mfug*(c/V)*sigmaaug_V*sqrt(2*V/Lg) mfag*(c/V)*sigmaag*sqrt(3*V/Lg);
  0  sigmaaug_V*sqrt(2*V/Lg)               0;
  0  0          sigmaag*sqrt(3*V/Lg);
  0  0          (1-2*sqrt(3))*sigmaag*sqrt((V/Lg)^3)];

% GAIN FACTORS FOR AUTOPILOT CHAPTER 7 AND DEFINITION OF MATRIX At
% (approximately "Dead Beat" damping)
Kt = -0.21; Kq = -3; % gains on "theta" and "q"
K = [0 0 Kt Kq 0 0 0]; % feedback matrix
At = A-B(:,1)*K; % new A matrix = (A - BK) because of feedback

% SAVE ALL TO FILE, THEN CLEAR, THEN READ AGAIN
save dumfile A At B sigmaaug_V sigmaag Lg V c
clear
load dumfile

```

Using the equations of motion (7.109), the response of the aircraft motion variables to vertical atmospheric turbulence can be computed by taking as input vector $\bar{u}(t) = [0 \ 0 \ w_3]^T$ where w_3 is a white noise input with intensity 1. The initial state is taken to be zero im-

plying that the turbulence starts acting on the aircraft at $t = 0$. The motions, simulated in this example, are therefore those of an aircraft that has been flying in undisturbed air until $t = 0$, encountering turbulence at $t = 0$.

The time histories of the aircraft responses are plotted in Figure 7.6. It can be observed that the responses are not stationary. This is particularly obvious with the time history of speed $u(t)$, Figure 7.6(a). Methods that can be used to calculate the (co-) variances of the motion variables in such a non-stationary situation have been discussed in Chapter 5 and will be used in the next example.

The MATLAB-file to produce the aircraft's responses is given below.

Listing 7.2: Example 7.1

```
% Filename : examp71.m
%
% Simulation of aircraft symmetric response to atmospheric turbulence.
%
% Chapter 7 of lecture notes ae4-304
%
% Revised: November 2014 [M Rodriguez]
%%

close all; clc; clear all;

disp(' Example 7.1 ');
disp(' ');
disp(' Simulation of symmetric gust response of the ');
disp(' Cessna Ce-500 "Citation" at an airspeed of 59.9 [m/s], ');
disp(' CRUISE condition. ');
disp(' ');
disp(' This program produces Figure 7-6 of the lecture notes: ');
disp(' Aircraft Responses to Atmospheric Turbulence. ');

cit2s      % loading A,B matrices

% TIME AXIS INPUT VECTOR DEFINITION
dt = input(' Give sampling time interval dt (0.01) : ');
T = 60; t = [0:dt:T]; N = length(t);

% INPUT VECTOR DEFINITION
nn = zeros(1,N);          % zero input elevator
w1 = randn(1,N)/sqrt(dt); % scaled input hor. turbulence,
                           % note the sqrt(dt) because of lsim
w3 = randn(1,N)/sqrt(dt); % scaled input vert. turbulence,
                           % note the sqrt(dt) because of lsim
u = [nn' nn' w3'];        % input vector definition (vertical
                           % turbulence only, can be changed).

% SIMULATION OF MOTION VARIABLES
C = eye(7); D = zeros(7,3);
y = lsim(A,B,C,D,u,t);
```

```
% PLOTTING RESULTS
subplot(4,1,1);
plot(t,y(:,1))
xlabel('time [s]'); ylabel('u/V [-]'); title('airspeed deviation');

subplot(4,1,2);
plot(t,y(:,2)*180/pi)
xlabel('time [s]'); ylabel('alpha [deg]'); title('angle of attack');

subplot(4,1,3);
plot(t,y(:,3)*180/pi)
xlabel('time [s]'); ylabel('theta [deg]'); title('pitch angle');

subplot(4,1,4);
plot(t,y(:,4)*180/pi)
xlabel('time [s]'); ylabel('qc/V [deg]'); title('pitch rate');
```

7.6.2 Example 7.2

In this example, the growth in time of the variances of the symmetric aircraft motion variables for an aircraft, responding to vertical atmospheric turbulence, will be calculated in two ways. The growth in time of the variances can be evaluated against the steady-state solution. The aircraft considered is taken to be the same as in Example 7.1; the input to the aircraft, vertical turbulence, is also taken the same as in the previous example.

The differential equations of the turbulence filter, combined with the symmetric aircraft motions can be written in state-space form, Equation (7.109):

$$\dot{\underline{x}} = A\underline{x} + B\underline{w}$$

where,

$$\underline{x} = \left[\hat{u} \ \alpha \ \theta \ \frac{q\bar{c}}{V} \ \hat{u}_g \ \alpha_g \ \alpha_g^* \right]^T$$

First we shall determine the steady-state solution of the (co)variances of the motion variables by either numerically integrating the power spectral densities of the motion variables, Equation (3.45),

$$\sigma_{\bar{x}}^2 = \frac{1}{\pi} \int_0^{+\infty} S_{\bar{x}\bar{x}}(\omega) d\omega$$

and as an alternative, solving the Lyapunov-matrix equation, Equation (5.37),

$$AC_{\bar{x}\bar{x},ss} + C_{\bar{x}\bar{x},ss}A^T = -BWB^T$$

Having done that, we shall calculate the growth in time of the covariance matrix using the two methods introduced in Chapter 5: the digital calculation of the growth in time of

the covariance matrix, Equation (5.41),

$$C_{\bar{x}\bar{x}}[k+1] = \Phi C_{\bar{x}\bar{x}}[k] \Phi^T + \Gamma \frac{W_{con}}{\Delta t} \Gamma^T$$

and using the ‘impulse response method’ (Section 5.7), Equation (5.52),

$$C_{\bar{x}\bar{x}}(t) = \int_0^t \underline{h}_i(\nu) \cdot \underline{h}_j^T(\nu) d\nu$$

The auto power spectral densities of a motion variable is related to the auto power spectral density of the input signal, Equation (3.44),

$$S_{\bar{y}\bar{y}}(\omega) = |H(\omega)|^2 S_{\bar{w}\bar{w}}(\omega)$$

In the case of Equation (7.109), the input signal is taken to be white noise with a spectral density,

$$S_{\bar{w}\bar{w}}(\omega) = 1$$

So in the case of a white noise input, the auto power spectral density of a motion variable equals the squared absolute value of the corresponding frequency response. The variance of the motion variable can be found by numerically integrating the auto power spectral density.

A MATLAB program to calculate the auto power spectral densities of the symmetric motion variables when vertical turbulence acts on the aircraft considered, is given. A numerical integration yields the steady state variances. In the program the steady state covariance matrix is calculated also by using the Lyapunov equation. Furthermore, the growth in time of the covariance matrix using the impulse response method and using the discrete system model description (Equation (5.41)).

The steady-state 7x7 covariance matrix (with the steady-state variances on the first four diagonal elements) can be obtained by solving the Lyapunov Equation (5.37) where the matrices A and B are given by (7.109).

Numerical methods to solve this equation have been developed, see e.g. (Bryson Jr. & Ho, 1975), and using the MATLAB command `lyap` the solution can be found to be (see also program `examp72.m`):

```
% Find solution of Lyapunov equation
cit2s
Css=lyap(A,B(:,3)*B(:,3)');
```

The first four diagonal elements are found to be, inputting $\sigma_{w_g} = 1 \text{ m/s}$ and $L_g = 150 \text{ m}$ for the Cessna Ce-500 ‘Citation’,

$$\boxed{\begin{array}{llll} C_{ss}(1,1) & = & \sigma_{\hat{u}}^2 & = 1.0852 \cdot 10^{-4} \text{ [rad}^2\text{]} \\ C_{ss}(2,2) & = & \sigma_{\alpha}^2 & = 2.2087 \cdot 10^{-4} \text{ [rad}^2\text{]} \\ C_{ss}(3,3) & = & \sigma_{\theta}^2 & = 1.9821 \cdot 10^{-4} \text{ [rad}^2\text{]} \\ C_{ss}(4,4) & = & \sigma_{\frac{q_c}{V}}^2 & = 5.3085 \cdot 10^{-8} \text{ [rad}^2\text{]} \end{array}}$$

The differences between the results found are a result of numerical errors in the integration of the spectra and in the solving of the Lyapunov equation.

Next, the calculation of the growth in time of the covariance matrix will be discussed, finally yielding a steady-state value as calculated above.

In Section 5.7 it was shown that the growth in time of the covariance matrix can be calculated by integrating the product of the impulse responses. An impulse response was found to be identical with a response to an initial condition, Equation (5.50),

$$\underline{x}(0) = \underline{B}_i$$

As vertical turbulence only is considered, in this case, the vector \underline{B} is the last column of the B matrix of the state-space Equation (7.109). The responses of the first four elements of the state vector to this initial condition, equaling the impulse responses, are plotted in Figure 7.8. Their cross products,

$$\underline{h}_i(t) \cdot \underline{h}_j(t)$$

are plotted in Figure 7.9. Notice that the diagonal elements are all equal to or larger than zero for all t . The integrated elements of the matrix given in Figure 7.9 are plotted in Figure 7.10. In Figure 7.10 the growth in time of the covariance matrix of the symmetric motion variables due to vertical atmospheric turbulence is given according to Equation (5.52),

$$C_{\bar{x}\bar{x}}(t) = \int_0^t \underline{h}_i(\nu) \cdot \underline{h}_j^T(\nu) d\nu$$

The diagonal elements $C_{\bar{x}\bar{x}}(1,1)$ through $C_{\bar{x}\bar{x}}(4,4)$ represent the variances of the symmetrical variables \hat{u} , α , θ and $\frac{q_c}{V}$ respectively. It can be seen that the variances $C_{\bar{x}\bar{x}}(2,2)$ and $C_{\bar{x}\bar{x}}(4,4)$ of the motion variables α and $\frac{q_c}{V}$, merely dependent of the short period motion, have reached their stationary values after about 7 seconds. The variances $C_{\bar{x}\bar{x}}(1,1)$ and $C_{\bar{x}\bar{x}}(3,3)$ of the motion variables \hat{u} and θ however, merely dependent of the phugoid, have not become stationary after 100 seconds.

Another method to calculate the growth in time of the covariance matrix was given in Section 5.6.2, Equation (5.41),

$$C_{\bar{x}\bar{x}}[k+1] = \Phi C_{\bar{x}\bar{x}}[k] \Phi^T + \Gamma \frac{W_{con}}{\Delta t} \Gamma^T$$

The discretized matrices Φ and Γ have been obtained from A and B by using the MATLAB program package. The calculated growth in time of the covariance matrix of the motion variables has been plotted in Figure 7.11. Also, the steady-state solutions as obtained

before, are plotted in Figure 7.11 with a dashed line. Here the off-diagonal elements have not been normalized by dividing each element $C_{\bar{x}\bar{x}}(i,j)$ $i \neq j$ by the steady state standard deviations:

$$\sqrt{C_{\bar{x}\bar{x}}(i,i)(t) C_{\bar{x}\bar{x}}(j,j)(t)} \quad t = 150 \text{ sec.}$$

Two variables are fully uncorrelated if their covariance equals zero. In the opposite case, if the absolute value of two (normalized) variables equals one, those variables are fully correlated. The values of the normalized off-diagonal elements then vary between -1 and 1 .

An effect worth noting is the zero stationary value of element $C_{\bar{x}\bar{x}_{ss}}(4,3)$ indicating a zero correlation between the motion variables $\frac{q\bar{c}}{V}$ and θ . This observation is in accordance with the theory, stating that a stochastic variable is uncorrelated with its time derivative, see also Example 5.2. The MATLAB program used is self explanatory and is given below.

Listing 7.3: Example 7.2

```
% Filename : exampl72.m
%
% Calculation of covariance matrix of the (non-dimensional)
% motion variables.
%
% Steady-state (co)variances are calculated by solving the
% Lyapunov-equation AC+CA'+BWB'=0 or by integrating the power
% spectral density.
%
% Transient behaviour may be calculated with either the recursive
% relation C(k+1)=PHI C(k) PHI' + GAMMA Wdis GAMMA' or using the
% impulse response method.
%
% Chapter 7 of lecture notes ae4-304
%
% Revised: November 2014 [M Rodriguez]
%%

clc; close all; clear all;

disp(' Example 7.2');
disp(' ');
disp(' Calculation of covariance matrix of the (non-dimensional)');
disp(' motion variables. Steady-state (co)variances are calculated');
disp(' by solving the Lyapunov-equation AC+CA' +BWB' =0 or by');
disp(' integrating the power spectral density. Transient behaviour');
disp(' may be calculated with either the recursive relation');
disp(' C(k+1)=PHI C(k) PHI' + GAMMA Wdis GAMMA' or using the');
disp(' impulse response method.');
disp(' ');
disp(' This program produces Figures 7-7 to 7-11 in the lecture');
disp(' notes: Aircraft Responses to Atmospheric Turbulence.');

% COMPUTE A/C DYNAMICS
```

```

cit2s          % loading A,B matrices

% GET INPUT PARAMETERS
Wc = input('      Give noise intensity           ( 1.0 ) : ');
dt = input('      Give sampling time interval dt   ( 0.01) : ');
T = input('      Give total time interval T_end    (150.0 ) : ');
Nf = input('      Give number of points in frequency axis ( 200 ) : ');

% DEFINE NOISE INTENSITY
W = Wc/dt;    % discrete time covariance, remember?

% DEFINE TIME AXIS
t = [0:dt:T]; N = length(t);

%%%%%%%%%%%%%
% COMPUTE THE STEADY-STATE SOLUTION
%%%%%%%%%%%%%

%%%%%%%%%%%%%
% Method 1. SOLVING THE LYAPUNOV-EQUATION
%%%%%%%%%%%%%
disp(,          );
disp('Method 1. SOLVING THE LYAPUNOV-EQUATION' );

Bin = B(:,3);
L = lyap(A, Bin*Wc*Bin );
% take only the part that belongs to the 4 states
L = L(1:4 ,1:4);

disp(,          );
disp(,          );
disp('    Display solution Lyapunov equation' );
disp(L);
disp('    Note: the diagonal elements are the variances: ' );
disp(diag(L));
pause

%%%%%%%%%%%%%
% Method 2. INTEGRATING THE ANALYTICAL POWER SPECTRAL DENSITIES
%%%%%%%%%%%%%
disp(,          );
disp('Method 2. INTEGRATING THE ANALYTICAL POWER SPECTRAL DENSITIES ' );

% The motion variables u/V, alpha, theta and qc/V are the first four
% elements of the seventh order state vector.

% Input vector u=[0 0 w3].
D = zeros(4 ,3);
C = [eye(4) zeros(4 ,3)];

% DEFINE FREQUENCY AXIS
omega = logspace(-2,2,Nf);

```

```
% COMPUTE FREQUENCY RESPONSE
mag = bode(A,B,C,D,3 ,omega);

% COMPUTE POWER SPECTRA OF u/V, ALPHA, THETA AND qc/V
Suu = mag(:,1).^2;
Saa = mag(:,2).^2;
Stt = mag(:,3).^2;
Sqq = mag(:,4).^2;

% PLOT POWER SPECTRA
figure
subplot(2,2,1);
loglog(omega,Suu); xlabel('omega [rad/sec]'); ylabel('Suu [rad^2/Hz]');
subplot(2,2,2);
loglog(omega,Saa); xlabel('omega [rad/sec]'); ylabel('Saa [rad^2/Hz]');
subplot(2,2,3);
loglog(omega,Stt); xlabel('omega [rad/sec]'); ylabel('Stt [rad^2/Hz]');
subplot(2,2,4);
loglog(omega,Sqq); xlabel('omega [rad/sec]'); ylabel('Sqq [rad^2/Hz]');

% NUMERICAL INTEGRATION OF PSD's
do = diff(omega)'; % compute "difference vector" in omega
% i.e., omega(k+1)-omega(k);
% then perform (very crude) integration
var(1) = sum(do.*Suu(1:Nf-1));
var(2) = sum(do.*Saa(1:Nf-1));
var(3) = sum(do.*Stt(1:Nf-1));
var(4) = sum(do.*Sqq(1:Nf-1));

disp(' Numerical integration of PSD yields the variances: ')
var = var/pi;
disp([' ', num2str(var) ])
disp(' Note that when we have more frequency points the ')
disp(' integration will become more accurate and the ')
disp(' variances will approximate the Lyapunov solution. ')

hh=ones(1,N);
var1 = var(1)*hh; var2 = var(2)*hh; var3 = var(3)*hh; var4 = var(4)*hh;
pause

%%%%%%%%%%%%%
% CALCULATION OF GROWTH IN TIME OF COVARIANCE MATRIX
%%%%%%%%%%%%%
% Method 1. BY RECURSIVE CALCULATION
%
% Cxx(k+1) = PHI Cxx(k) PHI' + GAMMA Wdis GAMMA'
%%%%%%%%%%%%%
```

```
% Discretize the system matrices
[Phi, Gamma] = c2d(A,B(:,3), dt);

% Initial conditions
Cxx = zeros(7,7);

% Discrete Solution of response equation
disp('') % Method 1. Computing response by recursive calculation
disp('') % hh=2;
hh=2;

% Remember: Cxx[k+1] = Phi*Cxx[k]*PhiT + Gamma*W*GammaT
for k=2:N
    Cxx=Phi*Cxx*Phi' + Gamma*W*Gamma';
    Cx1x1(k)=Cxx(1,1); Cx1x2(k)=Cxx(1,2); Cx1x3(k)=Cxx(1,3); Cx1x4(k)=Cxx(1,4);
    Cx2x2(k)=Cxx(2,2); Cx2x3(k)=Cxx(2,3); Cx2x4(k)=Cxx(2,4);
    Cx3x3(k)=Cxx(3,3); Cx3x4(k)=Cxx(3,4);
    Cx4x4(k)=Cxx(4,4);
    if hh > 100, hh=1; fprintf('step %g\n',k); end;
    hh=hh+1;
end
fprintf('ready')

I=ones(1,N);
Css11=L(1,1)*I; Css12=L(1,2)*I; Css13=L(1,3)*I; Css14=L(1,4)*I;
Css22=L(2,2)*I; Css23=L(2,3)*I; Css24=L(2,4)*I;
Css33=L(3,3)*I; Css34=L(3,4)*I;
Css44=L(4,4)*I;

%%%%%%%%%%%%%
% Method 2. USING THE IMPULSE RESPONSE METHOD
%%%%%%%%%%%%%
disp('') % Method 2. Using the impulse response method
disp('') % % ZERO INPUT, INITIAL CONDITION EQUALS B (for input 3 in this case)
u = zeros(3,N); x0=B(:,3);

% CALCULATION OF IMPULSE RESPONSES
h = lsim(A,B,C,D,u,t,x0);

% PLOT IMPULSE RESPONSE
figure
subplot(2,1,1)
plot(t,h(:,1)); xlabel('Time [sec]'); ylabel('h u w3(t)');
subplot(2,1,2)
plot(t,h(:,2)); xlabel('Time [sec]'); ylabel('h alpha w3(t)');
pause

figure
subplot(2,1,1)
```

```

plot(t,h(:,3)); xlabel('Time [sec]'); ylabel('h theta w3(t)');
subplot(2,1,2)
plot(t,h(:,4)); xlabel('Time [sec]'); ylabel('h qc/V w3(t)');
pause

% CALCULATION OF PRODUCT MATRIX OF IMPULSE RESPONSES
h11=h(:,1).*h(:,1); h12=h(:,1).*h(:,2); h13=h(:,1).*h(:,3); h14=h(:,1).*h(:,4);
h22=h(:,2).*h(:,2); h23=h(:,2).*h(:,3); h24=h(:,2).*h(:,4);
h33=h(:,3).*h(:,3); h34=h(:,3).*h(:,4);
h44=h(:,4).*h(:,4);

close all;
% PLOT (CROSS) PRODUCTS OF IMPULSE RESPONSES
disp('')')
disp(' PLOT (CROSS) PRODUCTS OF IMPULSE RESPONSES')
disp('')')
clf
subplot(2,2,1)
plot(t,h11); xlabel('Time [sec]'); ylabel('h1*h1(t)');
subplot(2,2,2)
plot(t,h12); xlabel('Time [sec]'); ylabel('h1*h2(t)');
subplot(2,2,4)
plot(t,h22); xlabel('Time [sec]'); ylabel('h2*h2(t)');
pause

figure
subplot(2,2,1)
plot(t,h13); xlabel('Time [sec]'); ylabel('h1*h3(t)');
subplot(2,2,2)
plot(t,h14); xlabel('Time [sec]'); ylabel('h1*h4(t)');
subplot(2,2,3)
plot(t,h23); xlabel('Time [sec]'); ylabel('h2*h3(t)');
subplot(2,2,4)
plot(t,h24); xlabel('Time [sec]'); ylabel('h2*h4(t)');
pause

figure
subplot(2,2,1)
plot(t,h33); xlabel('Time [sec]'); ylabel('h3*h3(t)');
subplot(2,2,2)
plot(t,h34); xlabel('Time [sec]'); ylabel('h3*h4(t)');
subplot(2,2,4)
plot(t,h44); xlabel('Time [sec]'); ylabel('h4*h4(t)');
pause

% INTEGRATION OF PRODUCT MATRIX OF IMPULSE RESPONSES
var11(1)=0; var12(1)=0; var13(1)=0; var14(1)=0;
var22(1)=0; var23(1)=0; var24(1)=0;
var33(1)=0; var34(1)=0;
var44(1)=0;

dth11 = dt*h11; dth12 = dt*h12; dth13 = dt*h13; dth14 = dt*h14;

```

```

dth22 = dt*h22; dth23 = dt*h23; dth24 = dt*h24;
dth33 = dt*h33; dth34 = dt*h34;
dth44 = dt*h44;

for i=1:N-1
    var11(i+1) = var11(i) + dth11(i);
    var12(i+1) = var12(i) + dth12(i);
    var13(i+1) = var13(i) + dth13(i);
    var14(i+1) = var14(i) + dth14(i);
    var22(i+1) = var22(i) + dth22(i);
    var23(i+1) = var23(i) + dth23(i);
    var24(i+1) = var24(i) + dth24(i);
    var33(i+1) = var33(i) + dth33(i);
    var34(i+1) = var34(i) + dth34(i);
    var44(i+1) = var44(i) + dth44(i);
end

close all;
% PLOT VARIANCES FROM IMPULSE RESPONSE METHOD
disp(' PLOT VARIANCES FROM IMPULSE RESPONSE METHOD ')
disp(' ')
clf
subplot(2,2,1)
plot(t,Css11,'--',t,var11); xlabel('time [s]'); ylabel('Cx1x1');
subplot(2,2,2)
plot(t,Css12,'--',t,var12); xlabel('time [s]'); ylabel('Cx1x2');
subplot(2,2,4)
plot(t,Css22,'--',t,var22); xlabel('time [s]'); ylabel('Cx2x2');
pause

clf
subplot(2,2,1)
plot(t,Css13,'--',t,var13); xlabel('time [s]'); ylabel('Cx1x3');
subplot(2,2,2)
plot(t,Css14,'--',t,var14); xlabel('time [s]'); ylabel('Cx1x4');
subplot(2,2,3)
plot(t,Css23,'--',t,var23); xlabel('time [s]'); ylabel('Cx2x3');
subplot(2,2,4)
plot(t,Css24,'--',t,var24); xlabel('time [s]'); ylabel('Cx2x4');
pause

clf
subplot(2,2,1)
plot(t,Css33,'--',t,var33); xlabel('time [s]'); ylabel('Cx3x3');
subplot(2,2,2)
plot(t,Css34,'--',t,var34); xlabel('time [s]'); ylabel('Cx3x4');
subplot(2,2,4)
plot(t,Css44,'--',t,var44); xlabel('time [s]'); ylabel('Cx4x4');
pause

close all;
% PLOT RESULTS FROM RECURSIVE EQUATION WITH STEADY-STATE DASHED
disp(' PLOT RESULTS FROM RECURSIVE EQUATION WITH STEADY-STATE DASHED')

```

```

disp('
clf
subplot(2,2,1)
plot(t,Cx1x1,t,Css11,'--'); xlabel('time [s]'); ylabel('Cx1x1');
subplot(2,2,2)
plot(t,Cx1x2,t,Css12,'--'); xlabel('time [s]'); ylabel('Cx1x2');
subplot(2,2,4)
plot(t,Cx2x2,t,Css22,'--'); xlabel('time [s]'); ylabel('Cx2x2')
pause

clf
subplot(2,2,1)
plot(t,Cx1x3,t,Css13,'--'); xlabel('time [s]'); ylabel('Cx1x3');
subplot(2,2,2)
plot(t,Cx1x4,t,Css14,'--'); xlabel('time [s]'); ylabel('Cx1x4');
subplot(2,2,3)
plot(t,Cx2x3,t,Css23,'--'); xlabel('time [s]'); ylabel('Cx2x3');
subplot(2,2,4)
plot(t,Cx2x4,t,Css24,'--'); xlabel('time [s]'); ylabel('Cx2x4');
pause

clf
subplot(2,2,1)
plot(t,Cx3x3,t,Css33,'--'); xlabel('time [s]'); ylabel('Cx3x3');
subplot(2,2,2)
plot(t,Cx3x4,t,Css34,'--'); xlabel('time [s]'); ylabel('Cx3x4');
subplot(2,2,4)
plot(t,Cx4x4,t,Css44,'--'); xlabel('time [s]'); ylabel('Cx4x4');
pause
')

```

7.6.3 Example 7.3

The primary design aim for a pitch-hold autopilot is often to damp the aircraft's short period and phugoid mode. In this example, the influence of an autopilot, designed by using this criterium only, on the aircraft behaviour in atmospheric turbulence will be investigated. To this end, the normal acceleration of an aircraft, encountering vertical turbulence, will be regarded, as the normal acceleration is an important measure for crew and passenger comfort. The aircraft is again the Cessna Ce-500 'Citation'. The damping coefficients of the uncontrolled aircraft can be calculated from the eigenvalues of the system matrix, resulting in,

$$\zeta_{ph} = 0.044054 \quad \zeta_{sp} = 0.71821$$

for the phugoid (ph) and short period (sp) mode, respectively. The phugoid mode appears to be almost undamped. The eigenfrequencies of the modes are respectively,

$$\omega_{ph} = 0.19573 \text{ rad/s} \quad \omega_{sp} = 1.6153 \text{ rad/s}$$

A simple lag-free autopilot is now applied, based on the following control law,

$$\delta_e = K_\theta \theta + K_q \frac{q\bar{c}}{V}$$

The gain factors K_θ and K_q are determined by a root-locus investigation in such a way that both the phugoid and the short period mode become well-damped, yielding damping coefficients,

$$\zeta_{ph} = 0.70578 \quad \zeta_{sp} = 0.70187$$

and eigenfrequencies,

$$\omega_{ph} = 0.20816 \text{ rad/s} \quad \omega_{sp} = 1.9408 \text{ rad/s}$$

for the phugoid and the short period mode, respectively.

Next, the influence of this autopilot on the normal acceleration of the aircraft, responding to atmospheric turbulence, will be investigated. Only vertical turbulence will be considered; variations in horizontal airspeed will be neglected.

The vertical acceleration of the aircraft (in g units) can be calculated by,

$$n(t) = \frac{V}{g} \dot{\gamma}(t) = -\frac{V}{g} [\dot{\alpha}(t) - \dot{\theta}(t)] = -\frac{V^2}{g\bar{c}} D_c [\alpha(t) - \theta(t)] \quad (7.142)$$

The transfer function H_{nw_3} for the vertical acceleration, due to vertical turbulence ($\alpha_g = \frac{w_g}{V}$) can be determined by performing the Laplace transformation to the equations of motion and solving for α and θ ,

$$n(s) = \frac{V}{g} s [\theta(s) - \alpha(s)] \quad (7.143)$$

or by defining an output element by, Equation (7.142),

$$n = y = C \underline{x} + D \underline{u}$$

and substituting for $\dot{\alpha}$ and $\dot{\theta}$ respectively the second and third row of Equation (7.109). The C and D matrices will then be functions of z_u , z_α , etc.

The influence of the autopilot can be investigated by comparing the power spectral densities of the normal acceleration for the aircraft with and without autopilot, which can be calculated by,

$$S_n(\omega) = |H_{nw_3}(\omega)|^2 S_{w_3}(\omega)$$

where $S_{w_3}(\omega)$ is the power spectral density of the white noise input, which is unity over the frequency range.

The resulting power spectrum S_n has been plotted in Figure 7.12, where the continuous line represents the uncontrolled aircraft and the dashed line represents the controlled aircraft. As can be seen, the phugoid excitation for the controlled aircraft is well damped.

This results in a smaller variance of the normal acceleration, which can be calculated by numerically integrating the spectrum,

$$\sigma_n^2 = \frac{1}{\pi} \int_0^{+\infty} S_n(\omega) d\omega$$

With $a_z = g \cdot n$ this results in $\sigma_{a_z}^2 = 2.8680 * 10^{-1} [m^2 s^{-4}]$ and $\sigma_{a_z}^2 = 2.4736 * 10^{-1} [m^2 s^{-4}]$ for the uncontrolled- and controlled aircraft, respectively. The variance due to horizontal turbulence u_g for the uncontrolled aircraft is found to be $\sigma_{a_z}^2 = 2.7918 * 10^{-1} [m^2 s^{-4}]$.

The following MATLAB program calculates the power spectral density of the normal acceleration for the controlled- and uncontrolled aircraft.

Listing 7.4: Example 7.3

```
% Filename : examp173.m
%
% Calculates the power spectral density of the normal acceleration.
%
% Chapter 7 of lecture notes ae4-304
%
% Revised: November 2014 [M Rodriguez]
%%

close all; clc; clear all;

disp(' Example 7.3 ');
disp(' Calculation of the power spectral density of the normal ');
disp(' acceleration due to longitudinal and vertical turbulence. ');
disp(' Also, the effect of a lagfree autopilot will be investigated.');
disp(' This program produces Figures 7-12 and 7-13 of the lecture ');
disp(' notes: Aircraft Responses to Atmospheric Turbulence. ');

% GET AIRCRAFT DYNAMICS
cit2s

% DEFINE FREQUENCY AXES
N = 1000;
omega = logspace(-3,3,N); % frequency axis

% MISCELLANEOUS
D = [0 0 0];
g = 9.80665; % gravitational acc [N/kg]

% HORIZONTAL TURBULENCE
C = [0 1 0 0 0 0];
[numa,den] = ss2tf(A,B,C,D,2); % transfer function alpha-w1

C = [ 0 0 1 0 0 0 0];
```

```

[ numt,den ] = ss2tf(A,B,C,D,2); % transfer function theta-w1

% CALCULATION OF THE LOAD FACTOR: n = V/g*s*(theta-alpha)
numn = numt-numa; % transfer function an-w1
numn( length(numn)+1 ) = 0;
numn = (V/g)*numn;

% COMPUTE FREQUENCY RESPONSE FUNCTION
[mag,phase] = bode(numn,den,omega);
Snn = mag.*mag;

% VERTICAL TURBULENCE
C = [0 1 0 0 0 0];
[numa,den] = ss2tf(A,B,C,D,3); % transfer function alpha-w3

C = [0 0 1 0 0 0];
[numt,den] = ss2tf(A,B,C,D,3); % transfer function theta-w3

numn = numt-numa; % transfer function an-w3
numn( length(numn)+1 ) = 0;
numn = (V/g)*numn;

% COMPUTE FREQUENCY RESPONSE FUNCTION
[mag,phase] = bode(numn,den,omega);
Snn1 = mag.*mag;

% VERTICAL TURBULENCE AIRCRAFT WITH PITCH ATTITUDE HOLD SYSTEM
C = [0 1 0 0 0 0];
[numa,den] = ss2tf(At,B,C,D,3); % transfer function alpha-w3

C = [0 0 1 0 0 0];
[numt,den] = ss2tf(At,B,C,D,3); % transfer function theta-w3

numn = numt-numa; % transfer function an-w3
numn( length(numn)+1 ) = 0;
numn = (V/g)*numn;

% COMPUTE FREQUENCY RESPONSE FUNCTION
[mag,phase] = bode(numn,den,omega);
Snt1 = mag.*mag;

% PLOT POWER SPECTRAL DENSITIES
clf;
axis('square')
loglog(omega,Snn1,'--',omega,Snn);
xlabel('omega [rad/s]'); ylabel('Snn');
legend('Pitch attitude hold', 'Elevator fixed')
title('Power Spectral Density of Normal Acceleration');
pause

clf;
axis('square')

```

```

loglog(omega,Snn,'--',omega,Snn1);
xlabel('omega [rad/s]'); ylabel('Snn');
legend('Horizontal turbulence', 'Vertical turbulence')
title('Power Spectral Density of Normal Acceleration');
pause

% CALCULATION OF VARIANCES USING VERY CRUDE INTEGRATION
disp(' ') )
disp(' Calculation of the variances of n and az: ') )
disp(' ') )

dw = diff(omega);
dw(length(dw)+1) = 0; % make vector length equal to N again

disp(' ');
disp(' Variance of n due to horizontal turbulence')
varn = sum(Snn' .* dw)/pi;
disp(num2str(varn))
pause(0.5)
disp(' Variance of az due to horizontal turbulence')
varaz = sum(Snn' .* dw)*g^2/pi; % Remember: var_z = E[(n*g)^2 - mu_z]
disp(num2str(varaz))
pause(0.5)
disp(' Variance of n due to vertical turbulence')
varn1 = sum(Snn1' .* dw)/pi;
disp(num2str(varn1))
pause(0.5)
disp(' Variance of az due to vertical turbulence')
varaz1 = sum(Snn1' .* dw)*g^2/pi;
disp(num2str(varaz1))
pause(0.5)
disp(' Variance of n due to vertical turbulence for aircraft')
disp(' with pitch attitude hold system')
varnt1 = sum(Snnt1' .* dw)/pi;
disp(num2str(varnt1))
pause(0.5)
disp(' Variance of az due to vertical turbulence for aircraft')
disp(' with pitch attitude hold system')
varazt1 = sum(Snnt1' .* dw)*g^2/pi;
disp(num2str(varazt1))
pause(0.5)

```

7.6.4 Example 7.4

In this example we shall calculate the power spectral density of the variables \hat{u} , α , θ , $\frac{q\bar{c}}{V}$ and n_z due to horizontal turbulence again. The power spectral densities will be calculated from time domain data. First the MATLAB file which describes the calculation of the (analytical) auto spectra will be given. The file is almost equivalent to the previous files where transfer functions have been calculated.

Listing 7.5: Example 7.4a

```
% Filename : exempl74a.m
%
% Calculation of analytical power spectral densities and variance of
% motion variables
%
% Chapter 7 of lecture notes ae4-304
%
% Revised: November 2014 [M Rodriguez]
%%

close all; clc; clear all;

disp(' Example 7.3 ');
disp(' Calculation of analytical power spectral densities and variance ');
disp(' motion variables ');

% GET AIRCRAFT DYNAMICS
cit2s;

% DEFINE MISCELLANEOUS
g = 9.80665; % gravitational acc [N/kg]

% calculation of the frequency response of the normal acceleration factor
% horizontal turbulence : u=2, vertical turbulence u=3.

disp(' ');
disp(' Input 2 for horizontal turbulence and 3 for vertical turbulence ');
disp(' excitation ');

u = input(' Input 2 or 3 : ');

% FREQUENCY AXIS
Nomega = 300; w = logspace(-2,2,Nomega);

% C and D MATRICES
Cu = [1 0 0 0 0 0];
Calpha = [0 1 0 0 0 0];
Ctheta = [0 0 1 0 0 0];
Cq = [0 0 0 1 0 0];
Cug = [0 0 0 0 1 0];
Cag = [0 0 0 0 0 1];
D = [0 0 0];

Calphadot = A(2,:);
Dalphadot = B(2,:);

% COMPUTE FREQUENCY RESPONSE FUNCTION AND PSD
mag = bode(A,B,Cu,D,u,w); Suu = mag.*mag;
mag = bode(A,B,Calpha,D,u,w); Saa = mag.*mag;
mag = bode(A,B,Ctheta,D,u,w); Stt = mag.*mag;
mag = bode(A,B,Cq,D,u,w); Sqq = mag.*mag;
```

```

mag = bode(A,B,Cug,D,2,w);      Sugug = mag.*mag;
mag = bode(A,B,Cag,D,3,w);      Sagag = mag.*mag;

% COMPUTE FREQ. RESPONSE of NZ
sys    = ss(A,B(:,u),Calphadot,Dalphadot(:,u));
Hadotw = freqresp(sys,w);
sys    = ss(A,B(:,u),Cq,D(:,u));
Hqw    = freqresp(sys,w);

Hnz   = (V/g)*((V/c)*Hqw - Hadotw);
mag   = abs(squeeze(Hnz));
Sznz = mag.*mag;

Sxx = [Suu Saa Stt Sqq Snznz Sugug Sagag];

% COMPUTE VARIANCE THROUGH CRUDE INTEGRATION OF PSDs
var = zeros(1,7);
for j=1:7
  for i=1:Nomega-1
    var(j) = var(j)+(w(i+1)-w(i))*Sxx(i,j);
  end
end

var = var/pi;
disp(' ', ')')
disp(' Compute variances for n and a_z: ', ')
disp([' Variance of nz: ', num2str(var(5))]) ')
% Remember: var_az = E[(a*g)^2 - mu_az]
disp([' Variance of az = g*nz: ', num2str(var(5)*g^2)] ) '

```

The power spectral densities of the motion variables are known by calculating the analytical transfer functions. However, the power spectral densities will now be calculated in an additional way.

First, the time response of the motion variables is calculated, using MATLAB ‘white noise’ as input for the equations of motion according to Equation (7.109). The Fourier transform of the time domain response is calculated and the so called periodogram is obtained, see Chapter 4:

$$I_N[k] = \frac{1}{T} X^*[k] X[k], \quad (7.144)$$

where:

$$X[k] = dt \cdot \text{fft}(x(t)). \quad (7.145)$$

The periodogram is an approximation for the power spectral densities concerned. In the next MATLAB program the periodograms of the motion variables, which are approximations for the power spectral densities, are calculated and will be named in the software by P_u , P_{alpha} etc. instead of the usual notation I_N .

Listing 7.6: Example 7.4b

```
% Filename : exempl74b.m
%
% Calculation of the output spectral densities using the
% MATLAB FFT algorithm
%
% Chapter 7 of lecture notes ae4-304
%
% Revised: November 2014 [M Rodriguez]
%%
clc; close all; clear all;

disp(' Example 7.4' );
disp(' This program calculates the periodograms of time-domain' );
disp(' data using the MATLAB FFT algorithm. The experimentally' );
disp(' obtained PSD will be compared with the analytically derived' );
disp(' PSD of the motion variables.' );
disp(' This program produces Figures 7-14 to 7-17 of the lecture' );
disp(' notes: Aircraft Responses to Atmospheric Turbulence.' );
disp(' ');

% RUN EXAMPL74A
exempl74a

% DEFINE TIME AXIS
dt = 0.05; fs = 1/dt;
T = 200; t = [0:dt:T]; N = length(t);

% CREATE ZERO INPUT SIGNAL
delta = zeros(1,N);

% CREATE NORMAL WHITE NOISE SIGNALS
% if Vertical turbulence (u=3) : w1 = 0
% if Horizontal turbulence (u=2) : w3 = 0
if u == 2
    w1 = randn(1,N)/sqrt(dt); % sqrt(dt) because of lsim
    w3 = zeros(1,N);
else
    w1 = zeros(1,N);
    w3 = randn(1,N)/sqrt(dt); % sqrt(dt) because of lsim
end

inpsig = [delta' w1' w3'];

% DEFINE C and D MATRICES
C = [1 0 0 0 0 0 % u/V
      0 1 0 0 0 0 % alpha
      0 0 1 0 0 0 % theta
      0 0 0 1 0 0 % qc/V
```

```

0 0 0 0 1 0 0    % u_g/V
0 0 0 0 1 0]; % alpha_g
D = zeros(6,3);

% COMPUTE TIME RESPONSE
y      = lsim(A,B,C,D,inpsig,t);

hatu   = y(:,1);
alpha   = y(:,2);
theta   = y(:,3);
qcV    = y(:,4);
hatug  = y(:,5);
alphag = y(:,6);

% Add a trailing zero for alpha array. Because we use the routine
% diff(w) which fills a vector of length(w)-1 with w(i+1)-w(i) for i=1 to
% length(w).

alphanz          = alpha;
alphanz(length(alphanz)+1) = 0;

% Calculation of the normal load factor nz according to:
nz = (V/g)*( (V/c)*qcV - diff(alphanz)/dt );
nz(length(nz)) = nz(length(nz)-1);

% PLOT TIME RESPONSES
clf
subplot(3,2,1);
plot(t,hatu); xlabel('Time [s]'); ylabel('u/V [-]');
subplot(3,2,2);
plot(t,alpha); xlabel('Time [s]'); ylabel('alpha [rad]');
subplot(3,2,3);
plot(t,theta); xlabel('Time [s]'); ylabel('theta [rad]');
subplot(3,2,4);
plot(t,qcV); xlabel('Time [s]'); ylabel('qc/V [rad]');
subplot(3,2,5);
plot(t,nz); xlabel('Time [s]'); ylabel('nz');
subplot(3,2,6);
if u == 2
    plot(t,hatug); xlabel('Time [s]'); ylabel('ug/V [-]');
    print -depsc2 -r1200 fig7_14
else
    plot(t,alphag); xlabel('Time [s]'); ylabel('alphag [rad]');
    print -depsc2 -r1200 fig7_16
end
pause

% FFT ALL SIGNALS
U      = dt*fft(hatu);
ALPHA  = dt*fft(alpha);
THETA  = dt*fft(theta);
QCV    = dt*fft(qcV);

```

```

NZ      = dt*fft(nz);
Ug      = dt*fft(hatug);
ALPHAg = dt*fft(alphag);

% COMPUTE PSDs
Pu      = real((1/T)*      U.*conj(U));
Palpha = real((1/T)* ALPHA.*conj(ALPHA));
Ptheta = real((1/T)* THETA.*conj(THETA));
PqcV   = real((1/T)* QCV.*conj(QCV));
Pnz    = real((1/T)* NZ.*conj(NZ));
Pug    = real((1/T)* Ug.*conj(Ug));
Palphag = real((1/T)*ALPHAg.*conj(ALPHAg));

% DEFINE FREQUENCY VECTOR FOR PLOTTING
omega = 2*pi*fs*(0:(N/2)-1)/N;

% PLOT PSDs
clf
subplot(3,2,1)
loglog(w,Sxx(:,1), '--', omega, Pu(1:round(N/2)-1));
axis(10.^[-2,2,-15,0])
xlabel('omega [rad/s]'); ylabel('Suu [rad2/Hz]')

subplot(3,2,2)
loglog(w,Sxx(:,2), '--', omega, Palpha(1:round(N/2)-1));
axis(10.^[-2,2,-15,0])
xlabel('omega [rad/s]'); ylabel('Saa [rad2/Hz]')

subplot(3,2,3)
loglog(w,Sxx(:,3), '--', omega, Ptheta(1:round(N/2)-1));
axis(10.^[-2,2,-15,0])
xlabel('omega [rad/s]'); ylabel('Stt [rad2/Hz]')

subplot(3,2,4)
loglog(w,Sxx(:,4), '--', omega, PqcV(1:round(N/2)-1));
axis(10.^[-2,2,-20,-5])
xlabel('omega [rad/s]'); ylabel('Sqq [rad2/Hz]')

subplot(3,2,5)
loglog(w,Sxx(:,5), '--', omega, Pnz(1:round(N/2)-1));
axis(10.^[-2,2,-10,0])
xlabel('omega [rad/s]'); ylabel('Snznz [/Hz]')

if u == 2
    subplot(3,2,6)
    loglog(w,Sxx(:,6), '--', omega, Pug(1:round(N/2)-1));
    axis(10.^[-2,2,-15,0])
    xlabel('omega [rad/s]'); ylabel('Sugug [rad2/Hz]')
    print -depsc2 -r1200 fig7_15
else
    subplot(3,2,6)
    loglog(w,Sxx(:,6), '--', omega, Palphag(1:round(N/2)-1));

```

```

axis(10.^[-2,2,-15,0])
xlabel('omega [rad/s]'); ylabel('Sagag [rad2/Hz]')
print -depsc2 -r1200 fig7_17
end

```

The frequency response of the analytically derived power spectral densities and periodograms are plotted in Figure 7.15.

Compare the low frequency time histories of \hat{u} and θ with their relatively smooth power spectral densities versus the noisy time histories of α and $\frac{q\bar{c}}{V}$ and their noisy power spectral densities. What is the effect of the number of samples on the calculation of a periodogram?

7.6.5 Problem 7.1

The specific force in X -direction measured in an aircraft due to turbulence can be written as:

$$A_x = \ddot{x} + g \sin \theta \approx \ddot{x} + g\theta \quad (7.146)$$

Compare the influence of both horizontal- and vertical turbulence on the Cessna Ce-500 ‘Citation’, where it is assumed that vertical turbulence only excites the short-period acceleration, $\hat{u} = 0$, and horizontal turbulence only excites the phugoid ($\dot{q} = \dot{\alpha} = 0$). Calculate therefore the power spectral density $S_{A_x A_x}(\omega)$ due to horizontal- and vertical turbulence. Use the Dryden filters (Equations (6.39)-(6.41)) with $\sigma_{w_g} = \sigma_{u_g} = 1 \text{ m/s}$. Calculate the variance $\sigma_{A_x}^2$ by numerically integrating the power spectral density.

Compare the variance of \ddot{x} as well as the component $g\theta$ in the case of horizontal turbulence and calculate the cross power spectral density of \ddot{x} and $g\theta$. Give a physical explanation for the sign of the covariance.

7.7 Summary

In this chapter we have presented the symmetric equations of motion for a rigid aircraft flying in turbulent air. The mathematical model for the aerodynamic forces and moment has been derived, as well as new parameters which we called gust derivatives. The steady and the unsteady gust derivatives were calculated using aerodynamic frequency response functions, which describe the buildup in aerodynamic forces and the moment if the aircraft is to be considered a wing/fuselage-horizontal tailplane combination and the aerodynamics to be steady.

	X	Z	M
u	$\frac{V}{\bar{c}} \frac{C_{X_u}}{2\mu_c}$	$\frac{V}{\bar{c}} \frac{C_{Z_u}}{2\mu_c - C_{Z_{\dot{\alpha}}}}$	$\frac{V}{\bar{c}} \frac{C_{m_u} + C_{Z_u} \frac{C_{m_{\dot{\alpha}}}}{2\mu_c - C_{Z_{\dot{\alpha}}}}}{2\mu_c K_Y^2}$
α	$\frac{V}{\bar{c}} \frac{C_{X_\alpha}}{2\mu_c}$	$\frac{V}{\bar{c}} \frac{C_{Z_\alpha}}{2\mu_c - C_{Z_{\dot{\alpha}}}}$	$\frac{V}{\bar{c}} \frac{C_{m_\alpha} + C_{Z_\alpha} \frac{C_{m_{\dot{\alpha}}}}{2\mu_c - C_{Z_{\dot{\alpha}}}}}{2\mu_c K_Y^2}$
θ	$\frac{V}{\bar{c}} \frac{C_{Z_0}}{2\mu_c}$	$\frac{V}{\bar{c}} \frac{-C_{X_0}}{2\mu_c - C_{Z_{\dot{\alpha}}}}$	$\frac{V}{\bar{c}} \frac{-C_{X_0} \frac{C_{m_{\dot{\alpha}}}}{2\mu_c - C_{Z_{\dot{\alpha}}}}}{2\mu_c K_Y^2}$
q	$\frac{V}{\bar{c}} \frac{C_{X_q}}{2\mu_c}$	$\frac{V}{\bar{c}} \frac{2\mu_c + C_{Z_q}}{2\mu_c - C_{Z_{\dot{\alpha}}}}$	$\frac{V}{\bar{c}} \frac{C_{m_q} + C_{m_{\dot{\alpha}}} \frac{2\mu_c + C_{Z_q}}{2\mu_c - C_{Z_{\dot{\alpha}}}}}{2\mu_c K_Y^2}$
δ_e	$\frac{V}{\bar{c}} \frac{C_{X_{\delta_e}}}{2\mu_c}$	$\frac{V}{\bar{c}} \frac{C_{Z_{\delta_e}}}{2\mu_c - C_{Z_{\dot{\alpha}}}}$	$\frac{V}{\bar{c}} \frac{C_{m_{\delta_e}} + C_{Z_{\delta_e}} \frac{C_{m_{\dot{\alpha}}}}{2\mu_c - C_{Z_{\dot{\alpha}}}}}{2\mu_c K_Y^2}$
u_g	$\frac{V}{\bar{c}} \frac{C_{X_{u_g}}}{2\mu_c}$	$\frac{V}{\bar{c}} \frac{C_{Z_{u_g}}}{2\mu_c - C_{Z_{\dot{\alpha}}}}$	$\frac{V}{\bar{c}} \frac{C_{m_{u_g}} + C_{Z_{u_g}} \frac{C_{m_{\dot{\alpha}}}}{2\mu_c - C_{Z_{\dot{\alpha}}}}}{2\mu_c K_Y^2}$
\dot{u}_g	$\frac{V}{\bar{c}} \frac{C_{X_{\dot{u}_g}}}{2\mu_c}$	$\frac{V}{\bar{c}} \frac{C_{Z_{\dot{u}_g}}}{2\mu_c - C_{Z_{\dot{\alpha}}}}$	$\frac{V}{\bar{c}} \frac{C_{m_{\dot{u}_g}} + C_{Z_{\dot{u}_g}} \frac{C_{m_{\dot{\alpha}}}}{2\mu_c - C_{Z_{\dot{\alpha}}}}}{2\mu_c K_Y^2}$
α_g	$\frac{V}{\bar{c}} \frac{C_{X_{\alpha_g}}}{2\mu_c}$	$\frac{V}{\bar{c}} \frac{C_{Z_{\alpha_g}}}{2\mu_c - C_{Z_{\dot{\alpha}}}}$	$\frac{V}{\bar{c}} \frac{C_{m_{\alpha_g}} + C_{Z_{\alpha_g}} \frac{C_{m_{\dot{\alpha}}}}{2\mu_c - C_{Z_{\dot{\alpha}}}}}{2\mu_c K_Y^2}$
$\dot{\alpha}_g$	$\frac{V}{\bar{c}} \frac{C_{X_{\dot{\alpha}_g}}}{2\mu_c}$	$\frac{V}{\bar{c}} \frac{C_{Z_{\dot{\alpha}_g}}}{2\mu_c - C_{Z_{\dot{\alpha}}}}$	$\frac{V}{\bar{c}} \frac{C_{m_{\dot{\alpha}_g}} + C_{Z_{\dot{\alpha}_g}} \frac{C_{m_{\dot{\alpha}}}}{2\mu_c - C_{Z_{\dot{\alpha}}}}}{2\mu_c K_Y^2}$

Table 7.1: Symbols appearing in the general state-space representation (Equations (7.104) and (7.109)).

$C_{X_{u_g}} = C_{X_u}$	$C_{Z_{u_g}} = C_{Z_u}$	$C_{m_{u_g}} = C_{m_u}$
$C_{X_{\dot{u}_g}} = 0$	$C_{Z_{\dot{u}_g}} = 2 C_{m_{ac}}$	$C_{m_{\dot{u}_g}} = -2 C_{m_h} \frac{l_h}{c}$
$C_{X_{\alpha_g}} = C_{X_\alpha}$	$C_{Z_{\alpha_g}} = C_{Z_\alpha}$	$C_{m_{\alpha_g}} = C_{m_\alpha}$
$C_{X_{\dot{\alpha}_g}} = 0$	$C_{Z_{\dot{\alpha}_g}} = C_{Z_{\dot{\alpha}}} - C_{Z_q}$	$C_{m_{\dot{\alpha}_g}} = C_{m_{\dot{\alpha}}} - C_{m_q}$

Table 7.2: Calculation of the symmetric gust derivatives.

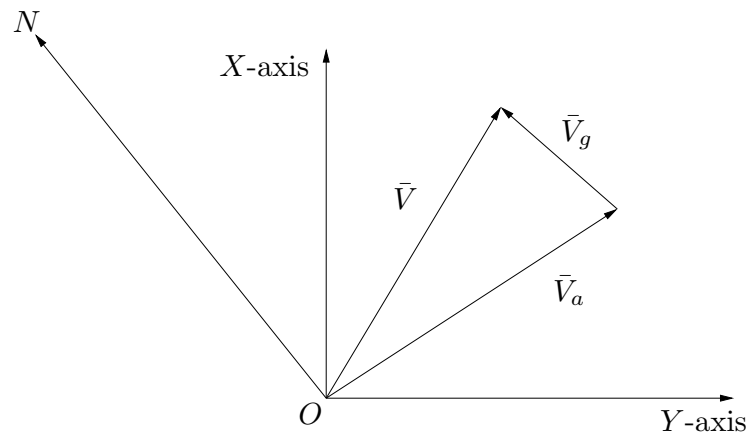


Figure 7.1: The velocities in the horizontal OXY -plane.

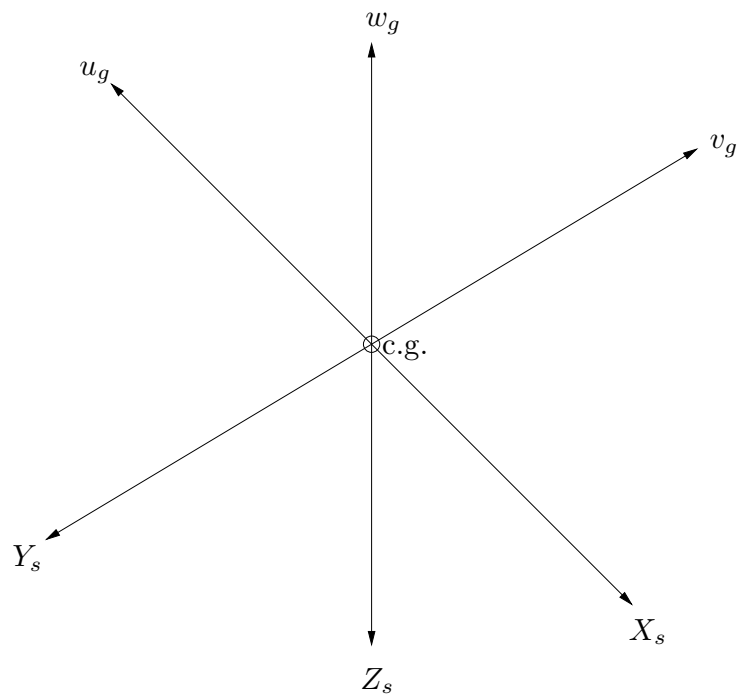


Figure 7.2: Positive directions of the gust velocities u_g , v_g and w_g .

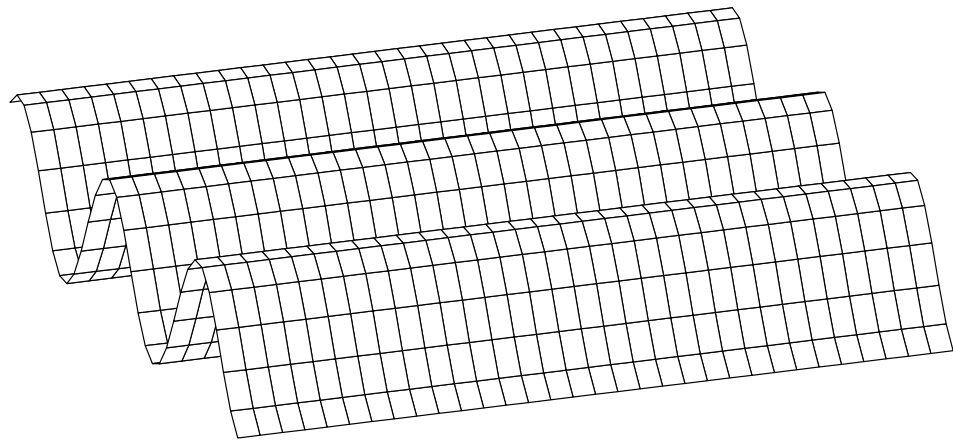


Figure 7.3: A sinusoidal elementary field of flow.

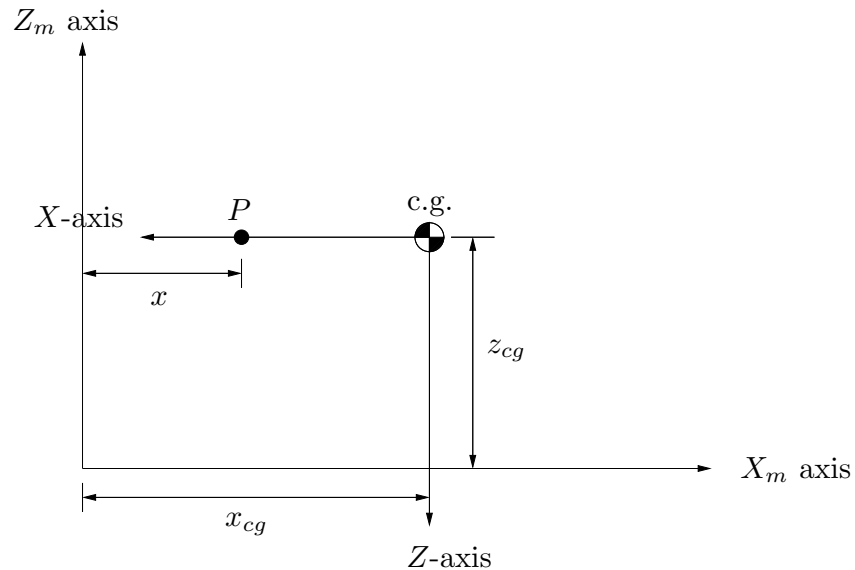


Figure 7.4: Positioning of the centre of gravity and arbitrary point P in a measurement frame of reference $OX_mY_mZ_m$.

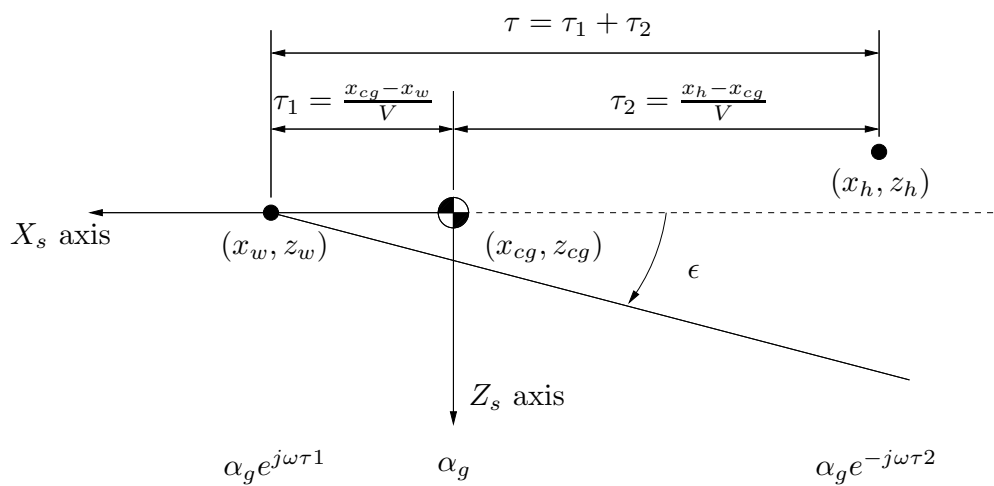


Figure 7.5: The influence of the finite dimensions of an aircraft.

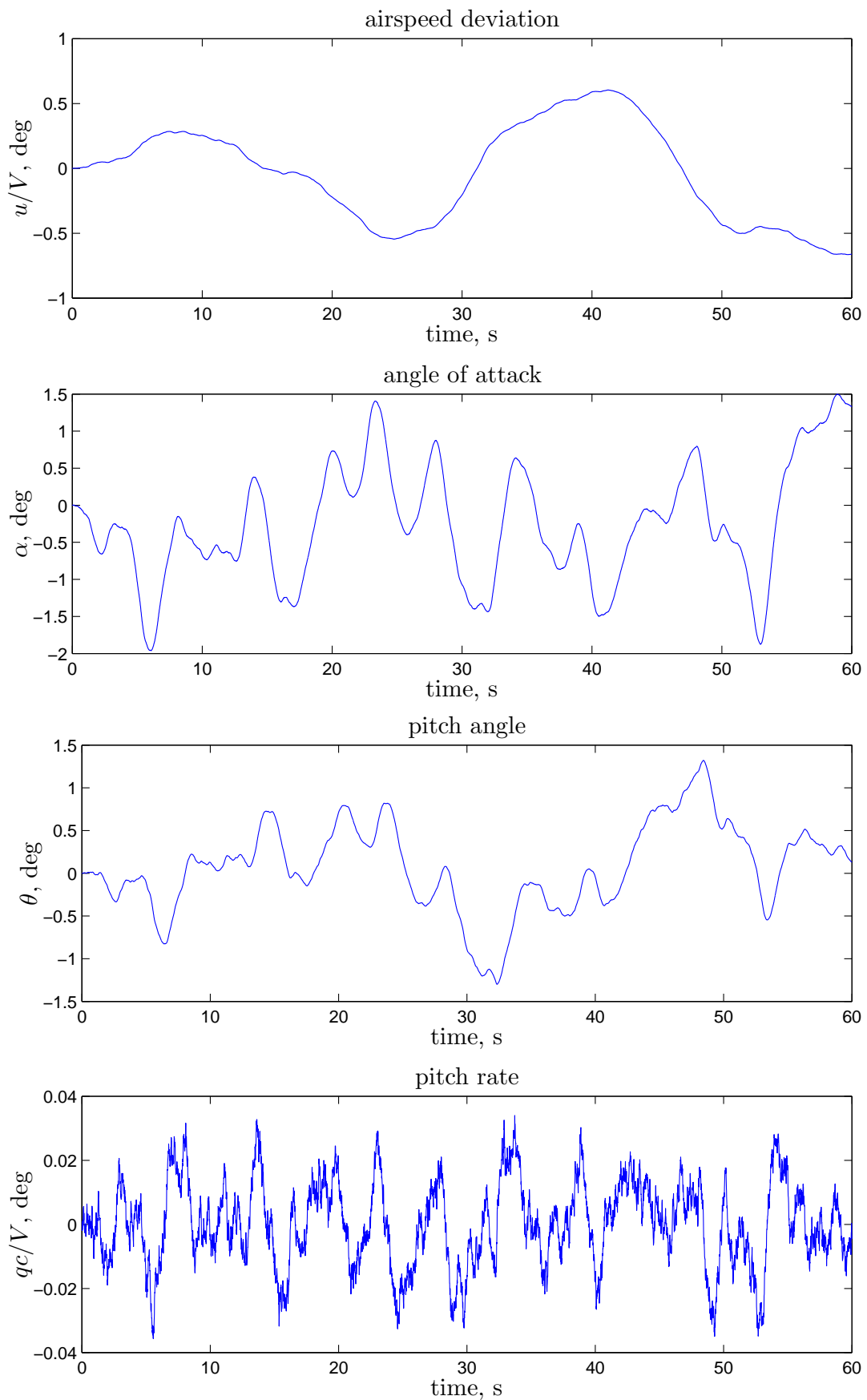


Figure 7.6: Aircraft responses to vertical turbulence for the Ce-500 ‘Citation’ for $V = 59.9 \text{ m/s}$ ($L_g=150 \text{ m}$, $\sigma=1 \text{ m/s}$).

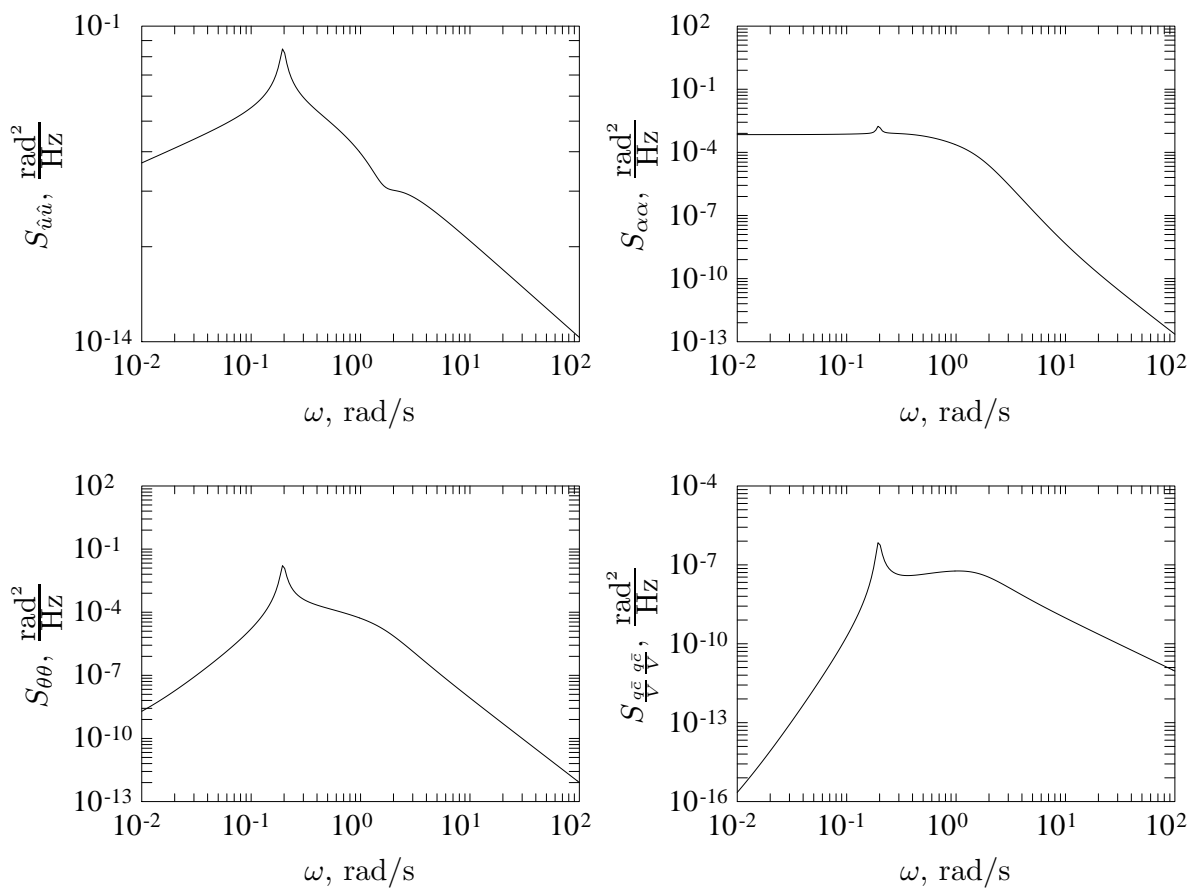


Figure 7.7: Auto power spectral densities of symmetric aircraft motion variables due to vertical turbulence for the Ce-500 ‘Citation’.

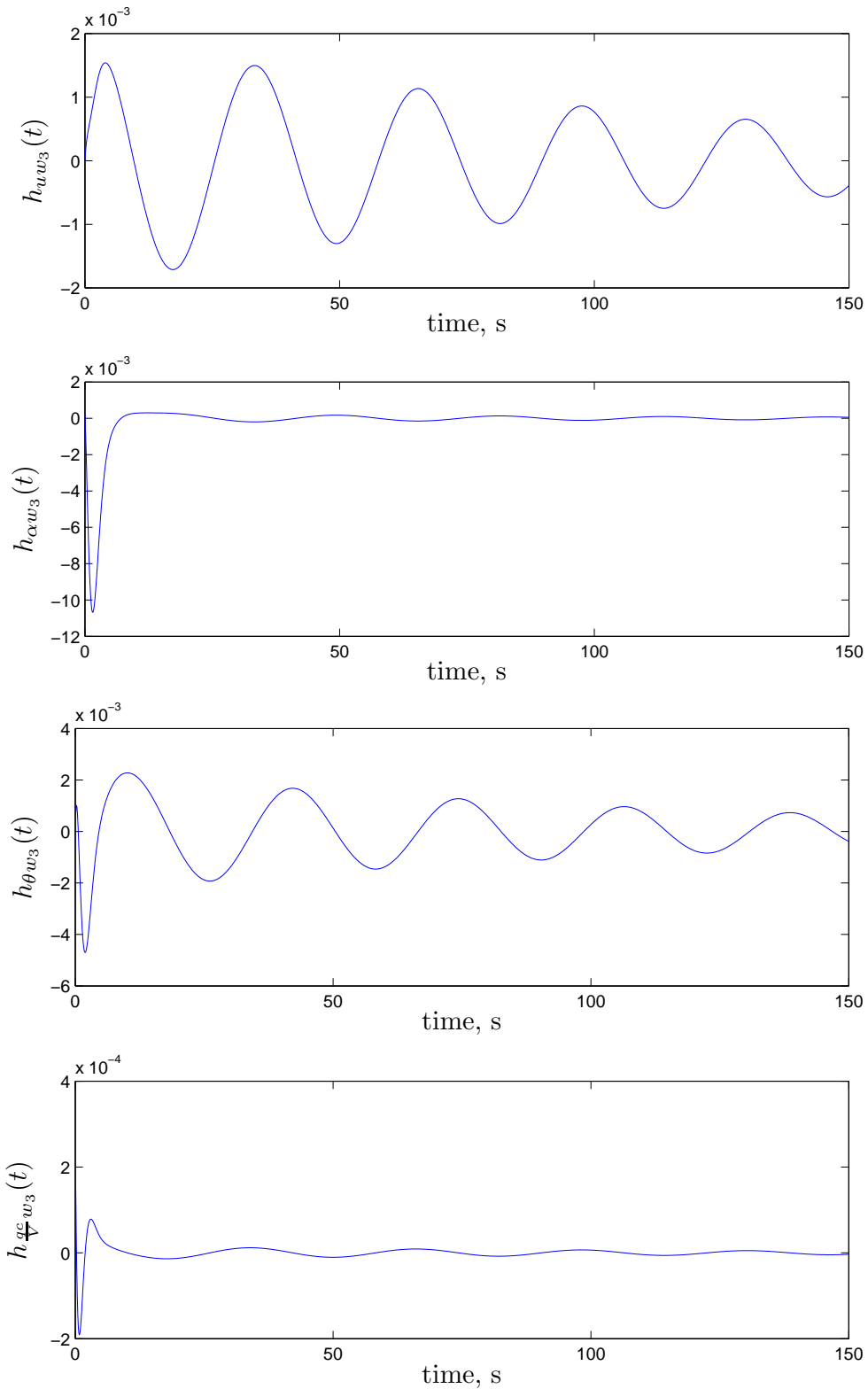


Figure 7.8: Impulse responses of symmetric aircraft motion variables (vertical turbulence) for the Ce-500 ‘Citation’.

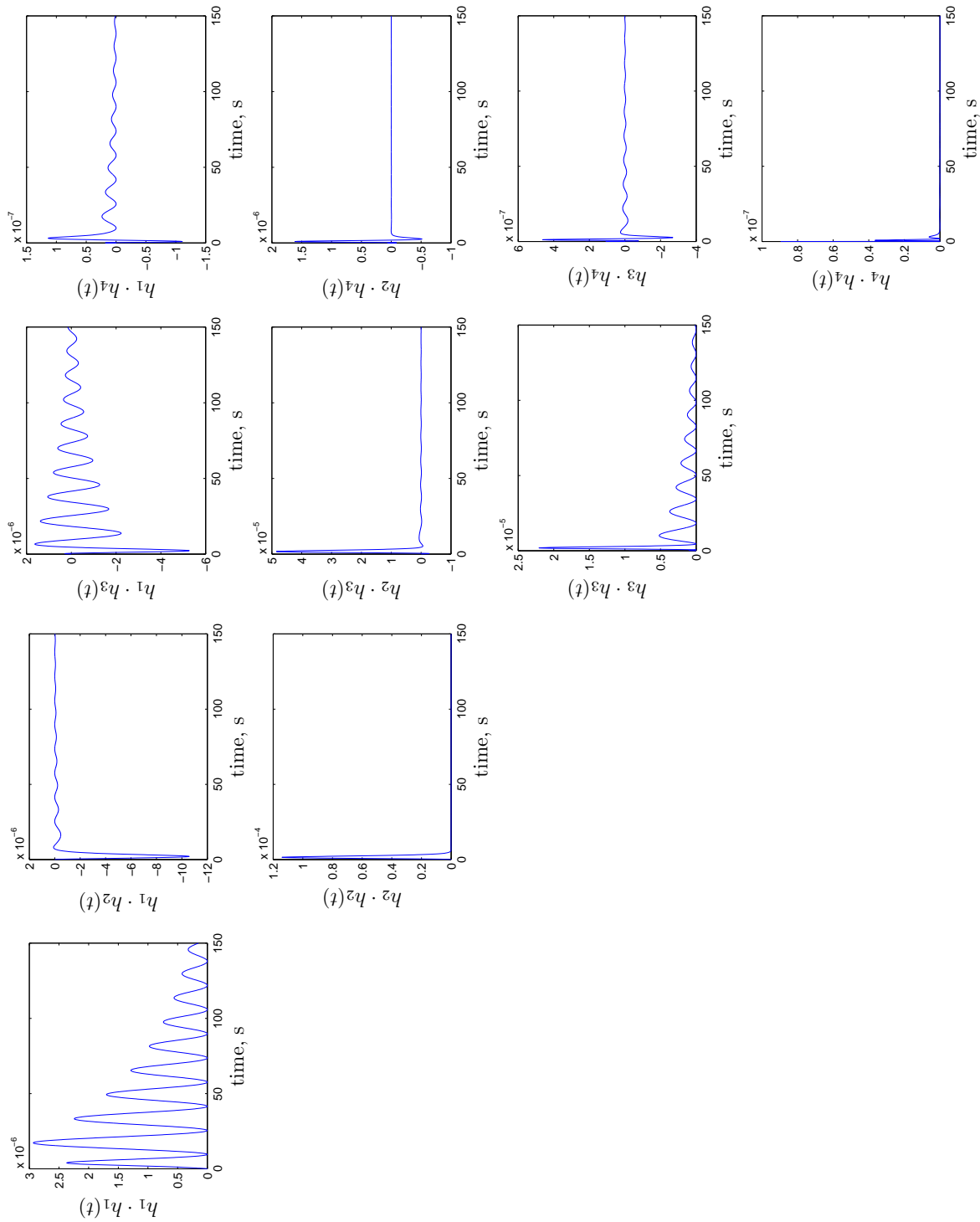


Figure 7.9: (Cross) products of impulse responses for the Ce-500 ‘Citation’.

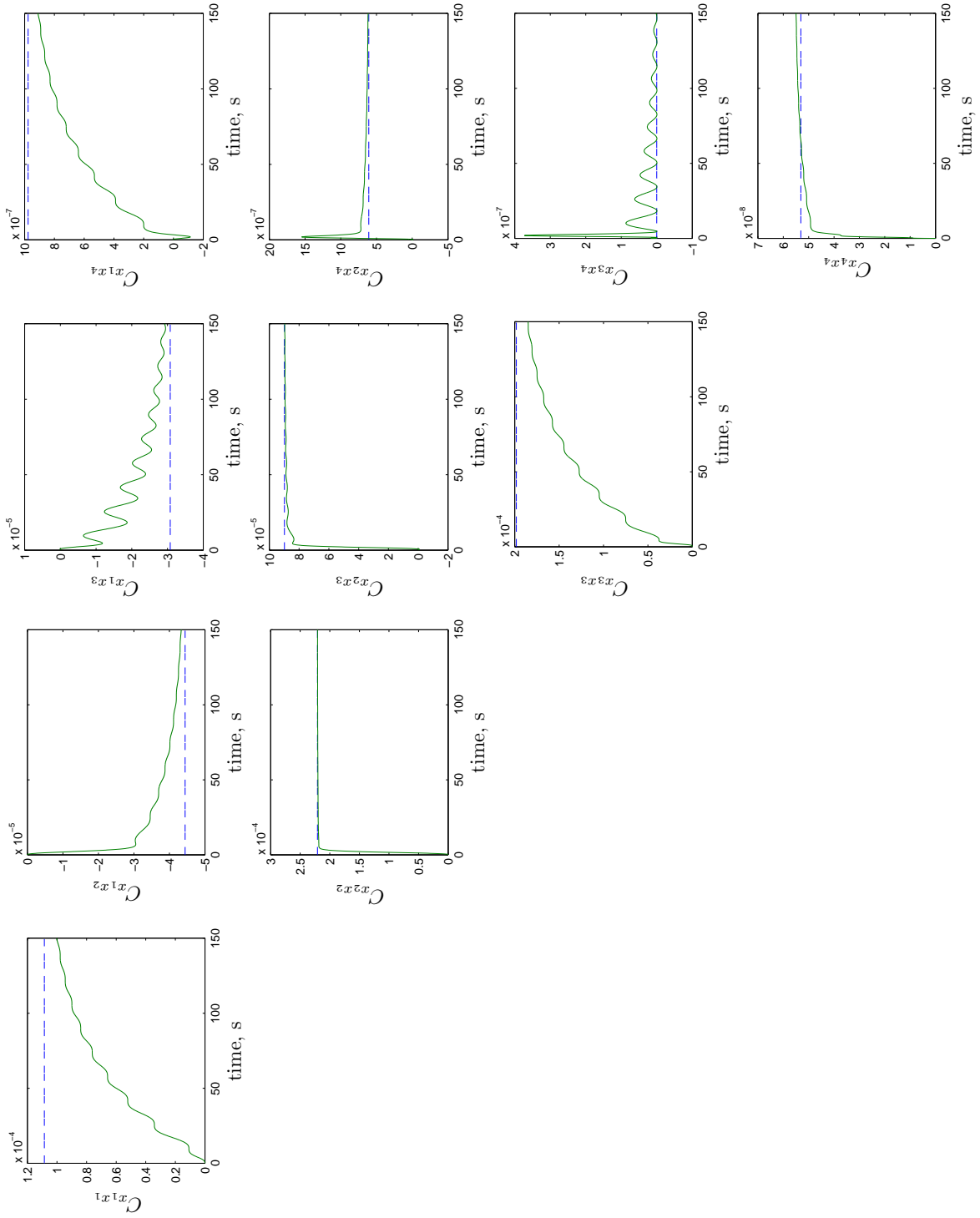


Figure 7.10: Growth in time of the covariance matrix calculated by integrating the (cross) products of the impulse responses (vertical turbulence) for the Ce-500 ‘Citation’.

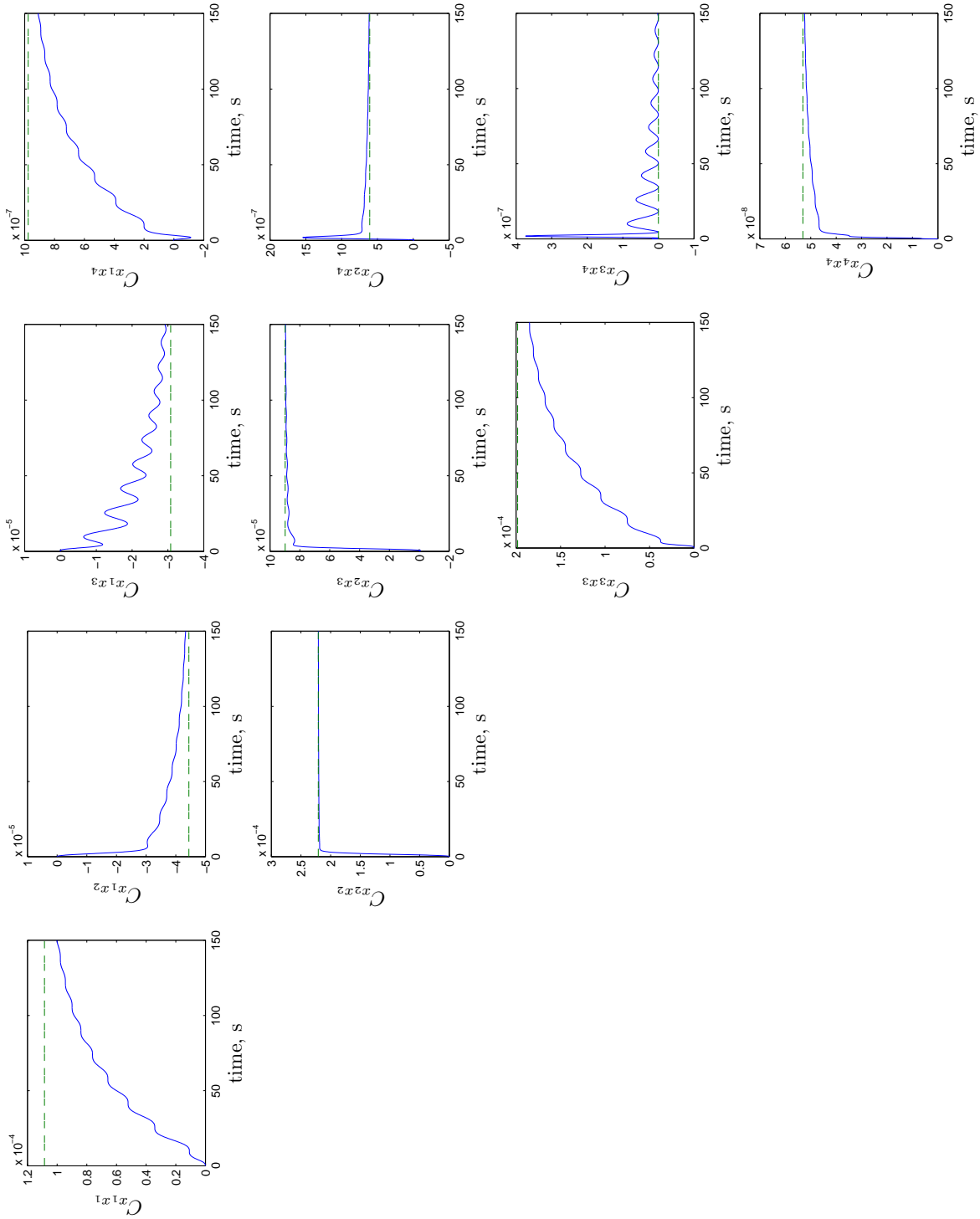


Figure 7.11: Growth in time of the covariance matrix of symmetric aircraft motion variables (response to vertical turbulence) for the Ce-500 'Citation'.

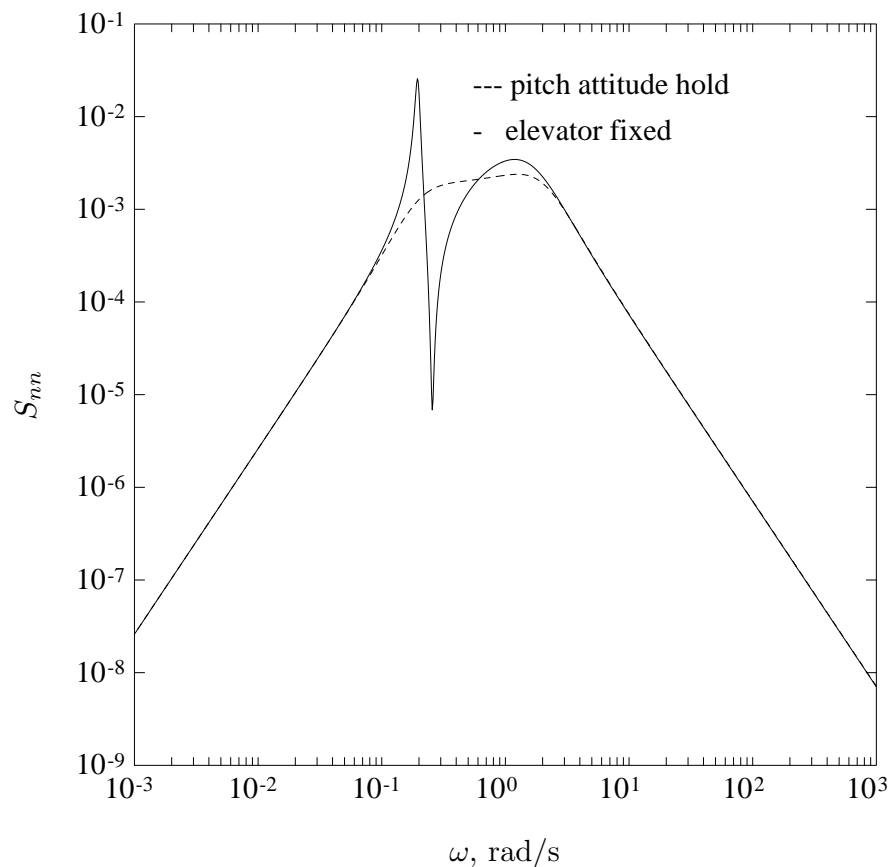


Figure 7.12: Power spectral density of the normal acceleration due to vertical turbulence for controlled (dashed line) and uncontrolled aircraft (continuous line) for the Ce-500 ‘Citation’.

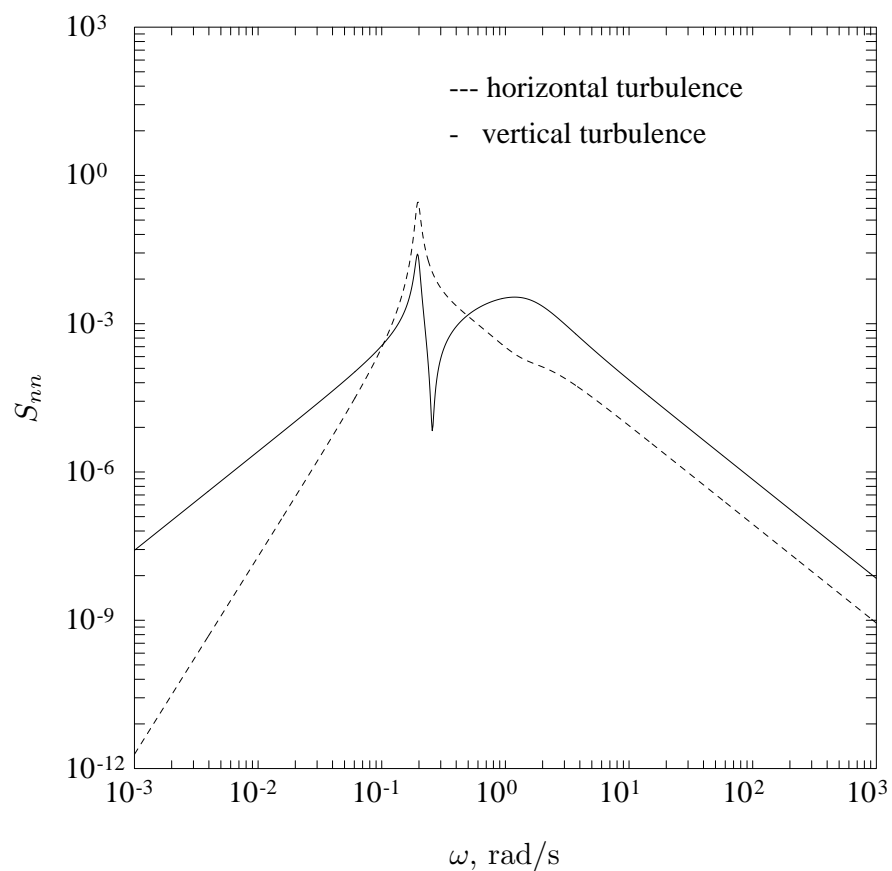


Figure 7.13: Power spectral density of the normal acceleration due to vertical (continuous line) and horizontal turbulence (dashed line) for the Ce-500 ‘Citation’.

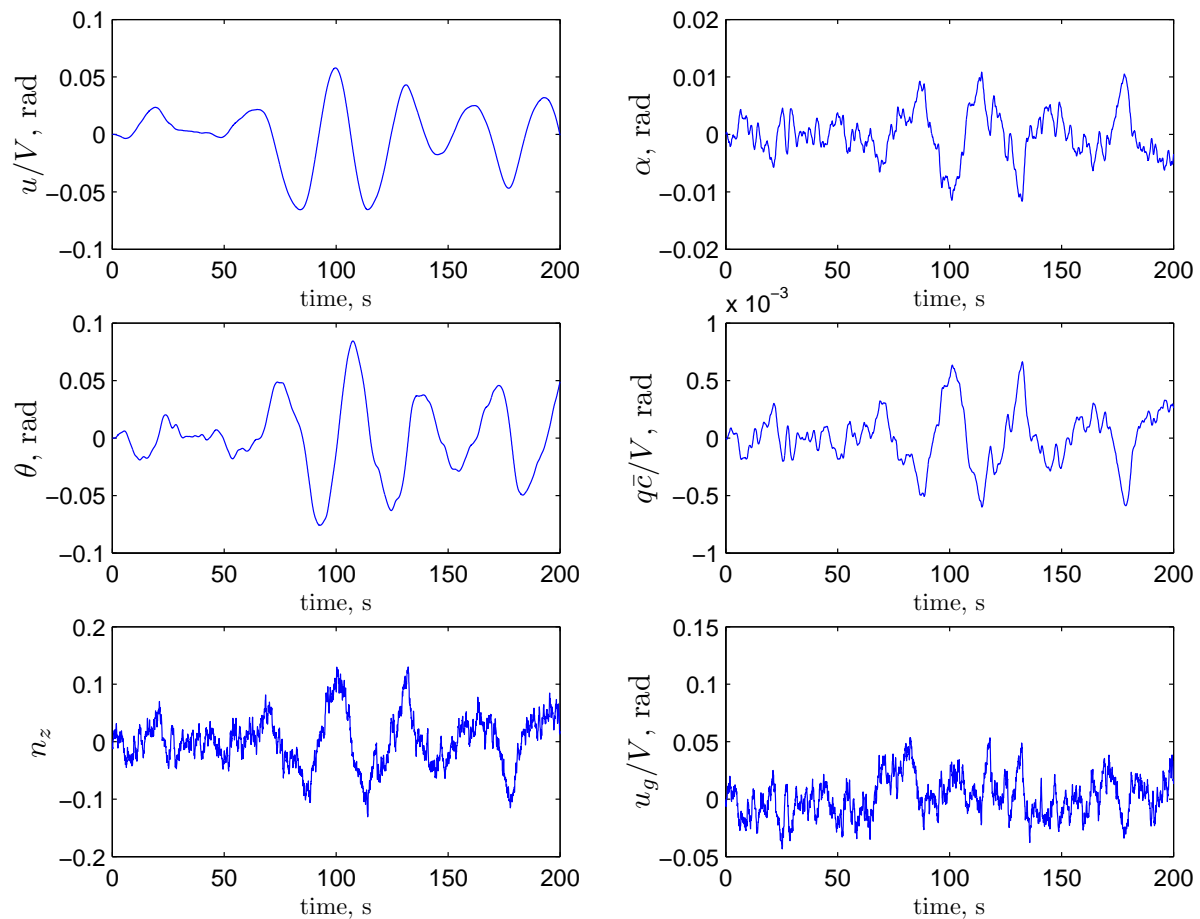


Figure 7.14: Aircraft responses due to horizontal turbulence for the Ce-500 ‘Citation’.

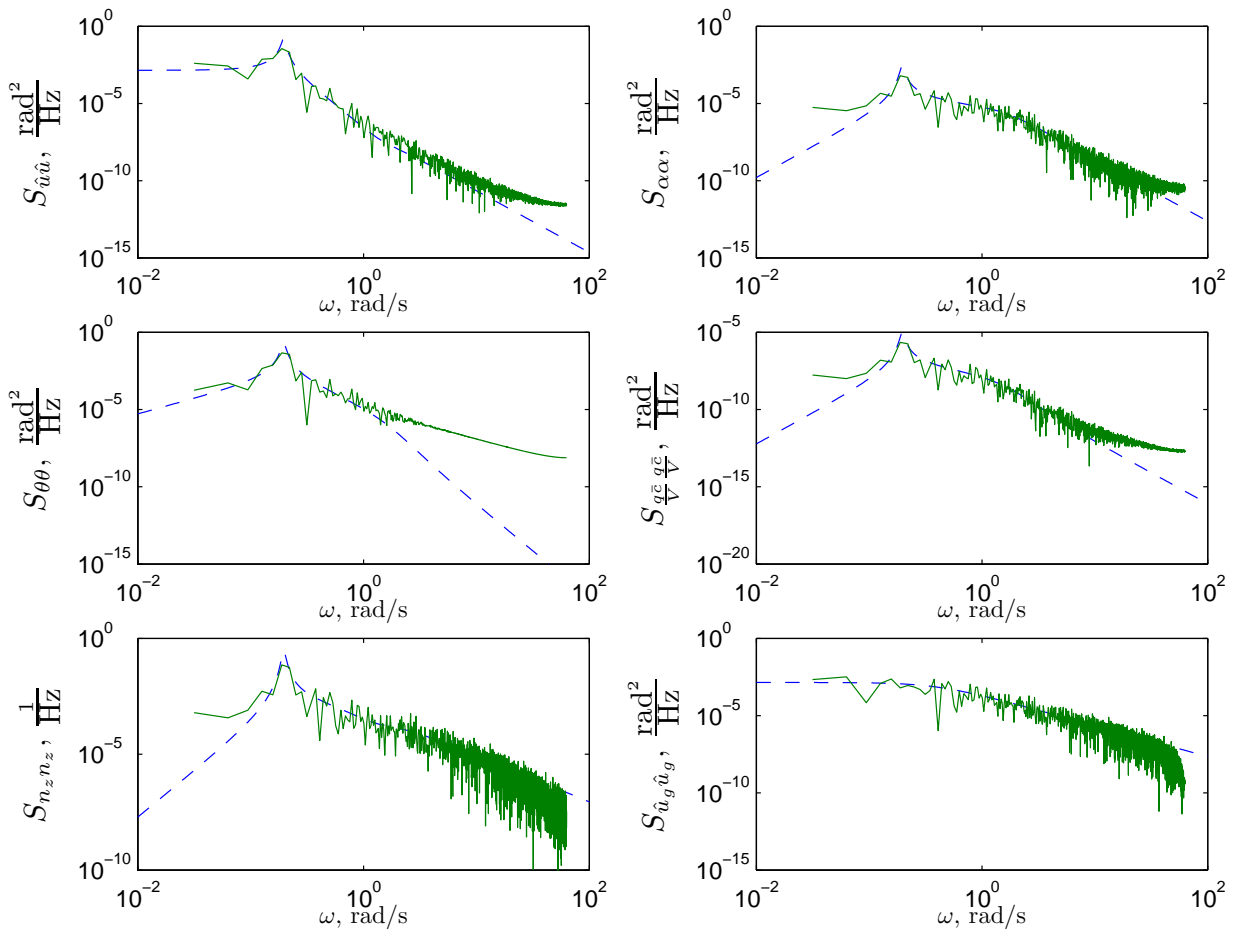


Figure 7.15: Analytically derived power spectral densities and periodograms of the motion variables for the Ce-500 ‘Citation’. The periodograms have been calculated from time-domain data (previous figure).

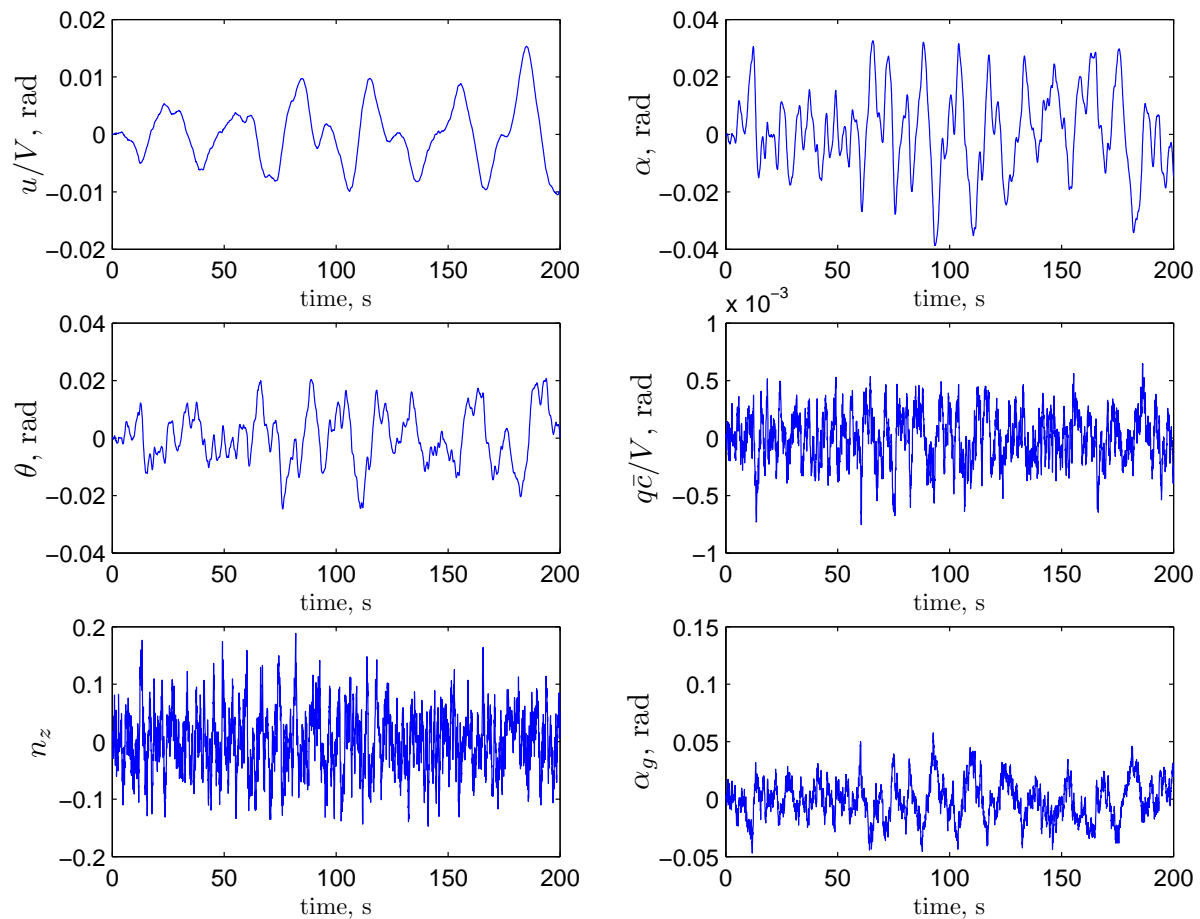


Figure 7.16: Aircraft responses due to vertical turbulence for the Ce-500 ‘Citation’.

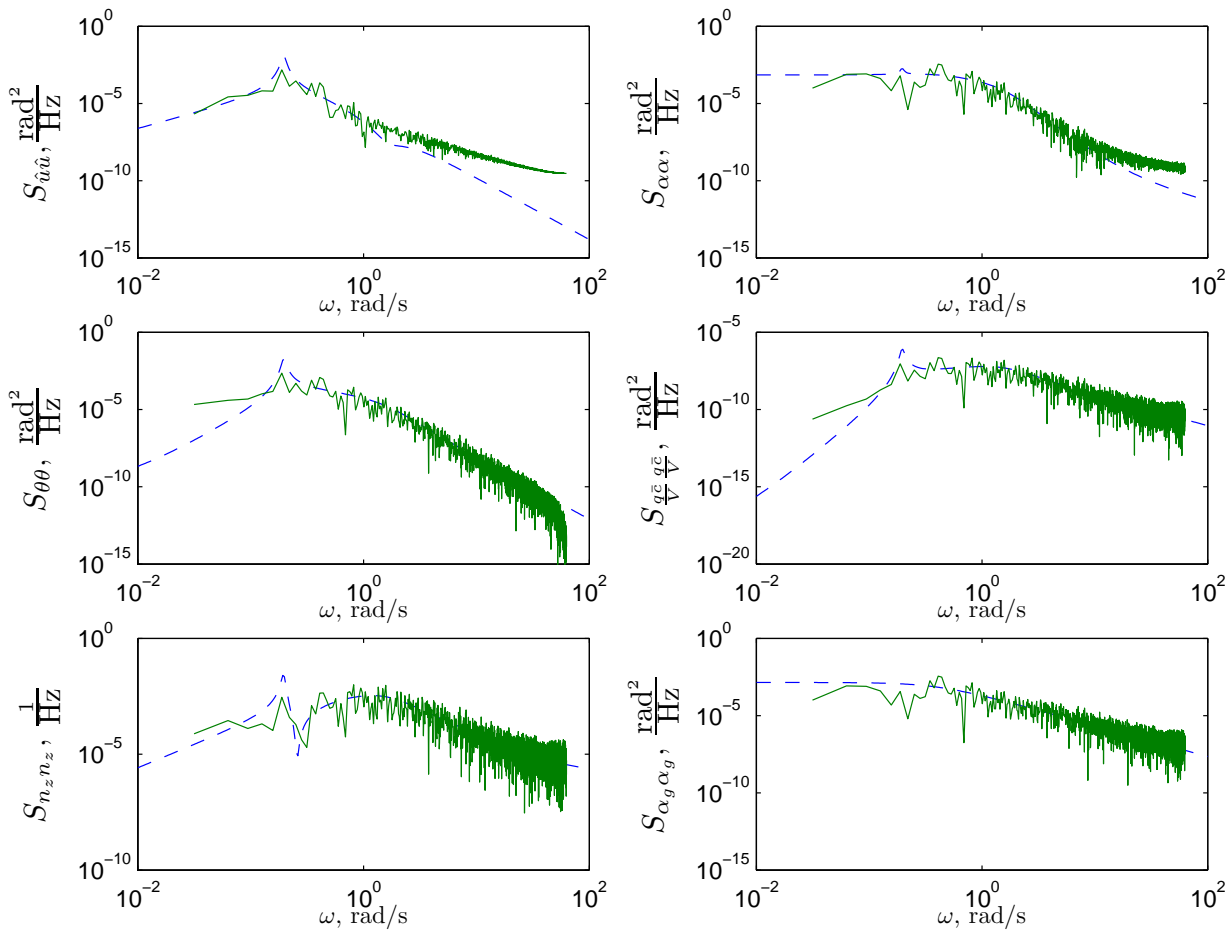


Figure 7.17: Analytically derived power spectral densities and periodograms of the motion variables for the Ce-500 ‘Citation’. The periodograms have been calculated from time-domain data (previous figure).

Chapter 8

Asymmetric Aircraft Response to Atmospheric Turbulence

8.1 Introduction

In this chapter a study will be made of the asymmetric motions of an aircraft in random atmospheric turbulence. As such it is an extension of the previous chapter, where the symmetric motions of an aircraft in atmospheric turbulence were discussed.

An essential difference between the symmetric and the asymmetric responses of an aircraft in turbulence is, that in the first case the gust velocity can be assumed to change only along the aircraft's longitudinal axis, whilst it is supposed constant along the lateral axis, see Figure 8.1(a). For the asymmetric aircraft motions, however, this assumption cannot be maintained. Due to the variations of the gust velocity along the longitudinal as well as along the lateral axis, the atmospheric turbulence now has to be considered as a two-dimensional process, Figure 8.1(b).

The statistical properties of the atmospheric turbulence are derived by considering the two-dimensional autocovariance functions, which express the average relations between the gust velocities in two different points of a two-dimensional stationary, homogeneous and isentropic field of flow. The autocovariance functions are transformed into power spectral density functions by applying the Fourier transform for two variables. From these spectral density functions the rolling and yawing moments due to longitudinal and vertical gusts are derived.

Finally, the model describing the asymmetric aircraft response to atmospheric turbulence will be derived.

8.2 The two-dimensional autocovariance functions of stationary homogeneous isentropic turbulence

This section deals with the autocovariance functions describing the statistical properties of atmospheric turbulence. The starting point in this discussion is the assumption that atmospheric turbulence may be considered as a stationary stochastic process. Also the turbulence is assumed to be homogeneous and isentropic.

In one respect, the description of atmospheric turbulence as required for the study of the asymmetric motions of an aircraft strongly deviates from that required for the symmetric motions, discussed in the previous chapter. The assumption that the gust velocity is constant along the wingspan, i.e. along the Y_e -axis, can no longer be maintained. In this chapter use is therefore made of the less restrictive assumption that the gust velocity changes in the horizontal plane both along the X_e - and the Y_e -axes. The dimensions of the aircraft in the direction of the Z_e -axis are considered to be sufficiently small to permit neglecting the variations of the gust velocity along the Z_e -axis. Therefore,

$$\begin{aligned} u_g &= u_g(x, y) \\ v_g &= v_g(x, y) \\ w_g &= w_g(x, y) \end{aligned} \quad (8.1)$$

From these equations it follows that atmospheric turbulence is considered here as a two-dimensional stochastic process. It will be shown that the one-dimensional process generally considered, can be described as a special case of the two-dimensional process to be discussed below.

Autocovariance functions express the average relations between the velocities in two different points in the turbulent field of flow. The two points to be considered here, lie in the horizontal $O_e X_e Y_e$ -plane of the $O_e X_e Y_e Z_e$ -frame of reference. They are the origin $O_e(0, 0)$ and the point $P(x, y)$, see Figure 8.2. The three autocovariance functions of interest are:

$$\begin{aligned} C_{u_g u_g} &= E\{u_g(0, 0) u_g(x, y)\} \\ C_{v_g v_g} &= E\{v_g(0, 0) v_g(x, y)\} \\ C_{w_g w_g} &= E\{w_g(0, 0) w_g(x, y)\} \end{aligned} \quad (8.2)$$

In stationary homogeneous isentropic turbulence the variations of the gust velocities u_g , v_g and w_g are mutually independent. As a consequence the crosscorrelation functions of these gust velocities are equal to zero.

The autocovariance functions expressed in (8.2) are therefore the diagonal elements of the covariance matrix of atmospheric turbulence $C_{\bar{u}\bar{u}}$, Equation (6.12) where the off-diagonal elements all equal zero. The three autocovariance functions will be expressed in the two basic one-dimensional autocovariance functions $f(r)$ and $g(r)$, see Section 6.4.4 and Figure

8.3.

To this end the velocities u_g and v_g in the $O_eX_eY_e$ -plane are resolved in components along and perpendicular to O_eP , see Figure 8.4,

$$u_g = u_1 \sin \alpha + u_2 \cos \alpha = u_1 \frac{x}{r} + u_2 \frac{y}{r} \quad (8.3)$$

$$v_g = v_1 \cos \alpha + v_2 \sin \alpha = v_1 \frac{y}{r} + v_2 \frac{x}{r} \quad (8.4)$$

The expression for $C_{u_g u_g}$ then reads,

$$\begin{aligned} C_{u_g u_g} &= E\{u_g(0,0) u_g(x,y)\} \\ &= E\left\{(u_1(0,0) \frac{x}{r} + u_2(0,0) \frac{y}{r}) (u_1(x,y) \frac{x}{r} + u_2(x,y) \frac{y}{r})\right\} \\ &= E\left\{u_1(0,0) u_1(x,y) \left(\frac{x}{r}\right)^2 + u_2(0,0) u_2(x,y) \left(\frac{y}{r}\right)^2\right. \\ &\quad \left.+ u_1(0,0) u_2(x,y) \left(\frac{xy}{r^2}\right) + u_2(0,0) u_1(x,y) \left(\frac{xy}{r^2}\right)\right\} \end{aligned} \quad (8.5)$$

Since,

$$E\{u_1(0,0) u_1(x,y)\} = \sigma_{u_g}^2 f(r) \quad (8.6)$$

$$E\{u_2(0,0) u_2(x,y)\} = \sigma_{u_g}^2 g(r) \quad (8.7)$$

$$E\{u_1(0,0) u_2(x,y)\} = E\{u_2(0,0) u_1(x,y)\} = 0 \quad (8.8)$$

it follows,

$$C_{u_g u_g}(x,y) = \sigma_{u_g}^2 \left\{ f(r) \left(\frac{x}{r}\right)^2 + g(r) \left(\frac{y}{r}\right)^2 \right\} \quad (8.9)$$

Similarly,

$$C_{v_g v_g}(x,y) = \sigma_{v_g}^2 \left\{ f(r) \left(\frac{y}{r}\right)^2 + g(r) \left(\frac{x}{r}\right)^2 \right\} \quad (8.10)$$

and,

$$C_{w_g w_g}(x,y) = \sigma_{w_g}^2 g(r) \quad (8.11)$$

In order to perform numerical calculations it is necessary to substitute explicit expressions for $f(r)$ and $g(r)$. In accordance with Chapter 6, using the Dryden covariance functions, the one-dimensional autocorrelation functions are written as, Equation (6.28),

$$\begin{aligned} f(r) &= e^{-\frac{r}{L_g}} \\ g(r) &= e^{-\frac{r}{L_g}} \left(1 - \frac{1}{2} \frac{r}{L_g}\right) \end{aligned}$$

where L_g is the longitudinal scale of turbulence defined for any longitudinal correlation function $f(r)$ as, Equation (6.16),

$$L_g = \int_0^\infty f(r) dr$$

Using these expressions for $f(r)$ and $g(r)$, the two-dimensional autocovariance functions now become,

$$C_{u_g u_g} \left(\frac{x}{L_g}, \frac{y}{L_g} \right) = \sigma_{u_g}^2 \left\{ e^{-\frac{r}{L_g}} \left(\frac{x}{r} \right)^2 + e^{-\frac{r}{L_g}} \left(1 - \frac{1}{2} \frac{r}{L_g} \right) \left(\frac{y}{r} \right)^2 \right\} \quad (8.12)$$

$$C_{v_g v_g} \left(\frac{x}{L_g}, \frac{y}{L_g} \right) = \sigma_{v_g}^2 \left\{ e^{-\frac{r}{L_g}} \left(\frac{y}{r} \right)^2 + e^{-\frac{r}{L_g}} \left(1 - \frac{1}{2} \frac{r}{L_g} \right) \left(\frac{x}{r} \right)^2 \right\} \quad (8.13)$$

$$C_{w_g w_g} \left(\frac{x}{L_g}, \frac{y}{L_g} \right) = \sigma_{w_g}^2 e^{-\frac{r}{L_g}} \left(1 - \frac{1}{2} \frac{r}{L_g} \right) \quad (8.14)$$

8.3 The two-dimensional power spectral density functions of stationary homogeneous turbulence

We found in Chapter 5 that the power spectral density function matrix could be obtained by applying the Fourier transform to the elements of the covariance matrix. The off-diagonal elements (cross power spectral densities) of the power spectral density matrix of atmospheric turbulence velocities are equal to zero, since the cross correlations are assumed to equal zero so the only three two-dimensional power spectral density functions of interest are:

$$\begin{aligned} S_{u_g u_g}(\Omega_x L_g, \Omega_y L_g) \\ S_{v_g v_g}(\Omega_x L_g, \Omega_y L_g) \\ S_{w_g w_g}(\Omega_x L_g, \Omega_y L_g) \end{aligned} \quad (8.15)$$

These power spectral density functions are obtained by applying the Fourier transform for two variables to the two-dimensional autocovariance functions, derived in the foregoing.

As an extension to the conventional expression for the Fourier transform, the expression for the Fourier transform $S(\Omega_x L_g, \Omega_y L_g)$ of the covariance function for two variables $\frac{x}{L_g}$ and $\frac{y}{L_g}$ reads,

$$S(\Omega_x L_g, \Omega_y L_g) = \int_{-\infty}^{+\infty} \int_{-\infty}^{+\infty} C \left(\frac{x}{L_g}, \frac{y}{L_g} \right) e^{-j(\Omega_x x + \Omega_y y)} d\frac{x}{L_g} d\frac{y}{L_g} \quad (8.16)$$

Since the autocovariance functions $C \left(\frac{x}{L_g}, \frac{y}{L_g} \right)$ are all strictly even functions, see Table

3.3, we can write this as, Equation (8.16),

$$S(\Omega_x L_g, \Omega_y L_g) = 4 \int_0^{+\infty} \int_0^{+\infty} C\left(\frac{x}{L_g}, \frac{y}{L_g}\right) \cos \Omega_x x \cos \Omega_y y d\frac{x}{L_g} d\frac{y}{L_g}$$

The resulting three power spectra (8.15) are obtained by substituting the autocovariance functions (8.12)-(8.14),

$$\begin{aligned} S_{u_g u_g}(\Omega_x L_g, \Omega_y L_g) &= 4 \int_0^{+\infty} \int_0^{+\infty} \sigma_{u_g}^2 \left\{ e^{-\frac{r}{L_g}} \left(\frac{x}{r} \right)^2 + e^{-\frac{r}{L_g}} \left(1 - \frac{1}{2} \frac{r}{L_g} \right) \left(\frac{y}{r} \right)^2 \right\} \\ &\quad \cos \Omega_x x \cos \Omega_y y d\frac{x}{L_g} d\frac{y}{L_g} \end{aligned} \quad (8.17)$$

$$\begin{aligned} S_{v_g v_g}(\Omega_x L_g, \Omega_y L_g) &= 4 \int_0^{+\infty} \int_0^{+\infty} \sigma_{v_g}^2 \left\{ e^{-\frac{r}{L_g}} \left(\frac{y}{r} \right)^2 + e^{-\frac{r}{L_g}} \left(1 - \frac{1}{2} \frac{r}{L_g} \right) \left(\frac{x}{r} \right)^2 \right\} \\ &\quad \cos \Omega_x x \cos \Omega_y y d\frac{x}{L_g} d\frac{y}{L_g} \end{aligned} \quad (8.18)$$

$$\begin{aligned} S_{w_g w_g}(\Omega_x L_g, \Omega_y L_g) &= 4 \int_0^{+\infty} \int_0^{+\infty} \sigma_{w_g}^2 e^{-\frac{r}{L_g}} \left(1 - \frac{1}{2} \frac{r}{L_g} \right) \\ &\quad \cos \Omega_x x \cos \Omega_y y d\frac{x}{L_g} d\frac{y}{L_g} \end{aligned} \quad (8.19)$$

The above integrals can all be expressed in closed form. The results are,

$$S_{u_g u_g}(\Omega_x L_g, \Omega_y L_g) = \pi \sigma_{u_g}^2 \frac{1 + \Omega_x^2 L_g^2 + 4\Omega_y^2 L_g^2}{(1 + \Omega_x^2 L_g^2 + \Omega_y^2 L_g^2)^{5/2}} \quad (8.20)$$

$$S_{v_g v_g}(\Omega_x L_g, \Omega_y L_g) = \pi \sigma_{v_g}^2 \frac{1 + 4\Omega_x^2 L_g^2 + \Omega_y^2 L_g^2}{(1 + \Omega_x^2 L_g^2 + \Omega_y^2 L_g^2)^{5/2}} \quad (8.21)$$

$$S_{w_g w_g}(\Omega_x L_g, \Omega_y L_g) = 3\pi \sigma_{w_g}^2 \frac{\Omega_x^2 L_g^2 + \Omega_y^2 L_g^2}{(1 + \Omega_x^2 L_g^2 + \Omega_y^2 L_g^2)^{5/2}} \quad (8.22)$$

A graphical representation of $S_{u_g u_g}(\Omega_x L_g, \Omega_y L_g)$ is given in Figure 8.5. There is a close relation between the above two-dimensional power spectral densities and the corresponding one-dimensional spectral density functions used to compute the symmetric motion of an aircraft in Chapter 6. The magnitude of a one-dimensional spectral density, i.e. $S'_{u_g u_g}$ at a certain value of $\Omega_x L_g$ can be considered to express the contribution to the total power contained in the fluctuations of u_g at this particular frequency, for a frequency range

$\Delta(\Omega_x L_g) = 1$. In the two-dimensional spectral density function $S_{u_g u_g}(\Omega_x L_g, \Omega_y L_g)$, at the $\Omega_x L_g$ considered, the same contribution to the power is provided by all frequencies $\Omega_y L_g$ together. The one-dimensional spectrum does not distinguish the value of $\Omega_y L_g$, at which the power is contributed. As a consequence the relation between $S'_{u_g u_g}(\Omega_x L_g)$ and $S_{u_g u_g}(\Omega_x L_g, \Omega_y L_g)$ is,

$$S'_{u_g u_g}(\Omega_x L_g) = \frac{1}{\pi} \int_0^{+\infty} S_{u_g u_g}(\Omega_x L_g, \Omega_y L_g) d(\Omega_y L_g) \quad (8.23)$$

Corresponding relations hold true for the power spectral density functions of v_g and w_g . If the integration (8.23) is carried out, the familiar one-dimensional spectral density function results,

$$S'_{u_g u_g}(\Omega_x L_g) = 2\sigma_{u_g}^2 \frac{1}{1 + \Omega_x^2 L_g^2} \quad (8.24)$$

which is indeed identical to the relevant one-dimensional Dryden power spectrum used in Section 6.6. Similar results are obtained for the power spectral density functions of v_g and w_g .

8.4 Elementary two-dimensional fields of flow

As in the case of the one-dimensional turbulence, the two-dimensional stochastic turbulence can be considered as a superposition of infinitely many elementary fields of flow. The one-dimensional elementary fields in Chapter 7 were represented by, Equations (7.16) and (7.17),

$$\begin{aligned} u_g &= u_{g_{max}} \operatorname{Re} \{ e^{j\Omega_x x} \} \\ w_g &= w_{g_{max}} \operatorname{Re} \{ e^{j\Omega_x x} \} \end{aligned}$$

The spatial circular frequency Ω_x [rad/m] or the wavelength $\lambda_x = \frac{2\pi}{\Omega_x}$ of these fields could assume any value between zero and infinity. In accordance with the foregoing, two-dimensional fields of flow will be considered now. These fields have a fixed orientation with respect to the $O_e X_e Y_e Z_e$ -frame of reference. In each of these elementary fields, the gust velocity varies sinusoidally along the X_e -axis as well as along the Y_e -axis.

The two-dimensional fields satisfy the expressions,

$$\begin{aligned} u_g &= u_{g_{max}} \operatorname{Re} \{ e^{j(\Omega_x x + \Omega_y y)} \} \\ v_g &= v_{g_{max}} \operatorname{Re} \{ e^{j(\Omega_x x + \Omega_y y)} \} \\ w_g &= w_{g_{max}} \operatorname{Re} \{ e^{j(\Omega_x x + \Omega_y y)} \} \end{aligned} \quad (8.25)$$

The one-dimensional fields, considered in Chapter 7, obviously are the two-dimensional fields for which $\Omega_y = 0$. In the following, another interpretation is given for the expressions

(8.25). The u_g Equation in (8.25) is therefore written as,

$$\begin{aligned}
 u_g &= u_{g_{max}} \operatorname{Re} \left\{ e^{j(\Omega_x x + \Omega_y y)} \right\} \\
 &= u_{g_{max}} \operatorname{Re} \{ (\cos \Omega_x x + j \sin \Omega_x x) (\cos \Omega_y y + j \sin \Omega_y y) \} \\
 &= u_{g_{max}} (\cos \Omega_x x \cos \Omega_y y - \sin \Omega_x x \sin \Omega_y y) \\
 &= u_{g_1}(x, y) - u_{g_2}(x, y)
 \end{aligned} \tag{8.26}$$

According to this expression the elementary field can be considered as the superposition of two separate fields in each of which the gust velocity varies sinusoidally in the X_e - as well as in the Y_e -direction, see Figure 8.6 and 8.7,

$$\begin{aligned}
 u_{g_1}(x, y) &= u_{g_{max}} \cos \Omega_x x \cos \Omega_y y \\
 u_{g_2}(x, y) &= u_{g_{max}} \sin \Omega_x x \sin \Omega_y y
 \end{aligned} \tag{8.27}$$

The characteristic difference between the two fields $u_{g_1}(x, y)$ and $u_{g_2}(x, y)$ is that the first one is symmetric with respect to the vertical $O_e X_e Z_e$ -plane and the second one is antisymmetric with respect to this plane. Quite similarly, the v_g - and w_g -fields can be separated in symmetric and antisymmetric parts:

$$\begin{aligned}
 v_{g_1}(x, y) &= v_{g_{max}} \cos \Omega_x x \cos \Omega_y y \quad (\text{antisymmetric}) \\
 v_{g_2}(x, y) &= v_{g_{max}} \sin \Omega_x x \sin \Omega_y y \quad (\text{symmetric})
 \end{aligned} \tag{8.28}$$

$$\begin{aligned}
 w_{g_1}(x, y) &= w_{g_{max}} \cos \Omega_x x \cos \Omega_y y \quad (\text{symmetric}) \\
 w_{g_2}(x, y) &= w_{g_{max}} \sin \Omega_x x \sin \Omega_y y \quad (\text{antisymmetric})
 \end{aligned} \tag{8.29}$$

The expressions (8.25) permit two apparently different interpretations of the way in which the gust velocity varies in the elementary field of flow. According to the view expressed by some researchers, the two-dimensional field is a one-dimensional field, which has been rotated about the Z_e -axis over an angle $\arctan(\frac{\Omega_y}{\Omega_x})$, such that the wave-heads and valleys are no longer perpendicular to the X_e -axis, see Figure 8.8. In order to gain more insight in the construction of the elementary flow field, Figure 8.9(a) and 8.9(b), which are computer generated, are numerically superimposed. The resulting image has been plotted in Figure 8.10, which corresponds to Figure 8.8 as expected.

In nominally steady straight flight, the aircraft's plane of symmetry usually coincides with the $O_e X_e Z_e$ -plane. As a consequence the symmetric parts $u_{g_1}(x, y)$, $v_{g_2}(x, y)$ and $w_{g_1}(x, y)$ of the elementary fields can cause only symmetric deviations from steady flight. In Chapter 7, Ω_y was in fact supposed to be zero. According to (8.28), this permitted the $v_{g_2}(x, y)$ -field to be omitted when considering the symmetric responses.

The three antisymmetric parts $u_{g_2}(x, y)$, $v_{g_1}(x, y)$ and $w_{g_2}(x, y)$ of the elementary fields give rise to asymmetric deviations from steady flight. In the following section the forces and moments due to these three elementary, antisymmetric fields are discussed.

8.5 The force and moments due to gust velocities parallel to the longitudinal axis

In the previous section it has been shown that only the antisymmetric part of the elementary u_g -field, Equation (8.27),

$$u_{g_2}(x, y) = u_{g_{max}} \sin \Omega_x x \sin \Omega_y y$$

has to be considered here. Suppose a wing has been placed in such a field. The plane of symmetry of the wing coincides with the $O_e X_e Z_e$ -plane. Due to the variations of u_g in the Y_e -direction, a rolling and a yawing moment will act on this wing. The sideforce, which in principle could arise, is supposed to be negligible. The aerodynamic force and moments exerted by the longitudinal field on other parts of the aircraft, other than the wing, are neglected. In the following, the longitudinal gust velocity in the $O_e X_e Z_e$ -plane will be referred to simply as u_g . Also the index 2 of $u_{g_2}(x, y)$ will be omitted, so,

$$u_g = u_{g_{max}} \sin \Omega_x x \quad (8.30)$$

and,

$$u_g(x, y) = u_g \sin \Omega_y y \quad (8.31)$$

The calculation of the rolling moment acting on the wing, is based on the assumption that the additional lift due to the turbulence can be computed by means of a strip-theory. A chordwise strip of the wing of width dy at a distance y from the plane of symmetry contributes to the rolling moment, see Figure 8.11,

$$dL_g = -c_l \frac{1}{2} \rho \left\{ [V + u_g(x, y)]^2 - V^2 \right\} c y dy = -\rho V u_{g_{max}} \sin \Omega_x x c_l c \sin \Omega_y y y dy \quad (8.32)$$

Consequently the total rolling moment due to the u_g -field is,

$$L_g = -2\rho V u_g \int_0^{\frac{b}{2}} c_l c \sin \Omega_y y y dy \quad (8.33)$$

This rolling moment can be expressed by means of a non-dimensional coefficient C_{l_g} ,

$$C_{l_g} = \frac{L_g}{\frac{1}{2} \rho V^2 S b} = -\frac{4}{S b} \frac{u_g}{V} \int_0^{\frac{b}{2}} c_l c \sin \Omega_y y y dy \quad (8.34)$$

Next the non-dimensional rolling moment coefficient C_{l_g} , is written by using a newly introduced gust derivative $C_{l_{u_g}}(\Omega_y \frac{b}{2})$,

$$C_{l_g} = C_{l_{u_g}}(\Omega_y \frac{b}{2}) \hat{u}_g \quad (8.35)$$

where,

$$\hat{u}_g = \frac{u_g}{V}$$

Hence,

$$C_{l_{u_g}}(\Omega_y \frac{b}{2}) = -\frac{4}{Sb} \int_0^{\frac{b}{2}} c_l c \sin \Omega_y y y dy \quad (8.36)$$

For sufficiently small values of $\Omega_y \frac{b}{2}$, i.e. for long wavelengths of $u_g(x, y)$ in the Y_e -direction, the velocity $u_g(x, y)$ varies approximately linearly along the wingspan. For these small values of $\Omega_y \frac{b}{2}$, $u_g(x, y)$ can be approximated, by replacing $\sin \Omega_y y$ by $\Omega_y y$,

$$u_g(x, y) = u_g \Omega_y y \quad (8.37)$$

This velocity distribution corresponds to the additional velocity due to a constant yawing velocity r ,

$$\Delta u = -ry \quad (8.38)$$

When further elaborating the expression for $C_{l_{u_g}}$, use is made of this similarity. The rolling moment acting on the wing due to a constant yawing velocity r can also be calculated by means of the strip-theory. An element of the wing of width dy at a distance y from the plane of symmetry contributes to the rolling moment,

$$dL = c_l \frac{1}{2} \rho 2V ry cy dy \quad (8.39)$$

The total rolling moment on the wing then is:

$$L = 2\rho V r \int_0^{\frac{b}{2}} c_l c y^2 dy = C_{l_{r_w}} \frac{rb}{2V} \frac{1}{2} \rho V^2 S b \quad (8.40)$$

The contribution of the wing to the stability derivative C_{l_r} is accordingly,

$$C_{l_{r_w}} = \frac{8}{Sb^2} \int_0^{\frac{b}{2}} c_l c y^2 dy \quad (8.41)$$

This expression for $C_{l_{r_w}}$ can be related to $C_{l_{u_g}}$ expressed by (8.36),

$$C_{l_{u_g}}(\Omega_y \frac{b}{2}) = -C_{l_{r_w}} \frac{\int_0^{\frac{b}{2}} c_l c \sin \Omega_y y y dy}{\int_0^{\frac{b}{2}} c_l c y^2 dy} \quad (8.42)$$

We will now introduce the non-dimensional function $h(\Omega_y \frac{b}{2})$,

$$h(\Omega_y \frac{b}{2}) = \frac{\int_0^{\frac{b}{2}} c_l c \sin \Omega_y y y dy}{\int_0^{\frac{b}{2}} c_l c y^2 dy} \quad (8.43)$$

In Figure 8.12 the function $h(\Omega_y \frac{b}{2})$ is plotted for three different spanwise distributions of the lift. It can be seen that the influence of the lift distribution increases with $\Omega_y \frac{b}{2}$. Using (8.43), $C_{l_{u_g}}$ can be written as,

$$C_{l_{u_g}}(\Omega_y \frac{b}{2}) = -C_{l_{r_w}} h(\Omega_y \frac{b}{2}) \quad (8.44)$$

It may be assumed, that the relation (8.44) between $C_{l_{u_g}}$ and $C_{l_{r_w}}$ holds true with some accuracy, also if $C_{l_{r_w}}$ is not obtained by means of the strip-theory.

In an identical manner the yawing moment acting on the wing due to the longitudinal gust velocity $u_g(x, y)$ is derived. This moment can be written as,

$$N_g = C_{n_g} \frac{1}{2} \rho V^2 S b \quad (8.45)$$

where,

$$C_{n_g} = C_{n_{u_g}}(\Omega_y \frac{b}{2}) \hat{u}_g \quad (8.46)$$

and,

$$C_{n_{u_g}}(\Omega_y \frac{b}{2}) = -C_{n_{r_w}} h(\Omega_y \frac{b}{2}) \quad (8.47)$$

In the latter expression the function $h(\Omega_y \frac{b}{2})$ again is represented by (8.43). Previously it was supposed that,

$$C_{Y_{u_g}} = 0 \quad (8.48)$$

corresponding to $C_{Y_{r_w}} = 0$.

8.6 The force and moments due to gust velocities parallel to the lateral axis

When considering the asymmetric force and moments exerted on the aircraft by the v_g -field, only the antisymmetric part of this flowfield is of interest. Omitting the index 1, this part is presented by, see (8.28),

$$v_g(x, y) = v_{g_{max}} \cos \Omega_x x \cos \Omega_y y$$

The variation of v_g along the wingspan will be neglected. This amounts to the assumption $\cos \Omega_y y = 1$.

Then v_g is written as,

$$v_g = v_{g_{max}} \cos \Omega_x x \quad (8.49)$$

The gust velocity v_g causes a gust angle of sideslip β_g ,

$$\beta_g = \frac{v_g}{V} \quad (8.50)$$

8.7 The force and moments due to gust velocities parallel to the vertical axis

which is quite analogous to the gust angle of attack. The gust angle of sideslip causes a force and moments which are computed in the same way as the forces and moments due to the gust angle of attack in Chapter 7. The results of such calculations are, see Section 8.13.5,

$$C_{Y_g} = \left(C_{Y_{\beta_g}} + C_{Y_{\dot{\beta}_g}} D_b \right) \beta_g \quad (8.51)$$

$$C_{l_g} = \left(C_{l_{\beta_g}} + C_{l_{\dot{\beta}_g}} D_b \right) \beta_g \quad (8.52)$$

$$C_{n_g} = \left(C_{n_{\beta_g}} + C_{n_{\dot{\beta}_g}} D_b \right) \beta_g \quad (8.53)$$

The gust derivatives $C_{Y_{\beta_g}}$, $C_{l_{\beta_g}}$ and $C_{n_{\beta_g}}$ can be expressed entirely in the stability derivatives C_{Y_β} , C_{l_β} , C_{n_β} and are equal to them. The derivatives $C_{Y_{\dot{\beta}_g}}$, $C_{l_{\dot{\beta}_g}}$ and $C_{n_{\dot{\beta}_g}}$ are determined as follows. Analogous to the corresponding expressions for the symmetric gust derivative $C_{m_{\dot{\alpha}_g}}$, $C_{Y_{\dot{\beta}_g}}$ may be written as,

$$C_{Y_{\dot{\beta}_g}} = C_{Y_{\dot{\beta}}} + C_{Y_r} \quad (8.54)$$

It should be remarked, that only the contribution of the fuselage and the vertical tailplane to C_{Y_r} have to be taken into account, since only these parts of the total C_{Y_r} arise as a result of a local velocity parallel to the Y -axis. Therefore,

$$\begin{aligned} C_{Y_{\beta_g}} &= C_{Y_\beta} & C_{Y_{\dot{\beta}_g}} &= C_{Y_{\dot{\beta}}} + \frac{1}{2} C_{Y_{r_f+v}} \\ C_{l_{\beta_g}} &= C_{l_\beta} & C_{l_{\dot{\beta}_g}} &= C_{l_{\dot{\beta}}} + \frac{1}{2} C_{l_{r_f+v}} \\ C_{n_{\beta_g}} &= C_{n_\beta} & C_{n_{\dot{\beta}_g}} &= C_{n_{\dot{\beta}}} + \frac{1}{2} C_{n_{r_f+v}} \end{aligned} \quad (8.55)$$

When considering aircraft having a straight wing and relatively small tailplanes, the derivatives $C_{Y_{\dot{\beta}}}$, $C_{l_{\dot{\beta}}}$ and $C_{n_{\dot{\beta}}}$ may usually be neglected. For the sake of simplicity, in the following it is supposed,

$$C_{Y_{\dot{\beta}_g}} = C_{l_{\dot{\beta}_g}} = C_{n_{\dot{\beta}_g}} = 0$$

8.7 The force and moments due to gust velocities parallel to the vertical axis

When considering the asymmetric force and moments exerted on the aircraft by the w_g -field, only the antisymmetric part of this field is of interest. Omitting the index 2, see (8.29), this part is represented by,

$$w_g(x, y) = w_{g_{max}} \sin \Omega_x x \sin \Omega_y y$$

This w_g -field causes a gust angle of attack α_g ,

$$\alpha_g(x, y) = \frac{w_g(x, y)}{V} \quad (8.56)$$

which varies in the direction of flight as well as along the wingspan. Denoting the gust angle of attack in the $O_eX_eZ_e$ -plane by α_g ,

$$\alpha_g = \alpha_{g_{max}} \sin \Omega_x x \quad (8.57)$$

it follows,

$$\alpha_g(x, y) = \alpha_g \sin \Omega_y y \quad (8.58)$$

The calculation of the rolling and yawing moments due to the α_g -field has a great similarity to the corresponding calculation for the \hat{u}_g -field in Section 8.5. The rolling moment can be written as,

$$L_g = C_{l_g} \frac{1}{2} \rho V^2 S b \quad (8.59)$$

where,

$$C_{l_g} = C_{l_{\alpha_g}} (\Omega_y \frac{b}{2}) \alpha_g \quad (8.60)$$

and likewise the coefficient for the yawing moment is,

$$C_{n_g} = C_{n_{\alpha_g}} (\Omega_y \frac{b}{2}) \alpha_g \quad (8.61)$$

For sufficiently small values of Ω_y , i.e. for long wavelengths in the Y_e -direction, the distribution of the gust angle of attack along the span of the wing (8.58) can again be approximated by replacing $\sin \Omega_y y$ by $\Omega_y y$,

$$\alpha_g(x, y) = \alpha_g \Omega_y y \quad (8.62)$$

This distribution of the angle of attack corresponds to the additional angle of attack due to a constant rolling velocity p ,

$$\Delta\alpha = \frac{p}{V} y \quad (8.63)$$

As a consequence, for sufficiently small values of Ω_y the gust derivatives $C_{l_{\alpha_g}} h(\Omega_y \frac{b}{2})$ and $C_{n_{\alpha_g}} h(\Omega_y \frac{b}{2})$ can be expressed in terms of parts of the stability derivatives C_{l_p} and C_{n_p} contributed by the wing, i.e. $C_{l_{p_w}}$ and $C_{n_{p_w}}$. After some elaboration, the following results are obtained,

$$C_{l_{\alpha_g}} (\Omega_y \frac{b}{2}) = C_{l_{p_w}} h(\Omega_y \frac{b}{2}) \quad (8.64)$$

and,

$$C_{n_{\alpha_g}} (\Omega_y \frac{b}{2}) = C_{n_{p_w}} h(\Omega_y \frac{b}{2}) \quad (8.65)$$

where the function $h(\Omega_y \frac{b}{2})$ has been given previously in (8.43). For the sake of simplicity the side force due to α_g will be neglected, so,

$$C_{Y_{\alpha_g}} = 0$$

This simplification corresponds to the assumption that $C_{Y_{p_w}} = 0$.

8.8 The power spectra of the rolling and yawing moments due to gust velocities parallel to the longitudinal and the vertical axes

The variables describing the aircraft's motions in turbulent air are stochastic functions of time. Therefore, the input signals to the aircraft can also be functions of time only.

These input signals are the gust velocities $u_g(x, y)$, $v_g(x, y)$ and $w_g(x, y)$ affecting the aircraft through the force C_{Y_g} and the moments C_{l_g} and C_{n_g} . In a certain way, C_{Y_g} , C_{l_g} and C_{n_g} may equally well be considered as input signals to the aircraft instead of the gust velocities.

In the foregoing it has been shown, that in the u_g - and w_g -fields the moments C_{l_g} and C_{n_g} are dependent on the two spatial circular frequencies Ω_x and Ω_y , see e.g. (8.30) and (8.46), the force C_{Y_g} being neglected in these fields. In the v_g -fields C_{Y_g} , C_{l_g} and C_{n_g} are functions of Ω_x only, see (8.49). Only Ω_x can directly be related to time. An aircraft flying with an airspeed V through an elementary field of flow of the spatial frequency Ω_x undergoes the changes of u_g , v_g and w_g with an angular frequency ω , Equation (6.25),

$$\omega = \Omega_x V$$

The influence of the second spatial circular frequency Ω_y on C_{l_g} and C_{n_g} is now studied in more detail for the u_g - and the w_g -fields. As an example the rolling moment due to $u_g(x, y)$ is considered here. In the turbulent atmosphere all values of Ω_y may be considered to occur simultaneously. It is, however, possible to evaluate the mean or effective value of the amplitude of C_{l_g} , due to $u_g(x, y)$ at a certain value of Ω_x . This mean value of C_{l_g} , caused by the contributions of all values of Ω_y , is determined with the aid of the two-dimensional power spectral density function of the gust velocity at the given Ω_x . According to (8.35), as a function of $\Omega_x L_g$, $\Omega_y L_g$ and $B = \frac{b}{2L_g}$ is,

$$C_{l_g} = C_{l_{u_g}}(\Omega_y \frac{b}{2}) \hat{u}_g(\Omega_x L_g)$$

Consequently the power spectral density of C_{l_g} is,

$$S_{C_{l_g}}(\Omega_x L_g, \Omega_y L_g, B) = C_{l_{u_g}}^2(\Omega_y \frac{b}{2}) S_{\hat{u}_g}(\Omega_x L_g, \Omega_y L_g) \quad (8.66)$$

where the duplication of indices has been omitted for the sake of simplicity. Substituting (8.44) for $C_{l_{u_g}}(\Omega_y \frac{b}{2})$ and (8.20) for $S_{\hat{u}_g}$, this power spectral density can be written as,

$$S_{C_{l_g}}(\Omega_x L_g, \Omega_y L_g, B) = C_{l_{rw}}^2 h^2(\Omega_y \frac{b}{2}) \pi \sigma_{\hat{u}_g}^2 \frac{1 + \Omega_x^2 L_g^2 + 4\Omega_y^2 L_g^2}{(1 + \Omega_x^2 L_g^2 + \Omega_y^2 L_g^2)^{5/2}} \quad (8.67)$$

The variance $\sigma_{C_{l_g}}^2 = E\{C_{l_g}^2\}$ ($\mu_{C_{l_g}} = 0$) is obtained by integrating this power spectral density function,

$$E\{C_{l_g}^2\} = \frac{1}{\pi} \sigma_{\hat{u}_g}^2 C_{l_{rw}}^2 \int_0^\infty \int_0^\infty h^2(\Omega_y \frac{b}{2}) \frac{1 + \Omega_x^2 L_g^2 + 4\Omega_y^2 L_g^2}{(1 + \Omega_x^2 L_g^2 + \Omega_y^2 L_g^2)^{5/2}} d(\Omega_x L_g) d(\Omega_y L_g) \quad (8.68)$$

The contributions to $E\{C_{l_g}^2\}$ effected - at a fixed Ω_x - by the elementary fields with different Ω_y , are taken together now. In this way the one-dimensional spectral density function of C_{l_g} results,

$$S_{C_{l_g}}(\Omega_x L_g, B) = \sigma_{\hat{u}_g}^2 C_{l_{rw}}^2 \int_0^\infty h^2(\Omega_y \frac{b}{2}) \frac{1 + \Omega_x^2 L_g^2 + 4\Omega_y^2 L_g^2}{(1 + \Omega_x^2 L_g^2 + \Omega_y^2 L_g^2)^{5/2}} d(\Omega_y L_g) \quad (8.69)$$

The new power spectral density function is a function of $\Omega_x L_g$ and $B = \frac{b}{2L_g}$. This one-dimensional power spectral density can be written as,

$$S_{C_{l_g}}(\Omega_x L_g, B) = C_{l_{rw}}^2 I_{\hat{u}_g}(\Omega_x L_g, B) \quad (8.70)$$

and $E\{C_{l_g}^2\}$ as,

$$E\{C_{l_g}^2\} = \frac{1}{\pi} C_{l_{rw}}^2 \int_0^\infty I_{\hat{u}_g}(\Omega_x L_g, B) d(\Omega_x L_g) \quad (8.71)$$

where,

$$I_{\hat{u}_g}(\Omega_x L_g, B) = \sigma_{\hat{u}_g}^2 \int_0^\infty h^2(\Omega_y \frac{b}{2}) \frac{1 + \Omega_x^2 L_g^2 + 4\Omega_y^2 L_g^2}{(1 + \Omega_x^2 L_g^2 + \Omega_y^2 L_g^2)^{5/2}} d(\Omega_y L_g) \quad (8.72)$$

The term $I_{\hat{u}_g}(\Omega_x L_g, B)$ may be considered as an effective one-dimensional power spectral density function of the input signal \hat{u}_g , as a function of $\Omega_x L_g$ and B . The relation between $\sigma_{\hat{u}_g}^2$ and $E\{C_{l_g}^2\}$ has been expressed by (8.71) and (8.72) as if the stochastic process were one-dimensional. The influence of Ω_y has entirely been taken into account in $I_{\hat{u}_g}$.

In an identical manner, the spectral density of the yawing moment due to \hat{u}_g can be written as,

$$S_{C_{n_g}}(\Omega_x L_g, B) = C_{n_{rw}}^2 I_{\hat{u}_g}(\Omega_x L_g, B) \quad (8.73)$$

and also (assuming $\mu_{C_{n_g}} = 0$),

$$E\{C_{n_g}^2\} = \frac{1}{\pi} C_{n_{rw}}^2 \int_0^\infty I_{\hat{u}_g}(\Omega_x L_g, B) d(\Omega_x L_g) \quad (8.74)$$

The foregoing derivation applies in principle also to the moments due to w_g . The one-dimensional power spectral density functions of the rolling moment and yawing moment coefficients due to the vertical gust velocity are,

$$S_{C_{l_g}}(\Omega_x L_g, B) = C_{l_{pw}}^2 I_{\alpha_g}(\Omega_x L_g, B) \quad (8.75)$$

and,

$$S_{C_{n_g}}(\Omega_x L_g, B) = C_{n_{pw}}^2 I_{\alpha_g}(\Omega_x L_g, B) \quad (8.76)$$

where the effective one-dimensional power spectral density function I_{α_g} is, see Equation (8.22),

$$I_{\alpha_g}(\Omega_x L_g, B) = 3 \sigma_{\alpha_g}^2 \int_0^\infty h^2(\Omega_y \frac{b}{2}) \frac{\Omega_x^2 L_g^2 + \Omega_y^2 L_g^2}{(1 + \Omega_x^2 L_g^2 + \Omega_y^2 L_g^2)^{5/2}} d(\Omega_y L_g) \quad (8.77)$$

The functions $I_{\hat{u}_g}(\Omega_x L_g, B)$ and $I_{\alpha_g}(\Omega_x L_g, B)$ for different values of B have been given in Figures 8.13 and 8.14.

8.9 Approximation of the effective one-dimensional power spectral densities

In the previous section we found that the power spectral densities of the rolling and yawing moments due to turbulence could be expressed using the effective one-dimensional power spectral densities $I_{\hat{u}_g}(\Omega_x L_g, B)$ and $I_{\alpha_g}(\Omega_x L_g, B)$, Equations (8.72) and (8.77),

$$\begin{aligned} I_{\hat{u}_g}(\Omega_x L_g, B) &= \sigma_{\hat{u}_g}^2 \int_0^\infty h^2(\Omega_y \frac{b}{2}) \frac{1 + \Omega_x^2 L_g^2 + 4\Omega_y^2 L_g^2}{(1 + \Omega_x^2 L_g^2 + \Omega_y^2 L_g^2)^{5/2}} d(\Omega_y L_g) \\ I_{\alpha_g}(\Omega_x L_g, B) &= 3 \sigma_{\alpha_g}^2 \int_0^\infty h^2(\Omega_y \frac{b}{2}) \frac{\Omega_x^2 L_g^2 + \Omega_y^2 L_g^2}{(1 + \Omega_x^2 L_g^2 + \Omega_y^2 L_g^2)^{5/2}} d(\Omega_y L_g) \end{aligned}$$

The non-dimensional function $h(\Omega_y \frac{b}{2})$ is given by Equation (8.43),

$$h(\Omega_y \frac{b}{2}) = \frac{b}{2} \frac{\int_0^{\frac{b}{2}} c_l c \sin \Omega_y y \, dy}{\int_0^{\frac{b}{2}} c_l c y^2 \, dy}$$

The assumption is now made that for not too large values of Ω_y , the spanwise lift distribution expressed by the product $c_l c$, will have negligible influence on the power spectral densities $I_{\hat{u}_g}(\Omega_x L_g, B)$ and $I_{\alpha_g}(\Omega_x L_g, B)$. In Figure 8.15 $I_{\hat{u}_g}(\Omega_x L_g, B)$ has been plotted for two extreme values of B for three different spanwise lift distributions. It can be seen that the influence of the lift distribution only becomes apparent either for large values of B , or for high frequencies $\Omega_x L_g$. Making this assumption, $h(\Omega_y \frac{b}{2})$ can be expressed in closed form:

$$h(\Omega_y \frac{b}{2}) = \frac{b}{2} \frac{\int_0^{\frac{b}{2}} \sin \Omega_y y \, dy}{\int_0^{\frac{b}{2}} y^2 \, dy} = 3 \frac{\sin(\Omega_y \frac{b}{2}) - (\Omega_y \frac{b}{2}) \cos(\Omega_y \frac{b}{2})}{(\Omega_y \frac{b}{2})^2} \quad (8.78)$$

The effective power spectral densities $I_{\hat{u}_g}(\Omega_x L_g, B)$ and $I_{\alpha_g}(\Omega_x L_g, B)$ (8.72) and (8.77) are not practical to use and have to be approximated with the following general expressions, (see (Gerlach & Baarspul, 1968)),

$$I_{\hat{u}_g}(\Omega_x L_g, B) = I_{\hat{u}_g}(0, B) \frac{1 + \tau_3^2 \Omega_x^2 L_g^2}{(1 + \tau_1^2 \Omega_x^2 L_g^2)(1 + \tau_2^2 \Omega_x^2 L_g^2)} \quad (8.79)$$

and,

$$I_{\alpha_g}(\Omega_x L_g, B) = I_{\alpha_g}(0, B) \frac{1 + \tau_6^2 \Omega_x^2 L_g^2}{(1 + \tau_4^2 \Omega_x^2 L_g^2)(1 + \tau_5^2 \Omega_x^2 L_g^2)} \quad (8.80)$$

In Section 8.12 we will use these approximated power spectral densities to derive a state-space filter in the time domain. Such an approximation proves to be quite acceptable, as will be shown below. The terms $I_{\hat{u}_g}(0, B)$ and $I_{\alpha_g}(0, B)$ are represented as functions of B in Table 8.1, τ_1 till τ_6 are given in Tables 8.2 and 8.3.

The values of τ_1 , τ_2 , τ_3 in (8.79) and Table 8.2 and τ_4 , τ_5 , τ_6 in (8.80) and Table 8.3 were obtained by equaling (8.79) and (8.80) each at three 'test frequencies' to the corresponding values of the exact functions (8.73) and (8.78) calculated with (8.72) and (8.77), see (Gerlach & Baarspul, 1968). The combination of values of the τ 's found in this way turned out to depend on the choice of the three test frequencies. The three test frequencies were chosen such as to minimize the value of the maximum error due to the approximation.

8.10 Summary of the expressions for the aerodynamic force and moments

The final expressions describing the asymmetric aerodynamic force and moments, acting on the aircraft due to atmospheric turbulence, can now be collected,

$$C_{Y_g} = C_{Y_\beta} \beta_g \quad (8.81)$$

$$C_{l_g} = -C_{l_{rw}} \hat{u}_g + C_{l_\beta} \beta_g + C_{l_{pw}} \alpha_g \quad (8.82)$$

$$C_{n_g} = -C_{n_{rw}} \hat{u}_g + C_{n_\beta} \beta_g + C_{n_{pw}} \alpha_g \quad (8.83)$$

As discussed in the foregoing, the contributions of the longitudinal and vertical gust velocities to C_{l_g} and C_{n_g} in the above expressions hold true only, if they are used in conjunction with the following one-dimensional power spectral densities of \hat{u}_g and α_g , Equations (8.72), (8.79), (8.77) and (8.80) respectively,

$$I_{\hat{u}_g}(\Omega_x L_g, B) = \sigma_{\hat{u}_g}^2 \int_0^\infty h^2(\Omega_y \frac{b}{2}) \frac{1 + \Omega_x^2 L_g^2 + 4 \Omega_y^2 L_g^2}{(1 + \Omega_x^2 L_g^2 + \Omega_y^2 L_g^2)^{5/2}} d(\Omega_y L_g)$$

approximated by,

$$I_{\hat{u}_g}(\Omega_x L_g, B) = I_{\hat{u}_g}(0, B) \frac{1 + \tau_3^2 \Omega_x^2 L_g^2}{(1 + \tau_1^2 \Omega_x^2 L_g^2)(1 + \tau_2^2 \Omega_x^2 L_g^2)}$$

and,

$$I_{\alpha_g}(\Omega_x L_g, B) = 3 \sigma_{\alpha_g}^2 \int_0^\infty h^2(\Omega_y \frac{b}{2}) \frac{\Omega_x^2 L_g^2 + \Omega_y^2 L_g^2}{(1 + \Omega_x^2 L_g^2 + \Omega_y^2 L_g^2)^{5/2}} d(\Omega_y L_g)$$

approximated by,

$$I_{\alpha_g}(\Omega_x L_g, B) = I_{\alpha_g}(0, B) \frac{1 + \tau_6^2 \Omega_x^2 L_g^2}{(1 + \tau_4^2 \Omega_x^2 L_g^2)(1 + \tau_5^2 \Omega_x^2 L_g^2)}$$

The power spectral density of β_g is,

$$S_{\beta_g \beta_g}(\Omega_x L_g) = \sigma_{\beta_g}^2 \frac{1 + 3 \Omega_x^2 L_g^2}{(1 + \Omega_x^2 L_g^2)^2} \quad (8.84)$$

The values of $I_{\hat{u}_g}(0, B)$ and τ_1, τ_2, τ_3 in the approximated power spectral density function for the longitudinal gust velocity and of $I_{\alpha_g}(0, B)$ and τ_4, τ_5, τ_6 in the approximated power spectral density function of the vertical gust velocity are represented as functions of B in Tables 8.1 and 8.2.

8.11 Equations for the asymmetric motions of an aircraft in atmospheric turbulence

In the following discussion, the simplifying but not essential assumption is made, that the aircraft may be considered as a rigid body. The asymmetric motions of the aircraft, considered as small deviations from steady, symmetric and level flight are described by the following four linear differential equations, (Mulder et al., 2013; Etkin, 1972), (with $D_b = \frac{b}{V} \frac{d(\cdot)}{dt}$),

$$\begin{bmatrix} C_{Y_\beta} - 2\mu_b D_b & C_L & C_{Y_p} & C_{Y_r} - 4\mu_b \\ 0 & -\frac{1}{2}D_b & 1 & 0 \\ C_{l_\beta} & 0 & C_{l_p} - 4\mu_b K_X^2 D_b & C_{l_r} + 4\mu_b K_{XZ} D_b \\ C_{n_\beta} & 0 & C_{n_p} + 4\mu_b K_{XZ} D_b & C_{n_r} - 4\mu_b K_Z^2 D_b \end{bmatrix} \begin{bmatrix} \beta \\ \varphi \\ \frac{pb}{2V} \\ \frac{rb}{2V} \end{bmatrix} = - \begin{bmatrix} 0 & C_{Y_{\delta_r}} & 0 & C_{Y_\beta} & 0 \\ 0 & 0 & 0 & 0 & 0 \\ C_{l_{\delta_a}} & C_{l_{\delta_r}} & C_{l_{u_g}}(\Omega_y \frac{b}{2}) & C_{l_\beta} & C_{l_{\alpha_g}}(\Omega_y \frac{b}{2}) \\ C_{n_{\delta_a}} & C_{n_{\delta_r}} & C_{n_{u_g}}(\Omega_y \frac{b}{2}) & C_{n_\beta} & C_{n_{\alpha_g}}(\Omega_y \frac{b}{2}) \end{bmatrix} \begin{bmatrix} \delta_a \\ \delta_r \\ \hat{u}_g \\ \beta_g \\ \alpha_g \end{bmatrix} \quad (8.85)$$

If these equations of motion are to be used in conjunction with the model of random atmospheric turbulence described in the previous sections, it is possible to modify the

right-hand side of these equations. Provided the power spectral density functions $I_{\hat{u}_g}$ and I_{α_g} are used for \hat{u}_g and α_g , the Equations (8.85) can be written as,

$$\begin{bmatrix} C_{Y_\beta} - 2\mu_b D_b & C_L & C_{Y_p} & C_{Y_r} - 4\mu_b \\ 0 & -\frac{1}{2}D_b & 1 & 0 \\ C_{l_\beta} & 0 & C_{l_p} - 4\mu_b K_X^2 D_b & C_{l_r} + 4\mu_b K_{XZ} D_b \\ C_{n_\beta} & 0 & C_{n_p} + 4\mu_b K_{XZ} D_b & C_{n_r} - 4\mu_b K_Z^2 D_b \end{bmatrix} \begin{bmatrix} \beta \\ \varphi \\ \frac{pb}{2V} \\ \frac{rb}{2V} \end{bmatrix} = \\ - \begin{bmatrix} 0 & C_{Y_{\delta_r}} & 0 & C_{Y_\beta} & 0 \\ 0 & 0 & 0 & 0 & 0 \\ C_{l_{\delta_a}} & C_{l_{\delta_r}} & -C_{l_{r_w}} & C_{l_\beta} & C_{l_{p_w}} \\ C_{n_{\delta_a}} & C_{n_{\delta_r}} & -C_{n_{r_w}} & C_{n_\beta} & C_{n_{p_w}} \end{bmatrix} \begin{bmatrix} \delta_a \\ \delta_r \\ \hat{u}_g \\ \beta_g \\ \alpha_g \end{bmatrix} \quad (8.86)$$

The general state-space representation, can be obtained by rearranging the Equations (8.86), see (Stevens & Lewis, 1992). The final result, in abbreviated notation, is,

$$\begin{bmatrix} \dot{\beta} \\ \dot{\varphi} \\ \frac{\dot{pb}}{2V} \\ \frac{\dot{rb}}{2V} \end{bmatrix} = \begin{bmatrix} y_\beta & y_\varphi & y_p & y_r \\ 0 & 0 & 2\frac{V}{b} & 0 \\ l_\beta & 0 & l_p & l_r \\ n_\beta & 0 & n_p & n_r \end{bmatrix} \begin{bmatrix} \beta \\ \varphi \\ \frac{pb}{2V} \\ \frac{rb}{2V} \end{bmatrix} + \begin{bmatrix} 0 & y_{\delta_r} & 0 & y_{\beta_g} & 0 \\ 0 & 0 & 0 & 0 & 0 \\ l_{\delta_a} & l_{\delta_r} & l_{u_g} & l_{\beta_g} & l_{\alpha_g} \\ n_{\delta_a} & n_{\delta_r} & n_{u_g} & n_{\beta_g} & n_{\alpha_g} \end{bmatrix} \begin{bmatrix} \delta_a \\ \delta_r \\ \hat{u}_g \\ \beta_g \\ \alpha_g \end{bmatrix} \quad (8.87)$$

The definition of the newly introduced symbols are recapitulated in Table 8.4.

8.12 Equations of motion in state-space form for asymmetric aircraft motions in atmospheric turbulence

Just as in Chapter 7 for symmetric motions, a general description in state-space form will be derived for the asymmetric motions of an aircraft flying in turbulent air.

First the turbulence forming filters will be derived for that purpose. Consider the equation, Equation (3.44),

$$S_{yy}(\omega) = |H(\omega)|^2 S_{uu}(\omega)$$

As input signal we choose white noise with spectral density:

$$S_{uu}(\omega) = 1 \quad (8.88)$$

As output signal consider the turbulence velocities u_g , v_g and w_g . In the previous paragraph it has been shown that the one-dimensional power spectral densities for \hat{u}_g and α_g can be approximated by, Equations (8.79) and (8.80),

$$I_{\hat{u}_g}(\Omega_x L_g, B) = I_{\hat{u}_g}(0, B) \frac{1 + \tau_3^2 \Omega_x^2 L_g^2}{(1 + \tau_1^2 \Omega_x^2 L_g^2)(1 + \tau_2^2 \Omega_x^2 L_g^2)}$$

$$I_{\alpha_g}(\Omega_x L_g, B) = I_{\alpha_g}(0, B) \frac{1 + \tau_6^2 \Omega_x^2 L_g^2}{(1 + \tau_4^2 \Omega_x^2 L_g^2)(1 + \tau_5^2 \Omega_x^2 L_g^2)}$$

It should be noted here that when these approximated power spectra are used for the derivation of the filters, the outputs \hat{u}_g and α_g cannot be regarded as (non-dimensional) wind velocities but rather as 'signals' used to calculate the influence of the wind velocities u_g and w_g on the equations of motion for asymmetric motions of aircraft, see Equations (8.81)-(8.83).

The power spectrum of β_g is, Equation (8.84):

$$S_{\beta_g \beta_g}(\Omega L_g) = \sigma_{\beta_g}^2 \frac{1 + 3 \Omega_x^2 L_g^2}{(1 + \Omega_x^2 L_g^2)^2}$$

Combining Equations (3.44), (8.79), (8.80) and (8.84) and using the radial frequency ω rather than the spatial circular frequency Ω_x yield:

$$|H_{\hat{u}_g w_1}(\omega)|^2 = \frac{L_g}{V} I_{\hat{u}_g}(0, B) \frac{1 + \tau_3^2 \left(\frac{\omega L_g}{V}\right)^2}{\left(1 + \tau_1^2 \left(\frac{\omega L_g}{V}\right)^2\right) \left(1 + \tau_2^2 \left(\frac{\omega L_g}{V}\right)^2\right)} \quad (8.89)$$

$$|H_{\alpha_g w_3}(\omega)|^2 = \frac{L_g}{V} I_{\alpha_g}(0, B) \frac{1 + \tau_6^2 \left(\frac{\omega L_g}{V}\right)^2}{\left(1 + \tau_4^2 \left(\frac{\omega L_g}{V}\right)^2\right) \left(1 + \tau_5^2 \left(\frac{\omega L_g}{V}\right)^2\right)} \quad (8.90)$$

$$|H_{\beta_g w_2}(\omega)|^2 = \frac{L_g}{V} \sigma_{\beta_g}^2 \frac{1 + 3 \left(\frac{\omega L_g}{V}\right)^2}{\left(1 + \left(\frac{\omega L_g}{V}\right)^2\right)^2} \quad (8.91)$$

Let's consider Equation (8.89) for the asymmetric turbulence field for horizontal turbulence parallel to the longitudinal axis. The frequency response function giving a stable filter with minimum-phase behaviour is given by:

$$H_{\hat{u}_g w_1}(\omega) = \sqrt{\frac{L_g}{V} I_{\hat{u}_g}(0, B)} \frac{1 + \tau_3 \frac{L_g}{V} j\omega}{\left(1 + \tau_1 \frac{L_g}{V} j\omega\right) \left(1 + \tau_2 \frac{L_g}{V} j\omega\right)} \quad (8.92)$$

Keeping in mind that $H_{\hat{u}_g w_1}(\omega) = \frac{\hat{U}_g(\omega)}{W_1(\omega)}$ where w_1 is the white noise input driving the filter for asymmetric \hat{u}_g and substituting $j\omega = \frac{d}{dt}(.)$, the differential equation describing the filter is found to be:

$$\begin{aligned} & \tau_1 \tau_2 \left(\frac{L_g}{V}\right)^2 \ddot{\hat{u}}_g(t) + (\tau_1 + \tau_2) \frac{L_g}{V} \dot{\hat{u}}_g(t) + \hat{u}_g(t) = \\ & = \sqrt{\frac{L_g}{V} I_{\hat{u}_g}(0, B)} w_1(t) + \tau_3 \sqrt{\left(\frac{L_g}{V}\right)^3 I_{\hat{u}_g}(0, B)} \dot{w}_1(t) \end{aligned} \quad (8.93)$$

To obtain a state-space description, an auxiliary variable \hat{u}_g^* is introduced:

$$\hat{u}_g^*(t) = \dot{\hat{u}}_g(t) - \frac{\tau_3}{\tau_1 \tau_2} \sqrt{\frac{V}{L_g}} I_{\hat{u}_g}(0, B) w_1(t) \quad (8.94)$$

Differentiating (8.94) and substituting (8.93) and (8.94) yields:

$$\begin{aligned} \dot{\hat{u}}_g^*(t) &= \frac{1}{\tau_1 \tau_2} \sqrt{\left(\frac{V}{L_g}\right)^3} I_{\hat{u}_g}(0, B) w_1(t) + \\ &- \frac{\tau_1 + \tau_2}{\tau_1 \tau_2} \frac{V}{L_g} \hat{u}_g^*(t) - \frac{\tau_3 (\tau_1 + \tau_2)}{(\tau_1 \tau_2)^2} \sqrt{\left(\frac{V}{L_g}\right)^3} I_{\hat{u}_g}(0, B) w_1(t) - \frac{1}{\tau_1 \tau_2} \left(\frac{V}{L_g}\right)^2 \hat{u}_g(t) \end{aligned} \quad (8.95)$$

In state-space form, using $[\hat{u}_g \ \hat{u}_g^*]^T$ as the state vector, this filter can be given by:

$$\begin{bmatrix} \dot{\hat{u}}_g \\ \dot{\hat{u}}_g^* \end{bmatrix} = \begin{bmatrix} 0 & 1 \\ -\frac{1}{\tau_1 \tau_2} \left(\frac{V}{L_g}\right)^2 & -\frac{\tau_1 + \tau_2}{\tau_1 \tau_2} \frac{V}{L_g} \end{bmatrix} \begin{bmatrix} \hat{u}_g \\ \hat{u}_g^* \end{bmatrix} + \begin{bmatrix} \frac{\tau_3}{\tau_1 \tau_2} \sqrt{\frac{V}{L_g}} I_{\hat{u}_g}(0, B) \\ \left(1 - \frac{\tau_3 (\tau_1 + \tau_2)}{\tau_1 \tau_2}\right) \frac{1}{\tau_1 \tau_2} \sqrt{\left(\frac{V}{L_g}\right)^3} I_{\hat{u}_g}(0, B) \end{bmatrix} w_1 \quad (8.96)$$

In a similar manner the filters for α_g and β_g are derived, yielding for α_g :

$$\begin{bmatrix} \dot{\alpha}_g \\ \dot{\alpha}_g^* \end{bmatrix} = \begin{bmatrix} 0 & 1 \\ -\frac{1}{\tau_4 \tau_5} \left(\frac{V}{L_g}\right)^2 & -\frac{\tau_4 + \tau_5}{\tau_4 \tau_5} \frac{V}{L_g} \end{bmatrix} \begin{bmatrix} \alpha_g \\ \alpha_g^* \end{bmatrix} + \begin{bmatrix} \frac{\tau_6}{\tau_4 \tau_5} \sqrt{\frac{V}{L_g}} I_{\alpha_g}(0, B) \\ \left(1 - \frac{\tau_6 (\tau_4 + \tau_5)}{\tau_4 \tau_5}\right) \frac{1}{\tau_4 \tau_5} \sqrt{\left(\frac{V}{L_g}\right)^3} I_{\alpha_g}(0, B) \end{bmatrix} w_3 \quad (8.97)$$

and for β_g :

$$\begin{bmatrix} \dot{\beta}_g \\ \dot{\beta}_g^* \end{bmatrix} = \begin{bmatrix} 0 & 1 \\ -\left(\frac{V}{L_g}\right)^2 & -2 \frac{V}{L_g} \end{bmatrix} \begin{bmatrix} \beta_g \\ \beta_g^* \end{bmatrix} + \begin{bmatrix} \sigma_{\beta_g} \sqrt{\frac{3V}{L_g}} \\ (1 - 2\sqrt{3}) \sigma_{\beta_g} \sqrt{\left(\frac{V}{L_g}\right)^3} \end{bmatrix} w_2 \quad (8.98)$$

Combining Equation (8.87) with the turbulence filters gives the equations of motion of an aircraft flying through turbulent air, as given on the next page.

(8.99)

8.13 Modeling the gust penetration-effect for asymmetric aircraft motions

8.13.1 Introduction

In Chapter 7 the term 'gust penetration effect' has been introduced. The gust penetration effect describes the aerodynamic phenomenon of a gust hitting parts of the aircraft on different instants in time: the gust is a moving front. Because of the finite dimensions of an aircraft the aerodynamic forces and moments will build up instead of instantly increasing of them. Because of the distinct contributions of the wing and the horizontal tailplane in the buildup of the aerodynamic forces and the moment caused by symmetric atmospheric turbulence, we were able to derive the so called 'aerodynamic frequency response functions' defining an aerodynamic model of the gust penetration effect in Chapter 7. For the asymmetric aircraft motions, caused by atmospheric turbulence, the principle of a gust penetration effect can also be introduced. In this section we will derive some aerodynamic frequency response functions describing the gust penetration effect for asymmetric aircraft motions. These aerodynamic frequency response functions will be a first order approximation because it is difficult to analytically describe the influence of the fuselage on the flowfield and the contribution of the fuselage to the aerodynamic forces and moments. We will derive some analytical expressions for the aerodynamic frequency response functions for the aerodynamic force Y and the moments L and N due to lateral horizontal atmospheric turbulence denoted by β_g . Of course, some simplifying assumptions have to be made. One of the assumptions is, that the aircraft's centre of gravity and the aerodynamic centre of the wing/fuselage combination coincide; if they do not we refer to Section 7.5.

8.13.2 Derivation of the aerodynamic frequency response function of the aerodynamic force coefficient C_Y with respect to β_g

The most important contributions to the gust-derivative $C_{Y_{\beta_g}}$ come from the wing, the fuselage and the vertical tailplane. If the aircraft has a straight wing, the contribution of the wing to the gust derivative is negligible. The aerodynamic force caused by atmospheric turbulence can be written as,

$$C_{Y_g} = C_{Y_{\beta_g}} \beta_g = C_{Y_{w_\beta}} \beta_g + C_{Y_{f_\beta}} \beta_g + C_{Y_{v_\beta}} \beta_g \quad (8.100)$$

If the gust derivative is assumed to be equal to the sum of the contributions of the wing, fuselage and the vertical tailplane, some analytical expressions for the aerodynamic frequency response functions can be derived. We emphasize that the contribution of wing-fuselage and the vertical tailplane-fuselage aerodynamic interference is neglected as well as the contribution of the (straight) wing. The aerodynamic force coefficient C_Y , caused by lateral atmospheric turbulence, is written as,

$$C_{Y_g} = C_{Y_{\beta_g}} \beta_g = C_{Y_{f_\beta}} \beta_g + C_{Y_{v_\beta}} \beta_g \quad (8.101)$$

For a finite aircraft this expression can be written in the frequency domain,

$$C_{Y_g} = C_{Y_{\beta_g}} \beta_g = C_{Y_{f_\beta}} \beta_g + C_{Y_{v_\beta}} \beta_g = C_{Y_{f_\beta}} \beta_g - C_{Y_{v_\alpha}} \left(\frac{V_v}{V} \right)^2 \frac{S_v}{S} \beta_{v_g} \quad (8.102)$$

With,

$$\beta_{v_g}(\omega) = \beta_g e^{-j\omega\tau} - \frac{\partial\sigma}{\partial\beta} \beta_g e^{-j\omega\tau} = \left(1 - \frac{\partial\sigma}{\partial\beta} \right) \beta_g e^{-j\omega \frac{l_v}{V}} \quad (8.103)$$

In the above equation the time-delay τ is equal to the distance between the aerodynamic centres of the wing/fuselage and the vertical tailplane divided by the airspeed V : $\tau = \frac{l_v}{V}$. Furthermore, the sidewash σ is assumed to have reached its stationary value at the wing/-fuselage's aerodynamic centre and is supposed to be merely dependent of the sideforce Y generated by the wing/fuselage. The aerodynamic sideforce Y can now be written as,

$$C_{Y_g}(\omega) = C_{Y_{f_\beta}} \beta_g - C_{Y_{v_\alpha}} \left(\frac{V_v}{V} \right)^2 \frac{S_v}{S} \left(1 - \frac{\partial\sigma}{\partial\beta} \right) \beta_g e^{-j\omega \frac{l_v}{V}} \quad (8.104)$$

The aerodynamic frequency response function becomes,

$$\frac{C_{Y_g}}{\beta_g}(\omega) = C_{Y_{f_\beta}} - C_{Y_{v_\alpha}} \left(\frac{V_v}{V} \right)^2 \frac{S_v}{S} \left(1 - \frac{\partial\sigma}{\partial\beta} \right) e^{-j\omega \frac{l_v}{V}} \quad (8.105)$$

8.13.3 Derivation of the aerodynamic frequency response function of the aerodynamic moment coefficient C_l with respect to β_g

The most important contributions to the gust derivative $C_{l_{\beta_g}}$ come from the wing, the vertical tailplane and the wing-fuselage aerodynamic interference. The aerodynamic moment, caused by atmospheric turbulence, can be written as,

$$C_{l_g} = C_{l_{\beta_g}} \beta_g = C_{l_{w_\beta}} \beta_g + C_{l_{f+w_\beta}} \beta_g + C_{l_{v_\beta}} \beta_g \quad (8.106)$$

In the following, the wing-fuselage aerodynamic interference will be neglected. The aerodynamic moment coefficient C_l caused by lateral atmospheric turbulence is written in the frequency domain as (see Figure 8.11),

$$C_{l_g} = C_{l_{w_\beta}} \beta_g - C_{Y_{v_\alpha}} \left(\frac{V_v}{V} \right)^2 \frac{S_v}{S} \left(\frac{z_v - z_{cg}}{b} \cos \alpha - \frac{x_v - x_{cg}}{b} \sin \alpha \right) \beta_{v_g}(\omega) \quad (8.107)$$

In the above equation is, again,

$$\beta_{v_g}(\omega) = \beta_g e^{-j\omega\tau} - \frac{\partial\sigma}{\partial\beta} \beta_g e^{-j\omega\tau} = \left(1 - \frac{\partial\sigma}{\partial\beta} \right) \beta_g e^{-j\omega \frac{l_v}{V}}$$

With the expression for β_{v_g} , the aerodynamic moment coefficient C_l , caused by lateral atmospheric turbulence, can be written as,

$$C_{l_g}(\omega) = C_{l_{w_\beta}} \beta_g - C_{Y_{v_\alpha}} \left(\frac{V_v}{V} \right)^2 \frac{S_v}{S} \left(\frac{z_v - z_{cg}}{b} \cos \alpha - \frac{x_v - x_{cg}}{b} \sin \alpha \right) \left(1 - \frac{\partial\sigma}{\partial\beta} \right) \beta_g e^{-j\omega \frac{l_v}{V}}$$

(8.108)

The aerodynamic frequency response function becomes,

$$\frac{C_{l_g}}{\beta_g}(\omega) = C_{l_{w\beta}} - C_{Y_{v\alpha}} \left(\frac{V_v}{V} \right)^2 \frac{S_v}{S} \left(\frac{z_v - z_{cg}}{b} \cos \alpha - \frac{x_v - x_{cg}}{b} \sin \alpha \right) \left(1 - \frac{\partial \sigma}{\partial \beta} \right) e^{-j\omega \frac{l_v}{V}} \quad (8.109)$$

8.13.4 Derivation of the aerodynamic frequency response function of the aerodynamic moment coefficient C_n with respect to β_g

The aerodynamic frequency response function for the aerodynamic moment coefficient C_n with respect to lateral atmospheric turbulence can be derived in a similar manner as in the previous section and is equal to,

$$\frac{C_{n_g}}{\beta_g}(\omega) = C_{n_{f\beta}} + C_{Y_{v\alpha}} \left(\frac{V_v}{V} \right)^2 \frac{S_v}{S} \left(\frac{x_v - x_{cg}}{b} \cos \alpha - \frac{z_v - z_{cg}}{b} \sin \alpha \right) \left(1 - \frac{\partial \sigma}{\partial \beta} \right) e^{-j\omega \frac{l_v}{V}} \quad (8.110)$$

8.13.5 Derivation of asymmetric steady and unsteady gust derivatives

In the derived aerodynamic frequency response functions,

$$\begin{aligned} \frac{C_{Y_g}}{\beta_g}(\omega) &= C_{Y_{f\beta}} - C_{Y_{v\alpha}} \left(\frac{V_v}{V} \right)^2 \frac{S_v}{S} \left(1 - \frac{\partial \sigma}{\partial \beta} \right) e^{-j\omega \frac{l_v}{V}} \\ \frac{C_{l_g}}{\beta_g}(\omega) &= C_{l_{w\beta}} - C_{Y_{v\alpha}} \left(\frac{V_v}{V} \right)^2 \frac{S_v}{S} \left(\frac{z_v - z_{cg}}{b} \cos \alpha - \frac{x_v - x_{cg}}{b} \sin \alpha \right) \left(1 - \frac{\partial \sigma}{\partial \beta} \right) e^{-j\omega \frac{l_v}{V}} \\ \frac{C_{n_g}}{\beta_g}(\omega) &= C_{n_{f\beta}} + C_{Y_{v\alpha}} \left(\frac{V_v}{V} \right)^2 \frac{S_v}{S} \left(\frac{x_v - x_{cg}}{b} \cos \alpha - \frac{z_v - z_{cg}}{b} \sin \alpha \right) \left(1 - \frac{\partial \sigma}{\partial \beta} \right) e^{-j\omega \frac{l_v}{V}} \end{aligned}$$

the time-delay appears again, which is a result of the finite dimensions of an aircraft. Again, we can approximate the time-delays by a first order Taylor polynomial, e.g.,

$$\begin{aligned} \frac{C_{Y_g}}{\beta_g}(\omega) &= C_{Y_{f\beta}} - C_{Y_{v\alpha}} \left(\frac{V_v}{V} \right)^2 \frac{S_v}{S} \left(1 - \frac{\partial \sigma}{\partial \beta} \right) \left(1 - j\omega \frac{l_v}{V} \right) \\ &= \left(C_{Y_{f\beta}} - C_{Y_{v\alpha}} \left(\frac{V_v}{V} \right)^2 \frac{S_v}{S} \left(1 - \frac{\partial \sigma}{\partial \beta} \right) \right) + \left(C_{Y_{v\alpha}} \left(\frac{V_v}{V} \right)^2 \frac{S_v l_v}{S b} \left(1 - \frac{\partial \sigma}{\partial \beta} \right) \right) \frac{j\omega b}{V} \\ &= C_{Y_{\beta_g}} + C_{Y_{\dot{\beta}_g}} \frac{j\omega b}{V} \end{aligned} \quad (8.111)$$

Or in the time domain,

$$C_{Y_g} = C_{Y_{\beta_g}} \beta_g + C_{Y_{\dot{\beta}_g}} \frac{b}{V} \dot{\beta}_g = C_{Y_{\beta_g}} \beta_g + C_{Y_{\dot{\beta}_g}} D_b \beta_g \quad (8.112)$$

with,

$$C_{Y_{\beta_g}} = C_{Y_{f_\beta}} - C_{Y_{v_\alpha}} \left(\frac{V_v}{V} \right)^2 \frac{S_v}{S} \left(1 - \frac{\partial \sigma}{\partial \beta} \right) \quad (8.113)$$

$$C_{Y_{\dot{\beta}_g}} = C_{Y_{v_\alpha}} \left(\frac{V_v}{V} \right)^2 \frac{S_v l_v}{S b} \left(1 - \frac{\partial \sigma}{\partial \dot{\beta}} \right) \quad (8.114)$$

The derivation of the other steady- and unsteady gust derivatives according to,

$$C_{l_g} = C_{l_{\beta_g}} \beta_g + C_{l_{\dot{\beta}_g}} \frac{b}{V} \dot{\beta}_g = C_{l_{\beta_g}} \beta_g + C_{l_{\dot{\beta}_g}} D_b \beta_g \quad (8.115)$$

$$C_{n_g} = C_{n_{\beta_g}} \beta_g + C_{n_{\dot{\beta}_g}} \frac{b}{V} \dot{\beta}_g = C_{n_{\beta_g}} \beta_g + C_{n_{\dot{\beta}_g}} D_b \beta_g \quad (8.116)$$

and the derivation of the steady- and unsteady gust derivatives according to,

$$C_{Y_g} = C_{Y_{\alpha_g}} \alpha_g + C_{Y_{\dot{\alpha}_g}} D_b \alpha_g \quad (8.117)$$

$$C_{l_g} = C_{l_{\alpha_g}} \alpha_g + C_{l_{\dot{\alpha}_g}} D_b \alpha_g \quad (8.118)$$

$$C_{n_g} = C_{n_{\alpha_g}} \alpha_g + C_{n_{\dot{\alpha}_g}} D_b \alpha_g \quad (8.119)$$

and,

$$C_{Y_g} = C_{Y_{\hat{u}_g}} \hat{u}_g + C_{Y_{\dot{\hat{u}}_g}} D_b \hat{u}_g \quad (8.120)$$

$$C_{l_g} = C_{l_{\hat{u}_g}} \hat{u}_g + C_{l_{\dot{\hat{u}}_g}} D_b \hat{u}_g \quad (8.121)$$

$$C_{n_g} = C_{n_{\hat{u}_g}} \hat{u}_g + C_{n_{\dot{\hat{u}}_g}} D_b \hat{u}_g \quad (8.122)$$

which will be frequency dependent of Ω_y , is left for the interested reader.

8.14 Examples and problems

8.14.1 Example 8.1

Using the state-space Equation (8.99), a simulation of asymmetric gust response can be made where the input consists of white noise and the output consists of the asymmetric aircraft motions due to atmospheric turbulence. The aircraft considered is, just as in the previous examples, the Cessna Ce-500 ‘Citation’. For the turbulence model, use will be made of the approximated effective one-dimensional power spectral densities as derived in Section 8.9. Values for the parameters describing the filter can be found in Tables 8.1 and 8.2.

- Aircraft data:

V	=	59.9 m/s	μ_b	=	15.5
S	=	24.2 m ²	K_X^2	=	0.012
b	=	13.36 m	K_Z^2	=	0.037
C_L	=	1.1360	K_{XZ}	=	0.002
C_{Y_β}	=	-0.9896	C_{l_β}	=	-0.0772
C_{Y_p}	=	-0.0870	C_{l_p}	=	-0.3444
C_{Y_r}	=	0.4300	C_{l_r}	=	0.2800
$C_{Y_{\delta_a}}$	=	0	$C_{l_{\delta_a}}$	=	-0.2349
$C_{Y_{\delta_r}}$	=	0.3037	$C_{l_{\delta_r}}$	=	0.0286
					$C_{n_\beta} = 0.1638$
					$C_{n_p} = -0.0108$
					$C_{n_r} = -0.1930$
					$C_{n_{\delta_a}} = 0.0286$
					$C_{n_{\delta_r}} = -0.1261$

- Turbulence model:

$$L_g = 150 \text{ m} \quad \sigma_{u_g} = \sigma_{w_g} = 1 \text{ m/s} \quad B \approx 0.045$$

Just as for the symmetric motions, a MATLAB .m file to define the A and B matrices has been written to be used throughout the examples. Adaption of this file will enable similar calculations for other aircraft or other flight conditions.

Listing 8.1: Citation Asymmetric motions

```
% Filename: cit2a.m
%
% Calculation of state matrix and input matrix for calculation
% of asymmetric aircraft response to atmospheric turbulence.
% The system model is in the form
%
%
%       .
%       x = Ax + Bu
%       -   -   -
% with x = [beta phi pb/2V rb/2V ug_ u_g* alpha_g alpha_g* beta_g betag*],
%
% and
%
% u = [delta_a delta_r w1 w3 w2].
%
%
% The turbulence filters are derived using the approximated
% effective one-dimensional power spectral densities for u_g, alpha_g and
% beta_g.
%
% Data for Cessna Citation Ce-500, landing (1)
%
% AIRCRAFT- AND FLIGHT CONDITION 'LANDING'.
V = 59.9;
S = 24.2;
b = 13.36;
```

```

mub = 15.5;
KX2 = 0.012;
KZ2 = 0.037;
KXZ = 0.002;
CL = 1.1360;

% TURBULENCE PARAMETERS APPROXIMATED POWER SPECTRAL DENSITIES
Lg = 150;
B = b/(2*Lg);
sigma = 1;
sigmaug_V = sigma/V;
sigmavg = sigma;
sigmabg = sigmavg/V;
sigmaag = sigma/V;

Iug0 = 0.0249*sigmaug_V^2;
Iag0 = 0.0182*sigmaag^2;
tau1 = 0.0991; tau2 = 0.5545; tau3 = 0.4159;
tau4 = 0.0600; tau5 = 0.3294; tau6 = 0.2243;

% AIRCRAFT ASYMMETRIC AERODYNAMIC DERIVATIVES
CYb = -0.9896; Clb = -0.0772; Cnb = 0.1638;
CYp = -0.0870; Clp = -0.3444; Cnp = -0.0108;
CYr = 0.4300; Clr = 0.2800; Cnr = -0.1930;
CYda = 0.0000; Clda = -0.2349; Cnda = 0.0286;
CYdr = 0.3037; Cldr = 0.0286; Cndr = -0.1261;

Clpw = 0.8*Clp; Cnpw = 0.9*Cnp;
Clrw = 0.7*Clr; Cnrw = 0.2*Cnr;

CYfb = 0;
Clfb = 0;
Cnfb = 0;

%CYfbg = CYfb+0.5*CYr;
%Clfbg = Clfb+0.5*Clr;
%Cnfbg = Cnfb+0.5*Cnr;

% CALCULATION OF AIRCRAFT ASYMMETRIC STABILITY DERIVATIVES
yb = (V/b)*CYb/(2*mub);
yphi = (V/b)*CL/(2*mub);
yp = (V/b)*CYp/(2*mub);
yr = (V/b)*(CYr-4*mub)/(2*mub);
ybg = yb;
ydr = (V/b)*CYdr/(2*mub);
den = b*4*mub*(KX2*KZ2-KXZ^2)/V;
lb = (Clb*KZ2+Cnb*KXZ)/den;
lp = (Clp*KZ2+Cnp*KXZ)/den;
lr = (Clr*KZ2+Cnr*KXZ)/den;
lda = (Clda*KZ2+Cnda*KXZ)/den;
ldr = (Cldr*KZ2+Cndr*KXZ)/den;
lug = (-Clrw*KZ2-Cnrw*KXZ)/den;
lbg = lb;

```

```

lag = (Clpw*KZ2+Cnpw*KXZ)/den;
nb = (Clb*KXZ+Cnb*KX2)/den;
np = (Clp*KXZ+Cnp*KX2)/den;
nr = (Clr*KXZ+Cnr*KX2)/den;
nda = (Clda*KXZ+Cnda*KX2)/den;
ndr = (Cldr*KXZ+Cndr*KX2)/den;
nug = (-Clrw*KXZ-Cnrw*KX2)/den;
nbg = nb;
nag = (Clpw*KXZ+Cnpw*KX2)/den;
aug1 = -(V/Lg)^2*(1/(tau1*tau2));
aug2 = -(tau1+tau2)*(V/Lg)/(tau1*tau2);
aag1 = -(V/Lg)^2*(1/(tau4*tau5));
aag2 = -(tau4+tau5)*(V/Lg)/(tau4*tau5);
abg1 = -(V/Lg)^2;
abg2 = -2*(V/Lg);
bug1 = tau3*sqrt(Iug0*V/Lg)/(tau1*tau2);
bug2 = (1-tau3*(tau1+tau2)/(tau1*tau2))*sqrt(Iug0*(V/Lg)^3)/(tau1*tau2);
bag1 = tau6*sqrt(Iag0*V/Lg)/(tau4*tau5);
bag2 = (1-tau6*(tau4+tau5)/(tau4*tau5))*sqrt(Iag0*(V/Lg)^3)/(tau4*tau5);
bbg1 = sigmabg*sqrt(3*V/Lg);
bbg2 = (1-2*sqrt(3))*sigmabg*sqrt((V/Lg)^3);

% STATE- AND INPUT MATRICES
A = [yb yphi yp yr 0 0 0 0 ybg 0;
      0 0 2*V/b 0 0 0 0 0 0 0;
      lb 0 lp lr lug 0 lag 0 lbg 0;
      nb 0 np nr nug 0 nag 0 nbg 0;
      0 0 0 0 1 0 0 0 0 0;
      0 0 0 0 aug1 aug2 0 0 0 0;
      0 0 0 0 0 0 1 0 0 0;
      0 0 0 0 0 aag1 aag2 0 0 0;
      0 0 0 0 0 0 0 0 0 1;
      0 0 0 0 0 0 0 0 abg1 abg2];

B = [0 ydr 0 0 0;
      0 0 0 0 0;
      lda ldr 0 0 0;
      nda ndr 0 0 0;
      0 0 bug1 0 0;
      0 0 bug2 0 0;
      0 0 0 bag1 0;
      0 0 0 bag2 0;
      0 0 0 0 bbg1;
      0 0 0 0 bbg2];

% SHOW EIGENVALUES OF THE UNCONTROLLED SYSTEM
eig(A)
pause
% check for yourself that the spiral mode is not stable, the
% corresponding pole lies in the right-half plane (s = 0.0764).

% THE CESSNA CITATION CE-500 IS NOT STABLE IN SPIRAL MODE (FOR THE cit2a.m

```

```
% FLIGHT CONDITION), HENCE THE FEEDBACK CONTROLLER TO THE AILERON FOR PHI IS
% USED AS IN :
%
%     delta_a = K_phi*phi      : (K_phi for THIS flight condition)
%
% THEREFORE, CONTROLLED AIRCRAFT SYSTEM MATRICES WILL BE USED FOR RESULTS;
%
%         A = At
%
% NO ALTERATIONS MADE FOR citia.m !
%
% NOTE: SPIRAL MODE IS JUST STABLE WITH K_phi ENTERED BELOW
Kphi = -0.025;
K    = [0 Kphi 0 0 0 0 0 0];
A1   = A-B(:,1)*K;
% SHOW EIGENVALUES OF THIS CONTROLLED SYSTEM
%eig(A1), pause
%
% FOR EFFECT OF K_phi ON AIRCRAFT RESPONSES, ONE OTHER K_phi IS USED
Kphi = -0.1;
K    = [0 Kphi 0 0 0 0 0 0];
A2   = A-B(:,1)*K;
% SHOW EIGENVALUES OF THIS CONTROLLED SYSTEM
%eig(A2), pause
%
save dumpfile A A1 A2 B sigmaug_V sigmabg sigmaag Lg V b
clear
load dumpfile
```

Assuming that the principle of superposition holds (linear systems theory) the influence of the turbulence velocities u_g , v_g and w_g on the motion variables β , φ , p and r can be investigated separately, and the influences summed to obtain the total asymmetric gust response. In practice, using Equation (8.99) we can apply the input vectors $[0 \ 0 \ w_1 \ 0 \ 0]^T$, $[0 \ 0 \ 0 \ w_3 \ 0]^T$, $[0 \ 0 \ 0 \ 0 \ w_2]^T$ and $[0 \ 0 \ w_1 \ w_3 \ w_2]^T$ consecutively to obtain the response to u_g , w_g , v_g and the total gust response. The results are given in Figures 8.16 and 8.17, where the following MATLAB program may be used:

Listing 8.2: Example 8.1

```
% Filename : examp81c.m
%
% Simulation of aircraft asymmetric response to atmospheric turbulence.
%
% Chapter 8 of lecture notes ae4-304
%
% Revised: November [M Rodriguez]
%%
%
clc; close all; clear all;
%
disp(' Example 8.1 ');
```

```

disp('
      Simulation of the motion variables for asymmetric aircraft      ');
disp('      motions.                                              ');
disp('                                              ');
disp('      This program produces Figures 8-16 and 8-17 of the lecture notes: ');
disp('      Aircraft Responses to Atmospheric Turbulence.          ');
disp('                                              ');

% GET SYSTEM DYNAMICS
cit2a;

% NOTE (see also cit2a.m)
%
% THE CESSNA CITATION CE-500 IS NOT STABLE IN SPIRAL MODE (FOR THE cit2a.m
% FLIGHT CONDITION), HENCE THE FEEDBACK CONTROLLER FOR PHI IS USED AS IN :
%
%     delta_a = K_phi*phi (K_phi for THIS flight condition)
%
% THEREFORE, CONTROLLED AIRCRAFT SYSTEM MATRICES WILL BE USED FOR RESULTS;
%
%     A = A2

% TIME AXIS AND INPUT VECTOR DEFINITION
dt = 0.05; T = 60; t = [0:dt:T]; N = length(t);
nn = zeros(1,N);

% TURBULENCE INPUTS
u_g = randn(1,N)/sqrt(dt);    % sqrt(dt) because of lsim characteristics
v_g = randn(1,N)/sqrt(dt);
w_g = randn(1,N)/sqrt(dt);

% INPUT VECTORS
u1 = [nn' nn' u_g' nn' nn'];
u2 = [nn' nn' nn' w_g' nn'];
u3 = [nn' nn' nn' nn' v_g'];

% DEFINE OUTPUT MATRICES
C = [1 0 0 0 0 0 0 0 0 0;
      0 1 0 0 0 0 0 0 0 0;
      0 0 1 0 0 0 0 0 0 0;
      0 0 0 1 0 0 0 0 0 0];
D = [0 0 0 0 0;
      0 0 0 0 0;
      0 0 0 0 0;
      0 0 0 0 0];

% RESPONSE to u_g
y1 = lsim(A2,B,C,D,u1,t);
% RESPONSE to w_g
y2 = lsim(A2,B,C,D,u2,t);
% RESPONSE to v_g

```

```

y3 = lsim(A2,B,C,D,u3 ,t );
% RESPONSE to all together (linear system!)
yt = y1+y2+y3;

% PLOT RESULTS
beta_axis = [0 60 -0.07 0.07];
phi_axis  = [0 60 -0.15 0.15];
pb_axis   = [0 60 -1e-2 1e-2];
rb_axis   = [0 60 -1e-2 1e-2];

% RESPONSE TO u_g
disp(' ')')
disp(' Response to u_g (see figures) ')
clf;
subplot(2,1,1); plot(t,y1(:,1)); axis(beta_axis);
ah=gca; set(ah,'Fontsize',14);
xlabel('time, s'); ylabel('beta [rad]');
subplot(2,1,2); plot(t,y1(:,2)); axis(phi_axis);
ah=gca; set(ah,'Fontsize',14);
xlabel('time, s'); ylabel('phi [rad]');
%print -depsc2 -r1200 fig8_16a1
pause

subplot(2,1,1); plot(t,y1(:,3)); axis(pb_axis);
xlabel('time, s'); ylabel('pb/2V [rad]');
subplot(2,1,2); plot(t,y1(:,4)); axis(rb_axis);
xlabel('time, s'); ylabel('rb/2V [rad]');
%print -depsc2 -r1200 fig8_16b1
pause

% RESPONSE TO w_g
disp(' ')')
disp(' Response to w_g (see figures) ')
subplot(2,1,1); plot(t,y2(:,1)); axis(beta_axis);
xlabel('time, s'); ylabel('beta [rad]');
subplot(2,1,2); plot(t,y2(:,2)); axis(phi_axis);
xlabel('time, s'); ylabel('phi [rad]');
%print -depsc2 -r1200 fig8_16a2
pause

subplot(2,1,1); plot(t,y2(:,3)); axis(pb_axis);
xlabel('time, s'); ylabel('pb/2V [rad]');
subplot(2,1,2); plot(t,y2(:,4)); axis(rb_axis);
xlabel('time, s'); ylabel('rb/2V [rad]');
%print -depsc2 -r1200 fig8_16b2
pause

% RESPONSE TO v_g
disp(' ')')
disp(' Response to v_g (see figures) ')
subplot(2,1,1); plot(t,y3(:,1)); axis(beta_axis);
xlabel('time, s'); ylabel('beta [rad]');

```

```

subplot(2,1,2); plot(t,y3(:,2)); axis(phi_axis);
xlabel('time, s'); ylabel('phi [rad]');
%print -depsc2 -r1200 fig8_17a3
pause

subplot(2,1,1); plot(t,y3(:,3)); axis(pb_axis);
xlabel('time, s'); ylabel('pb/2V [rad]');
subplot(2,1,2); plot(t,y3(:,4)); axis(rb_axis);
xlabel('time, s'); ylabel('rb/2V [rad]');
%print -depsc2 -r1200 fig8_17b3
pause

% RESPONSE TO all together
disp('
')
disp(' Response to u_g, v_g and w_g combined (see figures) ')
subplot(2,1,1); plot(t,yt(:,1)); axis(beta_axis);
xlabel('time, s'); ylabel('beta [rad]');
subplot(2,1,2); plot(t,yt(:,2)); axis(phi_axis);
xlabel('time, s'); ylabel('phi [rad]');
%print -depsc2 -r1200 fig8_17at
pause

subplot(2,1,1); plot(t,yt(:,3)); axis(pb_axis);
xlabel('time, s'); ylabel('pb/2V [rad]');
subplot(2,1,2); plot(t,yt(:,4)); axis(rb_axis);
xlabel('time, s'); ylabel('rb/2V [rad]');
%print -depsc2 -r1200 fig8_17bt
pause

```

From Figures 8.16 and 8.17 several conclusions can be drawn:

First, vertical gust w_g has virtually no influence on the sideslip angle, but it gives the largest contribution to the variance of the roll angle φ and the roll rate p , due to the large area of the wings perpendicular to the direction of w_g .

Second, the largest contribution to the yaw rate of an aircraft flying through turbulent air is due to sidegust. This is not surprising considering the yawing motion is mostly the result of a side gust hitting the vertical tailplane.

8.14.2 Example 8.2

In the previous example it was found that the roll angle becomes rather large for the Cessna Ce-500 ‘Citation’ flying in turbulence. This is because the spiral mode of this particular aircraft in this particular flight condition and configuration (landing) is unstable. A way to improve stability is to implement an autopilot wing leveler based on the following control law:

$$\delta_a = K_\varphi (\varphi_i - \varphi) \quad (8.123)$$

where the desired angle of roll is constant, therefore $\varphi_i = 0$. K_φ is a (negative) gain factor. We shall assume that the stabilization is done by an ideal lag-free autopilot. Due to this

idealized control law, two new derivatives can be introduced in Equation (8.99) (Gerlach & Baarspul, 1968):

$$l_\varphi = -K_\varphi l_{\delta_a} \quad (8.124)$$

$$n_\varphi = -K_\varphi n_{\delta_a} \quad (8.125)$$

With the same .m files as used in the previous Chapter (only the matrices A and B are different, symmetric: 7x7, asymmetric: 10x10) it is easy to investigate the influence of the autopilot on the variance of the roll angle. As shown in the previous example, vertical turbulence velocity yields by far the largest contribution to the variance of the roll angle, so only w_g will be considered. The resulting power spectral densities of the roll angle, with and without autopilot engaged for two values of K_φ , are given in Figure 8.18. Apparently the low-frequencies are filtered out with the autopilot and the variance reduces significantly. Integrating the power spectral densities, using Equation (3.45):

$$\sigma_\varphi^2 = \frac{1}{\pi} \int_0^\infty S_{\varphi\varphi}(\omega) d\omega$$

yielded the following results:

$\sigma_\varphi^2 = \infty$	$[rad^2]$	for	$K_\varphi = 0$
$\sigma_\varphi^2 = 5.5072 * 10^{-4}$	$[rad^2]$	for	$K_\varphi = -0.1$

In this case the transient behaviour as a function of K_φ is also interesting, as can be seen in Figure 8.19, where the growth in time of σ_φ^2 is plotted, digitally computed with Equation (5.41):

$$C_{\bar{x}\bar{x}}[k+1] = \Phi C_{\bar{x}\bar{x}}[k] \Phi^T + \Gamma \frac{W_{con}}{\Delta t} \Gamma^T$$

$$\sigma_\varphi^2[k] = C_{\bar{x}\bar{x}}(2, 2)[k]$$

In the case of $K_\varphi = -0.1$ the steady state is reached after about 10 seconds. The uncontrolled aircraft is unstable! The MATLAB program is given below.

Listing 8.3: Example 8.2

```
% Filename : exmpl82.m
%
% Calculation of the PSD functions for the controlled and uncontrolled
% aircraft. Also, numerical integration of the PSD is performed in order
% to determine the variances of phi for both cases. In this code figures
% 8.18 and 8.19 are generated.
%
% Chapter 8 of lecture notes ae4-304
```

```

%
% Revised: November 2014 [M Rodriguez]

%%

clc; close all; clear all;

disp(' Example 8.2 ') ;
disp('') ;
disp(' Calculation of the power spectral density of the roll angle ') ;
disp(' due to asymmetric vertical turbulence.') ;
disp('') ;
disp(' The effect of an autopilot which keeps the roll-angle constant ') ;
disp(' is also investigated.') ;
disp('') ;
disp(' This program produces Figures 8-18 and 8-19 of the lecture ') ;
disp(' notes: Aircraft Responses to Atmospheric Turbulence.') ;
disp('') ;

% COMPUTE SYSTEM DYNAMICS
% NOTE: A represents the UNCONTROLLED SYSTEM
% A2 represents the CONTROLLED SYSTEM with gain as in lecture notes
cit2a;

% FREQUENCY VECTOR
omega = logspace(-2,2,200);

% DEFINE C AND D MATRICES
C = [0 1 0 0 0 0 0 0 0];
D = [0 0 0 0 0];

% CALCULATION OF THE POWER SPECTRAL DENSITY FUNCTION OF PHI DUE TO
% VERTICAL TURBULENCE

% Uncontrolled aircraft
[numphi,den] = ss2tf(A,B,C,D,4);
[mag,phase] = bode(numphi,den,omega);
Sphi = mag.*mag;

% Controlled aircraft
[numphi,den] = ss2tf(A2,B,C,D,4);
[mag,phase] = bode(numphi,den,omega);
Sphit = mag.*mag;

clf
axis('square')
loglog(omega,Sphi,'-',omega,Sphit,'--');
xlabel('omega [rad/s]'); ylabel('Sphi [rad^2]');
legend('S_u_{\phi\phi}', 'S_c_{\phi\phi}');

pause

```

```
% CALCULATION OF THE COVARIANCE MATRIX
dt = 0.05; T = 300; t = [0:dt:T]; N = length(t);

Wdis = 1/dt; % discrete-time intensity of white noise

% Calculation of discrete time system matrices for the
% uncontrolled and controlled aircraft
[Phi, Gamma] = c2d(A,B(:,4), dt);
[Phit, Gammat] = c2d(A2,B(:,4), dt);

% Initial covariance matrices
Cx2x2 = zeros(10,10);
Cxxt = zeros(10,10);
Cx2x2t = zeros(N-1,1);

% Store only variance of phi
for k=2:N
    Cxx = Phi*Cxx*Phi' + Gamma*Wdis*Gamma';
    Cxxt = Phit*Cxxt*Phit' + Gammat*Wdis*Gammat';
    Cx2x2(k) = Cxx(2,2);
    Cx2x2t(k) = Cxxt(2,2);
end

% PLOT RESULTS
clf
subplot(2,1,1)
plot(t,Cx2x2); xlabel('time [s]'); ylabel('variance phi');
title('Uncontrolled aircraft');

subplot(2,1,2)
plot(t,Cx2x2t); xlabel('time [s]'); ylabel('variance phi');
title('Controlled aircraft');

% CHECK: CALCULATION OF THE VARIANCE BY NUMERICALLY INTEGRATING THE
% POWER SPECTRAL DENSITY FUNCTION OF THE ROLL ANGLE PHI.
dw = diff(omega);
varphi = sum(Sphi(1:length(dw)).*dw)/pi;
disp([' Variance of phi for the uncontrolled aircraft: ', num2str(varphi)]);
varphit = sum(Sphit(1:length(dw)).*dw)/pi;
disp([' Variance of phi for the controlled aircraft: ', num2str(varphi)]);
```

8.14.3 Example 8.3

In the next example the periodograms and the power spectral density of the state variables β , ϕ , $\frac{pb}{2V}$ and $\frac{rb}{2V}$ will be calculated. The analytical power spectral densities as well as the estimated PSDs are calculated.

Listing 8.4: Example 8.3

```
% Filename : examp183.m
%
% Computation of analytical PSDs and time-simulation of aircraft
% asymmetric response to atmospheric turbulence.
%
% Chapter 8 of lecture notes ae4-304
%
% Revised: November 2014 [M Rodriguez]
%
%%
clc; close all; clear all;

disp(' Example 8.3'); %)
disp(''); %)
disp(' This example compares analytically obtained auto power'); %)
disp(' spectral densities with experimentally obtained'); %)
disp(' periodograms of the asymmetric motion variables.'); %)
disp(''); %)
disp(' This program produces Figures 8-20 and 8-21 of the lecture'); %)
disp(' notes: Aircraft Responses to Atmospheric Turbulence.'); %)
disp(''); %)

% GET AIRCRAFT DYNAMICS
cit2a;

% NOTE (see also cit2a.m)
%
% THE CESSNA CITATION CE-500 IS NOT STABLE IN SPIRAL MODE (FOR THE cit2a.m
% FLIGHT CONDITION), HENCE THE FEEDBACK CONTROLLER FOR PHI IS USED AS IN :
%
% delta_a = K_phi*phi (K_phi for THIS flight condition)
%
% THEREFORE, CONTROLLED AIRCRAFT SYSTEM MATRICES WILL BE USED FOR RESULTS;
%
% A = A2

% DEFINE C and D MATRICES
C = [1 0 0 0 0 0 0 0 0 % beta
      0 1 0 0 0 0 0 0 0 % phi
      0 0 1 0 0 0 0 0 0 % pb/2V
      0 0 0 1 0 0 0 0 0 % rb/2V
      0 0 0 0 0 0 0 1 0]; % betag

D = [0 0 0 0 0
      0 0 0 0 0
      0 0 0 0 0
      0 0 0 0 0
      0 0 0 0 0];

% DEFINE FREQUENCY VECTOR
w = linspace(-2,2,300);
```

```
% COMPUTE ANALYTIC POWER SPECTRAL DENSITIES
% RESPONSE TO HORIZONTAL LATERAL TURBULENCE
temp = bode(A2,B,C(1,:),D(1,:),5,w); Sbeta = temp.*temp;
temp = bode(A2,B,C(2,:),D(2,:),5,w); Sphi = temp.*temp;
temp = bode(A2,B,C(3,:),D(3,:),5,w); Spp = temp.*temp;
temp = bode(A2,B,C(4,:),D(4,:),5,w); Srr = temp.*temp;
temp = bode(A2,B,C(5,:),D(5,:),5,w); Sbetag = temp.*temp;

Sxx = [Sbeta Sphi Spp Srr Sbetag];

% COMPUTE PSDS USING TIME DOMAIN DATA

% SET TIME AXIS
dt = 0.01; T = 60; t = [0:dt:T]; N = length(t);

% In this case responses to lateral gust vg are calculated (fifth input):
% no asymmetric vertical and longitudinal turbulence: u_g = w_g = 0.
vg = randn(N,1)/sqrt(dt); % sqrt(dt) because of lsim

nn = zeros(N,1);
u = [nn nn nn nn vg];

% COMPUTE SYSTEM RESPONSE
y = lsim(A2,B,C,D,u,t);

beta = y(:,1);
phi = y(:,2);
pbtV = y(:,3);
rbtV = y(:,4);
betag = y(:,5);

% PLOT TIME RESPONSES
disp(' ');
disp(' Aircraft response to atmospheric turbulence ');
title('Aircraft response to atmospheric turbulence ');
clf
subplot(2,2,1); plot(t,beta); xlabel('time, s'); ylabel('beta');
subplot(2,2,2); plot(t,phi); xlabel('time, s'); ylabel('phi');
subplot(2,2,3); plot(t,pbtV); xlabel('time, s'); ylabel('pb/2V');
subplot(2,2,4); plot(t,rbtV); xlabel('time, s'); ylabel('rb/2V');
pause

clf
title('Beta response to atmospheric turbulence ');
plot(t,betag); xlabel('time, s'); ylabel('betag');
pause

% COMPUTE PERIODOGRAM AND ESTIMATE PSD
% PERIODOGRAM
BETA = dt*fft(beta);
PHI = dt*fft(phi);
```

```

P      = dt*fft(pbtV);
R      = dt*fft(rbtV);
BETAG = dt*fft(betaG);

% PSD ESTIMATE
Pbeta = (1/T)*( BETA.* conj(BETA));
Pphi  = (1/T)*(  PHI.* conj(PHI));
Pp    = (1/T)*( P.* conj(P));
Pr    = (1/T)*( R.* conj(R));
Pbetag = (1/T)*(BETAG.* conj(BETAG));

% DEFINE FREQUENCY VECTOR
fs = 1/dt;                                % sample frequency
omega = 2*pi*fs*(0:(N/2)-1)/N;

% PLOT ANALYTIC AND ESTIMATED PSDS IN ONE PLOT
disp('');                                     );
disp(' Plot analytic and estimated PSD functions');   );
title(' Plot analytic and estimated PSD functions');  );
clf
subplot(2,2,1); loglog(w,Sxx(:,1), '--', omega, Pbeta(1:round(N/2)-1));
axis(10.^[-2 2 -12 -2]); xlabel('omega [rad/s]'); ylabel('Sbeta');
subplot(2,2,2); loglog(w,Sxx(:,2), '--', omega, Pphi(1:round(N/2)-1));
axis(10.^[-2 2 -12 -2]); xlabel('omega [rad/s]'); ylabel('Sphi');
subplot(2,2,3); loglog(w,Sxx(:,3), '--', omega, Pp(1:round(N/2)-1));
axis(10.^[-2 2 -14 -2]); xlabel('omega [rad/s]'); ylabel('Spp');
subplot(2,2,4); loglog(w,Sxx(:,4), '--', omega, Pr(1:round(N/2)-1));
axis(10.^[-2 2 -14 -2]); xlabel('omega [rad/s]'); ylabel('Srr');

pause

clf
title(' PSD for beta');                      );
loglog(w,Sxx(:,5), '--', omega, Pbetag(1:round(N/2)-1));
xlabel('omega [rad/s]'); ylabel('Sbetag [rad^2]');
legend('Analytic PSD', 'Estimated PSD')      );

```

The results are plotted in Figures 8.20 and 8.21. See also Example 7.4.

8.14.4 Problem 8.1

During a landing, the parameters describing the turbulence change as a function of altitude, see Figures 6.14 and 6.15. This influences the factor $B = \frac{b}{2L_g}$ in the filter description of the effective one-dimensional power spectral densities. Using the 11 points given in Figures 6.14 and 6.15, make plots of the variances of the motion variables at these 11 altitudes.

8.15 Summary

In this chapter we have presented the asymmetric equations of motion for a rigid aircraft flying in turbulent air. The mathematical model for the aerodynamic force and moments has been derived, as well as new parameters which we called gust derivatives. Some introductory remarks considering the gust penetration effect for asymmetric aircraft motions have been given. Despite the fact that it becomes more difficult to describe the gust penetration effect analytically for the asymmetric aircraft motions, some first order approximations of aerodynamic frequency response functions describing the aerodynamic force and moments buildup caused by lateral atmospheric turbulence have been derived.

B	$\frac{I_{\hat{u}_g}(0,B)}{\sigma_{\hat{u}_g}^2}$	$\frac{I_{\alpha_g}(0,B)}{\sigma_{\alpha_g}^2}$
0.50	0.7856621	0.5380229
0.45	0.7026423	0.4843205
0.40	0.6159092	0.4273037
0.35	0.5261885	0.3674375
0.30	0.4345357	0.3054225
0.25	0.3424367	0.2422765
0.20	0.2519903	0.1794823
0.15	0.1662091	0.1192077
0.125	0.1263831	0.0909742
0.10	0.0895637	0.0647137
0.075	0.0567340	0.0411580
0.0625	0.0422104	0.0306902
0.05	0.0292262	0.0212969
0.03125	0.0132418	0.0096887
0.015625	0.0039835	0.0029280

Table 8.1: $\frac{I_{\hat{u}_g}(0,B)}{\sigma_{\hat{u}_g}^2}$ and $\frac{I_{\alpha_g}(0,B)}{\sigma_{\alpha_g}^2}$ as a function of B .

B	τ_1	τ_2	τ_3
0.50	0.662562	2.311377	2.298718
0.45	0.607202	1.241514	1.204641
0.40	0.544252	1.016470	0.949548
0.35	0.472419	0.895606	0.793271
0.30	0.406748	0.832718	0.703821
0.25	0.346800	0.788367	0.642029
0.20	0.288690	0.747955	0.590821
0.15	0.231815	0.706023	0.545338
0.125	0.202945	0.682303	0.522628
0.10	0.172928	0.653908	0.497035
0.075	0.141145	0.618429	0.467082
0.0625	0.124455	0.596290	0.448961
0.05	0.106813	0.569551	0.427748
0.03125	0.077782	0.512936	0.383390
0.015625	0.048239	0.423350	0.312979

Table 8.2: τ_1 , τ_2 and τ_3 in the approximated power spectral density function of the horizontal gust velocity, as a function of B .

B	τ_4	τ_5	τ_6
0.50	0.480764	1.492572	1.527124
0.45	0.458294	1.332911	1.358464
0.40	0.426746	1.120000	1.140000
0.35	0.386097	0.787000	0.773000
0.30	0.337007	0.589747	0.552325
0.25	0.279943	0.551119	0.482539
0.20	0.218703	0.488882	0.390730
0.15	0.162684	0.440944	0.324153
0.125	0.136627	0.417279	0.296144
0.10	0.111941	0.392720	0.271229
0.075	0.087681	0.365723	0.247885
0.0625	0.076006	0.351389	0.237504
0.05	0.064521	0.336211	0.227862
0.03125	0.047613	0.310788	0.214478
0.015625	0.033226	0.283501	0.202983

Table 8.3: τ_4 , τ_5 and τ_6 in the approximated power spectral density function of the horizontal gust velocity, as a function of B .

	Y	L	N
β	$\frac{V}{b} \frac{C_{Y_\beta}}{2\mu_b}$	$\frac{V}{b} \frac{C_{l_\beta} K_Z^2 + C_{n_\beta} K_{XZ}}{4\mu_b(K_X^2 K_Z^2 - K_{XZ}^2)}$	$\frac{V}{b} \frac{C_{l_\beta} K_{XZ} + C_{n_\beta} K_X^2}{4\mu_b(K_X^2 K_Z^2 - K_{XZ}^2)}$
φ	$\frac{V}{b} \frac{C_L}{2\mu_b}$	0	0
p	$\frac{V}{b} \frac{C_{Y_p}}{2\mu_b}$	$\frac{V}{b} \frac{C_{l_p} K_Z^2 + C_{n_p} K_{XZ}}{4\mu_b(K_X^2 K_Z^2 - K_{XZ}^2)}$	$\frac{V}{b} \frac{C_{l_p} K_{XZ} + C_{n_p} K_X^2}{4\mu_b(K_X^2 K_Z^2 - K_{XZ}^2)}$
r	$\frac{V}{b} \frac{C_{Y_r} - 4\mu_b}{2\mu_b}$	$\frac{V}{b} \frac{C_{l_r} K_Z^2 + C_{n_r} K_{XZ}}{4\mu_b(K_X^2 K_Z^2 - K_{XZ}^2)}$	$\frac{V}{b} \frac{C_{l_r} K_{XZ} + C_{n_r} K_X^2}{4\mu_b(K_X^2 K_Z^2 - K_{XZ}^2)}$
δ_a	$\frac{V}{b} \frac{C_{Y_{\delta_a}}}{2\mu_b}$	$\frac{V}{b} \frac{C_{l_{\delta_a}} K_Z^2 + C_{n_{\delta_a}} K_{XZ}}{4\mu_b(K_X^2 K_Z^2 - K_{XZ}^2)}$	$\frac{V}{b} \frac{C_{l_{\delta_a}} K_{XZ} + C_{n_{\delta_a}} K_X^2}{4\mu_b(K_X^2 K_Z^2 - K_{XZ}^2)}$
δ_r	$\frac{V}{b} \frac{C_{Y_{\delta_r}}}{2\mu_b}$	$\frac{V}{b} \frac{C_{l_{\delta_r}} K_Z^2 + C_{n_{\delta_r}} K_{XZ}}{4\mu_b(K_X^2 K_Z^2 - K_{XZ}^2)}$	$\frac{V}{b} \frac{C_{l_{\delta_r}} K_{XZ} + C_{n_{\delta_r}} K_X^2}{4\mu_b(K_X^2 K_Z^2 - K_{XZ}^2)}$
u_g	0	$-\frac{V}{b} \frac{C_{l_{rw}} K_Z^2 + C_{n_{rw}} K_{XZ}}{4\mu_b(K_X^2 K_Z^2 - K_{XZ}^2)}$	$-\frac{V}{b} \frac{C_{l_{rw}} K_{XZ} + C_{n_{rw}} K_X^2}{4\mu_b(K_X^2 K_Z^2 - K_{XZ}^2)}$
β_g	$\frac{V}{b} \frac{C_{Y_\beta}}{2\mu_b}$	$\frac{V}{b} \frac{C_{l_\beta} K_Z^2 + C_{n_\beta} K_{XZ}}{4\mu_b(K_X^2 K_Z^2 - K_{XZ}^2)}$	$\frac{V}{b} \frac{C_{l_\beta} K_{XZ} + C_{n_\beta} K_X^2}{4\mu_b(K_X^2 K_Z^2 - K_{XZ}^2)}$
α_g	0	$\frac{V}{b} \frac{C_{l_{pw}} K_Z^2 + C_{n_{pw}} K_{XZ}}{4\mu_b(K_X^2 K_Z^2 - K_{XZ}^2)}$	$\frac{V}{b} \frac{C_{l_{pw}} K_{XZ} + C_{n_{pw}} K_X^2}{4\mu_b(K_X^2 K_Z^2 - K_{XZ}^2)}$

Table 8.4: Symbols appearing in the general state-space representation (Equations (8.87) and (8.99)).

$C_{Y_{u_g}}^{(*)} = 0$	$C_{l_{u_g}}^{(*)} = -C_{l_{rw}}$	$C_{n_{u_g}}^{(*)} = -C_{n_{rw}}$
$C_{Y_{\beta_g}} = C_{Y_\beta}$	$C_{l_{\beta_g}} = C_{l_\beta}$	$C_{n_{\beta_g}} = C_{n_\beta}$
$C_{Y_{\dot{\beta}_g}} = C_{Y_{\dot{\beta}}} + \frac{1}{2} C_{Y_{r_{f+v}}}$	$C_{l_{\dot{\beta}_g}} = C_{l_{\dot{\beta}}} + \frac{1}{2} C_{l_{r_{f+v}}}$	$C_{n_{\dot{\beta}_g}} = C_{n_{\dot{\beta}}} + \frac{1}{2} C_{n_{r_{f+v}}}$
$C_{Y_{\alpha_g}}^{(*)} = 0$	$C_{l_{\alpha_g}}^{(*)} = C_{l_{pw}}$	$C_{n_{\alpha_g}}^{(*)} = C_{n_{pw}}$

Table 8.5: Calculation of the asymmetric gust derivatives. The gust derivatives marked with an asterisk (*) should be used in conjunction with the effective one-dimensional input periodograms $I_{\hat{u}_g \hat{u}_g}(\omega)$ and $I_{\alpha_g \alpha_g}(\omega)$.

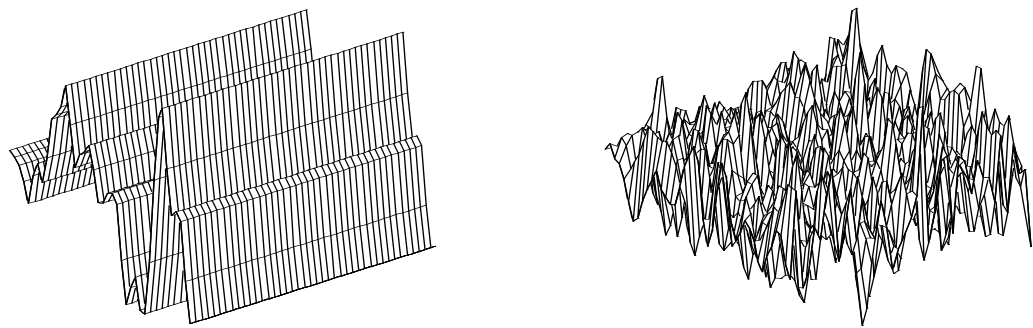


Figure 8.1: ‘Symmetric’ and ‘asymmetric’ gust.

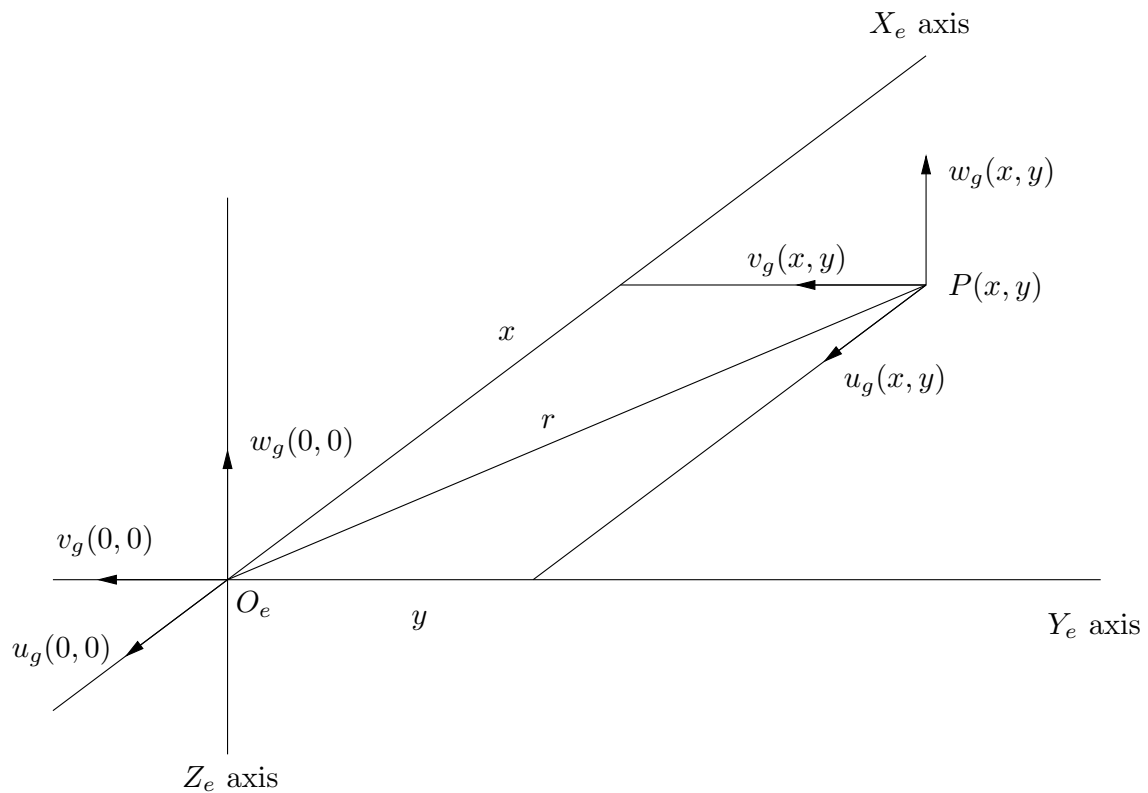


Figure 8.2: The components of the velocity in two points of the $O_eX_eY_e$ plane.

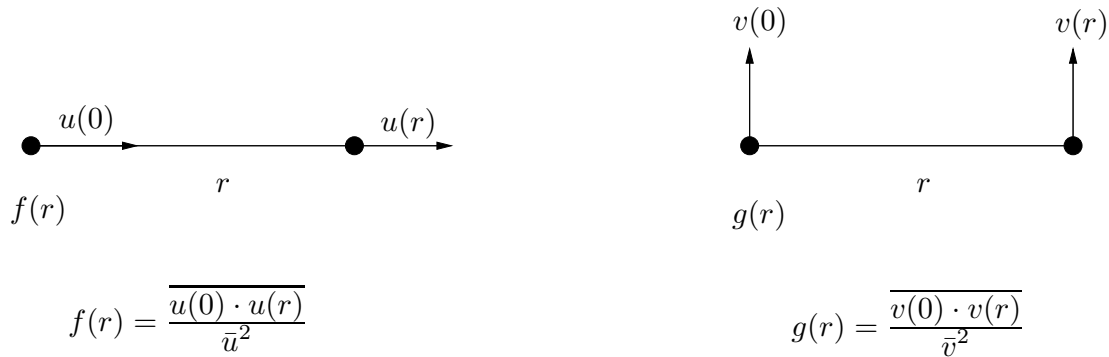


Figure 8.3: The one-dimensional covariance functions $f(r)$ and $g(r)$.

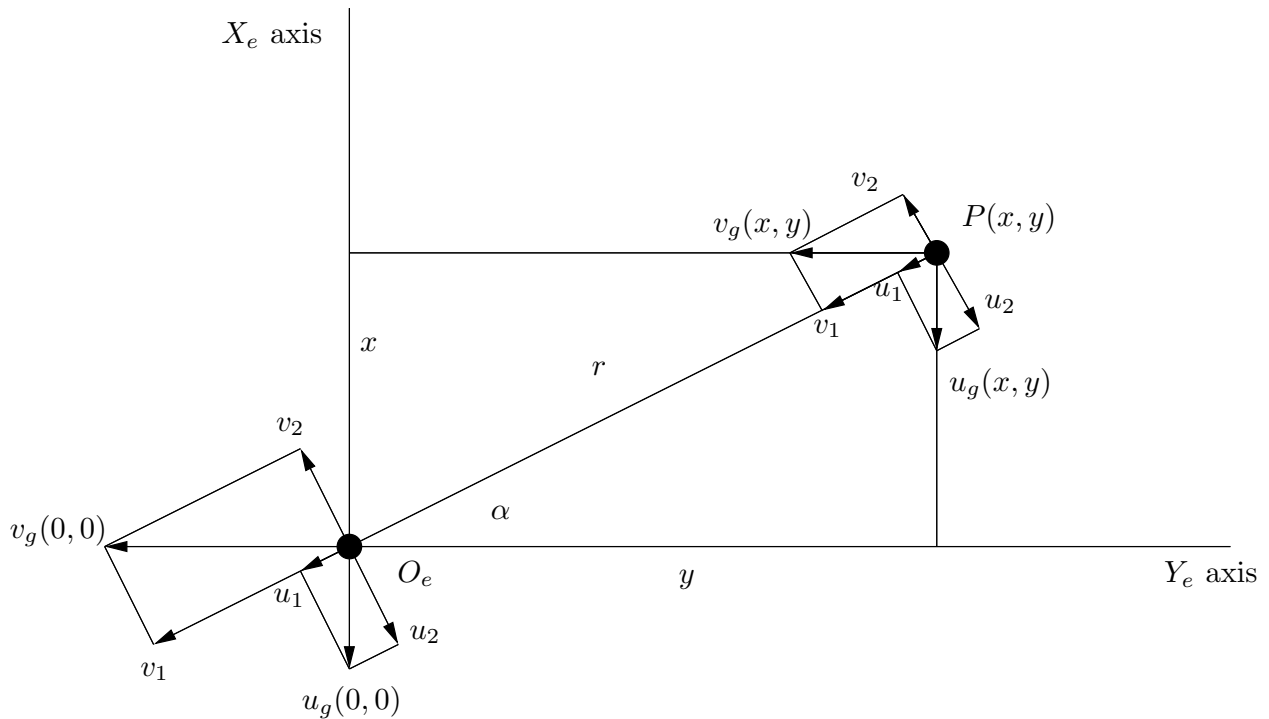


Figure 8.4: The velocities u_g and v_g in the $O_e X_e Y_e$ -plane, resolved in components along- and perpendicular to $O_e P$.

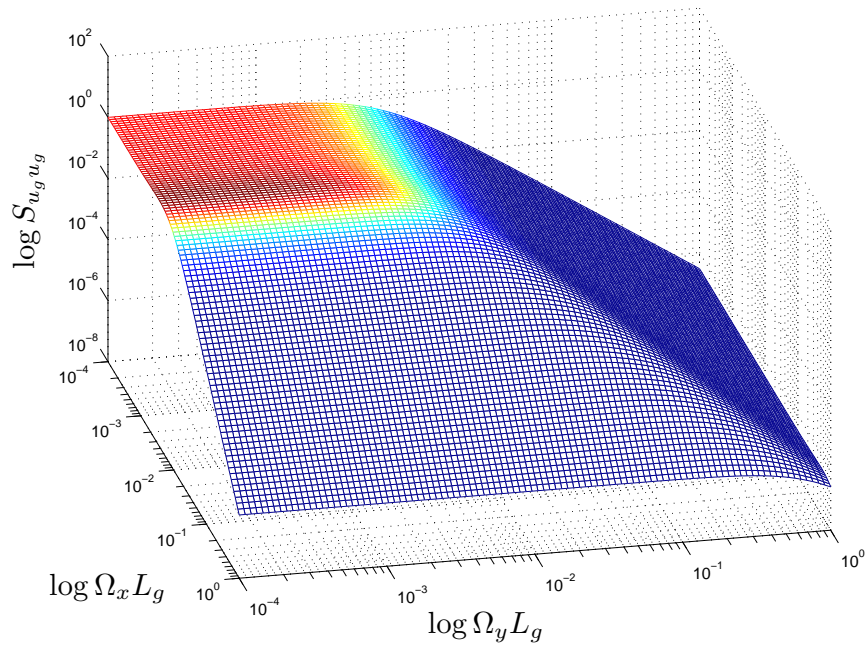


Figure 8.5: Graphical impression of the (2D) auto power spectral density $S_{u_g u_g}(\Omega_x L_g, \Omega_y L_g)$.

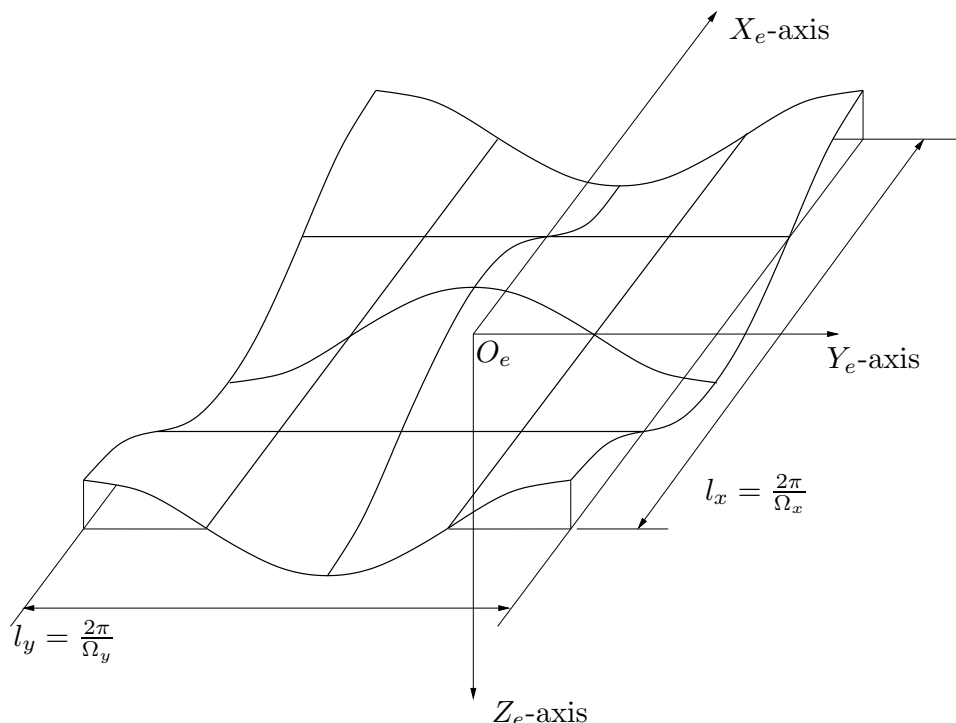


Figure 8.6: Two-dimensional elementary flowfield, symmetric with respect to the $O_e X_e Z_e$ -plane, in which the components of the gust velocity u_g , v_g or w_g change sinusoidally in the X_e - as well as in the Y_e -direction.

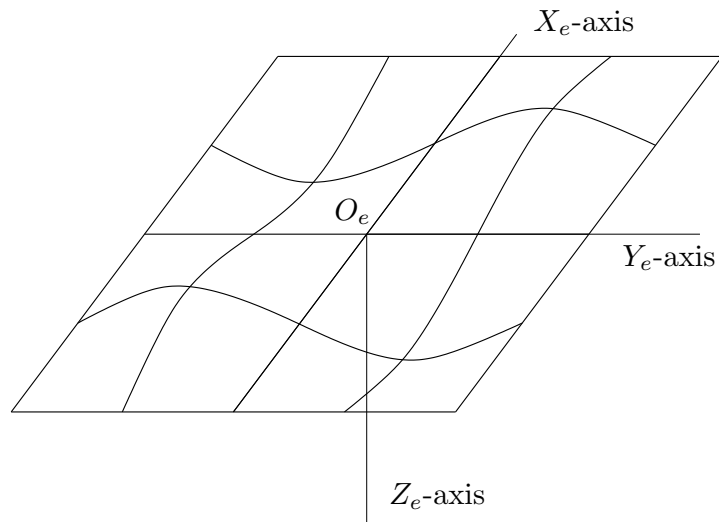


Figure 8.7: Two-dimensional elementary flowfield, antisymmetric with respect to the $O_eX_eZ_e$ -plane.

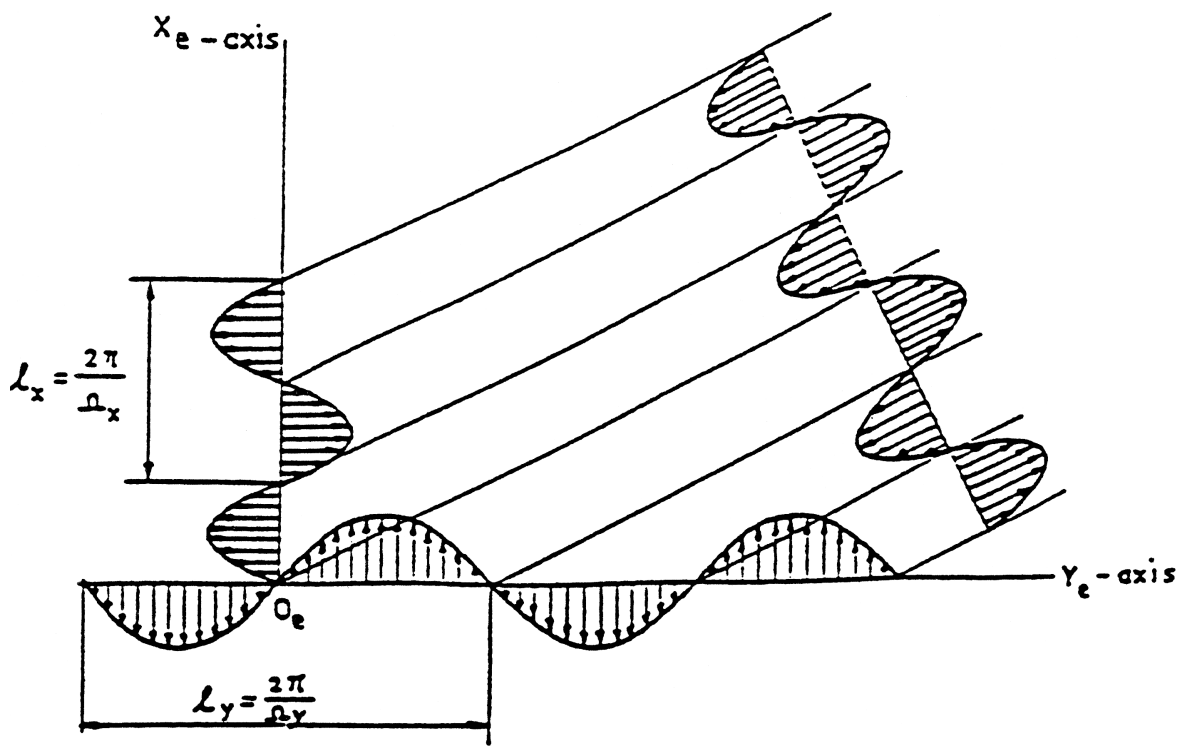


Figure 8.8: The two-dimensional flowfield, represented by a one-dimensional field rotated about the Z_e -axis over the angle $\arctan \frac{\Omega_y}{\Omega_x}$.

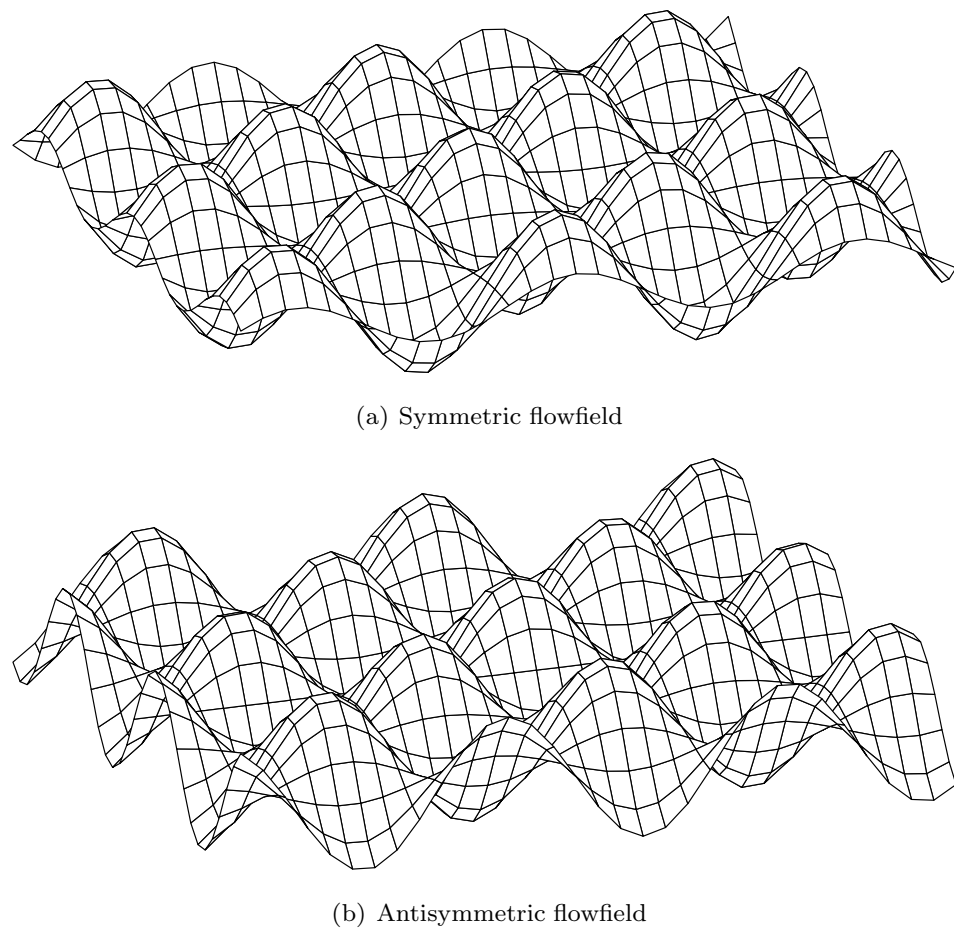


Figure 8.9: Two-dimensional symmetric (a) and antisymmetric flowfields (b).

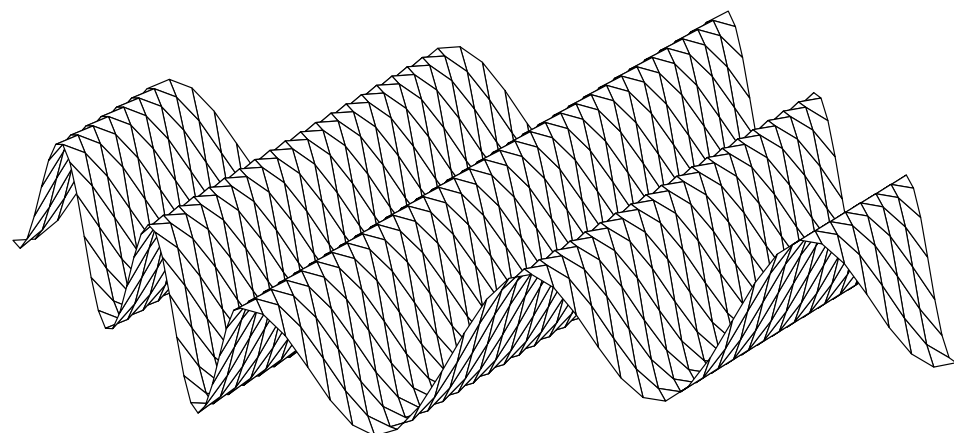


Figure 8.10: Two-dimensional elementary flowfield, resulting from the numerical superposition of Figures 8.9(a) and 8.9(b).

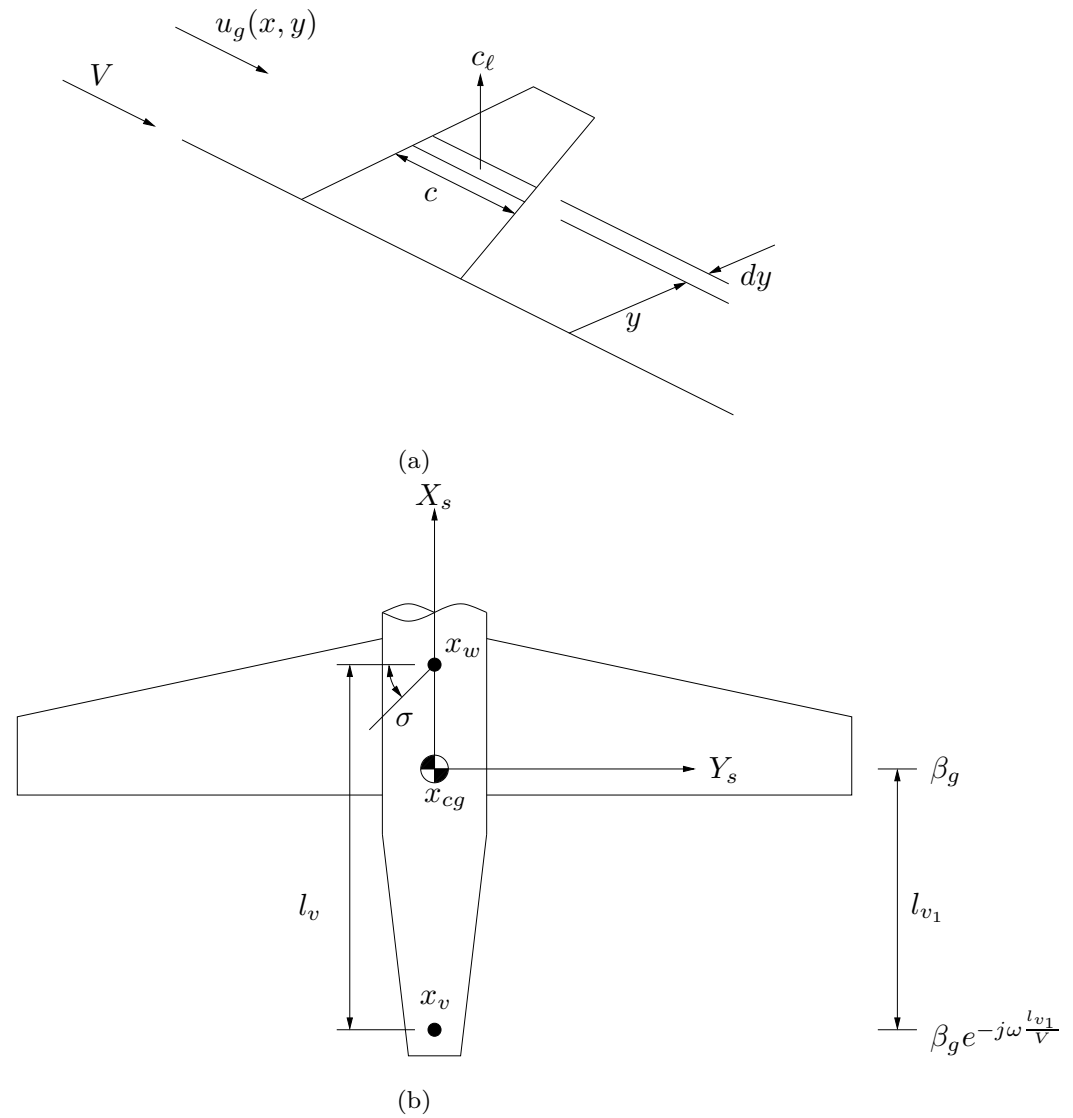


Figure 8.11: The contribution to the rolling moment by a chordwise strip of the wing of width dy at a distance y from the plane of symmetry (a), and description of the gust penetration effect for asymmetric aircraft motions (b).

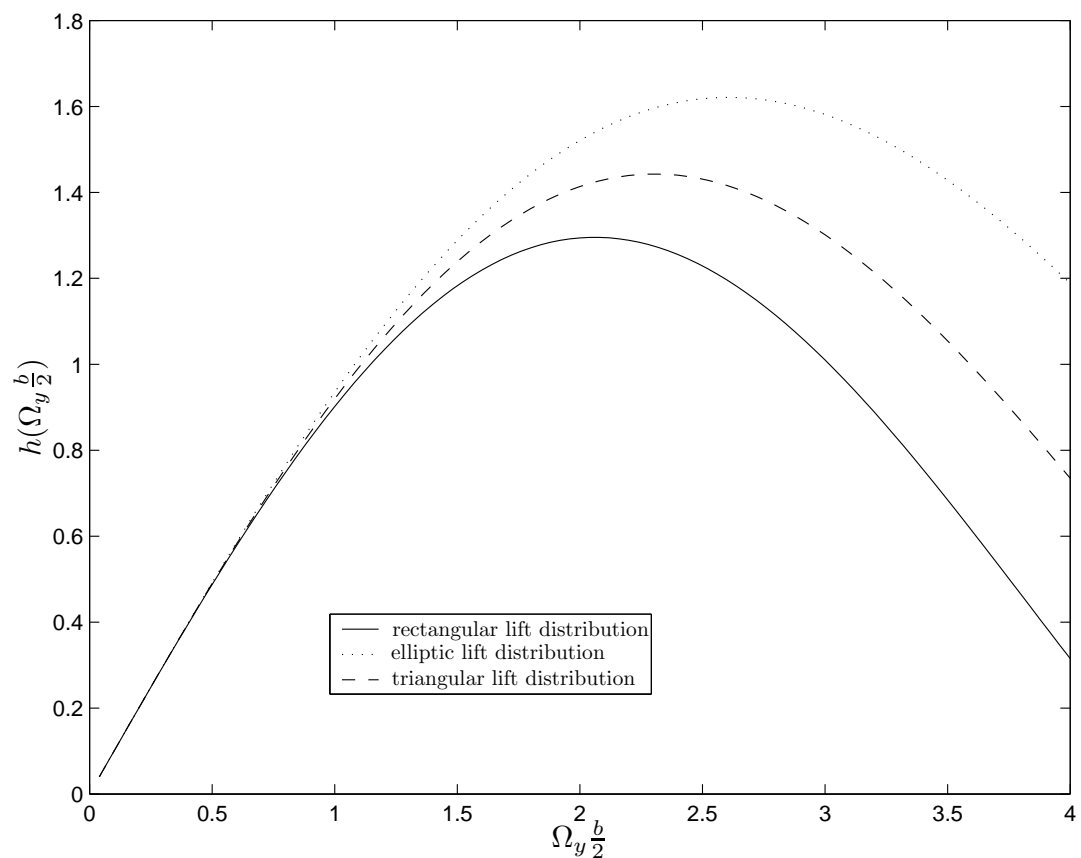


Figure 8.12: The non-dimensional function $h(\Omega_y \frac{b}{2})$ for three different spanwise lift distributions.

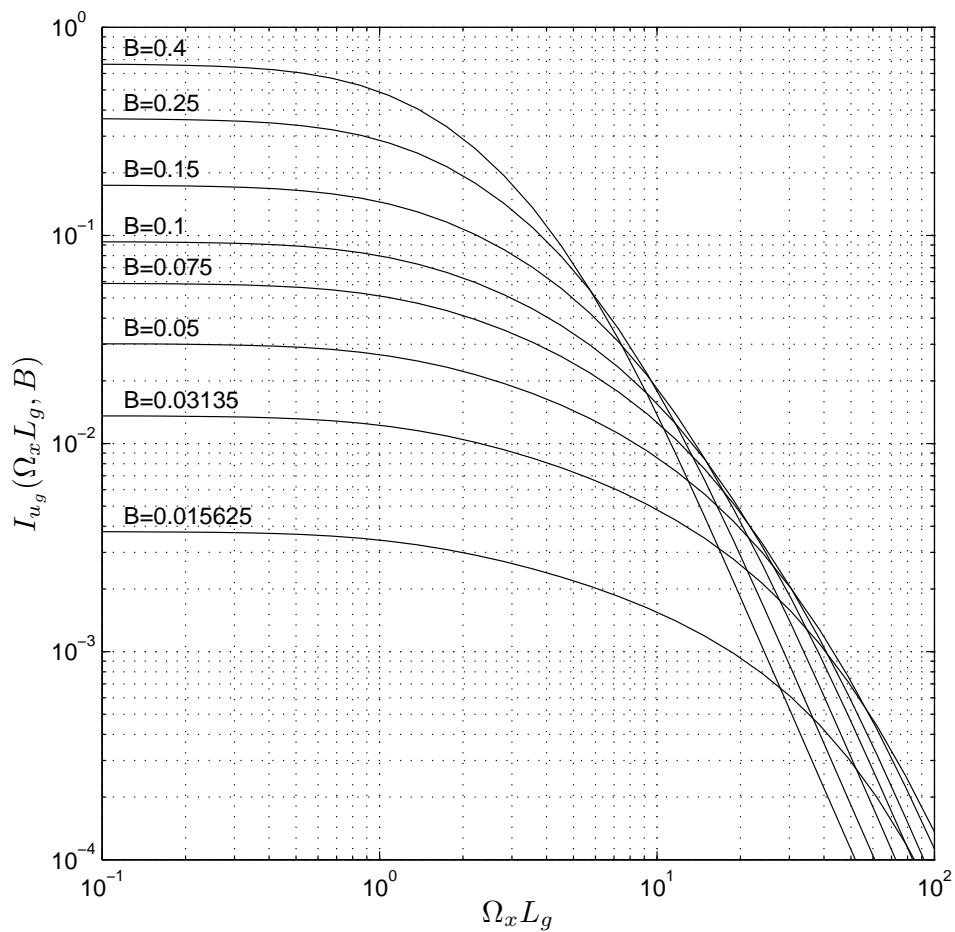


Figure 8.13: The effective one-dimensional power spectral density function of the horizontal gust velocity for different values of $B = \frac{b}{2L_g}$.

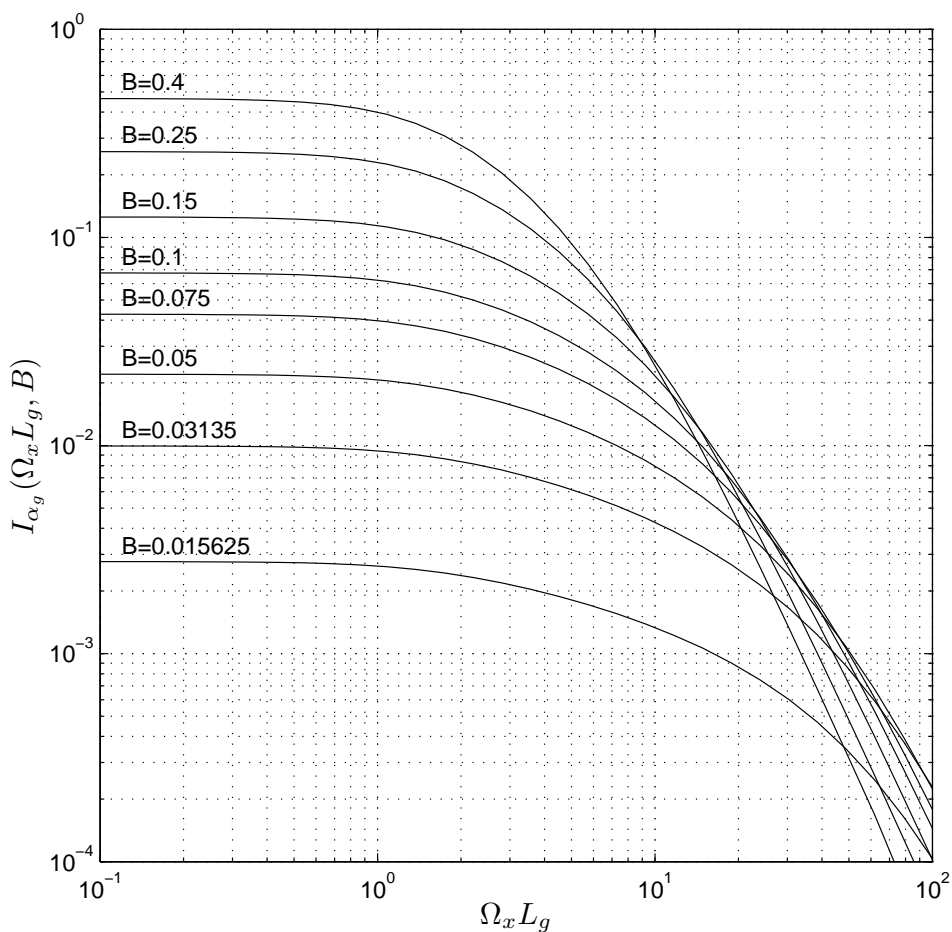


Figure 8.14: The effective one-dimensional power spectral density function of the vertical gust velocity for different values of $B = \frac{b}{2L_g}$.

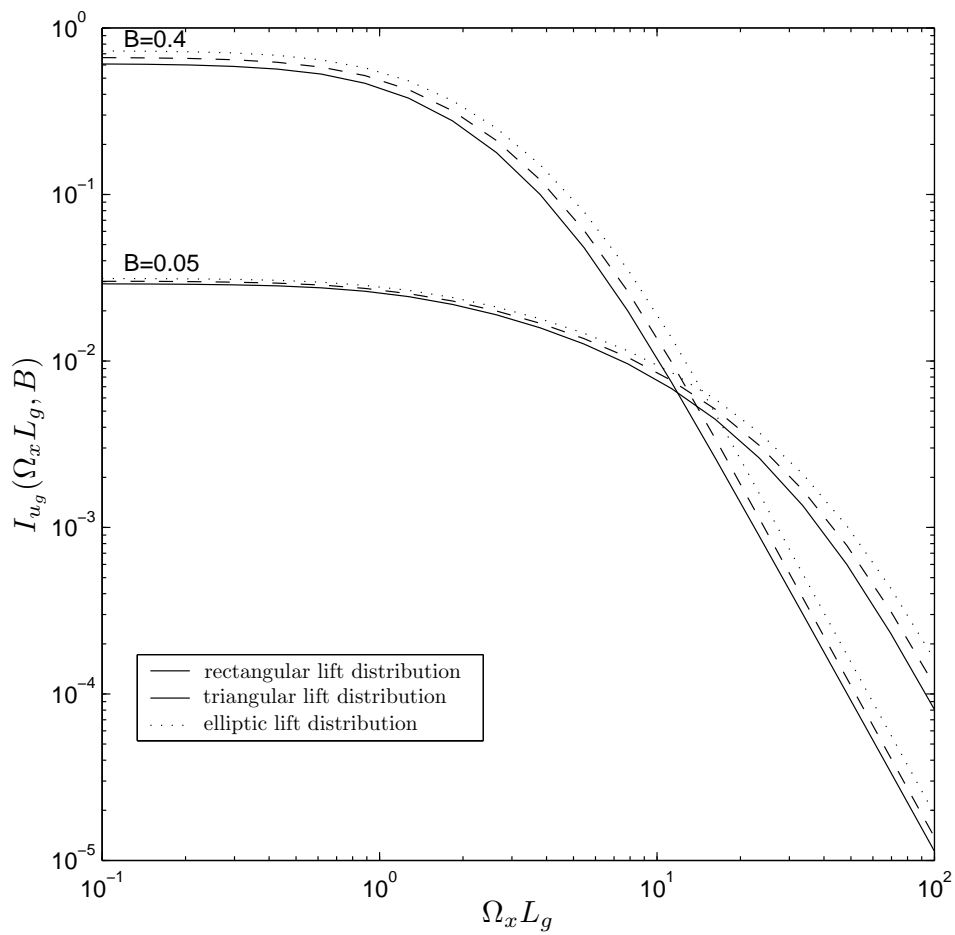


Figure 8.15: The effective one-dimensional power spectral density function of the horizontal gust velocity for three different spanwise lift distributions at two different values for B .

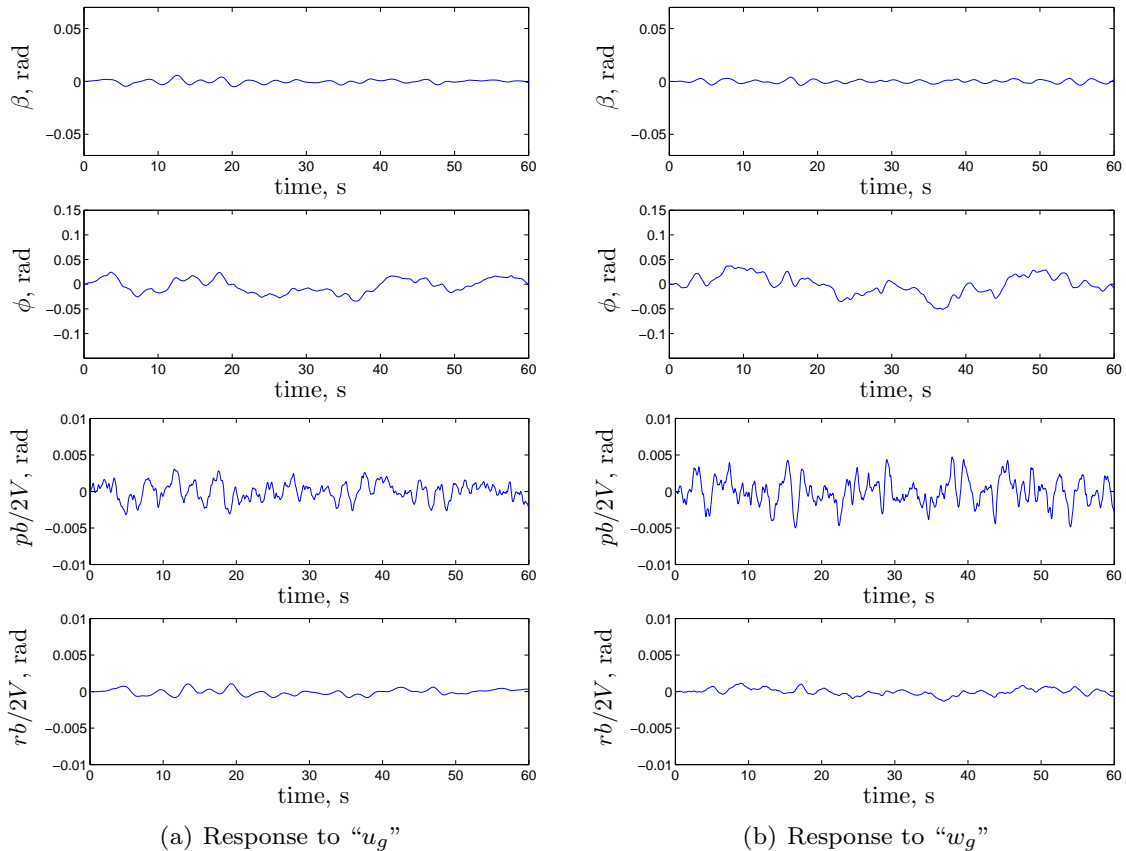


Figure 8.16: Gust responses of the asymmetric motion variables for the Ce-500 ‘Citation’.

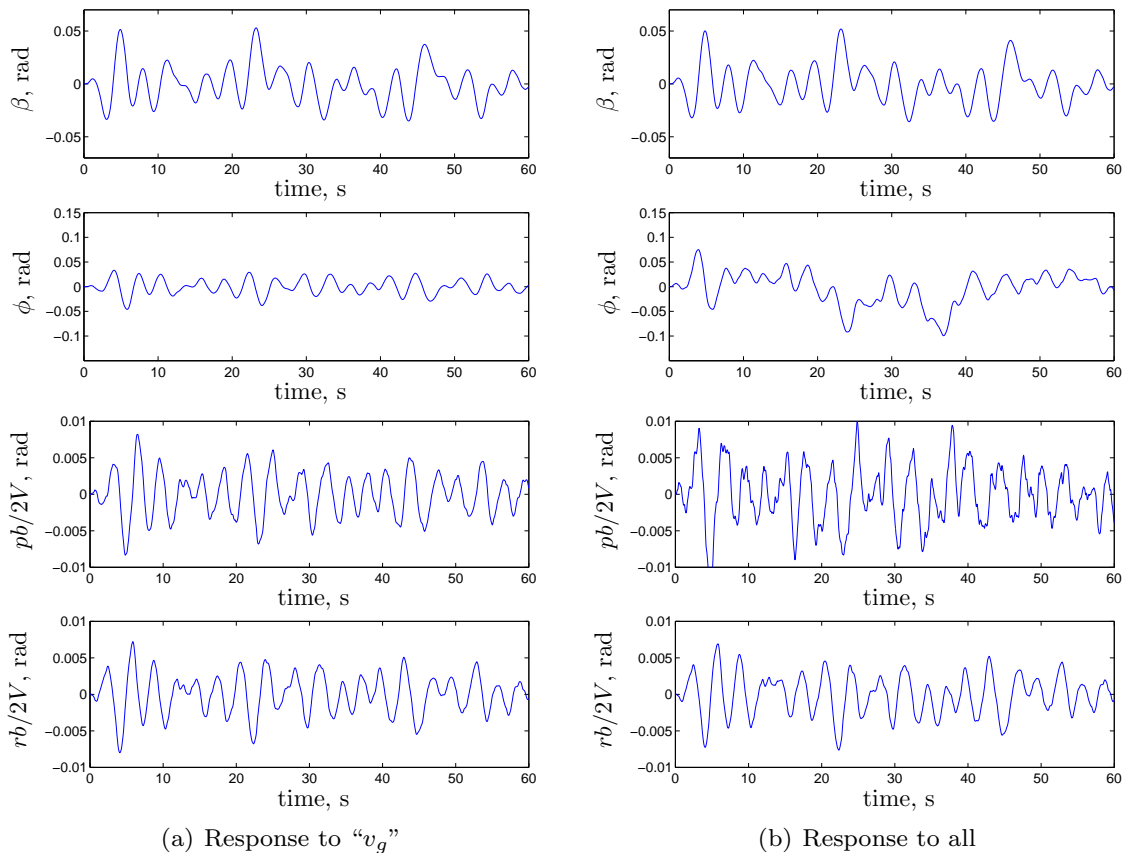


Figure 8.17: Gust responses of the asymmetric motion variables for the Ce-500 ‘Citation’ (continued).

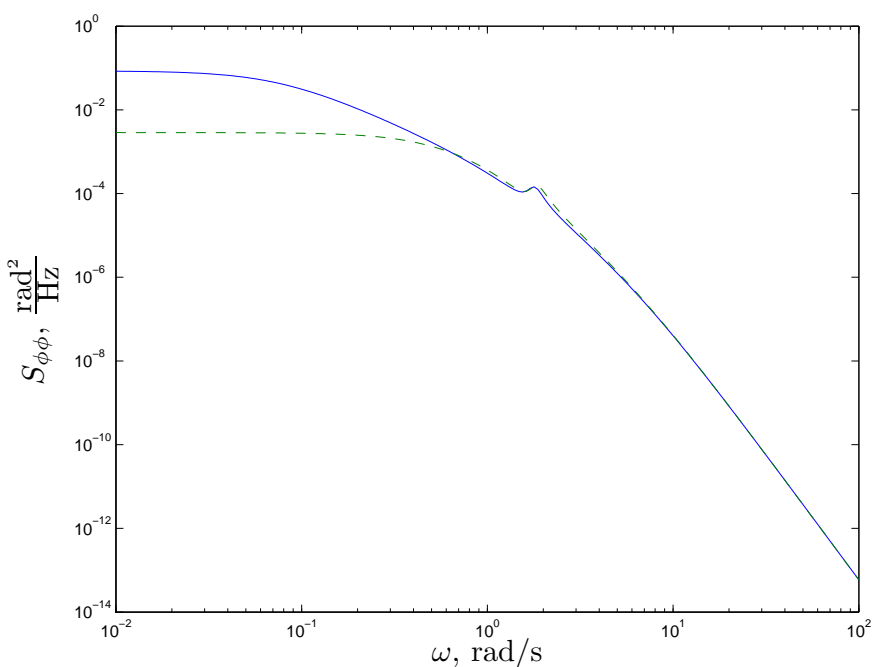


Figure 8.18: Power spectral density of the roll angle for the Ce-500 ‘Citation’ for two feedback gains. The dashed line represents the aircraft’s response with a wing-leveler active.

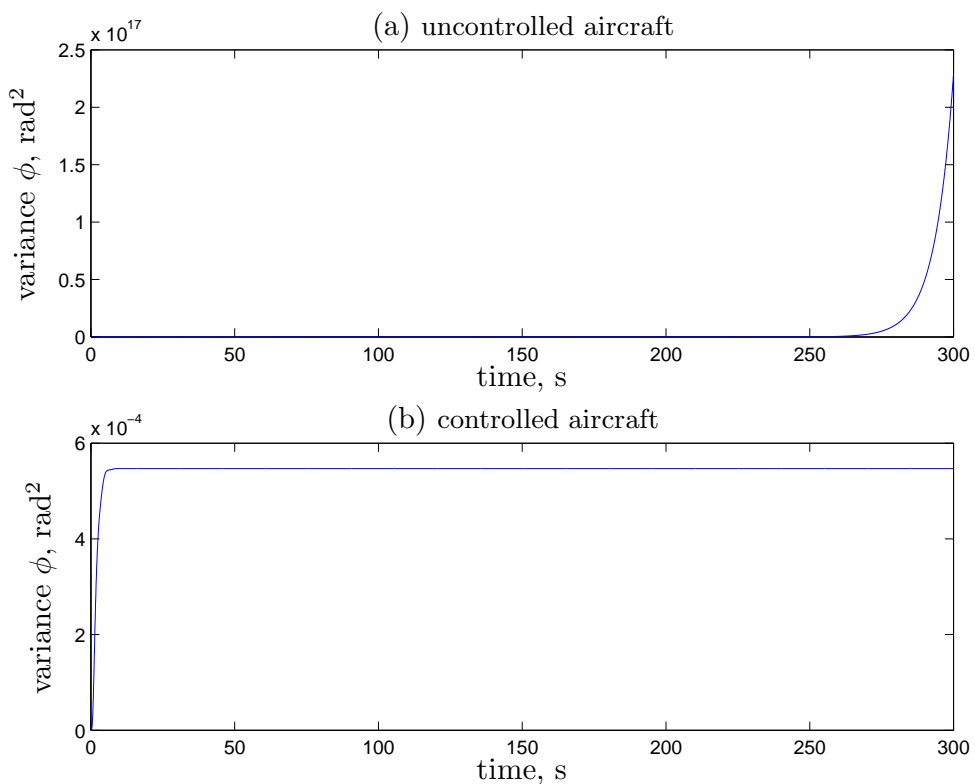
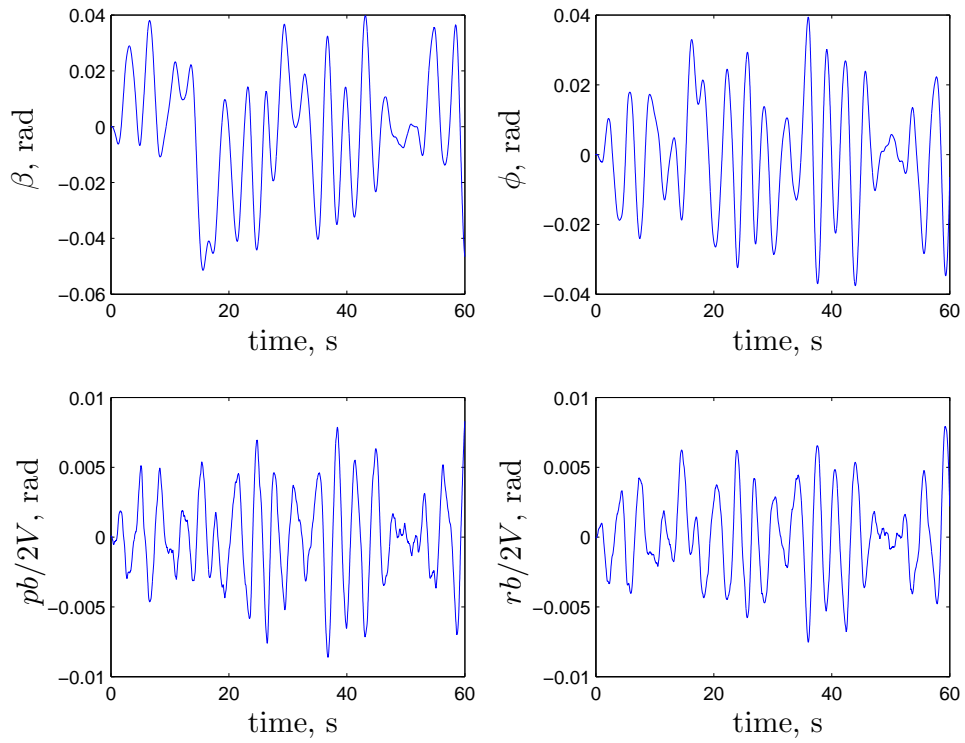
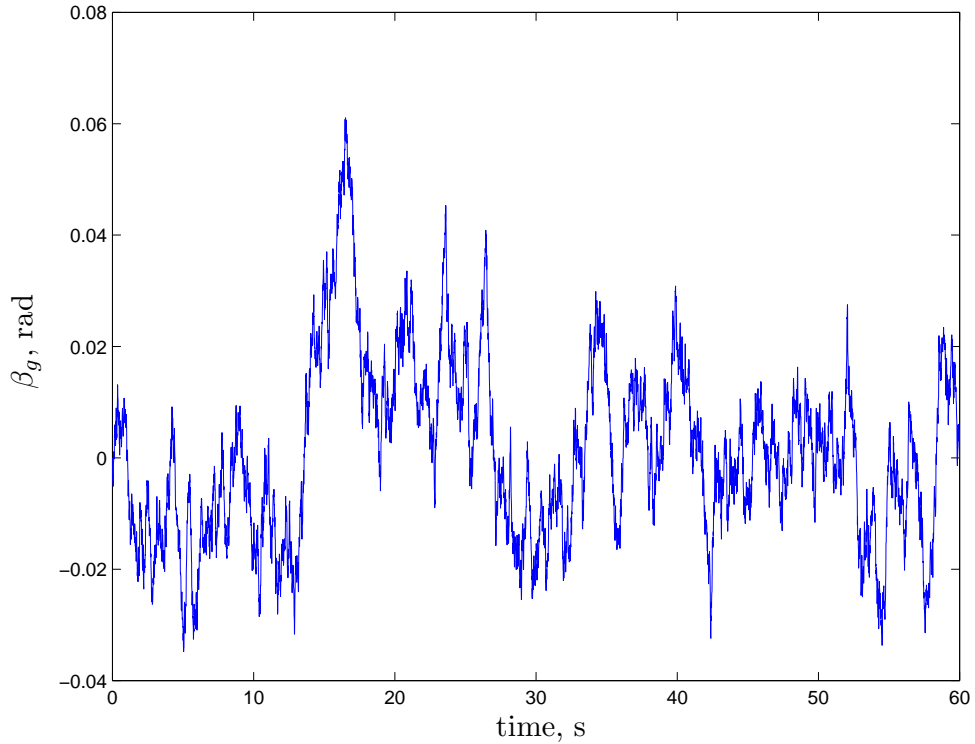


Figure 8.19: Growth in time of the covariance of the roll angle for $K_\varphi = 0$ (a) and $K_\varphi = -0.1$ (b).



(a) Output variables



(b) Asymmetric gust input

Figure 8.20: Aircraft responses due to lateral horizontal turbulence β_g for the Ce-500 ‘Citation’.

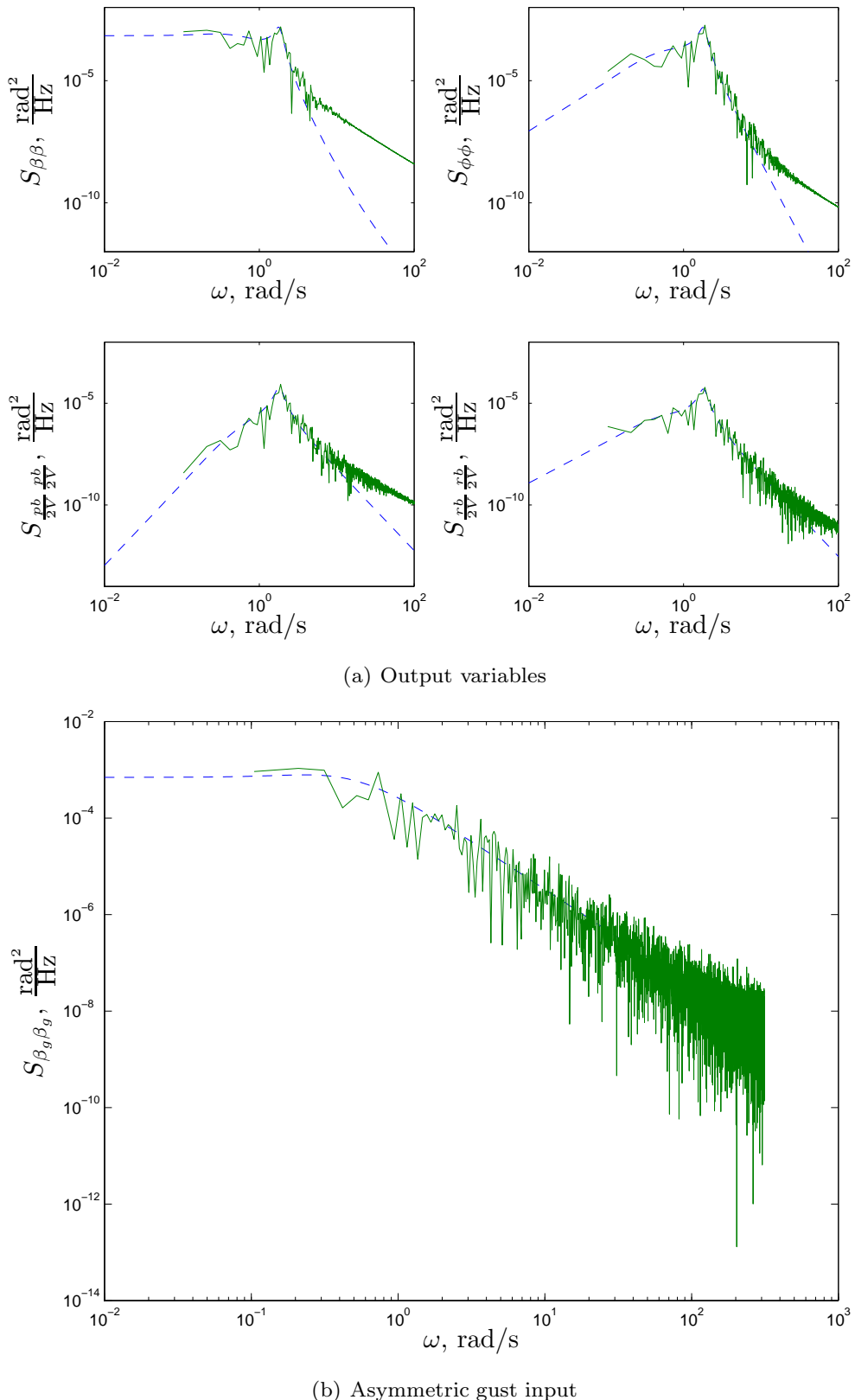


Figure 8.21: Analytically derived power spectral densities and periodograms of the motion variables. The periodograms have been calculated from time-domain data (previous figure).

Chapter 9

Aircraft Responses According to Etkin's 4 Point Model

9.1 Introduction

In the preceding chapters the description of the aircraft responses to atmospheric turbulence according to the Delft University of Technology model were presented. However, other authors propose their models and techniques for the calculation of aircraft responses to atmospheric turbulence. These techniques involve different turbulence models and different aircraft models.

In this chapter a description of the “four point” model according to (Etkin, 1980) will be presented for both the symmetrical and asymmetrical equations of motion. First of all, the relevant mathematical definitions and assumptions will be summarized in the following sections.

9.2 A general statistical description

It is considered that atmospheric turbulence is a random process with the random velocity vector \underline{u} of the air to be a function of the position $\underline{r} = (x_1, x_2, x_3)^T$ and time t ,

$$u(\underline{r}, t) = (u_1, u_2, u_3)^T \quad (9.1)$$

Note: the velocity vector \underline{u} is random, but will not be overstripped to simplify notations. The velocity vector, as in Equation (9.1), describes a multivariate (u_1, u_2, u_3) and multi-variable (x_1, x_2, x_3, t) process.

In the following we will be dealing with the relative, or separation, time τ instead of absolute times t and with the relative, or separation, distance vector $\underline{\xi} = (\xi_1, \xi_2, \xi_3)^T$ instead of the absolute positions $\underline{r} = (x_1, x_2, x_3)^T$.

The relevant correlation and spectrum functions can now be defined. The relevant definitions are summarized in the following.

The matrix of correlation functions is:

$$C_{\underline{u}\underline{u}}(\underline{r}, t; \underline{r} + \underline{\xi}, t + \tau) = E \{ \underline{u}(\underline{r}, t) \cdot \underline{u}(\underline{r} + \underline{\xi}, t + \tau) \} = \\ = \begin{bmatrix} E \{ u_1(\underline{r}, t) \cdot u_1(\underline{r} + \underline{\xi}, t + \tau) \} & E \{ u_1(\underline{r}, t) \cdot u_2(\underline{r} + \underline{\xi}, t + \tau) \} & E \{ u_1(\underline{r}, t) \cdot u_3(\underline{r} + \underline{\xi}, t + \tau) \} \\ E \{ u_2(\underline{r}, t) \cdot u_1(\underline{r} + \underline{\xi}, t + \tau) \} & E \{ u_2(\underline{r}, t) \cdot u_2(\underline{r} + \underline{\xi}, t + \tau) \} & E \{ u_2(\underline{r}, t) \cdot u_3(\underline{r} + \underline{\xi}, t + \tau) \} \\ E \{ u_3(\underline{r}, t) \cdot u_1(\underline{r} + \underline{\xi}, t + \tau) \} & E \{ u_3(\underline{r}, t) \cdot u_2(\underline{r} + \underline{\xi}, t + \tau) \} & E \{ u_3(\underline{r}, t) \cdot u_3(\underline{r} + \underline{\xi}, t + \tau) \} \end{bmatrix} \quad (9.2)$$

This correlation function, Equation (9.2), is a 3x3 matrix with each element an ensemble average of the product of two velocity components separated both in space and time. Equation (9.2) can describe unstationary flows, whose statistics may change with position (e.g. (turbulent) boundary layer flow, whether it is of a wing or the atmosphere) and time. However, if the statistical properties do not vary considerably in time, the random process is *stationary* and only the difference in time, as described by the variable τ , is important. Furthermore, for many applications it is acceptable to model the process as *homogeneous*, with no spatial variation of statistics, so the difference in space $\underline{\xi}$ is only important. Equation (9.2) will now be written as,

$$C_{\underline{u}\underline{u}}(\underline{\xi}, \tau) = E \{ \underline{u}(\underline{r}, t) \cdot \underline{u}(\underline{r} + \underline{\xi}, t + \tau) \} = \\ = \begin{bmatrix} E \{ u_1(\underline{r}, t) \cdot u_1(\underline{r} + \underline{\xi}, t + \tau) \} & E \{ u_1(\underline{r}, t) \cdot u_2(\underline{r} + \underline{\xi}, t + \tau) \} & E \{ u_1(\underline{r}, t) \cdot u_3(\underline{r} + \underline{\xi}, t + \tau) \} \\ E \{ u_2(\underline{r}, t) \cdot u_1(\underline{r} + \underline{\xi}, t + \tau) \} & E \{ u_2(\underline{r}, t) \cdot u_2(\underline{r} + \underline{\xi}, t + \tau) \} & E \{ u_2(\underline{r}, t) \cdot u_3(\underline{r} + \underline{\xi}, t + \tau) \} \\ E \{ u_3(\underline{r}, t) \cdot u_1(\underline{r} + \underline{\xi}, t + \tau) \} & E \{ u_3(\underline{r}, t) \cdot u_2(\underline{r} + \underline{\xi}, t + \tau) \} & E \{ u_3(\underline{r}, t) \cdot u_3(\underline{r} + \underline{\xi}, t + \tau) \} \end{bmatrix} \quad (9.3)$$

Fourier transformation of Equation (9.3) yields the spectral density matrix which is also a 3x3 matrix and is independent of absolute time and space,

$$S_{\underline{u}\underline{u}}(\Omega, \omega) = \int_{-\infty}^{+\infty} \int_{-\infty}^{+\infty} \int_{-\infty}^{+\infty} \int_{-\infty}^{+\infty} C_{\underline{u}\underline{u}}(\underline{r}, t; \underline{r} + \underline{\xi}, t + \tau) e^{-j(\Omega \cdot \underline{\xi} + \omega \tau)} d\xi_1 d\xi_2 d\xi_3 d\tau \quad (9.4)$$

with Ω and ω , respectively, the wave-number vector $\Omega = (\Omega_x, \Omega_y, \Omega_z)^T$ and circular frequency. An approximation almost universally accepted and quite valid for almost all cases of flight in a turbulent atmosphere is that temporal changes in the velocity field are negligible compared with the apparent temporal changes felt by the vehicle as it passes through spatial gradients. This implies that in flight at speed V on the x-axis (e.g. the stability frame of reference's x-axis), in which the actual perceived rate of change is,

$$\frac{D}{Dt} = \frac{\partial}{\partial t} + V \frac{\partial}{\partial x} \quad (9.5)$$

the partial time derivative can be neglected. This is known as the *frozen field* approximation. The approximation may not be valid when the airspeed V is very small in which case the first term may become dominant. The frozen field assumption has the result of reducing the three dimensional correlation and spectral functions summarized below,

$$C_{\underline{u}\underline{u}}(\underline{\xi}) = E \left\{ \underline{u}(\underline{r}) \cdot \underline{u}(\underline{r} + \underline{\xi}) \right\} = \quad (9.6)$$

$$= \begin{bmatrix} E \left\{ u_1(\underline{r}) \cdot u_1(\underline{r} + \underline{\xi}) \right\} & E \left\{ u_1(\underline{r}) \cdot u_2(\underline{r} + \underline{\xi}) \right\} & E \left\{ u_1(\underline{r}) \cdot u_3(\underline{r} + \underline{\xi}) \right\} \\ E \left\{ u_2(\underline{r}) \cdot u_1(\underline{r} + \underline{\xi}) \right\} & E \left\{ u_2(\underline{r}) \cdot u_2(\underline{r} + \underline{\xi}) \right\} & E \left\{ u_2(\underline{r}) \cdot u_3(\underline{r} + \underline{\xi}) \right\} \\ E \left\{ u_3(\underline{r}) \cdot u_1(\underline{r} + \underline{\xi}) \right\} & E \left\{ u_3(\underline{r}) \cdot u_2(\underline{r} + \underline{\xi}) \right\} & E \left\{ u_3(\underline{r}) \cdot u_3(\underline{r} + \underline{\xi}) \right\} \end{bmatrix}$$

$$S_{\underline{u}\underline{u}}(\underline{\Omega}) = \int_{-\infty}^{+\infty} \int_{-\infty}^{+\infty} \int_{-\infty}^{+\infty} \int_{-\infty}^{+\infty} C_{\underline{u}\underline{u}}(\underline{\xi}) e^{-j(\underline{\Omega} \cdot \underline{\xi})} d\xi_1 d\xi_2 d\xi_3 \quad (9.7)$$

9.3 Correlation functions and the integral scale of turbulence

At this moment, the correlation matrix C , Equation (9.6), and the power spectral density matrix S , Equation (9.7) are defined. At this point, however, a correlation matrix in analytical form is introduced,

$$C_{ij}(\xi) = \sigma^2 \left(\frac{f(\xi) - g(\xi)}{\xi^2} \xi_i \xi_j + g(\xi) \delta_{ij} \right) \quad (9.8)$$

with,

$$\xi^2 = \xi_1^2 + \xi_2^2 + \xi_3^2$$

and,

$$\underline{\xi} = (\xi_1, \xi_2, \xi_3)^T$$

The correlation function, Equation (9.8) holds for any model of homogeneous isotropic turbulence and is based on the correlation functions f and g , see also Chapter 6,

Von Karman correlation functions:

longitudinal:

$$f(\xi) = \frac{2^{\frac{2}{3}}}{\Gamma(\frac{1}{3})} \left(\frac{\xi}{1.339L_g} \right)^{\frac{1}{3}} K_{\frac{1}{3}} \left(\frac{\xi}{1.339L_g} \right) \quad (9.9)$$

lateral:

$$g(\xi) = \frac{2^{\frac{2}{3}}}{\Gamma(\frac{1}{3})} \left(\frac{\xi}{1.339L_g} \right)^{\frac{1}{3}} \left[K_{\frac{1}{3}} \left(\frac{\xi}{1.339L_g} \right) - \frac{1}{2} \left(\frac{\xi}{1.339L_g} \right) K_{\frac{2}{3}} \left(\frac{\xi}{1.339L_g} \right) \right] \quad (9.10)$$

Dryden correlation functions:

longitudinal:

$$f(\xi) = e^{-\frac{\xi}{L_g}} \quad (9.11)$$

lateral:

$$g(\xi) = e^{-\frac{\xi}{L'_g}} \left(1 - \frac{\xi}{2L_g}\right) \quad (9.12)$$

The longitudinal and lateral correlation functions f and g also define the longitudinal turbulence scale L_g and lateral scale L'_g by,

$$\text{longitudinal scale} : L_g = \int_0^\infty f(\xi) d\xi \quad (9.13)$$

$$\text{lateral scale} : L'_g = \int_0^\infty g(\xi) d\xi \quad (9.14)$$

Keep in mind that for *isotropic* turbulence, that is,

$$\sigma^2 = \overline{u_g^2} = \overline{v_g^2} = \overline{w_g^2} \quad (9.15)$$

or,

$$\sigma^2 = \sigma_{u_g}^2 = \sigma_{v_g}^2 = \sigma_{w_g}^2$$

the longitudinal scale L_g equals twice the lateral scale L'_g ,

$$L_g = 2L'_g \quad (9.16)$$

Finally, also for the four point model of Etkin, the turbulence is assumed to be Gaussian. Summarizing: atmospheric turbulence is, also for Etkin's four point model, to be considered stationary, isotropic, homogeneous with a Gaussian distribution.

Up till this point, we have considered an arbitrary frame of reference and a general separation vector $\underline{\xi}$. In Chapter 6 we have restricted ourselves to the stability frame of reference and selected the separation vector $\underline{\xi}$ along the aircraft's flight path ($\underline{\xi} = (V \cdot \tau, 0, 0)^T$). Hence, the spatial frequency Ω (rad/m) equals,

$$\omega = \Omega \cdot V. \quad (9.17)$$

And hence,

$$C(\tau) = R(\xi = V \cdot \tau) \quad (9.18)$$

$$S(\omega) = \frac{1}{V} S(\Omega = \frac{\omega}{V}). \quad (9.19)$$

If the separation vector is chosen as $\underline{\xi} = (V \cdot \tau, 0, 0)^T$, keep in mind that the spatial frequency $\Omega_x = \frac{\omega}{V}$ and the other two spatial frequencies Ω_y and Ω_z are zero. This way, we have derived the power spectral densities $S_{u_g u_g}(\omega)$, $S_{v_g v_g}(\omega)$ and $S_{w_g w_g}(\omega)$ in Chapter 6. These power spectral densities describe atmospheric turbulence which only varies along the aircraft's longitudinal axis. The ω in Equation (9.17) is not equal to the ω in Equation (9.4) since the latter describes a time dependency in the system, e.g. time-dependent parameters in the model. The ω in Equation (9.17) is related to the spatial frequency Ω_x and hence by time through the speed V and the separation vector $\underline{\xi} = (V \tau, 0, 0)^T$.

In the stability frame of reference the turbulence velocities are denoted as $\underline{u} = (u_g, v_g, w_g)^T$ instead of the general notation $\underline{u} = (u_1, u_2, u_3)^T$.

All of the above also holds for Etkin's four point model, except for the fact that the separation vector $\underline{\xi}$ will be chosen in different directions and other turbulence inputs will be considered. The choice of these new input variables will be discussed in the next section where the Linear Field Approximation model will be presented first.

9.4 The turbulence inputs for the linear field approximation

In the linear field approximation the turbulence inputs to the equations of motion, and hence the equations of motion themselves, differ from those as developed at the DUT. The gust velocities u_g , v_g and w_g are assumed to be linear functions of the ordinates x , y and z but since most aircraft may be assumed to be planar, the z gradients will be neglected. We are now only interested in x and y gradients of the three turbulence velocities in addition to their values at the mass centre.

The gust velocities, corrected for the value at the centre of gravity, are written as,

$$u_g = \frac{\partial u_g}{\partial x} x + \frac{\partial u_g}{\partial y} y \quad (9.20)$$

$$v_g = \frac{\partial v_g}{\partial x} x + \frac{\partial v_g}{\partial y} y \quad (9.21)$$

$$w_g = \frac{\partial w_g}{\partial x} x + \frac{\partial w_g}{\partial y} y \quad (9.22)$$

Of these six gradients, two of them ($\partial u_g / \partial x$, $\partial v_g / \partial y$) represent strains with velocity fields which have small effect on the longitudinal aerodynamics and none at all on the lateral aerodynamics. The gradient $\partial u_g / \partial x$ represents the difference in u_g along its longitudinal axis, hence, one can speak of a gust penetration effect for u_g which was neglected in Chapter 7. The gradient $\partial v_g / \partial y$ represents the difference in v_g along its lateral axis and has small effect on longitudinal and lateral aerodynamics.

Thus, four gust gradients remain: $\partial u_g / \partial y$, $\partial v_g / \partial x$, $\partial w_g / \partial x$ and $\partial w_g / \partial y$.

Considering a planar airplane, see Figure 9.1, we see that the gust downwash at coordinate (x, y) is equal to Equation (9.22). However, if the vehicle is pitching and rolling, the

contribution of its rates of rotation to the wings normal velocity at the same coordinate (x, y) is, see Figure 9.2,

$$w_{wing_n}(x, y) = py - qx, \quad (9.23)$$

with p and q the respective rates of rotation. Thus the wing boundary conditions (normal relative wind $w_g - w_{wing_n}$) produced by Equations (9.22) and (9.23) are identical if,

$$p = -\frac{\partial w_g}{\partial y}, \quad q = +\frac{\partial w_g}{\partial x},$$

and the wings pressure distributions will be the same whether it is rotating or exposed to a linear gust gradient. For this reason we can write,

$$p_g = \frac{\partial w_g}{\partial y}, \quad q_g = -\frac{\partial w_g}{\partial x}, \quad (9.24)$$

and treat the net effective pitch and roll rates (insofar as aerodynamic forces are concerned) as $(q - q_g)$ and $(p - p_g)$.

The remaining two gust gradients are, see Figure 9.3,

$$r_{1g} = -\frac{\partial u_g}{\partial y}, \quad r_{2g} = \frac{\partial v_g}{\partial x} \quad (9.25)$$

Note the minus sign in the q_g and r_{1g} turbulence inputs. The reason for this notation is made clear in Figures 9.2 and 9.3, showing an unswept wing and vertical tail system. The relative velocity distribution across the wing associated with $\partial u_g / \partial y$ and that associated with the yaw rate r are identical when $r = r_{1g}$, and the normal relative velocity at the fin associated with $\partial v_g / \partial x$ is the same as that for the yaw rate r when $r = r_{2g}$. The aerodynamic forces and moments due to these gust gradients are the same as the aerodynamic forces if the aircraft is pitching, rolling or yawing with rates equal to the gust gradients. The aerodynamic forces and moments due the gust gradients in non-dimensional form are given below, see also Chapters 7 and 8.

$$C_{Y_g} = C_{Y_p} \frac{p_g b}{2V} \quad (9.26)$$

$$C_{l_g} = C_{l_p} \frac{p_g b}{2V} \quad (9.27)$$

$$C_{n_g} = C_{n_p} \frac{p_g b}{2V} \quad (9.28)$$

$$C_{X_g} = -C_{X_q} \frac{q_g \bar{c}}{V} = 0 \quad (9.29)$$

$$C_{Z_g} = -C_{Z_q} \frac{q_g \bar{c}}{V} \quad (9.30)$$

$$C_{m_g} = -C_{m_q} \frac{q_g \bar{c}}{V} \quad (9.31)$$

$$C_{Y_g} = -C_{Y_{rw}} \frac{r_{1g} b}{2V} + C_{Y_{rv}} \frac{r_{2g} b}{2V} \quad (9.32)$$

$$C_{l_g} = -C_{l_{rw}} \frac{r_{1g} b}{2V} + C_{l_{rv}} \frac{r_{2g} b}{2V} \quad (9.33)$$

$$C_{n_g} = -C_{n_{rw}} \frac{r_{1g} b}{2V} + C_{n_{rv}} \frac{r_{2g} b}{2V} \quad (9.34)$$

where in the latter equations the subscripts w and v denote the contributions to the stability derivatives of the wing and the vertical tailplane respectively. Again, note the minus signs.

The non-dimensional aerodynamic forces and moments due to u_g , v_g and w_g are equal to those derived in Chapters 7 and 8, and are recapitulated as,

$$C_{X_g} = C_{X_u} \hat{u}_g + C_{X_\alpha} \alpha_g$$

$$C_{Z_g} = C_{Z_u} \hat{u}_g + C_{Z_\alpha} \alpha_g$$

$$C_{m_g} = C_{m_u} \hat{u}_g + C_{m_\alpha} \alpha_g$$

$$C_{Y_g} = C_{Y_\beta} \beta_g$$

$$C_{l_g} = C_{l_\beta} \beta_g$$

$$C_{n_g} = C_{n_\beta} \beta_g$$

Summarizing, the turbulence inputs for the linear field approximation become,

$$\underline{u} = [u_g \ v_g \ w_g \ p_g \ q_g \ r_{1g} \ r_{2g}]^T, \quad (9.35)$$

or for the non-dimensional symmetrical aircraft motions, with $\hat{u}_g = \frac{u_g}{V}$ and $\alpha_g = \frac{w_g}{V}$,

$$\underline{u}_{sym} = [\hat{u}_g \ \alpha_g \ \frac{q_g \bar{c}}{V}]^T, \quad (9.36)$$

and for the asymmetrical aircraft motions, with $\beta_g = \frac{v_g}{V}$,

$$\underline{u}_{asym} = [\beta_g \ \frac{p_g b}{2V} \ \frac{r_{1g} b}{2V} \ \frac{r_{2g} b}{2V}]^T. \quad (9.37)$$

Also, the time derivatives of the above input vectors can be considered, but only the time derivatives of v_g and w_g will not be neglected. The non-dimensional aerodynamic forces and moments for these inputs are,

$$C_{X_g} = C_{X_\dot{\alpha}} \frac{\dot{\alpha}_g \bar{c}}{V} = 0 \quad (9.38)$$

$$C_{Z_g} = C_{Z_{\dot{\alpha}}} \frac{\dot{\alpha}_g \bar{c}}{V} \quad (9.39)$$

$$C_{m_g} = C_{m_{\dot{\alpha}}} \frac{\dot{\alpha}_g \bar{c}}{V} \quad (9.40)$$

$$C_{Y_g} = C_{Y_{\dot{\beta}}} \frac{\dot{\beta}_g b}{V} \quad (9.41)$$

$$C_{l_g} = C_{l_{\dot{\beta}}} \frac{\dot{\beta}_g b}{V} \quad (9.42)$$

$$C_{n_g} = C_{n_{\dot{\beta}}} \frac{\dot{\beta}_g b}{V} \quad (9.43)$$

As described above, the effect of the above turbulence inputs can be described entirely by stability derivatives. Remember that the gust gradients or gust inputs are given by Equations (9.24) and (9.25). The equations of motion for the symmetric and asymmetric aircraft motions are given below:

Symmetric aircraft motions:

$$\begin{bmatrix} \dot{u} \\ \dot{\alpha} \\ \dot{\theta} \\ \frac{\dot{q}\bar{c}}{V} \end{bmatrix} = \begin{bmatrix} x_u & x_\alpha & x_\theta & 0 \\ z_u & z_\alpha & z_\theta & z_q \\ 0 & 0 & 0 & \frac{V}{\bar{c}} \\ m_u & m_\alpha & m_\theta & m_q \end{bmatrix} \begin{bmatrix} \hat{u} \\ \alpha \\ \theta \\ \frac{q\bar{c}}{V} \end{bmatrix} + \begin{bmatrix} x_u & x_\alpha & -x_{q_g} & x_{\dot{\alpha}} \\ z_u & z_\alpha & -z_{q_g} & z_{\dot{\alpha}} \\ 0 & 0 & 0 & 0 \\ m_u & m_\alpha & -m_{q_g} & m_{\dot{\alpha}} \end{bmatrix} \begin{bmatrix} \hat{u}_g \\ \alpha_g \\ \frac{q_g \bar{c}}{V} \\ \frac{\dot{\alpha}_g \bar{c}}{V} \end{bmatrix} \quad (9.44)$$

Asymmetric aircraft motions:

$$\begin{bmatrix} \dot{\beta} \\ \dot{\varphi} \\ \frac{\dot{p}b}{2V} \\ \frac{\dot{r}b}{2V} \end{bmatrix} = \begin{bmatrix} y_\beta & y_\varphi & y_p & y_r \\ 0 & 0 & 2\frac{V}{b} & 0 \\ l_\beta & 0 & l_p & l_r \\ n_\beta & 0 & n_p & n_r \end{bmatrix} \begin{bmatrix} \beta \\ \varphi \\ \frac{pb}{2V} \\ \frac{rb}{2V} \end{bmatrix} + \begin{bmatrix} y_\beta & y_p & y_{r_w} & y_{r_v} & y_{\dot{\beta}} \\ 0 & 0 & 0 & 0 & 0 \\ l_\beta & l_p & l_{r_w} & l_{r_v} & l_{\dot{\beta}} \\ n_\beta & n_p & n_{r_w} & n_{r_v} & n_{\dot{\beta}} \end{bmatrix} \begin{bmatrix} \frac{\beta_g}{p_g b} \\ \frac{r_1 g b}{2V} \\ \frac{r_2 g b}{2V} \\ \frac{\dot{\beta}_g b}{V} \end{bmatrix} \quad (9.45)$$

Most of the "derivatives" in the above equations are listed in the Tables 7.1 and 8.4. The following amendments to these tables are listed below (see also Tables 9.1 and 9.2):

$$x_{\dot{\alpha}} = \frac{V}{\bar{c}} \frac{C_{X_{\dot{\alpha}}}}{2\mu_c} = 0 \quad (9.46)$$

$$z_{\dot{\alpha}} = \frac{V}{\bar{c}} \frac{C_{Z_{\dot{\alpha}}}}{2\mu_c - C_{Z_{\dot{\alpha}}}} \quad (9.47)$$

$$m_{\dot{\alpha}} = \frac{V}{\bar{c}} \frac{C_{m_{\dot{\alpha}}} + C_{Z_{\dot{\alpha}}} \frac{C_{m_{\dot{\alpha}}}}{2\mu_c - C_{Z_{\dot{\alpha}}}}}{2\mu_c K_Y^2} \quad (9.48)$$

$$x_{q_g} = \frac{V}{\bar{c}} \frac{C_{X_q}}{2\mu_c} = 0 \quad (9.49)$$

$$z_{q_g} = \frac{V}{\bar{c}} \frac{C_{Z_q}}{2\mu_c - C_{Z_{\dot{\alpha}}}} \quad (9.50)$$

$$m_{q_g} = \frac{V}{\bar{c}} \frac{C_{m_q} + C_{Z_q} \frac{C_{m_{\dot{\alpha}}}}{2\mu_c - C_{Z_{\dot{\alpha}}}}}{2\mu_c K_Y^2} \quad (9.51)$$

$$y_{\dot{\beta}} = \frac{V}{b} \frac{C_{Y_{\dot{\beta}}}}{2\mu_b} \quad (9.52)$$

$$l_{\dot{\beta}} = \frac{V}{b} \frac{C_{l_{\dot{\beta}}} K_Z^2 + C_{n_{\dot{\beta}}} K_{XZ}}{4\mu_b (K_X^2 K_Z^2 - K_{XZ}^2)} \quad (9.53)$$

$$n_{\dot{\beta}} = \frac{V}{b} \frac{C_{l_{\dot{\beta}}} K_{XZ} + C_{n_{\dot{\beta}}} K_X^2}{4\mu_b (K_X^2 K_Z^2 - K_{XZ}^2)} \quad (9.54)$$

$$y_{r_w} = -\frac{V}{b} \frac{C_{Y_{r_w}}}{2\mu_b} \quad (9.55)$$

$$l_{r_w} = -\frac{V}{b} \frac{C_{l_{r_w}} K_Z^2 + C_{n_{r_w}} K_{XZ}}{4\mu_b (K_X^2 K_Z^2 - K_{XZ}^2)} \quad (9.56)$$

$$n_{r_w} = -\frac{V}{b} \frac{C_{l_{r_w}} K_{XZ} + C_{n_{r_w}} K_X^2}{4\mu_b (K_X^2 K_Z^2 - K_{XZ}^2)} \quad (9.57)$$

$$y_{r_v} = \frac{V}{b} \frac{C_{Y_{r_v}}}{2\mu_b} \quad (9.58)$$

$$l_{r_v} = \frac{V}{b} \frac{C_{l_{r_v}} K_Z^2 + C_{n_{r_v}} K_{XZ}}{4\mu_b (K_X^2 K_Z^2 - K_{XZ}^2)} \quad (9.59)$$

$$n_{r_v} = \frac{V}{b} \frac{C_{l_{r_v}} K_{XZ} + C_{n_{r_v}} K_X^2}{4\mu_b (K_X^2 K_Z^2 - K_{XZ}^2)} \quad (9.60)$$

In fact, the DUT's method and the linear field approximation method, as presented in (Etkin, 1980), are in theory the same except for the aircraft responses to asymmetrical u_g and α_g turbulence inputs which are the most difficult turbulence inputs for mathematical modeling. Compare the above equations with those presented in Chapters 7 and 8.

9.5 Etkin's four point model

9.5.1 Introduction

In the previous sections the foundations for a general statistical description have been presented. Also, the new turbulence inputs and the new equations of motion have been introduced. In this section Etkin's four point model will be introduced. The four point model is in fact the same as the linear field approximation, except that the input correlations and spectra differ.

One major drawback of the linear field approximation is the limited turbulence wave length, since for small wavelength, e.g. small λ_x , the linear field approximation exaggerates the response. For high turbulence wave lengths the linear field approximation is quite good, see for example Figure 9.4. If the wave length becomes smaller than, for example, the aircraft's length or wingspan, from Figure 9.4 it can be seen that the linear field approximation is no longer accurate. In fact, the correlation between turbulence speeds at the important aerodynamic surfaces and the centre of gravity is lost when we are using the linear field approximation. Therefore, the linear field approximation is valid up to a prescribed frequency or wave length. For longitudinal turbulence the wave length is limited to $\lambda_x \geq 10 l_h$ and for lateral turbulence the wave length is limited to $\lambda_y \geq 10 b$ with respectively l_h and b equal to the taillength and wingspan, see also for example Figure 9.5 where the effect of aircraft size is demonstrated.

Etkin's four point model, (Etkin, 1980), overcomes the above mentioned drawbacks of the linear field approximation. This four point model is a better approximation for lower turbulence wavelengths in both the x - (λ_x) and y - (λ_y) directions. In this model, the gust velocities are considered at four points, see Figure 9.6 and these four points are used to define the gust gradients introduced in the previous section. For u_g and v_g we use the values at the centre of gravity, but because the vertical turbulence velocity w_g is so important, we take it to be the average at the three wing points. By choosing the points 0, 1 and 2 on a straight line, as shown, sweepback is neglected.

The inputs considered in this section are,

$$\begin{aligned}
 u_g &= u_0 \\
 v_g &= v_0 \\
 w_g &= \frac{1}{3} (w_0 + w_1 + w_2) \\
 p_g &= \frac{w_1 - w_2}{b'} \\
 q_g &= \frac{w_3 - w_0}{l_h}
 \end{aligned} \tag{9.61}$$

$$r_{1g} = \frac{u_2 - u_1}{b'}$$

$$r_{2g} = \frac{v_0 - v_3}{l_v}$$

The subscripts 0, 1, 2 and 3 in the turbulence speeds refer to the points depicted in Figure 9.6. The parameters l_h and l_v are, respectively, the distance between the aerodynamic centres of the horizontal tailplane and the centre of gravity and the distance between the vertical tailplane and the centre of gravity. For the parameter b' a generally used value is $0.85b$ with b the wingspan, but this parameter may change considering the spanwise lift distribution (and hence, changes for different aircraft).

9.5.2 Correlations and spectra

In this section the correlation functions will be presented. Consider p_g for example,

$$p_g = \frac{w_1 - w_2}{b'}$$

The autocorrelation C is:

$$\begin{aligned} C_{p_g p_g}(\tau) &= E\{p_g(t) p_g(t + \tau)\} \\ &= \frac{1}{b'^2} E\{(w_1 - w_2)(w'_1 - w'_2)\} \\ &= \frac{1}{b'^2} [E\{w_1 w'_1\} + E\{w_2 w'_2\} - E\{w_1 w'_2\} - E\{w_2 w'_1\}] \end{aligned} \quad (9.62)$$

where w_1 and w_2 are values of w_g at points 1 and 2 at time t , and w'_1 and w'_2 are values of w_g at the same points at time $t+\tau$. The points 0, 1, 2 and 3 in Figure 9.7 respectively have the coordinates $(x_1, 0, 0)^T$, $(x_1, \frac{b'}{2}, 0)^T$, $(x_1, -\frac{b'}{2}, 0)^T$ and $(x_1 - l_v, 0, 0)^T$. The points 0', 1', 2' and 3' in Figure 9.7, respectively, have the coordinates $(x_1 + V\tau, 0, 0)^T$, $(x_1 + V\tau, \frac{b'}{2}, 0)^T$, $(x_1 + V\tau, -\frac{b'}{2}, 0)^T$ and $(V\tau x_1 - l_v, 0, 0)^T$. Hence, in Figure 9.7 the separation vectors become:

$$\underline{\xi}_{11'} = (V\tau, 0, 0)^T$$

$$\underline{\xi}_{12'} = (V\tau, -b', 0)^T$$

$$\underline{\xi}_{21'} = (V\tau, b', 0)^T$$

$$\underline{\xi}_{22'} = (V\tau, 0, 0)^T$$

Recalling the correlation matrix Equation (9.8),

$$E\{u_i u_j\} = C_{ij}(\xi) = \sigma^2 \left(\frac{f(\xi) - g(\xi)}{\xi^2} \xi_i \xi_j + g(\xi) \delta_{ij} \right)$$

and that we are dealing with the vertical gust velocity w (for p_g), in the correlation matrix Equation (9.8) $i = j = 3$ and the u_i and u_j both become u_3 (which corresponds to the vertical gust velocity w). Hence, the autocorrelation $C_{p_g p_g}$, Equation (9.63), becomes,

$$C_{p_g p_g}(\tau) = \frac{2}{b'^2} [C_{33}(V\tau, 0, 0) - C_{33}(V\tau, b', 0)] \quad (9.63)$$

or using Equation (9.8),

$$\frac{(b')^2}{2\sigma^2} C_{p_g p_g}(\tau) = g(\xi_1) - g(\xi_3) \quad (9.64)$$

with,

$$\frac{\xi_1}{aL_g} = \zeta_1 = \left| \frac{V\tau}{aL_g} \right| \quad (9.65)$$

$$\frac{\xi_3}{aL_g} = \zeta_3 = \sqrt{\left(\frac{V\tau}{aL_g} \right)^2 + \left(\frac{b'}{aL_g} \right)^2} \quad (9.66)$$

In a similar way, the other auto- and crosscorrelation functions can be derived. They are summarized in the following.

$$\frac{l_h^2 C_{q_g q_g}(\tau)}{\sigma^2} = 2g(\xi_1) - g(\xi_4) - g(\xi_5) \quad (9.67)$$

$$\frac{(b')^2 C_{r_{1g} r_{1g}}(\tau)}{2\sigma^2} = f(\xi_1) - K_1 f(\xi_3) - (1 - K_1) g(\xi_3) \quad (9.68)$$

$$\frac{l_v^2 C_{r_{2g} r_{2g}}(\tau)}{\sigma^2} = 2g(\xi_1) - g(\xi_6) - g(\xi_7) \quad (9.69)$$

$$\frac{C_{u_g u_g}(\tau)}{\sigma^2} = f(\xi_1) \quad (9.70)$$

$$\frac{C_{v_g v_g}(\tau)}{\sigma^2} = g(\xi_1) \quad (9.71)$$

$$\frac{C_{w_g w_g}(\tau)}{\sigma^2} = \frac{1}{3}g(\xi_1) + \frac{4}{9}g(\xi_2) + \frac{2}{9}g(\xi_3) \quad (9.72)$$

$$\frac{3l_h C_{w_g q_g}(\tau)}{\sigma^2} = g(\xi_5) - g(\xi_1) + 2g(\xi_8) - 2g(\xi_2) \quad (9.73)$$

$$\frac{b' C_{v_g r_{1g}}(\tau)}{\sigma^2} = 2K_2 [g(\xi_2) - f(\xi_2)] \quad (9.74)$$

$$\frac{l_v C_{v_g r_{2g}}(\tau)}{\sigma^2} = g(\xi_1) - g(\xi_7) \quad (9.75)$$

$$\frac{b' l_v C_{r_{1g} r_{2g}}(\tau)}{\sigma^2} = K_3 [g(\xi_9) - f(\xi_9)] + K_2 [f(\xi_2) - g(\xi_2)] \quad (9.76)$$

With,

$$K_1 = \frac{\left(\frac{V\tau}{L_g}\right)^2}{\left(\frac{V\tau}{L_g}\right)^2 + \left(\frac{b'}{2L_g}\right)^2} \quad (9.77)$$

$$K_2 = \frac{\left(\frac{V\tau}{L_g}\right) \left(\frac{b'}{2L_g}\right)}{\left(\frac{V\tau}{L_g}\right)^2 + \left(\frac{b'}{L_g}\right)^2} \quad (9.78)$$

$$K_3 = \frac{\left(\frac{V\tau}{L_g} - \frac{l_v}{L_g}\right) \left(\frac{b'}{2L_g}\right)}{\left(\frac{V\tau}{L_g} - \frac{l_v}{L_g}\right)^2 + \left(\frac{b'}{L_g}\right)^2} \quad (9.79)$$

$$\frac{\xi_2}{aL_g} = \zeta_2 = \sqrt{\left(\frac{V\tau}{aL_g}\right)^2 + \left(\frac{b'}{2aL_g}\right)^2} \quad (9.80)$$

$$\frac{\xi_4}{aL_g} = \zeta_4 = \left| \frac{V\tau}{aL_g} + \frac{l_h}{aL_g} \right| \quad (9.81)$$

$$\frac{\xi_5}{aL_g} = \zeta_5 = \left| \frac{V\tau}{aL_g} - \frac{l_h}{aL_g} \right| \quad (9.82)$$

$$\frac{\xi_6}{aL_g} = \zeta_6 = \left| \frac{V\tau}{aL_g} + \frac{l_v}{aL_g} \right| \quad (9.83)$$

$$\frac{\xi_7}{aL_g} = \zeta_7 = \left| \frac{V\tau}{aL_g} - \frac{l_f}{aL_g} \right| \quad (9.84)$$

$$\frac{\xi_8}{aL_g} = \zeta_8 = \sqrt{\left(\frac{V\tau}{aL_g} - \frac{l_h}{aL_g} \right)^2 + \left(\frac{b'}{2aL_g} \right)^2} \quad (9.85)$$

$$\frac{\xi_9}{aL_g} = \zeta_9 = \sqrt{\left(\frac{V\tau}{aL_g} - \frac{l_v}{aL_g} \right)^2 + \left(\frac{b'}{2aL_g} \right)^2} \quad (9.86)$$

Graphs of these correlations are given in Figures 9.8 to 9.18 in which the longitudinal and lateral correlation functions according to Dryden were used. From the above equations they are seen to be functions of $V\tau/L_g$ and the parameters b'/L_g , l_v/L_g and l_h/L_g , however, in these figures the time shift in seconds is used on the horizontal axes. The correlations are plotted in dimensional form however. The kinks in some of the correlation functions are the result of the four point model representation. They occur at that value of $V\tau/L_g$ for which the tail arrives at the position occupied τ seconds earlier by the centre of gravity (gust penetration effect).

For the calculation of the auto and cross spectral densities, the auto- and cross-correlation functions are Fourier transformed. For this purpose the MATLAB routine `fft` may be used. See also the examples in this chapter. The numerically calculated power spectral densities are given in Figures 9.19 to 9.29. These power spectral densities are given in non-dimensional form. See also the examples given in Section 9.6.

9.5.3 Equations of motion

The Equations (9.44) and (9.45) also hold for Etkin's four point model.

Symmetric aircraft motions:

$$\begin{bmatrix} \dot{\hat{u}} \\ \dot{\alpha} \\ \dot{\theta} \\ \frac{\dot{q}\bar{c}}{V} \end{bmatrix} = \begin{bmatrix} x_u & x_\alpha & x_\theta & 0 \\ z_u & z_\alpha & z_\theta & z_q \\ 0 & 0 & 0 & \frac{V}{\bar{c}} \\ m_u & m_\alpha & m_\theta & m_q \end{bmatrix} \begin{bmatrix} \hat{u} \\ \alpha \\ \theta \\ \frac{q\bar{c}}{V} \end{bmatrix} + \begin{bmatrix} x_u & x_\alpha & 0 & 0 \\ z_u & z_\alpha & -z_{q_g} & z_{\dot{\alpha}} \\ 0 & 0 & 0 & 0 \\ m_u & m_\alpha & -m_{q_g} & m_{\dot{\alpha}} \end{bmatrix} \begin{bmatrix} \hat{u}_g \\ \alpha_g \\ \frac{q_g\bar{c}}{V} \\ \frac{\dot{\alpha}_g\bar{c}}{V} \end{bmatrix}$$

Asymmetric aircraft motions:

$$\begin{bmatrix} \dot{\beta} \\ \dot{\varphi} \\ \frac{\dot{p}b}{2V} \\ \frac{\dot{r}b}{2V} \end{bmatrix} = \begin{bmatrix} y_\beta & y_\varphi & y_p & y_r \\ 0 & 0 & 2\frac{V}{b} & 0 \\ l_\beta & 0 & l_p & l_r \\ n_\beta & 0 & n_p & n_r \end{bmatrix} \begin{bmatrix} \beta \\ \varphi \\ \frac{pb}{2V} \\ \frac{rb}{2V} \end{bmatrix} + \begin{bmatrix} y_\beta & y_p & y_{r_w} & y_{r_v} & y_{\dot{\beta}} \\ 0 & 0 & 0 & 0 & 0 \\ l_\beta & l_p & l_{r_w} & l_{r_v} & l_{\dot{\beta}} \\ n_\beta & n_p & n_{r_w} & n_{r_v} & n_{\dot{\beta}} \end{bmatrix} \begin{bmatrix} \beta_g \\ \frac{p_g b}{2V} \\ \frac{r_{1g} b}{2V} \\ \frac{r_{2g} b}{2V} \\ \frac{\dot{\beta}_g}{V} \end{bmatrix}$$

9.5.4 Frequency domain simulations

For the frequency simulations the transfer functions of all motion variables to all gust inputs may be calculated using MATLAB. However, an important observation must be made; some of the inputs are correlated and hence cross power spectral densities exist. The transfer functions from all inputs to outputs are calculated using the `ss2tf` routine in MATLAB. An example is given below.

Example

Assume a three input/single output system according to,

$$Y(\omega) = H_{yu_1}(\omega)U_1(\omega) + H_{yu_2}(\omega)U_2(\omega) + H_{yu_3}(\omega)U_3(\omega) = H_{yu}(\omega)\underline{u}(\omega)$$

The power spectral density of this output is in general equal to,

$$S_{yy}(\omega) = H_{yu}(\omega) S_{\underline{u}\underline{u}}(\omega) H_{yu}^*(\omega)^T$$

with,

$$H_{yu}(\omega) = [H_{yu_1}(\omega) \ H_{yu_2}(\omega) \ H_{yu_3}(\omega)]$$

and,

$$S_{\underline{u}\underline{u}}(\omega) = \begin{bmatrix} S_{u_1 u_1}(\omega) & S_{u_1 u_2}(\omega) & S_{u_1 u_3}(\omega) \\ S_{u_2 u_1}(\omega) & S_{u_2 u_2}(\omega) & S_{u_2 u_3}(\omega) \\ S_{u_3 u_1}(\omega) & S_{u_3 u_2}(\omega) & S_{u_3 u_3}(\omega) \end{bmatrix}$$

If the inputs are uncorrelated, the cross power spectral densities are equal to zero and the power spectral density matrix becomes,

$$S_{\underline{u}\underline{u}}(\omega) = \begin{bmatrix} S_{u_1 u_1}(\omega) & 0 & 0 \\ 0 & S_{u_2 u_2}(\omega) & 0 \\ 0 & 0 & S_{u_3 u_3}(\omega) \end{bmatrix}$$

9.5.5 Time domain simulations

Although the model presented by Etkin can only be used for frequency domain simulations, time domain simulations may be performed as well.

Considering that the power spectral densities of the concerning input variables are calculated numerically, there seems to be no analytical form for them. However, it is always possible to approximate these power spectral densities by prescribed analytical formulae of which the unknown parameters are to be identified. This problem may be addressed as a curve fitting problem. In this section a linear least squares technique for fitting a real set of data will be presented.

Consider that the numerical frequency data set of a power spectral density is known and let this data be known as $S(\omega_i)$ for $i = 1$ to N (N are the number of frequency points considered). The power spectral density data is accompanied by a set of frequency data called $\omega(i)$, again for $i = 1$ to N . The power spectral density (PSD) data $S(\omega)$ will be approximated, or modelled, by the analytical PSD called $P(\omega)$, and $P(\omega)$ is assumed to have the form,

$$P(\omega) = \frac{K_1 + \gamma_3 \omega^2}{(1 + \gamma_1 \omega^2)(1 + \gamma_2 \omega^2)} \quad (9.87)$$

The analytical function $P(\omega)$ will now be defined as the fraction of two polynomials,

$$P(\omega) = \frac{N(\omega)}{D(\omega)} \quad (9.88)$$

with,

$$N(\omega) = K_1 + \gamma_3 \omega^2 \quad (9.89)$$

$$D(\omega) = (1 + \gamma_1 \omega^2)(1 + \gamma_2 \omega^2) \quad (9.90)$$

Now consider the error $\epsilon(\omega)$ between the actual data $S(\omega)$ and the approximating data $P(\omega)$ by,

$$\epsilon(\omega) = S(\omega) - P(\omega) = S(\omega) - \frac{N(\omega)}{D(\omega)} \quad (9.91)$$

and defining a cost function equal to,

$$J_1 = \sum_{i=1}^N (\epsilon(\omega_i))^2 \quad (9.92)$$

and to solve this problem for the unknown parameters K_1 , γ_1 , γ_2 and γ_3 for the smallest cost function J_1 , leads to a non-linear problem because of the non-linear parameters γ_1 and γ_2 . However, by introducing a new error function according to,

$$\varepsilon(\omega) = S(\omega) \cdot D(\omega) - N(\omega) \quad (9.93)$$

and a new cost function,

$$J = \sum_{i=1}^N (\varepsilon(\omega_i))^2 \quad (9.94)$$

this leads to a linear problem in all the unknown parameters K_1 , γ_1 , γ_2 and γ_3 ! A simple matrix inversion will provide these unknown parameters. Remember that, see also Chapter 8, the analytical power spectral density model,

$$P(\omega) = \frac{K_1 + \gamma_3 \omega^2}{(1 + \gamma_1 \omega^2)(1 + \gamma_2 \omega^2)}$$

can also be written in the form,

$$P(\omega) = K \frac{1 + \tau_3^2 \left(\frac{\omega L_g}{V}\right)^2}{\left(1 + \tau_1^2 \left(\frac{\omega L_g}{V}\right)^2\right) \left(1 + \tau_2^2 \left(\frac{\omega L_g}{V}\right)^2\right)} \quad (9.95)$$

with,

$$K = K_1 \quad (9.96)$$

$$\tau_1 = \sqrt{\gamma_1} \frac{V}{L_g} \quad (9.97)$$

$$\tau_2 = \sqrt{\gamma_2} \frac{V}{L_g} \quad (9.98)$$

$$\tau_3 = \sqrt{\frac{\gamma_3}{K_1}} \frac{V}{L_g} \quad (9.99)$$

This holds only if γ_1 , γ_2 and γ_3 are not negative.

A simple fit routine, based on the previous equations, was written for MAPLE. The listing is given in the following.

Listing 9.1: Fit routine

```
# Calculate the frequency response in e.g. MATLAB
# and fit this response using MAPLE for real data.
#
# This file calculates for the given data a filter which approximates
# the given frequency response data set.

V := 50;           # input airspeed
Lg := 150;         # input turbulence scale

#
#
# FIT ROUTINE
#
#
```

```

N := 50;                      # number of data points
w := array(1..N);             # initialize frequency array
H := array(1..N);             # initialize data array (data to be fitted)

read w;                      # read frequency points from file w
read h;                      # read data points from file h

nH := K1+gamma3*w[i]^2;        # numerator of model
dH := (1+gamma1*w[i]^2)*(1+gamma2*w[i]^2);    # denominator of model

e := H[i]*dH-nH;              # error function which results in a linear problem

J := sum( e^2 , i=1..N); # cost function

#
#
# partially differentiate J to each unknown parameter
#
#



eq1 := diff(J,K1);
eq2 := diff(J,gamma1);
eq3 := diff(J,gamma2);
eq4 := diff(J,gamma3);

#
#
# Solve for minimum in costfunction J
#
#



solution := solve({eq1=0,eq2=0,eq3=0,eq4=0},{K1,gamma1,gamma2,gamma3});

assign(solution);

K := K1;
tau1 := sqrt(gamma1)*V/Lg;
tau2 := sqrt(gamma2)*V/Lg;
tau3 := sqrt(gamma3/K1)*V/Lg;

```

Now that the unknown parameters of the power spectral density model are identified, a filter for the time domain can be calculated. The input for this filter is white noise with intensity equal to one. The output will be an equivalent turbulence velocity, or turbulence rate, of which the power spectral density is equal to the power spectral density model as in,

$$P(\omega) = K \frac{1 + \tau_3^2 \left(\frac{\omega L_g}{V} \right)^2}{\left(1 + \tau_1^2 \left(\frac{\omega L_g}{V} \right)^2 \right) \left(1 + \tau_2^2 \left(\frac{\omega L_g}{V} \right)^2 \right)}$$

See also Chapter 8.

9.6 Examples

9.6.1 Example 9.1

The calculation of the correlation functions and power spectral densities will be given in a sample MATLAB .m file. In this file, the correlation functions according to the equations given in Section 9.5 will be calculated. For the calculations in this chapter we have chosen the Dryden correlation functions f and g for economics in calculation time, the scale of turbulence L_g to equal 150 m and the standard deviations of all gust velocities to equal $\sigma = 1\text{m/s}$.

The program is self-explanatory. For the theory reference to the preceding sections is made.

Listing 9.2: Example 9.1

```
% Filename: examp91.m
%
%
% This program calculates the Correlation functions and Power Spectral
% Densities according to a 4 point model by Etkin, and using the Dryden
% correlation functions.

clc, clf, clear

% INPUT TURBULENCE PARAMETERS

Lg      = 150;
L       = Lg;
sigma   = 1;
sigma2  = sigma*sigma;
a       = 1.339;
b       = 0.85*14.63;    % in meters
lt      = 6;             % in meters
lf      = lt;
aL     = a*L;
bL     = b/L;
ltL    = lt/L;
lfL    = lf/L;
V      = 59.9;

i      = 0;
dtau   = 0.025;

for tau=-125:dtau:125,
    % Calculation of separation vectors xi:
```

```

i      = i+1
xi1(i) = abs(V*tau);
xi2(i) = sqrt((V*tau)^2 + (b/2)^2);
xi3(i) = sqrt((V*tau)^2 + b^2);
xi4(i) = abs(V*tau + lt);
xi5(i) = abs(V*tau - lt);
xi6(i) = abs(V*tau + lf);
xi7(i) = abs(V*tau - lf);
xi8(i) = sqrt((V*tau - lt)^2 + (b/2)^2);
xi9(i) = sqrt((V*tau - lf)^2 + (b/2)^2);

% Correlation functions f(xi) and g(xi) according to Dryden;
fd1(i) = exp(-xi1(i)/L);
gd1(i) = fd1(i)*(1-(xi1(i)/(2*L)));

fd2(i) = exp(-xi2(i)/L);
gd2(i) = fd2(i)*(1-(xi2(i)/(2*L)));

fd3(i) = exp(-xi3(i)/L);
gd3(i) = fd3(i)*(1-(xi3(i)/(2*L)));

fd4(i) = exp(-xi4(i)/L);
gd4(i) = fd4(i)*(1-(xi4(i)/(2*L)));

fd5(i) = exp(-xi5(i)/L);
gd5(i) = fd5(i)*(1-(xi5(i)/(2*L)));

fd6(i) = exp(-xi6(i)/L);
gd6(i) = fd6(i)*(1-(xi6(i)/(2*L)));

fd7(i) = exp(-xi7(i)/L);
gd7(i) = fd7(i)*(1-(xi7(i)/(2*L)));

fd8(i) = exp(-xi8(i)/L);
gd8(i) = fd8(i)*(1-(xi8(i)/(2*L)));

fd9(i) = exp(-xi9(i)/L);
gd9(i) = fd9(i)*(1-(xi9(i)/(2*L)));

Vtau = V*tau;

K1 = ((Vtau/L)^2) / ((Vtau/L)^2 + (b/L)^2);
K2 = ((Vtau/L)*(b/(2*L))) / ((Vtau/L)^2 + (b/(2*L))^2);
K3 = ((Vtau/L-lf/L)*(b/(2*L))) / (((Vtau/L)-lf/L)^2 + (b/(2*L))^2);

% Correlation functions of turbulence inputs according to Dryden
Ruud(i) = sigma2*fd1(i);
Rvvd(i) = sigma2*gd1(i);
Rwvd(i) = sigma2*((1/3)*gd1(i) + (4/9)*gd2(i) + (2/9)*gd3(i));
Rqqd(i) = (sigma2/lt^2)*(2*gd1(i) - gd4(i) - gd5(i));
Rppd(i) = (2*sigma2/b^2)*(gd1(i) - gd3(i));
Rr1r1d(i) = (2*sigma2/b^2)*(fd1(i) - K1*fd3(i) - (1-K1)*gd3(i));

```

```

Rr2r2d(i) = (sigma2/1f^2)*(2*gd1(i) - gd6(i) - gd7(i));
Rwqd(i)   = (sigma2/(3*1t))*(gd5(i) - gd1(i) + 2*gd8(i) - 2*gd2(i));
Rvr1d(i)  = (sigma2/b)*(2*K2*(gd2(i) - fd2(i)));
Rvr2d(i)  = (sigma2/1f)*(gd1(i) - gd7(i));
Rr1r2d(i) = (2*sigma2/(b*1f))*(K3*(gd9(i)-fd9(i))+K2*(fd2(i)-gd2(i)));

end

disp('I am ready with the calculation of the Correlation functions')

R1 = [Ruud(5002:10001) Ruud(1:4999)];
R2 = [Rvvd(5002:10001) Rvvd(1:4999)];
R3 = [Rwwd(5002:10001) Rwwd(1:4999)];
R4 = [Rppd(5002:10001) Rppd(1:4999)];
R5 = [Rqqd(5002:10001) Rqqd(1:4999)];
R6 = [Rr1r1d(5002:10001) Rr1r1d(1:4999)];
R7 = [Rr2r2d(5002:10001) Rr2r2d(1:4999)];
R8 = [Rwqd(5002:10001) Rwqd(1:4999)];
R9 = [Rvr1d(5002:10001) Rvr1d(1:4999)];
R10= [Rvr2d(5002:10001) Rvr2d(1:4999)];
R11= [Rr1r2d(5002:10001) Rr1r2d(1:4999)];

Suud    = fft(R1)*dtau;
Svvd    = fft(R2)*dtau;
Swwd    = fft(R3)*dtau;
Sppd    = fft(R4)*dtau;
Sqqd    = fft(R5)*dtau;
Sr1r1d  = fft(R6)*dtau;
Sr2r2d  = fft(R7)*dtau;
Swqd    = fft(R8)*dtau;
Svr1d   = fft(R9)*dtau;
Svr2d   = fft(R10)*dtau;
Sr1r2d  = fft(R11)*dtau;

save calc1150.mat

```

The results of this program are plotted in Figures 9.8 to 9.18 (correlation functions) and in Figures 9.19 to 9.29 (power spectral densities). Again, the chosen scale of turbulence equals $L_g = 150$ m. The correlation functions have been plotted in dimensional form, whereas the power spectral density functions have been plotted in non-dimensional form, e.g.,

$$S_{\alpha_g \alpha_g}(\omega) = \frac{1}{V^2} S_{w_g w_g}(\omega)$$

or,

$$S_{\frac{q_g \bar{c}}{V} \frac{q_g \bar{c}}{V}}(\omega) = \left(\frac{\bar{c}}{V}\right)^2 S_{q_g q_g}(\omega)$$

Etcetera.

9.6.2 Example 9.2

In this example, we will use the output of Example 9.1 for the calculation of the frequency response data of several variables for the Cessna Ce-500 'Citation'. In this example the symmetrical aircraft responses will be considered. The aircraft and turbulence data are equal to,

- Aircraft data:

V	=	59.9 m/s	m	=	4547.8 kg	\bar{c}	=	2.022 m
S	=	24.2 m ²	l_h	=	5.5 m	μ_c	=	102.7
K_Y^2	=	0.980	x_{cg}	=	0.30 \bar{c}			
C_{X_0}	=	0	C_{Z_0}	=	-1.1360			
C_{X_u}	=	-0.2199	C_{Z_u}	=	-2.2720	C_{m_u}	=	0
C_{X_α}	=	0.4653	C_{Z_α}	=	-5.1600	C_{m_α}	=	-0.4300
$C_{X_{\dot{\alpha}}}$	=	0	$C_{Z_{\dot{\alpha}}}$	=	-1.4300	$C_{m_{\dot{\alpha}}}$	=	-3.7000
C_{X_q}	=	0	C_{Z_q}	=	-3.8600	C_{m_q}	=	-7.0400
C_{X_δ}	=	0	C_{Z_δ}	=	-0.6238	C_{m_δ}	=	-1.5530

- Turbulence model:

$$\sigma_{u_g} = \sigma_{w_g} = 1 \text{ m/s} \quad L_g = 150 \text{ m}$$

Again, the program is self-explanatory. For the theory reference to the preceding sections is made.

Listing 9.3: Example 9.2

```
% Filename: examp92.m
%
%
% This program calculates the symmetrical aircraft response in the
% frequency domain for the Cessna Ce-500 Citation, using Etkin's
% 4 point model.

clc, clf, clear

% INPUT TURBULENCE- AND AIRCRAFT PARAMETERS

% AIRCRAFT FLIGHT CONDITION 'LANDING'.
V      = 59.9;
```

```

m      = 4547.8;
twmuc = 2*102.7;
KY2    = 0.980;
c      = 2.022;
S      = 24.2;
lh     = 5.5;
g      = 9.81;

% TURBULENCE PARAMETERS
sigmawg = 1;
Lg      = 150;
sigmaag = sigmawg/V;

% AIRCRAFT SYMMETRIC AERODYNAMIC DERIVATIVES :
CX0 = 0.0000;      CZ0  = -1.1360;      Cm0  = 0.0000;
CXu = -0.2199;     CZu  = -2.2720;     Cmu  = 0.0000;
CXa = 0.4653;      CZA   = -5.1600;     Cma  = -0.4300;
CXq = 0.0000;      CZq   = -3.8600;     Cmq  = -7.0400;
CXd = 0.0000;      CZd   = -0.6238;     Cmd  = -1.5530;
CXfa= 0.0000;     CZfa  = -1.4300;     Cmfa = -3.7000;
                  CZfug= 0.0000;     Cmfug= -Cm0*lh/c ;
                  CZfag= 0;        Cmfag= Cmfa-Cmq;

% CALCULATION OF AIRCRAFT SYMMETRIC STABILITY DERIVATIVES
xu   = (V/c)*(CXu/twmuc);
xa   = (V/c)*(CXa/twmuc);
xt   = (V/c)*(CZ0/twmuc);
xq   = 0;
xd   = (V/c)*(CXd/twmuc);
xug  = xu;
xfug = 0;
xag  = xa;
xflag = 0;
zu   = (V/c)*(CZu/(twmuc-CZfa));
za   = (V/c)*(CZa/(twmuc-CZfa));
zt   = (V/c)*(-CX0/(twmuc-CZfa));
zq   = (V/c)*((twmuc+CZq)/(twmuc-CZfa));
zd   = (V/c)*(CZd/(twmuc-CZfa));
zug  = zu;
zfug = (V/c)*(CZfug/(twmuc-CZfa));
zag  = za;
mu   = (V/c)*((Cmu+CZu*Cmfa/(twmuc-CZfa))/(twmuc*KY2));
ma   = (V/c)*((Cma+CZa*Cmfa/(twmuc-CZfa))/(twmuc*KY2));
mt   = (V/c)*((-CX0*Cmfa/(twmuc-CZfa))/(twmuc*KY2));
mq   = (V/c)*((Cmq+Cmfa*(twmuc+CZq)/(twmuc-CZfa))/(twmuc*KY2));
md   = (V/c)*((Cmd+CZd*Cmfa/(twmuc-CZfa))/(twmuc*KY2));
mug  = mu;
mfug = (V/c)*(Cmfug+CZfug*Cmfa/(twmuc-CZfa))/(twmuc*KY2);
mag  = ma;

xfa  = 0;
zfa  = (V/c)*(CZfa/(twmuc-CZfa));

```

```

mfa = (V/c)*((Cmfa+CZfa*Cmfa/(twmuc-CZfa))/(twmuc*KY2));

xqg = 0;
zqg = (V/c)*(CZq/(twmuc-CZfa));
mqg = (V/c)*((Cmq+Cmfa*CZq/(twmuc-CZfa))/(twmuc*KY2));

% STATE- AND INPUT MATRICES FOR 4 POINT MODEL

A=[xu xa xt 0
   zu za zt zq
   0 0 0 V/c
   mu ma mt mq ];

B=[xu xa -xqg xfa
   zu za -zqg zfa
   0 0 0 0
   mu ma -mqg mfa];

% SAVING RELEVANT DATA

save file1 A B sigmaawg sigmaag Lg V c g
clear

%-----%
% Load numerical data from saved mat files (see examp91.m).
%
%-----

load calcl150
save file2 Swqd Swwd Sqqd Suud dtau
clear

load file1
load file2

% define frequency vector
N = length(Suud);
w = 2*pi*(0:5000)/(dtau*10001);

% Auto and cross power spectral densities
Sugug = Suud(1:5001)/(V^2);
Sagqg = Swqd(1:5001)*(c/V^2);
Sagag = Swwd(1:5001)/(V^2);
Sqgqg = Sqqd(1:5001)*(c/V)^2;
Sfagfag = Sagag.* (w.^2);

% Output matrices
Cu = [1 0 0 0];
Ca = [0 1 0 0];
Ct = [0 0 1 0];
Cq = [0 0 0 1];

```

```

D = [0 0 0 0];

w=w(:);
%-----
%
% Response to ug put variable ug equal to 1 else to 0
%
%-----

ug = input(' Response to horizontal turbulence enter 1, else 0 : ');

if ug == 1,      % RESPONSE TO HORIZONTAL TURBULENCE

Sugug = Sugug';

% u
sys = ss(A,B(:,1),Cu,D(:,1));           % response u to ug
Htemp = squeeze(freqresp(sys,w));
Suu = Htemp.*conj(Htemp).*Sugug;

% alpha
sys = ss(A,B(:,1),Ca,D(:,1));           % response alpha to ug
Htemp = squeeze(freqresp(sys,w));
Saa = Htemp.*conj(Htemp).*Sugug;

% theta
sys = ss(A,B(:,1),Ct,D(:,1));           % response theta to ug
Htemp = squeeze(freqresp(sys,w));
Stt = Htemp.*conj(Htemp).*Sugug;

% qc/V
sys = ss(A,B(:,1),Cq,D(:,1));           % response qc/V to ug
Htemp = squeeze(freqresp(sys,w));
Sqq = Htemp.*conj(Htemp).*Sugug;

save 1150 Suu Saa Stt Sqq w Sagag Sqgqg Sfagfag Sagqg Sugug
clear, load 1150

% Plot the results
loglog(w,Suu); xlabel('Omega [rad/s]'); ylabel('Suu');
title('Response of u/V (to u_g)');
pause

loglog(w,Saa); xlabel('Omega [rad/s]'); ylabel('Saa');
title('Response of alpha (to u_g)');
pause

loglog(w,Stt); xlabel('Omega [rad/s]'); ylabel('Stt');
title('Response of theta (to u_g)');
pause

loglog(w,Sqq); xlabel('Omega [rad/s]'); ylabel('Sqq');

```

```

title('Response of qc/V (to u_g)');
pause

else % RESPONSE TO VERTICAL TURBULENCE

% Note here: put Ca for alpha, Ct for theta, Cq for q response,
% now only response of u is calculated
sys = ss(A,B(:,2),Cu,D(:,2)); % response u to alpha_g
Htemp1 = squeeze(freqresp(sys,w));

sys = ss(A,B(:,3),Cu,D(:,3)); % response u to q_g c/V
Htemp2 = squeeze(freqresp(sys,w));

sys = ss(A,B(:,4),Cu,D(:,4)); % response u to d alpha_g /d t
Htemp3 = squeeze(freqresp(sys,w));

% response of variable to alpha_g, which is correlated to
% d alpha_g/d t and q_g c/V
S1 = (Htemp1.*conj(Htemp2)).*Sagqg';
S2 = (Htemp1.*conj(Htemp3)).*(( -j*w)*(c/V).*conj(Sagag).');
S3 = (Htemp2.*conj(Htemp1)).*conj(Sagqg');
S4 = (Htemp2.*conj(Htemp3)).*(( -j*w)*(c/V).*conj(Sagqg'));
S5 = (Htemp3.*conj(Htemp1)).*(( j*w)*(c/V).*Sagag');
S6 = (Htemp3.*conj(Htemp2)).*(( j*w)*(c/V).*Sagqg');
S7 = Htemp1.*conj(Htemp1).*Sagag';
S8 = Htemp2.*conj(Htemp2).*Sqgqg';
S9 = Htemp3.*conj(Htemp3).*Sfagfag' .* (c/V)^2;

clear Htemp1 Htemp2 Htemp3

Suu = S1+S2+S3+S4+S5+S6+S7+S8+S9;

% Plot the result
loglog(w,Suu); xlabel('Omega [rad/s]'); ylabel('Suu');
title('Response of u/V (to alpha_g)');
pause

%loglog(w,Saa); xlabel('Omega [rad/s]'); ylabel('Saa');
%title('Response of alpha (to alpha_g)');
%pause
%loglog(w,Stt); xlabel('Omega [rad/s]'); ylabel('Stt');
%title('Response of theta (to alpha_g)');
%pause
%loglog(w,Sqq); xlabel('Omega [rad/s]'); ylabel('Sqq');
%title('Response of qc/V (to alpha_g)');
%pause

end

```

The results of this program are plotted in Figures 9.30 to 9.37. In these figures, the DUT results are plotted as well.

9.6.3 Example 9.3

In this example, again we will use the output of Example 9.1 for the calculation of the frequency response data of several variables for the Cessna Ce-500 Citation. In this example the asymmetrical aircraft responses will be considered. The aircraft and turbulence data are equal to,

- Aircraft data:

V	=	59.9 m/s	μ_b	=	15.5
S	=	24.2 m ²	K_X^2	=	0.012
b	=	13.36 m	K_Z^2	=	0.037
C_L	=	1.1360	K_{XZ}	=	0.002
C_{Y_β}	=	-0.9896	C_{l_β}	=	-0.0772
C_{Y_p}	=	-0.0870	C_{l_p}	=	-0.3444
C_{Y_r}	=	0.4300	C_{l_r}	=	0.2800
$C_{Y_{\delta_a}}$	=	0	$C_{l_{\delta_a}}$	=	-0.2349
$C_{Y_{\delta_r}}$	=	0.3037	$C_{l_{\delta_r}}$	=	0.0286
					$C_{n_\beta} = 0.1638$
					$C_{n_p} = -0.0108$
					$C_{n_r} = -0.1930$
					$C_{n_{\delta_a}} = 0.0286$
					$C_{n_{\delta_r}} = -0.1261$

- Turbulence model:

$$\sigma_{u_g} = \sigma_{v_g} = \sigma_{w_g} = 1 \text{ m/s} \quad L_g = 150 \text{ m} \quad B \approx 0.045$$

The program examp93.m is self-explanatory. For the theory reference to the preceding sections is made.

Listing 9.4: Example 9.3

```
% Filename: examp93.m
%
% This program calculates the asymmetrical aircraft response in the
% frequency domain for the Cessna Ce-500 Citation, using Etkin's
% 4 point model.

clc, clf, clear

% INPUT TURBULENCE- AND AIRCRAFT PARAMETERS

% AIRCRAFT FLIGHT CONDITION 'LANDING'.
V = 59.9;
S = 24.2;
b = 13.36;
```

```

mub = 15.5;
KX2 = 0.012;
KZ2 = 0.037;
KXZ = 0.002;
CL = 1.1360;

% TURBULENCE PARAMETERS APPROXIMATED POWER SPECTRAL DENSITIES
Lg = 150;
B = b/(2*Lg);
sigmaug = 1;
sigmavg = 1;
sigmawg = 1;

sigmaug = sigmaug/V;
sigmabg = sigmavg/V;
sigmaag = sigmawg/V;

Iug0 = 0.0249*sigmaug^2;
Iag0 = 0.0182*sigmaag^2;
tau1 = 0.0991; tau2 = 0.5545; tau3 = 0.4159;
tau4 = 0.0600; tau5 = 0.3294; tau6 = 0.2243;

% AIRCRAFT ASYMMETRIC AERODYNAMIC DERIVATIVES : Cessna Ce-500 Citation
CYb = -0.9896; Clb = -0.0772; Cnb = 0.1638;
CYp = -0.0870; Clp = -0.3444; Cnp = -0.0108;
CYr = 0.4300; Clr = 0.2800; Cnr = -0.1930;
CYda = 0.0000; Clda = -0.2349; Cnda = 0.0286;
CYdr = 0.3037; Cldr = 0.0286; Cndr = -0.1261;

Clpw = 0.8*Clp; Cnpw = 0.9*Cnp;
Clrw = 0.7*Clr; Cnrw = 0.2*Cnr;

CYfb = 0;
Clfb = 0;
Cnfb = 0;

% CYfbg = CYfb+0.5*CYr;
% CLfbg = Clfb+0.5*CLR;
% CNfbg = Cnfb+0.5*CNr;

% CALCULATION OF AIRCRAFT ASYMMETRIC STABILITY DERIVATIVES
yb = (V/b)*CYb/(2*mub);
yphi = (V/b)*CL/(2*mub);
yp = (V/b)*CYp/(2*mub);
yr = (V/b)*(CYr-4*mub)/(2*mub);
ybg = yb;
ydr = (V/b)*CYdr/(2*mub);
den = b*4*mub*(KX2*KZ2-KXZ^2)/V;
lb = (Clb*KZ2+Cnb*KXZ)/den;
lp = (Clp*KZ2+Cnp*KXZ)/den;
lr = (Clr*KZ2+Cnr*KXZ)/den;
lda = (Clda*KZ2+Cnda*KXZ)/den;
ldr = (Cldr*KZ2+Cndr*KXZ)/den;

```

```

lug = (-Clrw*KZ2-Cnrw*KXZ)/den ;
lbg = 1b ;
lag = (Clpw*KZ2+Cnpw*KXZ)/den ;
nb = (C1b*KXZ+Cnb*KX2)/den ;
np = (Clp*KXZ+Cnp*KX2)/den ;
nr = (Clr*KXZ+Cnr*KX2)/den ;
nda = (C1da*KXZ+Cnda*KX2)/den ;
ndr = (C1dr*KXZ+Cndr*KX2)/den ;
nug = (-Clrw*KXZ-Cnrw*KX2)/den ;
nbg = nb ;
nag = (Clpw*KXZ+Cnpw*KX2)/den ;
aug1 ==-(V/Lg)^2*(1/(tau1*tau2));
aug2 ==-(tau1+tau2)*(V/Lg)/(tau1*tau2);
aag1 ==-(V/Lg)^2*(1/(tau4*tau5));
aag2 ==-(tau4+tau5)*(V/Lg)/(tau4*tau5);
abg1 ==-(V/Lg)^2;
abg2 ==-2*(V/Lg);
bug1 = tau3*sqrt(Iug0*V/Lg)/(tau1*tau2);
bug2 = (1-tau3*(tau1+tau2)/(tau1*tau2))*sqrt(Iug0*(V/Lg)^3)/(tau1*tau2);
bag1 = tau6*sqrt(Iag0*V/Lg)/(tau4*tau5);
bag2 = (1-tau6*(tau4+tau5)/(tau4*tau5))*sqrt(Iag0*(V/Lg)^3)/(tau4*tau5);
bbg1 = sigmabg*sqrt(3*V/Lg);
bbg2 = (1-2*sqrt(3))*sigmabg*sqrt((V/Lg)^3);

ypg = 0;
lpg = (Clpw*KZ2+Cnpw*KXZ)/den ;
npg = (Clpw*KXZ+Cnpw*KX2)/den ;

yr1 = 0;
lr1 = (-Clrw*KZ2-Cnrw*KXZ)/den ;
nr1 = (-Clrw*KXZ-Cnrw*KX2)/den ;

yr2 = (V/b)*CYr/(2*mub);
lr2 = (Clr*KZ2+Cnr*KXZ)/den ;
nr2 = (Clr*KXZ+Cnr*KX2)/den ;

yfb = (V/b)*CYfb/(2*mub);
lfb = (Clfb*KZ2+Cnfb*KXZ)/den ;
nfb = (Clfb*KXZ+Cnfb*KX2)/den ;

% STATE- AND INPUT MATRICES
A = [yb yphi yp yr
      0 0 2*V/b 0
      lb 0 lp lr
      nb 0 np nr ];
B = [yb ypg yr1 yr2 yfb
      0 0 0 0 0
      lb lpg lr1 lr2 lfb
      nb npg nr1 nr2 nfb ];
% SAVING RELEVANT DATA

```

```

save file3 A B b V
clear

% Load numerical data from saved mat files (see examp91.m).
load calcl150
save file4 Sppd Sr1r1d Sr2r2d Sr1r2d Svr1d Svr2d Svvd dtau
clear

load file3
load file4

% Auto and cross power spectral densities
w = 2*pi*(0:5000)/(dtau*10001);
Spgpg = Sppd(1:5001)*( (b/(2*V))^2 );
Sr1gr1g = Sr1r1d(1:5001)*( (b/(2*V))^2 );
Sr2gr2g = Sr2r2d(1:5001)*( (b/(2*V))^2 );
Sbgbg = Svvd(1:5001)/(V^2);
Sbgr1g = Svr1d(1:5001)*( b/(2*(V^2)));
Sbgr2g = Svr2d(1:5001)*( b/(2*(V^2)));
Sr1gr2g = Sr1r2d(1:5001)*( (b/(2*V))^2 );
Sfbgfbg = Sbgbg.* (w.^2);

Spgpg = Spgpg';
Sr1gr1g = Sr1gr1g';
Sr2gr2g = Sr2gr2g';
Sbgbg = Sbgbg';
Sbgr1g = Sbgr1g';
Sbgr2g = Sbgr2g';
Sr1gr2g = Sr1gr2g';
Sfbgfbg = Sfbgfbg';

% Define C and D matrices
Cb = [1 0 0 0];      % beta
Cphi = [0 1 0 0];    % phi
Cp = [0 0 1 0];      % p
Cr = [0 0 0 1];      % r

D = [0 0 0 0 0];

% Compute response to the different turbulence inputs
disp(' Response to r1g (ug) enter 1, pg (wg) enter 2, ');
disp(' vg (etkin) (bg) enter 3 ');
disp(' or vg (dut) enter 4. ');
disp(' ');
ug = input(' Response to turbulence (1, 2, 3 or 4) : ');

om = w';

if ug == 1      % Response to r1g (ug in DUT model)

    % compute responses
    sys = ss(A,B(:,3),Cb,D(:,3));

```

```

Htemp = squeeze(freqresp(sys,om));
Sbb   = Htemp.*conj(Htemp).*Sr1gr1g;

sys   = ss(A,B(:,3),Cphi,D(:,3));
Htemp = squeeze(freqresp(sys,om));
Sphi  = Htemp.*conj(Htemp).*Sr1gr1g;

sys   = ss(A,B(:,3),Cp,D(:,3));
Htemp = squeeze(freqresp(sys,om));
Spp   = Htemp.*conj(Htemp).*Sr1gr1g;

sys   = ss(A,B(:,3),Cr,D(:,3));
Htemp = squeeze(freqresp(sys,om));
Srr   = Htemp.*conj(Htemp).*Sr1gr1g;

% plot results
loglog(om,Sbb); xlabel('Omega [rad/s]'); ylabel('Sbb');
title('Response of beta (to u_g)');
pause
loglog(om,Sphi); xlabel('Omega [rad/s]'); ylabel('Sphi');
title('Response of phi (to u_g)');
pause
loglog(om,Spp); xlabel('Omega [rad/s]'); ylabel('Spp');
title('Response of pb/2V (to u_g)');
pause
loglog(om,Srr); xlabel('Omega [rad/s]'); ylabel('Srr');
title('Response of rb/2V (to u_g)');
pause

elseif ug == 2      % Response to pg (alpha_g in DUT model)

% compute responses
sys   = ss(A,B(:,2),Cb,D(:,2));
Htemp = squeeze(freqresp(sys,om));
Sbb   = Htemp.*conj(Htemp).*Spgpg;

sys   = ss(A,B(:,2),Cphi,D(:,2));
Htemp = squeeze(freqresp(sys,om));
Sphi  = Htemp.*conj(Htemp).*Spgpg;

sys   = ss(A,B(:,2),Cp,D(:,2));
Htemp = squeeze(freqresp(sys,om));
Spp   = Htemp.*conj(Htemp).*Spgpg;

sys   = ss(A,B(:,2),Cr,D(:,2));
Htemp = squeeze(freqresp(sys,om));
Srr   = Htemp.*conj(Htemp).*Spgpg;

% plot results
loglog(om,Sbb); xlabel('Omega [rad/s]'); ylabel('Sbb');
title('Response of beta (to p_g)');
pause

```

```

loglog(om,Sphi); xlabel('Omega [rad/s]'); ylabel('Sphi');
title('Response of phi (to p_g)');
pause
loglog(om,Spp); xlabel('Omega [rad/s]'); ylabel('Spp');
title('Response of pb/2V (to p_g)');
pause
loglog(om,Srr); xlabel('Omega [rad/s]'); ylabel('Srr');
title('Response of rb/2V (to p_g)');
pause

elseif ug == 3      % Response to vg (beta_g in DUT model)

    % Note, beta_g is correlated to d beta_g/d t (Etkin 4 Point
    %       Model versus DUT model), (r1_g b)/(2V) and (r2_g b)/(2V).
    %
    % Put in for matrix C: Cb for beta; Cphi for phi;
    % Cp for (pb)/(2V) and Cr for (rb)/(2V). The D matrix is equal for
    % all outputs.
    %
    % Here only for beta.

    % compute responses
sys = ss(A,B(:,1),Cb,D(:,1));
Htemp1 = squeeze(freqresp(sys,om));
sys = ss(A,B(:,5),Cb,D(:,5));
Htemp2 = squeeze(freqresp(sys,om));
sys = ss(A,B(:,3),Cb,D(:,3));
Htemp3 = squeeze(freqresp(sys,om));
sys = ss(A,B(:,4),Cb,D(:,4));
Htemp4 = squeeze(freqresp(sys,om));

S1 = (Htemp1.*conj(Htemp2)).*(((-j*om)*(b/V)).*Sbgbg);
S2 = (Htemp1.*conj(Htemp3)).*Sbgr1g;
S3 = (Htemp1.*conj(Htemp4)).*Sbgr2g;
S4 = (Htemp2.*conj(Htemp1)).*((j*om)*(b/V).*conj(Sbgbg));
S5 = (Htemp2.*conj(Htemp3)).*((j*om)*(b/V).*Sbgr1g);
S6 = (Htemp2.*conj(Htemp4)).*((j*om)*(b/V).*Sbgr2g);
S7 = (Htemp3.*conj(Htemp1)).*conj(Sbgr1g);
S8 = (Htemp3.*conj(Htemp2)).*(((-j*om)*(b/V)).*conj(Sbgr1g));
S9 = (Htemp3.*conj(Htemp4)).*Sr1gr2g;
S10 = (Htemp4.*conj(Htemp1)).*conj(Sbgr2g);
S11 = (Htemp4.*conj(Htemp2)).*(((-j*om)*(b/V)).*conj(Sbgr2g));
S12 = (Htemp4.*conj(Htemp3)).*conj(Sr1gr2g);
S13 = (Htemp1.*conj(Htemp1)).*Sbgbg;
S14 = (Htemp2.*conj(Htemp2)).*((b/V)^2)*Sfbgfbg;
S15 = (Htemp3.*conj(Htemp3)).*Sr1gr1g;
S16 = (Htemp4.*conj(Htemp4)).*Sr2gr2g;

Sbb = S1+S2+S3+S4+S5+S6+S7+S8+S9+S10+S11+S12+S13+S14+S15+S16;

% plot results
loglog(om,Sbb); xlabel('Omega [rad/s]'); ylabel('Sbb');

```

```

title('Response of beta (to beta_g)');
pause
%loglog(om,Sphi); xlabel('Omega [rad/s]'); ylabel('Sphi');
%title('Response of phi (to beta_g)');
%pause
%loglog(om,Spp); xlabel('Omega [rad/s]'); ylabel('Spp');
%title('Response of pb/2V (to beta_g)');
%pause
%loglog(om,Srr); xlabel('Omega [rad/s]'); ylabel('Srr');
%title('Response of rb/2V (to beta_g)');
%pause

elseif ug == 4      % Response to vg (DUT model)

    % Put in for matrix C: Cb for beta; Cphi for phi; Cp for (pb)/(2V)
    % and Cr for (rb)/(2V)
    %
    % Here only for beta.

    sys = ss(A,B(:,1),Cb,D(:,1));
    Htemp1 = squeeze(freqresp(sys,om));
    sys = ss(A,B(:,5),Cb,D(:,5));
    Htemp2 = squeeze(freqresp(sys,om));
    sys = ss(A,B(:,4),Cb,D(:,4));
    Htemp3 = squeeze(freqresp(sys,om));

    S1 = (Htemp1.*conj(Htemp2)).*(((-j*om)*(b/V)).*Sbgbg);
    S2 = (Htemp1.*conj(Htemp3)).*Sbgr2g;
    S3 = (Htemp2.*conj(Htemp1)).*((j*om)*(b/V).*Sbgbg);
    S4 = (Htemp2.*conj(Htemp3)).*((j*om)*(b/V).*Sbgr2g);
    S5 = (Htemp3.*conj(Htemp1)).*conj(Sbgr2g);
    S6 = (Htemp3.*conj(Htemp2)).*(((-j*om)*(b/V)).*conj(Sbgr2g));
    S7 = (Htemp1.*conj(Htemp1)).*Sbgbg;
    S8 = (Htemp2.*conj(Htemp2)).*((b/V)^2)*Sfbgfbg;
    S9 = (Htemp3.*conj(Htemp3)).*Sr2gr2g;

    Sbb = S1+S2+S3+S4+S5+S6+S7+S8+S9;

    % plot results
    loglog(om,Sbb); xlabel('Omega [rad/s]'); ylabel('Sbb');
    title('Response of beta (to beta_g, DUT)');
    pause
    %loglog(om,Sphi); xlabel('Omega [rad/s]'); ylabel('Sphi');
    %title('Response of phi (to beta_g, DUT)');
    %pause
    %loglog(om,Spp); xlabel('Omega [rad/s]'); ylabel('Spp');
    %title('Response of pb/2V (to beta_g, DUT)');
    %pause
    %loglog(om,Srr); xlabel('Omega [rad/s]'); ylabel('Srr');
    %title('Response of rb/2V (to beta_g, DUT)');
    %pause

```

```
end
```

The results of this program are plotted in Figures 9.38 to 9.49. In these figures, the DUT results are plotted as well.

9.7 Summary

In this chapter Etkin's four point model was described. The correlation functions were calculated first, using four characteristic points distributed over the aircraft's fuselage, while afterwards the power spectral densities of the turbulence inputs were calculated numerically using MATLAB's Fast Fourier Transform routine `fft`. As compared to the DUT's aircraft models, Etkin's four point model is in fact the same, except for the asymmetrical aircraft responses to u_g and w_g , which are the most difficult to model.

	X	Z	M
$\dot{\alpha}$	$\frac{V}{\bar{c}} \frac{C_{X_{\dot{\alpha}}}}{2\mu_c}$	$\frac{V}{\bar{c}} \frac{C_{Z_{\dot{\alpha}}}}{2\mu_c - C_{Z_{\dot{\alpha}}}}$	$\frac{V}{\bar{c}} \frac{C_{m_{\dot{\alpha}}} + C_{Z_{\dot{\alpha}}} \frac{C_{m_{\dot{\alpha}}}}{2\mu_c - C_{Z_{\dot{\alpha}}}}}{2\mu_c K_Y^2}$
q_g	$\frac{V}{\bar{c}} \frac{C_{X_q}}{2\mu_c}$	$\frac{V}{\bar{c}} \frac{C_{Z_q}}{2\mu_c - C_{Z_{\dot{\alpha}}}}$	$\frac{V}{\bar{c}} \frac{C_{m_q} + C_{Z_q} \frac{C_{m_{\dot{\alpha}}}}{2\mu_c - C_{Z_{\dot{\alpha}}}}}{2\mu_c K_Y^2}$

Table 9.1: Additional symbols appearing in the general state-space representation for Etkin's Four Point Aircraft model. Symmetric aircraft models.

	Y	L	N
$\dot{\beta}$	$\frac{V}{b} \frac{C_{Y_{\dot{\beta}}}}{2\mu_b}$	$\frac{V}{b} \frac{C_{l_{\dot{\beta}}} K_Z^2 + C_{n_{\dot{\beta}}} K_{XZ}}{4\mu_b(K_X^2 K_Z^2 - K_{XZ}^2)}$	$\frac{V}{b} \frac{C_{l_{\dot{\beta}}} K_{XZ} + C_{n_{\dot{\beta}}} K_X^2}{4\mu_b(K_X^2 K_Z^2 - K_{XZ}^2)}$
r_w	$-\frac{V}{b} \frac{C_{Y_{rw}}}{2\mu_b}$	$-\frac{V}{b} \frac{C_{l_{rw}} K_Z^2 + C_{n_{rw}} K_{XZ}}{4\mu_b(K_X^2 K_Z^2 - K_{XZ}^2)}$	$-\frac{V}{b} \frac{C_{l_{rw}} K_{XZ} + C_{n_{rw}} K_X^2}{4\mu_b(K_X^2 K_Z^2 - K_{XZ}^2)}$
r_v	$\frac{V}{b} \frac{C_{Y_{rv}}}{2\mu_b}$	$\frac{V}{b} \frac{C_{l_{rv}} K_Z^2 + C_{n_{rv}} K_{XZ}}{4\mu_b(K_X^2 K_Z^2 - K_{XZ}^2)}$	$\frac{V}{b} \frac{C_{l_{rv}} K_{XZ} + C_{n_{rv}} K_X^2}{4\mu_b(K_X^2 K_Z^2 - K_{XZ}^2)}$

Table 9.2: Additional symbols appearing in the general state-space representation for Etkin's Four Point Aircraft model. Asymmetric aircraft models.

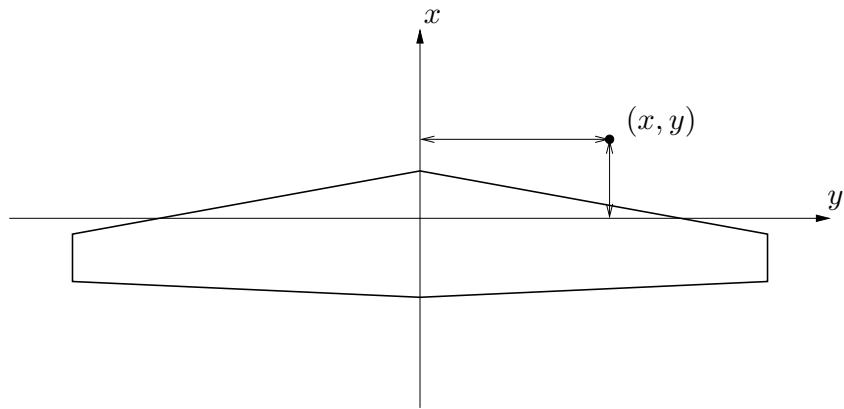


Figure 9.1: The downwash at point (x, y) of a planar aircraft.

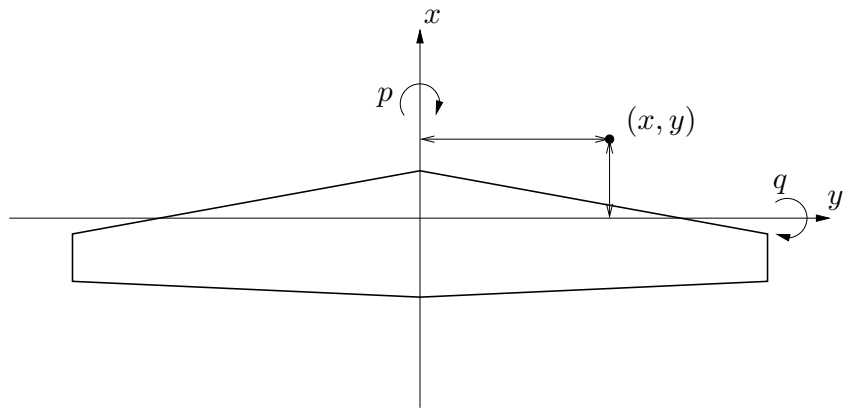


Figure 9.2: The downwash at point (x, y) of a planar aircraft due to rolling and yawing.

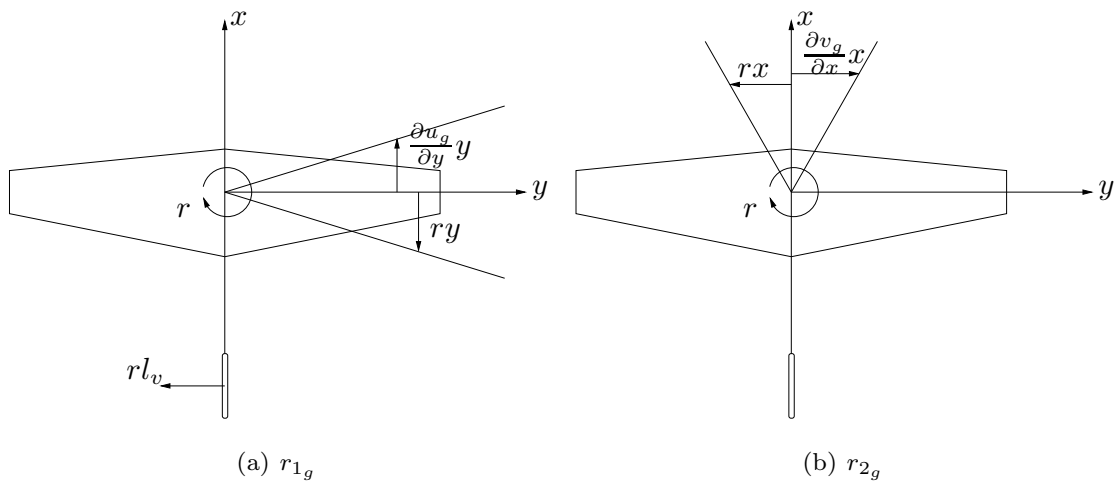


Figure 9.3: The turbulence inputs r_{1g} and r_{2g} .

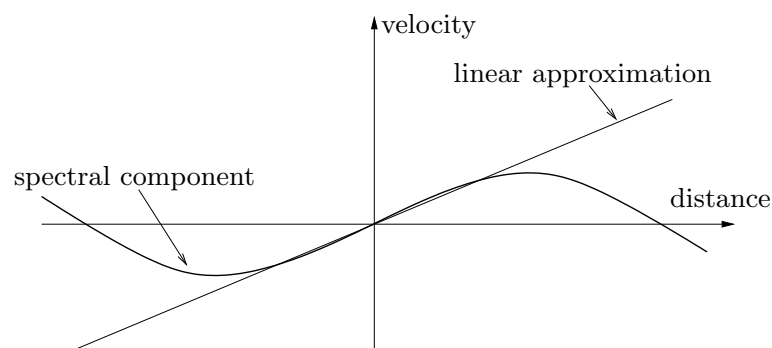


Figure 9.4: Linearization of the gust fields.

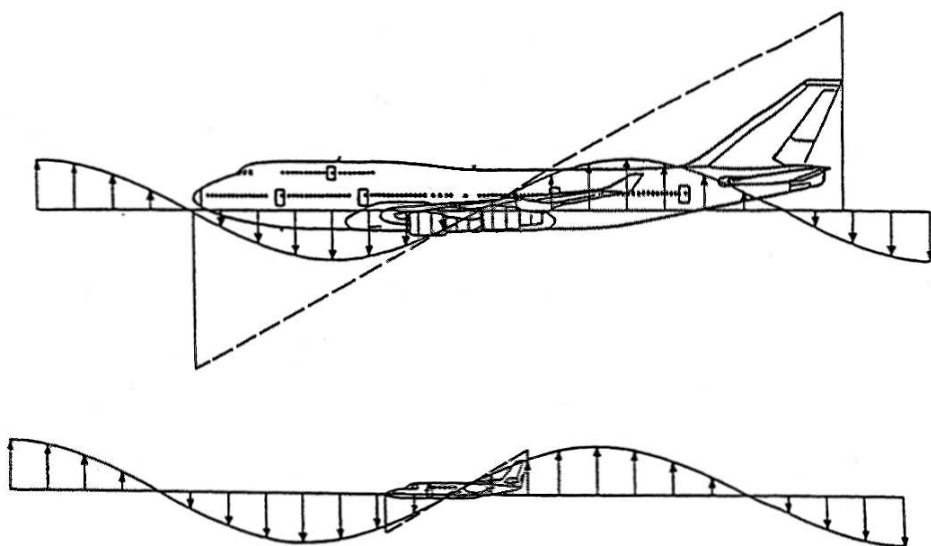


Figure 9.5: The influence of the dimensions of aircraft on the gust field linearization (747 and Cessna 'Citation II').

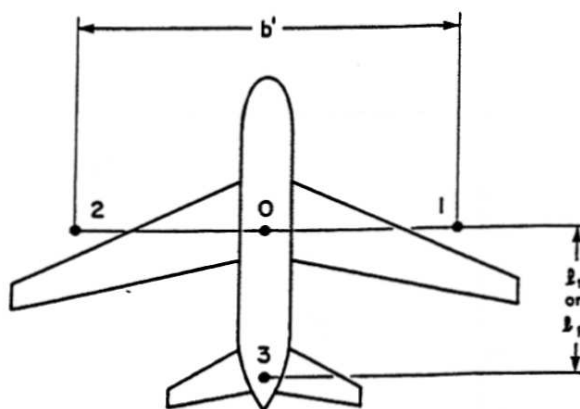


Figure 9.6: The "four point" aircraft model.

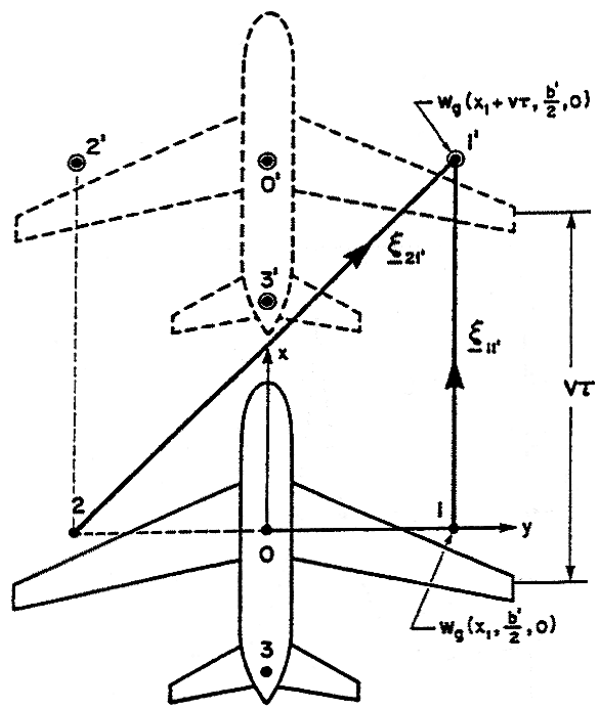


Figure 9.7: The “four point” model and separation vectors ξ .

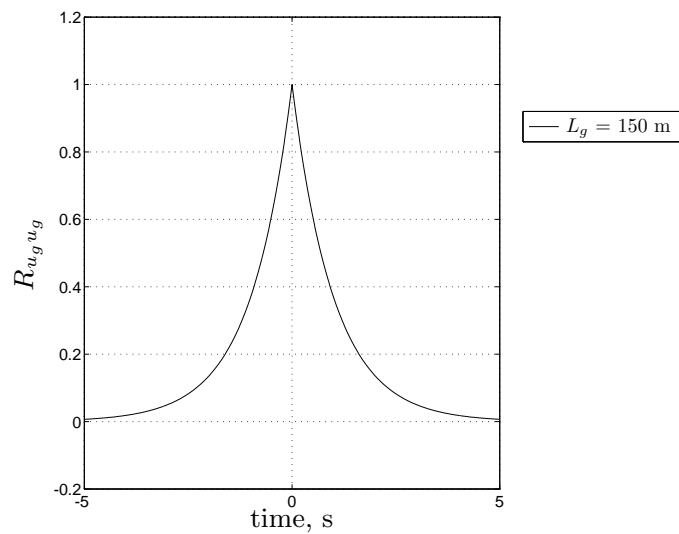


Figure 9.8: Dimensional autocorrelation function $R_{u_g u_g}$ for Etkin’s “four point” model.

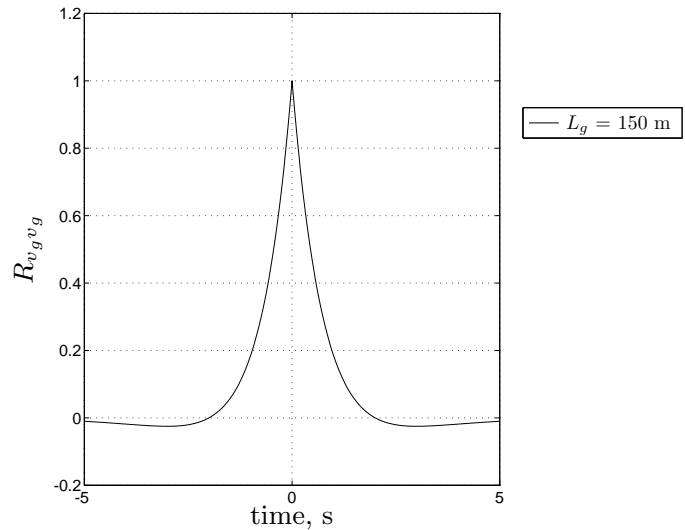


Figure 9.9: Dimensional autocorrelation function $R_{v_g v_g}$ for Etkin's "four point" model.

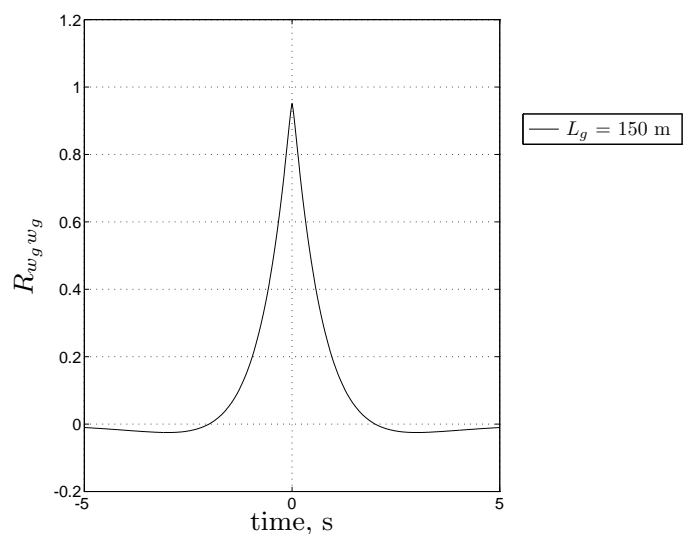


Figure 9.10: Dimensional autocorrelation function $R_{w_g w_g}$ for Etkin's "four point" model.

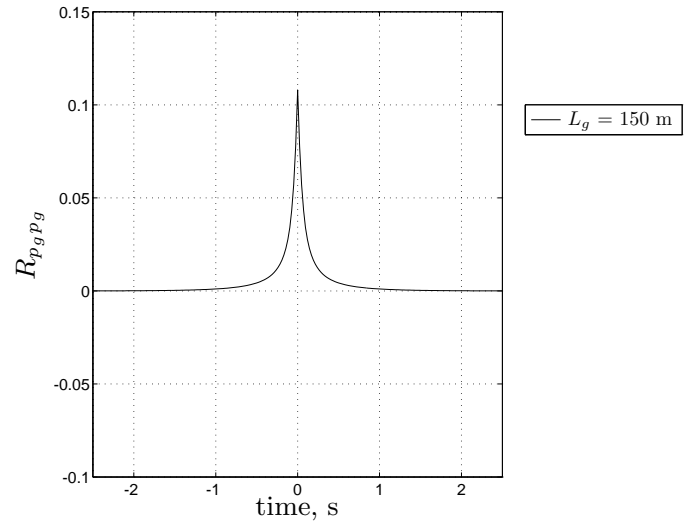


Figure 9.11: Dimensional autocorrelation function $R_{p_g p_g}$ for Etkin's "four point" model.

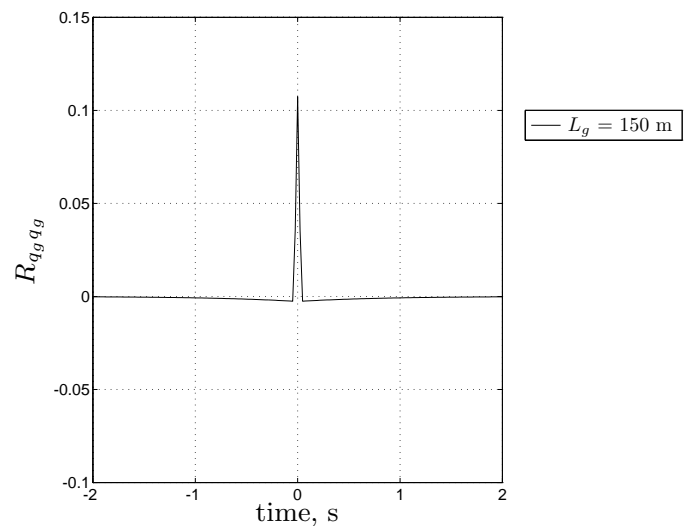


Figure 9.12: Dimensional autocorrelation function $R_{q_g q_g}$ for Etkin's "four point" model.

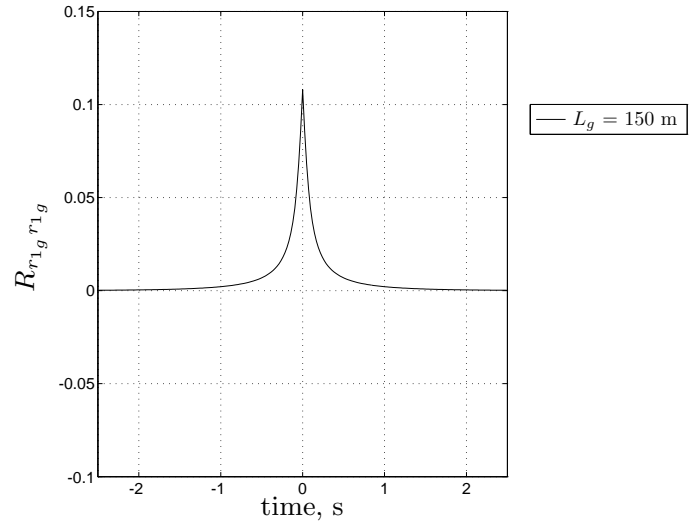


Figure 9.13: Dimensional autocorrelation function $R_{r1_g r1_g}$ for Etkin's "four point" model.

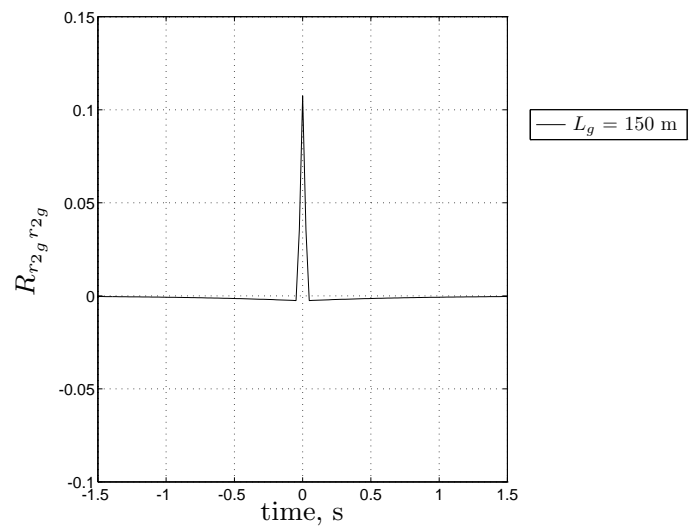


Figure 9.14: Dimensional autocorrelation function $R_{r2_g r2_g}$ for Etkin's "four point" model.

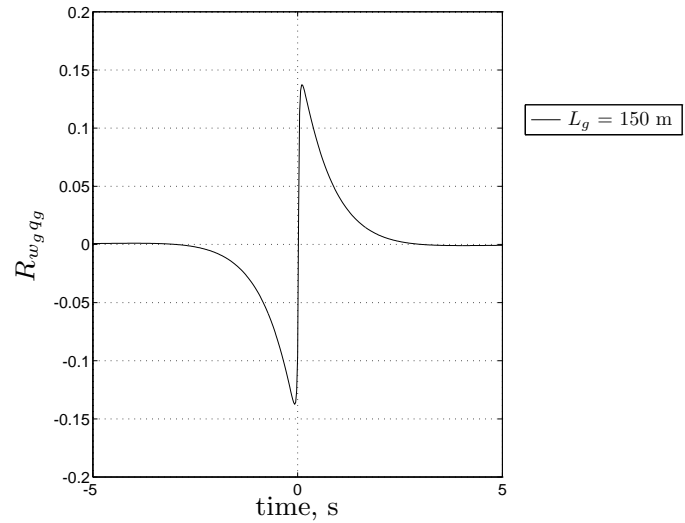


Figure 9.15: Dimensional crosscorrelation function $R_{w_g q_g}$ for Etkin's “four point” model.

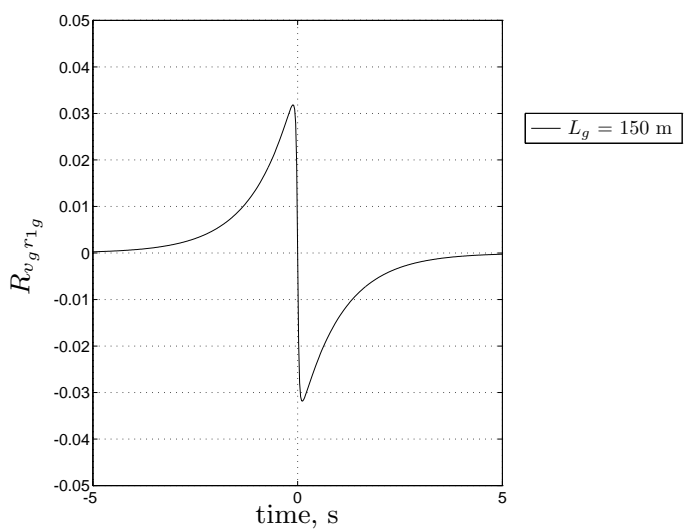


Figure 9.16: Dimensional crosscorrelation function $R_{v_g r_{1g}}$ for Etkin's “four point” model.

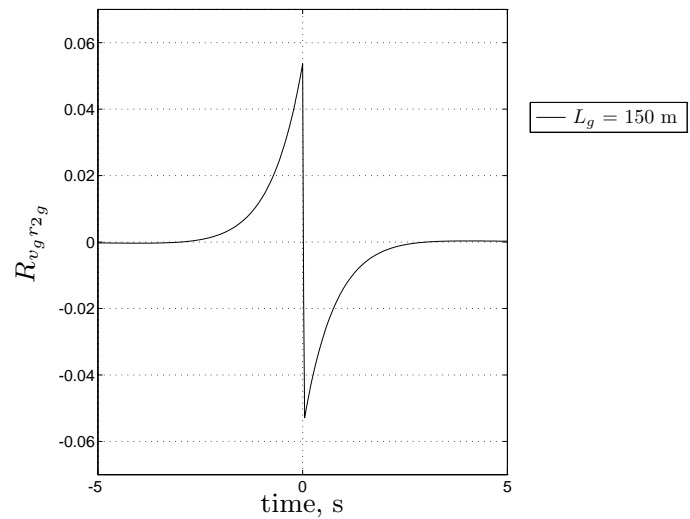


Figure 9.17: Dimensional crosscorrelation function $R_{v_g r_2 g}$ for Etkin's "four point" model.

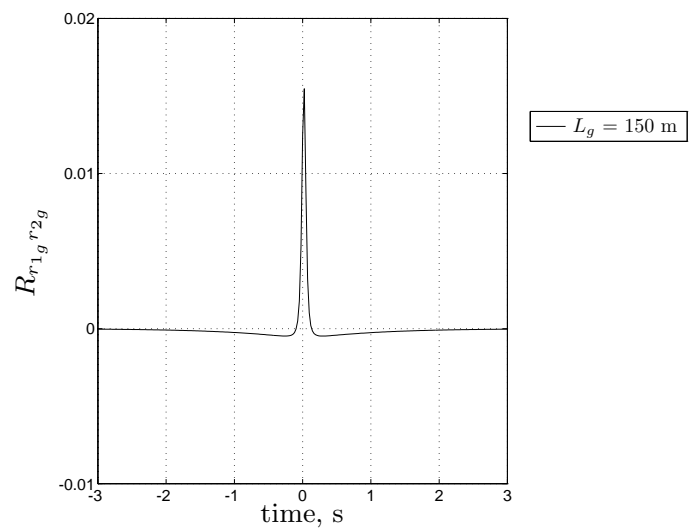


Figure 9.18: Dimensional crosscorrelation function $R_{r_1 g r_2 g}$ for Etkin's "four point" model.

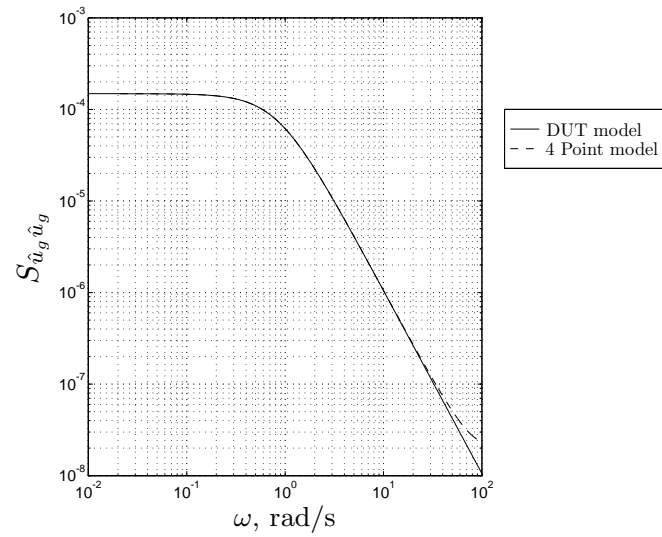


Figure 9.19: Auto power spectral density function $S_{\hat{u}_g \hat{u}_g}$ for Etkin's "four point" model ($L_g = 150$ m).

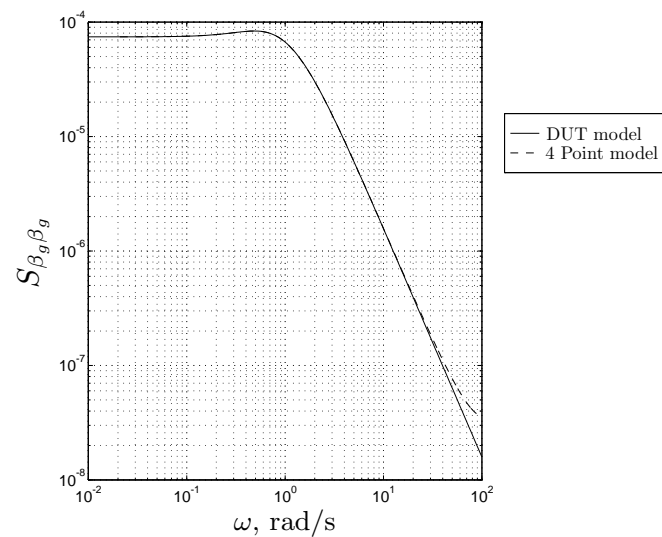


Figure 9.20: Auto power spectral density function $S_{\beta_g \beta_g}$ for Etkin's "four point" model ($L_g = 150$ m).

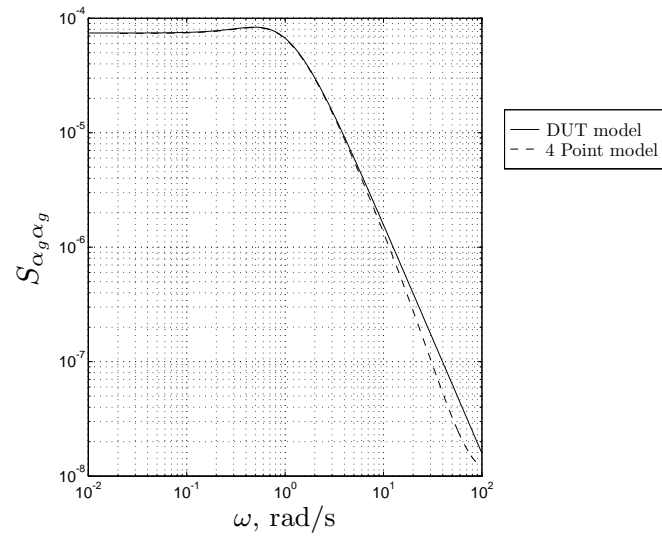


Figure 9.21: Auto power spectral density function $S_{\alpha_g \alpha_g}$ for Etkin's "four point" model ($L_g = 150$ m).

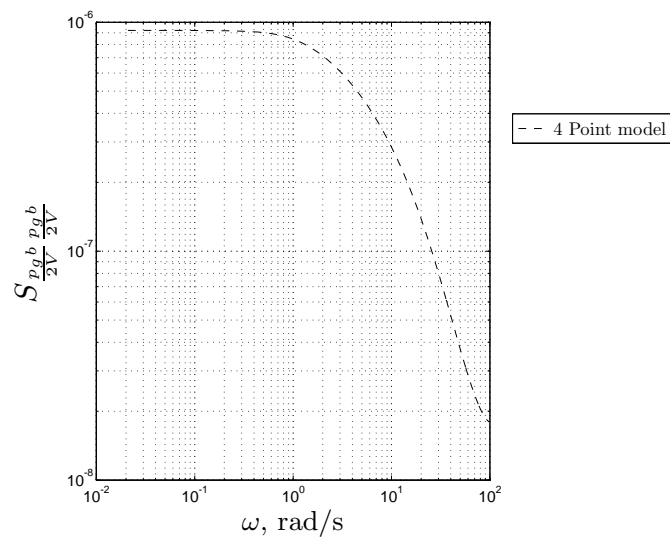


Figure 9.22: Auto power spectral density function $S_{\frac{pq}{2V} \frac{pq}{2V}}$ for Etkin's "four point" model ($L_g = 150$ m).

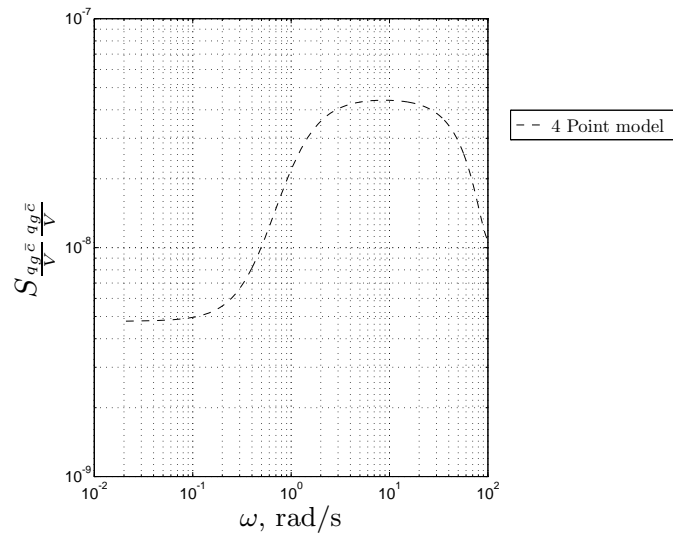


Figure 9.23: Auto power spectral density function $S_{qg\bar{c} qg\bar{c}} / V$ for Etkin's “four point” model ($L_g = 150$ m).

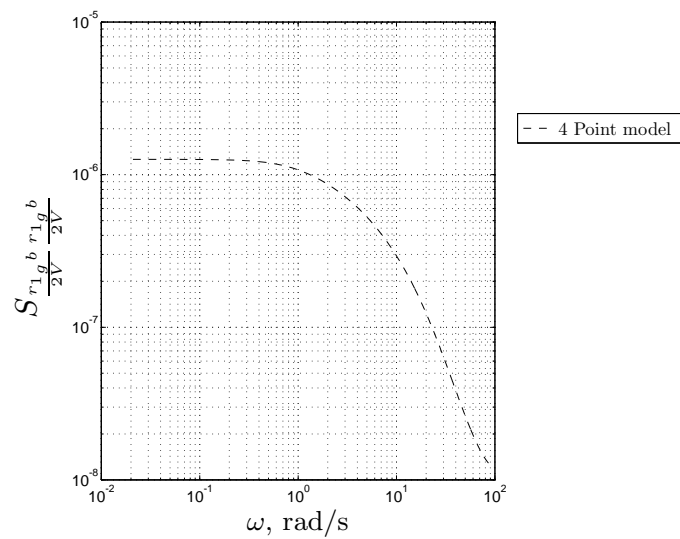


Figure 9.24: Auto power spectral density function $S_{r1g^b r1g^b} / (2V)$ for Etkin's “four point” model ($L_g = 150$ m).

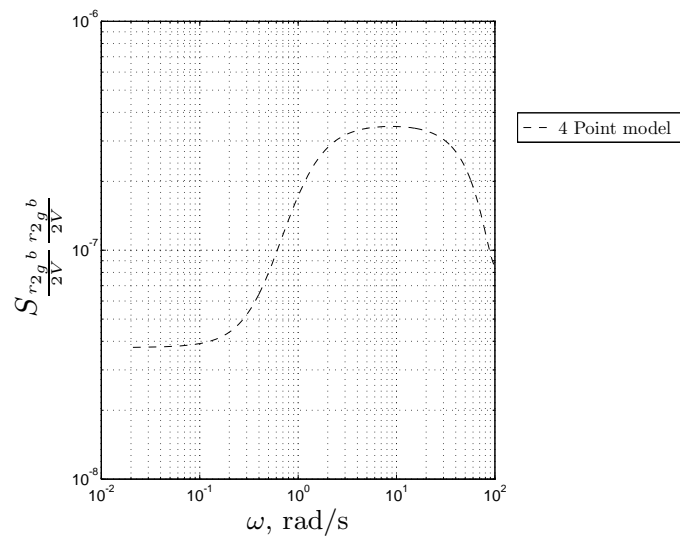


Figure 9.25: Auto power spectral density function $S_{r2g^b r2g^b} / (2V)$ for Etkin's “four point” model ($L_g = 150$ m).

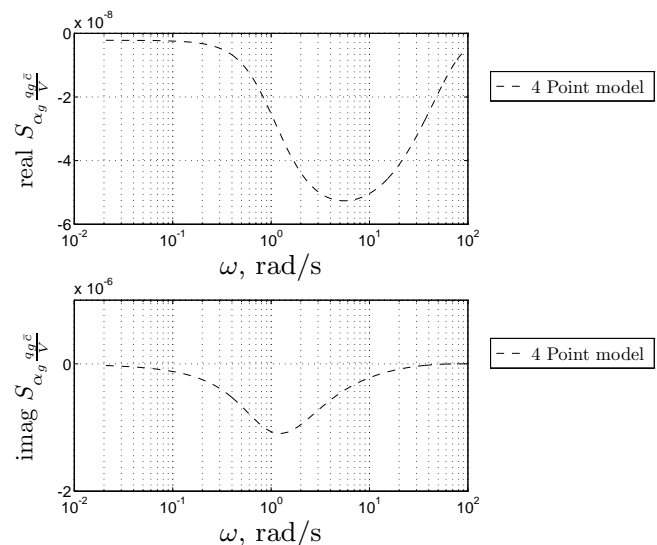


Figure 9.26: Cross power spectral density function $S_{\alpha_g qg^c} / V$ for Etkin's “four point” model ($L_g = 150$ m).

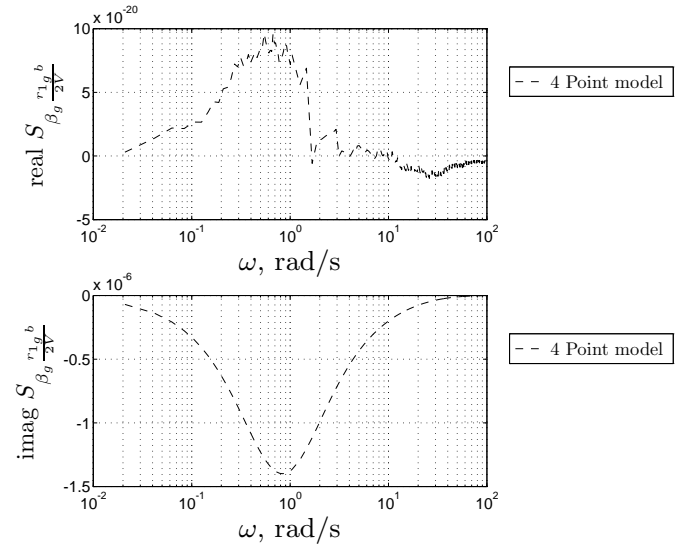


Figure 9.27: Cross power spectral density function $S_{\beta_g \frac{r_{1g}^b}{2V}}$ for Etkin's "four point" model ($L_g = 150$ m).

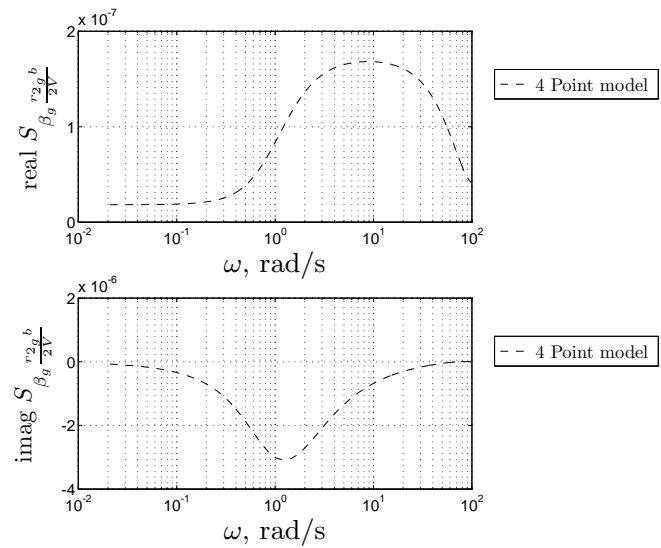


Figure 9.28: Cross power spectral density function $S_{\beta_g \frac{r_{2g}^b}{2V}}$ for Etkin's "four point" model ($L_g = 150$ m).

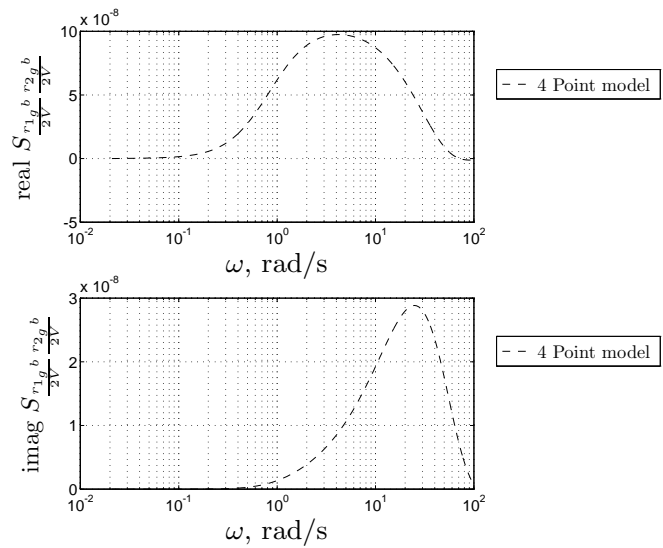


Figure 9.29: Cross power spectral density function $S_{\frac{r_1 g^b}{2V} \frac{r_2 g^b}{2V}}$ for Etkin's “four point” model ($L_g = 150$ m).

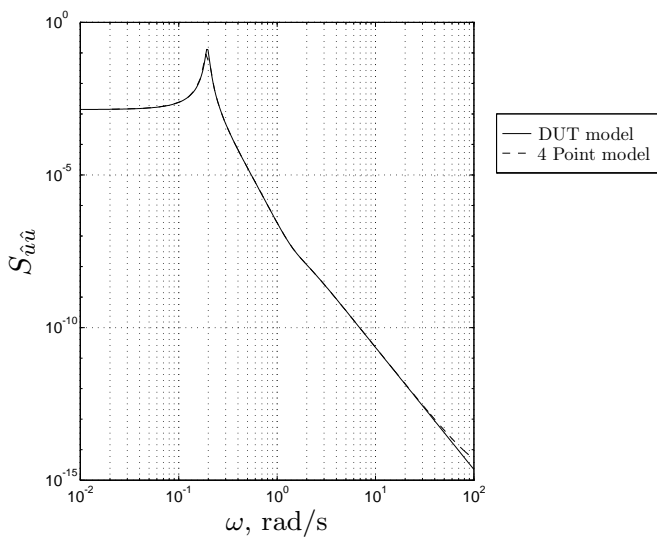


Figure 9.30: Power spectral density of \hat{u} for the Ce-500 'Citation' due to symmetrical gust u_g ($L_g = 150$ m).

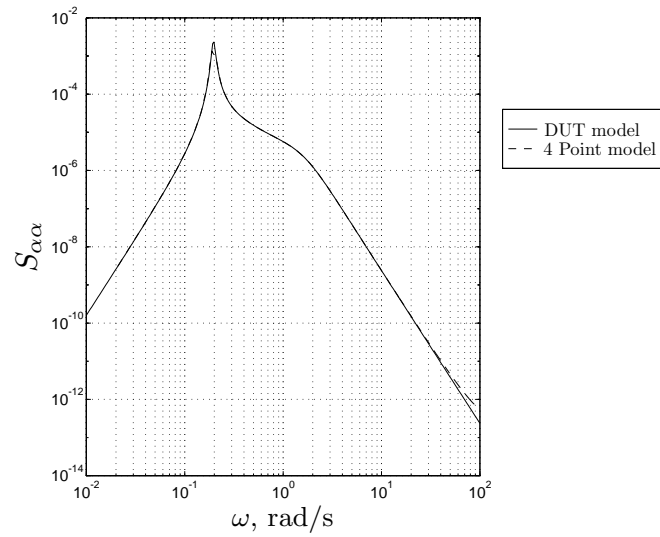


Figure 9.31: Power spectral density of α for the Ce-500 'Citation' due to symmetrical gust u_g ($L_g = 150$ m).

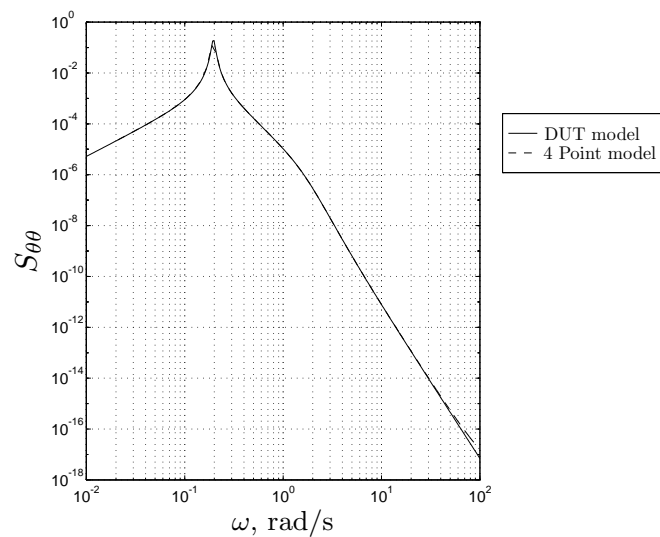


Figure 9.32: Power spectral density of θ for the Ce-500 'Citation' due to symmetrical gust u_g ($L_g = 150$ m).

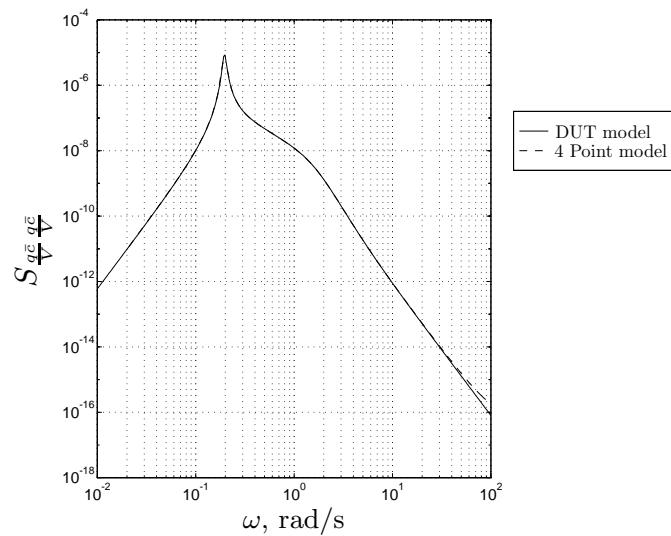


Figure 9.33: Power spectral density of $\frac{\bar{q}\bar{c}}{V}$ for the Ce-500 'Citation' due to symmetrical gust u_g ($L_g = 150$ m).

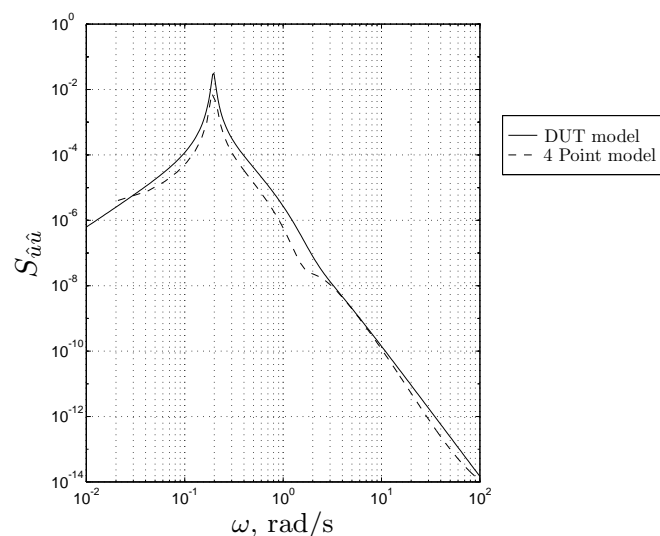


Figure 9.34: Power spectral density of \hat{u} for the Ce-500 'Citation' due to symmetrical gust w_g ($L_g = 150$ m).

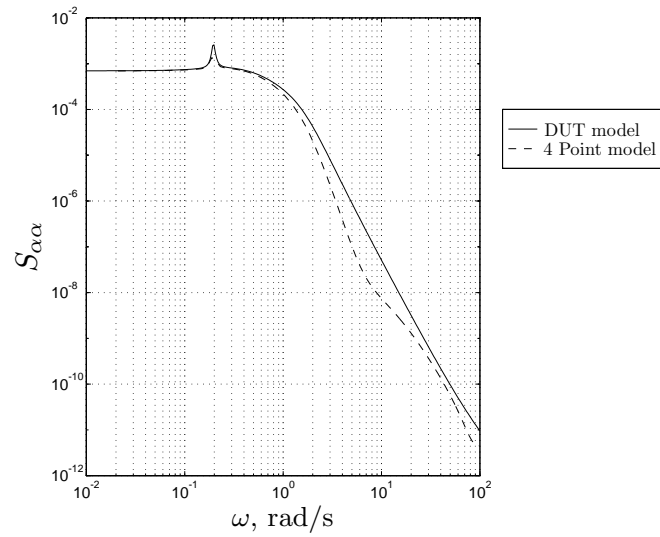


Figure 9.35: Power spectral density of α for the Ce-500 'Citation' due to symmetrical gust w_g ($L_g = 150$ m).

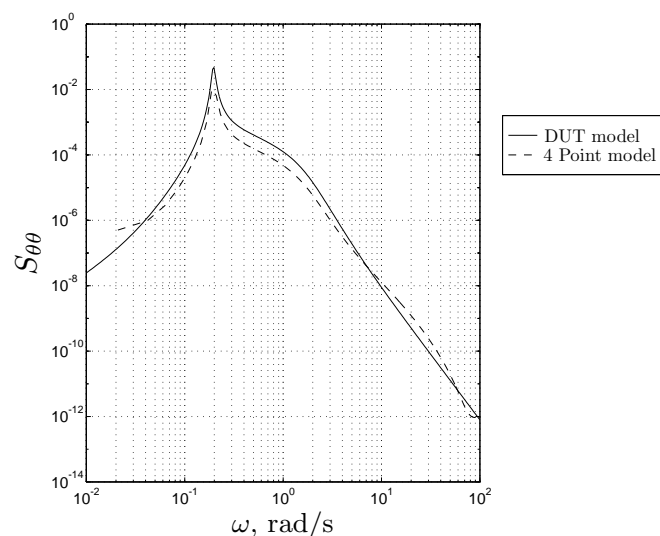


Figure 9.36: Power spectral density of θ for the Ce-500 'Citation' due to symmetrical gust w_g ($L_g = 150$ m).

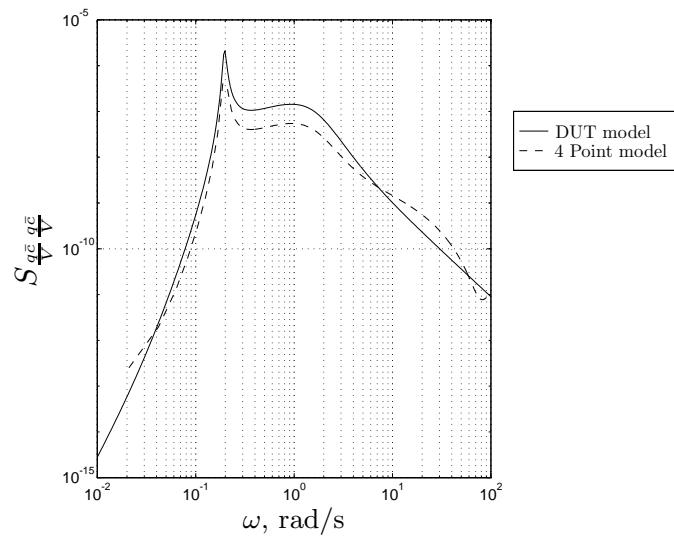


Figure 9.37: Power spectral density of $\frac{q\bar{c}}{V}$ for the Ce-500 'Citation' due to symmetrical gust w_g ($L_g = 150$ m).

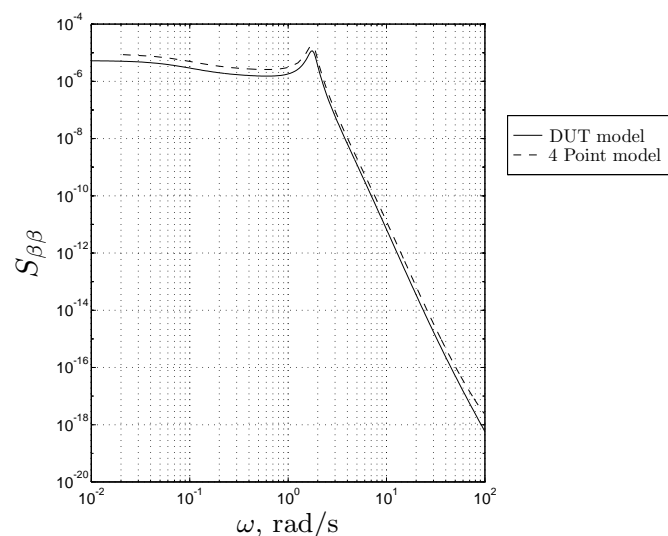


Figure 9.38: Power spectral density of β for the Ce-500 'Citation' due to asymmetrical gust u_g ($L_g = 150$ m).

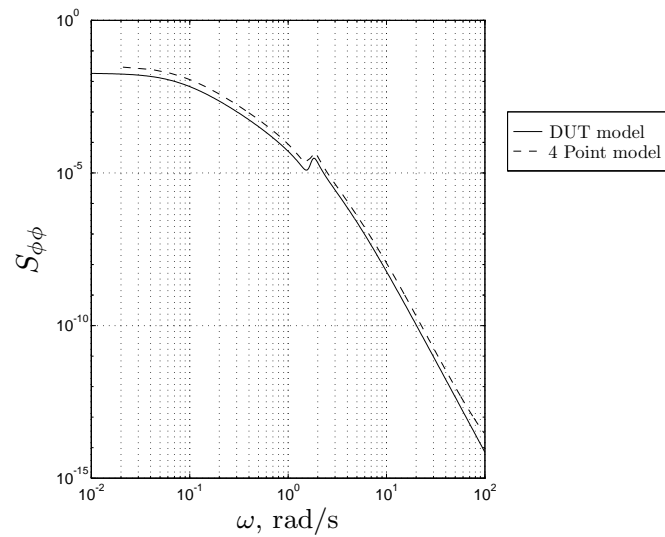


Figure 9.39: Power spectral density of ϕ for the Ce-500 'Citation' due to asymmetrical gust u_g ($L_g = 150$ m).

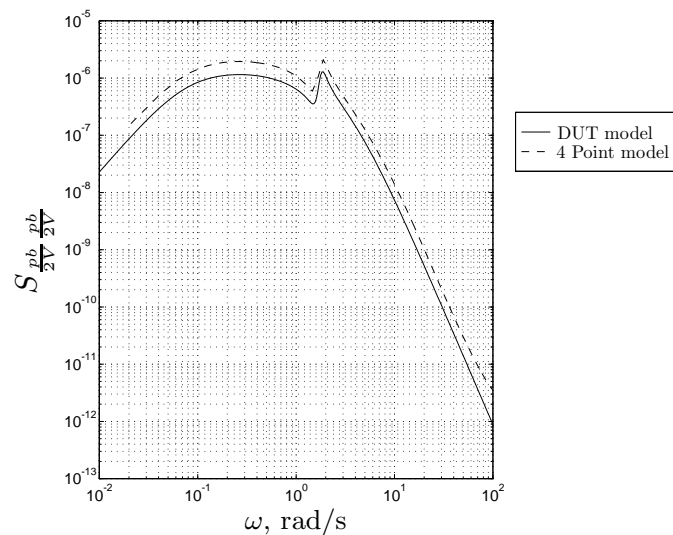


Figure 9.40: Power spectral density of $\frac{p_b}{2V}$ for the Ce-500 'Citation' due to asymmetrical gust u_g ($L_g = 150$ m).

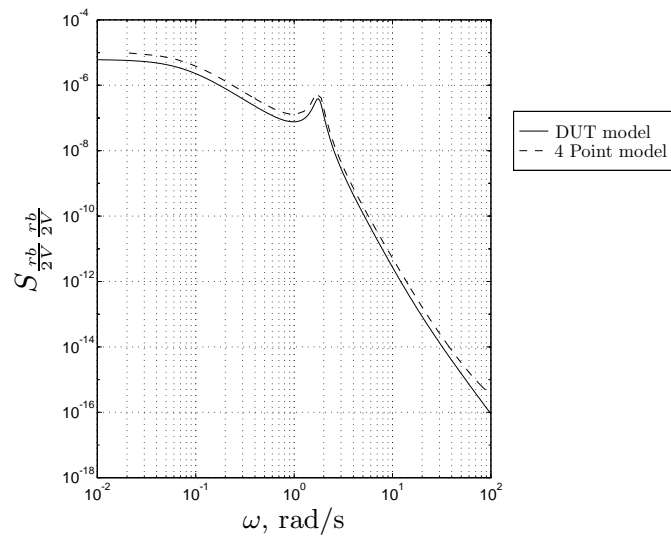


Figure 9.41: Power spectral density of $\frac{rb}{2V}$ for the Ce-500 'Citation' due to asymmetrical gust u_g ($L_g = 150$ m).

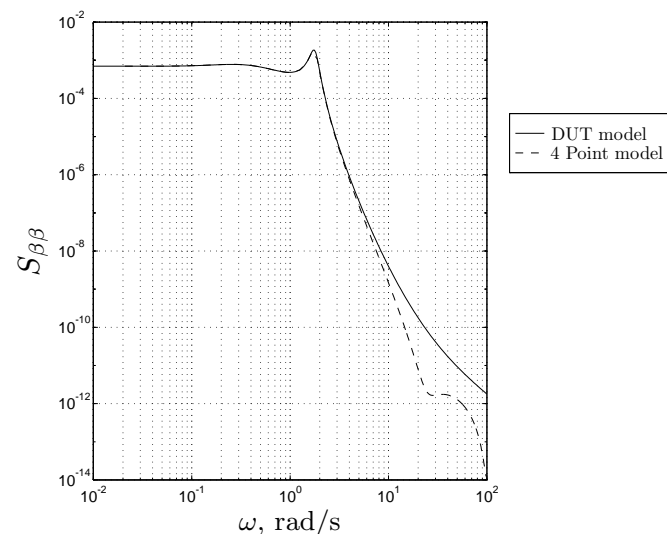


Figure 9.42: Power spectral density of β for the Ce-500 'Citation' due to asymmetrical gust v_g ($L_g = 150$ m).

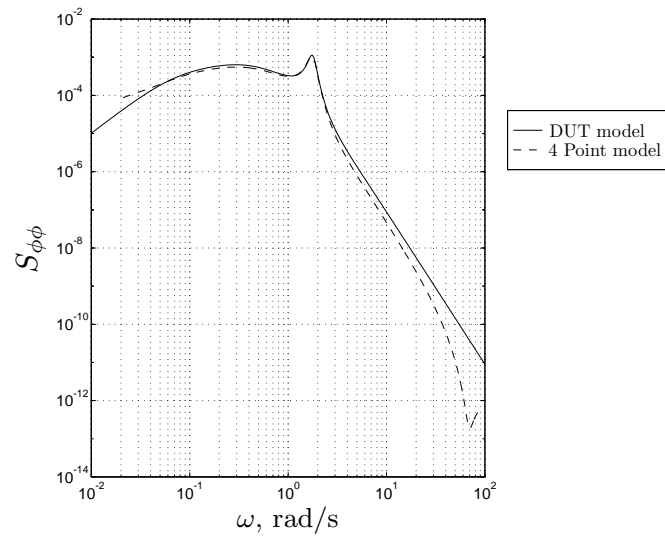


Figure 9.43: Power spectral density of ϕ for the Ce-500 'Citation' due to asymmetrical gust v_g ($L_g = 150$ m).

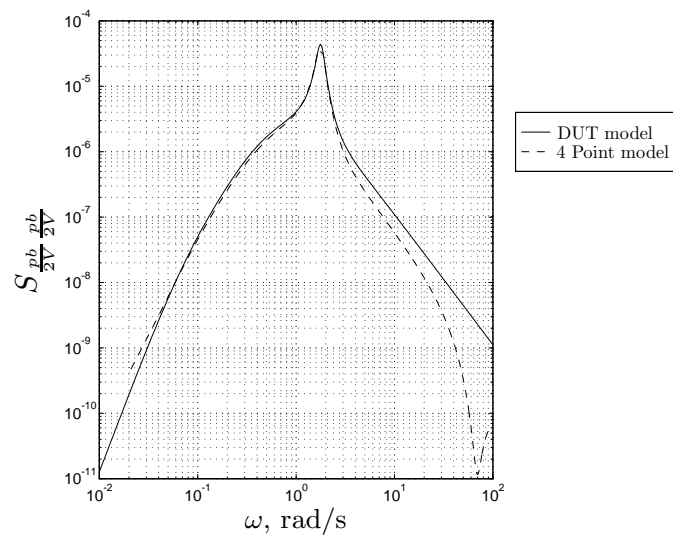


Figure 9.44: Power spectral density of $\frac{p_b}{2V}$ for the Ce-500 'Citation' due to asymmetrical gust v_g ($L_g = 150$ m).

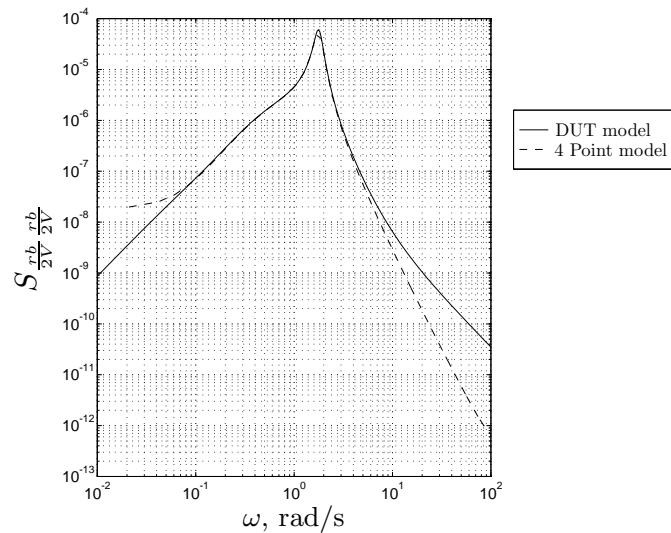


Figure 9.45: Power spectral density of $\frac{r_b}{2V}$ for the Ce-500 'Citation' due to asymmetrical gust v_g ($L_g = 150$ m).

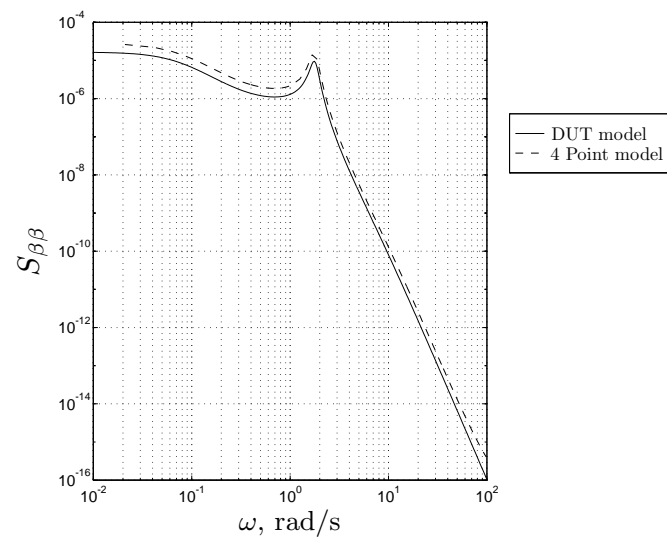


Figure 9.46: Power spectral density of β for the Ce-500 'Citation' due to asymmetrical gust w_g . ($L_g = 150$ m)

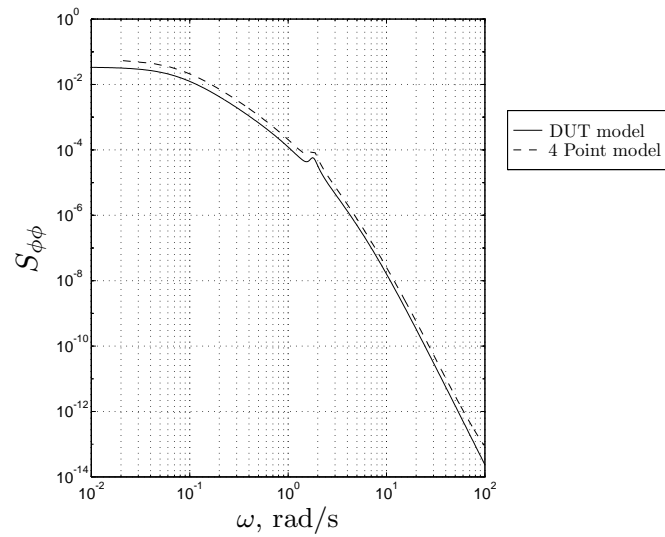


Figure 9.47: Power spectral density of ϕ for the Ce-500 'Citation' due to asymmetrical gust w_g ($L_g = 150$ m).

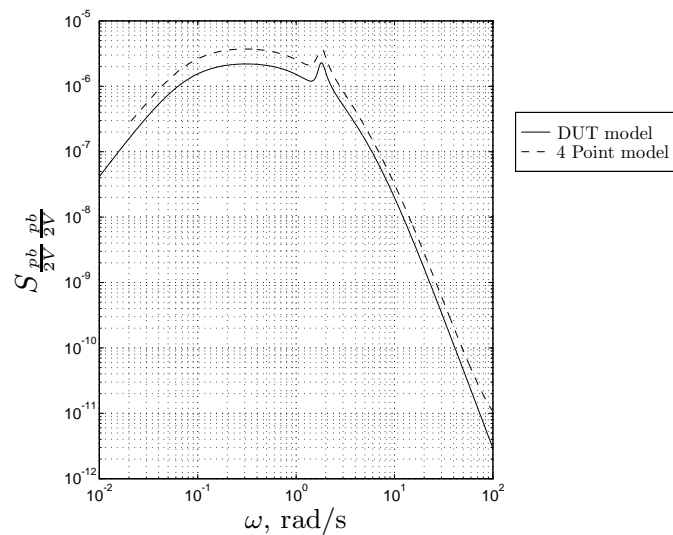


Figure 9.48: Power spectral density of $\frac{p_b}{2V}$ for the Ce-500 'Citation' due to asymmetrical gust w_g ($L_g = 150$ m).

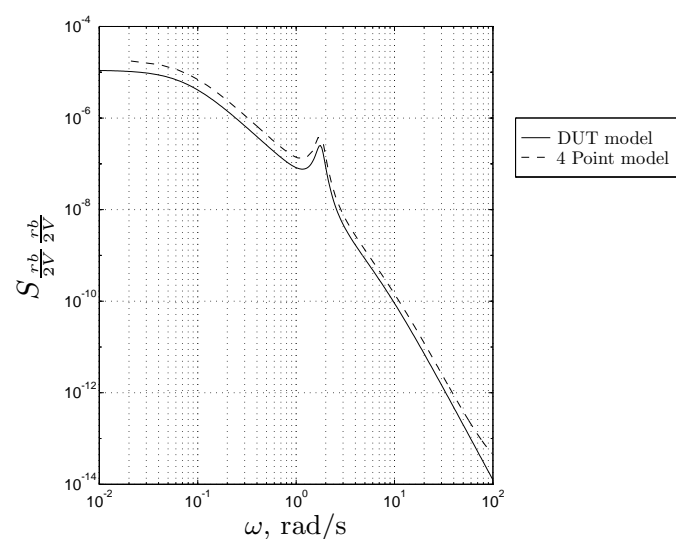


Figure 9.49: Power spectral density of $\frac{r^b}{2V}$ for the Ce-500 'Citation' due to asymmetrical gust w_g ($L_g = 150$ m).

References

- AGARD. (1975). *Approach and Landing Simulation* (AGARD-R No. 632). Neuilly-sur-Seine, France: Advisory Group for Aerospace Research and Development.
- Baarspul, M. (1990). A Review of Flight Simulation Techniques. *Progress in Aerospace Sciences*, 27(1), 1-120.
- Batchelor, G. K. (1953). *Theory of Homogeneous Turbulence*. Cambridge: Cambridge University Press.
- Billingsley, P. (1986). *Probability and Measure* (2nd. ed.). New York: Wiley.
- Boyce, W. E., & DiPrima, R. C. (1977). *Elementary Differential Equations and Boundary Value Problems* (3rd. ed.). New York: John Wiley & Sons.
- Bracewell, R. N. (1986). *The Fourier Transform and It's Application* (2nd. ed.). Stanford: McGraw-Hill.
- Brigham, E. O. (1974). *The Fast Fourier Transform*. New Jersey (NJ): Prentice-Hall.
- Bryson Jr., A. E., & Ho, Y. (1975). *Applied Optimal Control. Optimization, Estimation, and Control*. Washington (DC): Hemisphere Publishing Corporation.
- Burlington, R. S., & May Jr., D. C. (1970). *Handbook of Probability and Statistics with Tables* (2nd. ed.). New York: McGraw Hill.
- Chen, C. T. (1998). *Linear System Theory and Design* (3rd ed.). New York: Oxford University Press.
- Dwight, H. B. (1957). *Tables of Integrals and Other Mathematical Data*. New York: MacMillan.
- Endlich, R. M., & McLean, G. S. (1957). The Structure of the Jet Stream Core. *Journal of the Atmospheric Sciences*, 14(6), 543-552.
- Etkin, B. (1960). *A Simple Method for the Analogue Computation of the Mean-Square Response of Airplanes to Atmospheric Turbulence* (UTIA Technical Note No. 32).

- Etkin, B. (1972). *Dynamics of Atmospheric Flight*. New York: John Wiley and Sons.
- Etkin, B. (1980). *The Turbulent Wind and Its Effect on Flight* (UTIAS Report No. 44). University of Toronto.
- Fabian, V., & Hannan, J. (1985). *Introduction to Probability and Mathematical Statistics*. New York: Wiley.
- Gerlach, O. H. (1966). *Calculation of the Response of an Aircraft to Random Atmospheric Turbulence* (Delft University Report No. VTH-138). Delft.
- Gerlach, O. H., & Baarspul, M. (1968). *Calculation of the Response of an Aircraft to Random Atmospheric Turbulence* (Delft University Report No. VTH-139). TU Delft. (Part II: Asymmetric motions)
- Gerlach, O. H., & Schuring, J. (1970). *Mathematical Model of External Disturbances Acting on an Aircraft During an ILS Approach and Landing* (Delft University Report No. VTH-159). Delft.
- Houbolt, J. C., Steiner, R., & Pratt, K. G. (1964). *Dynamic Response of Airplanes to Atmospheric Turbulence Including Flight Data on Input and Response* (Tech. Rep. No. NASA-TR-R-199). Nasa Langley, Washington.
- Iribarne, J. V., & Cho, H. R. (1980). *Atmospheric Physics*. Dordrecht: Reidel Publishing Co.
- Jenkins, G. M., & Watts, D. G. (1968). *Spectral Analysis and its Application*. San Francisco: Holden Day Inc.
- Jonkers, H. L., Kappetijn, F. K., & Van der Vaart, J. C. (1981). *Digital Calculation of the Propagation in Time of the Aircraft Gust Response Covariance Matrix* (Delft University Report No. LR-266). Delft.
- Korn, G. A., & Korn, T. M. (1968). *Mathematical Handbook for Scientists and Engineers* (2nd. ed.). New York: McGraw Hill.
- Kuettner, J., & Jenkins, C. F. (1953). *Flight Aspects of the Mountain Wave* (USAF Cambridge Research Center). Washington.
- Kwakernaak, H., & Sivan, R. (1972). *Linear Optimal Control Systems*. New York: John Wiley & Sons.
- Ljung, L. (1987). *System Identification: Theory for the user* (1st ed.). New-Jersey: Prentice-Hall.
- Mathai, A. M., & Pederzoli, G. (1977). *Characterizations of the Normal Probability Law*. New Delhi: Wiley.

- Mulder, J. A., van Staveren, W. H. J. J., van der Vaart, J. C., de Weerdt, E., de Visser, C. C., in 't Veld, A. C., & Mooij, E. (2013). *Flight Dynamics* (Lecture notes No. AE3202). TU Delft.
- Newland, D. E. (1984). *An Introduction to Random Vibrations and Spectral Analysis* (2nd. ed.). New York: Longman Scientific and Engineering.
- Ogata, K. (2002). *Modern Control Engineering* (4th ed.). Upper Saddle River: Prentice-Hall Inc.
- Oppenheim, A. V., & Schafer, R. W. (1975). *Digital Signal Processing*. Englewood Cliffs (NJ): Prentice-Hall.
- Oppenheim, A. V., Willsky, A. S., & Hamid, N. S. (1997). *Signals and Systems* (2nd ed.). London: Prentice-Hall.
- Papoulis, A. (1991). *Probability, Random Variables, and Stochastic Processes* (3rd. ed.). New York: McGraw-Hill.
- Patel, J. K., & Read, C. B. (1982). *Handbook of the Normal Distribution*. New York: Dekkers.
- Priestley, M. B. (1981). *Spectral Analysis and Time Series*. London: Academic Press.
- Pritchard, F. E. (1966). *A Statistical Model of Atmospheric Turbulence and a Review of the Assumptions Necessary for Its Use* (AGARD No. CP.17 Pt.II). Paris: Advisory Group for Aerospace Research and Development.
- Ruygrok, G. J. J. (1970). *Gegevens van de Atmosfeer* (Delft University Report No. VTH-71). Delft.
- Stevens, B. L., & Lewis, F. L. (1992). *Aircraft Control and Simulation*. New York: John Wiley & Sons.
- Van der Vaart, J. C. (1975). *The Impulse Response Method for the Calculation of Statistical Properties of Aircraft Flying in Random Atmospheric Turbulence* (Delft University Report No. VTH-197). Delft.